

August 2024

**MODELING
EUTROPHICATION
PROCESSES IN THE
DELAWARE RIVER ESTUARY:
THREE-DIMENSIONAL
HYDRODYNAMIC MODEL**

Technical Report No. 2024-4

FINAL REPORT

Managing, Protecting and Improving
the Water Resources of the
Delaware River Basin since 1961



MODELING EUTROPHICATION PROCESSES IN THE DELAWARE RIVER ESTUARY: THREE-DIMENSIONAL HYDRODYNAMIC MODEL

This report was prepared by the following staff of the Delaware River Basin Commission (DRBC) who performed the work described herein at the direction of Executive Director Steve Tambini.

Fanghui Chen, Ph.D., P.E. (primary author)

Li Zheng, Ph.D.

Thomas Amidon, BCES

Namsu Suk, Ph.D.

Kristen Bowman Kavanagh, P.E.

Senior Water Resource Engineer

Senior Water Resource Modeler

Manager, Water Resource Modeling

Director, Science and Water Quality Management

Deputy Executive Director

SUGGESTED CITATION

Chen, F., Zheng, L., Amidon, T., Suk, N., & Kavanagh K.B. (2024). *Modeling Eutrophication Processes in the Delaware River Estuary: Three-Dimensional Hydrodynamic Model*. (DRBC Report No. 2024-4). Delaware River Basin Commission.

ACKNOWLEDGEMENTS AND DISCLAIMERS

This work was funded in part by grants from the United States Environmental Protection Agency, the New Jersey Department of Environmental Protection, the Pennsylvania Department of Environmental Protection, and the William Penn Foundation.

Critical datasets, without which this work could not have been performed, were obtained from the National Oceanic and Atmospheric Administration’s National Climatic Data Center as well as the United States Geological Survey (USGS).

The DRBC is grateful for the technical support and direction provided by its Model Expert Panel, composed of internationally renowned modelers: Dr. Steve Chapra, Dr. Carl Cerco, Dr. Bob Chant, and Tim Wool. In addition to the Model Expert Panel, DRBC acknowledges with appreciation its hydrodynamic modeling consultant, Dr. Hugo Rodrigues of GHD. Vince DePaul of USGS provided important technical support, in particular the estimation of boundary flows for unmonitored tributaries and watersheds. DRBC also acknowledges with appreciation the invaluable guidance received from the day-to-day interactions with its modeling consultants, Dr. Victor Bierman and Scott Hinz of LimnoTech.

DRBC acknowledges the various National Pollutant Discharge Elimination System (NPDES) permit-holders within the tidal estuary that provided critical discharge data for this work, with special appreciation to the Philadelphia Water Department for sharing current velocity data they collected at three buoy locations during DRBC’s simulation period.

Finally, Water Quality Advisory Committee members provided technical reviews and comments on the draft report released in December 2021 to improve both the model and this report.

EXECUTIVE SUMMARY

The hydrodynamic model described herein is one component of a larger eutrophication modeling study of the Delaware River Estuary, the goal of which is to develop and calibrate a water quality model of eutrophication processes in the Delaware River Estuary¹ from the head of the tide at Trenton, New Jersey, to the Atlantic Ocean. The purpose of the project is to provide the scientific basis for the Delaware River Basin Commission (DRBC) and others to evaluate management options for establishing water quality criteria for dissolved oxygen and nutrients as necessary to support higher aquatic life designated uses, and for establishing loading targets for point and non-point sources to achieve these criteria. This report documents the technical approach and fitness of a three-dimensional hydrodynamic model that was deemed by an external Model Expert Panel to be adequately calibrated for its intended purpose.

The DRBC developed the hydrodynamic model using the Environmental Fluid Dynamics Code (EFDC) to simulate transport information (water surface elevation, current velocity, salinity, and water temperature) over a range of hydrologic and boundary conditions with the degree of accuracy and confidence necessary to support calibration and application of the linked water quality model. The linked water quality model was developed using the Water Quality Analysis Simulation Program (WASP), and development and calibration of that model is documented in a separate report (Zheng et al., 2024). Both the EFDC and WASP models are supported by the U.S. Environmental Protection Agency (EPA).

The hydrodynamic model represents the estuary in three dimensions through a numerical grid comprised of 1,876 computational cells in the horizontal plane and 10 vertical layers in the navigation channel, resulting in a total of 11,490 cells throughout the domain (Figure ES-1). Within each cell, the model simulates time-variable flow by simultaneously solving, every 10 seconds, the fundamental physics equations that describe the movement of water in an estuary, namely the conservation of mass, momentum, and heat, as well as temperature and salinity throughout the domain.

The DRBC developed and calibrated the hydrodynamic model for the periods of 2018-2019 and 2012. For each calendar year, time-variable boundary conditions were assigned including: water surface elevations at the mouth of the Bay and the western end of the Chesapeake and Delaware (C&D) Canal; freshwater inflows into the mainstem of the Delaware River Estuary; salinity and water temperature at all inflow and open boundaries; and meteorological data at the water surface including air temperature, air pressure, dew point, precipitation, wind speed and direction, and solar radiation.

Boundaries generally vary spatially and temporally, making their specification over three calendar years a significant undertaking. Freshwater inflows, for example, include: flows from the upstream boundary and tributaries (gaged and ungaged), non-point sources and municipal separate storm sewer systems (MS4s), point source discharges, combined sewer overflows (CSOs), direct precipitation onto the water surface,

¹ The Delaware River Estuary includes the tidally-influenced Delaware River and the Delaware Bay.

and withdrawals. To accomplish this task, a statistical watershed sub-model based on a regional analysis of shared features was developed to estimate hydrologic inputs from unmonitored tributaries and watersheds. In addition, the DRBC performed a numerical evaluation that determined a three-dimensional grid consisting of 10 vertical layers in the navigation channel is needed to adequately simulate gradients and mass transfer in the system.

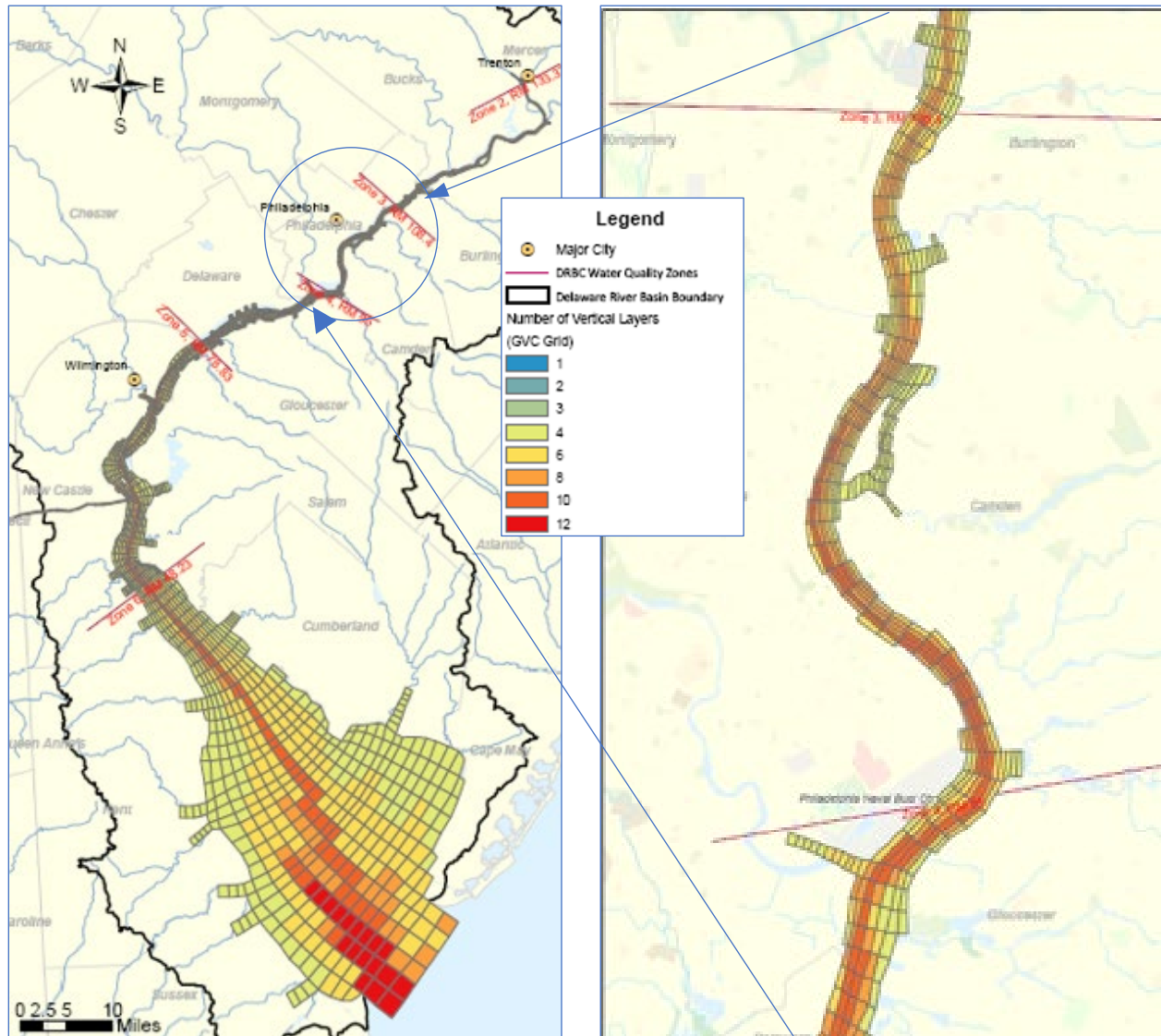


Figure ES- 1: Numerical Grid with Number of Vertical Layers

Hydrodynamic calibration was focused on reproducing observed water surface elevation (WSE), depth-averaged current velocity, and the longitudinal and vertical distribution of salinity and water temperature at various locations throughout the estuary during the calibration periods. Several parameters were adjusted based on system knowledge and typical ranges to calibrate the hydrodynamic model, the most

important being effective bed (or bottom) roughness (a friction factor that affects the propagation of tides) and the turbulent exchange coefficients for conduction and evaporation (factors that control heat loss to the air). Model performance was evaluated through both visual comparisons and quantitative, statistical measures. Visualizations of time histories of simulated results along with observed data, for instance, show the degree to which the model captures the general trends and overall magnitudes of the observed condition, while statistical measures were used to quantify the quality of fit between the observations and model predictions. Figures ES-2 and ES-3 provide examples of the types of visual comparisons performed to assess model predictions versus observed data.

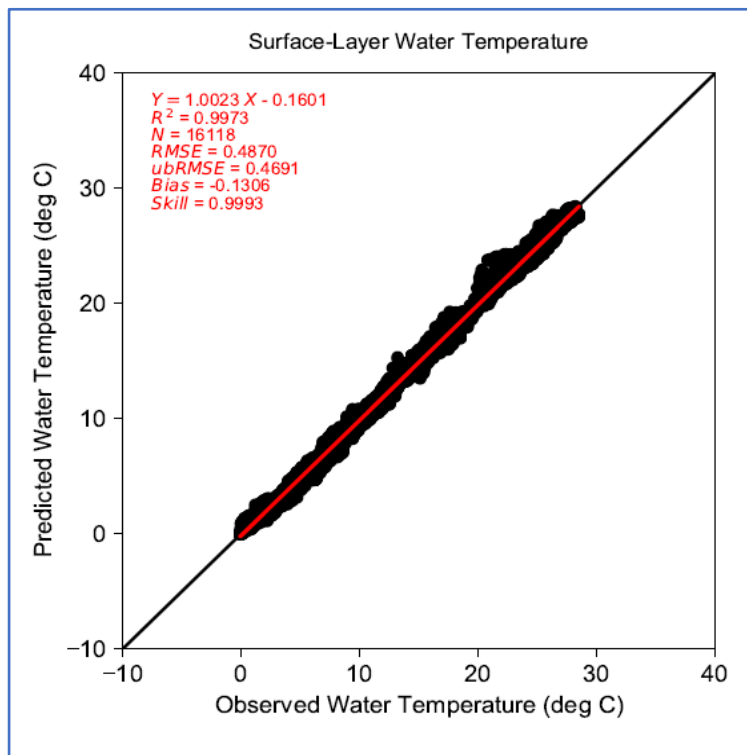


Figure ES-2: Predicted vs Observed Temperature

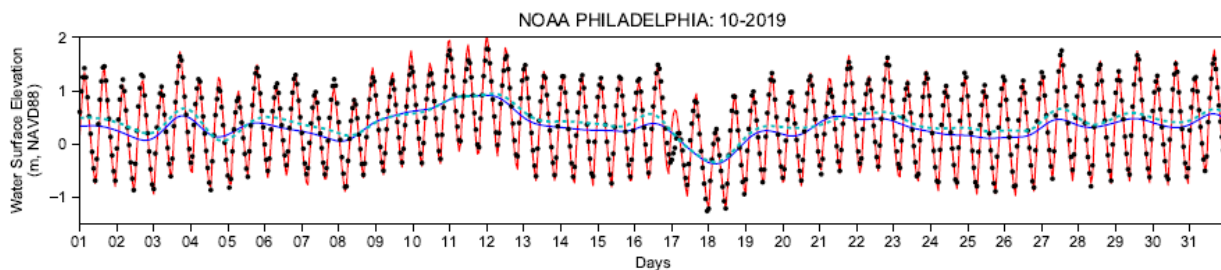


Figure ES-3: One-Month Time Series Showing Predicted and Observed Water Surface Elevations

Figure ES-4 is an example of one of the statistical analyses performed to evaluate the model calibration. As shown, model skill scores for predicted water surface elevation (WSE), velocity, water temperature, and salinity varied by location and year. Skill scores for WSE ranged from 0.982 to 0.996; skill scores for velocity ranged from 0.921 to 0.987; skill scores for water temperature varied from 0.988 to 0.999; and skill scores for salinity varied from 0.712 to 0.965. Skill scores of 1.0 represent a perfect fit; however, skill scores greater than 0.975 for WSE, 0.90 for velocity and temperature, and 0.85 for salinity, are considered accurate. For salinity, skill scores above 0.70 are considered acceptable. Thus, the model fitness reflected

in these skill scores represents a remarkable achievement. Model goodness of fit is also supported by the other statistical metrics as described in Section 3.1.

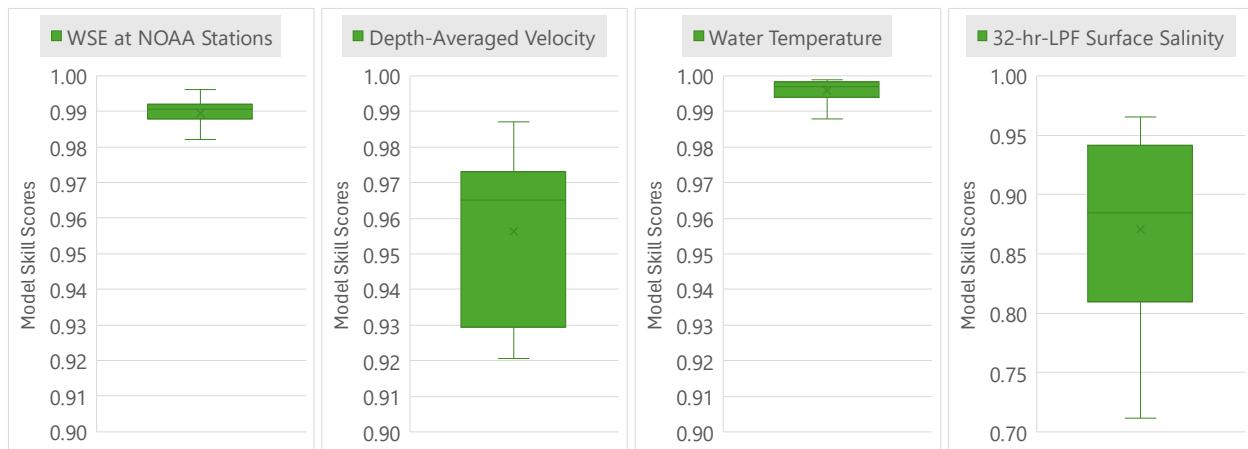


Figure ES-4: Model Skill Scores for WSE, Velocity, Temperature, and Salinity

In accordance with the established Quality Assurance Project Plan (DRBC, 2019) for this project, a “weight of evidence” approach for calibration was used in close coordination with the Model Expert Panel in order to judge the acceptability of the model for its intended purpose. DRBC’s Model Expert Panel unanimously agreed in May 2020, and submitted a report documenting their findings in October 2020², that the hydrodynamic model is appropriate and sufficiently calibrated to be used as the basis for the eutrophication model. With the guidance of the Model Expert Panel and the benefit of thoughtful comments provided by members of DRBC’s Water Quality Advisory Committee, DRBC has further enhanced the model and its documentation as reflected in this report.

While the development and calibration of this hydrodynamic model represents a significant milestone, it is important to recognize that this model is not intended to be merely a useful reference. The model as described is fully adequate for its purpose, namely, to provide dynamic inputs for a water quality model that relates specific water and pollutant loading scenarios with dissolved oxygen outcomes in the Delaware River Estuary. However, the DRBC is continuing to develop modifications and improvements to the model both for its primary purpose and for related purposes as appropriate. Documenting model development and calibration within this report is of course necessary, but the model is not a static tool. The DRBC is using the tool to better understand estuary dynamics and will continuously improve the model consistent with its goals and resources.

² The presentation report of the Model Expert Panel was delivered to the DRBC’s Water Quality Advisory Committee on October 29, 2020, and can be found on the DRBC website at https://www.nj.gov/drbc/library/documents/WQAC/102920/expert-panel_model-update.pdf

TABLE OF CONTENTS

Acknowledgements and Disclaimers	ii
Executive Summary.....	iii
Table of Contents.....	vii
1. Introduction	1
1.1 Objectives of Modeling Study.....	1
1.2 Study Area.....	2
1.2.1 Delaware River Basin	2
1.2.2 Delaware River Estuary	4
1.2.3 Chesapeake & Delaware Canal	5
1.3 Salinity Intrusion	6
1.4 Overview of Technical Approach	9
2. Hydrodynamic Model Development	11
2.1 Model Description	11
2.2 Model Domain and Numerical Grid.....	13
2.3 Bathymetry and Generalized Vertical Coordinate (GVC)	14
2.4 Boundary Conditions.....	18
2.4.1 Water Surface Elevations.....	18
2.4.2 Freshwater Inflows.....	19
2.4.3 Water Temperature and Salinity	27
2.4.4 Climate / Meteorological Forcing	32
2.4.5 Initial Conditions	34
3. Hydrodynamic Model Calibration.....	35
3.1 Calibration Approach, Model Accuracy, and Reliability	35
3.2 Calibration Parameters	42
3.2.1 Bottom Roughness Height Z_0	42
3.2.2 Turbulent Model Parameter	43
3.2.3 Adjustment to Tidal Surface Elevation in C&D Canal.....	44
3.2.4 Turbulent Exchange Coefficients for Conduction and Evaporation	45
3.2.5 Numerical Stability and Time Step.....	45



3.3 Calibration Results	45
3.3.1 Water Surface Elevation	46
3.3.2 Current Velocity	49
3.3.3 Water Temperature	52
3.3.4 Salinity.....	54
3.4 Sensitivity to Vertical Grid Resolution	56
4. Summary.....	59
References	60

LIST OF APPENDICES

- Appendix A: Numerical grid and projected bathymetry
- Appendix B: Development of watershed flows
- Appendix C: Meteorological data
- Appendix D: Summaries of NOAA and USGS calibration data
- Appendix E: Bottom roughness height
- Appendix F: Summary of tidal harmonic analysis based on 2019 simulation
- Appendix G: Tidal harmonics analysis based on predicted 2019 water surface elevation
- Appendix H: Time series of observed and predicted water surface elevation (2019)
- Appendix I: Comparison of observed and predicted water surface elevation
- Appendix J: Observed and predicted depth-averaged current velocity magnitude at NOAA current velocity stations
- Appendix K: Observed and predicted depth-averaged current velocity magnitude at PWD buoy locations
- Appendix L: Summary of harmonic analysis for current velocity at NOAA stations
- Appendix M: Harmonics analysis for current velocity at NOAA stations
- Appendix N: Summary of harmonic analysis for current velocity at PWD stations
- Appendix O: Harmonics analysis for current velocity at PWD stations
- Appendix P: Observed and predicted water temperature
- Appendix Q: Observed and predicted hourly and 32-hour-low-pass-filtered salinity for 2018, 2019, and 2012 periods
- Appendix R: Observed and predicted daily average chloride for 2018, 2019, and 2012
- Appendix S: Longitudinal profile of salinity in Delaware River and Bay for 2018, 2019, and 2012
- Appendix T: Evaluation of vertical resolution

LIST OF TABLES

Table 2-1: Summary of NOAA Stations and Datum Conversion	18
Table 2-2: Summary of Tributary Inflow Boundaries.....	20
Table 2-3 Summary of Point Source Discharges	24
Table 2-4 Consolidated CSO Discharge Locations.....	25
Table 2-5: Summary of Major Withdrawals.....	26
Table 2-6: Availability of Tributary Temperature Data for Simulation Periods	29
Table 2-7: Monthly Mean Water Temperature near the Mouth of Delaware Bay	30
Table 2-8: NOAA-NCDC Weather Stations	32
Table 3-1 Criteria to Assess Coastal Hydrodynamic Model Performance	42
Table 3-2 Bottom Roughness Height	43
Table 3-3: Harmonic Constituents for Model Performance Evaluation	47
Table 3-4: Model Performance Predicting Tidal Elevation at NOAA Stations (2018-2019).....	48
Table 3-5: Model Performance Predicting Tidal Elevation at NOAA Stations (2012)	49
Table 3-6: Model Performance Predicting Depth-Averaged Current Velocity at NOAA Stations	50
Table 3-7: Model Performance Predicting Depth-Averaged Current Velocity at PWD Buoy Locations.....	51
Table 3-8: Model Performance Predicting Water Temperature (2018-2019).....	53
Table 3-9: Model Performance Predicting Water Temperature (2012)	54
Table 3-10: Model Performance Predicting 32-hr-LPF Surface Salinity (2018-2019)	54
Table 3-11: Model Performance Predicting 32-hr-LPF Surface Salinity (2012)	55



LIST OF FIGURES

Figure ES- 1: Numerical Grid with Number of Vertical Layers iv

Figure ES-2: Predicted vs Observed Temperature v

Figure ES-3: One-Month Time Series Showing Predicted and Observed Water Surface Elevations v

Figure ES-4: Model Skill Scores for WSE, Velocity, Temperature, and Salinity vi

Figure 1-1: Delaware River Basin and Bay 3

Figure 1-2: Delaware River Estuary Map and Location of the Salt Front..... 8

Figure 1-3 Relationship between Chloride and Specific Conductance Developed using DRBC Boat Run Data (a), and Developed by USGS in the 1970s (b) 9

Figure 2-1: Numerical Grid and Projected Bathymetry 15

Figure 2-2: Example of GVC Grid..... 16

Figure 2-3 Number of Vertical Layers 17

Figure 2-4: Hydrograph of Delaware River at Trenton 21

Figure 2-5: Delineation of Watershed Drainage Areas 23

Figure 2-6 Consolidated CSO Discharge Locations..... 26

Figure 2-7: Freshwater Budget 2018-2019 27

Figure 2-8: Water Temperature and Salinity at Trenton During 2019..... 28

Figure 2-9: Predicted Daily Averaged Salinity at Chesapeake City. Predicted salinity at Chesapeake City was based on salinity at Reedy Island and Susquehanna River at Marietta..... 31

Figure 2-10: Locations of Five Weather Stations Used to Characterize Climatic Boundaries 33

Figure 3-1: Locations of NOAA Tide Stations 36

Figure 3-2: Locations of USGS Stations on Delaware River Mainstem 37

Figure 3-3: Locations of NOAA and PWD Stations for Current Velocity 38

Figure 3-4: DRBC Boat Run Sampling Locations..... 39

Figure 3-5: Distribution of M2, M4, and M6 Water Level Amplitudes 47

LIST OF ACRONYMS/ABBREVIATIONS

1D	one-dimensional
2D	two-dimensional
3D	three-dimensional
ADCP	acoustic Doppler current profiler
ASC	Average Seasonal Cycle
C&D Canal	Chesapeake and Delaware Canal
CCMUA	Camden County Municipal Utilities Authority
COSMIC	Conservative Operator Splitting for Multidimensions with Inherent Constancy
CoW	City of Wilmington
CSO	combined sewer overflow
DELCORA	Delaware County Regional Water Quality Control Authority
DEM	Digital Elevation Model
DO	dissolved oxygen
DRBC	Delaware River Basin Commission
EFDC	Environmental Fluid Dynamics Code
EPA	U.S. Environmental Protection Agency
ETM	estuarine turbidity maximum zone
FEMA	Federal Emergency Management Agency
FNC	Federal Navigation Channel
GVC	Generalized Vertical Coordinate (Grid)
LCL	laterally constrained and localized-sigma
ubRMSD	unbiased Root Mean Square Difference
M2	Principal lunar semidiurnal constituent
MHHW	mean higher high water
MLLW	mean lower low water
MS4	municipal separate storm sewer system
NAD83	North American Datum of 1983
NAVD88	North American Vertical Datum of 1988
NCDC	NOAA's National Climatic Data Center
NOAA	National Oceanic and Atmospheric Administration
NPDES	National Pollutant Discharge Elimination System

NPS	non-point source
PWD	Philadelphia Water Department
r	Correlation Coefficient
R-squared	Coefficient of determination
RM	River Mile
RMSE	Root Mean Square Error
USGS	U.S. Geological Survey
USACE	U.S. Army Corps of Engineers
WASP	Water Quality Analysis Simulation Program
WSE	water surface elevation
Z0	effective bottom (or bed) roughness height

1. INTRODUCTION

The Delaware River Basin Commission (DRBC or Commission) adopted a resolution on September 13, 2017, recognizing the significant water quality improvements in the Delaware River Estuary and the vital importance of determining the appropriate aquatic life designated uses and water quality criteria necessary to support these uses. The resolution specifically requires the development and calibration of a eutrophication model for the Delaware River Estuary, as well as the formation of an Expert Panel to provide input and advice to the DRBC.

A hydrodynamic model was developed as one component of the larger eutrophication modeling study of the Delaware River Estuary, the goal of which is to develop and calibrate a water quality model of eutrophication processes in the Delaware River Estuary from the head of the tide at Trenton, New Jersey, to the ocean. The eutrophication modeling study will enhance our understanding of the impact of nutrient loads on dissolved oxygen conditions in the tidal Delaware River and Bay, particularly in a 38-mile-long segment of the tidal river including Zone 3, Zone 4, and upper Zone 5 where a summertime dissolved oxygen (DO) sag (lower levels of dissolved oxygen than are observed elsewhere in the Estuary) is observed to occur every year. This effort includes: 1) the convening of an Expert Panel to guide the development of the eutrophication model; 2) the completion of a two-year monitoring program in partnership with wastewater authorities in order to obtain data on nutrient loadings from point sources; 3) the completion of two years of intensive monitoring of key tributaries and ambient waters to develop loadings from key tributaries and to establish model calibration targets; 4) field studies on primary productivity in the lower Delaware River Estuary; and 5) development of linked hydrodynamic and water quality models. The project will provide the scientific basis for the DRBC to evaluate management options in establishing water quality criteria for dissolved oxygen and nutrients as necessary, and for establishing loading targets for point and non-point sources into the Delaware River Estuary to achieve these criteria.

1.1 OBJECTIVES OF MODELING STUDY

The three-dimensional (3D) hydrodynamic model development and calibration described herein provides the foundation for the linked water quality model of the Delaware River Estuary. Specifically, the spatial resolution of the linked models is generally dictated by the needs of the hydrodynamic model, while information from the 3D hydrodynamic model, including water volume, current velocity, flow, mixing characteristics, salinity, and water temperature, is transferred to the water quality model for use in simulating water column transport of constituents. The objective of the hydrodynamic model, therefore, is to simulate transport information over a range of hydrologic and boundary conditions with the degree of accuracy and confidence necessary to drive the water quality model calibration and application.

1.2 STUDY AREA

The study area encompasses the entire Delaware River drainage basin, while the Delaware River Estuary (the tidal Delaware River and Bay) defines the extent of the hydrodynamic model domain. The Chesapeake and Delaware (C&D) Canal is a unique boundary to the hydrodynamic model and warrants a brief description as well (see Section 1.2.3).

1.2.1 Delaware River Basin

The Delaware River extends 330 miles from Hancock, New York, in the Catskill Mountains to the mouth of the Delaware Bay where it enters the Atlantic Ocean between Cape May, New Jersey, and Cape Henlopen, Delaware (Figure 1-1). It is the longest un-dammed river on the Atlantic coast of the United States. The entire Delaware River basin comprises 13,539 square miles in four states (New York, New Jersey, Pennsylvania, and Delaware), including the 782 square miles of the Delaware Bay itself. Approximately 14.2 million people (almost 5% of the U.S. population) rely on the waters of the Delaware River Basin for multiple uses including drinking water, irrigation, power generation, and industry. In addition to the more than 8.6 million people in the Delaware River Basin itself, the Catskill Mountain Region of New York State supplies approximately half of New York City's drinking water from three basin reservoirs (Cannonsville, Pepacton, and Neversink).

Situated in the Mid-Atlantic temperate zone, the Delaware River Basin is influenced by two major North American weather systems: 1) low pressure systems originating in the south that move along the coast bringing substantial rainfalls, and 2) Canadian high-pressure systems that bring heavy snowfall and cold temperatures to the upper northwest portions of the basin. Coastal influences are more significant in the south and east portions of the basin. Average annual precipitation ranges from 40 inches in southern New Jersey to about 50 inches in the Catskill Mountains of southern New York; annual snowfall ranges from 13 inches in southern New Jersey to about 80 inches in the Catskill Mountains (Dolgoplova, 2014). Precipitation is approximately evenly distributed throughout the year, with a little higher average precipitation occurring in March and again from July to September; however, it is not uncommon for the highest rainfall to occur in July or August due to sporadic summer storms. The mean air temperature at the Philadelphia airport is -4.0°C in winter and $+23^{\circ}\text{C}$ from June to September. The mean annual precipitation amount is 41.6 inches: July averages 4.3 inches while January and February average 2.7 inches per month.

The East and West Branches of the Delaware River combine at River Mile (RM) 330 in Hancock, New York, to form the mainstem Delaware River, which flows 197 miles south to the head of tide at Trenton, New Jersey (RM 133). Below Trenton, the river is tidally influenced for 133 miles down to the mouth of the Delaware Bay (RM 0). The drainage area at Trenton, New Jersey, is approximately 6,780 square miles, whereas the total watershed downstream of Trenton to the mouth of the bay is 7,541 square miles. This includes the Schuylkill and Christina River basins (1,911 and 755 mi^2 , respectively), which contribute the

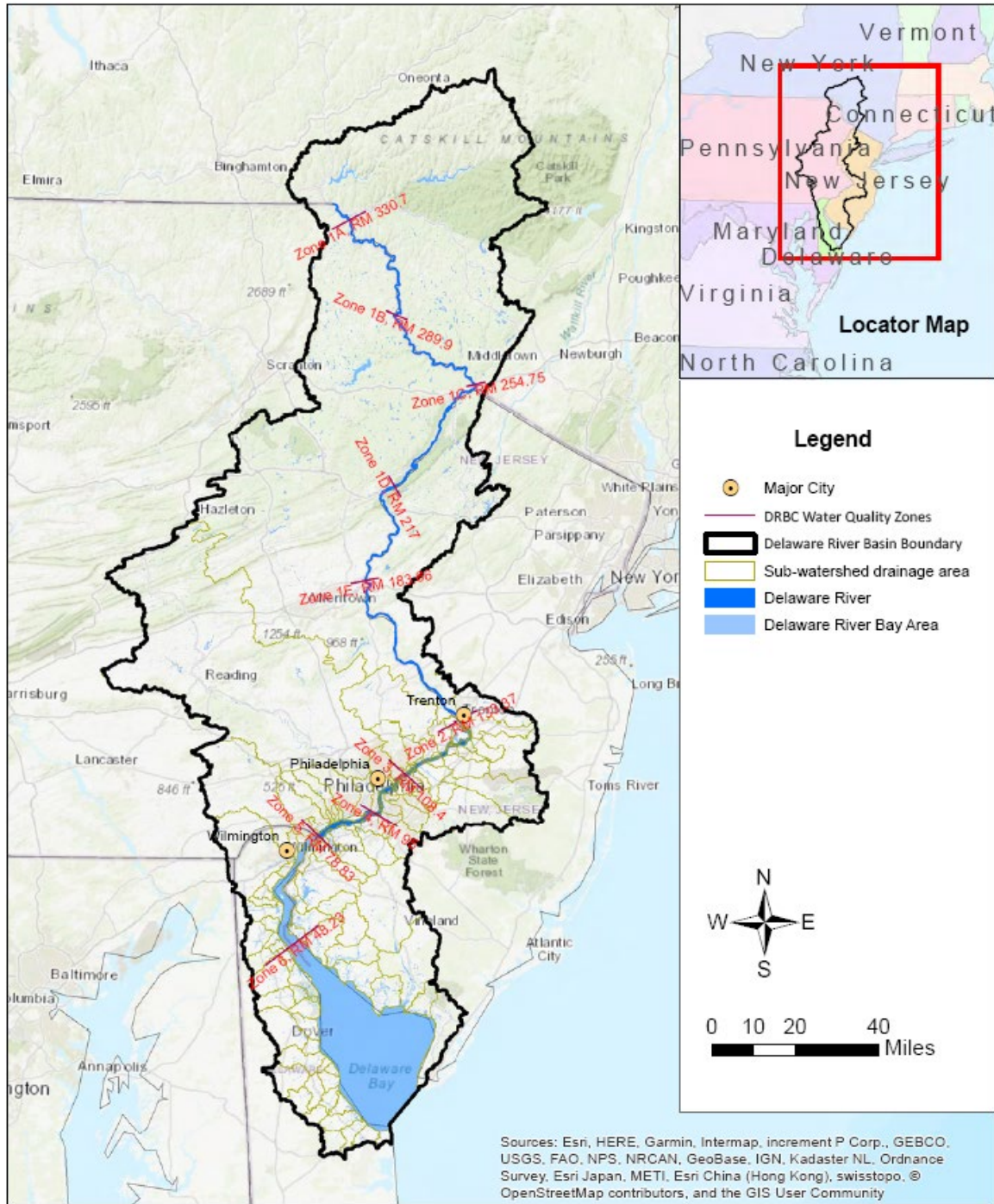


Figure 1-1: Delaware River Basin and Bay

most freshwater flow to the tidal system, and the Delaware Bay itself (782 mi²). The hydrodynamic model domain extends from the head of tide at Trenton to the mouth of the bay into the Atlantic Ocean.

The average annual water discharge at Trenton is approximately 12,055 cfs based on data from 1912 to 2023. The monthly statistics of river discharge show a clear flow seasonality, with the two highest monthly mean flows in March and April (20,400 and 21,900 cfs, respectively) and the two lowest in July and August

(6,420 and 6,680 cfs, respectively). The average annual water discharge from the Schuylkill River over the period 1932 to 2018 was approximately 2,850 cfs.

According to a U.S. Geological Survey (USGS) study prepared for the Federal Emergency Management Agency (FEMA) in 2008, the flood frequencies of the Delaware River at Trenton, New Jersey, are estimated as follows: 94,900 (2-year), 138,000 (5-year), 169,000 (10-year), 211,000 (25-year), 245,000 (50-year), and 280,000 (100-year) in units of cfs (Schopp and Firda, 2008).

1.2.2 Delaware River Estuary

The tidal portion of the Delaware River is a typical coastal plain estuary with a relatively homogeneous shallow depth of about 26 to 33 feet. Eighty percent of the estuary has a depth of less than 30 feet, except for the Federal Navigation Channel (FNC), which was deepened most recently in 2016 to a depth of 45 feet below Mean Lower Low Water (MLLW) level. The width of the Delaware Bay at its mouth is 11 miles, and the widest part of the bay is about 27 miles. The width decreases precipitously from the bay area toward the upriver: 2.4 miles wide in the reach from Delaware City just inland of the C&D Canal (RM 60); a half-mile wide in Philadelphia at the Ben Franklin Bridge (RM 100); about a quarter-mile wide at Burlington (RM 117.5); and less than 1,000 feet wide at Trenton (RM 134). The geometry and the rate of estuary narrowing along the river affect the amplitude and shape of the tidal wave, which changes as it propagates along the estuary. According to the National Oceanic and Atmospheric Administration (NOAA), the observed M2 (Principal lunar semidiurnal constituent, and the dominant tidal harmonic constituent) tide amplitude increases from 2.02 feet at Lewes, Delaware, to 2.75 feet at Philadelphia and 3.51 feet at Newbold, Pennsylvania, which is 1.7 times larger than at the mouth of the bay. The range of the tidal surface elevation between Mean Higher High Water (MHHW) and MLLW is 4.65 feet at the bay mouth, 6.69 feet at Philadelphia, and 8.39 feet at Newbold.

The seasonal and interannual variability in wind and tides near the mouth of the Delaware Bay exerts significant influence on salinity and transport of any chemical in the estuary. A consistent seasonality named the Average Seasonal Cycle (ASC) in the observed tides is reported at the Lewes, Cape May, and Atlantic City NOAA tide gage stations. The mean sea level tends to be lower during winter periods (from December to March) and relatively higher during summer periods (from July to October). According to NOAA, ASC is caused by regular fluctuations in coastal temperatures, salinities, winds, atmospheric pressures, and ocean currents. This pattern seems consistent with the observations that wind-induced downwelling occurs more often in the winter, and upwelling may be the dominating phenomenon for the summer period. Near the mouth of the Delaware Bay, relatively stable winter northern winds may cause downwelling (i.e., ocean water sinks along the continental shelf), while southern and southwestern winds that primarily blow over the summer and fall may cause upwelling (i.e., rise of ocean water with higher salinity). Persistent downwelling will contribute to weaker salinity intrusion and relatively stronger vertical stratification. Conversely, upwelling will strengthen salinity intrusion into the estuary. Seasonal changes in seawater temperature also make a difference in the water surface elevation due to the change in water

density. Near the mouth of the bay, a difference of 10 degrees Celsius in water temperature may cause a 20 cm difference in water surface elevation³.

Regarding water column stratification or salinity vertical structure, the temperate Delaware Bay is categorized as a weakly stratified or partially mixed estuary resulting from moderate tidal forcing and weak to moderate river discharge (Valle-Levinson, 2010). The tidally averaged mean salinity profile has either a weak or no stratification from surface to bottom, which indicates vigorous vertical mixing between riverine and oceanic waters. The salinity structure results from competition between river flow forcing, which drives the saltwater seaward, and tidal forcing, which drives the saltwater landward into the Delaware Bay and estuary.

Dolgoplova (2014) classified the estuary zone using the long-term averaged and depth-averaged salinity with units in parts per thousand (ppt)⁴. Using long-term averaged information, the region can be characterized by four large zones: 1) A 53-mile river reach from the fall line near Trenton at RM 132 to the Marcus Hook gage at RM 79, where salinity is less than 0.25 psu; 2) the upper Delaware Bay estuary, a 54-mile reach where salinity ranges from 0.25 to 25 psu, from the Marcus Hook gage to the transect between Port Mahon and Gandys Beach at RM 25; 3) the lower Delaware Bay estuary, a 25-mile reach where salinity exceeds 25 psu, from RM 25 to the mouth of the bay; and 4) the coastal zone of the ocean (Dolgoplova, 2014).

1.2.3 Chesapeake & Delaware Canal

The Chesapeake & Delaware Canal (C&D Canal) is a ship channel 18 miles in length that connects the Delaware River Estuary with the Chesapeake Bay through the states of Delaware and Maryland. In 1954, the United States Congress authorized further expansion of the channel to 450 wide (bottom width) and 35 feet deep. These improvements began in the 1960s and were completed in the mid-1970s. Today's canal is a modern, electronically controlled commercial waterway, carrying 40 percent of all ship traffic in and out of the Port of Baltimore (Ward et al., 2009).

³ Based on personal discussion with Dr. Robert Chant (Rutgers University) during an expert panel meeting in December 2019 at DRBC.

⁴ Salinity unit:

PPT was used for the salinity unit before 1978 by oceanographers and referred to the physical quantity, i.e., “the total amount of [dissolved] solid material, in grams, contained in one kilogram of sea water, or kg salt per kg water in parts per thousand”.

In 1978 (PSS-78) the practical salinity unit (or practical salinity scale) was introduced. This is non-dimensional. (PSS-78) suggested salinity should be written without the unit. <https://salinometry.com/pss-78/>. Since salinity is a ratio, the value is actually dimensionless (no units). (PSS-78) suggested the practical salinity should be expressed by a dimensionless number only and should be written as, for example, $S = 35.034$.

Salinity values in ppt and psu are nearly equivalent numerically.

The flow magnitude, flow direction, and the net flow in the canal are controlled by the amplitude and phase of tides and water density at the eastern and western ends of the canal. According to information from NOAA, the MLLW level at Chesapeake City near the western boundary (the Chesapeake Bay end) is over 16 inches higher than at Reedy Point near the eastern boundary (the Delaware River Estuary end). In addition, about 10 hours tidal phase difference is observed between the Delaware and Chesapeake ends of the C&D Canal. The salinity at the eastern end of the canal is higher than the western end by 2 to 3 psu. The U.S. Army Corps of Engineers (USACE) conducted a hydraulic study of the C&D Canal in 2009 using data collected from 1992 to 1993, which concluded that the average net flow in the C&D Canal is normally from the Chesapeake Bay to the Delaware River Estuary. During the time period of their study, the mean net flow ranged from 3,000 to 4,000 cfs moving from west to east; however, a reversed flow direction during the winter period of November and December 1992 was also observed.

In a 3D hydrodynamic and water quality modeling study conducted for Chesapeake Bay (Wang and Johnson, 2000), the C&D Canal was treated as a river boundary with a constant outflow of 750 cfs specified at the eastern end of the C&D Canal. This information was also used by DRBC staff for developing its one-dimensional (1D) hydrodynamic model DYNHYD5 (Suk, 2003). In reality, flows are dynamic and can occur in excess of 100,000 cfs through the canal. Normally, the flow reverses direction every 6 hours or so as the tide changes. However, during episodic events, large flows can continue in the same direction for two to three days. Thus, the treatment of the C&D Canal as a river with a constant outflow in the 3D Chesapeake Bay hydrodynamic model is a simplification, and the resulting estimated long-term average net flow differs from the USACE study significantly. A more thorough study may be needed over a longer time span, considering the large net flow from the Chesapeake Bay to the Delaware River Estuary through the C&D Canal. In the DRBC model, the C&D Canal is treated as an open boundary to allow flows in and out of the Delaware River Estuary system.

1.3 SALINITY INTRUSION

Salinity gradients are complex in the Delaware River Estuary, and the ability of the model to simulate them with sufficient accuracy provides an important demonstration of fitness for the hydrodynamic model. Understanding the salinity structure, salinity transport, and seasonal to inter-annual variability, as well as the underlying principle driving forces, is critical to advance our understanding of the hydrodynamics in the Delaware River Estuary. In addition, the simulation of salinity is directly relevant to the water quality modeling processes in the linked model, including light extinction and phytoplankton toxicity.

With nearly zero salinity from upland freshwater inflows at Trenton and close to constant salinity of about 32 to 35 psu in ocean water 40 to 50 miles from the bay mouth on the continental shelf, a temporally variable longitudinal salinity profile is formed and is the unique characteristic that differentiates tidal rivers and estuaries from any other type of surface waters. The salinity structure is maintained mainly by two competing forces: a) river flow, which tends to drive saltwater seaward; and b) tidal forcing and gravitational circulation, which tends to drive saltwater landward. Other influential factors that affect the salinity structure include turbulent shear and meteorological forcings such as precipitation, evaporation,

and wind. Although most of the upper portion of the tidal river upstream of Marcus Hook (RM 79) is typically well-mixed, a clear vertical stratification exists in the lower portion of the estuary, especially near the entrance of the bay. During low-flow and spring tide periods, stratification weakens due to the relatively stronger tidal forcing against the smaller river inflows, while high-flow and neap tide periods cause a stronger vertical stratification. Following a strong high-flow event, the salt front location usually retreats quickly in the seaward direction.

Salinity in the estuary is monitored by tracking the location of the salt front. The salt front represents the interface of salt water and fresh water in the estuary as well as the extent of salinity intrusion into the estuary. It is defined as the 7-day average of the 250 mg/l chloride concentration (isochlor). The value of 250 mg/l is a secondary drinking water standard, used as a guideline to assist public water systems in managing their drinking water for aesthetic considerations, such as taste, color, and odor. The 7-day average 250 mg/l chloride concentration was selected as a criterion for salinity monitoring and reservoir operations. It is a more stable indicator of the trend in the movement of the salt front, given the variability of day-to-day measurements. DRBC calculates the salt front location daily and reports it on a weekly basis on its website using the map of the estuary presented in Figure 1-2. The normal range of the salt front is between River Mile 67 and 76. For reference, RM 67 is near Pennsville, New Jersey; RM 68.7 is the Delaware Memorial Bridge; and RM 76 is near Marcus Hook, Pennsylvania.

Since specific conductance is tightly correlated with chloride concentration, salinity can be derived from chloride concentration or chlorinity. The empirical relationship between salinity (in psu) and chlorinity (chlorides) is given as:

$$\text{Salinity} = 0.03 + 1.805 \times \text{Chlorinity (g/kg sea water); or}$$

$$\text{Salinity} = 0.0018066 \times \text{Chlorinity (mg/l)}.$$

For example, 250 ppm chlorinity is equivalent to 0.45 psu salinity. It should be noted that although the empirical relationship between chloride and salinity has been used for seawater and estuaries, the relationship breaks when salinity is lower than 2 psu (APHA, 1995).

The Salt Front: Current Location

The below graphic shows the current location of the salt front in relation to several other sites along the river. Estimates of the salt front are based on provisional data and subject to change if better data becomes available.

Salt Front Location: December 5, 2022

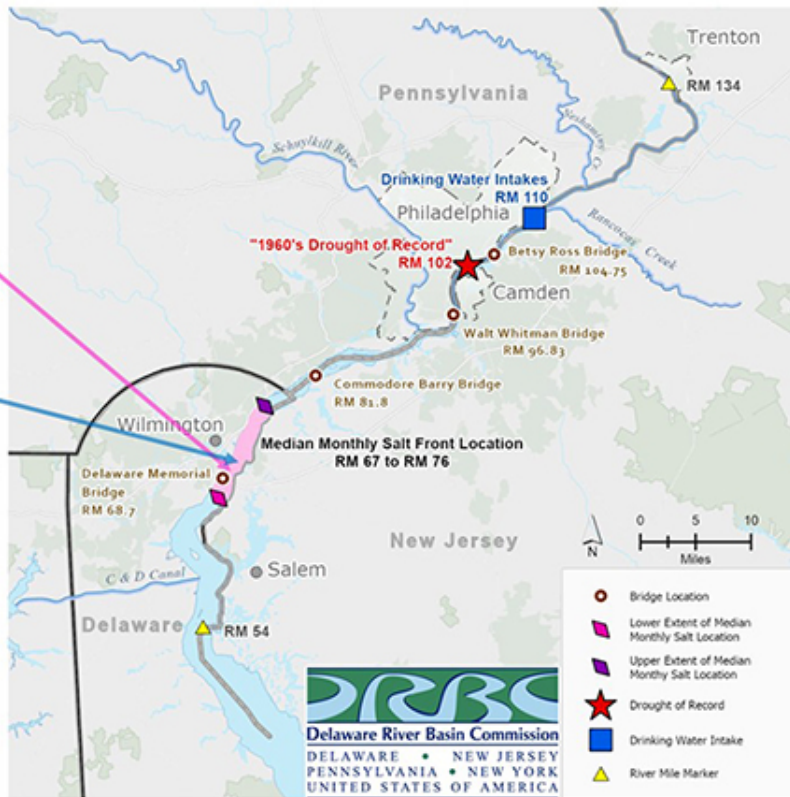
Normal December Location: RM 69

12/5/2022 Location: RM 69.8

Salt front not tracked below RM 54.

Median Monthly Salt Front Locations

January	69
February	71
March	70
April	67
May	68
June	69
July	70
August	74
September	76
October	72
November	70
December	69



(RM= river mile)

One important metric for understanding salinity concentrations in the Delaware River Estuary (the tidal Delaware River & Bay) is the seven-day average location of the salt front, the 250 mg/L chloride concentration based on drinking water quality standards. Chloride concentrations indicate the degree to which ocean derived saltwater has moved into the upper portion of the estuary; freshwater flowing downstream from the non-tidal Delaware River helps repel, or flush back, the salt-laced water. While you cannot see the salt front, its location fluctuates in response to changing freshwater inflows, which either dilute or concentrate chlorides in the river.

DRBC website for salt front information: <https://www.state.nj.us/drbc/programs/flow/salt-front.html>

Figure 1-2: Delaware River Estuary Map and Location of the Salt Front

Based on site specific data collected by DRBC between 2000 to 2018 as part of its long-running Estuary Water Quality Monitoring Program (i.e., Boat Run), the relationship between specific conductance and chloride concentration was re-evaluated and the results are similar to the USGS study from the early 1970s (Paulson, 1970) (Figure 1-3). The relationship exhibits a bi-linearity between specific conductance and chlorinity with a cutoff value at 320 ($\mu\text{S}/\text{cm}$ at 25 °C). These relationships were used when making model-

to-data comparisons of chloride concentrations reported at several USGS water quality monitoring gage locations on the Delaware River mainstem.

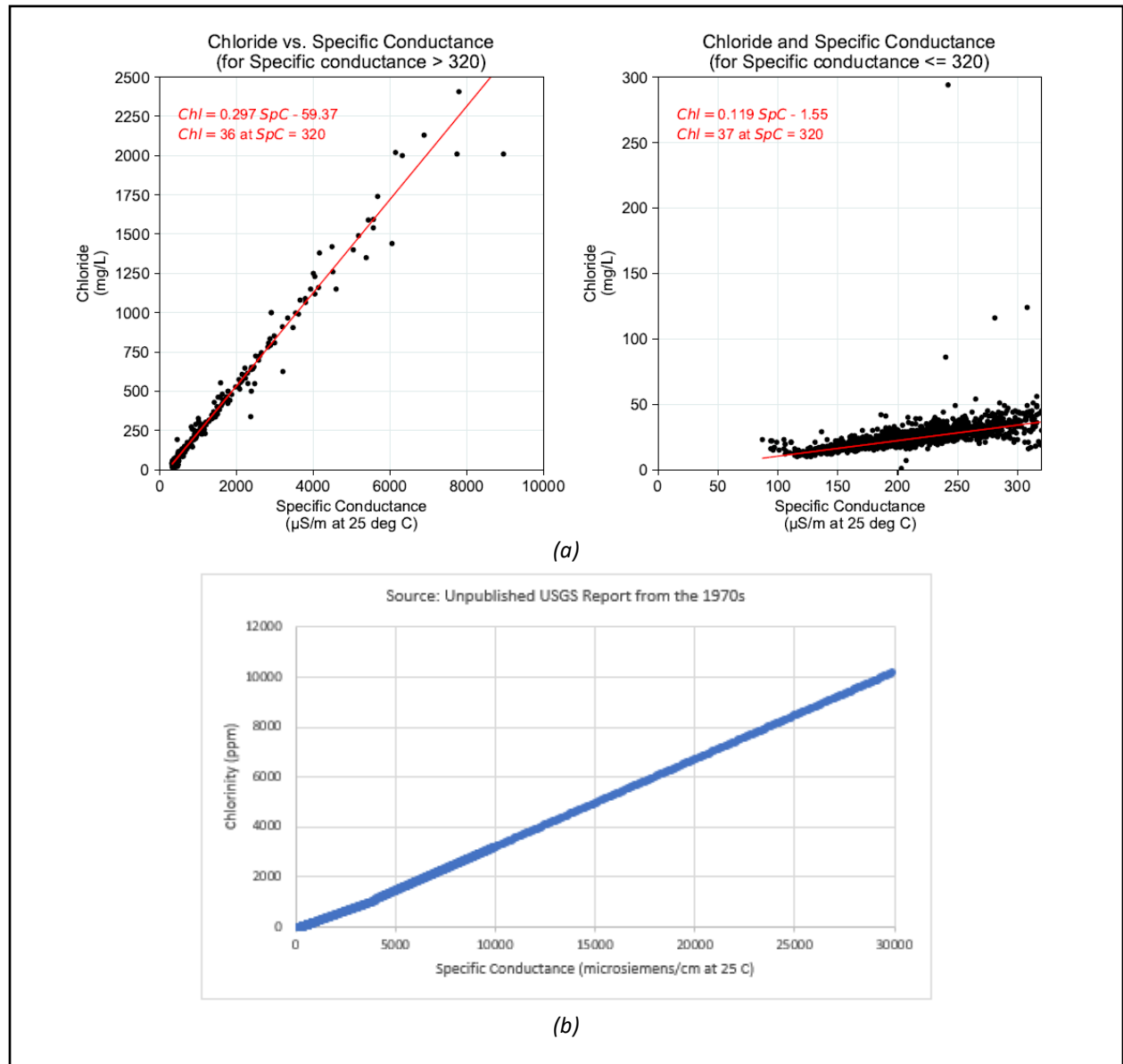


Figure 1-3 Relationship between Chloride and Specific Conductance Developed using DRBC Boat Run Data (a), and Developed by USGS in the 1970s (b)

1.4 OVERVIEW OF TECHNICAL APPROACH

The hydrodynamics and salinity transport in the Delaware River Estuary have been studied in the past through simplified analytical methods. For example, the relative importance of tidal advective diffusion to the residual salt transport was investigated by coupling the width-averaged, shallow-water equation and the salinity equation with the well-mixed assumption and excluding lateral transport processes (Wei 2014). This type of model excludes the influence of local bed friction variations on water motion and salt

dynamics among other important factors. Full 3D numerical simulation takes more physical processes into consideration, including buoyancy forcing due to river discharges, tidal forcing, meteorological forcing, surface heat exchange, wind forcing (local and remote), wind-wave induced current, and etc., and has been used to study the vertical stratification and its variability during flood-tide and ebb-tide and cross-channel momentum balance (Aristizábal and Chant, 2012), the salt fluxes (Aristizábal and Chant, 2013), thermal circulations (Salehi, 2017), the effect of wind waves on momentum budget and subtidal exchange (Fernando Pareja-Roman et al., 2019), wave energy and interactions between bathymetry and wave processes (Jia-Lin Chen et al., 2018), and the processes responsible for coastal changes including sediment transport (Warner, 2010).

The DRBC developed a 3D hydrodynamic model of the Delaware River Estuary based on the Environmental Fluid Dynamics Code (EFDC), which is supported by EPA. The model was calibrated and validated for the years 2018 to 2019 and 2012 to demonstrate fitness over a range of hydrologic conditions. The primary focus of the hydrodynamic model calibration was for the years 2018 and 2019 when continuous conductivity and other water quality data were collected through DRBC's intensive eutrophication modeling study sampling program; however, the 2012 year was added to the calibration in order to incorporate a year with drier hydrologic conditions than occurred in 2018 and 2019.

This study used available data and information to the fullest extent possible, while acknowledging that data gaps exist in the present state of knowledge about the Delaware River Estuary study area and that all hydrodynamic models are numerical approximations of, and not exact replicas of, natural systems. Therefore, multiple lines of evidence were used to evaluate the reliability of the model during the calibration and validation process, since model fitness is impacted not just by the quality of the calibration but also by the quality of boundary and field data, neither of which are perfectly known. Model performance was evaluated for major parameters, such as tidal harmonic constituents, water surface elevation, water temperature, and salinity, through model to data comparisons.

Before the hydrodynamic model was successfully calibrated and finalized, a sensitivity analysis was also conducted to evaluate the effects of several alternative vertical resolutions of the numerical grid on model predictions in order to select an appropriate vertical resolution. The findings from the vertical resolution sensitivity analysis are included in this report.

2. HYDRODYNAMIC MODEL DEVELOPMENT

2.1 MODEL DESCRIPTION

The hydrodynamic model code applied for this study is the Environmental Fluid Dynamics Code (EFDC), which was originally developed by Dr. John Hamrick (Hamrick, 1992) and is supported by the U.S. Environmental Protection Agency (EPA). EFDC is a general purpose hydrodynamic model code capable of three-dimensional simulation of time-variable flow in stratified rivers, lakes, reservoirs, estuaries, and coastal areas. It solves the conservation of mass and momentum equations, as well as transport equations for temperature and salinity, which are the fundamental equations governing the movement of water in an estuary. The state equation links the water density to salinity and water temperature. The EFDC model has been applied to a wide range of environmental studies. A complete description of EFDC is given in Hamrick (1992) and Tetra Tech (2007).

The version of EFDC used in this study was provided by EPA Region 4 and is equivalent to the public release version of EFDC 2007 via the EPA website. A high-order advection scheme, Conservative Operator Splitting for Multidimensions with Inherent Constancy (COSMIC) (Leonard et al., 1996), was adopted because: 1) in theory, the COSMIC scheme limits numerical diffusion better than the Euler scheme (the other option available in EFDC); 2) numerical test results indicate that the COSMIC scheme better predicts transport than the Euler scheme in both the hydrodynamic (EFDC) model and linked water quality model, the Water Quality Analysis Simulation Program (WASP); and 3) the COSMIC scheme is preferred⁵ for the water quality model, and consistent numerical schemes between the hydrodynamic and water quality models helps maintain consistent transport calculations. Furthermore, DRBC staff and its consultant, GHD, have made improvements to this version of EFDC in two major aspects: 1) enhancement of the mass balance when choosing the COSMIC scheme with a generalized vertical coordinate grid (see Section 2.3); and 2) enhancement of the hydrodynamic linkage file to the water quality model.

Although the Delaware River Estuary is commonly considered as weakly stratified, vertical mixing and along-channel salinity structure vary in time depending on river discharge, tidal forcing, and meteorological forcing (Aristizabal and Chant, 2013 and 2015). Furthermore, reaeration at the water surface and sediment oxygen demand at the bed may cause dissolved oxygen stratification in the water column. These conditions make it necessary to use a three-dimensional (3D) mode in EFDC to accurately simulate transport in the Delaware River Estuary. EFDC implements the Mellor-Yamada level 2.5 turbulence closure scheme (Mellor and Yamada, 1982) as modified by Galperin et al. (1988) to parameterize vertical mixing.

⁵ Personal communication with Expert Panel member Tim Wool, EPA (retired) regarding the use of the eutrophication (Eutro) module within WASP.

The continuity, momentum, and state equations used in EFDC are:

$$\frac{\partial u}{\partial x} + \frac{\partial v}{\partial y} + \frac{\partial w}{\partial z} = 0 \quad (\text{Eqn 2.1-1})$$

$$\frac{\partial u}{\partial t} + \frac{\partial u^2}{\partial x} + \frac{\partial uv}{\partial y} + \frac{\partial uw}{\partial z} - fv + g \frac{\partial \eta}{\partial x} = \frac{\partial}{\partial z} \left(K_M \frac{\partial u}{\partial z} \right) - \frac{g}{\rho_0} \frac{\partial}{\partial x} \int_z^\eta \rho dz + F_x \quad (\text{Eqn 2.1-2})$$

$$\frac{\partial v}{\partial t} + \frac{\partial uv}{\partial x} + \frac{\partial v^2}{\partial y} + \frac{\partial vw}{\partial z} + fu + g \frac{\partial \eta}{\partial y} = \frac{\partial}{\partial z} \left(K_M \frac{\partial v}{\partial z} \right) - \frac{g}{\rho_0} \frac{\partial}{\partial y} \int_z^\eta \rho dz + F_y \quad (\text{Eqn 2.1-3})$$

$$\frac{\partial T}{\partial t} + \frac{\partial uT}{\partial x} + \frac{\partial vT}{\partial y} + \frac{\partial wT}{\partial z} = \frac{\partial}{\partial z} \left(K_H \frac{\partial T}{\partial z} \right) + \frac{1}{\rho_0 c_p} \frac{\partial I}{\partial z} + F_T \quad (\text{Eqn 2.1-4})$$

$$\frac{\partial S}{\partial t} + \frac{\partial uS}{\partial x} + \frac{\partial vS}{\partial y} + \frac{\partial wS}{\partial z} = \frac{\partial}{\partial z} \left(K_H \frac{\partial S}{\partial z} \right) + F_S \quad (\text{Eqn 2.1-5})$$

$$\rho = F(S, T, P) \quad (\text{Eqn 2.1-6})$$

where:

η = water surface elevation;

$u, v,$ and w = velocity components along the $x, y,$ and z directions, respectively;

ρ_0 and ρ = reference density and in situ density of water;

g = gravitational acceleration;

f = Coriolis parameter;

K_M = vertical viscosity for momentum mixing;

F_x and F_y = horizontal momentum diffusion in x and y directions, respectively;

T = water temperature;

S = salinity;

K_H = vertical diffusivity for turbulent mixing of temperature and salinity;

F_T and F_S = horizontal diffusion terms for temperature and salinity, respectively;

$\partial I / \partial z$ = solar radiation forcing term;

c_p = specific heat; and

P = pressure.

The state equation (Eqn. 2.1-6) indicates that the water density is a function of salinity and water temperature. It is critically important for the model to correctly represent the effects of water density on the estuary hydrodynamics, such as the density-driven estuary exchange flow pattern. This is also a reason why a 3D model was developed instead of a two-dimensional (2D) model with vertical average circulations.

Certain physical processes, such as groundwater-surface water interactions, wave-induced currents, and wave-current interactions, are not included in this eutrophication study because their impacts on long-term salinity and water quality transport in the Delaware River Estuary are considered to be insignificant. Horizontal diffusion terms for temperature (F_T) and salinity (F_S) in Eqns. 2.1-4 and 2.1-5 are not activated in this study because the horizontal diffusion calculations are not sufficiently developed in EFDC. However, given the high-energy nature of the Delaware River Estuary, horizontal diffusion can be expected to exert relatively minor impacts compared to advection. Improvements to the EFDC code may be contemplated in future model updates.

2.2 MODEL DOMAIN AND NUMERICAL GRID

The model domain extends from just upstream of the head of tide on the Delaware River at Trenton (River Mile [RM] 135)⁶ to the mouth of the Delaware Bay (RM 0). The C&D Canal is also included in the domain as far westward as the NOAA tide gage station at Chesapeake City. Inflows from 33 major tributaries and 124 sub-basin drainage areas are incorporated for freshwater inflows, as described in Section 2.4 below.

Curvilinear and orthogonal numerical grids were created to represent the geometry of the study area (Appendix A). The discretization of the model domain was accomplished with a fixed grid. Floodplain areas and marshes were excluded from the model domain to conserve computational time for the water quality model (Zheng et al., 2024), which utilizes the same numerical grid as the hydrodynamic model except that two rows of grid cells at each of the two open boundaries are clipped for the water quality model domain. The reason for clipping the grid at the open boundaries is that EFDC does not calculate flows at its open boundaries; clipping allows the water quality model to receive flow information for its open boundaries from within the EFDC grid. The EFDC model domain contains a total of 1,890 grid cells in the horizontal plane, with the upper portion (Zones 2, 3 and 4) of the tidal river being discretized by 946 grid cells and the lower portion (Zones 5 and 6) by 944 grid cells. The river was generally delineated by four to seven grid cells in the cross-channel (bank to bank) direction, and the navigational channel was represented by one to two cells in the horizontal plane. Grid resolution is higher in the tidal river than in the Bay in order to provide higher resolution in Zone 3 and upper Zone 4 in particular where the dissolved oxygen (DO) sag has been observed. For example, in the Philadelphia area (i.e., $91 < \text{RM} < 104$), the average horizontal grid sizes are 760 m and 150 m in the longitudinal and lateral directions, respectively. There are about six to seven cells across the river in the urban area (see Figure A-5 in Appendix A). The average grid cell sizes downstream of Philadelphia (i.e., $70 < \text{RM} < 91$) are 580 m and 190 m in the longitudinal and lateral directions, respectively. Grid cells in the downstream Zone 6 are much coarser, with an average of 2,020 m and 1,900 m in the longitudinal and lateral directions, respectively. There are about 12 to 14 cells across the Bay.

⁶ Note: While the exact head of tide at Trenton, New Jersey, is at RM 133, the model extends to RM 135 in order to capture the boundary flows at the USGS continuous gage #01463500 (Delaware River at Trenton).

Major tributaries (e.g., the Schuylkill River) are represented by four to ten longitudinal grid cells. This simplified delineation is designed to balance representation of the tributaries with model computation time while still honoring the net loadings and residence time to the Delaware River. As such, the model is not intended to fully resolve tributary hydrodynamics to the same degree of certainty as in the mainstem Delaware River Estuary.

Regarding the horizontal grid cell sizes used in the model, it is important to note that the significance of lateral transport depends on the intended use of the model. Dissolved oxygen is the primary constituent of concern, and the urban estuary is the primary area of concern. Lateral transport is less significant because of the time scale for the oxidation of oxygen-demanding substances from multiple locations of continuous discharges. This statement is supported by the observation of measured transect DO and other data, which show only minor gradients across the river channel within the urban portion of the estuary. Overall, model-data comparisons of salinity, water temperature, nutrients, and DO in the hydrodynamic and water quality modeling (Zheng et al., 2024) reports indicate that 1) longitudinal and lateral grid resolutions are adequate to represent tidal transport in the model domain, including in the vicinity of the DO sag; and 2) the simplified delineation of tributaries exerts an insignificant impact on the results predicted for the mainstem.

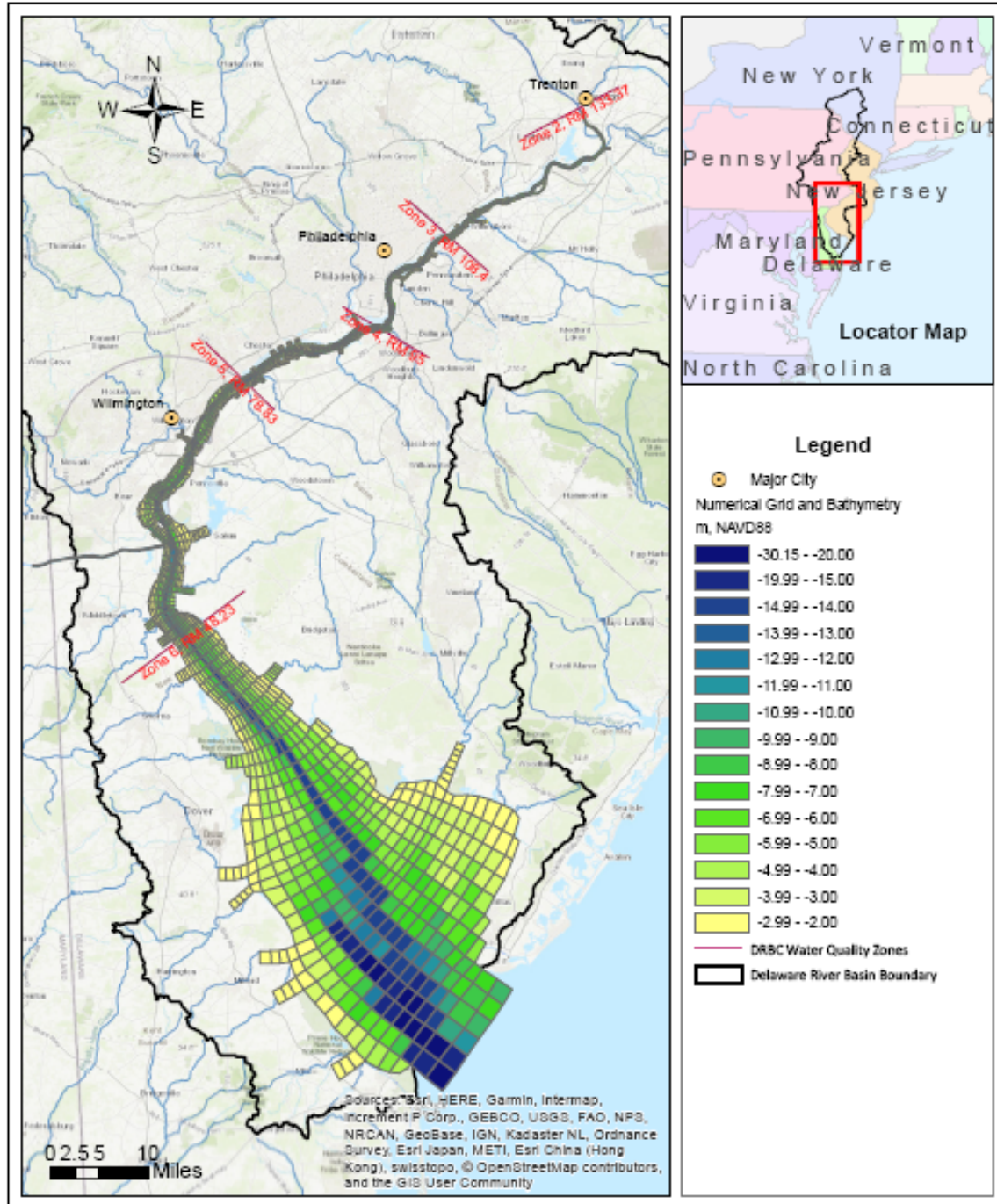
2.3 BATHYMETRY AND GENERALIZED VERTICAL COORDINATE (GVC)

Bathymetry data were based on a Digital Elevation Model (DEM) from the Federal Emergency Management Agency (FEMA) (Forte et al., 2011), in which the horizontal datum is the North American Datum of 1983 (NAD83) and the vertical datum is the North American Vertical Datum of 1988 (NAVD88). The DEM incorporated the latest coastal Lidar and other topographic survey data sets with the most reliable bathymetric datasets of the region. The raster grid resolution in the DEM is 1/3 arc-seconds (~10 meters). Bathymetry in the C&D Canal was set to 35 feet below Mean Lower Low Water (MLLW) according to the NOAA nautical chart for the canal.

The U.S. Army Corps of Engineers (USACE) completed a 102.5-mile long channel deepening project in 2016^{7,8}. The previous 40-foot deep federal navigation channel, extending from Philadelphia Harbor in Pennsylvania and Beckett Street Terminal in Camden, New Jersey, to the Delaware Bay, was deepened to 45 feet. This dredging project was reflected in the model bathymetry setup; the navigation channel was set to 45 feet below MLLW for simulations of years after 2016 and 40 feet below MLLW for earlier years. The final post-dredging bathymetry as projected on the numerical grid is shown in Figure 2-1.

⁷ <https://www.nap.usace.army.mil/Missions/Civil-Works/Delaware-River-Main-Channel-Deepening/>

⁸ <https://www.philaport.com/delaware-river-deepening-30-years-and-16-million-cubic-later/>



Note: Figures showing more details for each DRBC water quality zone are presented in Appendix A.

Figure 2-1: Numerical Grid and Projected Bathymetry

According to Tetra Tech (2006), the EFDC model was originally formulated with a sigma stretched vertical coordinate. In the sigma coordinate formulation, the number of vertical layers is the same at all horizontal locations in the model domain. This formulation is widely accepted, conceptually attractive, and adequate for a large range of applications. However, in the Delaware River Estuary, bathymetry may vary rapidly in

the lateral direction, from a deep navigational channel to a much shallower flank, resulting in V- or T-shaped cross-sections. Therefore, a traditional Z or hybrid coordinate is more desirable.

For this study, a generalized vertical coordinate (GVC) was chosen to represent the lateral bathymetry variation more efficiently and accurately. This approach allows the horizontal model domain to be represented by laterally constrained and localized-sigma regions (LCL sigma) (Figure 2-2). In the LCL region, the number of active vertical layers varies at different horizontal locations, as opposed to a traditional sigma coordinate in which the number of vertical layers is constant throughout. At any given horizontal location, the number of vertical layers is fixed during simulation, though the water level rises and falls. Theoretical and computational aspects of the generalized vertical coordinate are described in Tetra Tech (2006).

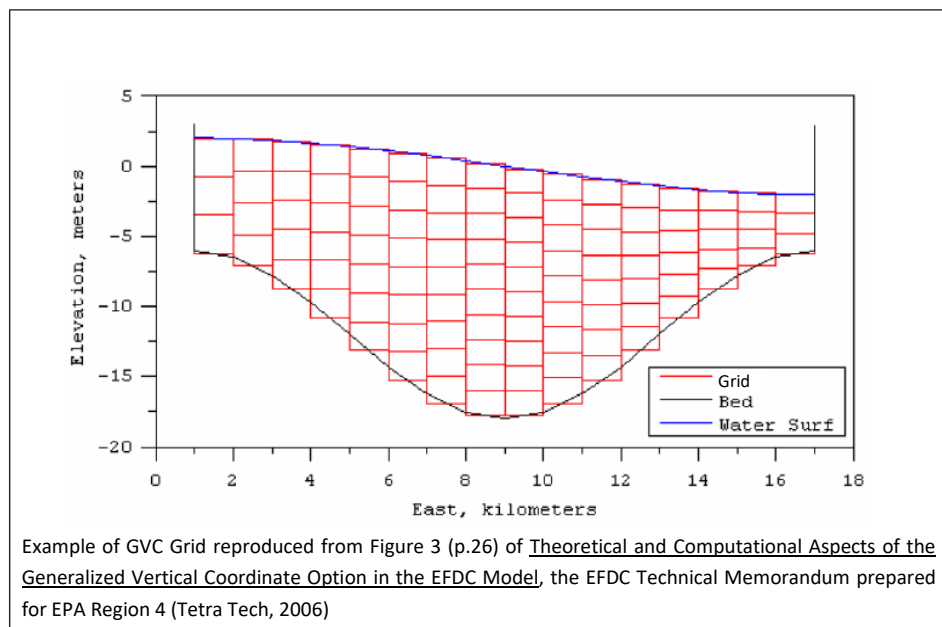


Figure 2-2: Example of GVC Grid

In this study, a maximum of 12 vertical layers were assigned to a few of the deepest cells near the ocean boundary and within the navigational channel near this boundary. Ten vertical layers were maintained in most of the cells inside the navigational channel. The spatial variation in the number of vertical layers is shown in Figure 2-3. A finer scale graphic of the number of vertical layers around the urban area is presented in Figure A-10 in Appendix A. Sensitivity tests with regard to vertical layer resolution (see Section 3.4 for details) indicated that the number of layers inside the navigational channel should be greater than five but need not be more than 10 in order for the model to perform adequately.

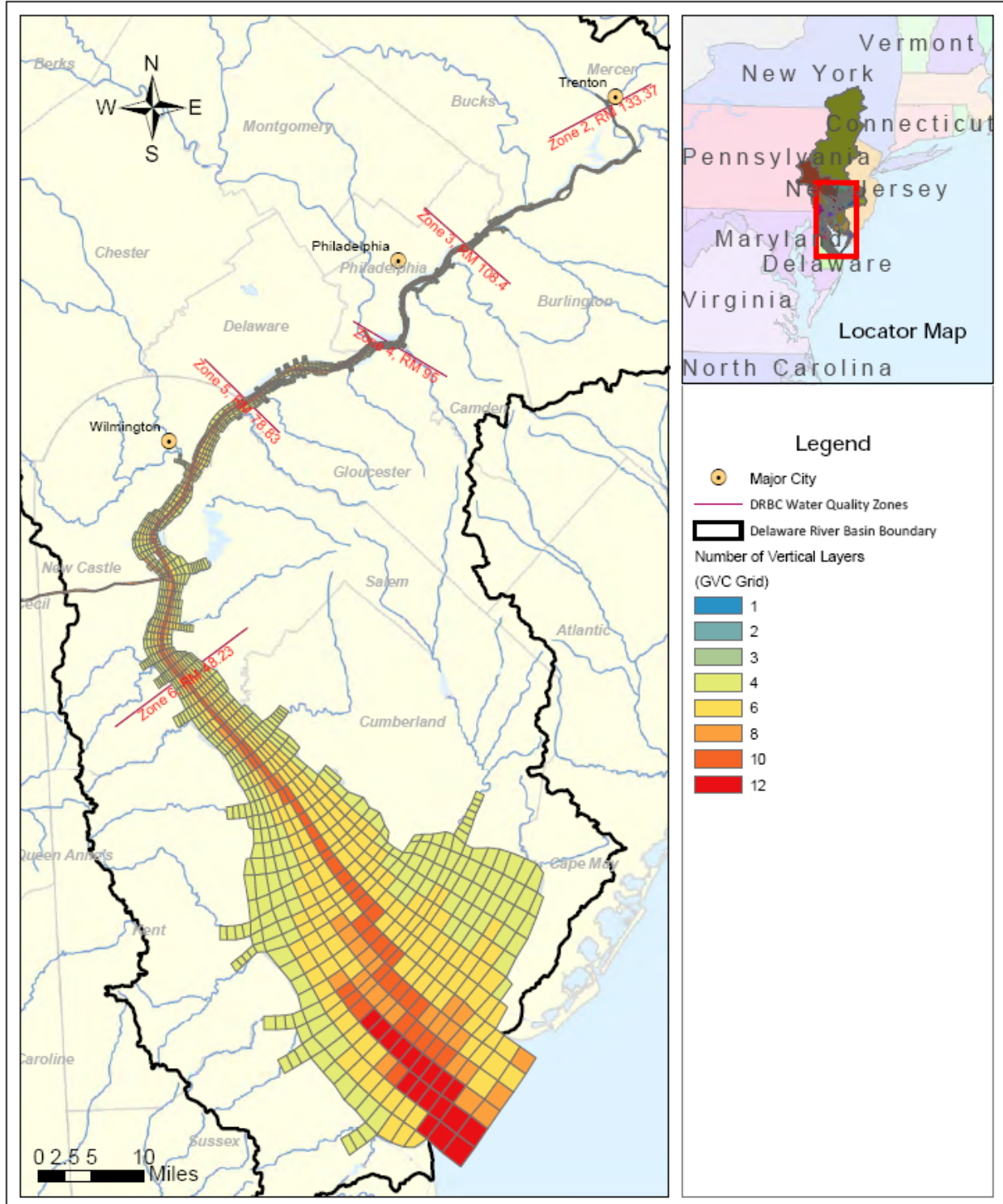


Figure 2-3 Number of Vertical Layers

2.4 BOUNDARY CONDITIONS

The hydrodynamic model requires specification of the following boundary conditions:

- Water surface elevations at the open boundaries at the mouth of the Bay and the western end of the C&D Canal;
- Freshwater inflows into the mainstem of the Delaware River Estuary;
- Salinity and water temperature at all inflow and open boundaries; and
- Climate/meteorological forcings at the water surface including air temperature, air pressure, dew point, precipitation, wind speed and direction, and solar radiation.

2.4.1 Water Surface Elevations

In this study, verified hourly data of water surface elevations collected at NOAA stations at Lewes, Delaware, (8557380) and Chesapeake City, Maryland, (8573927) were used to specify the open boundary conditions at the mouth of the Bay and the west end of the C&D Canal, respectively. Since the open boundary at the mouth of the Bay is 14.6 km downstream of Lewes station, trial-and-error exercises were conducted by adjusting the tidal amplitude and phases to ensure the model reproduces the observed data at Lewes station. These data include the signals of astronomical tides and meteorological forcing (i.e., sub-tidal signal), which are the two major components of water surface elevation. The dominant astronomical tidal constituent in the model domain is the principal lunar semi-diurnal (M2). All water surface elevation data were converted to the vertical datum of NAVD88 in meters to be consistent with the bathymetry (Table 2-1).

Table 2-1: Summary of NOAA Stations and Datum Conversion

No.	Station	Station ID	Vertical Datum	Conversion Factor to NAVD88 m
1	Lewes, DE	8557380	NAVD88	0.000
2	Cape May, NJ	8536110	NAVD88	0.000
3	Brandywine Shoal Light, DE	8555889	MLLW	-0.872
4	Ship John Shoal, NJ	8537121	MLLW	-0.963
5	Reedy Point, DE	8551910	NAVD88	0.000
6	Chesapeake City, MD	8573927	MLLW	-0.474
7	Delaware City, DE	8551762	MLLW	-0.887
8	Marcus Hook, PA	8540433	MLLW	-0.890
9	Philadelphia, PA	8545240	NAVD88	0.000
10	Burlington, Delaware River, NJ	8539094	MLLW	-1.016
11	Newbold, PA	8548989	MLLW	-1.152

*Notes: NAVD 88 meter = MLLW meter + Conversion Factor
Conversion factor values are based on NOAA's Vertical Datum Transformation, V.3.6.1*

2.4.2 Freshwater Inflows

Freshwater inflows into the mainstem of the Delaware River Estuary include the flows from the upstream boundary, tributaries (gaged and ungaged), non-point sources and municipal separate storm sewer systems (MS4s), point source discharges, combined sewer overflows (CSOs), direct precipitation onto the water surface, and withdrawals. Groundwater and surface water interactions were not explicitly considered in this study.

The flow rate at the upstream boundary represents the inflow from the non-tidal Delaware River and was specified based on data collected at USGS gaging station 01463500 (Delaware River at Trenton, New Jersey). Flow at Trenton during 2012, 2018, and 2019 are presented in Figure 2-4. Inflows from 32 other major tributaries were specified using available USGS gaging station data. Hourly flow data were utilized for the Delaware River at Trenton and for the Schuylkill River because of their significant contributions to the total freshwater input, while daily flows were utilized for the remaining tributary inflows. Missing streamflow values were imputed by fitting a structural time series model to the data followed by a smoothing function. Average flow rates of the tributaries during the 2018-2019 model calibration period are provided in Table 2-2 below.

Table 2-2: Summary of Tributary Inflow Boundaries

Count	Tributaries	Mean flow during 2018-2019 (cfs)	RM	USGS Gauge
1	Delaware River at Trenton (mainstem)	17,877	134.3	USGS01463500
2	Assunpink Creek	220	133.8	USGS01464000
3	Crosswicks Creek	217	128.41	USGS01464500
4	Neshaminy Creek	526	115.63	USGS01465500
5	Rancocas Creek North Branch	295	111.06	USGS01467000
6	Rancocas Creek South Branch	260	111.06	USGS01465850
7	Poquessing Creek	44	111.66	USGS01465798
8	Pennypack Creek	135	109.75	USGS01467048
9	Pennsauken Creek South Branch	34	105.4	USGS01467081
10	Pennsauken Creek North Branch	37	105.4	N/A
11	Frankford Creek	30	104.6	USGS01467087
12	Cooper River	67	101.58	USGS01467150
13	Big Timber Creek	83	95.46	N/A
14	Schuylkill River	5,176	92.47	USGS01474500
15	Mantua Creek	86	89.66	N/A
16	Darby Creek	154	85.28	N/A
17	Crum Creek	73	84.9	USGS01475850
18	Ridley Creek	78	84.2	USGS01476480
19	Chester Creek	151	82.93	USGS01477000
20	Raccoon Creek	66	80.66	USGS01477120
21	Oldman Creek	69	77	N/A
22	Christina River	570	70.73	USGS01478000
23	Brandywine Creek	757	70.73	USGS01481500
24	Salem River	145	58.37	USGS01482500
25	Alloway Creek	54	54.45	N/A
26	Appoquinimink River	58	51.2	N/A
27	Blackbird Creek	38	49.25	N/A
28	Smyrna River	116	45	N/A
29	Cohansey River	73	37.8	USGS01412800
30	Leipsic River	78	35	USGS01483500
31	St. Jones River	145	23.7	USGS01483700
32	Murderkill River	84	23.14	USGS01484000
33	Maurice River	387	21.03	USGS01411500

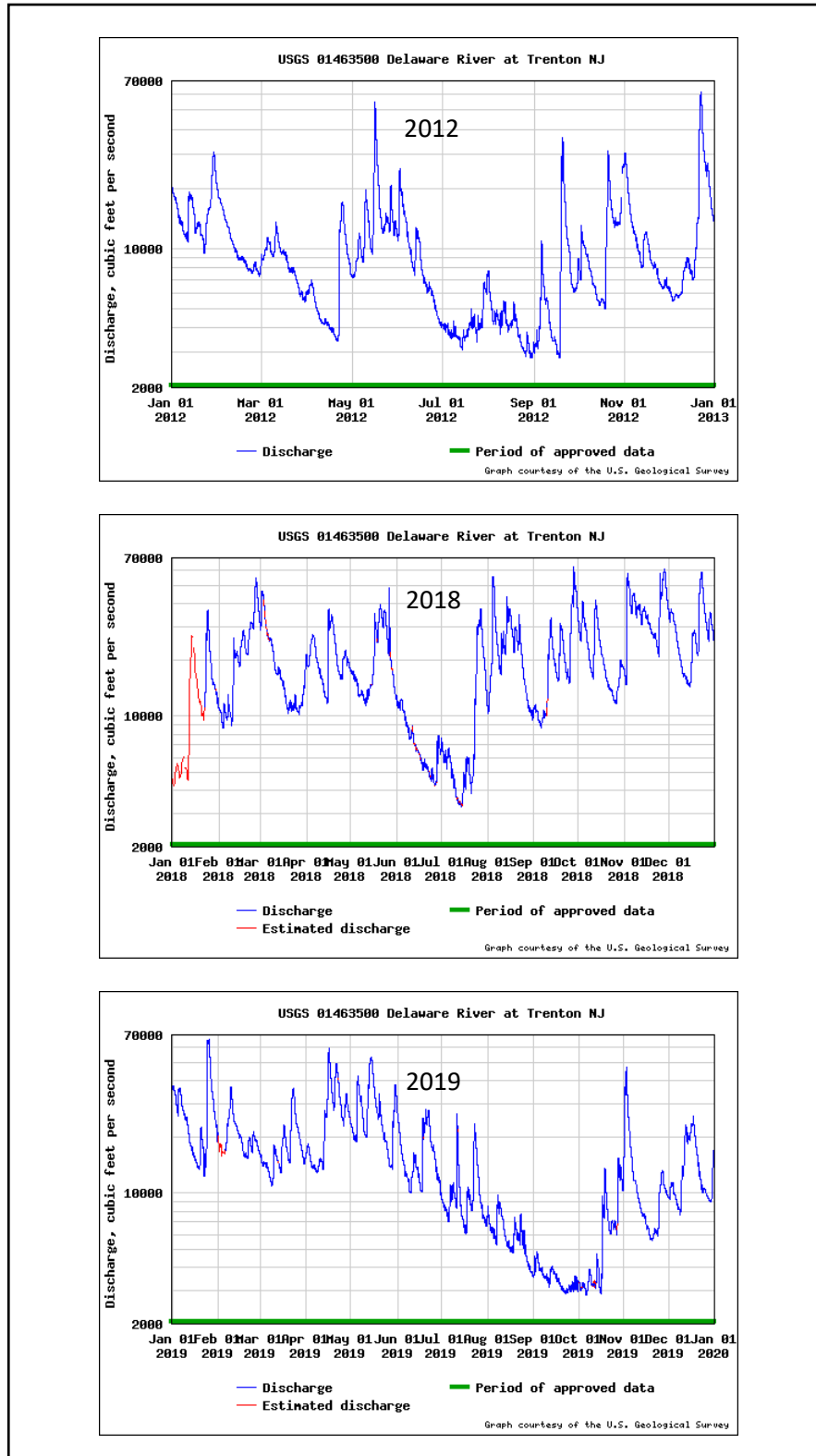


Figure 2-4: Hydrograph of Delaware River at Trenton

Discharge gaging stations are often located at or above the head of tide, often leaving substantial portions of the watershed ungaged. For these areas and upland tributaries absent of flow data, flow rates for each were estimated based on data from a similar watershed. Similarity among gaged and ungaged catchments was determined by environmental classification owing to the availability of high-quality, hydrologically relevant digital datasets; classes are defined based on physical and climatic attributes that are assumed to produce a similar hydrologic response independent of geographic location. Basin characteristics were chosen among broad categories such as morphology (channel length and slope, basin shape, drainage density, etc.), soil properties, land use/land cover, geology, and climate and constitute a subset of those typically used in the regionalization of streamflow statistics. A hierarchical agglomerative clustering technique (HACA) was used to objectively determine the optimal number of clusters with similar descriptive attributes and to assign membership of 124 sub watersheds (gaged and ungaged; Figure 2-5) to seven general landscape types. Reference gages were assigned to ungaged watersheds within their respective clusters. The daily hydrograph at each reference gage was partitioned into baseflow and runoff components using standard hydrograph separation techniques prior to transfer of flow information using the drainage-area-ratio approach. Low-gradient, tidally influenced basins directly adjacent to the river and bay were assigned runoff only, all others were assigned the full hydrograph. The inflow boundary of a tributary was set at the DRBC monitoring stations, whereas inflow boundaries for all others were set at the outlet point of the sub watershed, i.e., estimated flows for the ungaged areas (including direct runoff) were input to the model at downstream watershed boundaries. This approach results in 104 aggregated non-point sources (NPS) and MS4 freshwater inputs, in addition to 33 major tributaries. Additional information on the development of watershed flows is presented in Appendix B.

A point discharge monitoring program was conducted to estimate loadings of nutrients from individual wastewater treatment plant facilities during the model calibration period of 2018-2019. A total of 71 major point source discharges were selected (Table 2-3). These discharges were categorized into Tiers 1, 2, and 3 according to their nutrient loadings. Tier 1 and 2 dischargers collected nutrient samples weekly and monthly, respectively. No additional monitoring was required from Tier 3 dischargers. Daily measured flow rates during this monitoring period were used to specify freshwater inflows from Tier 1 and 2 discharges. Flow rates from Tier 3 discharges were based on monthly data obtained from National Pollutant Discharge Elimination System (NPDES) reports. Point discharge flow rates during the model calibration period of 2012 were based on point discharge monitoring performed from 2011 to 2015, in which Tier 1 and Tier 2 discharges were monitored daily; Tier 3 discharge rates were estimated as constant monthly values reflecting median flows.

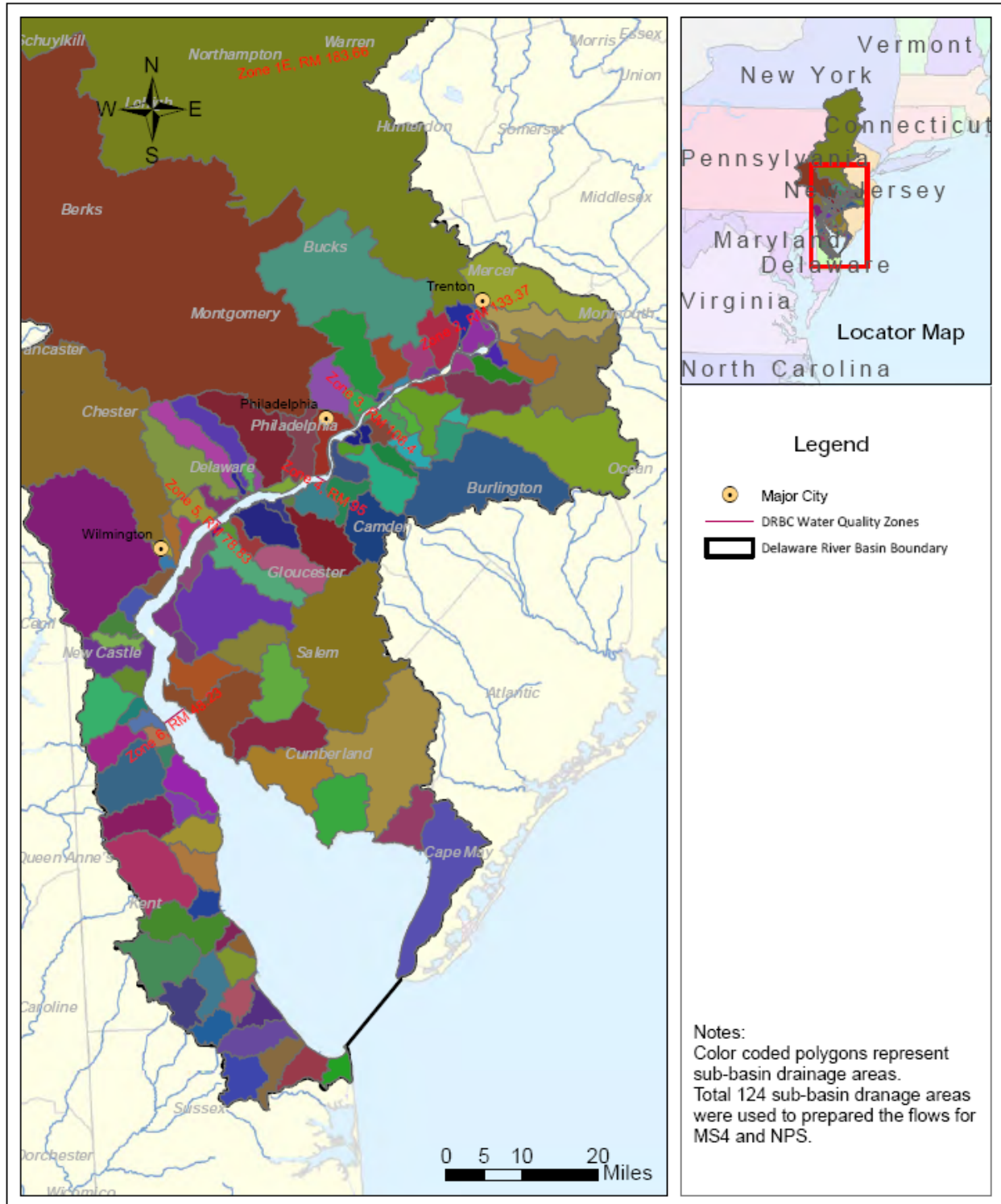


Figure 2-5: Delineation of Watershed Drainage Areas

Table 2-3 Summary of Point Source Discharges

Count	NPDES ID	Facility Names	Tiers
1	PA0026701-201	Morrisville Borough Municipal Authority	1
2	NJ0020923-001A	Trenton Sewer Utility	1
3	NJ0026301-001A	Hamilton TWP WPCF	1
4	PA0026468-001	Lower Bucks County JMA	1
5	NJ0023361-001A	Willingboro Water Pollution Control Plt	1
6	PA0026689-001	PWD Northeast	1
7	NJ0026182-001A	Delaware 1 WPCF (Camden)	1
8	PA0026662-001	PWD Southeast	1
9	PA0026671-001	PWD Southwest	1
10	NJ0024686-001A	GCUA	1
11	PA0027103-001	Delcora	1
12	DE0020320-001	City of Wilmington	1
13	NJ0024678-001A	Bordentown SA Black's Creek STP	2
14	PA0043818-001	GROWS Landfill, Waste Management	2
15	NJ0023701-001A	Florence Township STP	2
16	NJ0021709-002A	Central Ave. WTP, Burlington TWP	2
17	PA0027294-001	Bristol Borough Water & Sewer Authority	2
18	NJ0024660-002A	Burlington City STP	2
19	NJ0025178-001A	Hartford RD WPCF	2
20	NJ0024015-001A	Mount Holly WPCF	2
21	NJ0022519-001A	Riverside Sewerage Authority	2
22	NJ0023507-001A	Delran TWP Sewer Utility Department	2
23	NJ0024007-001A	Cinnaminson Sewerage Authority T2	2
24	NJ0024996-001	Moorestown TWP WWTP	2
25	NJ0005029-001	Paulsboro Refining Company	2
26	NJ0005045-001A	Polymer Additives Inc. (VSC)	2
27	NJ0005100-662A	Chambers Works, Tier-2	2
28	NJ0021598-001A	Pennsville Sewerage Authority	2
29	DE0000256-601	Delaware City Refining	2
30	NJ0024651-001A	Cumberland County Utilities Authority	2
31	DE0020338-001	Kent County Levy Court	2
32	NJ0029467-001A	Millville WTP	2
33	NJ0004995-441A	Mercer Generating Station	3
34	PA0013463-203	US Steel, Fairless-203	3
35	PA0013463-103	US Steel, Fairless-103	3
36	PA0012769-009	Rohm & Haas Chemicals, Bristol	3
37	NJ0005002-WTPA	PSEG Fossi,Burlington Generating Sta	3
38	NJ0027481-001	Beverly Sewerage Authority	3
39	NJ0004375-001A	Hoeganaes Corporation	3
40	NJ0021610-001A	Riverton STP	3
41	NJ0024449-001A	Palmyra STP	3
42	NJ0031216-001B	Menu Food Inc	3
43	NJ0004090-001A	MAFCO Worldwide Corp	3
44	NJ0005584-003A	FORMER BP PAULSBORO TERMINAL NO 4555	3
45	NJ0004219-001	Chemours Company Repauno	3
46	PA0028380-001A	Tinicum TWP	3
47	PA0013323-001	Boeing	3
48	PA0013714-107	Exelon Generating Company, Eddystone	3
49	PA0051713-001	Evonik Degussa	3
50	NJ0005240-001A	Bridgeport Disposal LLC	3
51	NJ0027545-001A	Logan Township MUA	3
52	PA0012637-201	Monroe Energy	3
53	DE0000655-001	General Chemical	3
54	PA0244449-001	FPL Energy Marcus Hookl	3
55	DE0050911-001	Occidental	3
56	NJ0004286-001	Mexichem Specialty Resins	3
57	DE0000051-001	DuPont Edgemoor	3
58	DE0000558-016	Calpine Mid-Atlantic Generation	3
59	NJ0024023-001A	Penns Grove Sewerage Authority	3
60	NJ0021601-001A	Carneys Point STP	3
61	DE0000612-001	Formosa Plastics	3
62	DE0021555-001	Delaware City STP	3
63	NJ0024856-001A	Salem City Wastewater Treatment Facility	3
64	DE0021539-001	Port Penn STP	3
65	DE0050547-001	Middletown-Odessa-Townsend	3
66	NJ0005622-048C	PSEG Nuclear Salem Generating Station	3
67	NJ0025411-461A	Hope Creek Generating Station	3
68	NJ0062201-001A	Canton Village STP	3
69	NJ0004766-001A	SURFSIDE PRODUCTS LLC	3
70	DE0021491-001	Milton STP	3
71	DE0021512-001	City of Lewes	3

Freshwater inflows from CSOs during the model calibration periods were provided at various degrees of resolution by four dischargers (i.e., municipalities): Philadelphia Water Department (PWD), Camden County Municipal Utilities Authority (CCMUA), Delaware County Regional Water Quality Control Authority (DELCORA), and City of Wilmington (CoW). For simplification all CSO outfalls were aggregated into 14 model inflow locations (Table 2-4 and Figure 2-6): five for PWD CSOs; three for CCMUA CSOs; three for DELCORA CSOs; and three for CoW CSOs. Mapping information used to route CSO flows was obtained from long term control plan documents for each of the CSO authorities. CSO outfalls located upstream of tributary monitoring locations were excluded to avoid double counting of flows and loads.

Table 2-4 Consolidated CSO Discharge Locations

No.	Location	Municipalities	CSO Outfalls
1	Poquessing Creek Downstream	PWD	Not Used (no flow)
2	Pennypack Creek Downstream	PWD	D02, D03, D04, D05, D06, D07, D08, D09, D11, D12, D13, D15, F21, F23, F24, F25, P03, P05
3	Frankford Creek Downstream	PWD	D_FRW, D17, D18, D19, D20, D21, D22, D23, D25, F11, F12, F13, F_FRFG, F09, F10
4	Camden, Cooper River Downstream	CCMUA	C15, C16, C17, C18C19, C22, Thorndyke, C22A, C23A, C24, C27, C28, C32
5	Philadelphia	PWD	D37, D38, D39, D40, D41, D42, D43, D44, D45, D46, D47, D48, D49, D50, D51, D51A, D52, D53, D54, D58, D61, D62, D63, D64, D65, D66, D67, D68, D69, D70, D71, D72, D73
6	Camden, Newtown Creek Downstream	CCMUA	CFA, C01, C02, C03, C05, C7C6, C08, C09, C10, C11, C13A
7	Gloucester	CCMUA	G01, G02, G03, G04, G05, G06, G07
8	Schuylkill River Downstream	PWD	S_FRM, S01, S02, S03, S04, S05, S06, S07, S08, S09, S10, S11, S12A, S13, S14, S15, S16, S17, S18, S19, S20, S21, S22, S23, S24, S25, S26, S30, S31, S32, S33, S36A, S37, S38, S42, S42A, S44, S45, S46, S50
9	Ridley Creek Downstream	DELCORA	14, 15, 16, 17, 18, 33
10	Chester Creek Downstream	DELCORA	12, 13, 22, 23, 24, 25, 26, 32
11	Delcora, to Delaware River mainstem	DELCORA	2, 3, 4, 5, 7, 8, 9, 10, 11
12	Shellpot Creek, Delaware River mainstem	CoW	CS031
13	Christina River Downstream	CoW	CSO09A, CSO09C, CSO10, CSO13, CSO14, CSO15, CSO16, CSO17
14	Brandywine River Downstream	CoW	CSO01, CSO03, CSO04A, CSO04B, CSO04C, CSO04D, CSO04E, CSO04F, CSO18, CSO19, CSO20, CSO21A, CSO21B, CSO21C, CSO22B, CSO22C, CSO23, CSO24, CSO25, CSO26

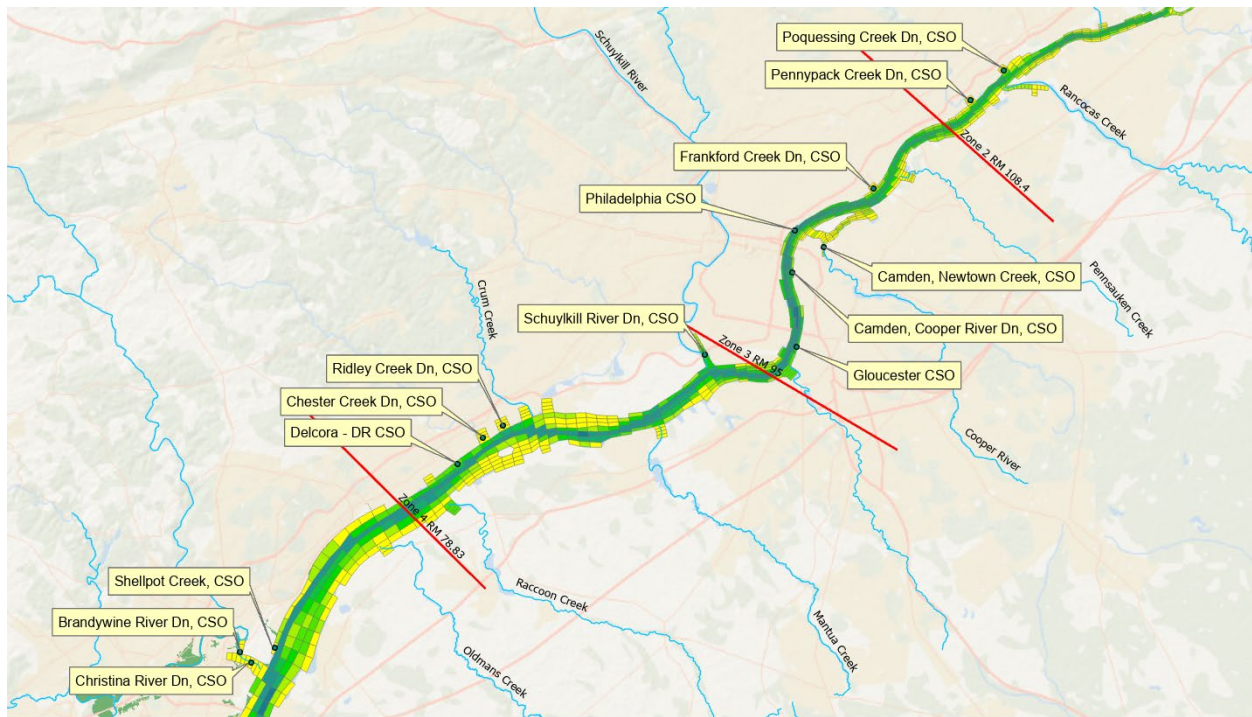


Figure 2-6 Consolidated CSO Discharge Locations

Eight major withdrawal facilities were included in the model and are listed in Table 2-5. The monthly withdrawal rates were based on the DRBC Water Use database for 2012 and assumed the same for the period of 2018-2019, since reported data for 2018-2019 were not available during model development.

Table 2-5: Summary of Major Withdrawals

Count	Facility Names
1	USX-US Steel Division
2	Lower Bucks County Joint Municipal Authority
3	Aqua Pennsylvania, Inc.
4	BURLINGTON CITY WATER DEPT
5	Philadelphia City
6	Kimberly-Clark Corporation
7	Chemours Company, FC, LLC., - Edge Moor
8	Chambers_Dupont_Chemours_Combined

As shown in Figure 2-7, based on boundary conditions developed for 2018 – 2019, the contribution of freshwater to the total water inflow budget from the mainstem at Trenton, Schuylkill River, the combined Christina and Brandywine Rivers, and remaining tributaries is 51%, 15%, 3.8%, and 11%, respectively. Point source (PS) discharges contribute 3.7%, and direct watershed contributions from NPS discharges, including MS4s and CSOs, contribute 5.0%. Direct precipitation onto Delaware River Estuary surface waters contributed another 10% of the total water load.

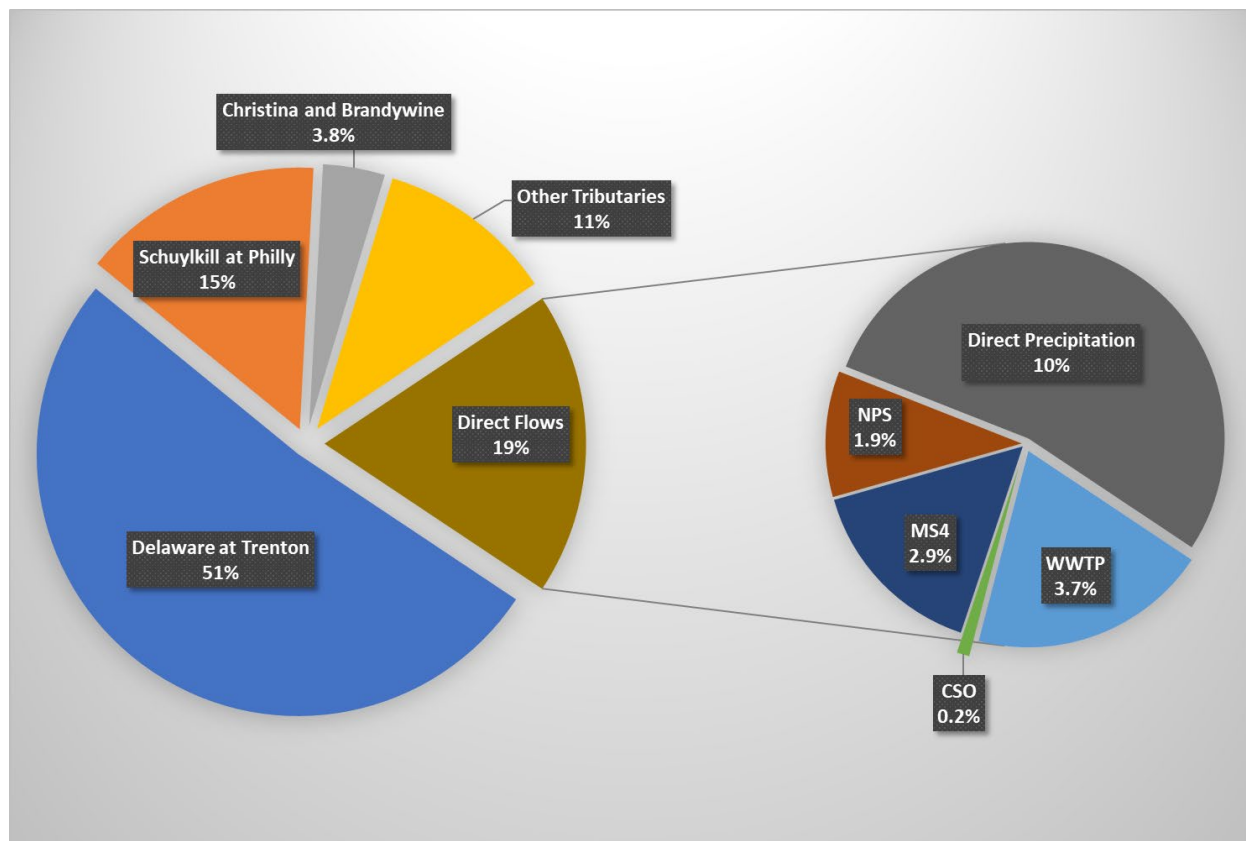


Figure 2-7: Freshwater Budget 2018-2019

2.4.3 Water Temperature and Salinity

Water temperature and specific conductance data collected at USGS gaging stations were used to specify the water temperature and salinity boundary conditions at the Delaware River at Trenton and all tributaries. Salinity can be calculated based on specific conductance (i.e., conductivity at 25°C). The conversion from USGS specific conductance or from NOAA conductivity measurements to salinity is summarized in the book “Standard Methods for the Examination of Water and Wastewater” 19th Ed. 1995 (American Public Health Association, 1995). Temperature in the Delaware River at Trenton varies seasonally, with minimum temperatures of 1 to 5° C during winter and maximum temperatures of approximately 25° C during summer. Temporal variations in water temperature, specific conductance, and salinity at the USGS station (1463500) at Trenton, New Jersey, during 2019, for example, are shown in Figure 2-8.

For tributaries without specific conductance data available, salinity was assigned the values from the Delaware River at Trenton gage and from the Schuylkill River gage for tributaries located upstream and downstream, respectively, of the Schuylkill River. The data gap for the Schuylkill River specific conductance dataset from January 1 to March 5 of 2018 was filled with 2019 data for the same period.

The salinity from point source discharges was set to zero all the time. While this assumption is imperfect, treatment plant salinity will have a negligible impact on salinity intrusion and stratification. From a water quality perspective, salinity predictions get passed to the water quality model for the purpose of estimating freshwater toxicity (for marine species) and salinity toxicity (for freshwater species); the assumption of zero salinity from point sources exerts a minimal impact on algal predictions. DRBC may improve this boundary condition assumption for future upgrades.

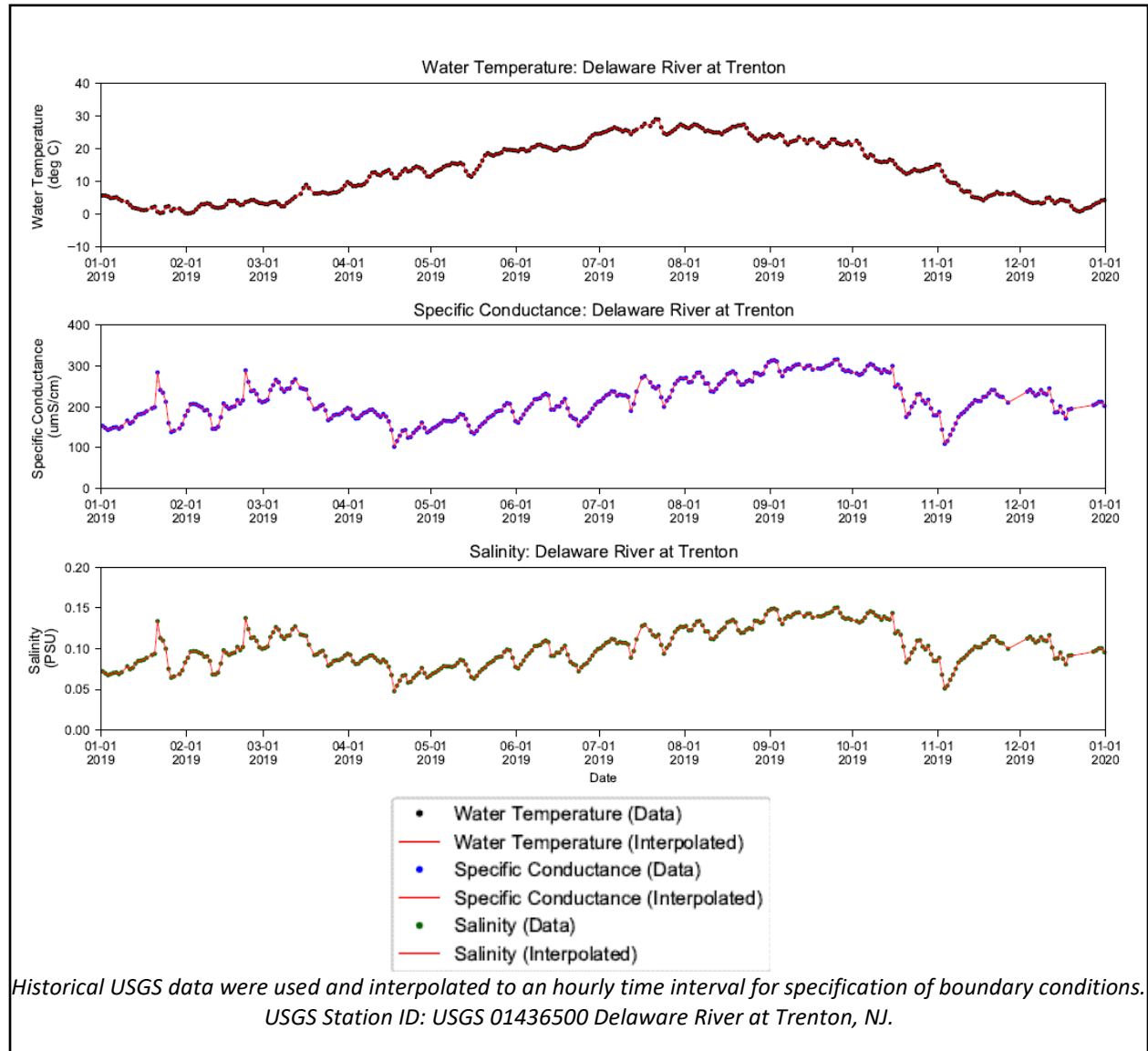


Figure 2-8: Water Temperature and Salinity at Trenton During 2019

Temperatures at tributary boundaries are critical to model performance and will be even more so when applied to the water quality model, since dissolved oxygen solubility varies with temperature, and all biological and chemical processes are impacted by temperature. Tributary temperatures were assigned based on continuous temperature measurements available as shown in Table 2-6. Tributaries with grab

sample temperature measurements were assigned temperatures from representative tributaries with continuous temperature based on a correlation matrix developed for this purpose. R-squared (coefficient of determination) values all exceeded 0.95. Tributaries without continuous or grab sample temperature data were assigned values based on geographic proximity. Daily or weekly effluent data from Tier 1 and Tier 2 point source discharges were used to assign effluent temperatures, while Tier 3 discharges were assigned the temperatures recorded at the Delaware River at Trenton or at the Schuylkill River based on their location upstream or downstream of the Schuylkill River.

Table 2-6: Availability of Tributary Temperature Data for Simulation Periods

USGS	Location	Temperature Data	CY2019	CY2018	CY2012
01464290	Crosswicks Ck at Hockamik Rd near Cookstown NJ	10/31/2019 through present			
01464500	Crosswicks Creek at Extonville NJ	01/31/2020 through present			
01465500	Neshaminy Creek near Langhorne, PA	12/19/2018 through present	X		
01465850	South Branch Rancocas Creek at Vincentown NJ	11/14/2019 through present			
01466500	McDonalds Branch in Byrne State Forest NJ	02/08/2012 through present	X	X	X
01466900	Greenwood Branch at New Lisbon NJ	11/12/2019 through present			
01467000	North Branch Rancocas Creek at Pemberton NJ	01/06/2020 through present			
01467005	NB Rancocas C at Iron Works Park at Mount Holly NJ	01/30/2020 through present			
01467024	Rancocas Creek at Bridgeboro NJ	09/25/2019 through present			
01467081	South Branch Pennsauken Creek at Cherry Hill NJ	11/07/2019 through present			
01467087	Frankford Creek at Castor Ave, Philadelphia, PA	10/01/2018 through present	X		
01467150	Cooper River at Haddonfield NJ	02/25/2020 through present			
01475510	Darby Creek near Darby, PA	11/19/2018 through present	X		
01475530	Cobbs Cr at U.S. Hghwy No. 1 at Philadelphia, PA (winter gaps)	10/01/2018 through present	X		
01477070	Raccoon Creek at Wrights Mill NJ	01/29/2020 through present			
01412000	Menantico Creek near Millville NJ	09/24/2019 through present			
01412080	Manumuskin River at Cumberland NJ	10/01/2019 through present			
01483050	Alloway Creek at Hancocks Bridge NJ	10/12/2018 through present	X		
01484080	Murderkill River at Frederica, DE	06/11/2010 through present	X	X	X
01484272	Broadkill River near Milton, DE	12/21/2016 through present	X	X	
01463500	Delaware River at Trenton NJ	10/01/2007 through present	X	X	X
01474500	Schuylkill River at Philadelphia, PA	10/01/2018 through present	X		
01483177	Appoquinimink River Near Odessa, DE	10/26/2011 through present	X	X	X
01481500	Brandywine Creek at Wilmington, DE	10/01/2007 through present	X	X	X
01480065	Christina River at Newport, DE	10/01/2007 through present	X	X	X

The surface water temperature and salinity at the ocean open boundary was established based on water temperature and conductivity data collected at NOAA Station (8557380) at Lewes, Delaware. For the year 2012, the data from Lewes were not available; data collected at NOAA Station (8555889) at Brandywine Shoal Light (which is about 10 miles from the mouth of the bay) was adjusted to represent year 2012 surface salinity at the ocean open boundary by adding 3 psu to reflect the salinity gradient in the estuary. For all years, the boundary salinity was further adjusted based on the surface salinity values by adding a small adjustment of +3.5 psu to reflect the vertical stratification at lower depths. The adjustment was applied to the third layer from the top and to all lower layers, and a linear transition was made for the top three layers.

A similar approach was used for water temperature at the boundaries. Water temperature varies significantly over the course of a year. It was assumed that the near-surface water temperature at the ocean open boundary is about the same as the observed water temperature recorded at NOAA station (8557380) at Lewes, Delaware. The water temperature below the surface was adjusted based on the

World Ocean Atlas 2013 (Locarnini et al., 2013) database of monthly mean data near the mouth of the Delaware Bay, which is shown in Table 2-7. The average difference in monthly mean water temperature ranged from -0.3° C in February at the surface to 4.3° C in July at a depth of 10 m.

Table 2-7: Monthly Mean Water Temperature near the Mouth of Delaware Bay

Month	Water Temp. (surface)	Water Temp. (Depth = 5 m)	Water Temp. (Depth = 10 m)	Difference (surface - D10m)
1	7.11	7.15	7.19	-0.08
2	5.08	5.12	5.38	-0.3
3	5.63	5.58	5.5	0.13
4	10.42	9.19	8.68	1.74
5	14.76	14.24	12.79	1.97
6	20.45	19.76	17.21	3.24
7	23.93	23.09	19.67	4.26
8	24.35	23.94	21.74	2.61
9	21.9	21.81	21.67	0.23
10	16.29	16.42	16.44	-0.15
11	15.1	15.15	15.25	-0.15
12	10.14	10.39	10.39	-0.25

* This is based on WOA13 database

The water temperature and salinity boundary conditions at the C&D Canal were established based on water temperature and conductivity data collected at NOAA Station (8573927) at Chesapeake City, Maryland. For periods when conductivity data were not available (e.g., 2012), a rating curve was used to specify the salinity boundary conditions. Multiple-linear regression analysis was conducted using data collected at NOAA Station Chesapeake City, USGS Station at Reedy Island, and USGS Station (01576000) at Susquehanna River at Marietta, Pennsylvania, from April 1, 2017, to May 31, 2019. The 30-day moving average salinity data were used in the analysis and resulted in a regression correlation coefficient R-squared of 0.77. The observed and predicted salinity at Chesapeake City during the same period are presented in Figure 2-9. The salinity (psu) rating curve is given as:

$$S = 0.1832 + 0.40083 S_r + 0.00885 \times 10^6 \times Q_m^{-1} \quad (\text{Eqn 2.4-1})$$

where S = Daily averaged salinity at Chesapeake City (western end of C&D canal); S_r = Salinity at Reedy Island; and Q_m = flow rate (in cfs) at USGS Station at Susquehanna River at Marietta. Daily averaged salinity at Chesapeake City is about half of that observed at Reedy Point; however, the salinity is quite low when there is high flow from the Susquehanna River, indicating an inverse relationship between the salinity at Chesapeake City and the salinity at the Susquehanna River at Marietta.

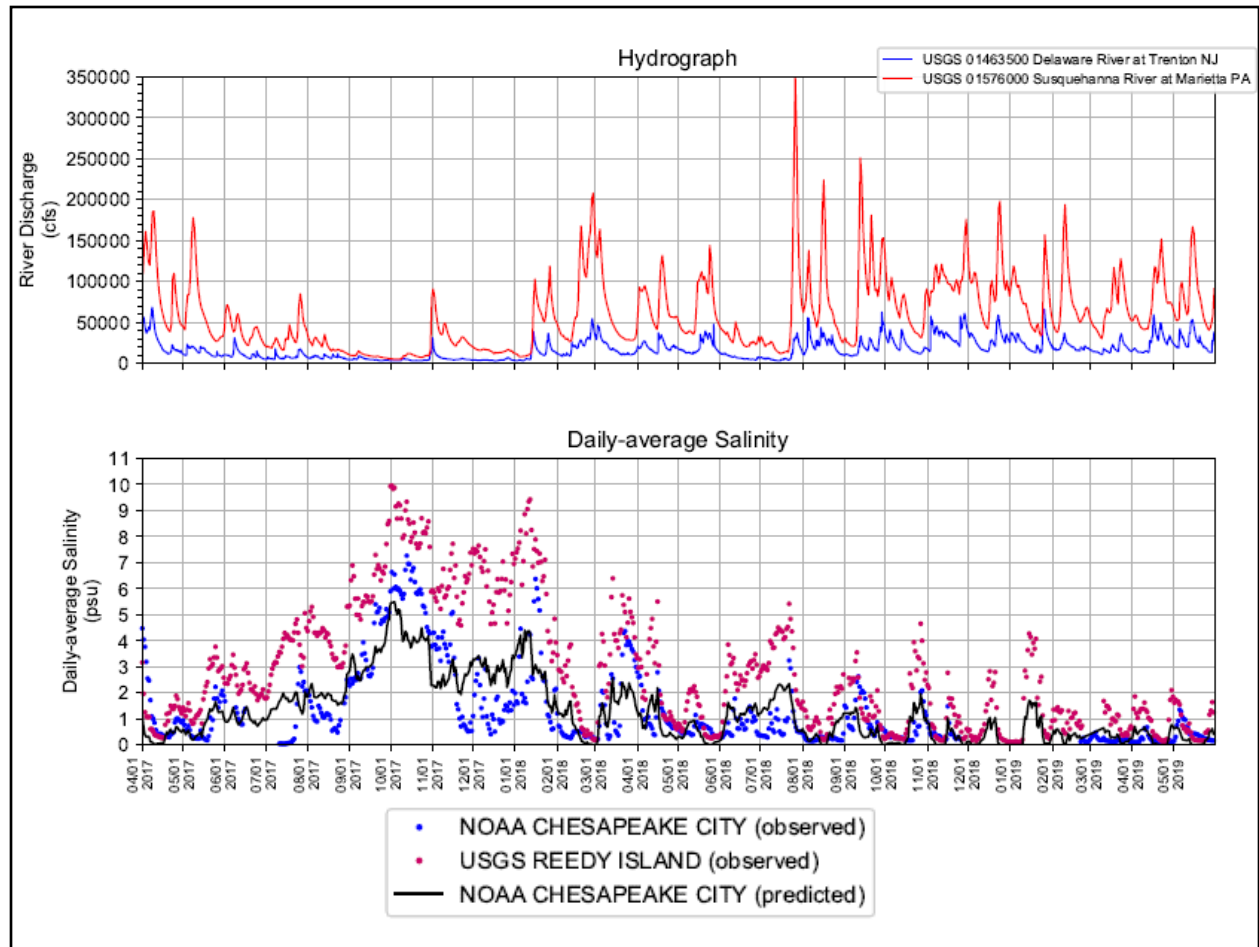


Figure 2-9: Predicted Daily Averaged Salinity at Chesapeake City. Predicted salinity at Chesapeake City was based on salinity at Reedy Island and Susquehanna River at Marietta.

2.4.4 Climate / Meteorological Forcing

Climate/Meteorological forcing boundary conditions include air temperature, air pressure, dew point, cloud conditions, wind speed, wind direction, precipitation, and net shortwave solar radiation. This information is used by EFDC to calculate the heat flux at the water surface, and it affects the vertical distribution of water temperature in the water column. Since surface heat flux was spatially variable over the large model domain, meteorological data collected at multiple NOAA National Climatic Data Center (NOAA-NCDC) weather stations were considered for the climate forcing boundary conditions. Locations of five weather stations that were considered by the model are shown in Figure 2-10 and summarized in Table 2-8. Temporal variations in meteorological data for 2018 and 2019 are shown in the meteorological data graphs provided in Appendix C. Note that (1) the direct measurements of net shortwave solar radiation were not available at the NOAA-NCDC weather stations; (2) the inputs of net shortwave solar radiation to EFDC were calculated using a procedure in Iqbal (1983) based on latitude, longitude, and cloud cover⁹; and (3) no adjustments were made to the solar radiation inputs during model calibration. Besides the shortwave solar radiation, EFDC also internally calculates the long-wave radiation (a heat loss emitted from water to air as gray body), as well as conductive heat loss and heat loss due to evaporation, in the surface heat flux computation.

Table 2-8: NOAA-NCDC Weather Stations

Count	STATION	USAF	WBAN	LAT	LON
1	TRENTON MERCER AIRPORT	724095	14792	40.277	-74.816
2	PHILADELPHIA INTERNATIONAL AIR	724080	13739	39.873	-75.227
3	NEW CASTLE COUNTY AIRPORT	724180	13781	39.674	-75.606
4	DOVER AFB AIRPORT	724088	13707	39.133	-75.467
5	CAPE MAY COUNTY AIRPORT	745966	03726	39.008	-74.908

The wind roses for years 2018 and 2019 shown in Appendix C depict temporal frequencies of wind speed and wind directions at NOAA-NCDC stations at Trenton, Philadelphia, New Castle, Dover, and Cape May. Overall, wind over the bay area usually comes from the north or northwest direction during the wintertime, while most of the winds blow in from the south, southeast, or southwest directions during the summertime.

Heat flux into and out of the sediment bed was not incorporated into the hydrodynamic model because limited data were available to specify or calculate this heat flux. Typically, heat flux at the sediment bed is not included in estuarine hydrodynamic model simulations.

⁹ The net shortwave solar radiation can be calculated as the difference between the in-coming shortwave solar radiation and the amount being reflected back to the atmosphere. The incoming shortwave solar radiation was calculated using the method described in Iqbal (1983).

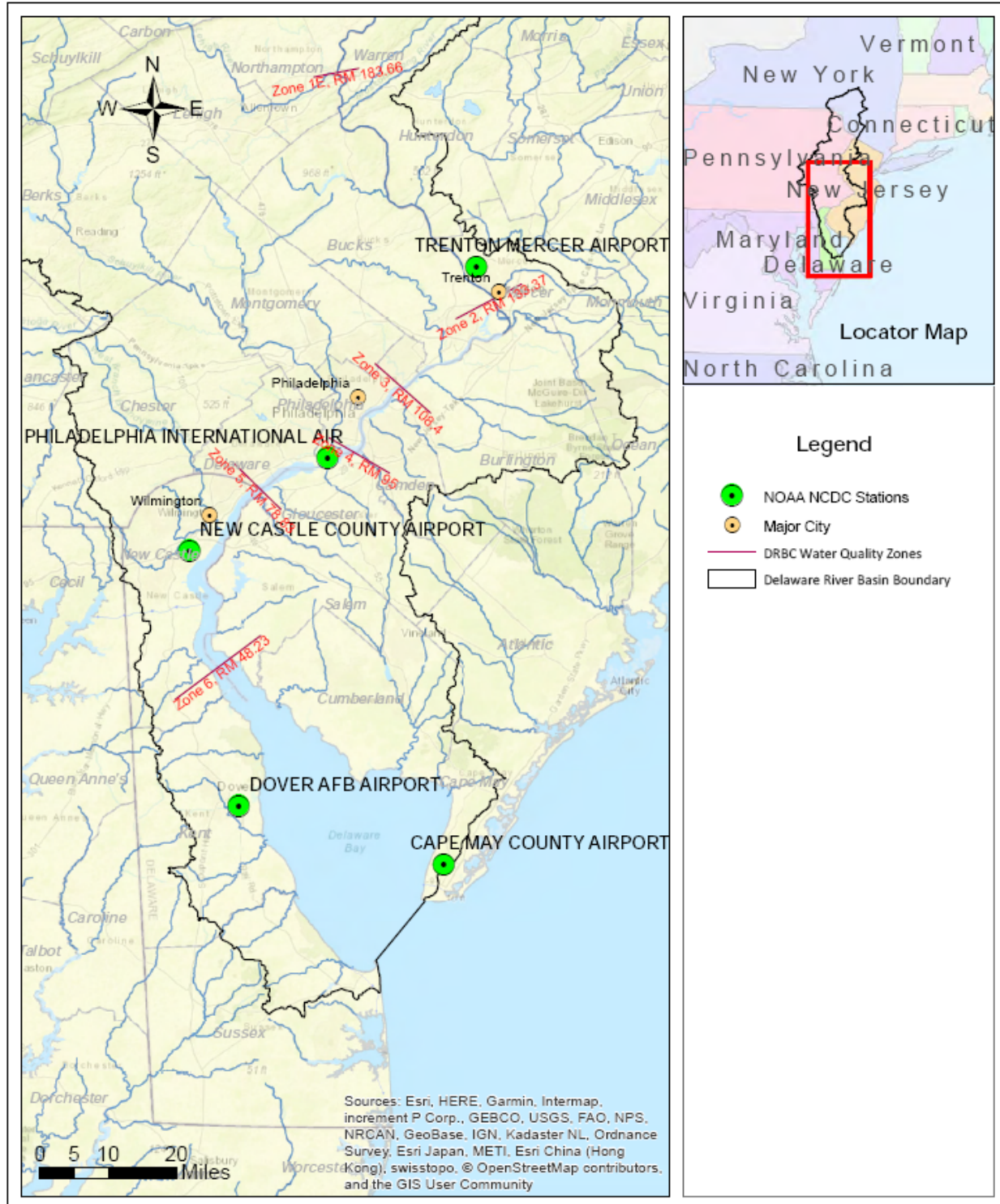


Figure 2-10: Locations of Five Weather Stations Used to Characterize Climatic Boundaries

2.4.5 Initial Conditions

Model simulations were set to start on January 1 of each year. The model can be simulated with a ‘null’ (i.e., zero) or user-specified starting values for every grid cell for all modeling variables (state variables) including water surface elevation, current velocity, water temperature, salinity, etc. This type of initial condition setup is called “cold-start”. With a cold-start condition, the model takes a certain simulation time period to reach realistic values of each state variable. An alternative is to run the model from “cold-start” for a short period of time (called a “spin-up” period) until all variables reach realistic values. Model predictions at the end of the “spin-up” period are saved to a restart file as initial conditions for future simulations. This approach is called “hot-start”, which is adopted in this project.

A model spin-up period of 31 days was conducted before the January 1 start date of the 2012 and 2018 hydrodynamic model simulations; the simulation of year 2019 was set up using a “hot-start” procedure in which the hydrodynamic parameters at the end of 2018 were taken as the initial conditions for 2019. Flow rates at Trenton, as well as inflows from all other flow boundaries, were held constant throughout the spin-up periods at the flow rate on January 1 of the simulated year. The initial conditions for water surface elevation, water temperature, and salinity for the spin-up periods were set as interpolated values between the upstream boundary at Trenton and the ocean open boundary at the beginning of the spin-up simulation. The 31-day spin-up period was sufficient to ensure that any transient effects on model predictions due to the initial conditions were eliminated prior to the start of a model calibration simulation.

3. HYDRODYNAMIC MODEL CALIBRATION

3.1 CALIBRATION APPROACH, MODEL ACCURACY, AND RELIABILITY

Calibration of the hydrodynamic model was accomplished by comparing model predictions to observed water surface elevation (WSE), current velocity, temperature, and salinity data collected at various locations within the Delaware River Estuary study area during the 2018 through 2019 period, as well as the drier 2012 period. Hydrodynamic calibration focused on reproducing observed WSE, depth-averaged current velocity, and the longitudinal and vertical distribution of salinity and water temperature. Detailed summaries of model calibration periods and the data from NOAA and USGS used to calibrate the hydrodynamic model are provided in Appendix D, which along with the DRBC boat run dataset formed the basis for model calibration metrics. Locations of NOAA tide and current velocity stations are shown in Figure 3-1 and Figure 3-3; USGS stations are shown in Figure 3-2; and DRBC Boat Run sampling locations are presented in Figure 3-4. The calibration metrics are listed below:

- Predicted water surface elevation (astronomic tidal and sub-tidal fluctuations) at NOAA stations;
- Predicted current velocity at NOAA stations and Philadelphia Water Department (PWD) buoy locations;
- Predicted salinity at NOAA stations;
- Predicted salinity (chlorinity) at USGS gaging stations;
- Predicted salinity (chlorinity) at DRBC boat run sampling stations;
- Predicted water temperature at various NOAA and USGS stations; and

The City of Philadelphia Water Department (PWD) contracted the Woods Hole Group Inc. (WHG) to measure Delaware River current velocities in 2012. Three long-term current monitoring stations were located at: a) Burlington, New Jersey (upstream station), b) Eagle Point, across from Philadelphia, Pennsylvania, and c) Marcus Hook Bar in Chester, Pennsylvania (downstream station). The locations of the three long-term data collection stations are shown in Figure 3-3. At each station, WHG deployed a surface-buoy data collection system equipped with an acoustic Doppler current profiler (ADCP). These data were obtained from PWD in December 2022, after model calibration was completed. Comparisons between these data and model predictions are included in this report as additional model validation.

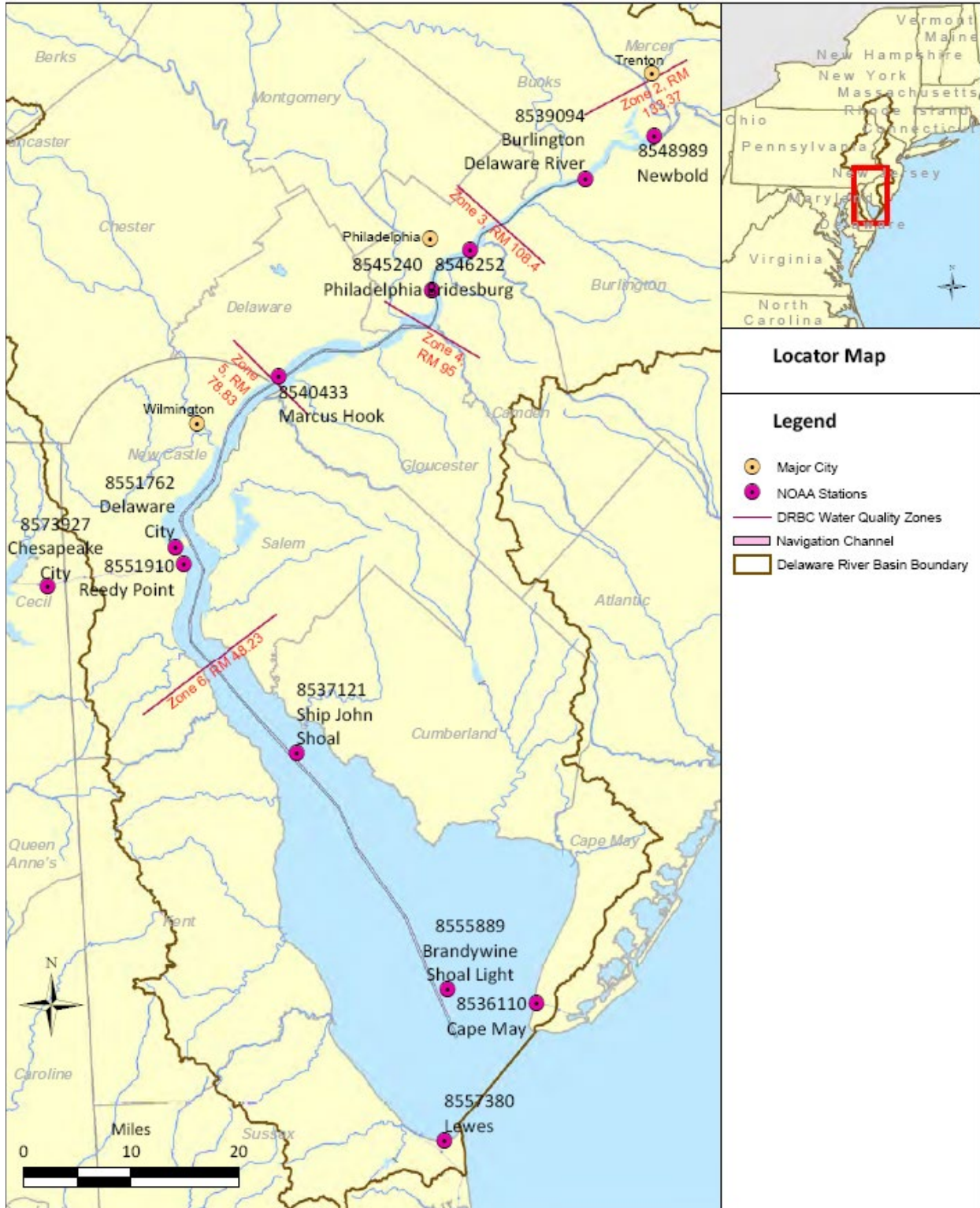


Figure 3-1: Locations of NOAA Tide Stations

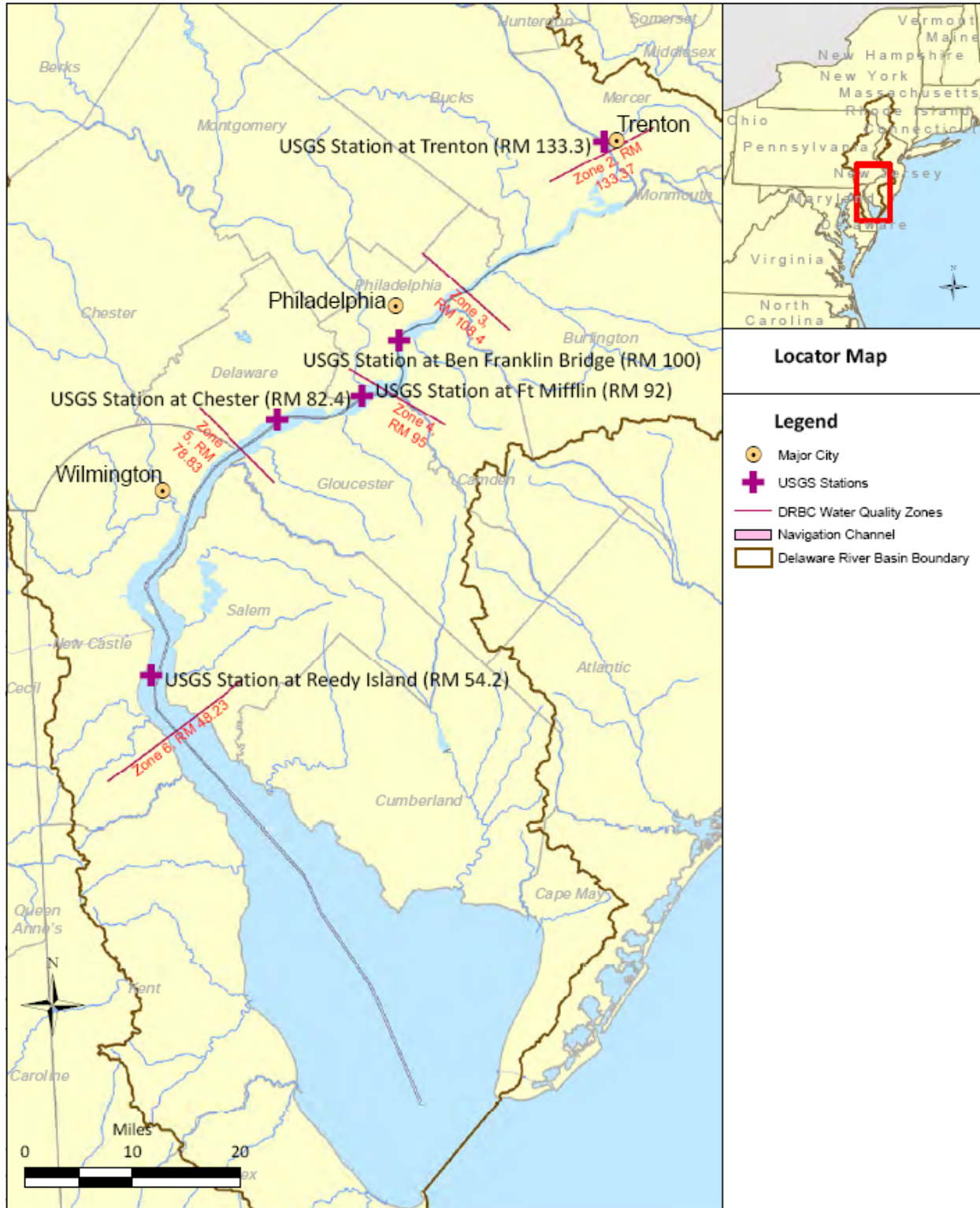


Figure 3-2: Locations of USGS Stations on Delaware River Mainstem

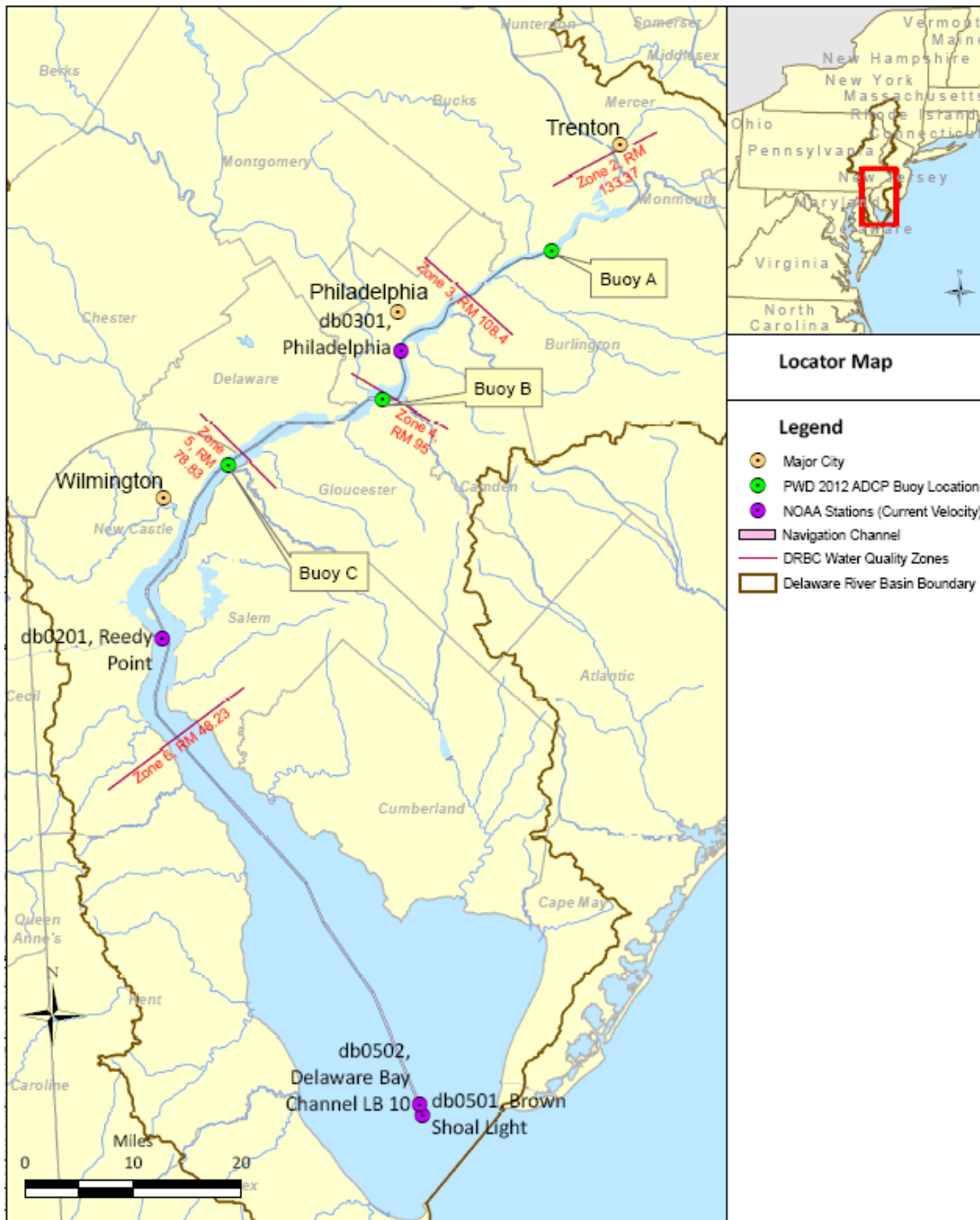


Figure 3-3: Locations of NOAA and PWD Stations for Current Velocity

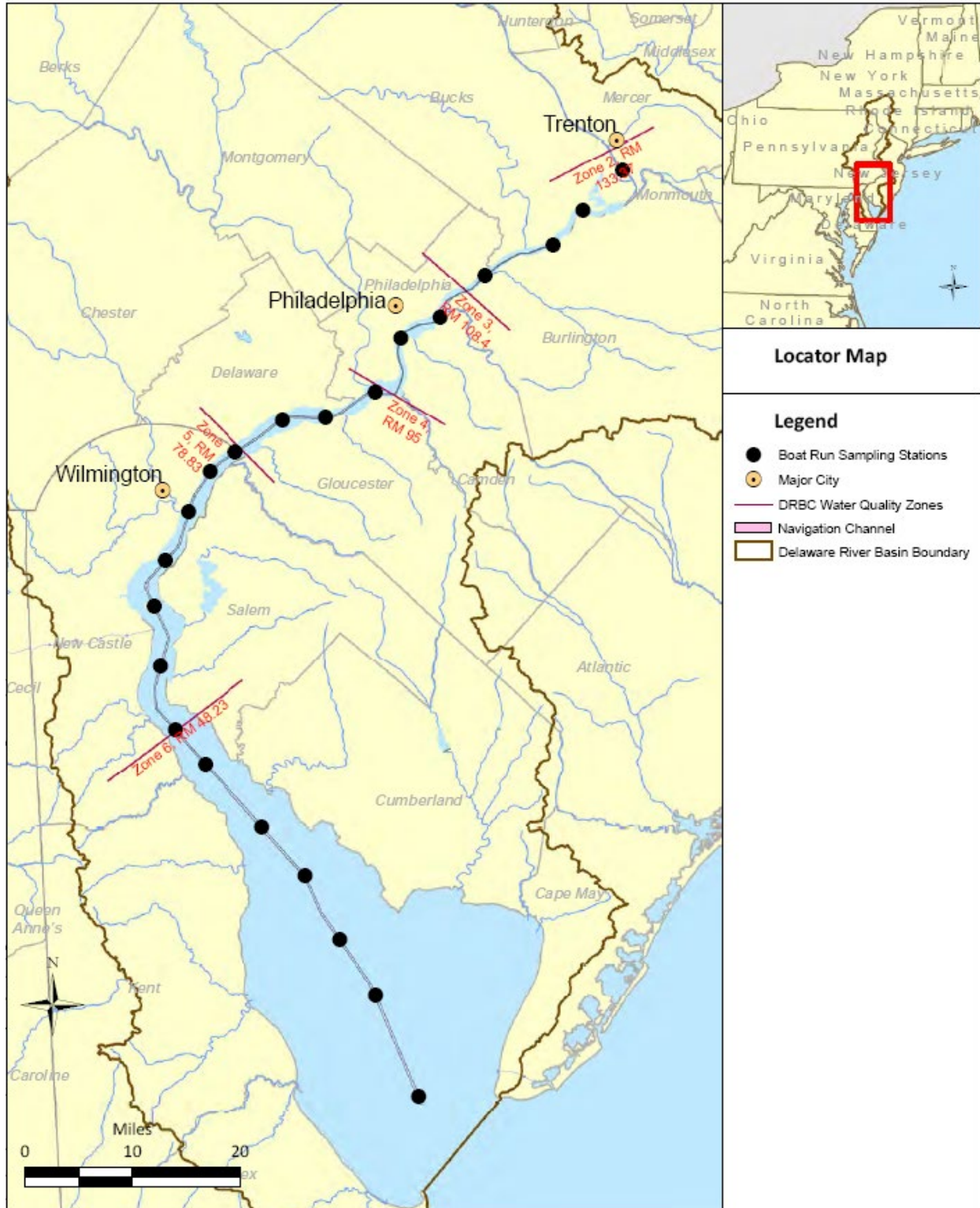


Figure 3-4: DRBC Boat Run Sampling Locations

In this study, the hydrodynamic model performance was evaluated through both visual comparisons and quantitative measures to differentiate among calibration runs and to provide sufficient evidence upon which to base a decision of model acceptance or rejection for its intended use. Visualization of a time history of simulated results against observed data shows the degree to which the model captures the general trend and overall magnitude of the observed condition. To quantify the quality of fit between the observations and model predictions of water surface elevation, current velocity, salinity, and water temperature, a series of statistical measures similar to those utilized in MacWilliams et al. (2015) were used. Statistical measures that characterize the model accuracy and reliability include: 1) Model Skill, 2) Correlation Coefficient (r), 3) Bias and normalized bias of model estimates by the standard deviation of the observed data, 4) Root Mean Square Error (RMSE), and 5) unbiased Root Mean Square Difference (ubRMSD) and normalized ubRMSD by the standard deviation of the observed data.

Model skill is calculated as:

$$Skill = 1 - \left[\sum_{n=1}^N |X_{Mi} - X_{Oi}|^2 \right] / \left[\sum_{n=1}^N (|X_{Mi} - \bar{X}_O| + |X_{Oi} - \bar{X}_O|)^2 \right] \quad (Eqn 3.1-1)$$

The bias of model estimates is calculated as

$$bias = \frac{1}{N} \sum_{n=1}^N X_{Mi} - \frac{1}{N} \sum_{n=1}^N X_{Oi} \quad (Eqn 3.1-2)$$

Negative bias indicates that the model underpredicts relative to data; positive bias indicates that the model overpredicts relative to data.

The ubRMSD is calculated as

$$ubRMSD = \left[\frac{1}{N} \sum_{n=1}^N [(X_{Mi} - \bar{X}_M) - (X_{Oi} - \bar{X}_O)]^2 \right]^{0.5} \quad (Eqn 3.1-3)$$

The ubRMSD metric quantifies the model-data differences with the bias removed. It is similar to a root-mean-square error analysis, but the effects of bias are removed from the calculation. As ubRMSD increases, the difference between oscillations in the predicted and observed variable becomes larger. Formulations of the commonly used parameters Correlation Coefficient (or coefficient of determination, R^2) and RMSE are widely known and not documented here.

While there is no consensus¹⁰ amongst practitioners on hydrodynamic model performance criteria, guidelines of model acceptance have been recommended by some researchers and agencies (e.g., Willmott 1981, Hess et al. 2003, Zhang et al. 2006, Patchen 2007, and Bever et al. 2013). NOAA (Hess et al. 2003 and Zhang et al. 2006) proposed acceptable error bounds for predicting water level (15 cm),

¹⁰ This statement is attributed to DRBC's Model Expert Panel and is based on members' experiences.

current velocity (26 cm/s), phase (0.5 hrs.), water temperature (7.7 °C), and salinity (3.5 psu). The criterion for water temperature became stricter as 3.0 °C (Patchen 2007). Note that these criteria were designed for the operational nowcast and forecast models used to support navigational application. Some of the bounding values (e.g., salinity and water temperature) may be too imprecise for the water quality study of the Delaware River Estuary. To provide a succinct method to evaluate and report the accuracy of a large number of comparisons, MacWilliams et al. (2015) established a standardized set of cutoff values for both the skill scores and target diagram (See Table 1 in MacWilliams et al., 2015). Skill scores greater than 0.975 have been used to show that a model accurately predicts the water surface elevation. Skill scores of greater than 0.85 have been used to show accurate modeling of salinity, with scores between 0.7 and 0.85 representing “acceptable” values. Skill scores greater than 0.9 have been used to indicate accurate modeling of current speed or velocity, with scores between 0.8 and 0.9 indicating “acceptable” model predictions. The thresholds for classifying model performance using the target statistics were based on the distance from the origin of target diagram plots, and thresholds applied to classify the accuracy of model predictions based on the target statistics were the same for each variable. It is classified as acceptable if all predictions are inside a radius of 1 and considered as accurate if all predictions fall inside a radius of 0.5.

In this study, statistical measures such as bias, RMSE, ubRMSE, Correlation Coefficient (r) or R-squared, and target diagram are used to quantitatively evaluate the model performance. In accordance with the established Quality Assurance Project Plan (DRBC, 2019) for this project, a “weight of evidence” approach was used in close coordination with the Model Expert Panel in order to judge the acceptability of the model for its intended purpose. The referenced standards or thresholds for error tolerance to assess the model performance are summarized in Table 3-1.

Table 3-1 Criteria to Access Coastal Hydrodynamic Model Performance

Model accuracy		Water Level	Harmonic Tide		Current Speed	Current Speed		Salinity	Water Temp.
		Magnitude	Amp.	Phase	Magnitude	Amp.	Phase	Magnitude	Magnitude
NOAA	Acceptable		< 15 cm	< 0.5 hr		< 26 cm/s	< 0.5 hr	< 3.5 psu	< 3 degree C
Skill accuracy	Accurate	>0.975			>0.9			>0.85	
	Acceptable	0.95 – 0.975			0.8 – 0.9			0.7 – 0.85	
	Poor agreement	<0.95			<0.8			<0.7	
Target accuracy	Very accurate	0.0 - 0.25							
	Accurate	0.25 - 0.50							
	Acceptable	0.5 - 1.0							
	Poor agreement	> 1.0							

Note that the NOAA standards are for assessing the performance of coastal models and mostly for navigation purposes. In the table, Amp. = Amplitude; Temp. = Temperature; and hr = hour.

3.2 CALIBRATION PARAMETERS

There were five major parameters adjusted to calibrate the hydrodynamic model, described as follows in the same sequential steps used during the calibration process.

3.2.1 Bottom Roughness Height Z0

The model was first calibrated against tidal water surface elevation, using the data collected at total of nine NOAA tide stations along the river, by adjusting the effective bottom (or bed) roughness height, Z0, which accounts for the friction from the bed in the hydrodynamic model. It affects the current circulation in the system as well as the amplitude and phase of the progressive wave that propagates from the mouth of the Bay towards upstream.

The composition of bottom sediments in the upper estuary includes fine sands, coarse sediment, and gravel with silt accumulated in spots. Muddy and fine sediments are found in the estuarine turbidity maximum zone (ETM), located approximately from RM 55 to 75. This spatial variability made it necessary to implement a spatially variable effective bottom roughness height throughout the model domain, ranging from 2 to 20 mm. The range of effective bed roughness values typically used in estuarine hydrodynamic models is 1 to 100 mm (Blumberg and Mellor, 1987). Summarized Z0 values used in the model are presented in Table 3-2 and Appendix E. Bottom roughness height was set to be small in Zone 5, where the ETM is located, to reflect the clay and silt sediment bed locally. The bottom roughness height was set to be slightly higher in the deeper navigation channel than the shallower area adjacent to it in

Zones 5 and 6 to reflect a relatively rougher sediment bed due to a higher current velocity and near-bed shear stress. Lateral variation in bottom roughness was not established for most of the tidal river (e.g., Zones 2 to 4), because (1) there is not enough information on the lateral distribution of current velocity data to validate this setup, (2) lateral gradients of DO, conductivity, and water temperature data are not significant in the tidal river, and (3) the model does not simulate floodplain inundation (i.e., the wetting and drying process over floodplain areas was turned off), where bottom roughness values are typically higher than the those in the river channel.

Table 3-2 Bottom Roughness Height

Zone	In Channel (mm)	Outside Channel (mm)
2 (upstream RM 132)	12	12
2 (downstream RM132, except Burlington Is. Area)	8	8
2 (Burlington Is. Area, RM 118 to 195)	12	12
3	5	5
4	2	2
5 (upstream RM 68)	1.6	1.5
5 (downstream RM 68)	1.5	1.2
6	2.2	2
C&D Canal	20	
Tributary	10	

Maximum Active Layer, KC = 12

Total Number of Cells = 1890

3.2.2 Turbulent Model Parameter

The EFDC hydrodynamic model utilizes the Mellor and Yamada (1982) turbulence model to calculate the eddy viscosity and eddy diffusivity, which governs the vertical mixing process due to turbulent shear and buoyancy from vertical stratification of water temperature and salinity. The original model of Mellor and Yamada (1982) considered equal contribution of turbulent shear and buoyancy to the length scale equation. Burchard (2001) demonstrated that: 1) all empirical parameters in the Mellor and Yamada (1982) model were calibrated except the buoyancy term E3 (or here in EFDC named as CTE3); and 2) CTE3 was set equal to the shear production term CTE1 as 1.8 in Mellor and Yamada (1982) as the default value due to lack of information. This constant has been the subject of specific studies (e.g., Burchard, 2001) since the value suggested by the original authors (Mellor and Yamada, 1982) has not been thoroughly studied. Literature values for CTE3 (Mellor and Yamada, 1982; and Burchard, 2001) range from 1.8 to 7.784. The study by Burchard (2001) paid special attention to this variable and proposed a narrower range

for this value from 4.752 to 5.634. The CTE3 value ranges should be considered as a reference and not as absolute.

In this study, CTE3 was adjusted through model-to-data comparison of salinity. A final CTE3 value of 12 was selected, which is outside the range of 1.8 to 7.8 suggested in the literature. Numerical tests indicate that varying the CTE3 value exerted minimal impact on the simulated tidal water surface elevation but more noticeable impact on salinity intrusion; increasing CTE3 enhanced salinity vertical stratification as well as salinity intrusion farther upstream. For this study, the use of a value outside the range analyzed by Burchard's was deemed acceptable under the conditions of the simulation. The end use of this hydrodynamic model when linked with DRBC's water quality model (Zheng et al., 2024), demonstrates that: 1) observed nutrients and DO in the Delaware River Estuary are weakly stratified, especially in the urban area (about 0.5 mg/L difference in dissolved oxygen concentrations from the surface to bottom); and 2) vertical gradients of predicted DO and nutrients were consistent with observations. This indicates that vertical mixing was not unrealistically restricted by the use of a CTE3 value of 12.

3.2.3 Adjustment to Tidal Surface Elevation in C&D Canal

As discussed in Section 2.4.1, vertical datums used in the model were all relative to NAVD88 and apply to all model inputs and model outputs. NOAA tide data collected at Station (8573927) Chesapeake City, Maryland¹¹, were based on MLLW datum. Tidal water surface elevation was converted from MLLW to NAVD88 in meters as follows: $\text{NAVD88} = \text{MLLW} - 0.474$. The uncertainty in the NOAA provided vertical datum that is associated with datum conversion is about +/- 10 cm (based on https://vdatum.noaa.gov/docs/est_uncertainties.html).

Given the relatively large uncertainty in the vertical datum conversion of the NOAA tide data, adjustments to the tidal water surface elevation at the C&D canal western boundary within the uncertainty range were made as an additional calibration parameter. A preliminary sensitivity analysis showed that the model prediction of net flow in the C&D canal may be sensitive to the tidal water surface elevation at both ends of the canal, and the net flow moving from Chesapeake Bay to the Delaware River Estuary (or vice versa) may have a significant impact on salinity intrusion in the Delaware River Estuary. A final adjustment of -2 cm was selected for the calibrated model in this study. The resulting average monthly residual flows in the C&D canal are 8.5, 5.7, and 55.7 m³/s for the years 2018, 2019, and 2012, respectively. These predicted net flows are in good agreement with the data-driven estimations in the literature (Ward et al., 2009). Numerical tests of tracers released from the C&D Canal suggests that discharges from the C&D

¹¹ At the time this model was developed, the tidal water surface elevation data using NAVD 88 datum, as well as the datum conversion between MLLW datum and NAVD88, were not available from the NOAA site. This information has only become available since after year 2020 on NOAA's updated website: <https://tidesandcurrents.noaa.gov/datums.html?id=8573927>. The updated conversion is $\text{NAVD88 (m)} = \text{MLLW (m)} - 0.487\text{m}$. This is 1.3 cm lower than the value used to convert NOAA tide data for this model and very close to the value (-2 cm) used to adjust the water surface elevation at the western end of the C&D canal as part of model calibration.

Canal could affect the mainstem of Delaware River around $40 < RM < 75$. USGS is collecting current velocity data, and both hourly and tidally filtered flow rate have been reported in the C&D Canal since late 2019¹². These data will be helpful in refining the C&D Canal boundary during future model enhancements.

3.2.4 Turbulent Exchange Coefficients for Conduction and Evaporation

Heat transfer simulation in EFDC is based on the algorithms proposed by Rosati and Miyakoda (1988), in which turbulent exchange coefficients C_H and C_E for conduction and evaporation control the heat loss from the water column to air. Through a series of numerical tests, C_H and C_E were selected as 1.1×10^{-3} (dimensionless) in the hydrodynamic model to achieve optimum comparisons between predicted and observed water temperatures. These values are consistent with those in Rosati and Miyakoda (1988). Heat transfer between the water column and the riverbed is not considered in this study.

3.2.5 Numerical Stability and Time Step

Preliminary diagnostic simulations were conducted with the hydrodynamic model to ensure that the numerical grid structure and resolution did not produce localized numerical instabilities or unrealistic results. The preliminary simulations were also used to determine the optimum timestep for numerical stability, which was determined to be 10 seconds for the 3D hydrodynamic model. With the 10 second time step, it takes about 8 hours for a workstation (Precision 5820 Tower) to finish a one-year hydrodynamic simulation. In this study, the wetting and drying option was turned off, since the flooding and inundation of low-lying marsh areas in Zone 6 is of minimal concern in the water quality study. Excluding the wetting and drying enhances the efficiency and speed of the model simulations and minimizes the error introduced into the hydro-linkage file between the hydrodynamic EFDC model and the WASP water quality model.

3.3 CALIBRATION RESULTS

Representative results from the calibration simulations for the hydrodynamic model are presented in this section.

¹² Newly established USGS gage in C&D Canal:

https://waterdata.usgs.gov/nwis/inventory/?site_no=01482695&agency_cd=USGS

3.3.1 Water Surface Elevation

3.3.1.1 Astronomical Tide

Evaluating model performance with respect to water surface elevation was the first step during model calibration. The tidal wave enters the estuary at the mouth near Cape May and progresses upstream to the head of tide at Trenton. The measured WSE (total water level) is the sum of the astronomical tide and subtidal fluctuations at a given location. The dominant tidal constituent is the principal lunar semi-diurnal (M2, 12.42-hour period). In addition to M2, eight other constituents (S2, N2, K2, K1, O1, Q1, M4 and M6, Table 3-3) were also included in the analysis. According to NOAA, the mean tidal range¹³ observed at the mouth of the estuary at RM 0 is 4.07 feet (1.24 m), increasing to a local maximum of 5.57 feet (1.70 m) at RM 37 (Ship John Shoal, New Jersey) and a local maximum of 7.84 feet (2.39 m) at Newbold, Pennsylvania, which is approximately 8 miles downstream from the USGS gage at Trenton. The tidal range is about 10 feet at Trenton. Tidal harmonic analyses were performed using the observed data and model predictions for a 1-year (2019) period. The model-data comparisons of amplitude and phase of major harmonic constituents are summarized in the tables in Appendix F. The spatial distribution of the amplitudes of M2, and shallow water constituents M4 and M6, are presented in Figure 3-5, with the focus being on the amplification of tidal amplitude of the dominant harmonic constituent M2. The tidal amplitude of M2 increased from 0.6 m at the mouth of the Bay (RM 0) to about 0.85-0.9 m at RM 37, then decreased to about 0.8 m at RM 79 near Marcus Hook, and then increased again all the way to the head of tide at Trenton (RM 133) to about 1.1 m. The M2 amplitude at Newbold (located approximately 126 mi from the mouth of the Bay) is about 1.1 m, which is about a factor of 2 increase. The maximum error in predicted M2 tidal amplitude is 8.8 cm at NOAA Station Ship John Shoal, likely attributed to the inundation of low-lying marsh areas in Zone 6 that is not included in the model. M4 and M6 reflect the influence of river inflows as well as impact from bathymetry. A complete set of model-to-data comparison plots of the amplitude and phase of nine major harmonic constituents at the nine NOAA tide stations is presented in Appendix G. The comparison errors listed in Appendices F and G all fall within the acceptable error bounds of 15 cm for water level and 0.5 hour for phase as recommended by NOAA (Hess et al., 2003 and Zhang et al., 2006), except for a few phase comparisons of the non-dominant constituents. These comparisons indicate that the hydrodynamic model adequately reproduces the amplitude and phase of the astronomical tide components.

¹³ Mean Tidal Range (or range of tide) —The difference in height between consecutive high and low waters. The mean range is the difference in height between mean high water and mean low water. See <https://tidesandcurrents.noaa.gov/publications/glossary2.pdf>, on page 20.

Table 3-3: Harmonic Constituents for Model Performance Evaluation

No.	Name	Description
1	M2	Principal lunar semidiurnal constituent
2	S2	Principal solar semidiurnal constituent
3	N2	Larger lunar elliptic semidiurnal constituent
4	K1	Lunar diurnal constituent
5	M4	Shallow water overtides of principal lunar constituent
6	O1	Lunar diurnal constituent
7	M6	Shallow water overtides of principal lunar constituent
8	Q1	Larger lunar elliptic diurnal constituent
9	K2	Lunisolar semidiurnal constituent

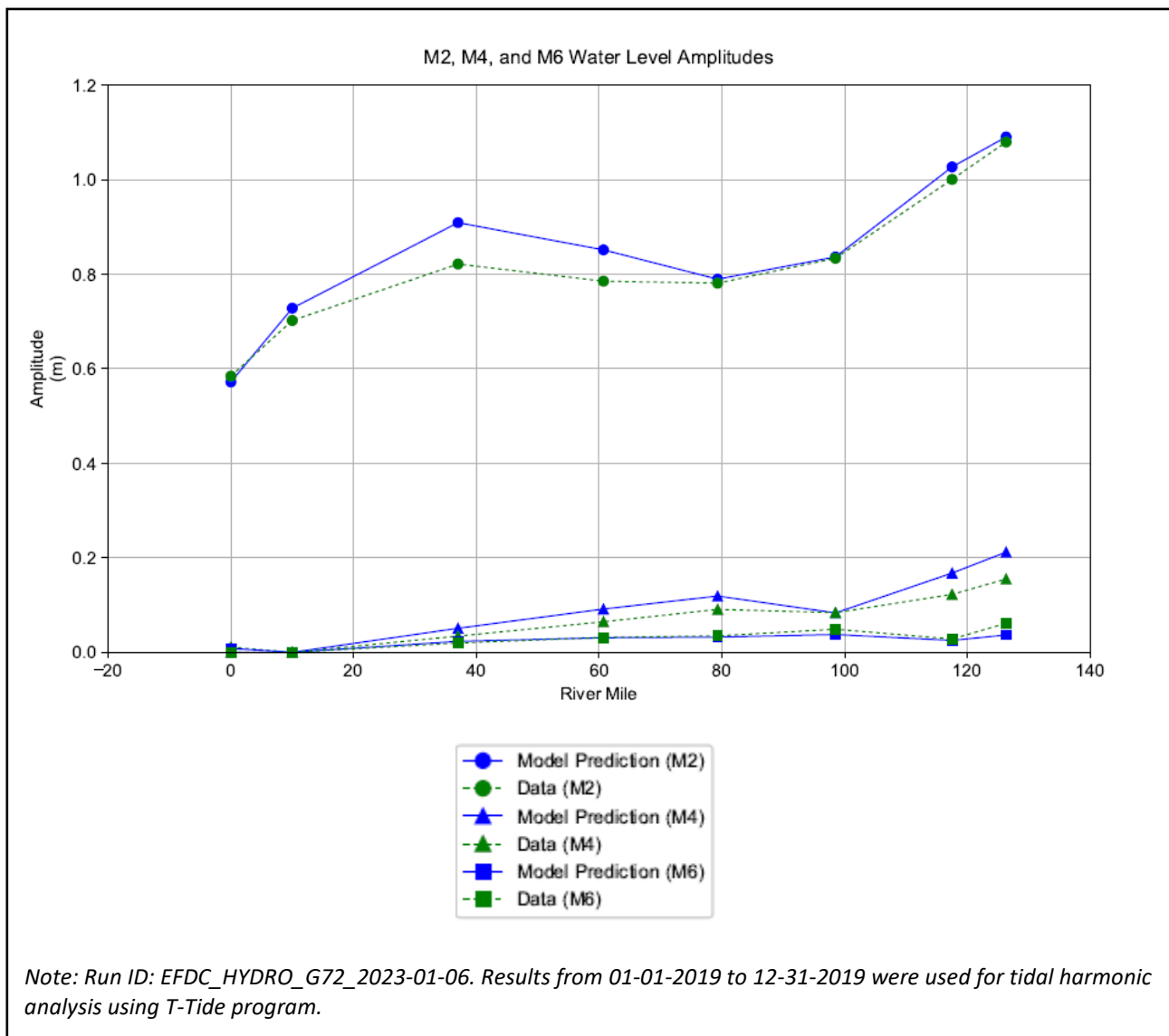


Figure 3-5: Distribution of M2, M4, and M6 Water Level Amplitudes

3.3.1.2 Water Surface Elevation

Appendix H shows time history graphs of predicted and observed water surface elevations at nine NOAA tide stations for the period of October through December of 2019 as examples to visualize the model predictions qualitatively. A more thorough statistical analysis was used to evaluate 1-to-1 comparisons based on two-year simulations of 2018 and 2019 (Appendix I). Results of statistical measures are summarized in Table 3-4 and Table 3-5 to quantify the model performance for the 2018-2019 and 2012 periods, respectively.

Table 3-4: Model Performance Predicting Tidal Elevation at NOAA Stations (2018-2019)

Station	State	NOAA ID	N	R ²	Bias (m)	RMSE (m)	ubRMSE (m)	Skill Score
Lewes*	DE	8557380	17519	0.995	0.010	0.036	0.035	0.999
Cape May*	NJ	8536110	17514	0.978	-0.008	0.089	0.088	0.994
Brandywine	NJ	8555889	17183	0.986	-0.022	0.076	0.072	0.996
Ship John Shoal	NJ	8537121	17514	0.984	-0.052	0.121	0.109	0.992
Reedy Point	DE	8551910	16487	0.979	-0.044	0.117	0.108	0.992
Delaware City	DE	8551762	17514	0.976	-0.038	0.119	0.113	0.992
Marcus Hook	PA	8540433	17514	0.966	-0.053	0.130	0.119	0.990
Philadelphia	PA	8545240	17514	0.960	-0.049	0.143	0.134	0.989
Burlington	NJ	8539094	17514	0.971	-0.100	0.173	0.141	0.988
Newbold	PA	8548989	17514	0.967	-0.033	0.161	0.158	0.991

* These stations are close to the ocean boundary and should be viewed more as boundary conditions than as calibration stations.

Based on these results, the hydrodynamic model simulates water surface elevation with sufficient accuracy to satisfy the objectives of this study. For the 2018-2019 period, predicted tidal elevations have minimal bias (typically less than 0.1 m) and low ubRMSD (ranging from 0.04 to 0.16 m). For example, the model Bias and ubRMSE error at Philadelphia are -0.05 m and 0.13 m, respectively. Overall model skill score ranged from 0.988 to 0.999. Skill scores greater than 0.975 have been used to show that a model accurately predicts the water surface elevation (MacWilliams et al., 2015). A value of 1 in skill score indicates a perfect fit between model predictions and observed data. The comparison at Burlington station is slightly worse compared to other stations. This station, with the lowest skill score of 0.988, is close to the downstream end of Burlington Island where bottom roughness was smoothly transitioned from 2 mm to a relatively high value of 5 mm upstream. A target diagram based on the predicted and observed hourly and 32-hour-lowpass-filtered water surface elevation for the 2018-2019 period is presented in Appendix I. All comparison results are inside the circle with a radius of 0.5, which indicates that the model accurately predicted the water surface elevation for both the tidal and non-tidal components throughout the Delaware River Estuary during 2018-2019 period.

Model performance for predicted water surface elevation for 2012 is summarized in Table 3-5, and a target diagram is shown in Appendix I. Predicted tidal water surface elevation has minimal bias (-0.13 to 0.005 m) and low ubRMSD (ranging from 0.03 to 0.17 m). For example, the model Bias and ubRMSE error at Philadelphia are -0.08 m and 0.15 m, respectively. Model skill score ranged from 0.982 to 0.999 for

2012, close to the value of 1 that indicates a perfect fit between model predictions and observed data (MacWilliams et al., 2015). In the target diagram for 2012, the comparison results of hourly data fall within the 0.5-radius, and the comparison results of the 32-hour-lowpass-filtered data fall within a radius of 1, indicating that the model predicted tidal elevations accurately and non-tidal components acceptably throughout the estuary during 2012 (MacWilliams et al., 2015).

Overall, the model adequately captured the progressive wave that propagates from the mouth of the Bay all the way to Trenton as well as the increase in the amplitude as observed in the data. These statistical measures demonstrate that the model accurately predicts tidal water surface elevation throughout the entire system.

Table 3-5: Model Performance Predicting Tidal Elevation at NOAA Stations (2012)

Station	State	NOAA ID	N	R ²	Bias (m)	RMSE (m)	ubRMSE (m)	Skill Score
Lewes*	DE	8557380	17519	0.996	0.005	0.031	0.030	0.999
Cape May*	NJ	8536110	17514	0.979	-0.019	0.087	0.085	0.994
Brandywine	NJ	8555889	17183	0.986	-0.059	0.092	0.070	0.994
Ship John Shoal	NJ	8537121	17514	0.981	-0.067	0.130	0.111	0.991
Reedy Point	DE	8551910	16487	0.978	-0.053	0.119	0.106	0.991
Delaware City	DE	8551762	17514	0.973	-0.053	0.128	0.116	0.990
Marcus Hook	PA	8540433	17514	0.955	-0.067	0.159	0.133	0.984
Philadelphia	PA	8545240	17514	0.947	-0.082	0.172	0.152	0.982
Burlington	NJ	8539094	17514	0.963	-0.127	0.199	0.152	0.984
Newbold	PA	8548989	17514	0.959	-0.062	0.184	0.173	0.988

* These stations are close to the ocean boundary and should be viewed more as boundary conditions than as calibration stations. A target diagram for predicted WSE for 2012 is shown in Figure I-12 in Appendix I.

3.3.2 Current Velocity

3.3.2.1 Along-channel Depth Averaged Current Velocity

Limited current velocity measurements from a few NOAA stations were used for model calibration of predicted current velocity, including db0502 at Brown Shoal Light for the period of 2018-2019, as well as db0301 at Philadelphia, db0201 at Reedy Point, and db0501 at Brown Shoal Light for 2012. Current velocity data collected at NOAA station db0301 were compared with model predictions; however, the ADCP at this station is shore-mounted and, thus, lacks vertical profile information. Recently, PWD provided detailed vertical velocity measurements for locations in the Burlington area (PWD Buoy A), south of the Navy Yard (PWD Buoy B), and at Marcus Hook (PWD Buoy C) for 2012; comparisons with model predictions are provided below.

Representative comparisons of observed and predicted depth-averaged velocity along-channel and cross-channel at NOAA station db0502 (Delaware Bay Channel LB 10), which is located about approximately

7 miles from the mouth of the Bay at the starting point of the federal navigation channel, are provided in Figure J-1 in Appendix J for the period of October 1 to 7, 2018. A 1-to-1 model-to-data comparison and a target diagram of the velocity magnitude for a longer time period, from September 6, 2018, to February 25, 2019, are presented Figures J-2 and J-3. Figure J-4 in Appendix J shows the comparisons of temporal variation of the depth-averaged current velocity at db0501 for the period of June 18 to 25, 2012. A 1-to-1 comparison and a target diagram based on the entire dataset for the June 2012 period are presented in Figures J-5 and J-6. The comparison results in the target diagrams (Figures J-3 and J-6) all fall within the 0.5-radius, indicating the model predicted current velocities well at these two stations during the periods of 2012 and 2018-2019.

Moving further upstream from the mouth of the Bay, representative comparisons of observed and predicted depth-averaged along-channel and cross-channel current velocity at Reedy Point, NOAA station db0201, which is located 58 miles from the bay mouth in the mainstem near the eastern end of the C&D canal, is shown in Figure J-7 in Appendix J for the period of January 30 to February 5, 2012. A 1-to-1 comparison of the velocity magnitude for a longer time period from January 1 to May 5, 2012, is shown in Figure J-8. The statistical measures for predicted depth-averaged current velocity at db0201 for this four-month period are ubRMSE (14.3 cm/s), bias (-2.8 cm/s), and skill score of 0.97. These statistical measures indicate that the model adequately predicted depth-averaged current velocity magnitude at this location. A target diagram based on the data during this four-month period is presented in Figure J-9, in which the comparison result falls within the 0.5-radius, indicating the model-data comparison of current velocity at db0201 is accurate.

Similarly, model-data comparisons of depth-averaged current velocity at NOAA station db0301 during June 2012 are presented in Figures J-10 through J-12 in Appendix J in the formats of time history comparisons, a 1-to-1 comparison, and a target diagram, respectively. Again, all comparisons indicate that the model accurately predicted the depth-averaged current velocity at this station.

The results of statistical measures for predicted along-channel depth-averaged current velocity at the four ADCP station locations are summarized in Table 3-6. Skill scores greater than 0.9 have been used to indicate accurate modeling of current speed or velocity, with scores between 0.8 and 0.9 indicating “acceptable” model predictions (MacWilliams et al., 2015). Overall, the model skill scores for predicted depth-averaged current velocity ranged from 0.965 to 0.987, and the unbiased error ubRMSE ranged from 14.3 to 22.3 cm/s. These statistical measures indicate that the hydrodynamic model simulates current velocity with sufficient accuracy to satisfy the objectives of this study.

Table 3-6: Model Performance Predicting Depth-Averaged Current Velocity at NOAA Stations

Station	Source	ID	Period of Records	N	R ²	Bias (cm/s)	RMSE (cm/s)	ubRMSE (cm/s)	Skill Score
Delaware Bay Channel LB 10	NOAA	db0502	09-06-2018 to 02-25-2019	4075	0.914	-2.858	14.648	14.366	0.973
Brown Shoal Light	NOAA	db0501	06-01-2012 to 06-30-2012	719	0.951	-1.031	10.749	10.699	0.987

Station	Source	ID	Period of Records	N	R ²	Bias (cm/s)	RMSE (cm/s)	ubRMSE (cm/s)	Skill Score
Reedy Point	NOAA	db0201	01-01-2012 to 05-05-2012	2811	0.906	8.084	22.451	20.946	0.965
Philadelphia*	NOAA	db0301	06-01-2012 to 06-30-2012	714	0.838	4.340	22.732	22.314	0.953

Note: Use caution for model-to-data comparisons of depth-averaged current velocity collected at NOAA Philadelphia (db0301). Current velocity data were collected at a fixed depth, and the sensor is shooting sideways across the river. Sensor depth is 4.5 m, and it is located at the west bank (PA side). Signals from bin# 34, which is approximately 138 m from the sensor, were used for the comparison with model results for predicted depth-averaged velocity at cell (32, 154) inside the ship channel. It was assumed that the ADCP depth of 4.5 m is representative of the depth-averaged value at that location. The depth of the ship channel is approximately 45 ft (13.7 m) below MLLW. Although model skill score is acceptable, large uncertainty exists at this location because of this assumption and the grid resolution.

Model performance for predicted along-channel depth-averaged current velocity for three PWD buoy stations is summarized in Table 3-7. The time history and 1-to-1 model-data comparison plots, as well as target statistics, are presented in Appendix K. ADCP current velocity data collected from the three buoys over a common period from August 21 through September 20, 2012, were used for this analysis. For all comparisons, RMSE are less than 25 cm/s, skill scores are above 0.90, and target diagram results are within the 0.5-radius circle, which indicates good accuracy for predicted depth averaged current speeds at these buoy locations (MacWilliams et al., 2015).

The 1-to-1 comparisons in Appendix K indicate that there are phase shifts between the predicted and observed data at all three buoys. These mismatches could be caused by (1) the imperfect specifications of spatial variations of bottom roughness; (2) the simplified delineation of model geometry/bathymetry around the upper portion of the model domain near Trenton; and (3) the exclusion of floodplains (i.e., wetting and drying cells) in the model domain. However, the relatively small phase shift in the current velocity does not significantly affect long-term water quality constituent transport.

Table 3-7: Model Performance Predicting Depth-Averaged Current Velocity at PWD Buoy Locations

Station	Source	Period of Records	N	R ²	Bias (cm/s)	RMSE (cm/s)	ubRMSE (cm/s)	Skill Score
Buoy A	PWD	08-21-2012 to 09-20-2012	720	0.7762	-1.9351	21.8254	21.7394	0.9206
Buoy B	PWD	08-21-2012 to 09-20-2012	721	0.7468	0.0519	24.4338	24.4337	0.9293
Buoy C	PWD	08-21-2012 to 09-20-2012	721	0.8821	-5.1205	21.7571	21.146	0.9664

3.3.2.2 Harmonic Analysis for Current Velocity

Similar to the tidal harmonic analysis for water surface elevation in Section 3.3.1.1, this section examines the tidal component of the current velocity at four NOAA current gage stations (db0501, db0502, db0201, and db0301) as well as at the three PWD buoy stations. The harmonic analysis was performed for the

along-channel depth-averaged current velocity using T-Tide program. The results are summarized in Table L-1 in Appendix L, and comparisons between EFDC predictions and observations are presented graphically in Appendix M. M2 is the dominant component, and the difference in the amplitude between model predictions and observations are 7, 12, -12, and 11 cm/s at db0501, db0502, db0201, and db0301, respectively. The differences in the velocity amplitude were all close to or less than 10 cm/s for other major harmonic constituents. The absolute differences are all within the acceptable error bound of 26 cm/s for predicting current speed recommended by NOAA (Hess et al., 2003 and Zhang et al., 2006). The phase differences between EFDC predictions and observations for the M2 component are 0.62, 0.73, 0.43, and 0.55 hours at db0501, db0502, db0201, and db0301, respectively, which are close to or slightly larger than the acceptable error bound of 0.5 hour for predicting the time of maximum flood or ebb suggested by NOAA (Hess et al., 2003 and Zhang, et al., 2006). Exclusion of the floodplain in this study is a possible cause contributing to the phase mismatch at these locations.

Harmonic analysis for the ADCP data collected at the three PWD buoys in 2012 are presented in Appendix N and Appendix O. The absolute errors in the amplitude of the M2 constituents are 16, 2, and -5 cm/s for Buoy A, Buoy C, and Buoy C, respectively. These errors are all within the 26 cm/s threshold recommended by NOAA (Hess et al., 2003 and Zhang et al., 2006) for evaluating model performance for current velocity. The errors in phases are larger than the 0.5-hour threshold suggested by NOAA. For example, the differences in phase for the dominant constituent M2 are 0.6, 0.9, and 0.6 hours for Buoy A, Buoy C, and Buoy C, respectively. Generally, a phase mismatch of 0.5 up to about 1 hours is not substantial for long-term water quality constituent transport, whereas it might be expected to be more important in the context of navigation applications for which NOAA's tolerance suggestions may be more relevant.

3.3.3 Water Temperature

The hydrodynamic model is capable of simulating density-driven flows in the estuary. The water density is calculated as a function of salinity and water temperature. As water temperature changes, so does the water density. Although the impact of water temperature change on salinity transport is considered a secondary factor, the accurate prediction of water temperature is important for addressing its impact on water quality in the linked WASP water quality model. Comparisons of near surface water temperature at various NOAA and USGS gaging stations, in the form of time history comparisons (Figures P-1 to P-11 and P-24 to P-35), 1-to-1 comparisons (Figures P-12 to P-22), and target diagrams (Figures P-23 and P-36), are presented in Appendix P for the period 2018-2019 and 2012. Summaries of the statistical measures are presented in Table 3-8 based on analysis of the 2018-2019 period and in Table 3-9 for the analysis of 2012. Model bias at all locations ranged from -0.65 to 1.31°C for the period of 2018-2019 and -1.61 to 0.17°C for 2012. The unRMSE ranged from 0.41 to 1.36 °C for 2018-2019 and 0.51 to 1.29°C for 2012. Model skill scores for predicted water temperature ranged from 0.993 to 0.999 for the period of 2018-2019 and 0.993 to 0.998 for 2012, all close to the value of 1 for a perfect fit in model-data comparison. The comparison results in the target diagrams in Figure P-23 and P-36 fall within the 0.25-radius, indicating that the model predicted well the water temperature throughout the Delaware River Estuary during the periods of 2012

and 2018-2019. Overall, these results show that the model was able to simulate the seasonal variation in temperature at all stations.

The model over-predicts water temperature by 1-3° C at the NOAA Delaware City station during summer 2018 (Figure P-5) for unknown reasons. Water temperature data at this station during the summer of 2018 are about 1-3° C lower than those at its neighboring stations, e.g., NOAA Marcus Hook station located about 19 miles upstream and NOAA Reedy Point station located about two miles downstream.

For 2012, water temperatures collected by NOAA and USGS are inconsistent in the upstream portion of the river. For example, water temperatures at the USGS Trenton station are usually consistent with those at the NOAA Newbold station (Figure P-37 for the period of 2017-2019), since these two stations are located only about eight miles apart in a relatively narrow and fast-moving reach of the river. However, the water temperatures measured at NOAA Newbold station in 2012 are systematically higher than those measured at the USGS Trenton station (Figure P-37) in 2012, especially after July 1. There is also seemingly a vertical shift in the dataset for the second half of the year, which could be attributed to a data quality control issue. These inconsistencies in measured data between the two different agencies may have contributed to the mismatches between the predicted and observed water temperatures at some NOAA stations in 2012, because the water temperatures at the upstream boundary were specified based on the USGS data at Trenton.

The model over-predicts water temperatures somewhat in the Bay (e.g., NOAA Ship John Shoal station). This is likely because the inputs used for wind speed and other meteorological forcings for the Bay were based on a land station (i.e., Dover airport), while the actual wind speed over the Bay would be expected to be stronger than that observed on land. Stronger wind causes more heat loss through evaporation and conduction and subsequently lower water temperatures.

Table 3-8: Model Performance Predicting Water Temperature (2018-2019)

Agency	Station	State	NOAA ID	N	R ²	Bias (C)	RMSE (C)	ubRMSE (C)	Skill Score
NOAA	Lewes	DE	8557380	16131	0.975	0.097	1.366	1.363	0.993
NOAA	Ship John Shoal	NJ	8537121	11780	0.991	-0.176	1.027	1.012	0.997
NOAA	Reedy Point	DE	8551910	15987	0.996	-0.155	0.663	0.644	0.999
NOAA	Delaware City	DE	8551762	14931	0.982	1.307	1.886	1.360	0.988
NOAA	Marcus Hook	PA	8540433	17280	0.996	-0.651	0.890	0.608	0.998
NOAA	Philadelphia	PA	8545240	16118	0.997	-0.131	0.487	0.469	0.999
NOAA	Burlington	NJ	8539094	11245	0.998	-0.041	0.417	0.414	0.999
NOAA	Newbold	PA	8548989	17229	0.997	-0.227	0.537	0.486	0.997
USGS	Reedy Island	DE	USGS 01482800	17006	0.997	-0.200	0.719	0.690	0.999
USGS	Chester	PA	USGS 01477050	14310	0.996	-0.406	0.702	0.573	0.998
USGS	Ben Franklin Bridge	PA	USGS 01467200	15012	0.997	-0.195	0.493	0.453	0.999

Table 3-9: Model Performance Predicting Water Temperature (2012)

Agency	Station	State	NOAA ID	N	R ²	Bias (C)	RMSE (C)	ubRMSE (C)	Skill Score
NOAA	Lewes	DE	8557380	8766	0.978	-0.140	1.210	1.202	0.993
NOAA	Ship John Shoal	NJ	8537121	8512	0.991	0.173	1.300	1.289	0.995
NOAA	Reedy Point	DE	8551910	8688	0.993	-0.246	0.988	0.957	0.997
NOAA	Delaware City	DE	8551762	8758	0.992	-0.618	1.269	1.109	0.995
NOAA	Marcus Hook	PA	8540433	8760	0.988	-1.610	1.973	1.140	0.988
NOAA	Philadelphia	PA	8545240	8702	0.995	-0.347	0.891	0.821	0.998
NOAA	Burlington	NJ	8539094	8762	0.997	-0.824	0.966	0.505	0.997
NOAA	Newbold	PA	8548989	8740	0.994	-1.235	1.411	0.683	0.994
USGS	Reedy Island	DE	USGS 01482800	8467	0.994	-0.461	1.240	1.151	0.995
USGS	Chester	PA	USGS 01477050	5861	0.990	-0.603	1.023	0.826	0.994
USGS	Ben Franklin Bridge	PA	USGS 01467200	5989	0.991	-0.522	0.945	0.788	0.995

Note: Target diagram for predicted water temperature for 2012 is shown in Figure P-36 in Appendix P.

3.3.4 Salinity

Prediction of salinity intrusion and salinity structure in the estuary is important for the hydrodynamic model because salinity is essentially a natural tracer that allows us to evaluate transport. Salinity in the estuary is monitored by tracking the location of the salt front, as described previously in Section 1.3. The observed extent of the salinity intrusion during the 2018-2019 calibration period ranged from below RM 50 to RM 84.6 (observed on October 15, 2019), and the maximum intrusion during 2012 reached to approximately RM 76 (observed on September 1, 2012).

The following two types of salinity data were used to evaluate hydrodynamic model performance:

- Continuous salinity (conductivity or specific conductance) measurements at multiple NOAA and USGS locations; and
- Discrete sampling of along-channel salinity profiles (DRBC boat run survey data).

Predicted salinity at the NOAA stations at Lewes (at the mouth of the Bay), Brandywine, and Ship John Shoal (RM 37), and at the USGS station at Reedy Island, are presented in Appendix Q for 2018-2019 and 2012 in the form of time history comparisons, 1-to-1 comparisons, and target diagrams. Results of statistical measures are summarized in Table 3-10 and Table 3-11 for 2018-2019 and 2012, respectively.

Table 3-10: Model Performance Predicting 32-hr-LPF Surface Salinity (2018-2019)

Agency	Station	State	NOAA ID	N	R ²	Bias (C)	RMSE (C)	ubRMSE (C)	Skill Score
NOAA	Lewes	DE	8557380	13884	0.436	-0.689	2.578	2.484	0.712
NOAA	Brandywine	NJ	8555889	N/A	N/A	N/A	N/A	N/A	N/A
NOAA	Ship John Shoal	NJ	8537121	2684	0.752	-0.626	2.061	1.963	0.915
USGS	Reedy Island	DE	USGS 01482800	16863	0.888	0.093	1.034	1.031	0.965

Table 3-11: Model Performance Predicting 32-hr-LPF Surface Salinity (2012)

Agency	Station	State	NOAA ID	N	R ²	Bias (C)	RMSE (C)	ubRMSE (C)	Skill Score
NOAA	Lewes	DE	8557380	N/A	N/A	N/A	N/A	N/A	N/A
NOAA	Brandywine	NJ	8555889	6636	0.590	0.588	2.213	2.134	0.854
NOAA	Ship John Shoal	NJ	8537121	4026	0.697	-1.075	2.479	2.234	0.842
USGS	Reedy Island	DE	USGS 01482800	8324	0.842	-0.301	1.208	1.170	0.934

Generally, the model agreed well with the observed salinity at the NOAA and USGS stations. The model skill scores for predicted surface salinity at the NOAA and USGS stations range from 0.71 to 0.97 for the period of 2018-2019, and 0.84 to 0.93 for 2012, respectively. MacWilliams et al. (2015) suggested that skill scores of greater than 0.85 had been used to show accurate modeling of salinity, with scores between 0.7 and 0.85 representing “acceptable” values. Most comparison results in the target diagrams (Figure Q-9 for 2018-2019 and Figure Q-18 for 2012) fall within a radius of 1 or even 0.5 (i.e., within the acceptable, or even accurate ranges suggested by MacWilliams et al. 2015), except for the NOAA Lewes station (hourly comparison for 2018-2019 at 1.5-radius in Figure Q-9) and the USGS Chester station (both hourly and 32-hour-LPF comparisons for 2012 are around the 1.5-radius in Figure Q-18). Salinity measurements from Chester are usually low values (e.g., < 0.45 psu), and relevant chloride comparisons converted from salinity (Appendix R) provide better resolution of the comparisons at this station. The relatively large value of ubRMSE for salinity at Lewes station for 2018-2019 (Figure Q-9) is caused by the larger tidal fluctuations in the model predictions compared with observations (Figure Q-1). The long-term trend and sub-tidal salinity comparisons at this station are reasonable. Overall, the results demonstrate that the model adequately predicts salinity throughout the Delaware River Estuary. Note that 2018 to 2019 were relatively wet years in terms of freshwater flows, and 2012 was a normal year in terms of hydrologic conditions. In the future, the model might be further calibrated against salinity intrusion data during a drought year if time and resources allow.

From the perspective of further evaluating water quality and salinity results in the upper portion of the tidal river (upstream of Reedy Island), model predicted salinity was also converted to chloride concentration (chlorinity) and compared with measured USGS data at four sites. Data-based chlorinity was calculated using the empirical relationship between specific conductance and chloride concentration developed using DRBC boat run data, as discussed previously in Section 1.3. Temporal variations of predicted and observed daily-averaged chloride concentration at Reedy Island (RM 54), Chester (RM 83.6), Fort Mifflin (RM 92) and Ben Franklin Bridge (RM 100) are presented in Appendix R. Predicted chloride concentrations are generally in good agreement with the observed data, except at Chester during low flow periods (e.g., Figure R-2 during October 2019 and Figure R-6 during July-August 2012). These discrepancies between predicted and observed salinity/chloride during low flow periods are likely due to the uncertainty in the background salinity/chloride. Salinity/chloride concentrations in the tributaries, from non-point sources in the watershed, and from point source discharges around and upstream of

Chester are normally low (i.e., salinity < 0.45 psu and chloride < 250 mg/L). Uncertainties exist when specifying salinity inputs from these boundaries due to insufficient data, which in turn may result in some uncertainty when predicting low salinity concentrations around Chester.

DRBC staff developed the Delaware River Estuary Water Quality Monitoring Program (Boat Run), and regular boat run surveys have been performed since 1967. During the modeled years of 2012 and 2018-2019, samples were collected monthly during a short 4-to-5-hour time window at 22 locations (Figure 3-4). This dataset essentially provides a snapshot of profiles of various water quality parameters, including salinity or specific conductance. Comparison of 21 predicted and observed longitudinal salinity profiles during 2018 and 2019 are presented in Appendix S. The predicted tidally-averaged salinity longitudinal profile agreed with the boat run data reasonably well over a wide range of flow and tidal conditions.

Overall, the results discussed above show that the hydrodynamic model simulates salinity adequately for the model purposes, though with less accuracy for certain periods of time. Further investigation to improve salinity simulation might be needed as time and resources allow. Simulations and calibrations with data collected from more “normal” and drought years would help to enhance the model performance.

3.4 SENSITIVITY TO VERTICAL GRID RESOLUTION

Model predicted salinity transport is three-dimensional in nature. Near the mouth of the bay, a typical two-layer vertical current and salinity structure exists (also known as tidal exchange flow structure) as a result of the competing forcings from the upstream inflows and from the ocean tidal forcing. During a high-flow event, fresher and less dense water flushes out seaward on the surface layer, and saltier and denser water moves landward in the bottom layer. As a result, a relatively strong vertical stratification in salinity is often observed in the lower bay area. Moving upstream from the mouth of the Bay, the vertical stratification becomes weaker. Upstream of RM 79 near Marcus Hook, the tidal river becomes nearly well-mixed with a uniform vertical salinity profile. Since vertical stratification interrupts the mixing process and affects salinity transport in the estuary, it is important for the model to represent the vertical structure correctly. More vertical layers in the model increase overall simulation time dramatically. Thus, the appropriate vertical grid resolution for the model must be determined before setting up the model boundary conditions and carrying out any model calibration and simulations.

To determine the appropriate vertical grid resolution, three different models were set up with five, ten, and fifteen vertical layers in the navigation channel. Sensitivity simulations were then conducted for the period of August 2012, which was a relatively calm and dry period with average flow from the Delaware River at Trenton around 4,200 to 4,800 cfs. Model results (current velocity, water temperature, and salinity) were analyzed for a spring-tide period (08-19-2012 16:00 to 08-21-2012 16:00) and a neap-tide period (08-10-2012 10:00 to 08-12-2012 10:00). Simulation conditions of flow and tide are shown in Figure T-1 of Appendix T. Model results from the navigational channel as well as from three cross-sections (shown in Figure T-2 of Appendix T) were used in the sensitivity analysis. Diagnostic analyses were conducted at selected locations as listed below:

- Three transects (cross-sections) at RM 37, 42, and 69; and
- Three cells in the navigation channel at RM 37, 42, and 69.

Diagnostic analysis focused on predicted water surface elevation, current velocity, salinity, and water temperature. Tidally-averaged longitudinal and vertical structures of the current velocity and salinity were investigated by obtaining and comparing the residual signals, which were calculated as the average of the 32-hour low pass filtered results over a 48-hour window for neap and spring tides, respectively. Model-to-model comparisons were focused on the velocity and salinity structures (i.e., the gradient and shape of the vertical and longitudinal profiles rather than the absolute values).

Models with three different vertical resolutions (5-layer model, 10-layer model, and 15-layer model) all produced nearly identical results for the water surface elevation at the three selected cell locations at RM 37, 42, and 69 shown in Figure T-3 through Figure T-5, respectively, of Appendix T.

The spatial and vertical distributions of predicted tidally-averaged 32-low-pass filtered salinity results are presented as contours on a vertical slide that cuts through the FNC in Figure T-6 and Figure T-7 during a 48-hour time window during a spring and a neap tide period, respectively. Model-to-model comparisons of the gradient of the predicted 32-low-pass filtered depth-averaged salinity longitudinal profiles are shown in Figure T-8 and Figure T-9 of Appendix T for the same spring and neap tide period. The higher vertical resolution grid tends to predict less saltwater intrusion in terms of the longitudinal residual salinity profile. The longitudinal residual salinity profiles seem to start deviating from each other at RM 25 in the lower bay area. The differences in predicted depth-averaged salinity seem to be larger around RM 40 to 60, where the 15-layer model predicted salinity being less than predicted by the 5-layer model by about 2 to 3 psu.

Note that the degree of salinity intrusion was not the same amongst the three scenarios because the three models were not calibrated for these diagnostic simulations. These vertical resolution test models are not therefore directly comparable. To further investigate the sensitivity to the vertical grid resolution, predicted current and salinity structures at given cross-sections were compared among the three models. Normalization was therefore applied to the cross-sectional salinity and velocity outputs to make comparable results among scenarios. Each model result was divided by the maximum value of this cross-section to provide an intensity with values ranging from 0 to 1. A similar approach was applied to the current velocity analysis.

The predicted distribution of the 'raw' and normalized tidally-averaged 32-hour-lowpass filtered salinity on the cross-sections at RM 37, 42, and 69 are presented in Figure T-10 through Figure T-15, respectively, of Appendix T. At RM 69, the river exhibited a typical riverine well-mixed environment with an almost uniform vertical profile of salinity, and the absolute salinity value was very small. Stronger vertical stratification of salinity was observed at both cross-sections at RM 37 and RM 42, with saltier water at the bottom. At these two locations, the vertical stratification was stronger during neap tide than spring tide. The water near the Delaware side of the cross-section was relatively fresher than the water closer to the

New Jersey side. The normalized salinity distribution produced by the three models showed a very consistent pattern, with the 10-layer model results being closer to the 15-layer model than the 5-layer model.

The predicted distribution of the ‘raw’ and normalized tidally-averaged 32-hour-lowpass filtered along-channel current velocity on the cross-sections at RM 37, 42, and 69 are presented in Figure T-16 through Figure T-21, respectively of Appendix T. A clear typical estuary exchange flow structure was observed at RM 37 and RM 42, with the fresher water moving in the seaward direction on the top and the saltier water moving landward from the ocean. At RM 69, the velocity profile became the typical logarithmic profile with unidirectional flow. During neap tide, the model predicted a net landward movement of water near the New Jersey side and a net seaward movement of water near the Delaware side in the mid and upper Bay, while during spring tide the model predicted net seaward-moving water on the top from shore to shore. Comparing the normalized current velocity at these locations, the 10-layer model and 15-layer models produced very similar results.

Vertical profiles of the tidally-averaged 32-hour-lowpass filtered current velocity, salinity, and water temperature in the FNC from the three cross-sections were also presented in Figure T-22 through Figure T-39, respectively, of Appendix T without normalization. Without calibrating the three models, qualitative comparison was done by visualizing the shape and gradient of the vertical profiles. Based on this sensitivity study on the grid vertical resolution, the 10-layer model and 15-layer model produced very similar results, and the 10-layer model was considered more desirable because of its faster run time and efficiency to store and process the model output.

Sensitivity tests to vertical layer resolution indicated that: a) a 10-layer model in the navigational channel adequately captures the vertical structures of salinity and current; b) a 5-layer model performed well in most respects but might not adequately capture all gradients; and c) it is likely that a number of layers greater than five but less than 10 would also perform adequately.

4. SUMMARY

The primary objective of this hydrodynamic modeling study was to develop a well-calibrated, three-dimensional hydrodynamic model for use in the eutrophication modeling study of the Delaware River Estuary, the goal of which is to understand and evaluate eutrophication processes in the Delaware River Estuary from the head of tide at Trenton, New Jersey, to the Atlantic Ocean. The 3D hydrodynamic model described herein provides the necessary foundation for the linked WASP water quality model of the Delaware River Estuary (Zheng et al., 2024).

The hydrodynamic model was developed and calibrated for the periods of 2018-2019 and 2012. A statistical sub-model based on a regional analysis of shared features was developed in order to estimate hydrologic inputs for unmonitored tributaries and watersheds. Model performance was evaluated for water surface elevation, current velocity, water temperature, and salinity in the estuary. The calibrated hydrodynamic model simulated observed data reasonably well, as documented in this report. The external Model Expert Panel unanimously agreed in May 2020 that the calibrated EFDC hydrodynamic model is sufficient to be used as the basis of the WASP water quality model in the eutrophication modeling study (Expert Panel report to WQAC, October 29, 2020).

In the course of the model calibration, a detailed evaluation was performed to determine the extent of vertical resolution needed to adequately simulate gradients and mass transfer in the system. Based on this evaluation, it was determined that more than five, but fewer than 10, vertical layers in the navigation channel would be adequate for the model purposes. While a coarser degree of vertical resolution was deemed sufficient, a three-dimensional grid with 10 vertical layers in the navigation channel was selected as the vertical resolution for the hydrodynamic and water quality models.

Preliminary findings are summarized in this report. The hydrodynamic model calibration showed a very good prediction for tidal water surface elevation and adequate performance for predicted water temperature and salinity. Results of the calibration process and sensitivity analyses indicate that the performance of the 3D hydrodynamic model is adequate to meet the objectives of the modeling study, namely that the model can be used to evaluate large-scale hydrodynamic circulation processes within the Delaware River Estuary system to the degree necessary to drive water quality modeling of eutrophication processes.

The DRBC is continuing to develop modifications to improve model reliability and reduce uncertainties, consistent with its goals and resources. Several potential modifications were noted in this report: improvements to EFDC code to better account for horizontal diffusion; more realistic estimates of treatment plant salinity inputs; improvements to C&D Canal flow dynamics based on newly available velocity data; and improvements to salinity predictions by making use of data from drier years, for instance.

REFERENCES

- APHA. (1995). *Standard Methods for the Examination of Water and Wastewater (19th ed.)*. American Public Health Association.
- Aristizabal, M., & Chant, R. (2013). A Numerical Study of Salt Fluxes in Delaware Bay Estuary. *Journal of Physical Oceanography*, 43, 1572-1588. <https://doi.org/10.1175/JPO-D-12-0124.1>
- Aristizabal, M.F., & Chant, R.J. (2015). An observational study of salt fluxes in Delaware Bay. *Journal of Geophysical Research: Oceans*, 120(4), 2751-2768. <https://doi.org/10.1002/2014JC010680>
- Bever, A.J., & MacWilliams, M.L. (2013). Simulating sediment transport processes in San Pablo Bay using coupled hydrodynamic, wave, and sediment transport models. *Marine Geology*, 345, 235-253. <https://doi.org/10.1016/j.margeo.2013.06.012>
- Burchard, H. (2001). Notes and Correspondence on the q2l Equation by Mellor and Yamada (1982). *Journal of Physical Oceanography*, 31, 1377-1387.
- Dolgoplova, E.N. (2014). Sediment Transport and Saltwater Intrusion into the Weakly Stratified Estuary of the Delaware River. *Water Resources*, 41(2), 143-162. <https://doi.org/10.1134/S0097807814020067>
- DRBC. (2019). *Modeling Eutrophication Processes in the Delaware River Estuary: Quality Assurance Project Plan*. Delaware River Basin Commission.
- Forte, M.F., Hanson, J.L., Stillwell, L., Blanchard-Montgomery, M. (2011). *Coastal Storm Surge Analysis System Digital Elevation Model: Report 1: Intermediate Submission No. 1.1*. FEMA Region III Storm Surge Study, Prepared by USACE ERDC.
- Galperin, B., Kantha, L.H., Hassid, S., Rosati, A. (1988). A Quasi-equilibrium Turbulent Energy Model for Geophysical Flows. *Journal of the Atmospheric Sciences*, 45(1), 55-62.
- Hamrick, J.M. (1992). *A Three-Dimensional Environmental Fluid Dynamics Code: Theoretical and Computational Aspects*. Special Report 317 in Applied Marine Science and Ocean Engineering, Virginia Institute of Marine Science, College of William and Mary. <https://doi.org/10.21220/V5TT6C>
- Hess, K.W., Gross, T.F., Schmalz, R.A., Kelley, J.G.W., Aikman, F. III, Wei, E. (2003). *NOS Standards for Evaluating Operational Nowcast and Forecast Hydrodynamic Model Systems*. (NOAA Technical Report NOS CS 17). National Oceanic and Atmospheric Administration. <https://repository.library.noaa.gov/view/noaa/2460>

- Iqbal, M. (1983). *An Introduction to Solar Radiation*. Academic Press Canada.
<https://doi.org/10.1016/B978-0-12-373750-2.50002-1>
- Leonard, B.P., Lock, A.P., MacVean, M.K. (1996). Conservative Explicit Unrestricted-Time-Step Multidimensional Constancy-Preserving Advection Schemes. *Monthly Weather Review*, 124(11), 2588-2606. [https://doi.org/10.1175/1520-0493\(1996\)124%3C2588:CEUTSM%3E2.0.CO;2](https://doi.org/10.1175/1520-0493(1996)124%3C2588:CEUTSM%3E2.0.CO;2)
- Locarnini, R.A., Mishonov, A.V., Antonov, J.I., Boyer, T.P., Garcia, H.E., Baranova, O.K., Zweng, M.M., Paver, C.R., Reagan, J.R., Johnson, D.R., Hamilton, M., Seidov, D. (2013). World Ocean Atlas 2013, Volume 1: Temperature. In S. Levitus (Ed.), & A. Mishonov (Technical Ed.), *NOAA Atlas NESDIS 73*. <http://www.nodc.noaa.gov/OC5/indprod.html>
- MacWilliams, M.L., Bever, A.J., Gross, E.S., Ketefian, G.S., Kimmerer, W.J. (2015). Three-Dimensional Modeling of Hydrodynamics and Salinity in the San Francisco Estuary: An Evaluation of Model Accuracy, X2, and the Low-Salinity Zone. *San Francisco Estuary and Watershed Science*, 13(1). <https://doi.org/10.15447/sfews.2015v13iss1art2>
- Mellor, G.L., & Yamada, T. (1982). Development of a Turbulence Closure Model for Geophysical Fluid Problems. *Reviews of Geophysics*, 20(4), 851-875. <https://doi.org/10.1029/RG020i004p00851>
- Patchen, R. (2007). Establishment of a Delaware Bay Model Evaluation Environment. *Proceedings of the 10th International Conference in Estuarine and Coastal Modeling (ECM10)*, M.L. Spaulding (Ed), 783-818.
- Paulson, R.W. (1970). *A graphical summary of specific conductance data for the Delaware River estuary as correlated with Delaware River flow at Trenton, New Jersey*. (USGS Open-File Report 70-260). United States Geological Survey. <https://doi.org/10.3133/ofr70260>
- Rosati A., & Miyakoda, K. (1988). A general circulation model for upper ocean simulation. *Journal of Physical Oceanography*, 18(11), 1601-1626. [https://doi.org/10.1175/1520-0485\(1988\)018<1601:AGCMFU>2.0.CO;2](https://doi.org/10.1175/1520-0485(1988)018<1601:AGCMFU>2.0.CO;2)
- Schopp, R.D., & Firda, G.D. (2008). *Flood magnitude and frequency of the Delaware River in New Jersey, New York, and Pennsylvania*. (USGS Open-File Report 2008-1203). United States Geological Survey. <https://pubs.usgs.gov/of/2008/1203/>
- Szpilka, C., Dresback, K., Kolar, R., Feyen, J., & Wang, J. (2016). Improvements for the Western North Atlantic, Caribbean and Gulf of Mexico ADCIRC Tidal Database (EC2015). *J. Mar. Sci. Eng.* 4(4), 72. <https://doi.org/10.3390/jmse4040072>
- Suk, N. (2003). *DYNHYD5 Hydrodynamic Model (version 2.0) and Chloride Water Quality Model for the Delaware River Estuary*. Delaware River Basin Commission.

- Tetra Tech, Inc. (2006). *Theoretical and Computational Aspects of the Generalized Vertical Coordinate Option in the EFDC Model*. EFDC Technical Memorandum, Prepared for US Environmental Protection Agency Region 4.
- Tetra Tech, Inc. (2007). *The Environmental Fluid Dynamics Code User's Manual: USEPA Version 1.01*. https://www.epa.gov/sites/production/files/2016-01/documents/efdc_user_manual_epa_ver-101.pdf
- Valle-Levinson, A. (2010). Definition and classification of estuaries. Chapter 1 in A. Valle-Levinson (Ed.), *Contemporary Issues in Estuarine Physics*, 978-0-521-89967-3. https://assets.cambridge.org/97805218/99673/frontmatter/9780521899673_frontmatter.pdf
- Wang, H.V., & Johnson, B.H. (2000). Validation and Application of the Second Generation Three Dimensional Hydrodynamic Model of Chesapeake Bay. *Water Quality and Ecosystem Modeling*, 1, 51–90. <https://doi.org/10.1023/A:1013982515467>
- Ward ND, Gebert JA, Weggel JR. 2009. *Hydraulic Study of the Chesapeake and Delaware Canal*. Journal of Waterway, Port, Coastal, and Ocean Engineering. ASCE. 135(1) Technical Note. [https://doi.org/10.1061/\(ASCE\)0733-950X\(2009\)135:1\(24\)](https://doi.org/10.1061/(ASCE)0733-950X(2009)135:1(24))
- Willmott, C.J. (1981). On the Validation of Models. *Physical Geography*, 2(2), 184-194. <https://doi.org/10.1080/02723646.1981.10642213>
- Zhang, A., Hess, K.W., Wei, E., & Myers, E. (2006). *Implementation of Model Skill Assessment Software for Water Level and Current in Tidal Regions*. (NOAA Technical Report NOS CS 24). National Oceanic and Atmospheric Administration. <https://repository.library.noaa.gov/view/noaa/2204>
- Zheng, L., Chen, F., Bransky, J., Panuccio, E., Beganskas, S., Amidon, T., Yagecic, J., Suk, N., & Kavanagh, K.B. (2024). *Modeling Eutrophication Processes in the Delaware River Estuary: Three-Dimensional Water Quality Model*. (DRBC Report No. 2024-5). Delaware River Basin Commission.

Appendix A: Numerical grid and projected bathymetry

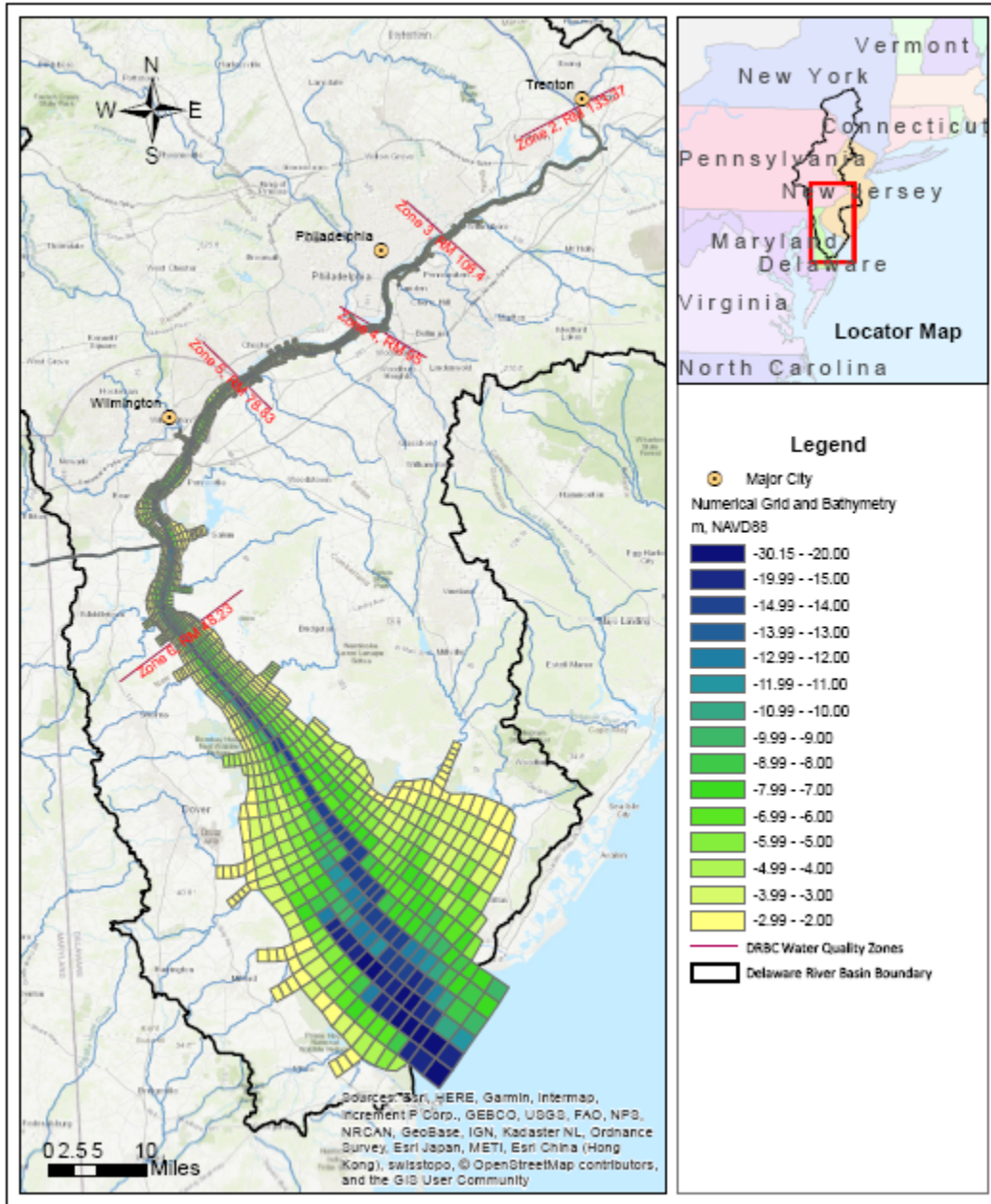


Figure A-1: Numerical Grid and Projected Bathymetry

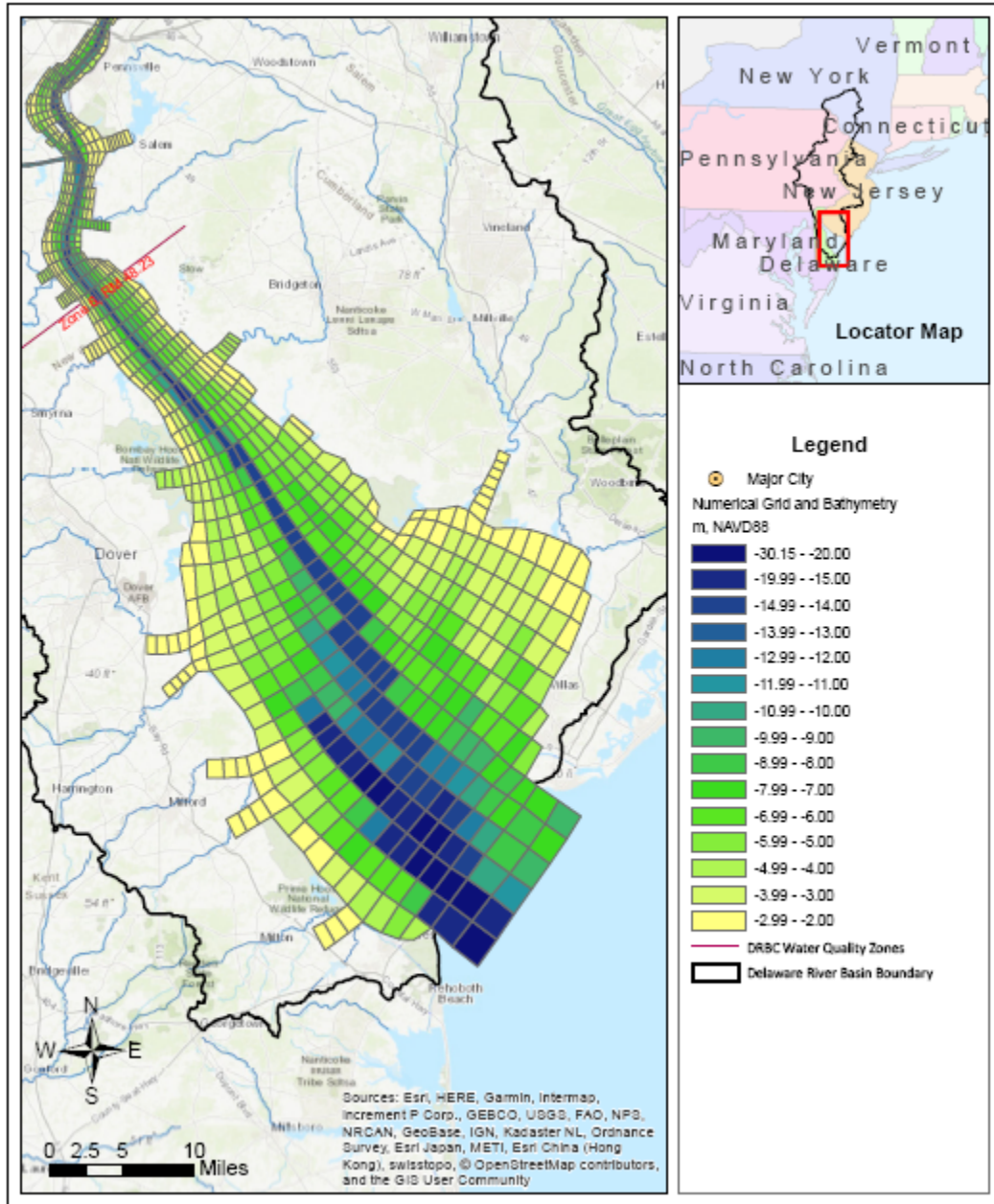


Figure A-2: Numerical Grid and Projected Bathymetry, Zone 6

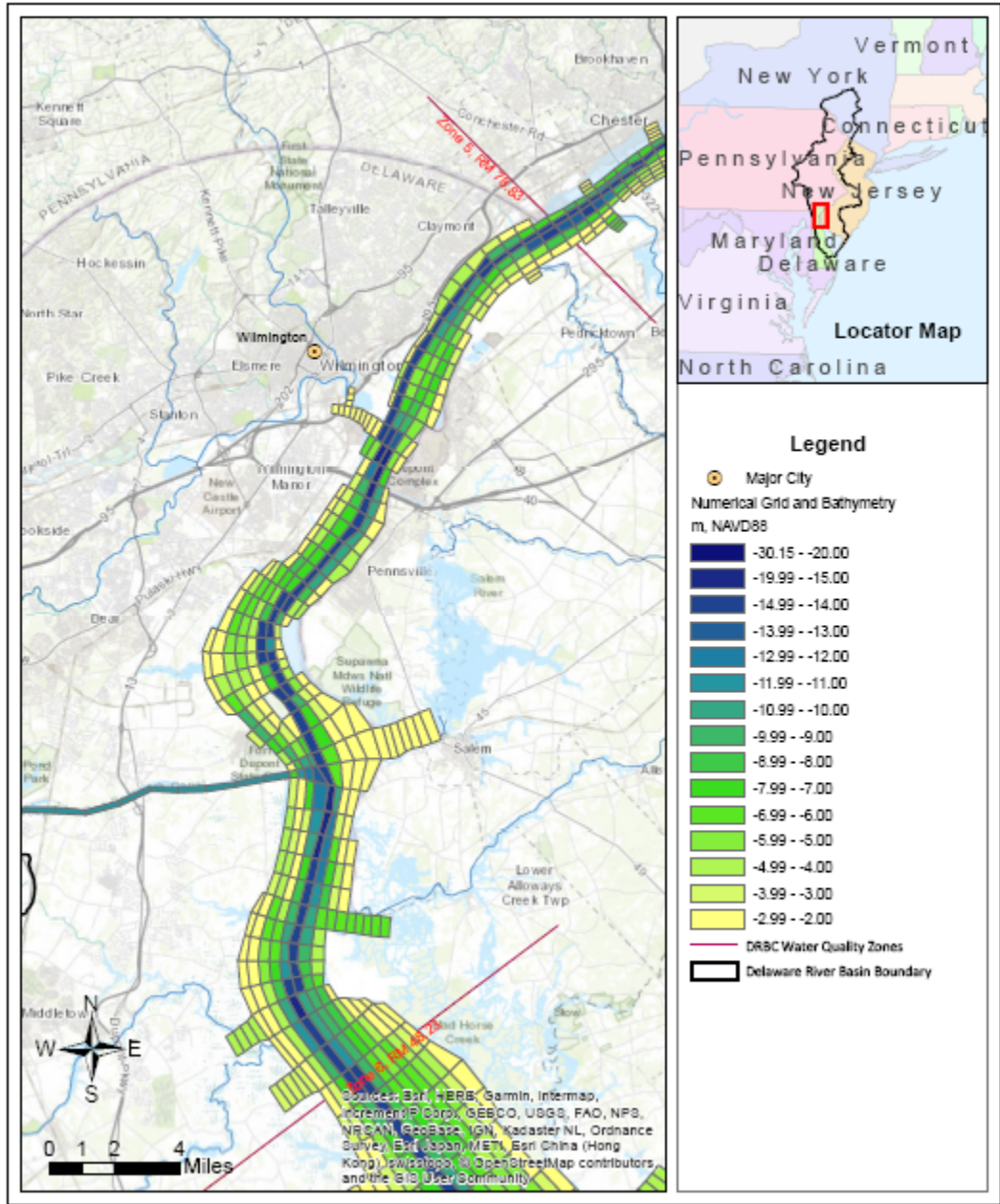


Figure A-3: Numerical Grid and Projected Bathymetry, Zone 5

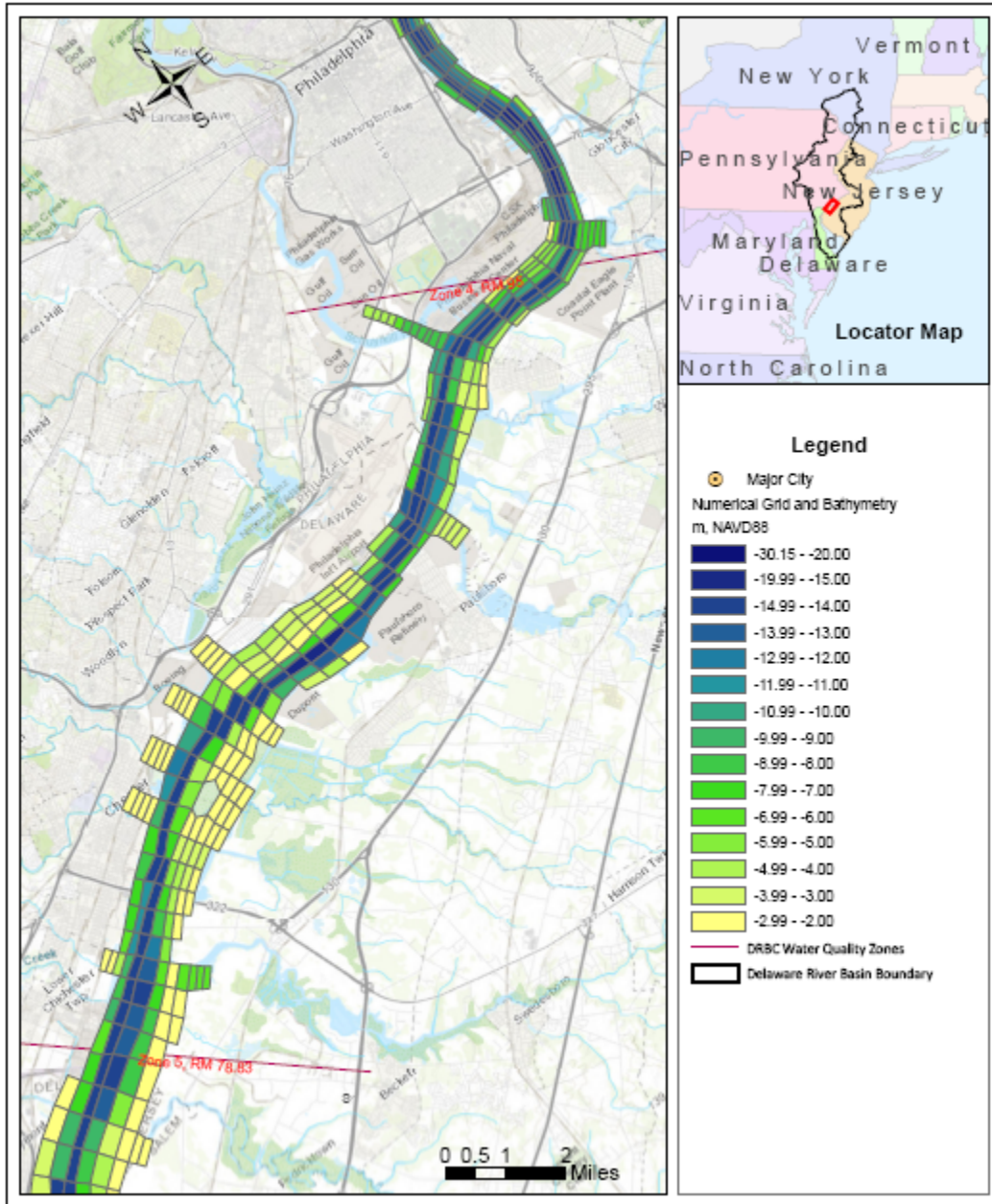


Figure A-4: Numerical Grid and Projected Bathymetry, Zone 4

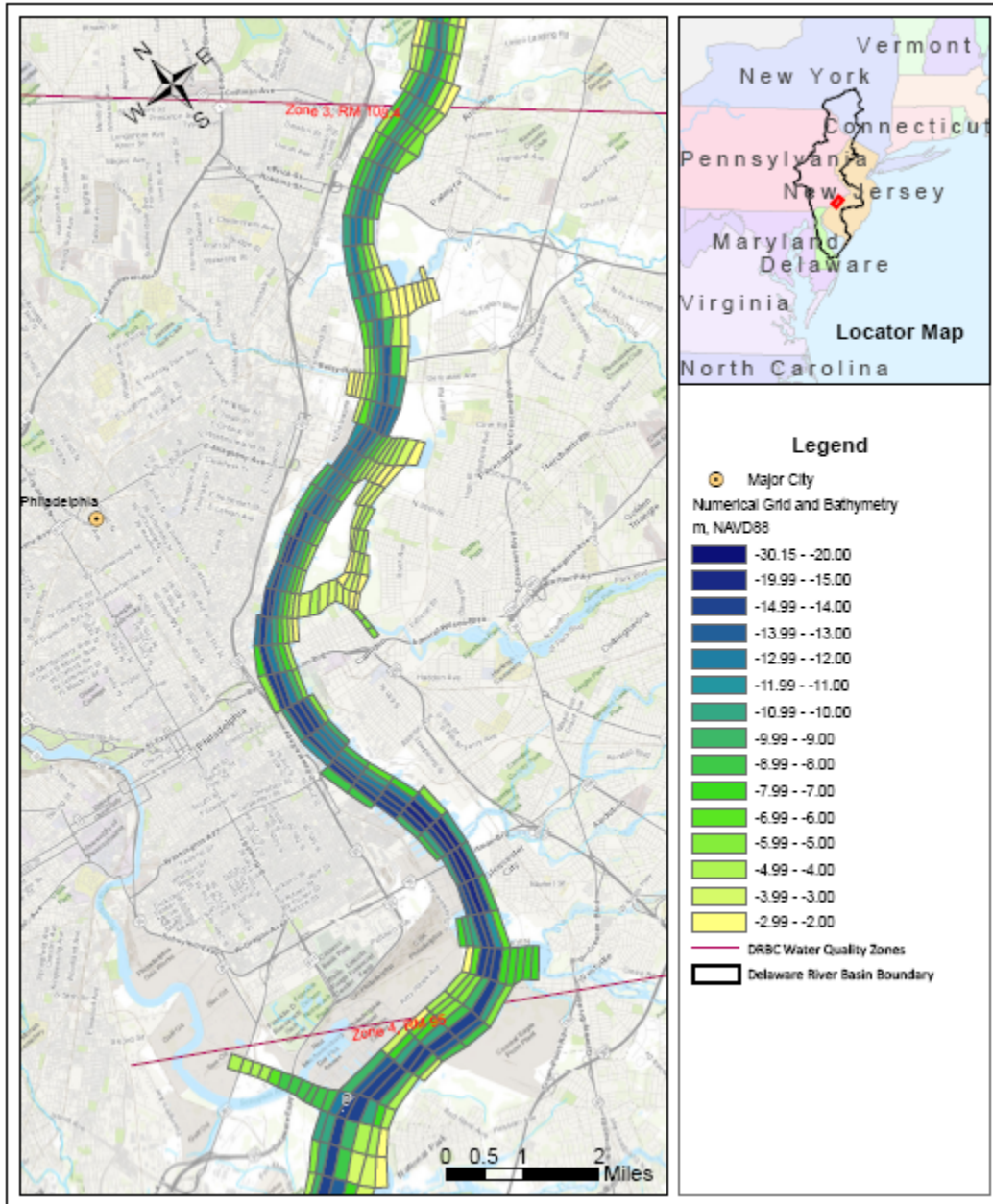


Figure A-5: Numerical Grid and Projected Bathymetry, Zone 3

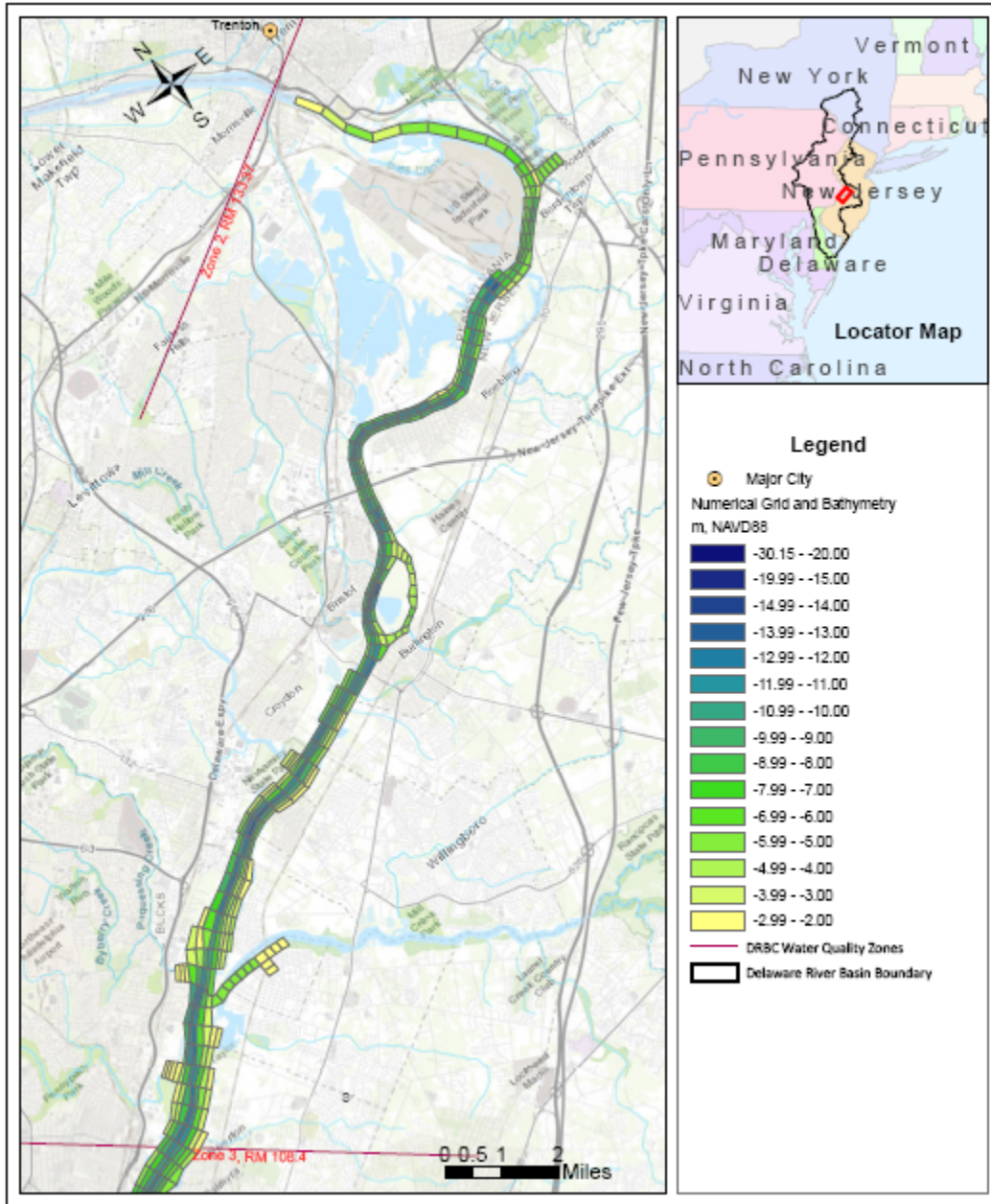


Figure A-6: Numerical Grid and Projected Bathymetry, Zone 2

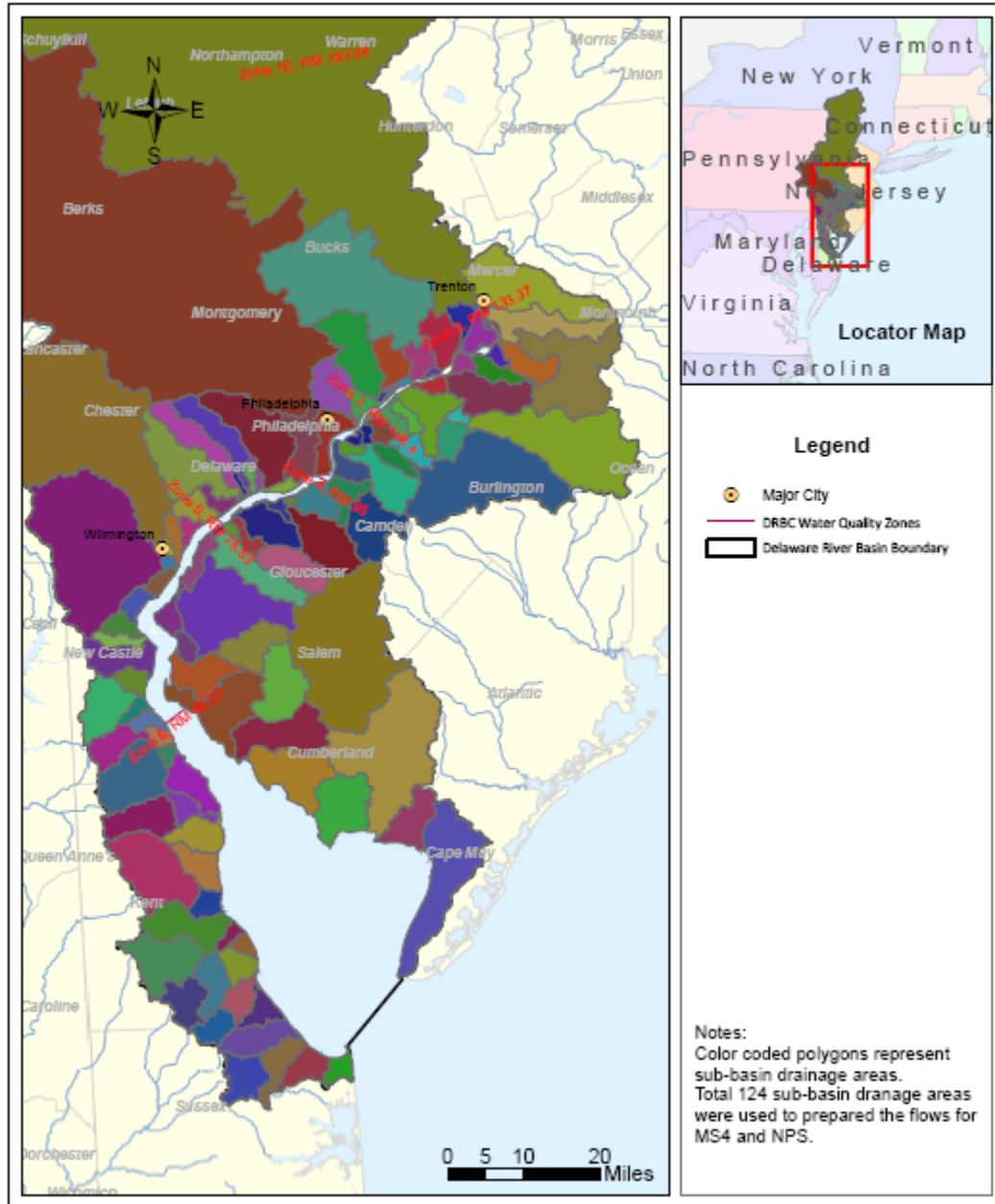


Figure A-7: Delineation of Watershed Drainage Areas

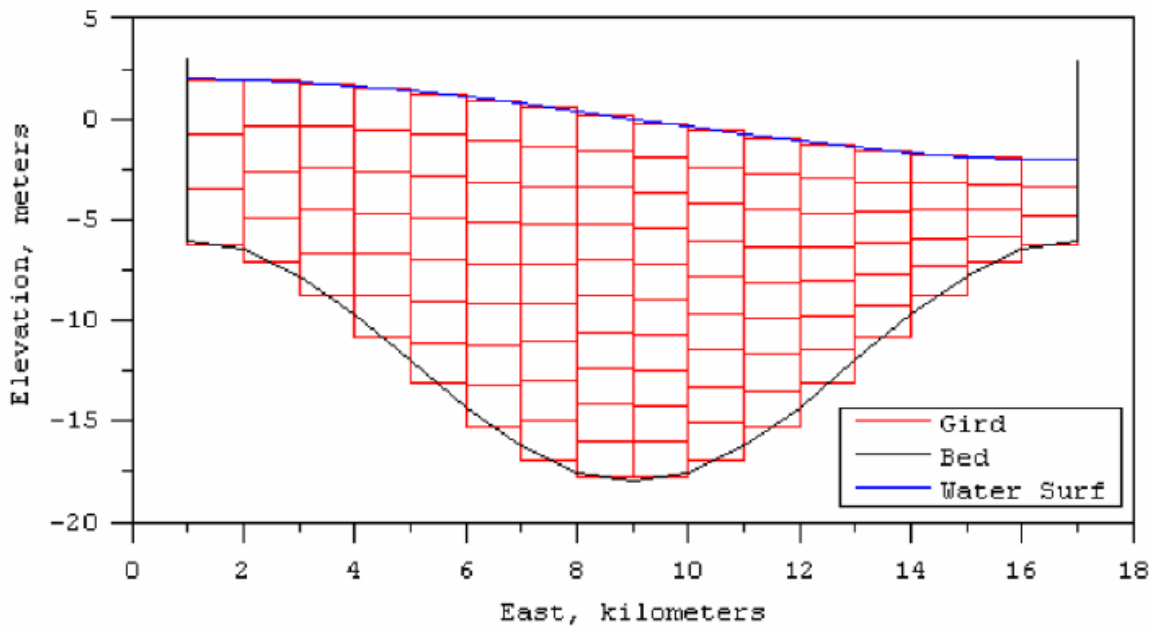


Figure A-8: Example of GVC Grid Cited from EFDC Technical Memorandum, Theoretical and Computational Aspects of the Generalized Vertical Coordinate Option in the EFDC Model (Tetra Tech, 2006)

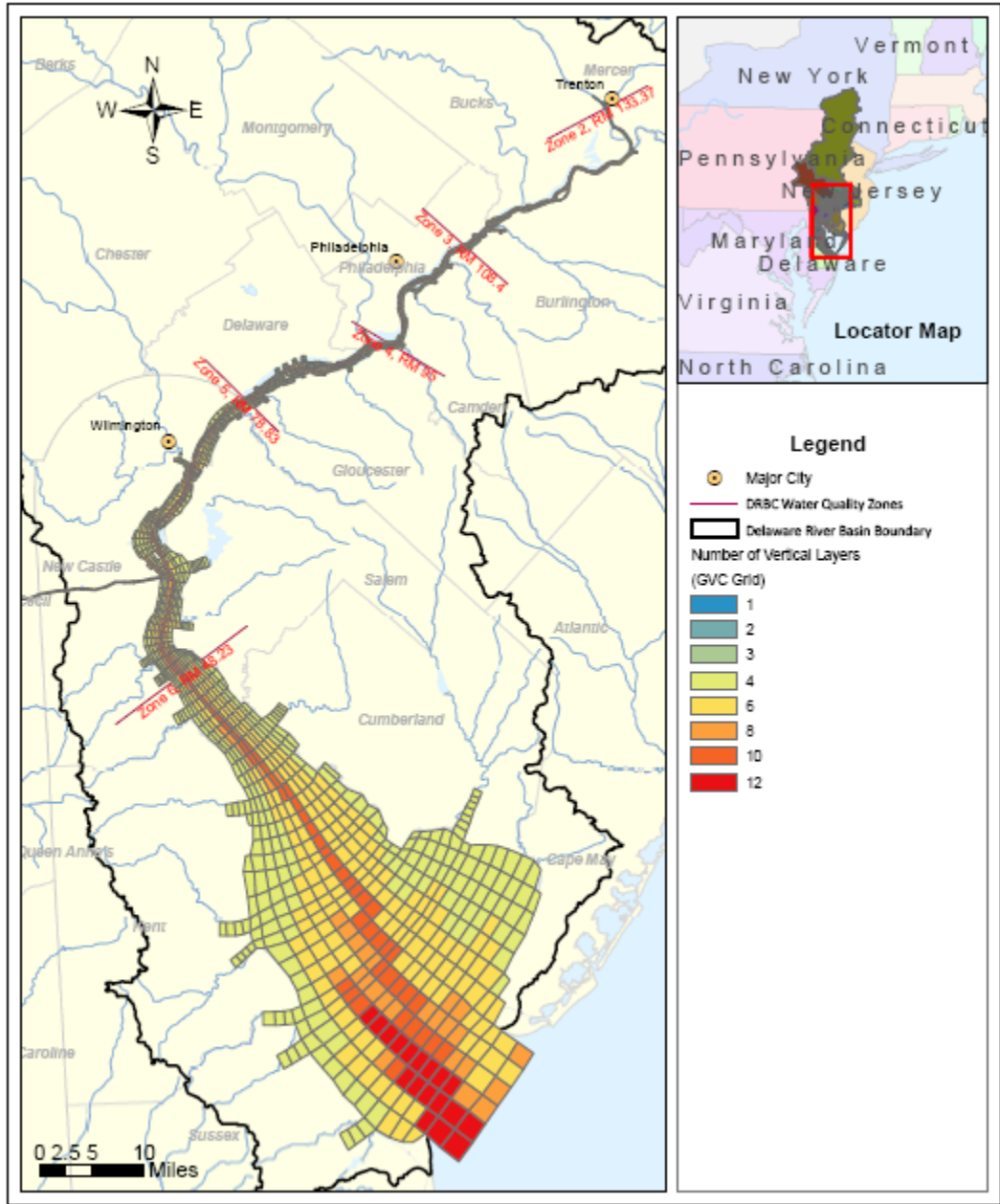


Figure A-9: Numerical Grid with Number of Vertical Layers

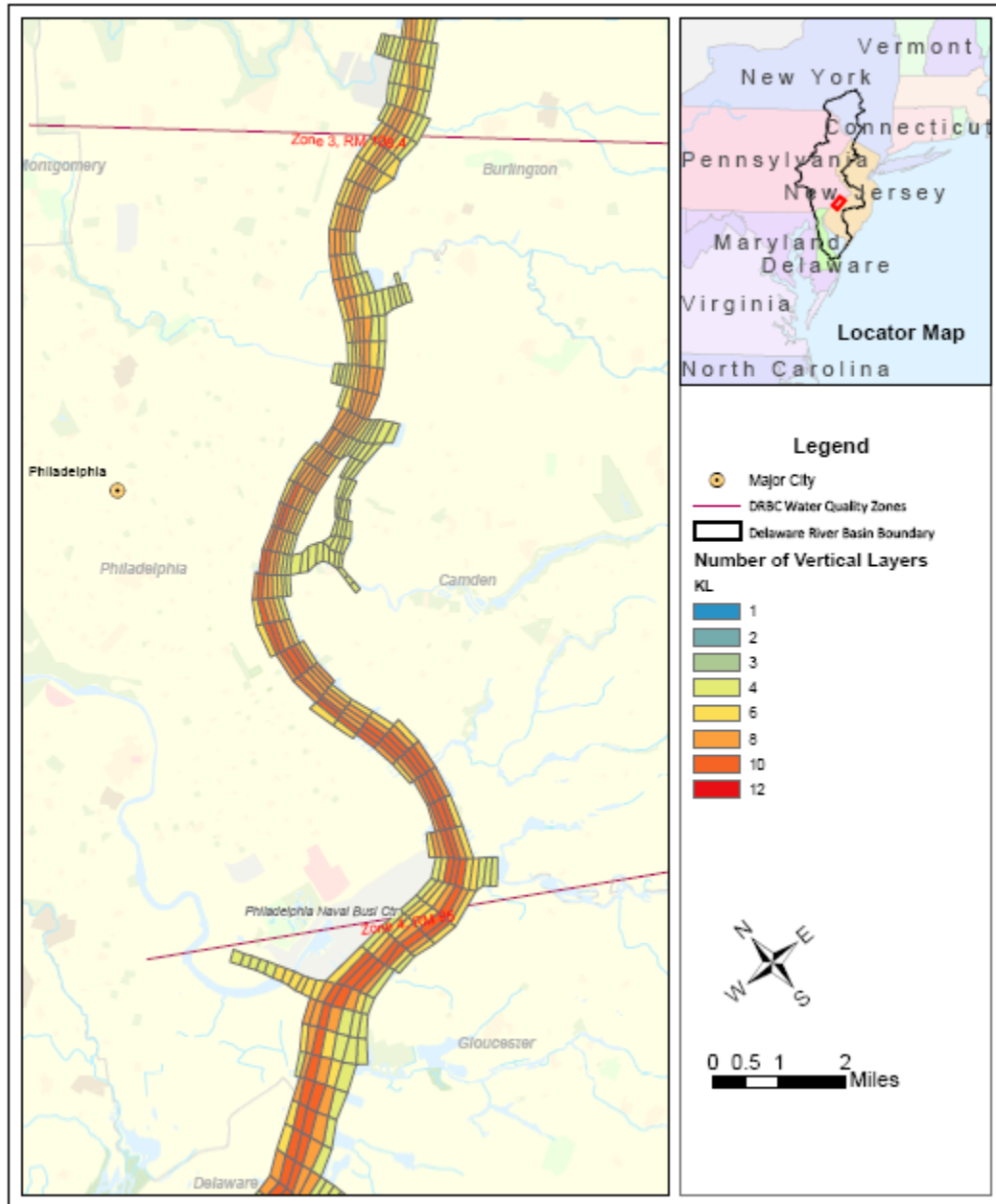


Figure A-10: Numerical Grid with Number of Vertical Layers around Philadelphia Area

Appendix B: Development of watershed flows

Appendix B: Development of Watershed Flows

This appendix is in connection with Section 2.4.2 in the main report – Freshwater Inflows. It is compiled from DRBC' presentations to its Model Expert Panel. The appendix aims to provide additional information on developing watershed inflows.

1. Continuously Gaged Watersheds

For this study measurements from 105 active USGS stream gages with periods of record from 1911 to present were examined (figure 1-1). Time-series input for 26 model inflow boundaries were constructed using direct discharge measurements, averaged on an hourly or daily basis. If stream gage stations were not coincident with model water-quality boundaries, input flows were adjusted on a per-unit-area basis. Exclusive of the upstream boundary at Trenton, these direct measurements account for more than 80 percent of total influent surface water to the lower Delaware River/Estuary.

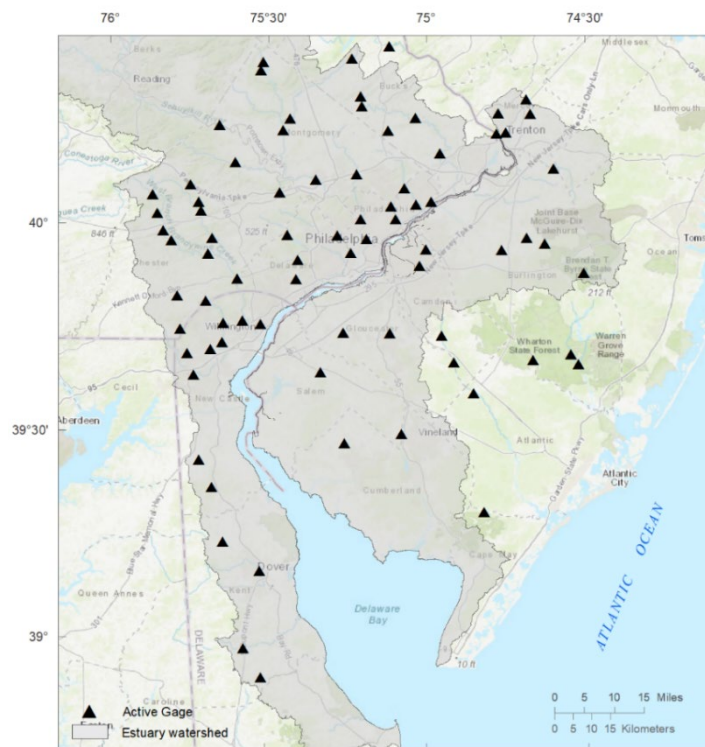


Figure 1-1. Location of USGS active stream gages, Lower Delaware River Basin and vicinity, 2019.

Contributing watersheds were delineated for all established DRBC nutrient monitoring stations using a geographic information system (GIS) with specific hydrologic toolsets (ArcHydro) coupled with the New Jersey-Delaware coastal topo bathymetric elevation model (spatial resolution of 1 meter). Drainage basins for USGS stream gaging stations were reviewed for accuracy and, if needed, were similarly re-delineated. The remaining downstream or other un-gaged portions of the watersheds were delineated by appending

the National Hydrography Dataset (NHD) sub-watersheds and aggregating at an approximate HUC12 scale (Figure 1-2).

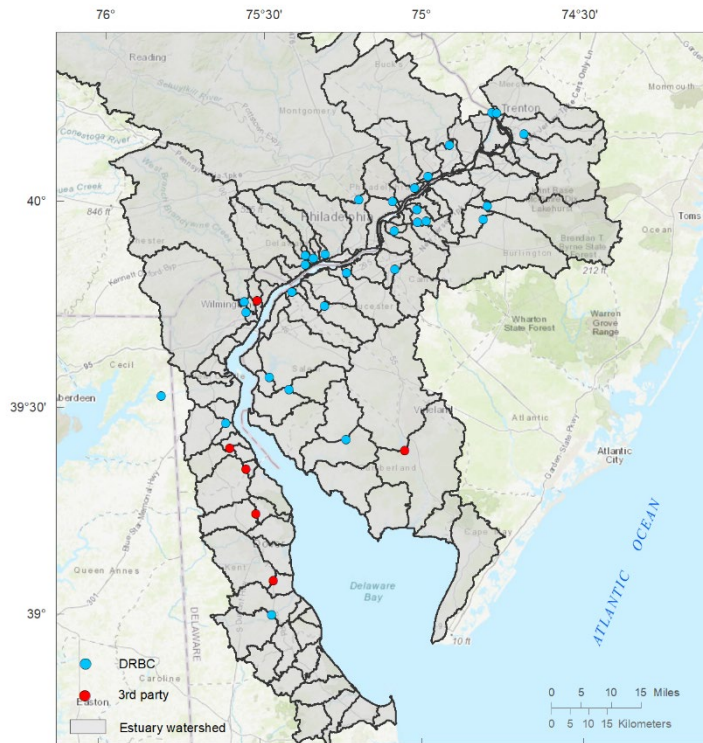


Figure 1-2. Sub-watersheds of the Lower Delaware River Basin.

2. Un-gaged Watersheds

For sub-watersheds where direct measurements were absent, input flows were estimated using index or reference watersheds as described in the following passage.

Because spatial proximity is not always a reliable indicator of hydrologic similarity, a method was needed for the transfer of flow from gaged to un-gaged watersheds. Similarity among gaged and un-gaged catchments was determined via environmental classification. Geomorphological and climatic characteristics that are assumed to produce similar hydrologic responses independent of geographic location were determined and attributed to all catchments using a GIS. Data for all catchments, both gaged and un-gaged were compiled, and watersheds were classified into similar landscapes or hydrologic response units. Candidate basin characteristics are provided in table 2-1.

Hydrodynamic Model of the Delaware River Estuary

Table 2-1. Basin and associated characteristics used for classification of Delaware River Basin watersheds

Label	Description	Units
DA_M2	Drainage Area in square miles	mi ²
DA_KM2	Drainage Area in square kilometers	km ²
fDev	Fraction of basin with urban development	fraction
aDev	Area of basin with urban development	mi ²
fFor	Fraction of basin covered by forest	fraction
aFor	Area of basin covered by forest	mi ²
fAgr	Fraction of basin with agricultural landuse	fraction
aAgr	Area of agricultural land use within basin	mi ²
fUndev	Fraction of undeveloped land within basin	fraction
AUndev	Area of undeveloped land within basin	mi ²
fWet	Fraction of wetlands within basin	fraction
aWet	Area of wetlands within basin	mi ²
fls	Fraction of impervious surface	fraction
als	Area of impervious surface within basin	mi ²
fQcp	Fraction of basin underlain by Quaternary Coastal Plain sediments	fraction
fTM_cp	Fraction of basin underlain by Tertiary Coastal Plain sediments	fraction
fUCret_cp	Fraction of basin Upper Cretaceous Inner Coastal Plain sediments	fraction
fLCret_cp	Fraction of basin underlain by Lower Cretaceous Inner Coastal Plain sediments	fraction
fNewk	Fraction of basin underlain by consolidated rocks of the Newark Basin	fraction
fOther	Fraction of basin underlain by consolidated rocks (other)	fraction
ppt_ann	Average annual precipitation (30y normals) computed from 1981-2010 PRISM datasets	millimeters
degC_ann	Mean annual temperature (30y normals) computed from 1981-2010 PRISM datasets	degrees C
bas_slp	Mean basin slope computed from 1 ft DEM	percent rise
bas_rlf	Basin relief (maximum - minimum elevation)	feet, meters
BFI	Base flow Index- Proportion of mean annual flow that is from groundwater, from Wolock (2003)	fraction; percent
bas_shp	Shape Factor for Area--basin area divided by (main channel length) ²	dimensionless
strmden	Total length of mapped streams in basin divided by basin area	mi per mi ²
storage	Fraction of area of storage (lakes ponds reservoirs wetlands)	fraction
CSL10_85	Change in elevation between points at 10 and 85 percent of length along main channel to basin divide divided by length between points	feet, meters
f_C	Fraction hydrologic soil group C, moderately high runoff potential	fraction
f_B	Fraction hydrologic soil group B, moderately low runoff potential	fraction
f_Urb	Fraction Urban Complex soils	fraction
f_D	Fraction hydrologic soil group D, high runoff potential	fraction
f_BD	Fraction hydrologic soil group BD	fraction
f_A	Fraction hydrologic soil group A, low runoff potential	fraction
f_CD	Fraction hydrologic soil group CD	fraction
f_AD	Fraction hydrologic soil group AD, low runoff potential when dry, high when saturated	fraction

The classification methodology employs hierarchical agglomerative clustering using Ward's algorithm. Agglomerative clustering works from the bottom-up, with each element or site considered a leaf, and with each algorithmic step, the two clusters are combined into another (nodes) until all leaves are part of one large cluster, which is represented as the dendrogram. An advantage to using Ward's method is that the algorithm identifies the strongest clustering structures and minimizes total within-cluster variance. The number of appropriate clusters is not determined from the dendrogram itself, but rather by examination of other statistical measures such as the within-cluster sum of squares, which is a measure of the variability in observations within each cluster. The k-curve is plotted and the point where k (clusters) diminishes indicates the point at which the observed difference in within-cluster dissimilarity is not significant, thus the optimal number of clusters should not go beyond seven (Figure 2-1). The dendrogram in Figure 2-2 shows

the hierarchical relationship between watersheds of the DRB based on a subset of basin characteristics.

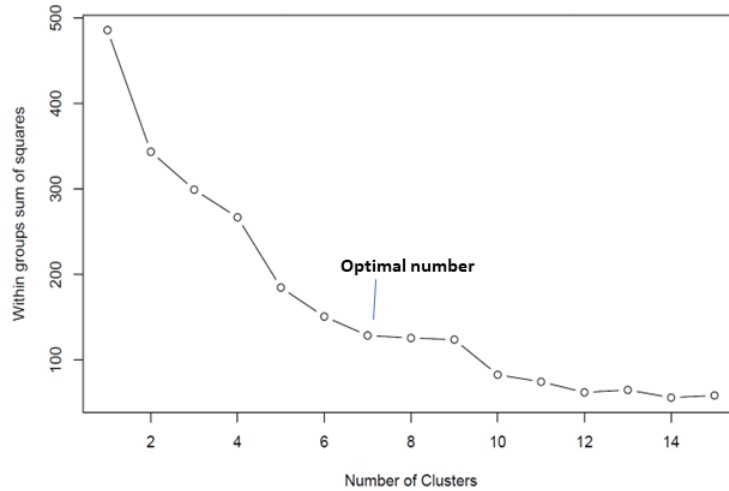


Figure 2-1. Plot of within groups sum of squares against number of clusters.

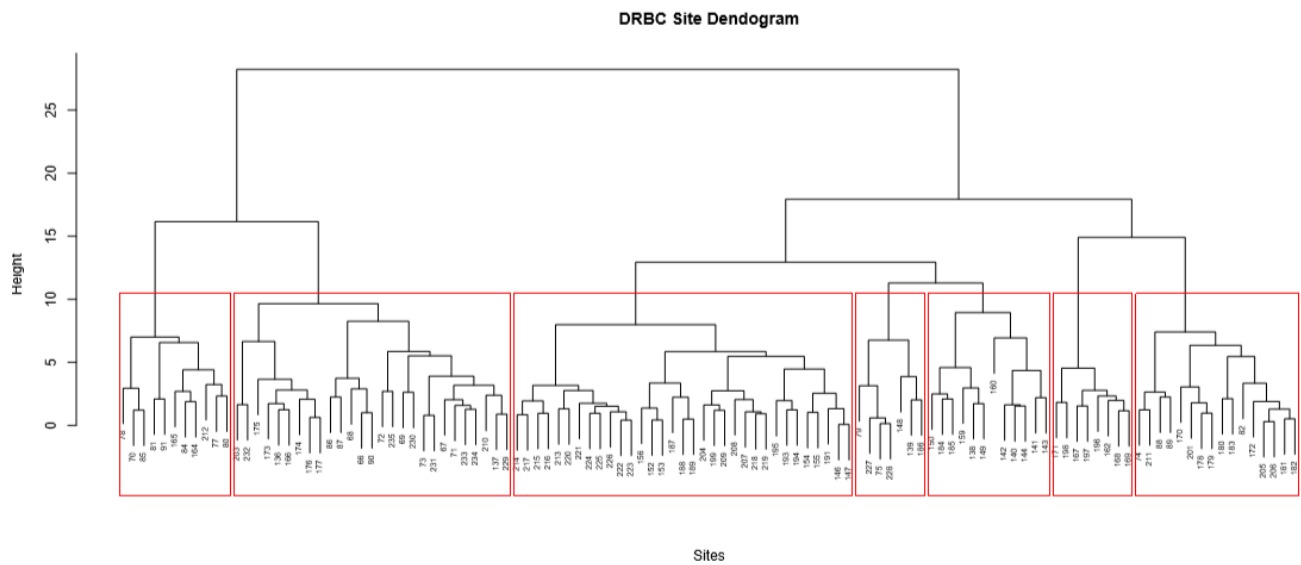


Figure 2-2. Dendrogram showing hierarchical relationship among watersheds of the Delaware River Basin. (Numbers on each limb are serial numbers from each of the Delaware Estuary sub-watersheds and potential reference gages.)

Index gages were assigned to un-gaged watersheds by distance within their respective clusters. Prior to the transfer of flow information, the daily hydrograph for each index gage was partitioned into the groundwater-discharge (baseflow) and runoff components using standard USGS hydrograph separation techniques – PART methods, HYSEP (Fixed Interval, Sliding Interval, and Local Minimum), and BFI (Standard). Detailed information

on these methods can be found in Barlow and others (2015), Rutledge (1998), Sloto and Crouse (1996), and Wahl and Wahl, 1995. Figure 2-3 shows the flow duration curves for measured streamflow and the components of baseflow and runoff for the Maurice River at Norma, NJ estimated by three methods.

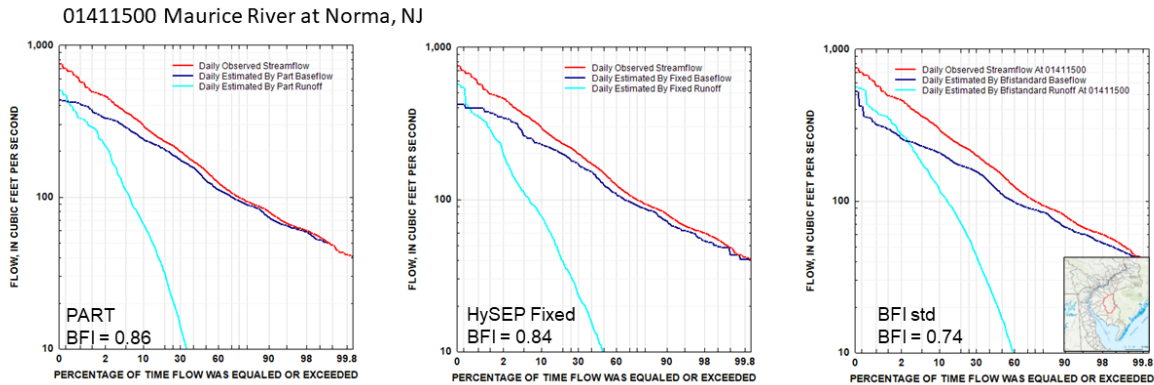


Figure 2-3. Flow duration curves for measured streamflow and estimated baseflow and runoff at Maurice River at Norma, NJ using three hydrograph separation methods.

Following the assignment of index stations to all un-gaged areas, the drainage-area-ratio (DAR) method was used for streamflow transference. The DAR method is commonly used to estimate streamflow where no data are available, equating the ratio of streamflow at two locations to the ratio of the respective drainage areas using the following formulation,

$$Y = X(A_y/A_x)^\Phi \quad (1)$$

where Y is the streamflow at the un-gaged site, X is the streamflow at the gaged site, and A_y and A_x are the drainage areas for the un-gaged and gaged sites, respectively. In most applications, unity is assumed for Φ . In this application, Φ is a function of the streamflow percentile and thus scales the flow on a fractional power of drainage area ($\Phi < 1$). Exponents range from 0.74 to 0.94, with smaller exponents associated with the highest percentiles of flow. For a more thorough explanation, see Asquith and others (2006). The DAR routines were run subsequent to hydrograph separation, and the full hydrograph or runoff component was transferred to the target catchment as appropriate.

References:

Asquith, W.H., Roussel, M.C., and Vrabel, Joseph, 2006, Statewide analysis of the drainage-area ratio method for 34 streamflow percentile ranges in Texas: U.S. Geological Survey Scientific Investigations Report 2006–5286, 34 p., 1 appendix.

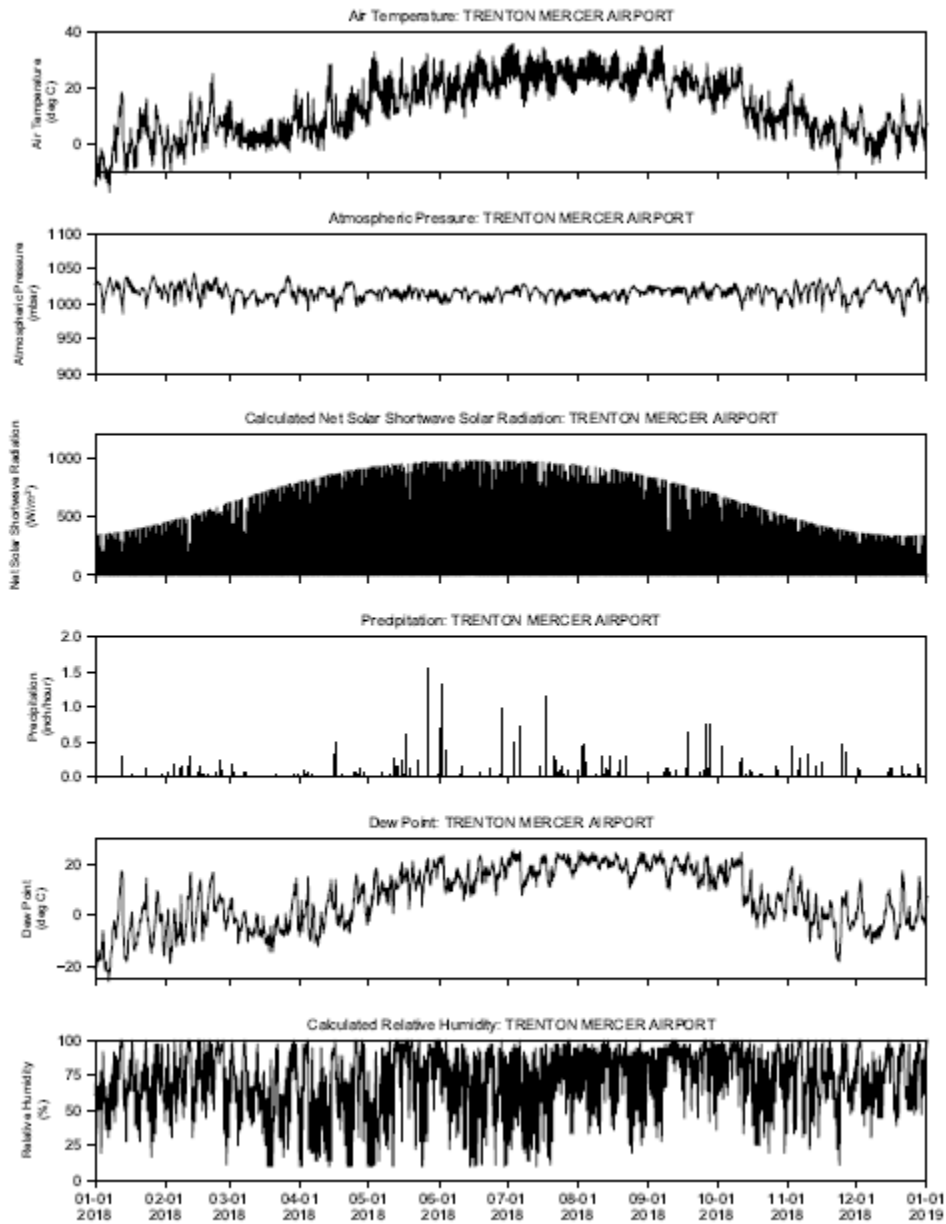
Barlow, P.M., Cunningham, W.L., Zhai, Tong, and Gray, Mark, 2015, U.S. Geological Survey Groundwater Toolbox, a graphical and mapping interface for analysis of hydrologic data (version 1.0)—User guide for estimation of base flow, runoff, and groundwater recharge from streamflow data: U.S. Geological Survey Techniques and Methods, book 3, chap. B10, 27 p., <http://dx.doi.org/10.3133/tm3B10>.

Rutledge, A.T., 1998, Computer programs for describing the recession of ground-water discharge and for estimating mean ground-water recharge and discharge from streamflow records—Update: U.S. Geological Survey Water-Resources Investigations Report 98–4148, 43 p., <http://pubs.usgs.gov/wri/wri984148>.

Sloto, R.A., and Crouse, M.Y., 1996, HYSEP—A computer program for streamflow hydrograph separation and analysis: U.S. Geological Survey Water-Resources Investigations Report 96–4040, 46 p., <http://pubs.er.usgs.gov/publication/wri964040>

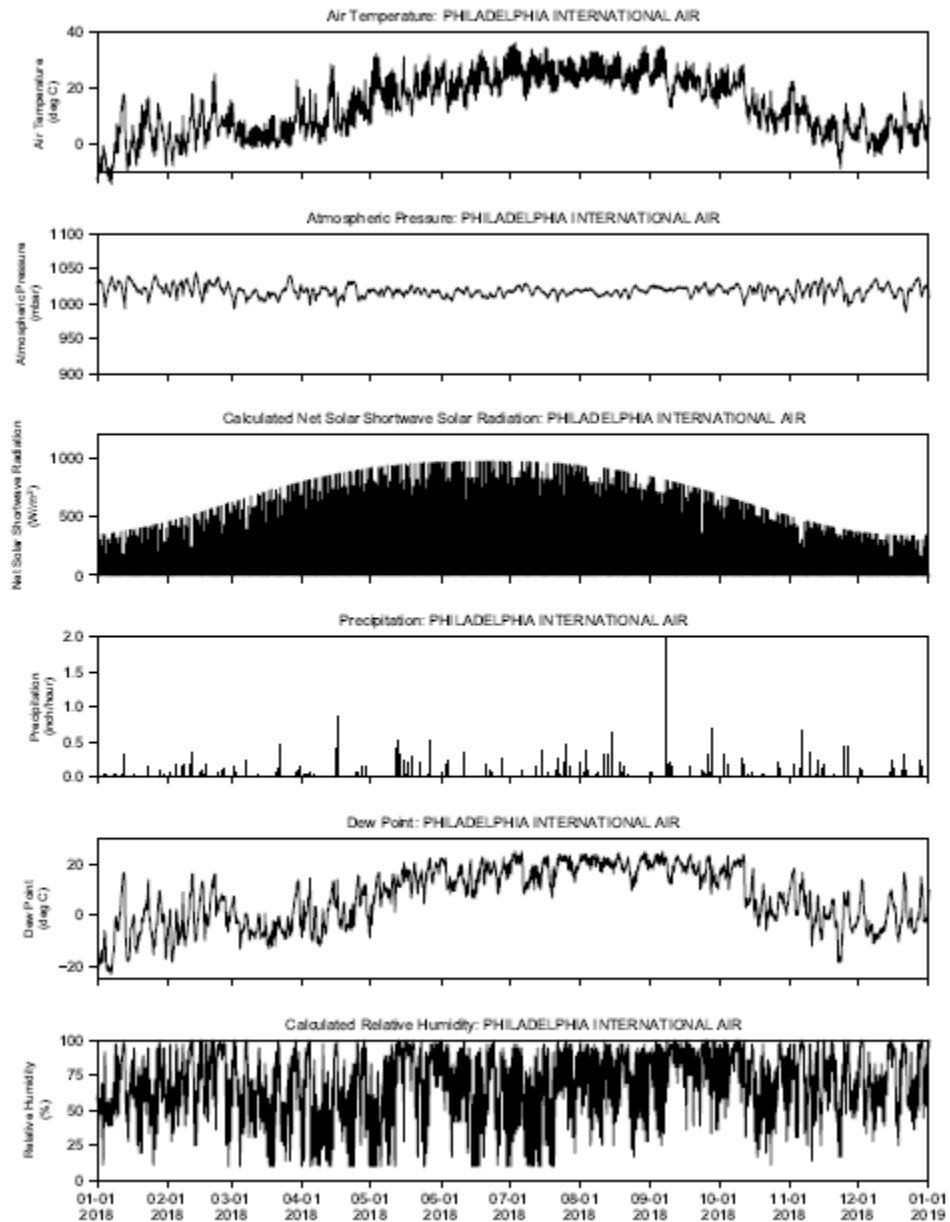
Wahl, K.L., and Wahl, T.L., 1995, Determining the flow of Comal Springs at New Braunfels, Texas, in Proceedings of Texas Water 95, August 16–17, 1995, San Antonio, Tex.: American Society of Civil Engineers, p. 77–86.

Appendix C: Meteorological data



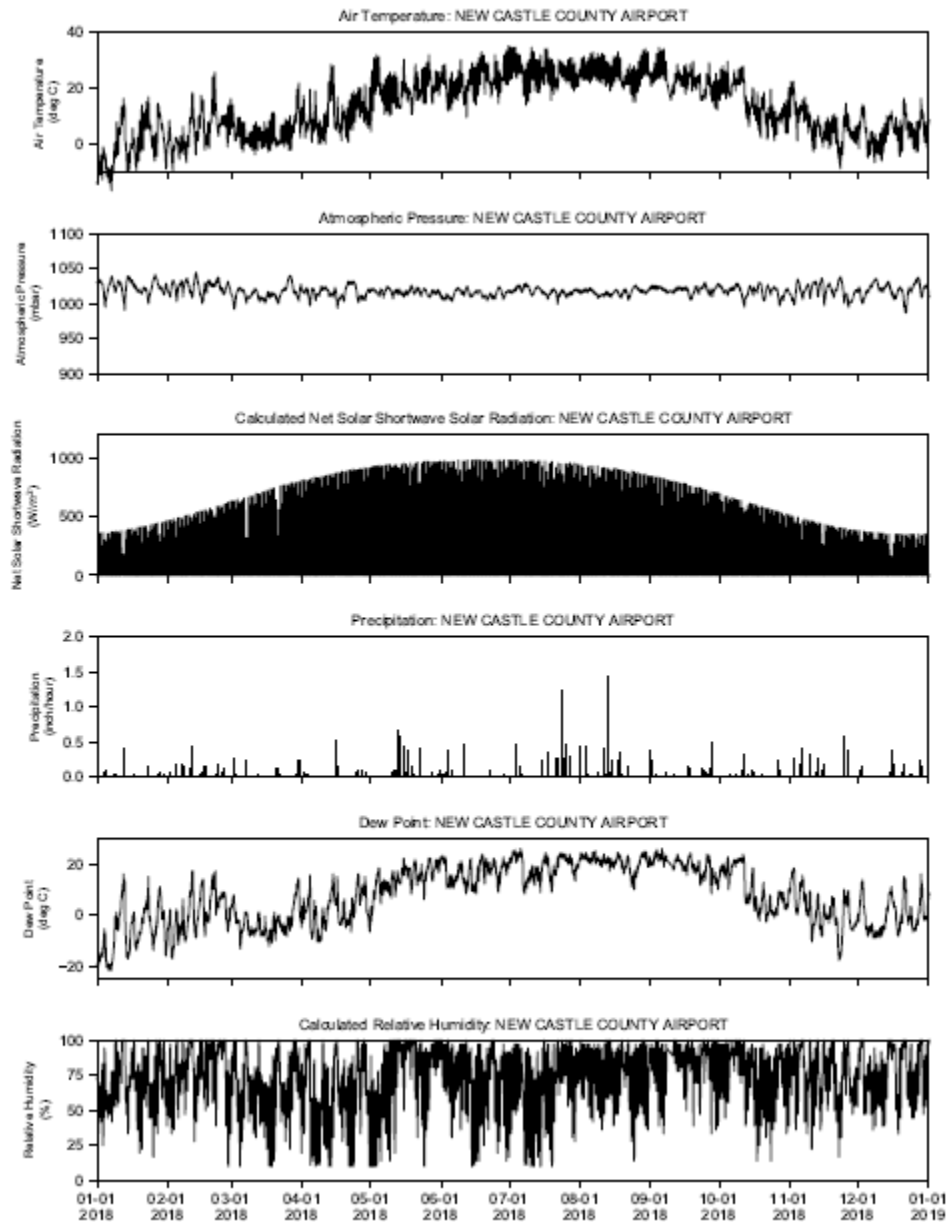
Notes: Meteorological data were downloaded from NOAA NCDC website.
<https://gis.ncdc.noaa.gov/maps/ncei/cdo/hourly>.
Net solar shortwave radiation and relative humidity were calculated as best estimate.

Figure C-1: Meteorological Data from TRENTON MERCER AIRPORT During 2018



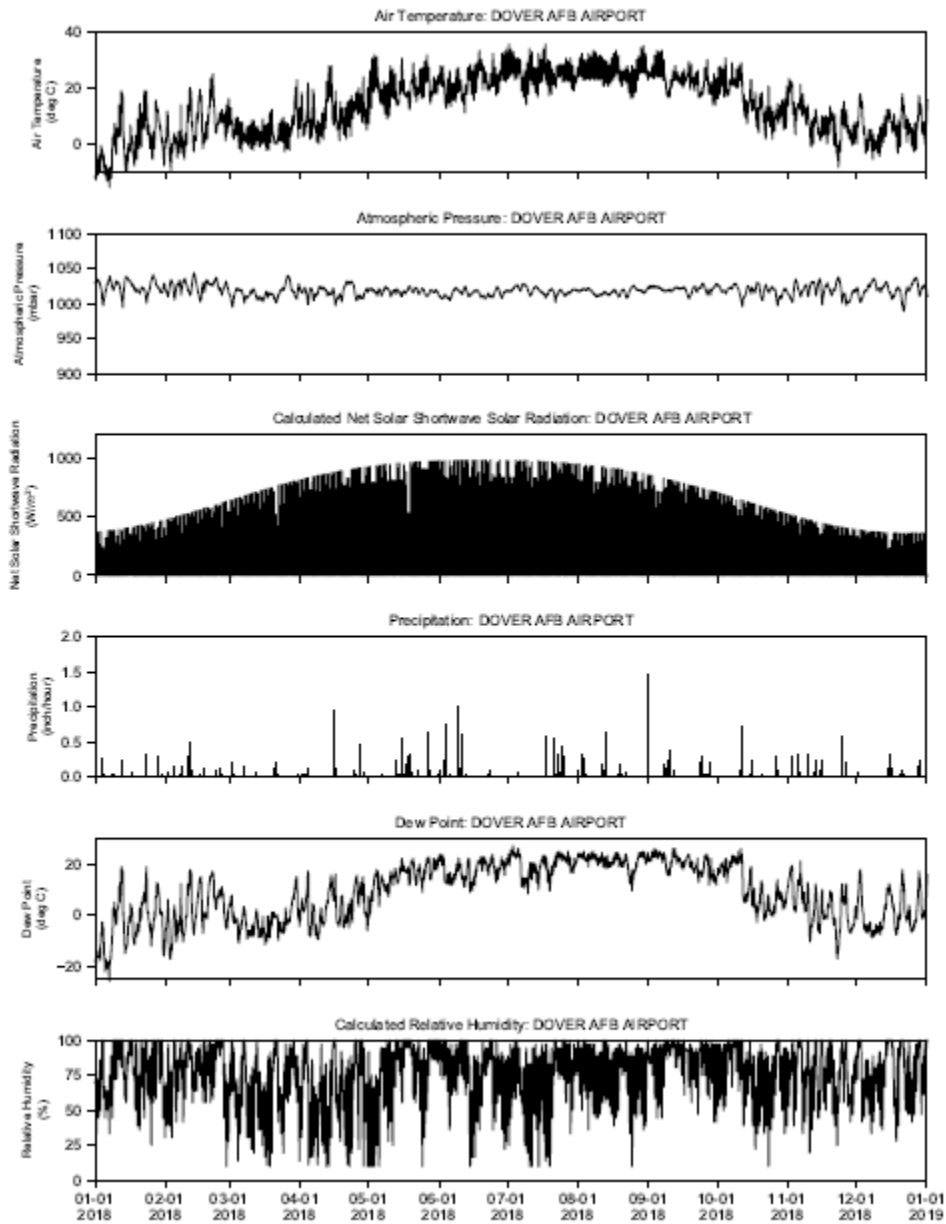
Notes: Meteorological data were downloaded from NOAA NCDC website.
<https://gis.ncdc.noaa.gov/maps/ncei/cdo/hourly>.
 Net solar shortwave radiation and relative humidity were calculated as best estimate.

Figure C-2: Meteorological Data from PHILADELPHIA INTERNATIONAL AIR During 2018



Notes: Meteorological data were downloaded from NOAA NCDC website.
<https://gis.ncdc.noaa.gov/maps/ncei/cdo/hourly>.
 Net solar shortwave radiation and relative humidity were calculated as best estimate.

Figure C-3: Meteorological Data from NEW CASTLE COUNTY AIRPORT During 2018

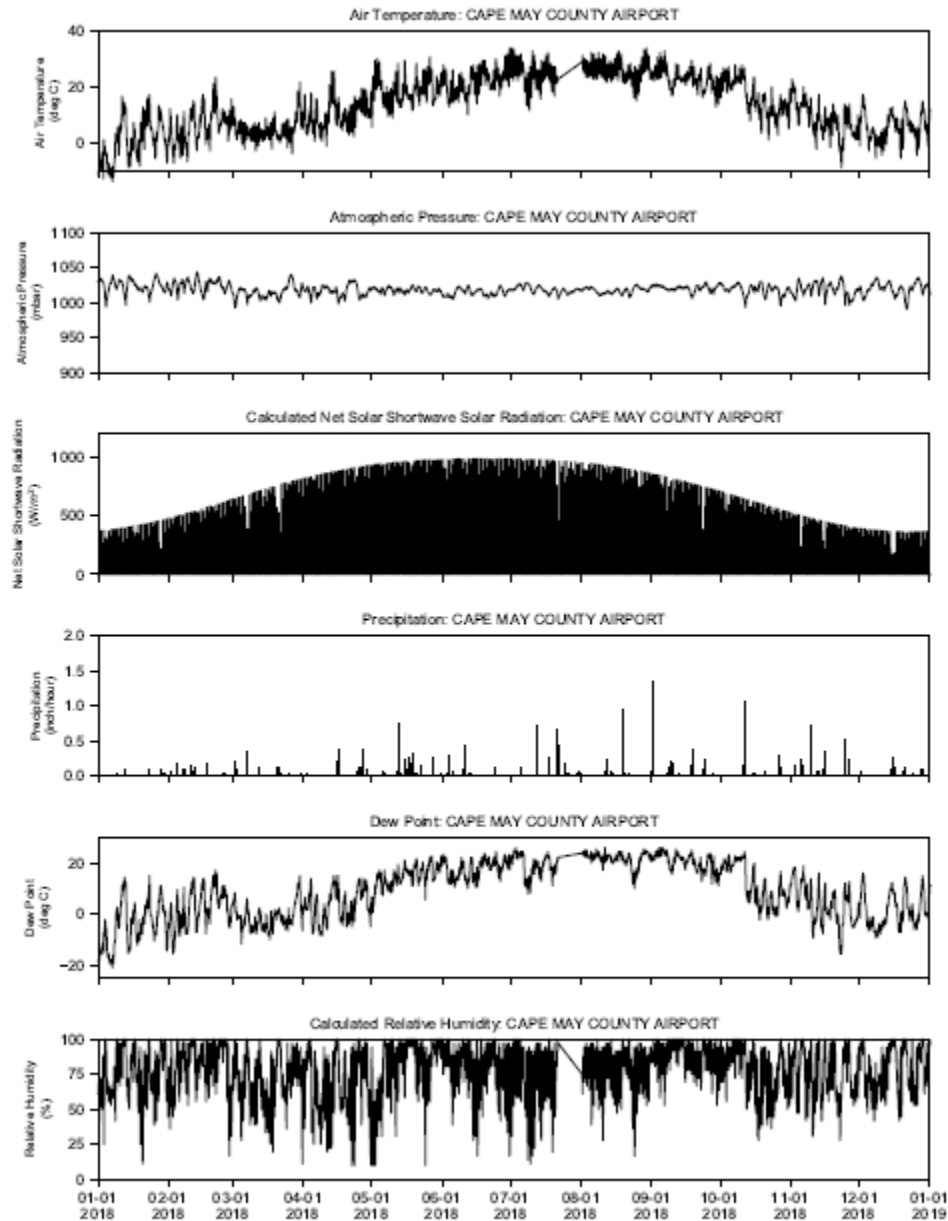


Notes: Meteorological data were downloaded from NOAA NCDC website.

<https://gis.ncdc.noaa.gov/maps/ncei/cdo/hourly>.

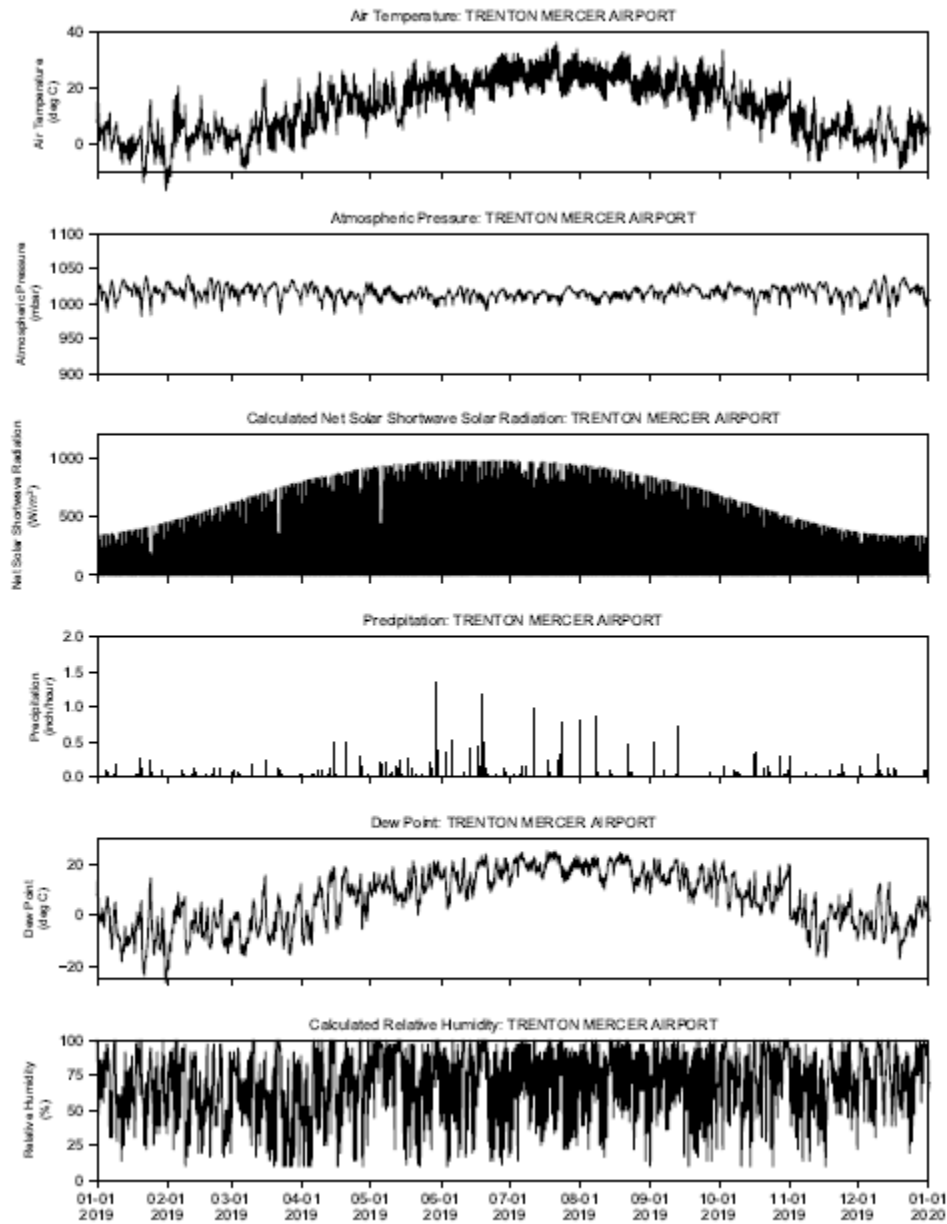
Net solar shortwave radiation and relative humidity were calculated as best estimate.

Figure C-4: Meteorological Data from DOVER AFB AIRPORT During 2018



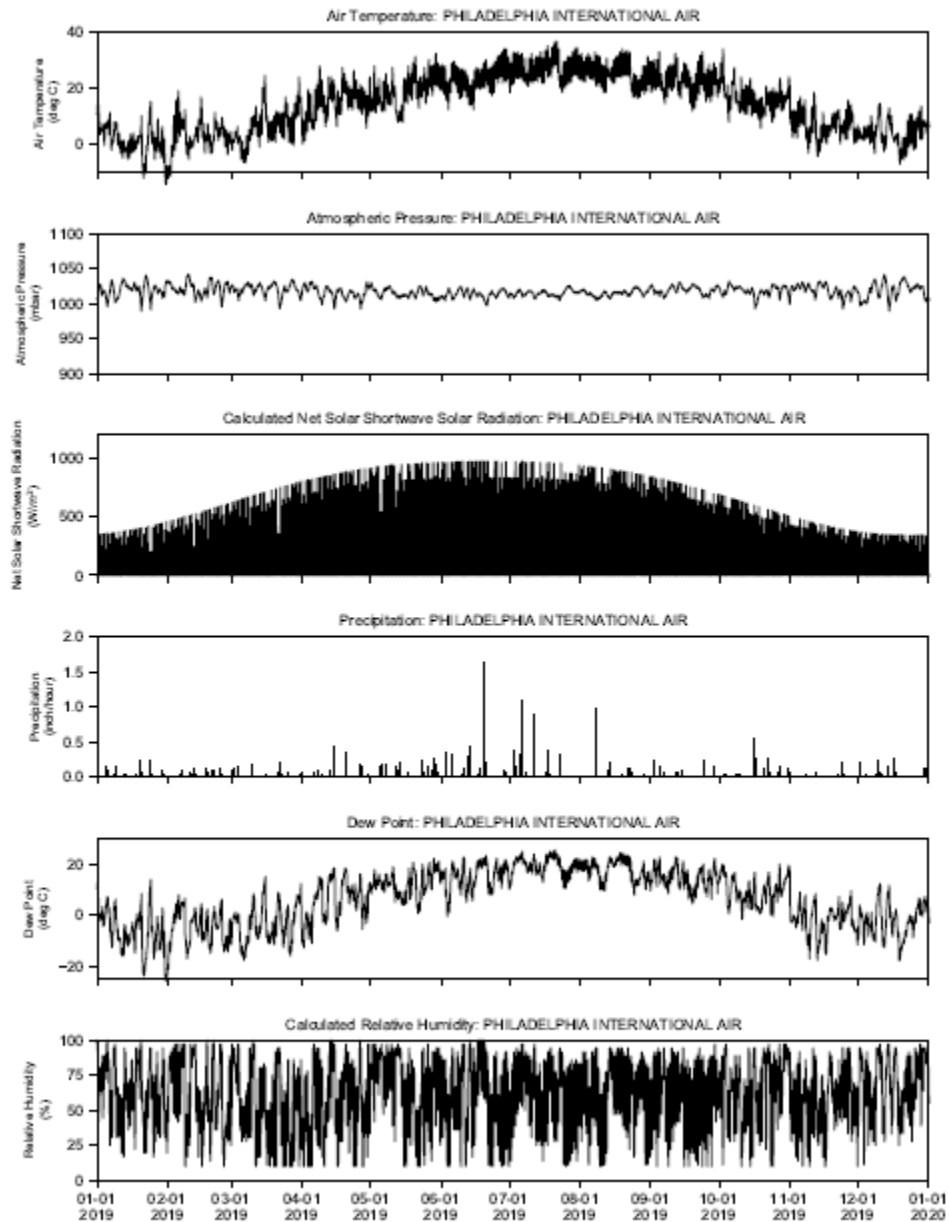
Notes: Meteorological data were downloaded from NOAA NCDC website.
<https://gis.ncdc.noaa.gov/maps/ncei/cdo/hourly>.
Net solar shortwave radiation and relative humidity were calculated as best estimate.

Figure C-5: Meteorological Data from CAPE MAY COUNTY AIRPORT During 2018



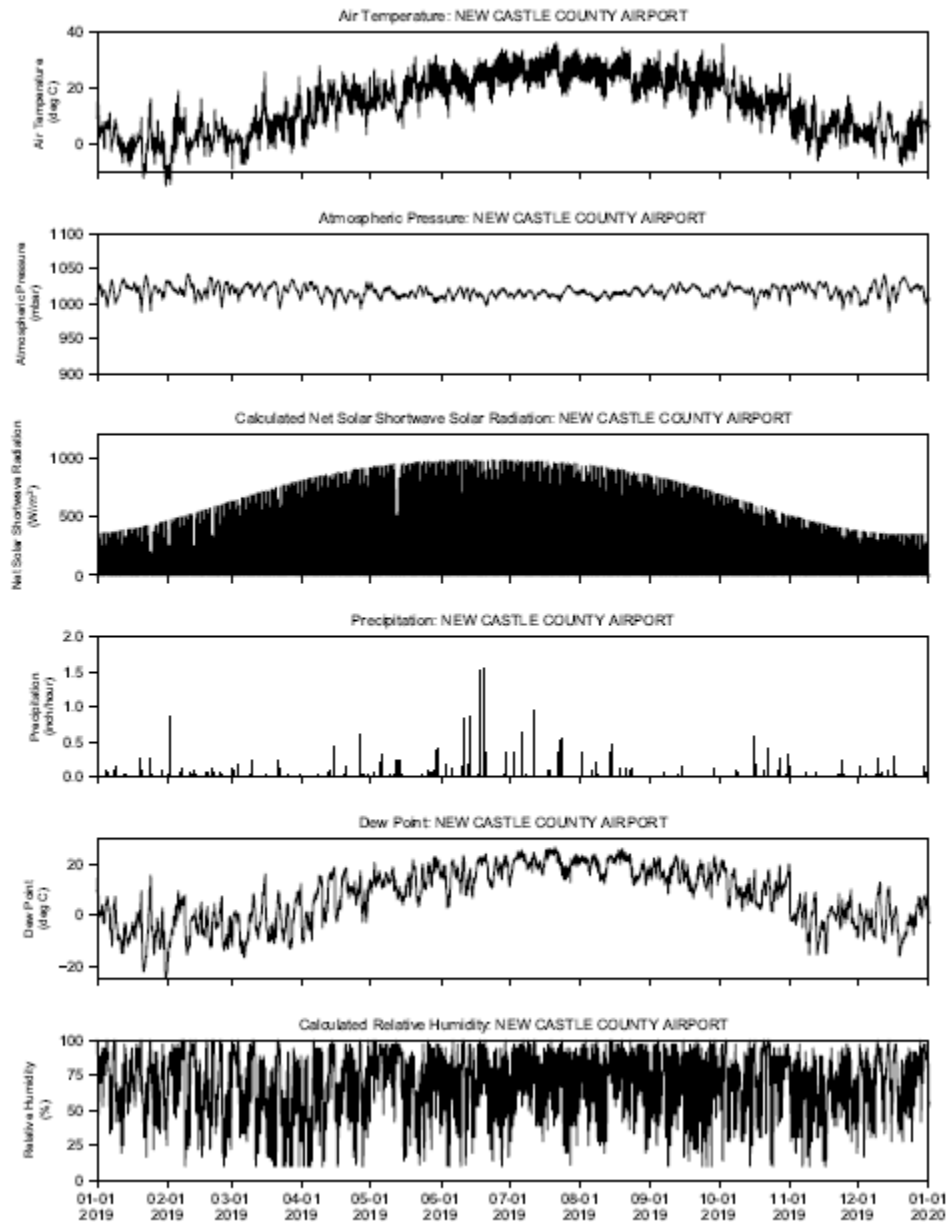
Notes: Meteorological data were downloaded from NOAA NCDC website.
<https://gis.ncdc.noaa.gov/maps/ncei/cdo/hourly>.
 Net solar shortwave radiation and relative humidity were calculated as best estimate.

Figure C-6: Meteorological Data from TRENTON MERCER AIRPORT During 2019



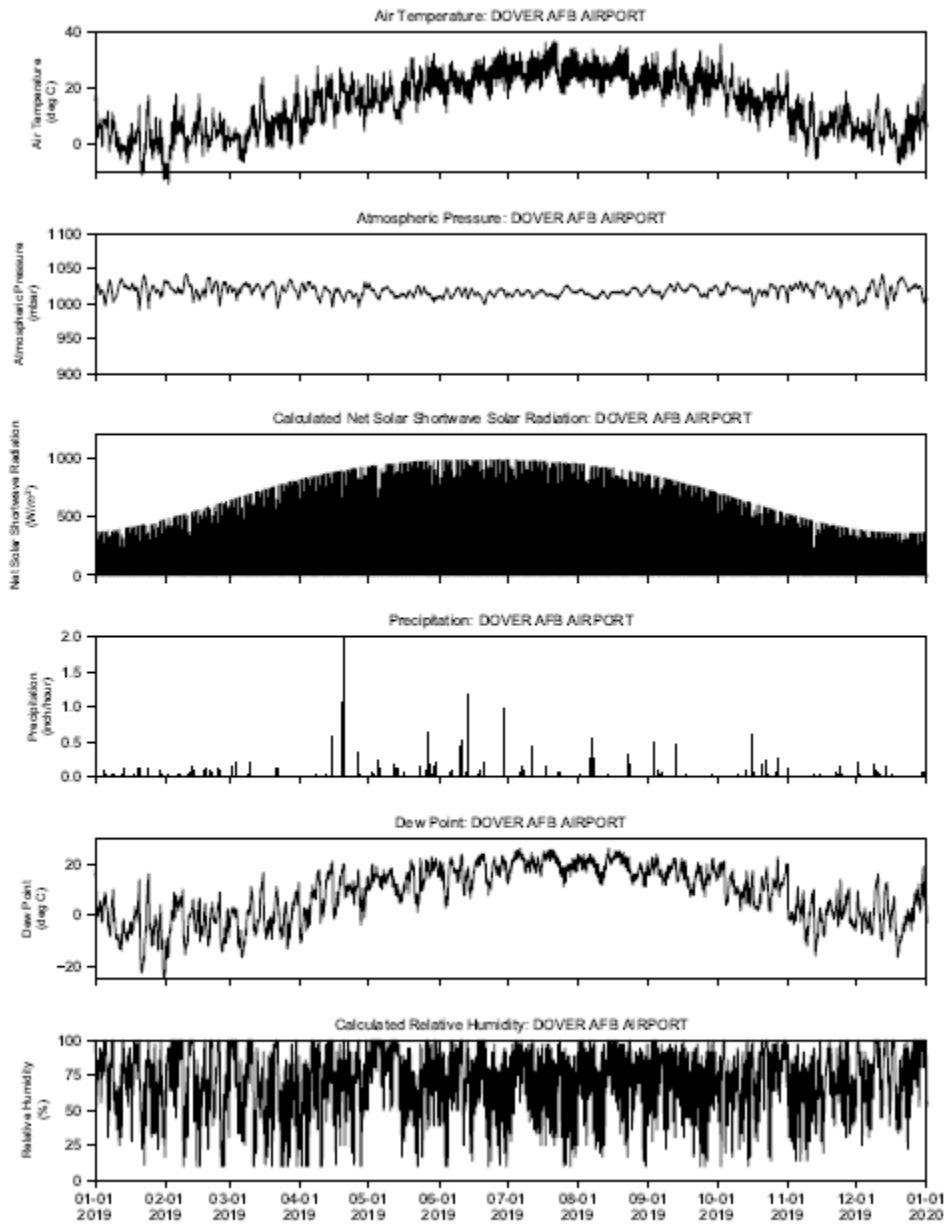
Notes: Meteorological data were downloaded from NOAA NCDC website.
<https://gis.ncdc.noaa.gov/maps/ncei/cdo/hourly>.
 Net solar shortwave radiation and relative humidity were calculated as best estimate.

Figure C-7: Meteorological Data from PHILADELPHIA INTERNATIONAL AIR During 2019



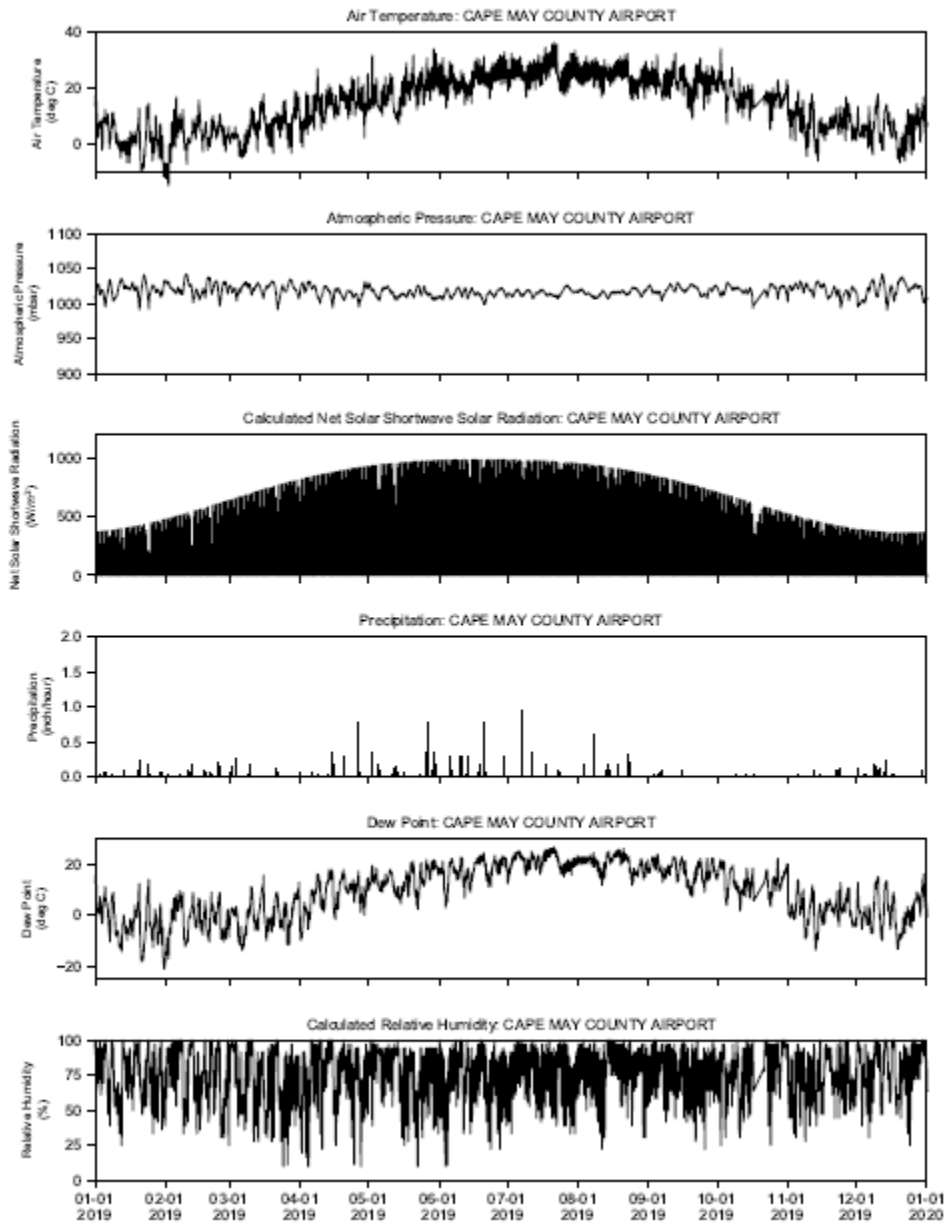
Notes: Meteorological data were downloaded from NOAA NCDC website.
<https://gis.ncdc.noaa.gov/maps/ncei/cdo/hourly>.
Net solar shortwave radiation and relative humidity were calculated as best estimate.

Figure C-8: Meteorological Data from NEW CASTLE COUNTY AIRPORT During 2019



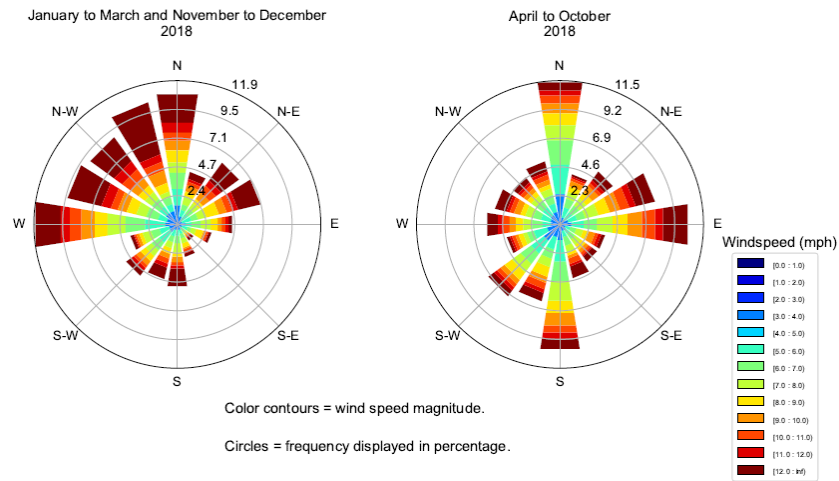
Notes: Meteorological data were downloaded from NOAA NCDC website.
<https://gis.ncdc.noaa.gov/maps/ncei/cdo/hourly>.
Net solar shortwave radiation and relative humidity were calculated as best estimate.

Figure C-9: Meteorological Data from DOVER AFB AIRPORT During 2019



Notes: Meteorological data were downloaded from NOAA NCDC website.
<https://gis.ncdc.noaa.gov/maps/ncei/cdo/hourly>.
 Net solar shortwave radiation and relative humidity were calculated as best estimate.

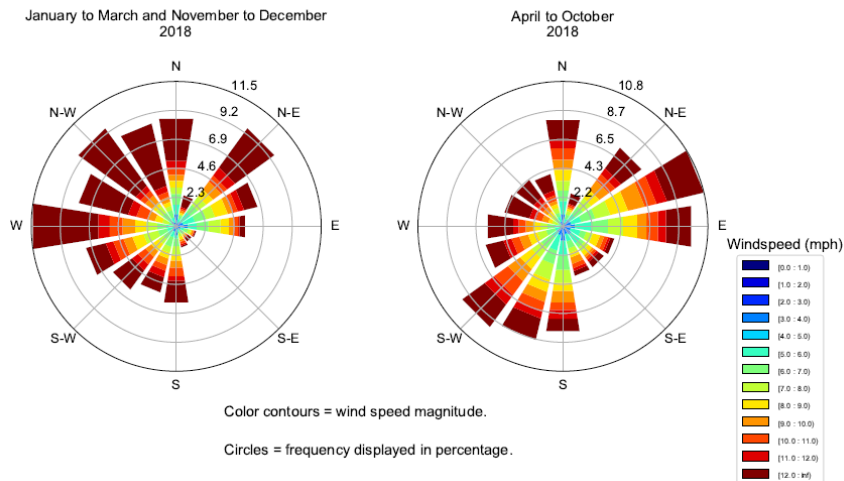
Figure C-10: Meteorological Data from CAPE MAY COUNTY AIRPORT During 2019



Notes:

1. Direction angle is measured from true north clockwise to the wind vector (blowing from) in degrees
2. Data were downloaded from NOAA NCDC website, <https://gis.ncdc.noaa.gov/maps/ncei/cdo/hourly>

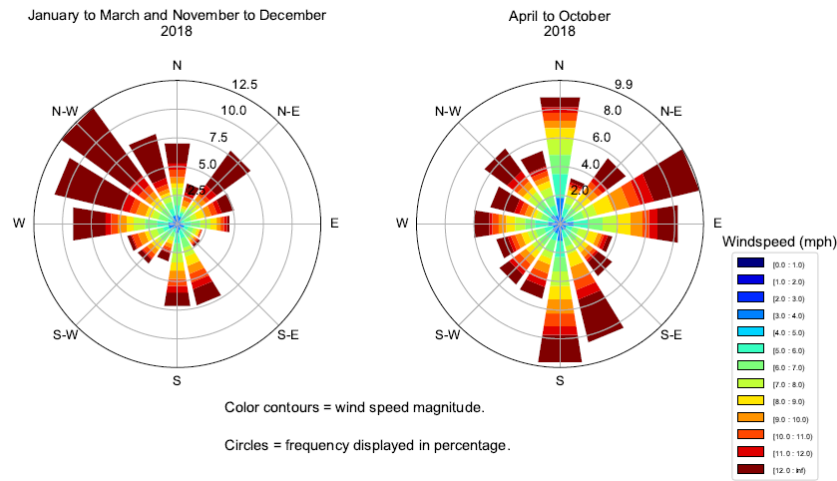
Figure C-11: Wind Rose Plot Based on 2018 Data Collected at Station TRENTON MERCER AIRPORT, Station ID: 724095



Notes:

1. Direction angle is measured from true north clockwise to the wind vector (blowing from) in degrees
2. Data were downloaded from NOAA NCDC website, <https://gis.ncdc.noaa.gov/maps/ncei/cdo/hourly>

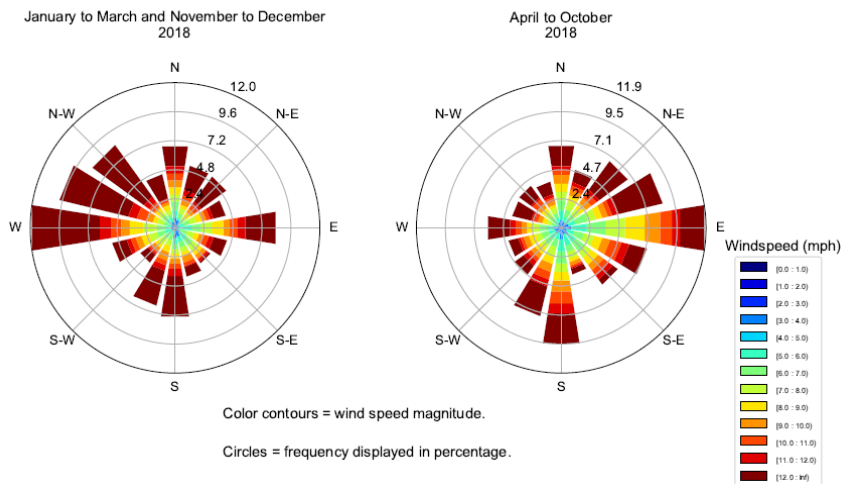
Figure C-12: Wind Rose Plot Based on 2018 Data Collected at Station PHILADELPHIA INTERNATIONAL AIR, Station ID: 724080



Notes:

1. Direction angle is measured from true north clockwise to the wind vector (blowing from) in degrees
2. Data were downloaded from NOAA NCDC website, <https://gis.ncdc.noaa.gov/maps/ncei/cdo/hourly>

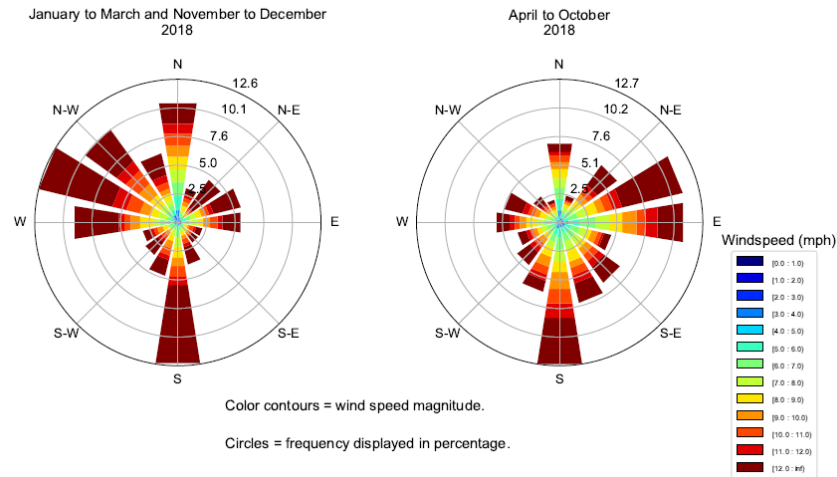
Figure C-13: Wind Rose Plot Based on 2018 Data Collected at Station NEW CASTLE COUNTY AIRPORT, Station ID: 724180



Notes:

1. Direction angle is measured from true north clockwise to the wind vector (blowing from) in degrees
2. Data were downloaded from NOAA NCDC website, <https://gis.ncdc.noaa.gov/maps/ncei/cdo/hourly>

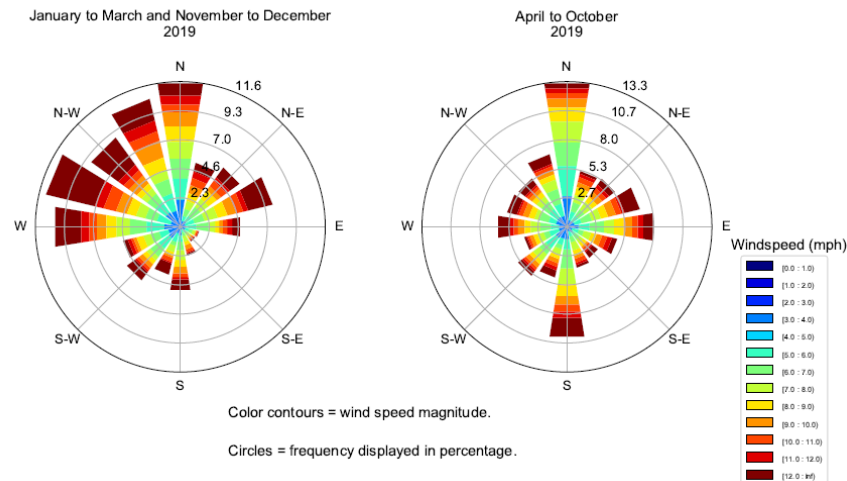
Figure C-14: Wind Rose Plot Based on 2018 Data Collected at Station DOVER AFB AIRPORT, Station ID: 724088



Notes:

1. Direction angle is measured from true north clockwise to the wind vector (blowing from) in degrees
2. Data were downloaded from NOAA NCDC website, <https://gis.ncdc.noaa.gov/maps/ncei/cdo/hourly>

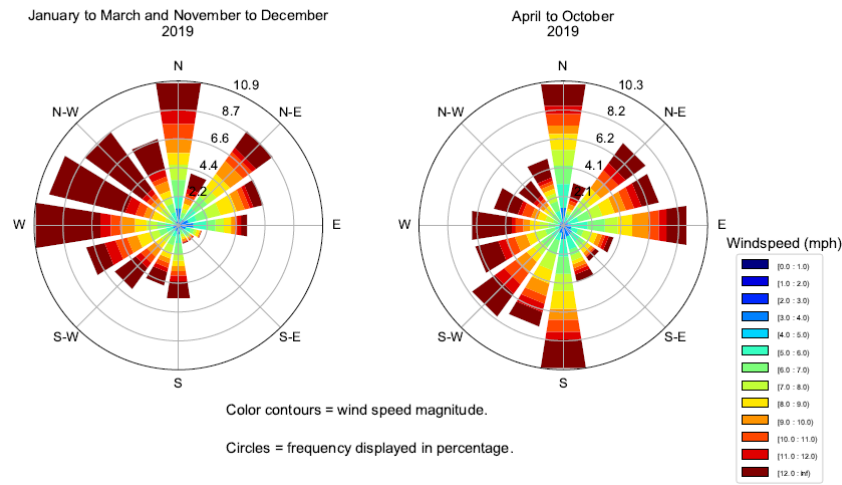
Figure C-15: Wind Rose Plot Based on 2018 Data Collected at Station CAPE MAY COUNTY AIRPORT, Station ID: 745966



Notes:

1. Direction angle is measured from true north clockwise to the wind vector (blowing from) in degrees
2. Data were downloaded from NOAA NCDC website, <https://gis.ncdc.noaa.gov/maps/ncei/cdo/hourly>

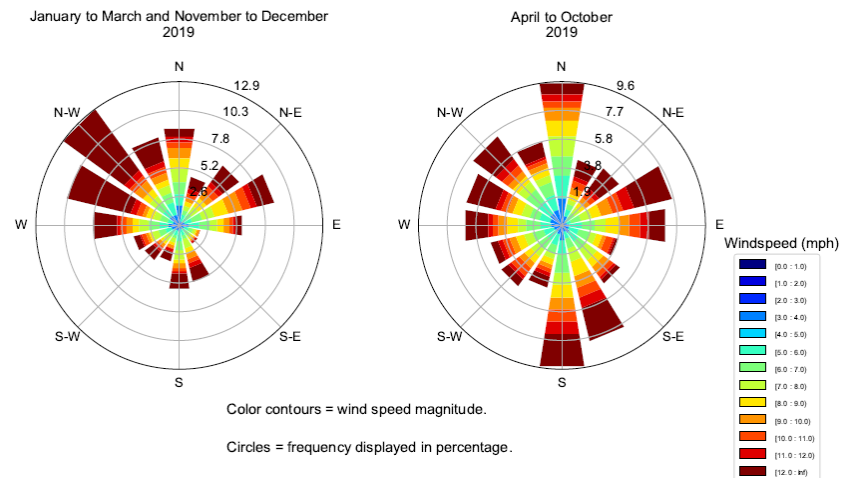
Figure C-16: Wind Rose Plot Based on 2019 Data Collected at Station TRENTON MERCER AIRPORT, Station ID: 724095



Notes:

1. Direction angle is measured from true north clockwise to the wind vector (blowing from) in degrees
2. Data were downloaded from NOAA NCDC website, <https://gis.ncdc.noaa.gov/maps/ncei/cdo/hourly>

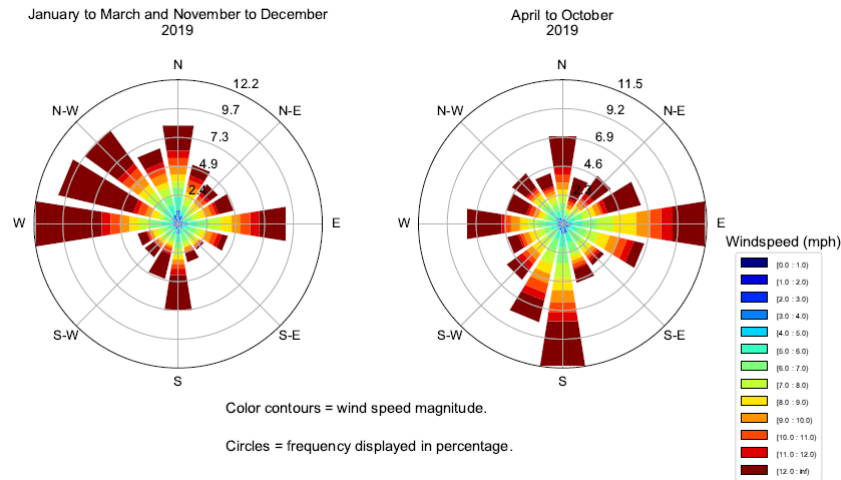
Figure C-17: Wind Rose Plot Based on 2019 Data Collected at Station PHILADELPHIA INTERNATIONAL AIR, Station ID: 724080



Notes:

1. Direction angle is measured from true north clockwise to the wind vector (blowing from) in degrees
2. Data were downloaded from NOAA NCDC website, <https://gis.ncdc.noaa.gov/maps/ncei/cdo/hourly>

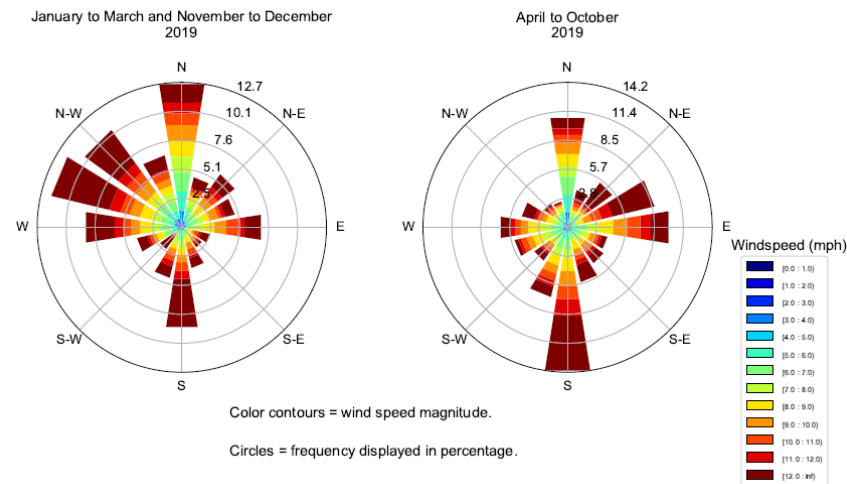
Figure C-18: Wind Rose Plot Based on 2019 Data Collected at Station NEW CASTLE COUNTY AIRPORT, Station ID: 724180



Notes:

1. Direction angle is measured from true north clockwise to the wind vector (blowing from) in degrees
2. Data were downloaded from NOAA NCDC website, <https://gis.ncdc.noaa.gov/maps/ncei/cdo/hourly>

Figure C-19: Wind Rose Plot Based on 2019 Data Collected at Station DOVER AFB AIRPORT, Station ID: 724088



Notes:

1. Direction angle is measured from true north clockwise to the wind vector (blowing from) in degrees
2. Data were downloaded from NOAA NCDC website, <https://gis.ncdc.noaa.gov/maps/ncei/cdo/hourly>

Figure C-20: Wind Rose Plot Based on 2019 Data Collected at Station CAPE MAY COUNTY AIRPORT, Station ID: 745966

Appendix D: Summaries of NOAA and USGS calibration data

Table D-1: Summary of Data from NOAA Stations Used for Model Calibration

No.	Station	Station ID	Data Type	Data Inventory for Period Covers Calibration	DRBC River Mile	Comments
1	Lewes, DE	8557380	Verified Hourly Water Level	1975-02-26 14:00 to Present (2019)	~ 0	Subtidal fluctuations and water temperature were used for specification of tidal forcing and temperature boundary conditions.
			Water Conductivity	2017-04-05 19:48 to Present (2019)		
			Water Temperature	2000-04-10 14:00 to Present (2019)		
2	Cape May, NJ	8536110	Verified Hourly Water Level	1972-04-06 09:00 to 2002-12-10 23:00 2003-04-01 00:00 to Present (2019)	~ 4	The data collected at Cape May were not considered for calibration due to the configuration of the model grid.
			Water Conductivity	2017-04-26 18:18 to Present (2019)		
			Water Temperature	1997-05-22 15:00 to Present (2019)		
3	Brandywine Shoal Light, DE	8555889	Verified Hourly Water Level	2002-07-01 00:00 to 2012-10-29 12:00 2014-11-12 20:00 to 2016-06-23 17:00 2017-06-20 18:00 to Present (2019)	10.0	
			Water Conductivity	2002-06-24 07:00 to 2002-09-09 15:06 2002-12-13 16:00 to 2012-10-29 12:00 2014-11-12 18:24 to 2016-01-23 12:06		
			Water Temperature	2002-11-06 19:54 to 2004-04-30 23:00 2004-08-26 13:42 to 2012-10-29 12:00 2014-11-21 19:30 to 2016-01-23 12:06		
4	Ship John Shoal, NJ	8537121	Verified Hourly Water Level	2002-08-14 19:00 to 2009-05-11 14:00 2009-11-07 16:00 to Present (2019)	37.0	
			Water Conductivity	2002-07-17 21:00 to 2009-05-11 14:42 2009-11-09 17:18 to 2014-09-20 00:30 2015-12-16 18:24 to 2018-02-03 08:54 2018-07-27 15:42 to 2018-10-18 07:36		

No.	Station	Station ID	Data Type	Data Inventory for Period Covers Calibration	DRBC River Mile	Comments
			Water Temperature	2002-07-17 21:00 to 2002-07-24 14:00 2002-11-06 19:00 to 2003-10-02 12:54 2004-05-24 01:00 to 2004-05-25 01:00 2006-03-21 20:54 to 2009-05-11 14:42 2009-11-07 15:30 to 2018-02-03 08:54 2018-07-27 13:42 to Present (2019)		
5	Reedy Point, DE	8551910	Verified Hourly Water Level	1980-05-13 17:06 to Present (2019)	~ 58.5 East end of C&D Canal	
			Water Conductivity	N/A		
			Water Temperature	1994-06-22 15:00 to Present (2019)		
6	Chesapeake City, MD	8573927	Verified Hourly Water Level	2003-08-29 19:00 to Present (2019)	West end of C&D Canal	
			Water Conductivity	2017-03-22 13:24 to Present (2019)		
			Water Temperature	2003-08-29 20:24 to Present (2019)		
7	Delaware City, DE	8551762	Verified Hourly Water Level	2001-10-16 15:00 to Present (2019)	60.5	Data were used for specification of model boundary conditions.
			Water Conductivity	N/A		
			Water Temperature	2001-10-16 11:00 to Present (2019)		
8	Marcus Hook, PA	8540433	Verified Hourly Water Level	2002-07-19 22:00 to 2015-07-07 14:00 2017-02-01 23:00 to Present (2019)	79.3	
			Water Conductivity	2002-06-14 20:00 to 2004-03-25 08:48 2004-07-03 08:00 to Present (2019)		
			Water Temperature	2002-09-23 13:18 to 2003-05-21 23:00 2004-05-24 01:00 to 2004-05-25 01:00 2006-03-21 20:54 to 2015-07-07 16:42 2017-02-01 23:00 to Present (2019)		
9	Philadelphia, PA	8545240	Verified Hourly Water Level	1989-03-01 00:00 to Present (2019)	98.5	
			Water Conductivity	N/A		
			Water Temperature	1997-06-06 18:00 to Present (2019)		
10	Bridesburg, PA	8546252	Verified Hourly Water Level	2016-01-04 18:00 tp present (2019)	104.4	Data were not considered for model calibration.
			Water Conductivity	N/A		

No.	Station	Station ID	Data Type	Data Inventory for Period Covers Calibration	DRBC River Mile	Comments
			Water Temperature	2016-01-04 17:24 to Present (2019)		
11	Burlington, Delaware River, NJ	8539094	Verified Hourly Water Level	2002-06-10 18:00 to Present (2019)	117.5	
			Water Conductivity	2002-08-15 18:48 to 2011-12-30 21:12		
			Water Temperature	2002-08-15 18:48 to 2004-04-01 12:06 2004-08-25 12:54 to Present (2019)		
12	Newbold, PA	8548989	Verified Hourly Water Level	2001-11-14 18:00 to Present (2019)	126.3	
			Water Conductivity	N/A		
			Water Temperature	2001-11-14 20:00 to Present (2019)		
<p><i>Notes:</i></p> <ol style="list-style-type: none"> <i>Bridesburg, PA (8546252) was not used for model calibration. This location of this station is close to the station at Philadelphia.</i> <i>Model calibration and validation periods are 2018-2019 and 2012.</i> <i>Data collected outside the model calibration periods were not included in the data inventory in this table and are not used in this study.</i> 						

Table D-2: Summary of Data from USGS Stations Used for Model Calibration

No.	Station	Station ID	Data Type	Data Inventory for Period Covers Calibration and Validation	DRBC River Mile	Comments
1	Delaware River at Trenton, NJ	USGS 01463500	Discharge	1981-10-01 to Present (2019)	134.3	15-min discharge data are available. Hourly discharge, water temperature and specific conductance were used for specification of river inflow boundary conditions.
			Specific conductance	2007-10-01 to Present (2019)		
			Water Temperature	2007-10-01 to Present (2019)		
2	Delaware River at Ben Franklin Bridge at Philadelphia, PA	USGS 01467200	Specific conductance	2007-10-01 to Present (2019)	100.1	
			Water Temperature	2007-10-01 to Present (2019)		
3	Delaware River at Fort Mifflin at Philadelphia, PA	USGS 01474703	Specific conductance	2007-10-01 to Present (2019)	91.9	
			Water Temperature	2007-10-01 to Present (2019)		
4	Delaware River at Chester, PA	USGS 01477050	Specific conductance	2007-10-01 to Present (2019)	83.6	
			Water Temperature	2007-10-01 to Present (2019)		
5	Delaware River at Reedy Island Jetty, DE	USGS 01482800	Specific conductance	2007-10-01 to Present (2019)	54.1	
			Water Temperature	2007-10-01 to Present (2019)		

Notes:

1. There are data gaps within the time period listed in the data inventory column.
2. Model calibration and validation periods are 2018-2019 and 2012.
3. Data collected outside model calibration and validation periods may not be included in the data inventory in this table and are not used in this study.

Table D-3: Summary of NOAA Current Velocity Data Used for Model Calibration

No.	Station	Station ID	Latitude	Logitude	Data Type	Sensor Type	Sensor Orientation	Period of Records for Calibration	DRBC River Mile	Comments
1	Philadelphia	db0301	39.946	-75.140	Current Velocity	Sontek ADP	Side (Shore-Mounted)	2012-05-31 to 2012-06-30	99.5	Approximate Sensor Depth = 4.57 m
2	Reedy Point	db0201	39.559	-75.551	Current Velocity	Workhorse ADCP	up	2012-01-01 to 2012-05-05	58	
3	Brown Shoal Light	db0501	38.922	-75.101	Current Velocity	Sontek ADP	up	2012-05-02 to 2012-07-13	6	
4	Delaware Bay Channel LB 10	db0502	38.939	-75.105	Current Velocity	Nortek ADP	down	2018-09-06 to 2019-02-25	6.5	

Notes:
 1. Station at Philadelphia has sensor orientated side way at a fixed depth.
 2. Model calibration and validation periods are 2018-2019 and 2012.
 3. Data collected outside model calibration and validation periods may not be included in the data inventory in this table and are not used in this study.

Appendix E: Bottom roughness height

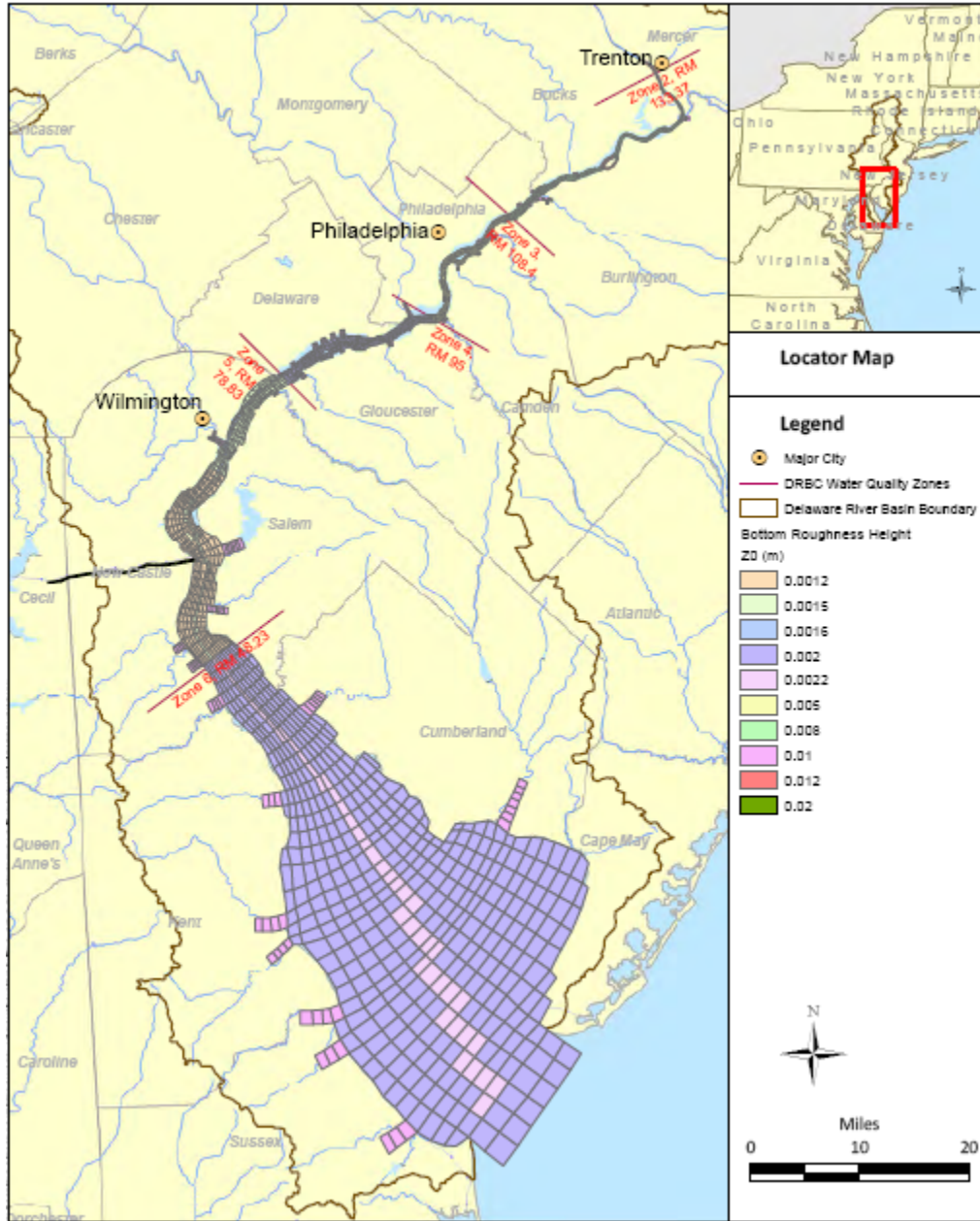


Figure E-1: Bottom Roughness Height

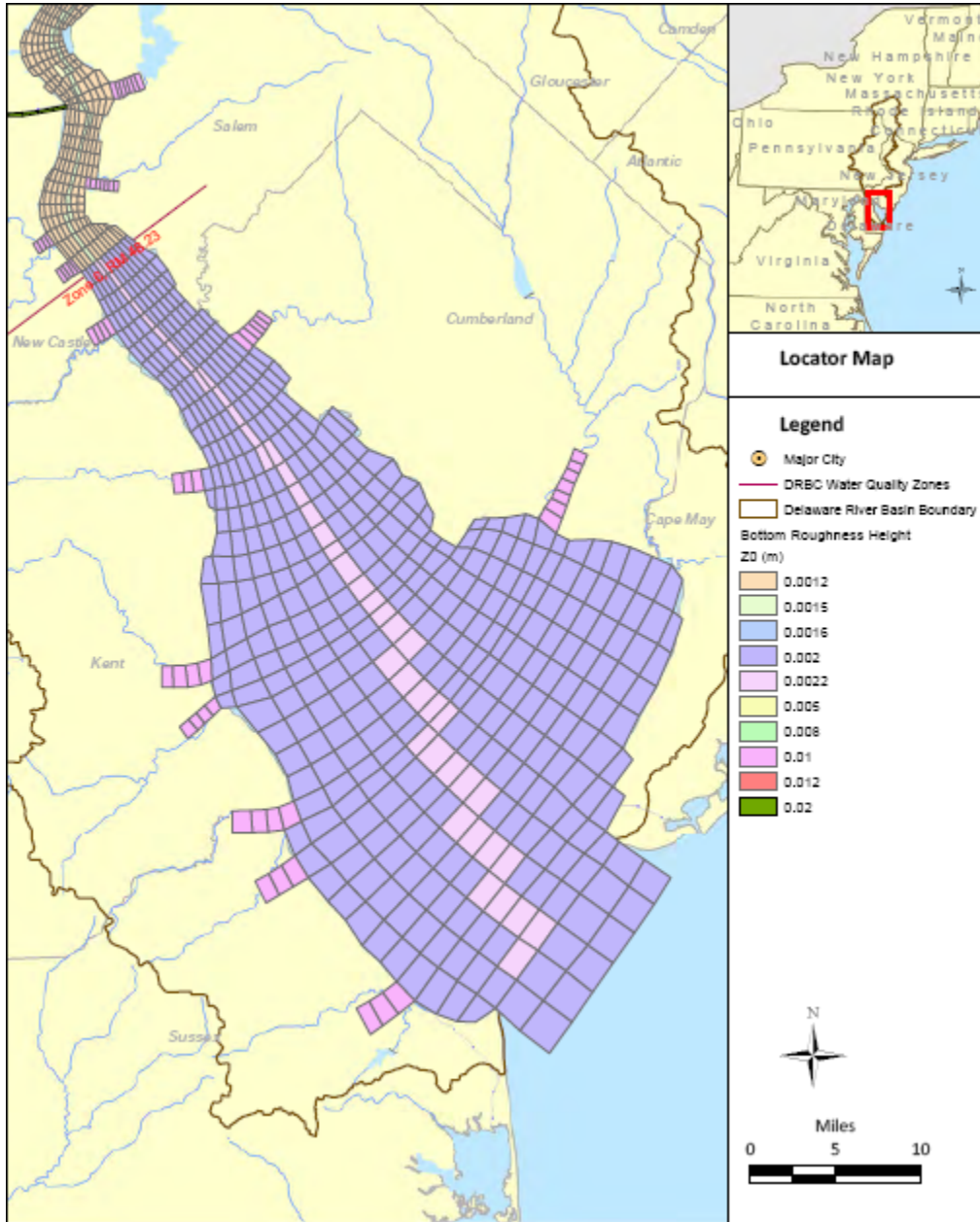


Figure E-2: Bottom Roughness Height, Zone 6

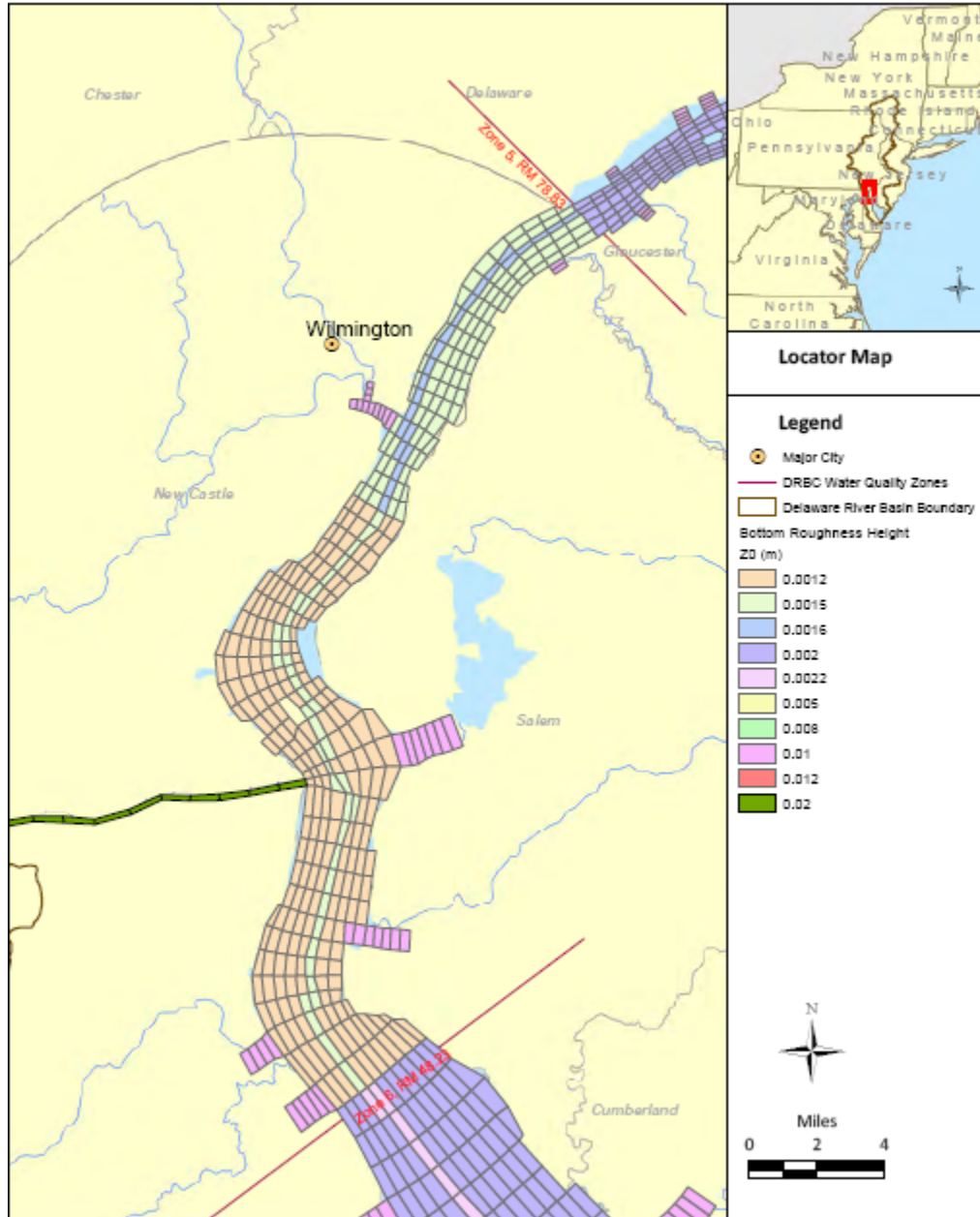


Figure E-3: Bottom Roughness Height, Zone 5

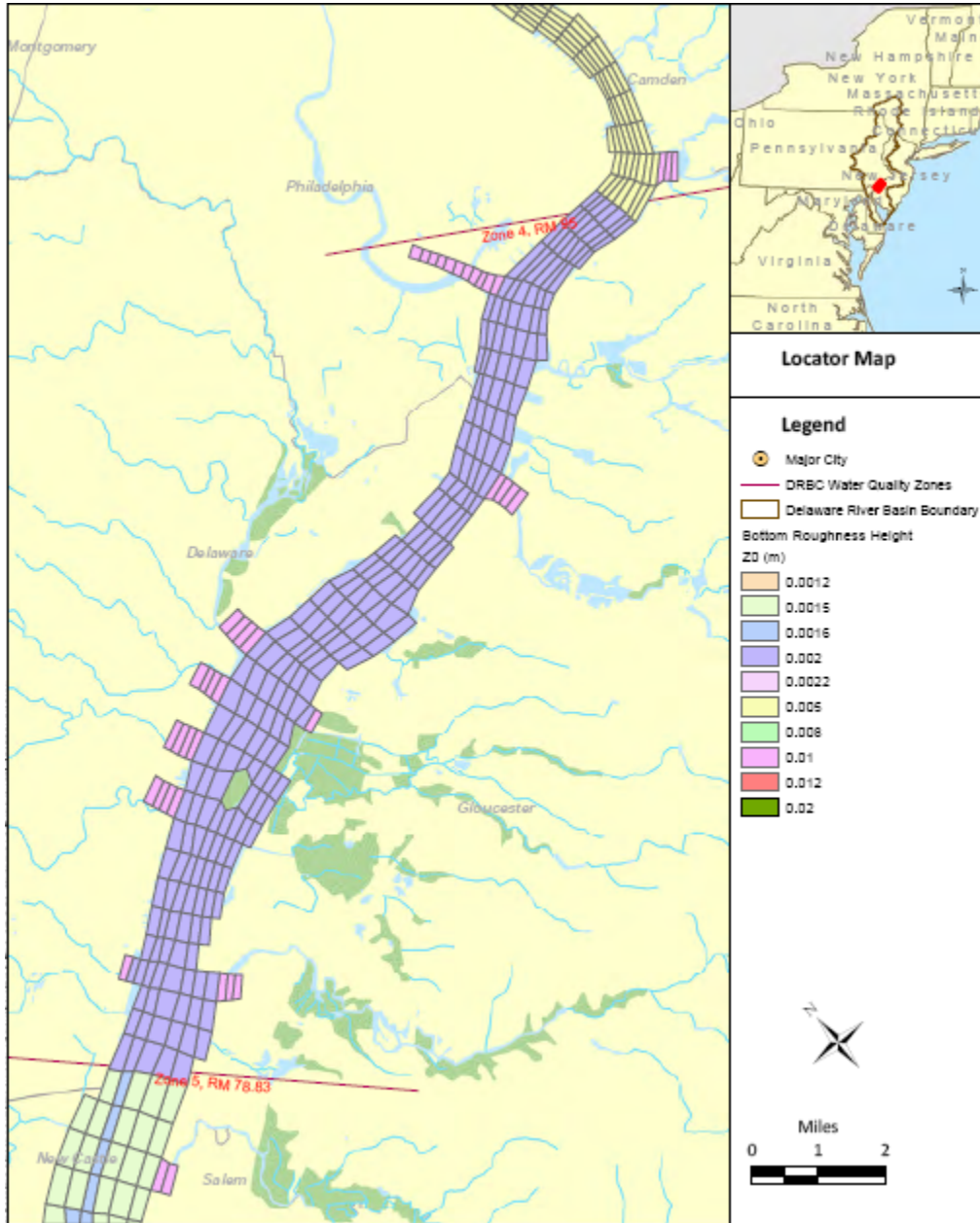


Figure E-4: Bottom Roughness Height, Zone 4

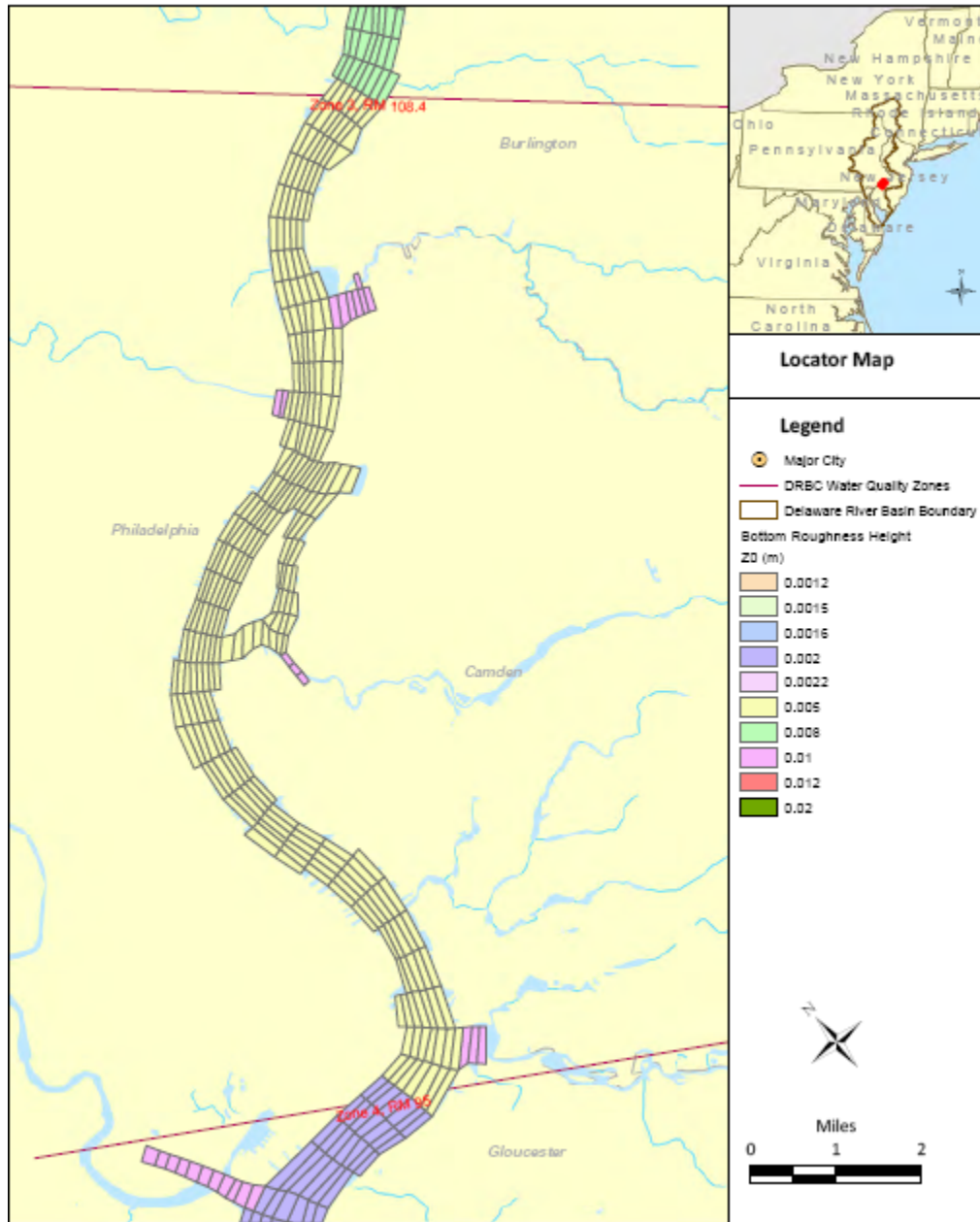


Figure E-5: Bottom Roughness Height, Zone 3

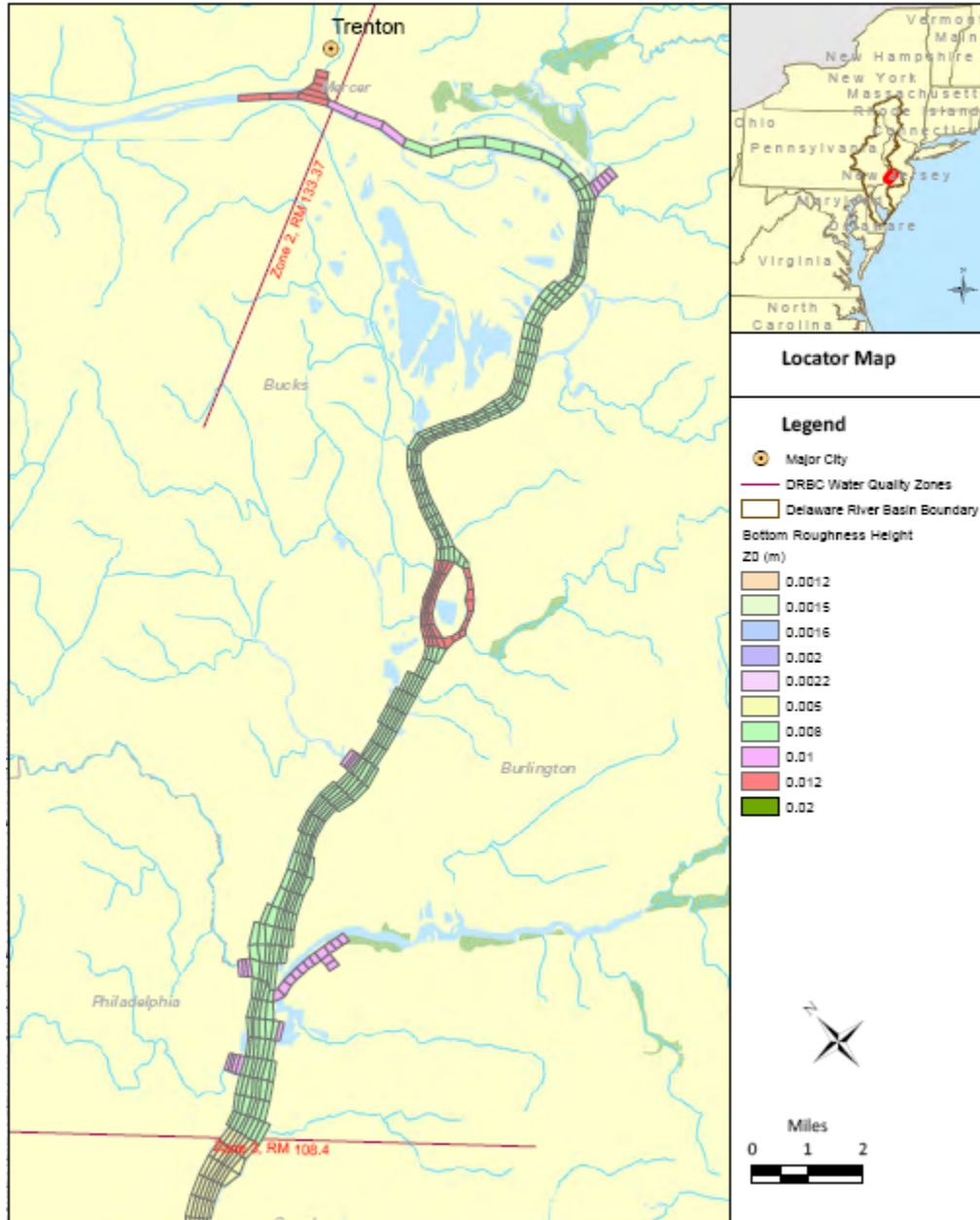


Figure E-6: Bottom Roughness Height, Zone 2

Appendix F: Summary of tidal harmonic analysis based on 2019 simulation

Table F-1: Summary of Tidal Harmonic Analysis based on Simulation of Year 2019

Note: Run id: EFDC_HYDRO_G72_2023-01-06

Station	Station ID	Tide	River Mile	Amplitude (m)			Phase (degree)			Phase (hours)		
				EFDC Predicted	Data	Difference (cm)	EFDC Predicted	Data	Difference (deg.)	EFDC Predicted	Data	Difference (hr.)
NOAA LEWES	8557380	M2	0	0.572	0.584	-1.230	34.400	31.550	2.850	1.187	1.089	0.098
NOAA LEWES	8557380	S2	0	0.099	0.106	-0.720	60.690	57.190	3.500	2.023	1.906	0.117
NOAA LEWES	8557380	N2	0	0.131	0.136	-0.500	12.100	8.890	3.210	0.425	0.313	0.113
NOAA LEWES	8557380	K1	0	0.110	0.104	0.570	202.810	201.420	1.390	13.484	13.391	0.092
NOAA LEWES	8557380	M4	0	0.000	0.011	-1.090	0.000	188.710	171.290	0.000	3.255	2.955
NOAA LEWES	8557380	O1	0	0.089	0.084	0.540	191.410	189.990	1.420	13.728	13.626	0.102
NOAA LEWES	8557380	M6	0	0.008	0.000	0.000	27.200	0.000	0.000	0.313	0.000	0.000
NOAA LEWES	8557380	Q1	0	0.015	0.014	0.090	182.220	179.930	2.290	13.600	13.429	0.171
NOAA LEWES	8557380	K2	0	0.028	0.029	-0.160	61.850	57.950	3.900	2.056	1.926	0.130
NOAA CAPE MAY	8536110	M2	2	0.713	0.696	1.680	36.850	28.850	8.000	1.271	0.995	0.276
NOAA CAPE MAY	8536110	S2	2	0.117	0.121	-0.410	67.620	55.860	11.760	2.254	1.862	0.392
NOAA CAPE MAY	8536110	N2	2	0.154	0.155	-0.060	16.390	8.440	7.950	0.576	0.297	0.280
NOAA CAPE MAY	8536110	K1	2	0.115	0.106	0.840	202.100	199.300	2.800	13.437	13.250	0.186
NOAA CAPE MAY	8536110	M4	2	0.016	0.012	0.400	108.020	101.380	6.640	1.863	1.749	0.115
NOAA CAPE MAY	8536110	O1	2	0.091	0.085	0.590	190.870	186.930	3.940	13.689	13.407	0.283
NOAA CAPE MAY	8536110	M6	2	0.000	0.000	0.000	0.000	0.000	0.000	0.000	0.000	0.000
NOAA CAPE MAY	8536110	Q1	2	0.015	0.014	0.130	184.030	180.060	3.970	13.735	13.439	0.296
NOAA CAPE MAY	8536110	K2	2	0.032	0.034	-0.170	66.540	53.850	12.690	2.212	1.790	0.422
NOAA BRANDYWINE	8555889	M2	10	0.728	0.702	2.610	43.320	37.550	5.770	1.495	1.296	0.199
NOAA BRANDYWINE	8555889	S2	10	0.118	0.120	-0.170	74.160	63.890	10.270	2.472	2.130	0.342
NOAA BRANDYWINE	8555889	N2	10	0.157	0.155	0.180	22.590	16.250	6.340	0.794	0.571	0.223
NOAA BRANDYWINE	8555889	K1	10	0.117	0.109	0.790	204.580	202.480	2.100	13.601	13.462	0.140
NOAA BRANDYWINE	8555889	M4	10	0.000	0.000	0.000	0.000	0.000	0.000	0.000	0.000	0.000

Hydrodynamics Model of the Delaware River Estuary

Station	Station ID	Tide	River Mile	Amplitude (m)			Phase (degree)			Phase (hours)		
				EFDC Predicted	Data	Difference (cm)	EFDC Predicted	Data	Difference (deg.)	EFDC Predicted	Data	Difference (hr.)
NOAA BRANDYWINE	8555889	O1	10	0.094	0.086	0.740	193.430	190.420	3.010	13.873	13.657	0.216
NOAA BRANDYWINE	8555889	M6	10	0.000	0.000	0.000	0.000	0.000	0.000	0.000	0.000	0.000
NOAA BRANDYWINE	8555889	Q1	10	0.016	0.014	0.140	186.900	183.140	3.760	13.949	13.669	0.281
NOAA BRANDYWINE	8555889	K2	10	0.032	0.034	-0.190	73.560	63.740	9.820	2.445	2.119	0.326
NOAA SHIP JOHN SHOAL	8537121	M2	37	0.909	0.822	8.760	74.280	71.760	2.520	2.563	2.476	0.087
NOAA SHIP JOHN SHOAL	8537121	S2	37	0.133	0.122	1.110	115.050	104.350	10.700	3.835	3.478	0.357
NOAA SHIP JOHN SHOAL	8537121	N2	37	0.176	0.162	1.420	56.400	53.690	2.710	1.983	1.888	0.095
NOAA SHIP JOHN SHOAL	8537121	K1	37	0.120	0.114	0.600	218.280	220.370	-2.090	14.512	14.651	-0.139
NOAA SHIP JOHN SHOAL	8537121	M4	37	0.051	0.034	1.660	75.760	32.310	43.450	1.307	0.557	0.750
NOAA SHIP JOHN SHOAL	8537121	O1	37	0.095	0.087	0.750	206.480	207.760	-1.280	14.809	14.901	-0.092
NOAA SHIP JOHN SHOAL	8537121	M6	37	0.023	0.020	0.340	277.150	274.790	2.360	3.187	3.160	0.027
NOAA SHIP JOHN SHOAL	8537121	Q1	37	0.014	0.014	0.000	208.320	199.270	9.050	15.548	14.872	0.675
NOAA SHIP JOHN SHOAL	8537121	K2	37	0.036	0.037	-0.070	110.540	103.650	6.890	3.675	3.446	0.229
NOAA REEDY POINT	8551910	M2	58.5	0.849	0.780	6.860	107.510	107.960	-0.450	3.709	3.725	-0.016
NOAA REEDY POINT	8551910	S2	58.5	0.113	0.102	1.020	151.700	142.100	9.600	5.057	4.737	0.320
NOAA REEDY POINT	8551910	N2	58.5	0.152	0.144	0.810	91.630	90.230	1.400	3.222	3.173	0.049
NOAA REEDY POINT	8551910	K1	58.5	0.094	0.096	-0.270	238.450	242.860	-4.410	15.853	16.146	-0.293
NOAA REEDY POINT	8551910	M4	58.5	0.085	0.053	3.170	149.660	125.320	24.340	2.582	2.162	0.420
NOAA REEDY POINT	8551910	O1	58.5	0.074	0.072	0.190	223.690	228.540	-4.850	16.043	16.391	-0.348
NOAA REEDY POINT	8551910	M6	58.5	0.030	0.031	-0.120	53.520	51.650	1.870	0.616	0.594	0.022
NOAA REEDY POINT	8551910	Q1	58.5	0.010	0.012	-0.210	234.780	228.430	6.350	17.523	17.049	0.474
NOAA REEDY POINT	8551910	K2	58.5	0.032	0.034	-0.200	141.290	139.290	2.000	4.697	4.630	0.066
NOAA DELAWARE CITY	8551762	M2	60.7	0.852	0.785	6.630	114.200	113.210	0.990	3.940	3.906	0.034
NOAA DELAWARE CITY	8551762	S2	60.7	0.112	0.103	0.900	159.300	147.460	11.840	5.310	4.915	0.395
NOAA DELAWARE CITY	8551762	N2	60.7	0.152	0.144	0.760	98.470	95.190	3.280	3.462	3.347	0.115
NOAA DELAWARE CITY	8551762	K1	60.7	0.107	0.107	-0.050	242.450	244.580	-2.130	16.119	16.261	-0.142

Hydrodynamics Model of the Delaware River Estuary

Station	Station ID	Tide	River Mile	Amplitude (m)			Phase (degree)			Phase (hours)		
				EFDC Predicted	Data	Difference (cm)	EFDC Predicted	Data	Difference (deg.)	EFDC Predicted	Data	Difference (hr.)
NOAA DELAWARE CITY	8551762	M4	60.7	0.092	0.065	2.690	162.490	139.340	23.150	2.803	2.404	0.399
NOAA DELAWARE CITY	8551762	O1	60.7	0.086	0.085	0.120	228.900	231.470	-2.570	16.417	16.601	-0.184
NOAA DELAWARE CITY	8551762	M6	60.7	0.031	0.032	-0.060	54.930	59.280	-4.350	0.632	0.682	-0.050
NOAA DELAWARE CITY	8551762	Q1	60.7	0.012	0.013	-0.140	237.500	225.230	12.270	17.726	16.810	0.916
NOAA DELAWARE CITY	8551762	K2	60.7	0.032	0.034	-0.280	148.820	142.820	6.000	4.947	4.748	0.199
NOAA MARCUS HOOK	8540433	M2	79.3	0.790	0.781	0.840	151.190	146.700	4.490	5.216	5.061	0.155
NOAA MARCUS HOOK	8540433	S2	79.3	0.097	0.096	0.120	198.000	181.890	16.110	6.600	6.063	0.537
NOAA MARCUS HOOK	8540433	N2	79.3	0.137	0.140	-0.370	134.760	127.490	7.270	4.738	4.483	0.256
NOAA MARCUS HOOK	8540433	K1	79.3	0.107	0.108	-0.140	262.610	262.240	0.370	17.460	17.435	0.025
NOAA MARCUS HOOK	8540433	M4	79.3	0.119	0.091	2.830	220.880	194.840	26.040	3.810	3.361	0.449
NOAA MARCUS HOOK	8540433	O1	79.3	0.086	0.086	0.070	247.610	248.320	-0.710	17.759	17.810	-0.051
NOAA MARCUS HOOK	8540433	M6	79.3	0.032	0.035	-0.260	151.100	158.200	-7.100	1.738	1.819	-0.082
NOAA MARCUS HOOK	8540433	Q1	79.3	0.011	0.013	-0.170	256.230	244.220	12.010	19.124	18.227	0.896
NOAA MARCUS HOOK	8540433	K2	79.3	0.028	0.033	-0.530	186.020	176.840	9.180	6.184	5.879	0.305
NOAA PHILADELPHIA	8545240	M2	98.5	0.837	0.834	0.280	189.700	183.760	5.940	6.545	6.340	0.205
NOAA PHILADELPHIA	8545240	S2	98.5	0.097	0.094	0.370	241.950	222.670	19.280	8.065	7.422	0.643
NOAA PHILADELPHIA	8545240	N2	98.5	0.139	0.143	-0.420	173.330	164.590	8.740	6.095	5.787	0.307
NOAA PHILADELPHIA	8545240	K1	98.5	0.110	0.112	-0.200	280.100	281.310	-1.210	18.622	18.703	-0.080
NOAA PHILADELPHIA	8545240	M4	98.5	0.083	0.084	-0.050	289.540	252.610	36.930	4.995	4.358	0.637
NOAA PHILADELPHIA	8545240	O1	98.5	0.087	0.087	-0.010	262.960	265.850	-2.890	18.860	19.067	-0.207
NOAA PHILADELPHIA	8545240	M6	98.5	0.038	0.049	-1.100	235.830	246.240	-10.410	2.712	2.832	-0.120
NOAA PHILADELPHIA	8545240	Q1	98.5	0.011	0.013	-0.190	272.440	263.630	8.810	20.333	19.676	0.658
NOAA PHILADELPHIA	8545240	K2	98.5	0.027	0.033	-0.550	228.130	215.220	12.910	7.584	7.154	0.429
NOAA BURLINGTON	8539094	M2	117.5	1.027	1.001	2.640	213.220	213.460	-0.240	7.356	7.365	-0.008
NOAA BURLINGTON	8539094	S2	117.5	0.123	0.117	0.650	269.830	258.390	11.440	8.994	8.613	0.381
NOAA BURLINGTON	8539094	N2	117.5	0.167	0.166	0.130	198.470	196.140	2.330	6.979	6.897	0.082

Station	Station ID	Tide	River Mile	Amplitude (m)			Phase (degree)			Phase (hours)		
				EFDC Predicted	Data	Difference (cm)	EFDC Predicted	Data	Difference (deg.)	EFDC Predicted	Data	Difference (hr.)
NOAA BURLINGTON	8539094	K1	117.5	0.117	0.115	0.120	290.420	296.200	-5.780	19.308	19.693	-0.384
NOAA BURLINGTON	8539094	M4	117.5	0.168	0.123	4.510	6.020	338.140	27.880	0.104	5.833	0.481
NOAA BURLINGTON	8539094	O1	117.5	0.090	0.089	0.120	272.510	279.370	-6.860	19.545	20.037	-0.492
NOAA BURLINGTON	8539094	M6	117.5	0.025	0.028	-0.310	329.020	347.770	-18.750	3.784	4.000	-0.216
NOAA BURLINGTON	8539094	Q1	117.5	0.012	0.014	-0.200	282.620	277.470	5.150	21.093	20.709	0.384
NOAA BURLINGTON	8539094	K2	117.5	0.033	0.038	-0.480	256.330	248.510	7.820	8.521	8.261	0.260
NOAA NEWBOLD	8548989	M2	126.3	1.090	1.080	1.060	217.070	218.320	-1.250	7.489	7.532	-0.043
NOAA NEWBOLD	8548989	S2	126.3	0.133	0.123	1.020	273.660	263.300	10.360	9.122	8.777	0.345
NOAA NEWBOLD	8548989	N2	126.3	0.178	0.180	-0.190	203.060	201.630	1.430	7.140	7.090	0.050
NOAA NEWBOLD	8548989	K1	126.3	0.119	0.117	0.160	292.260	297.720	-5.460	19.431	19.794	-0.363
NOAA NEWBOLD	8548989	M4	126.3	0.212	0.155	5.690	13.960	346.680	27.280	0.241	5.981	0.471
NOAA NEWBOLD	8548989	O1	126.3	0.091	0.093	-0.150	274.740	281.930	-7.190	19.704	20.220	-0.516
NOAA NEWBOLD	8548989	M6	126.3	0.037	0.062	-2.470	12.480	31.730	-19.250	0.144	0.365	-0.221
NOAA NEWBOLD	8548989	Q1	126.3	0.000	0.014	-1.380	0.000	280.550	79.450	0.000	20.939	5.930
NOAA NEWBOLD	8548989	K2	126.3	0.034	0.039	-0.480	260.210	254.090	6.120	8.650	8.447	0.203

Appendix G: Tidal harmonics analysis based on predicted 2019 water surface elevation

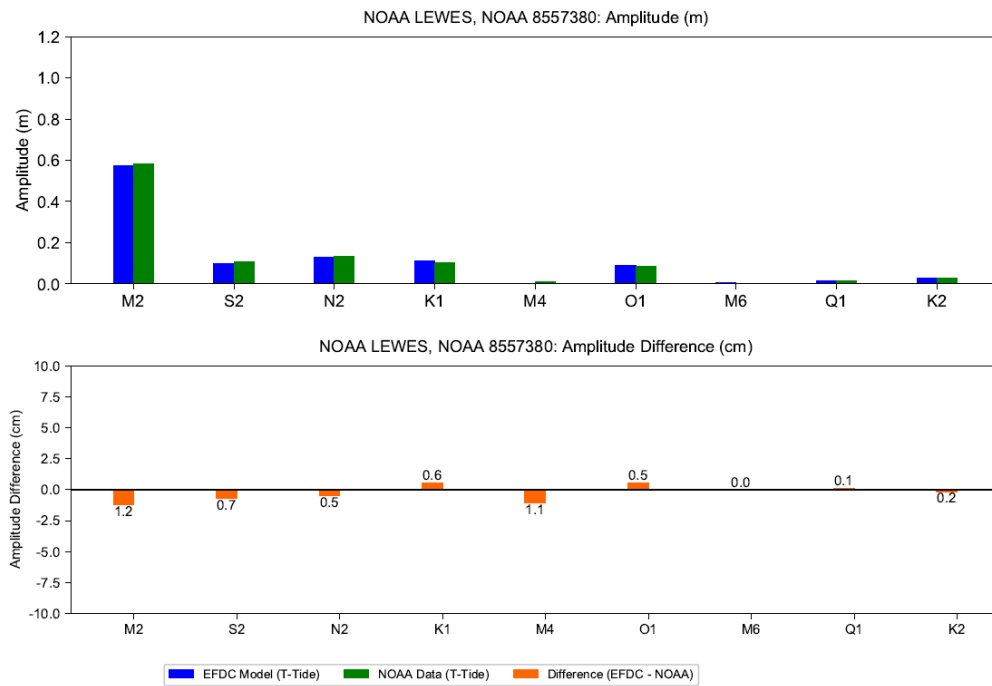


Figure G-1: Tidal Harmonics Analysis Based on Predicted Water Surface Elevation: Amplitude at NOAA LEWES, NOAA Station 8557380

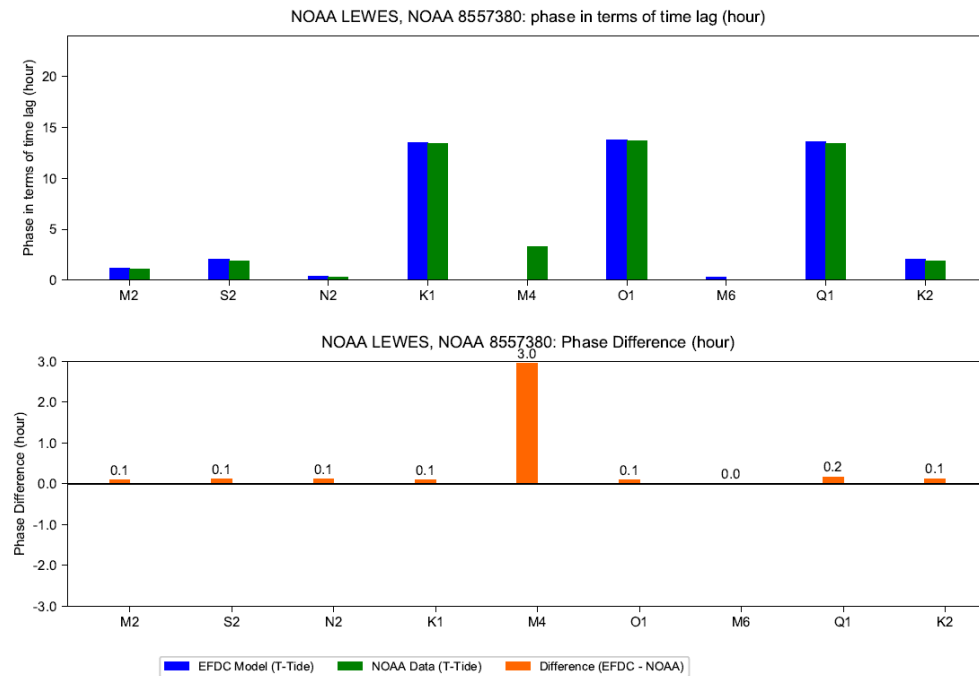


Figure G-2: Tidal Harmonics Analysis Based on Predicted Water Surface Elevation: Phase at NOAA LEWES, NOAA Station 8557380

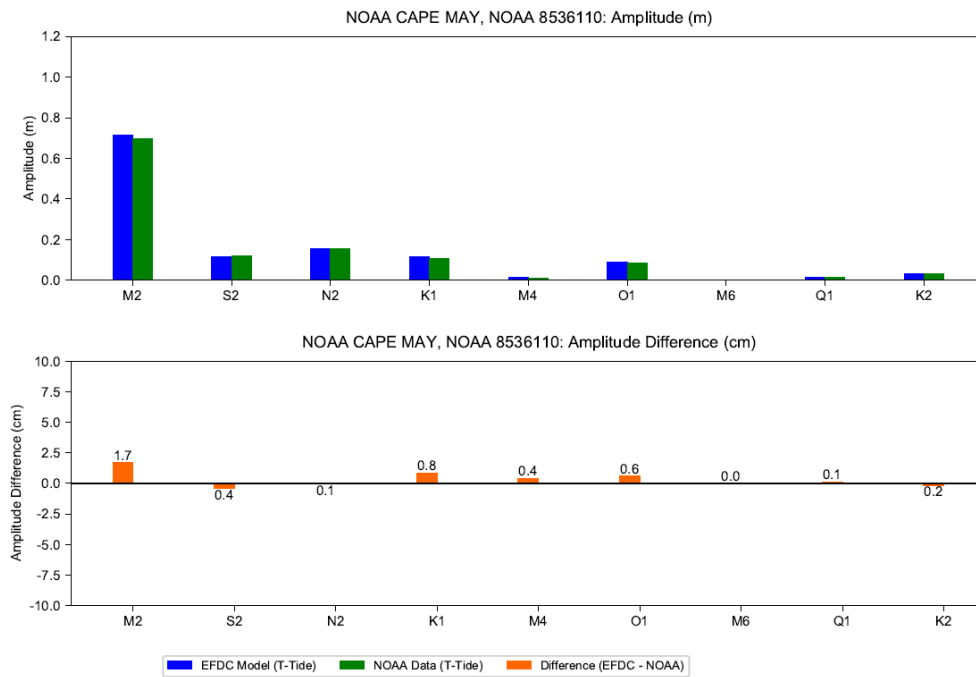


Figure G-3: Tidal Harmonics Analysis Based on Predicted Water Surface Elevation: Amplitude at NOAA CAPE MAY, NOAA Station 8536110

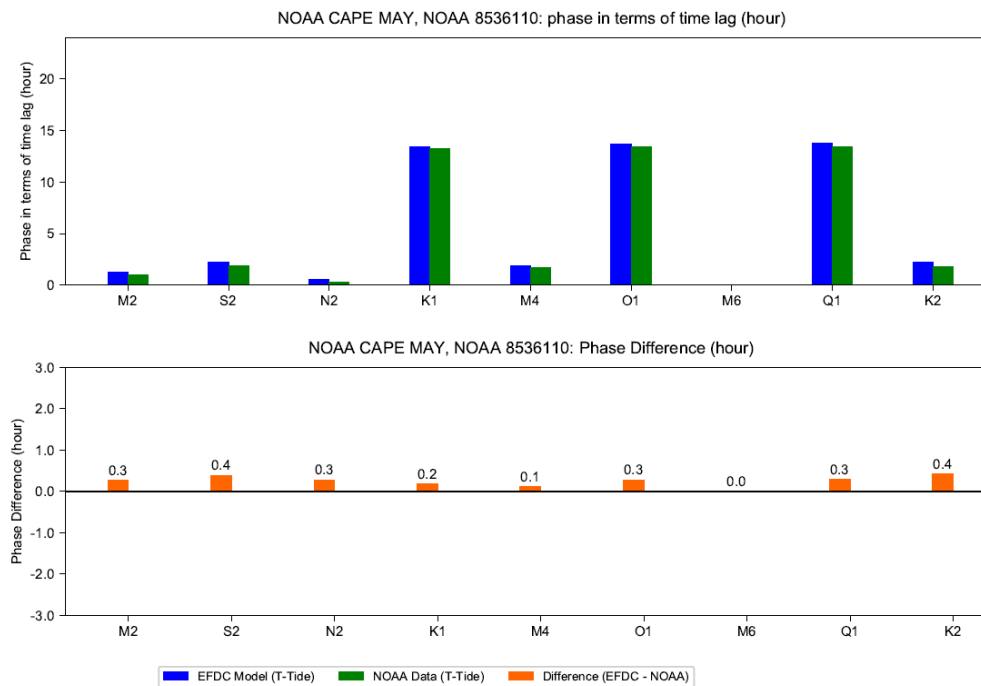


Figure G-4: Tidal Harmonics Analysis Based on Predicted Water Surface Elevation: Phase at NOAA CAPE MAY, NOAA Station 8536110

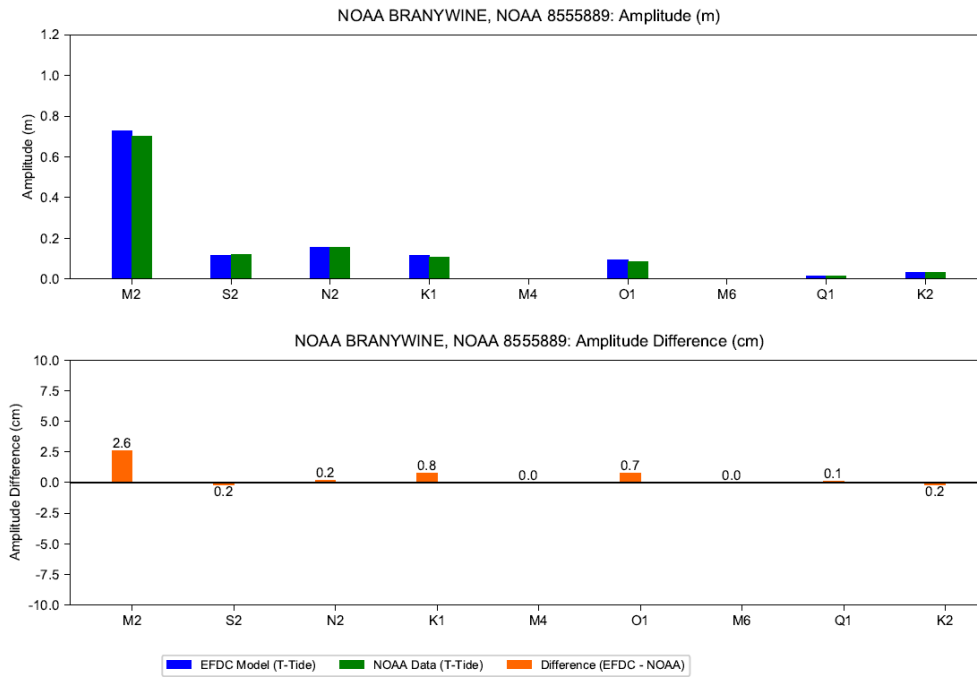


Figure G-5: Tidal Harmonics Analysis Based on Predicted Water Surface Elevation: Amplitude at NOAA BRANDYWINE, NOAA Station 8555889

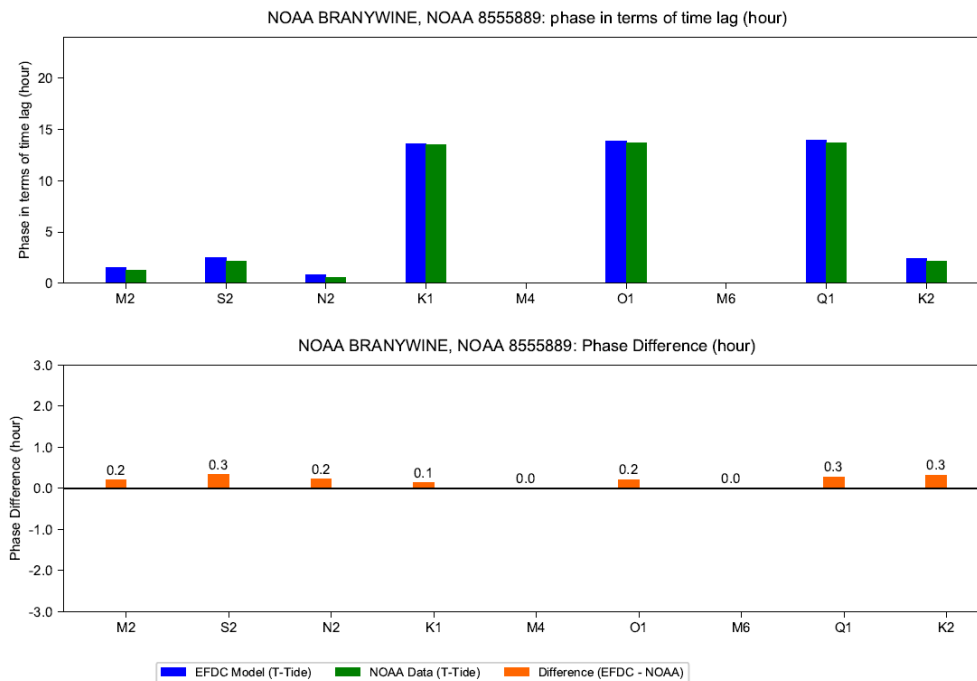


Figure G-6: Tidal Harmonics Analysis Based on Predicted Water Surface Elevation: Phase at NOAA BRANDYWINE, NOAA Station 8555889

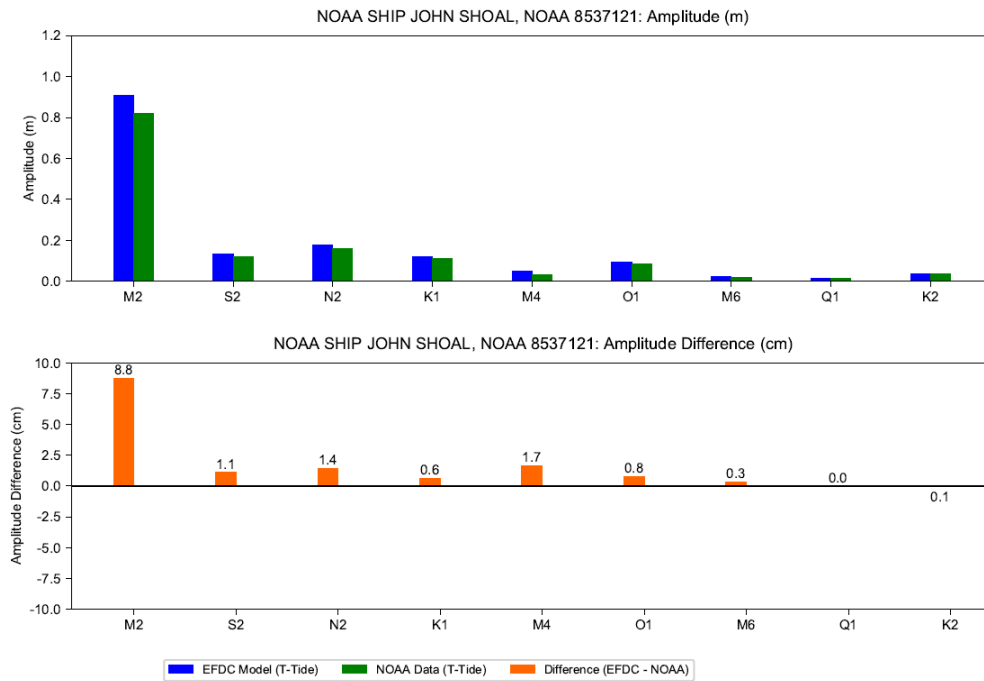


Figure G-7: Tidal Harmonics Analysis Based on Predicted Water Surface Elevation: Amplitude at NOAA SHIP JOHN SHOAL, NOAA Station 8537121

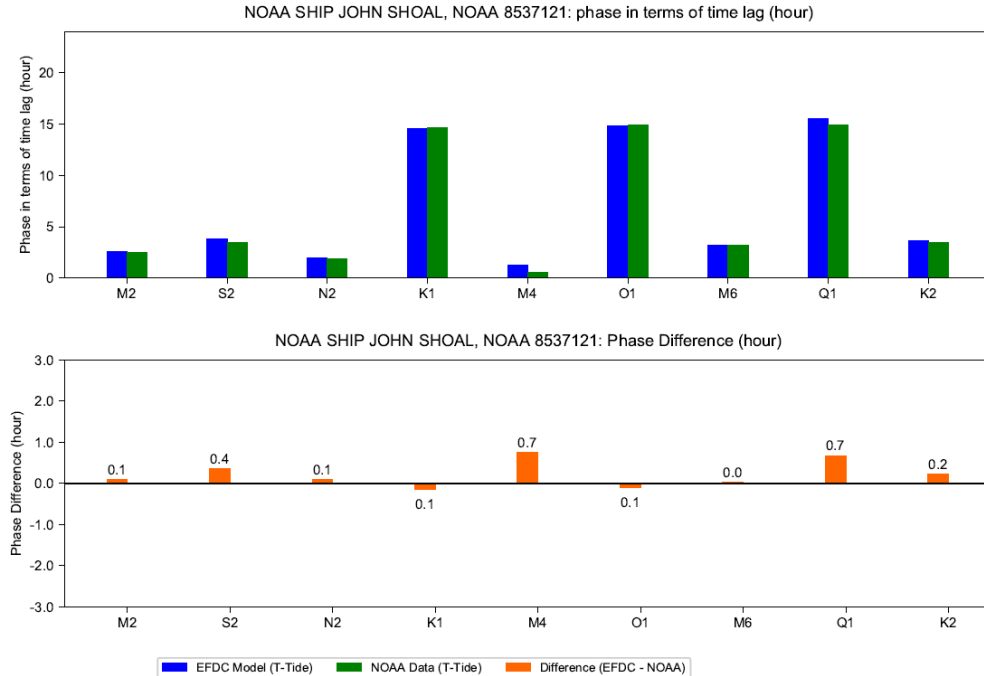


Figure G-8: Tidal Harmonics Analysis Based on Predicted Water Surface Elevation: Phase at NOAA SHIP JOHN SHOAL, NOAA Station 8537121

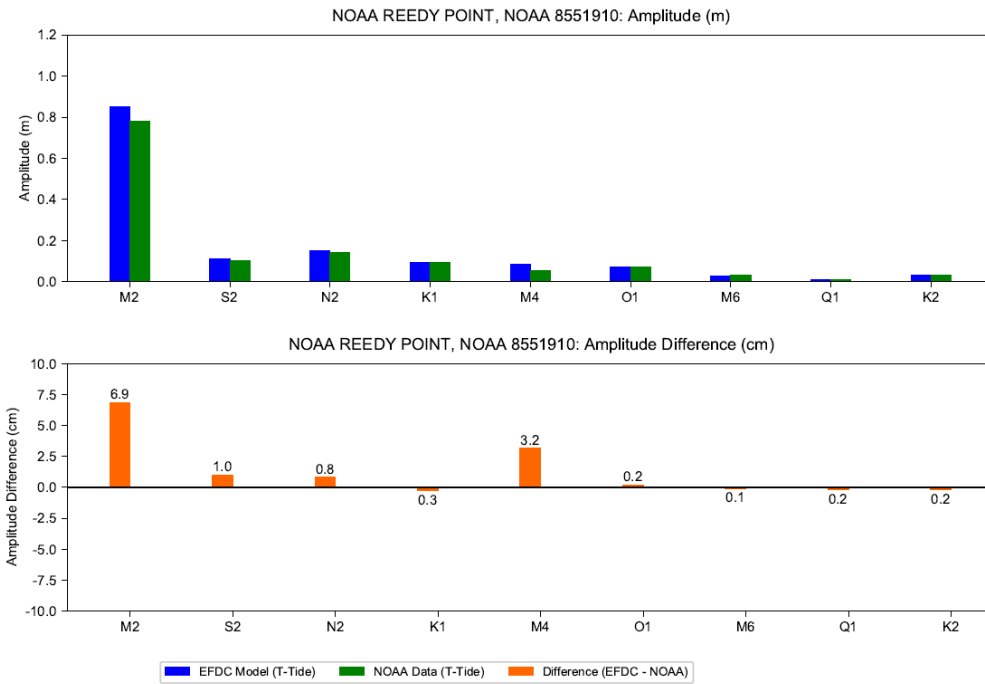


Figure G-9: Tidal Harmonics Analysis Based on Predicted Water Surface Elevation: Amplitude at NOAA REEDY POINT, NOAA Station 8551910

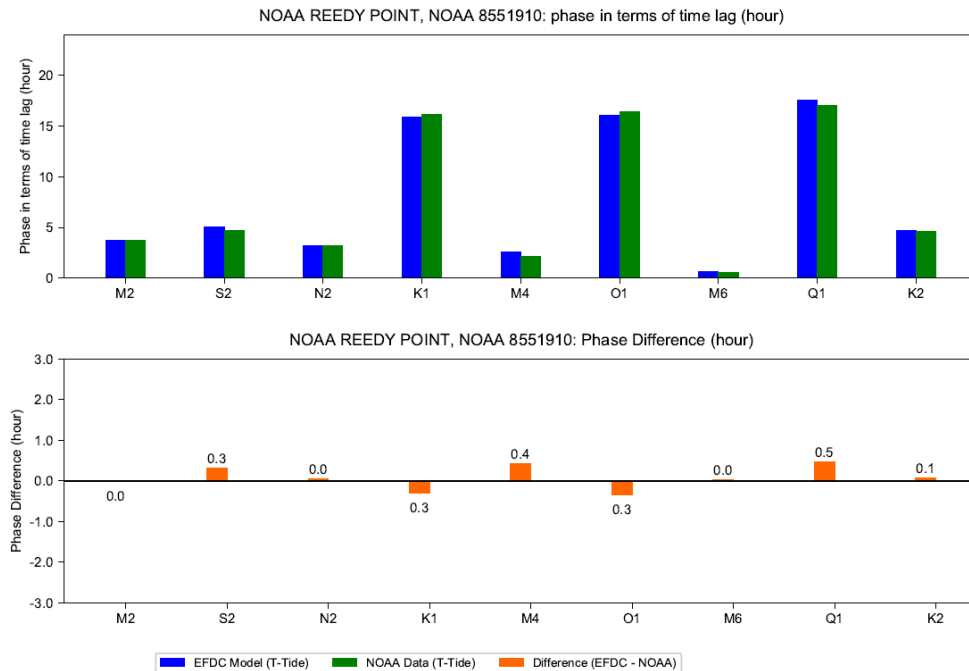


Figure G-10: Tidal Harmonics Analysis Based on Predicted Water Surface Elevation: Phase at NOAA REEDY POINT, NOAA Station 8551910

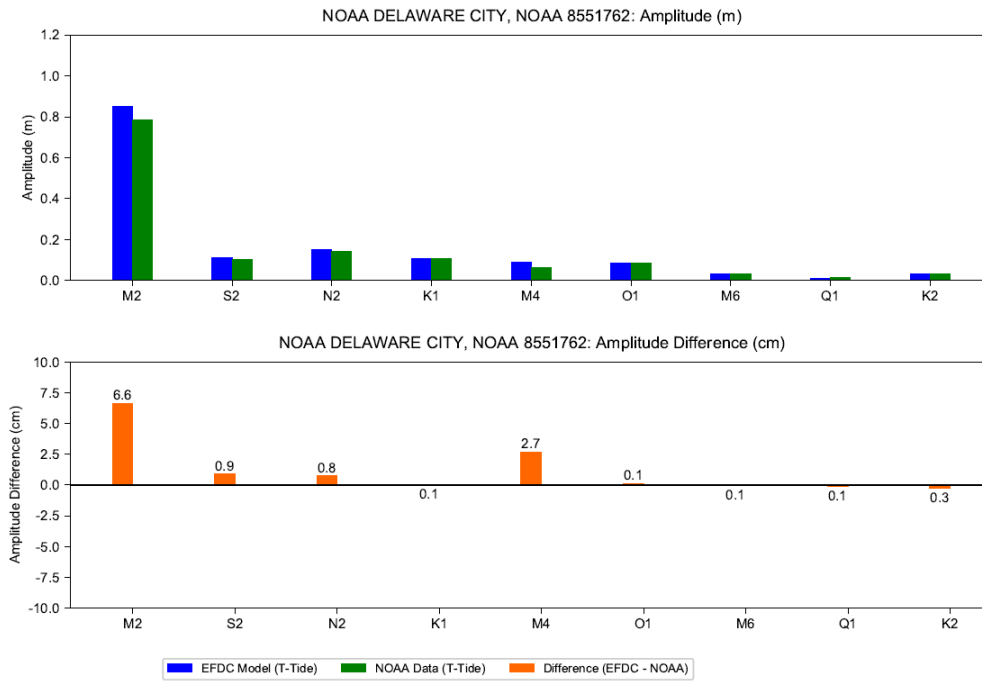


Figure G-11: Tidal Harmonics Analysis Based on Predicted Water Surface Elevation: Amplitude at NOAA DELAWARE CITY, NOAA Station 8551762

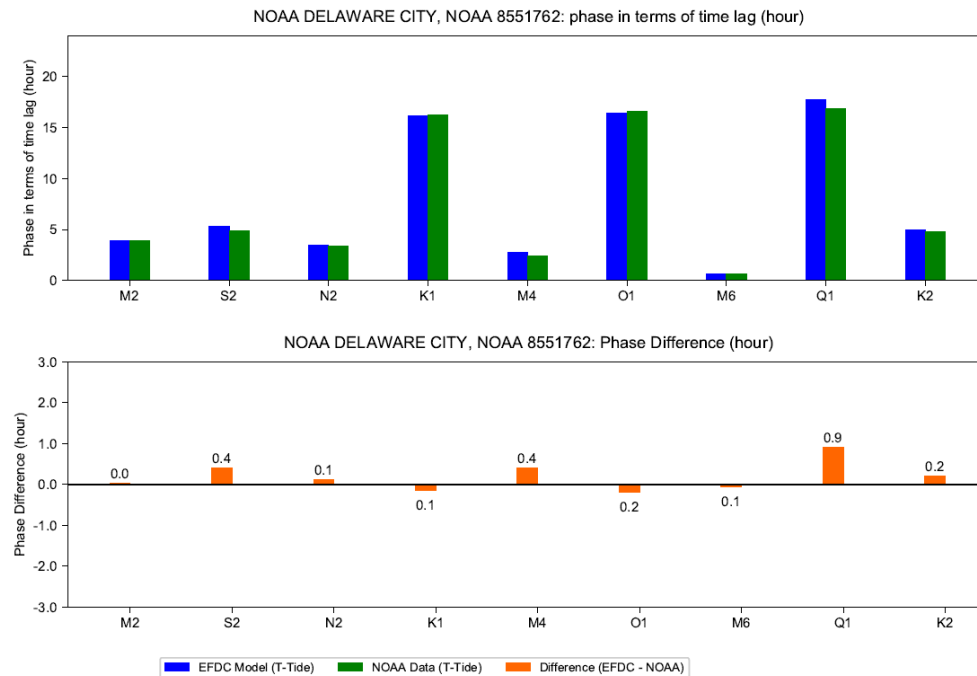


Figure G-12: Tidal Harmonics Analysis Based on Predicted Water Surface Elevation: Phase at NOAA DELAWARE CITY, NOAA Station 8551762

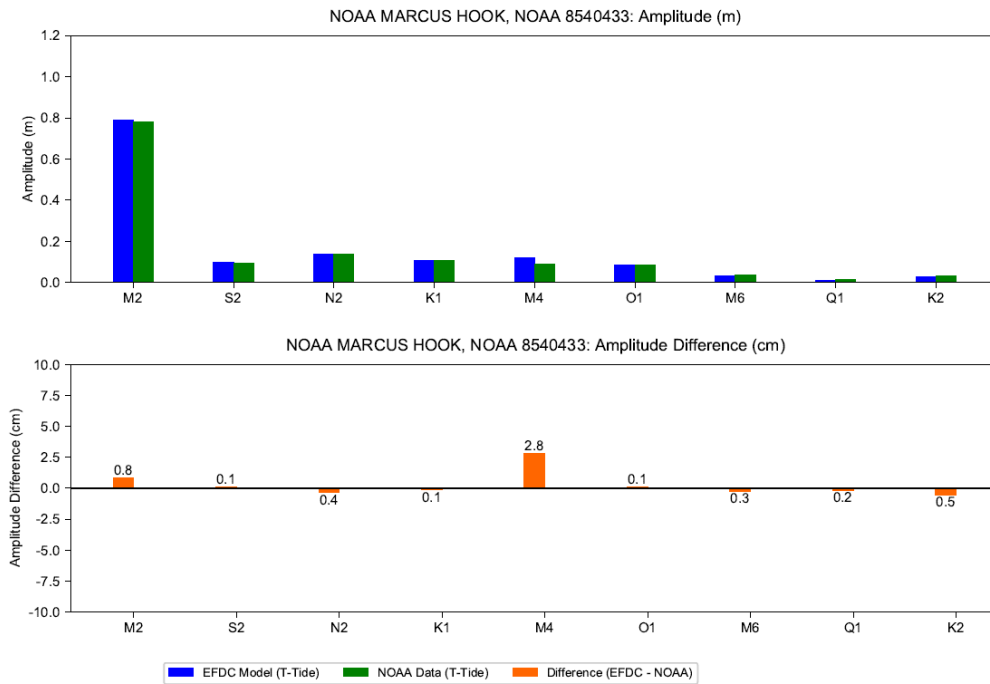


Figure G-13: Tidal Harmonics Analysis Based on Predicted Water Surface Elevation: Amplitude at NOAA MARCUS HOOK, NOAA Station 8540433

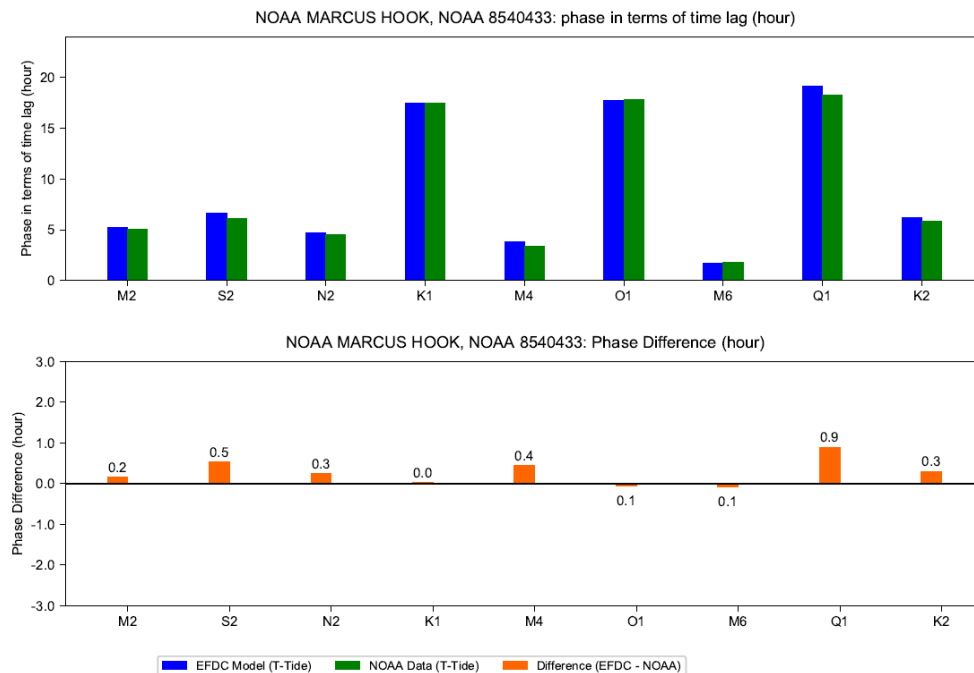


Figure G-14: Tidal Harmonics Analysis Based on Predicted Water Surface Elevation: Phase at NOAA MARCUS HOOK, NOAA Station 8540433

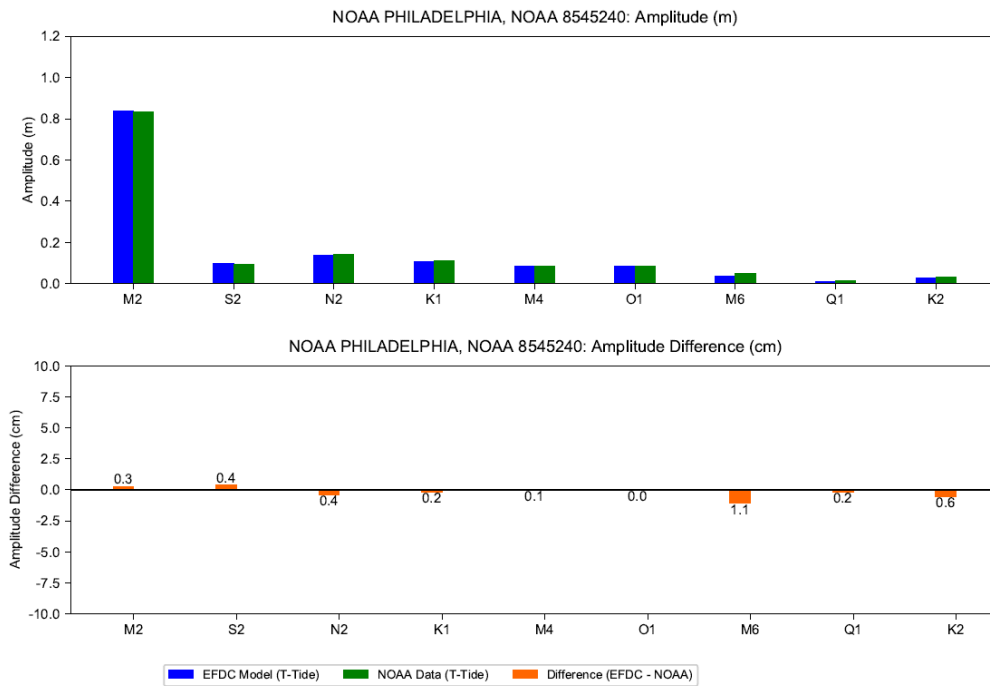


Figure G-15: Tidal Harmonics Analysis Based on Predicted Water Surface Elevation: Amplitude at NOAA PHILADELPHIA, NOAA Station 8545240

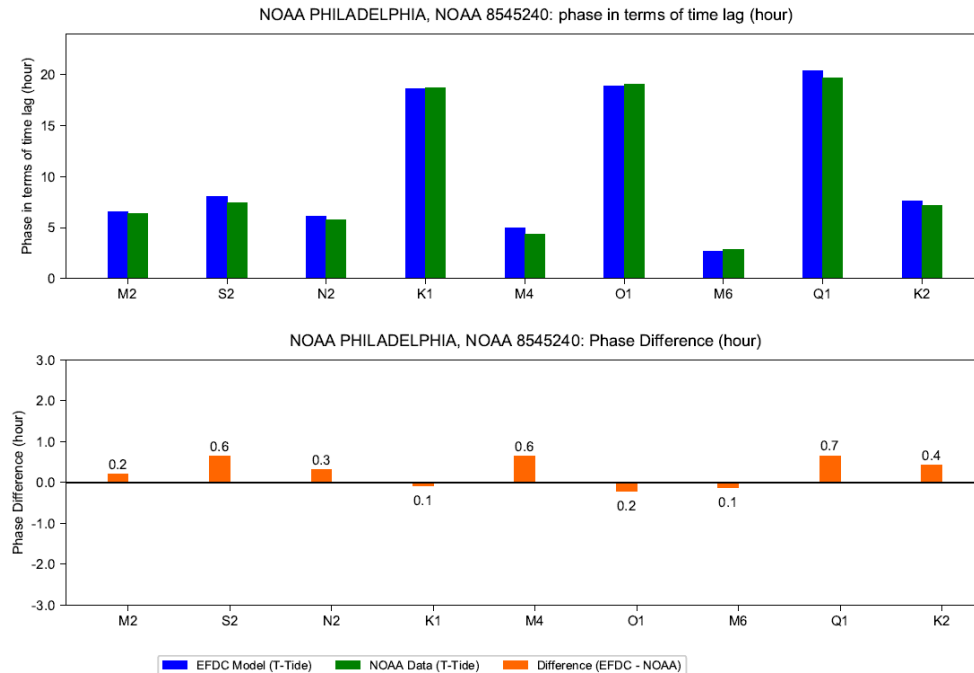


Figure G-16 Tidal Harmonics Analysis Based on Predicted Water Surface Elevation: Phase at NOAA PHILADELPHIA, NOAA Station 8545240

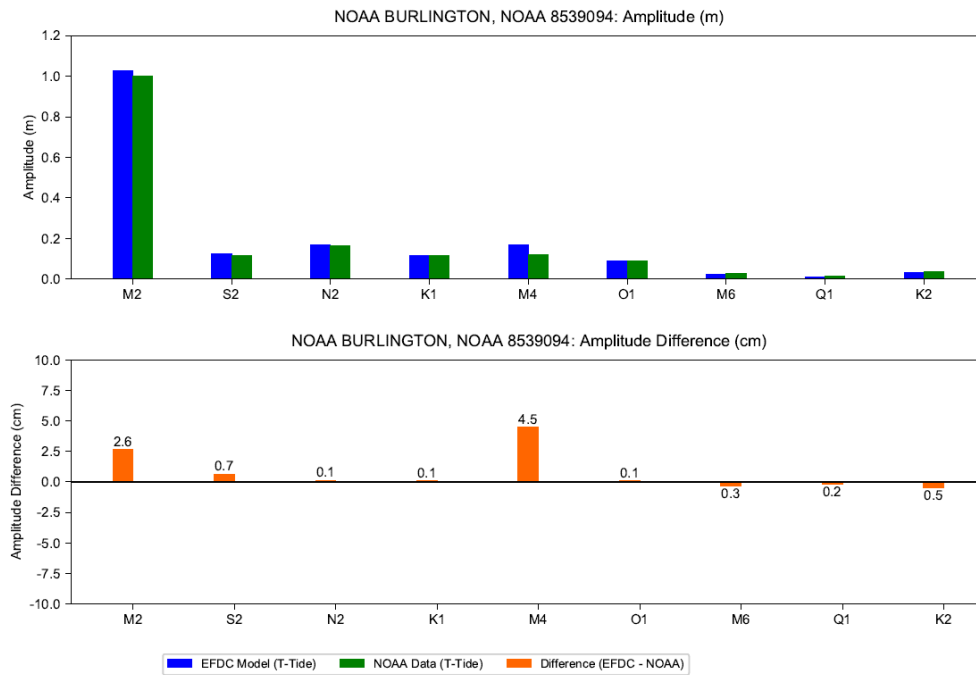


Figure G-17: Tidal Harmonics Analysis Based on Predicted Water Surface Elevation: Amplitude at NOAA BURLINGTON, NOAA Station 8539094

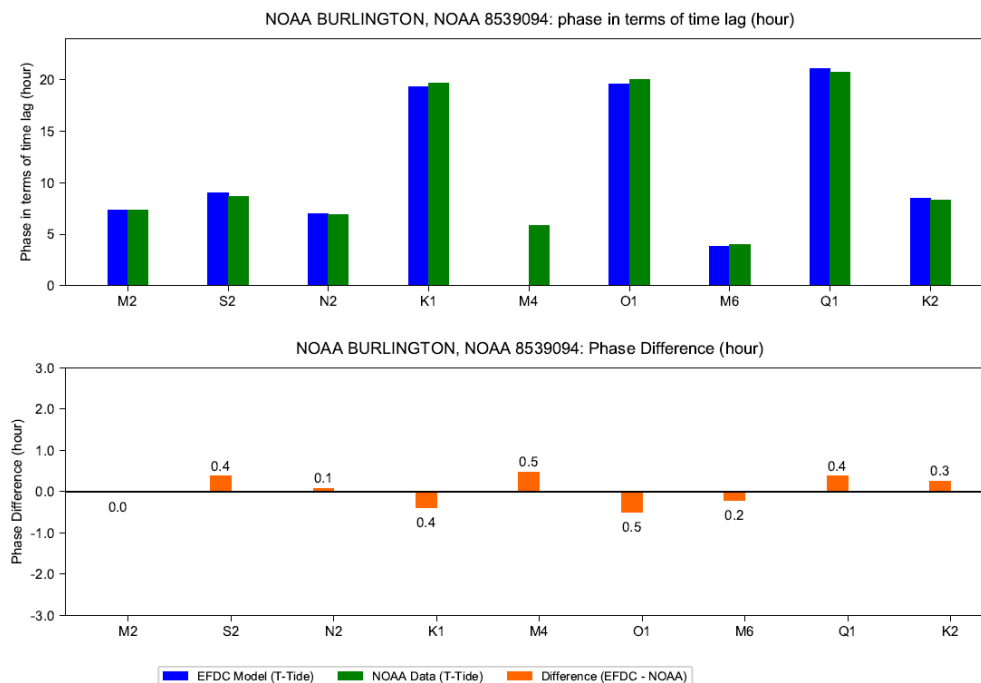


Figure G-18: Tidal Harmonics Analysis Based on Predicted Water Surface Elevation: Phase at NOAA BURLINGTON, NOAA Station 8539094

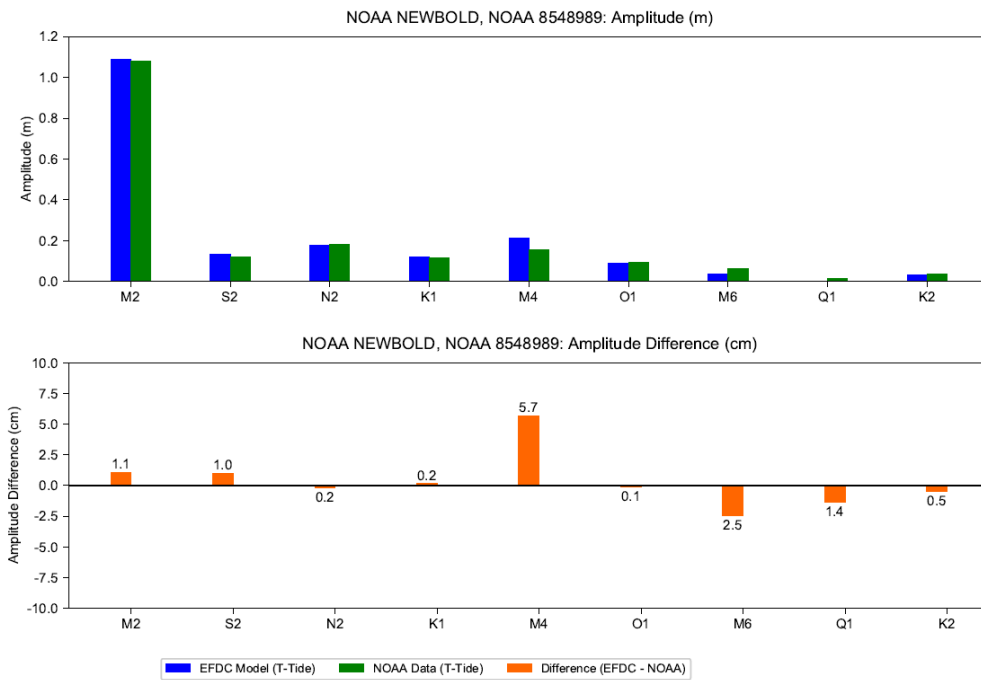


Figure G-19: Tidal Harmonics Analysis Based on Predicted Water Surface Elevation: Amplitude at NOAA NEWBOLD, NOAA Station 8548989

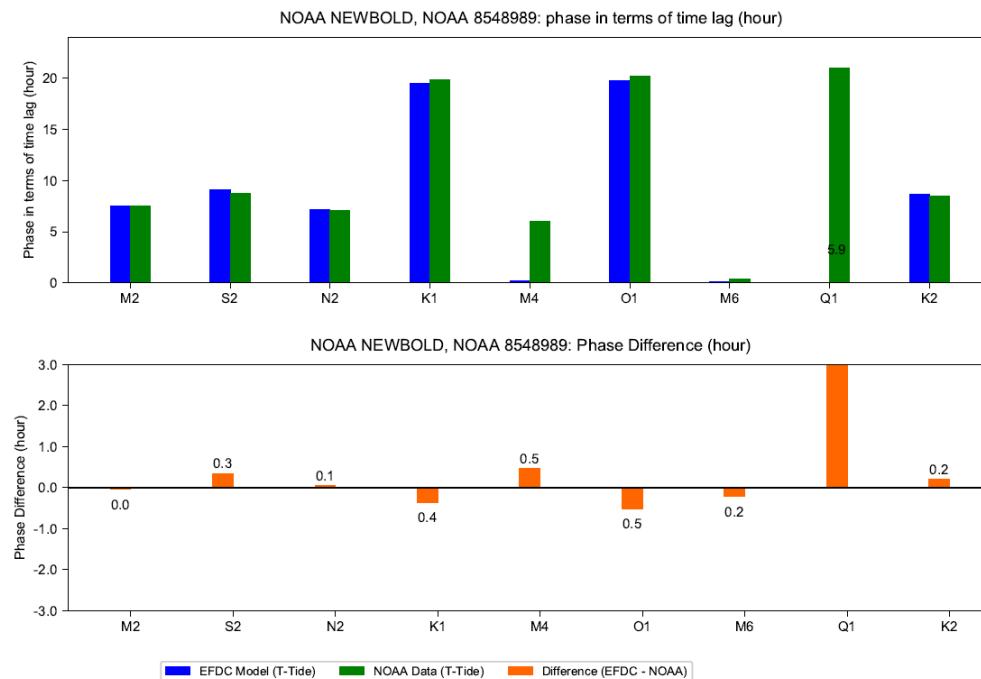
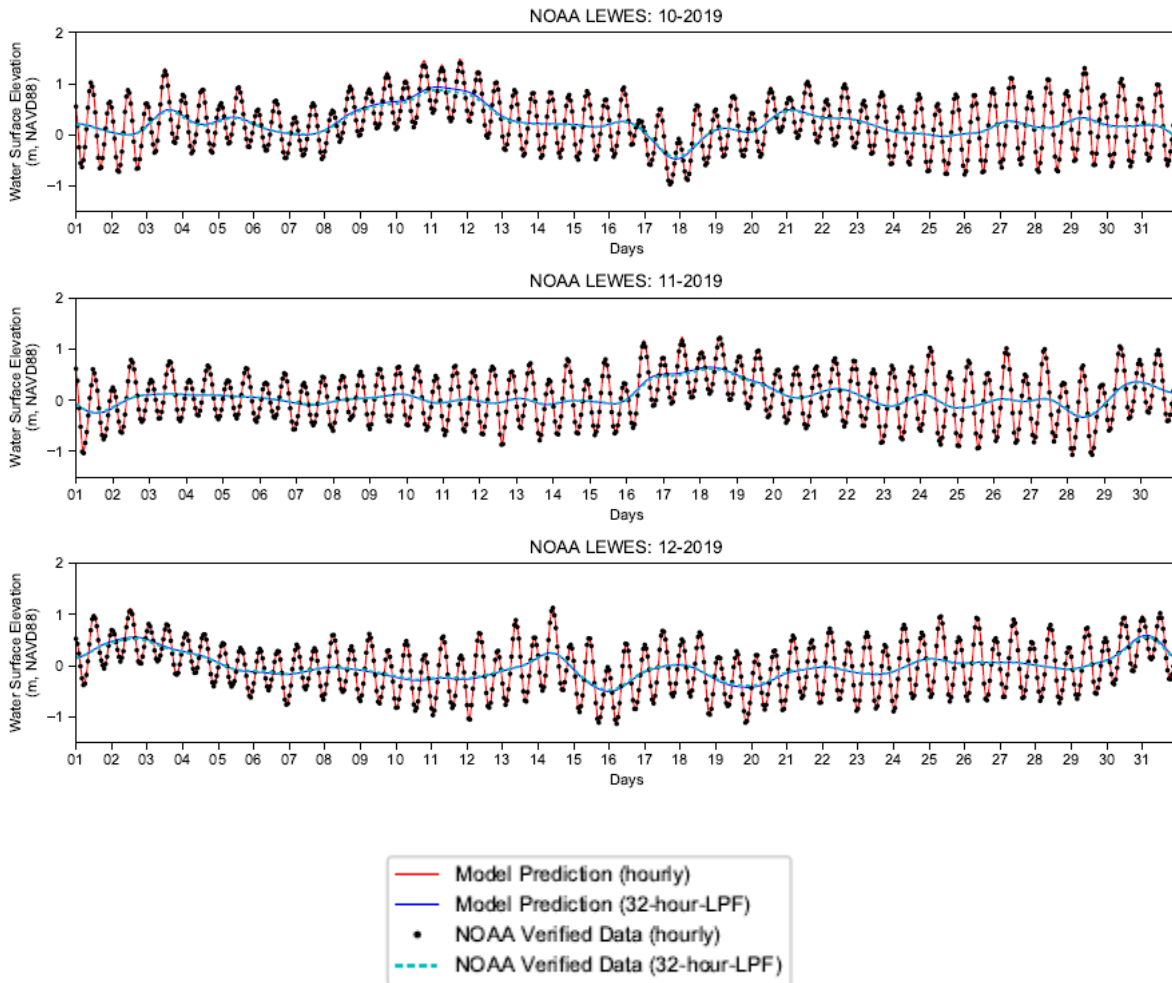


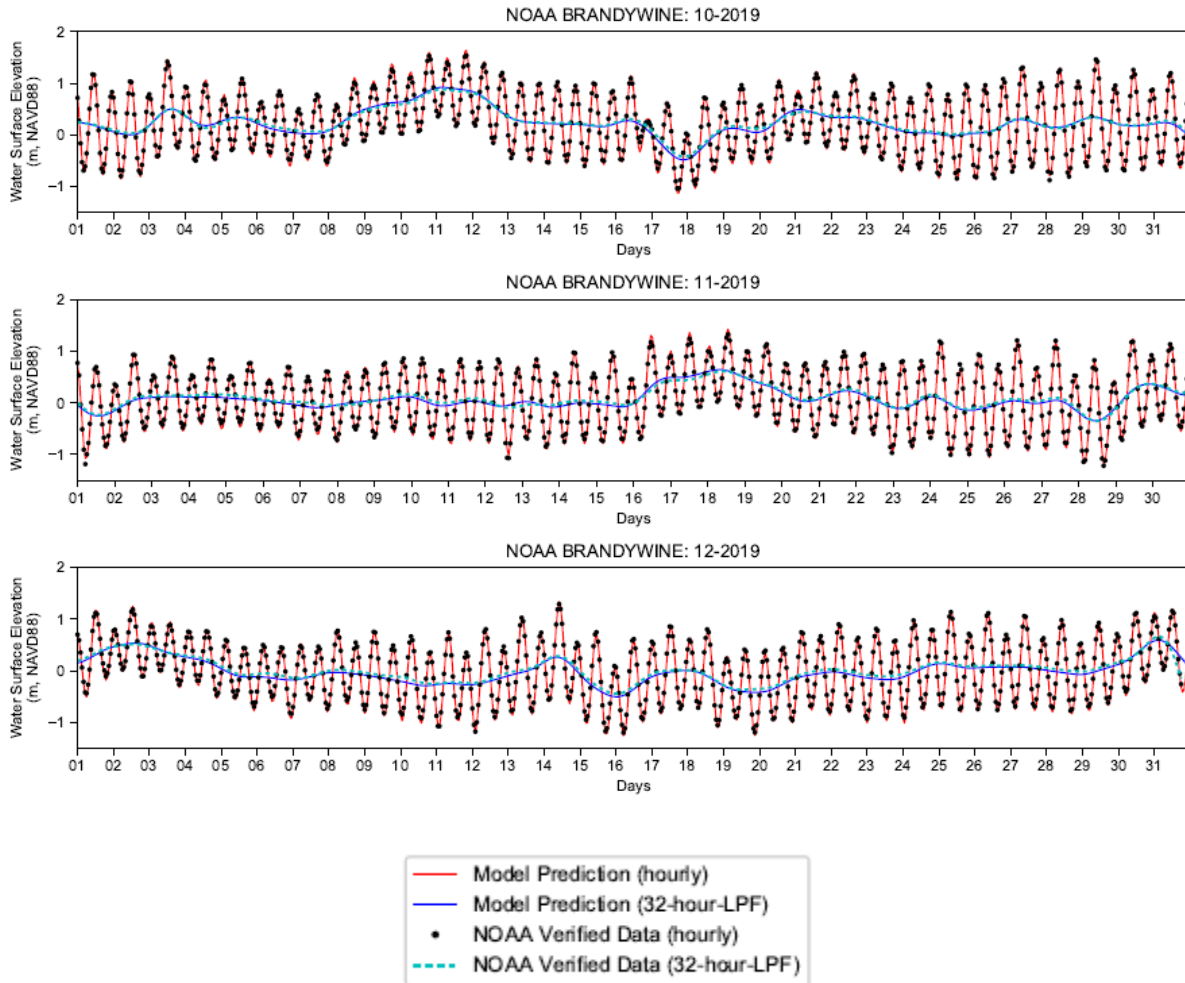
Figure G-20: Tidal Harmonics Analysis Based on Predicted Water Surface Elevation: Phase at NOAA NEWBOLD, NOAA Station 8548989

Appendix H: Time series of observed and predicted water surface elevation (2019)



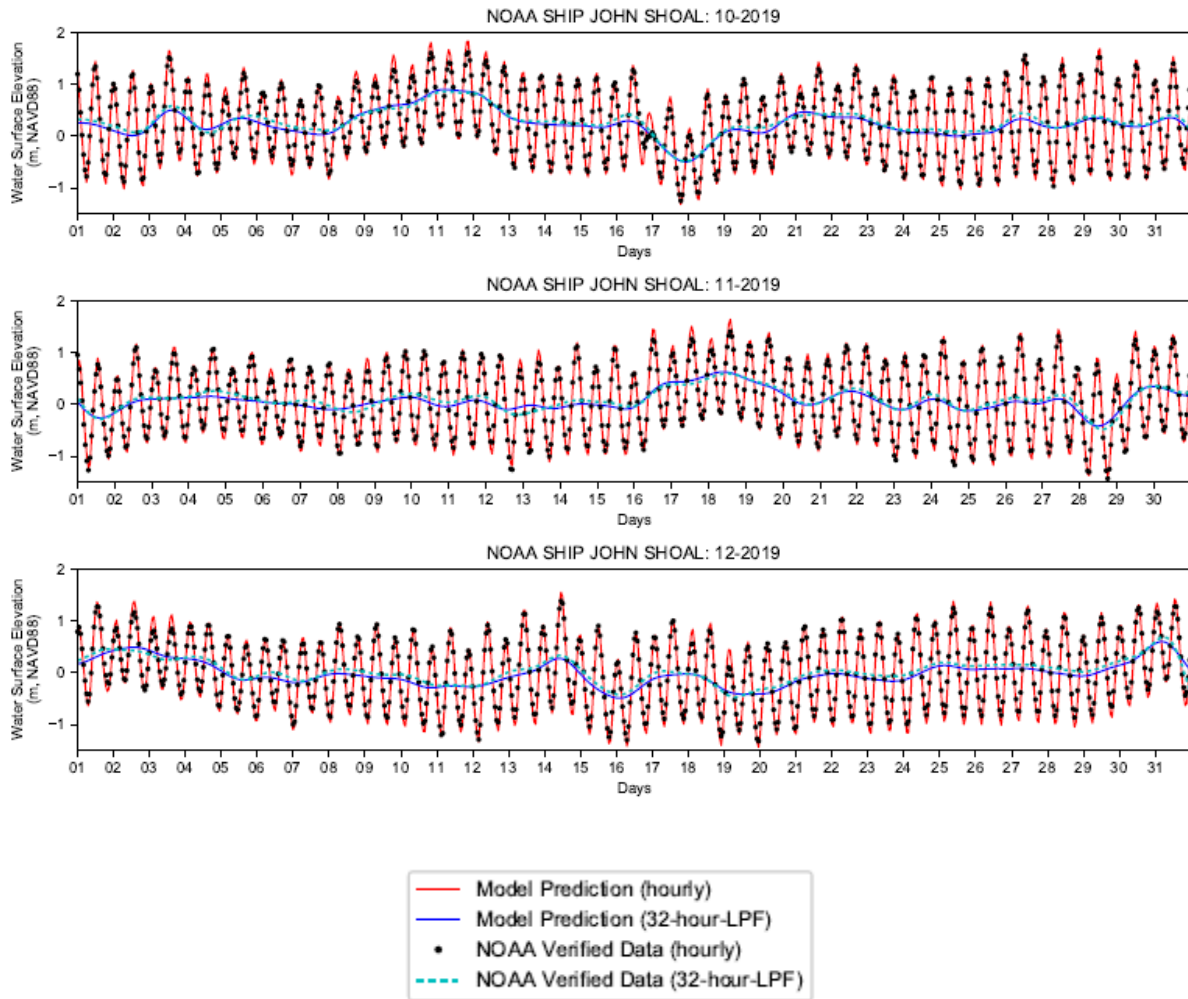
NOAA hourly verified data were used. Station ID: 8557380
Run ID: EFDC_HYDRO_G72_2023-01-06.

Figure H-1: Observed and Predicted Water Surface Elevation at NOAA LEWES



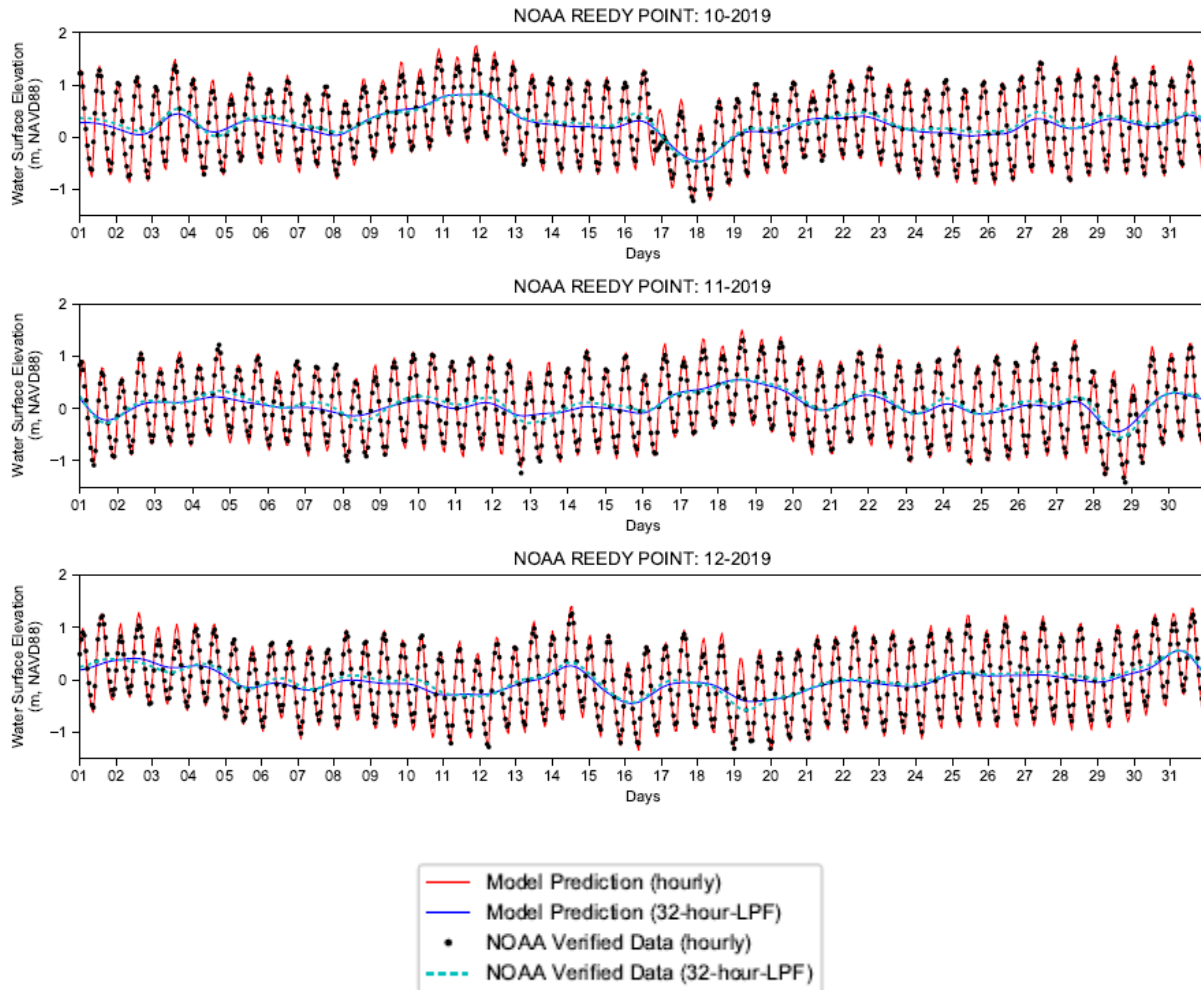
NOAA hourly verified data were used. Station ID: 8555889
Run ID: EFDC_HYDRO_G72_2023-01-06

Figure H-2: Observed and Predicted Water Surface Elevation at NOAA BRANDYWINE



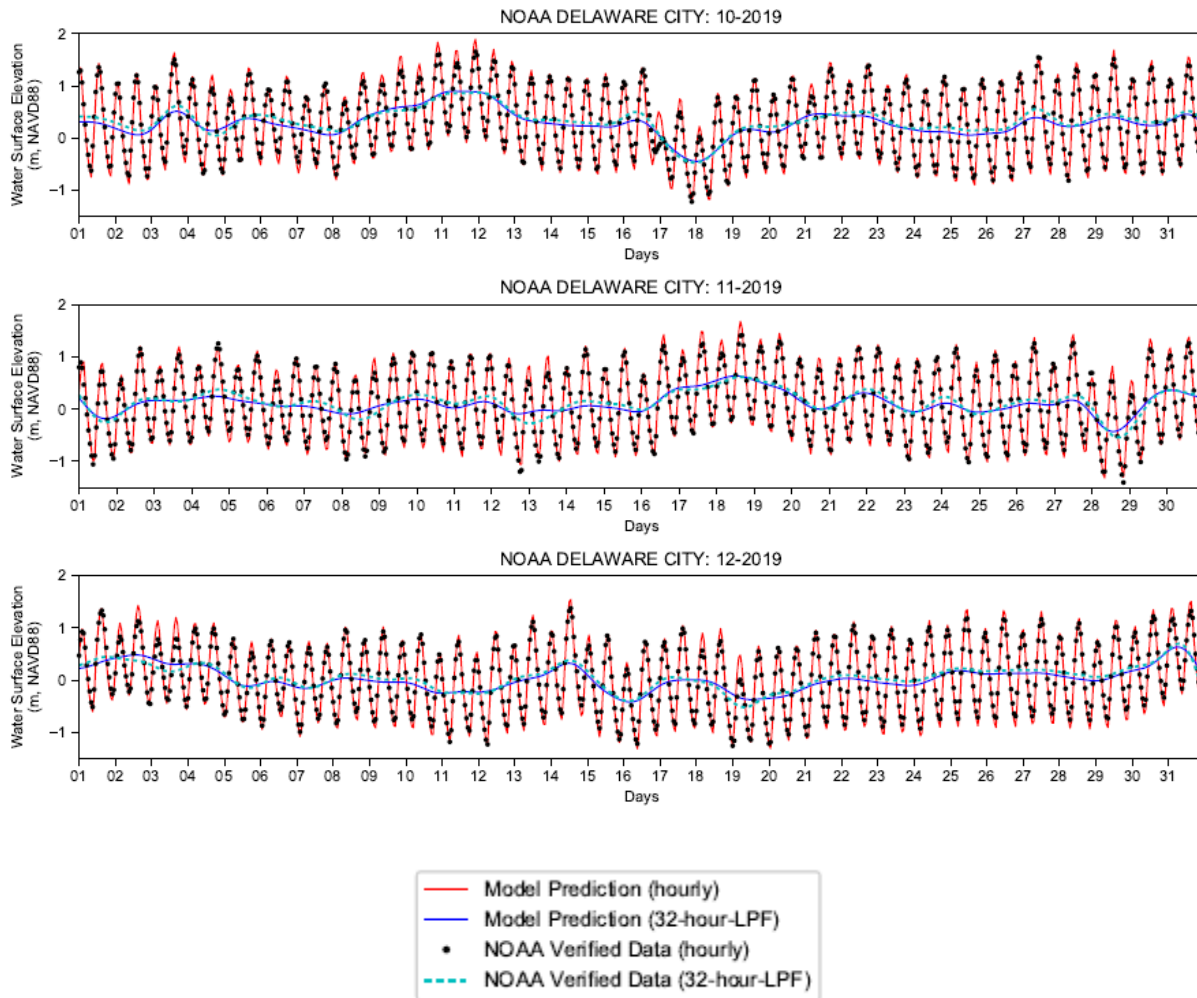
NOAA hourly verified data were used. Station ID: 8537121
Run ID: EFDC_HYDRO_G72_2023-01-06

Figure H-3: Observed and Predicted Water Surface Elevation at NOAA SHIP JOHN SHOAL



NOAA hourly verified data were used. Station ID: 8551910
Run ID: EFDC_HYDRO_G72_2023-01-06

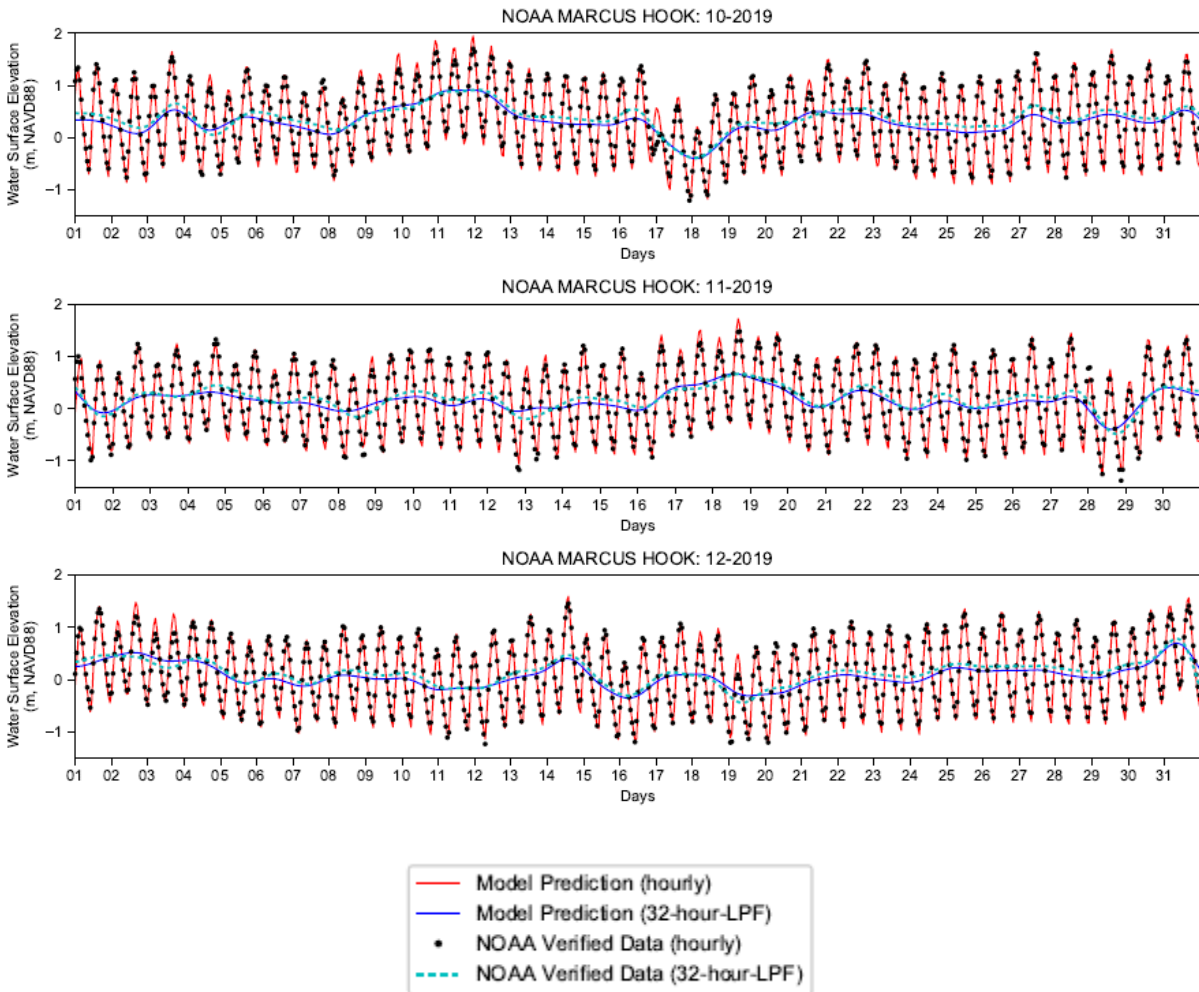
Figure H-4: Observed and Predicted Water Surface Elevation at NOAA REEDY POINT



NOAA hourly verified data were used. Station ID: 8551762

Run ID: EFDC_HYDRO_G72_2023-01-06

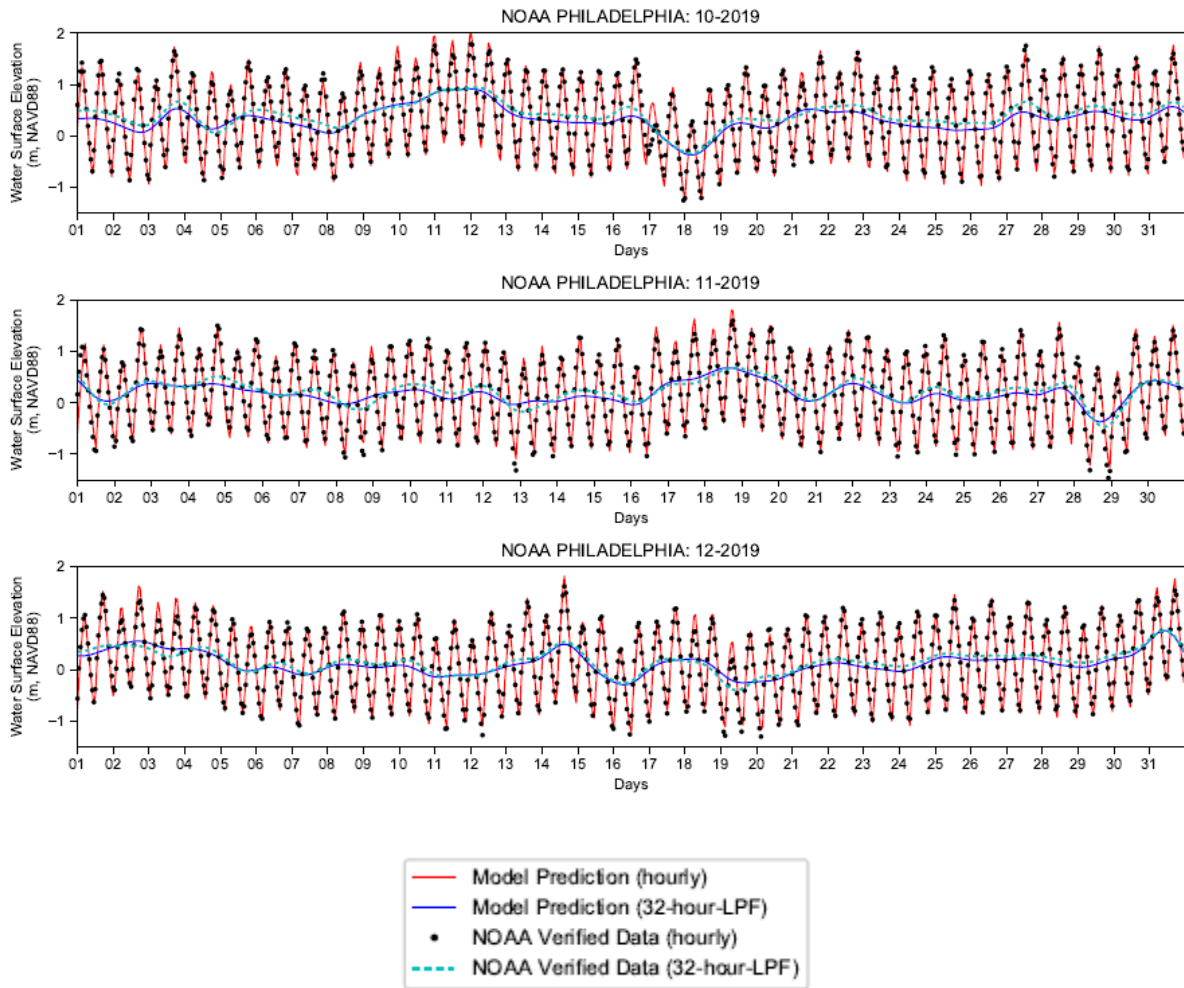
Figure H-5: Observed and Predicted Water Surface Elevation at NOAA DELAWARE CITY



NOAA hourly verified data were used. Station ID: 8540433

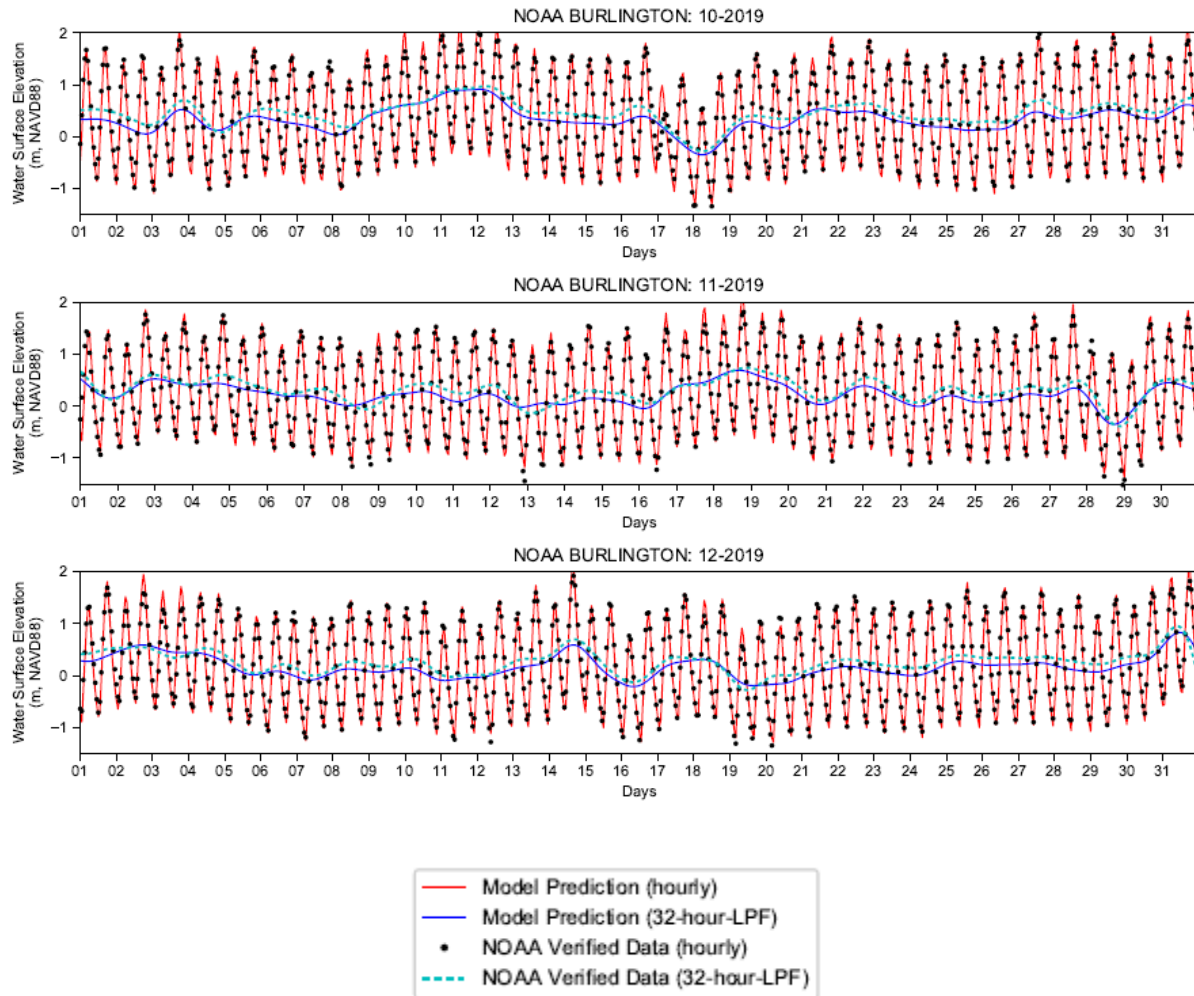
Run ID: EFDC_HYDRO_G72_2023-01-06

Figure H-6: Observed and Predicted Water Surface Elevation at NOAA MARCUS HOOK



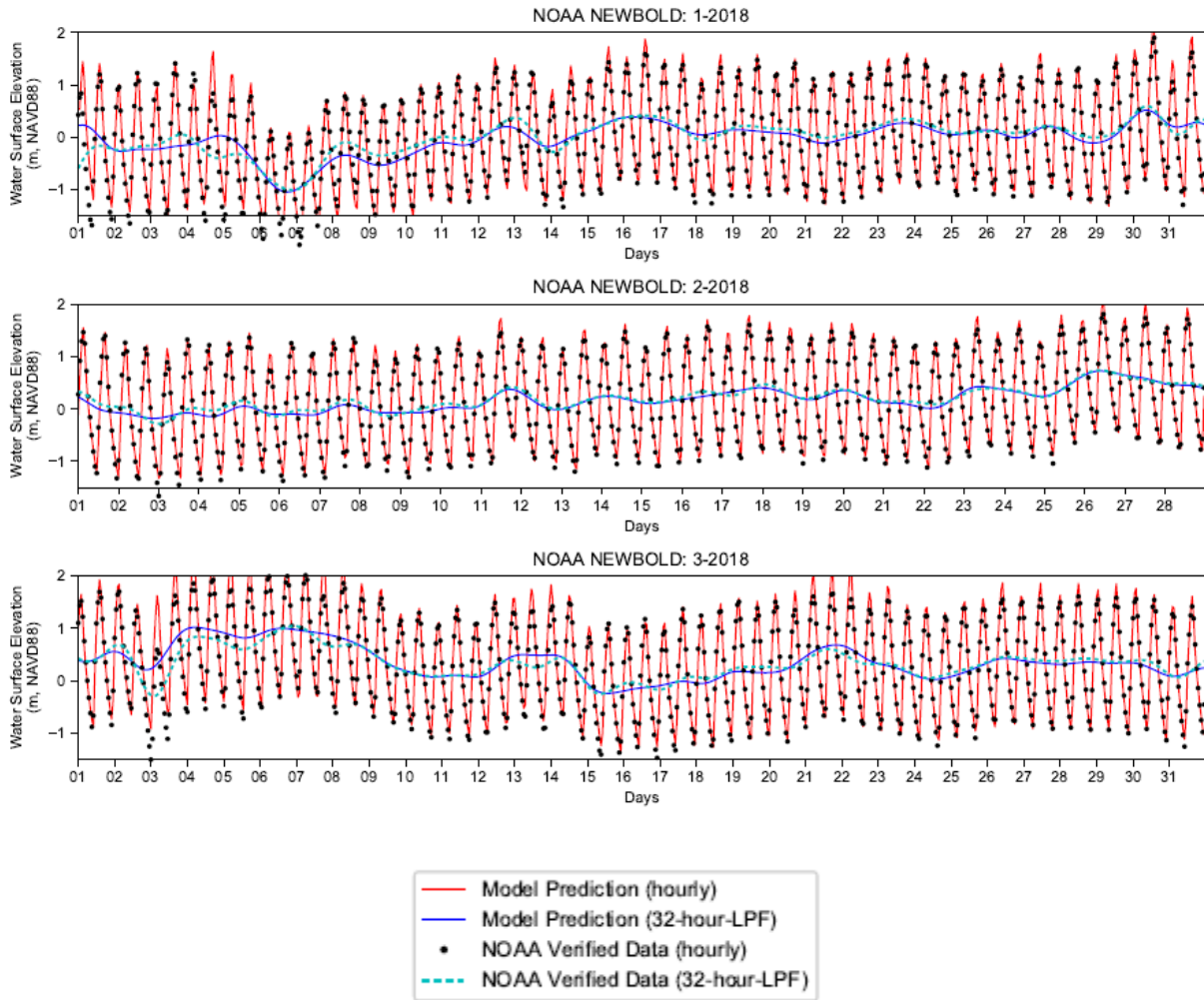
NOAA hourly verified data were used. Station ID: 8545240
Run ID: EFDC_HYDRO_G72_2023-01-06

Figure H-7: Observed and Predicted Water Surface Elevation at NOAA PHILADELPHIA



NOAA hourly verified data were used. Station ID: 8539094
Run ID: EFDC_HYDRO_G72_2023-01-06

Figure H-8: Observed and Predicted Water Surface Elevation at NOAA BURLINGTON

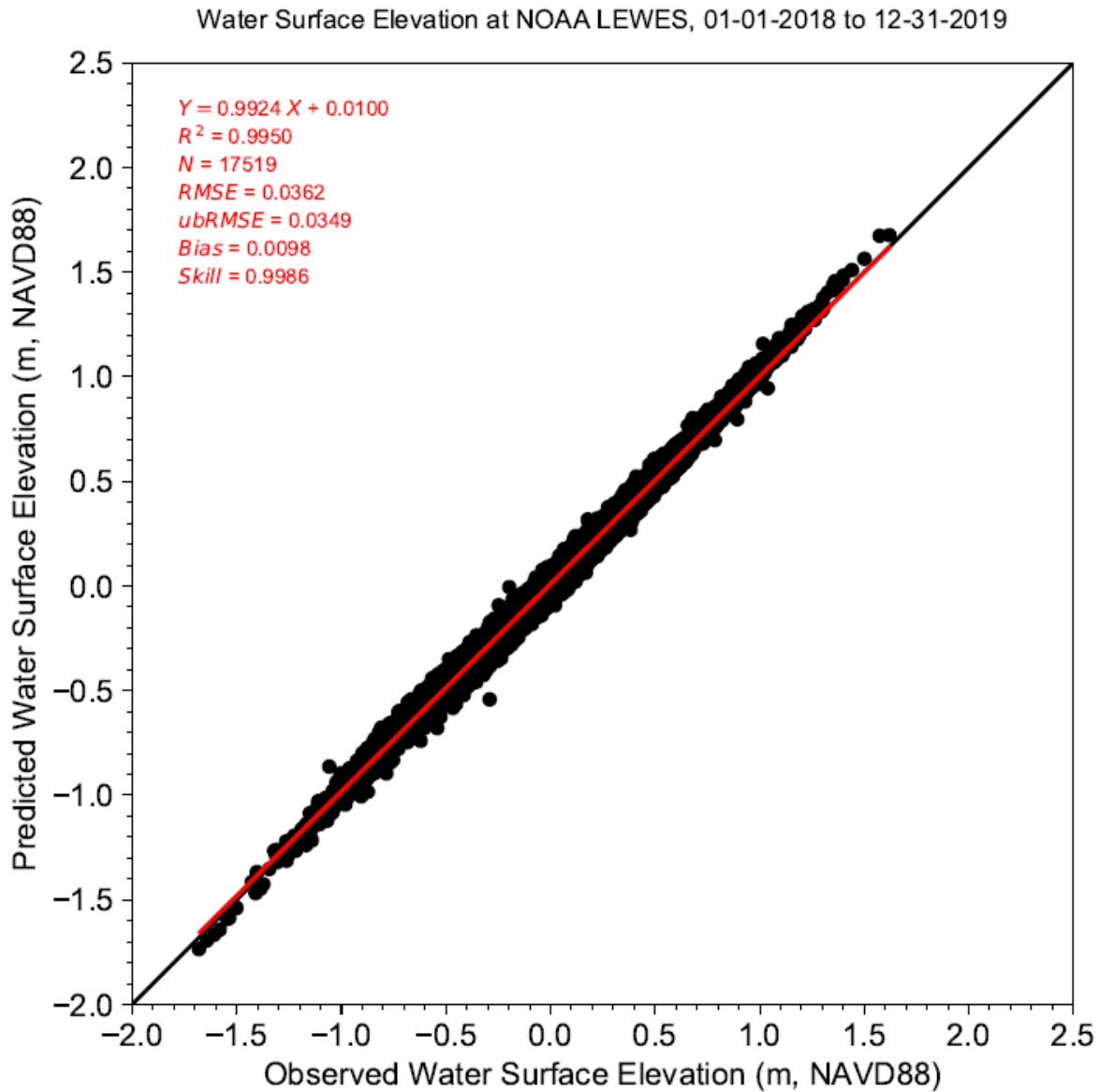


NOAA hourly verified data were used. Station ID: 8548989

Run ID: EFDC_HYDRO_G72_2023-01-06

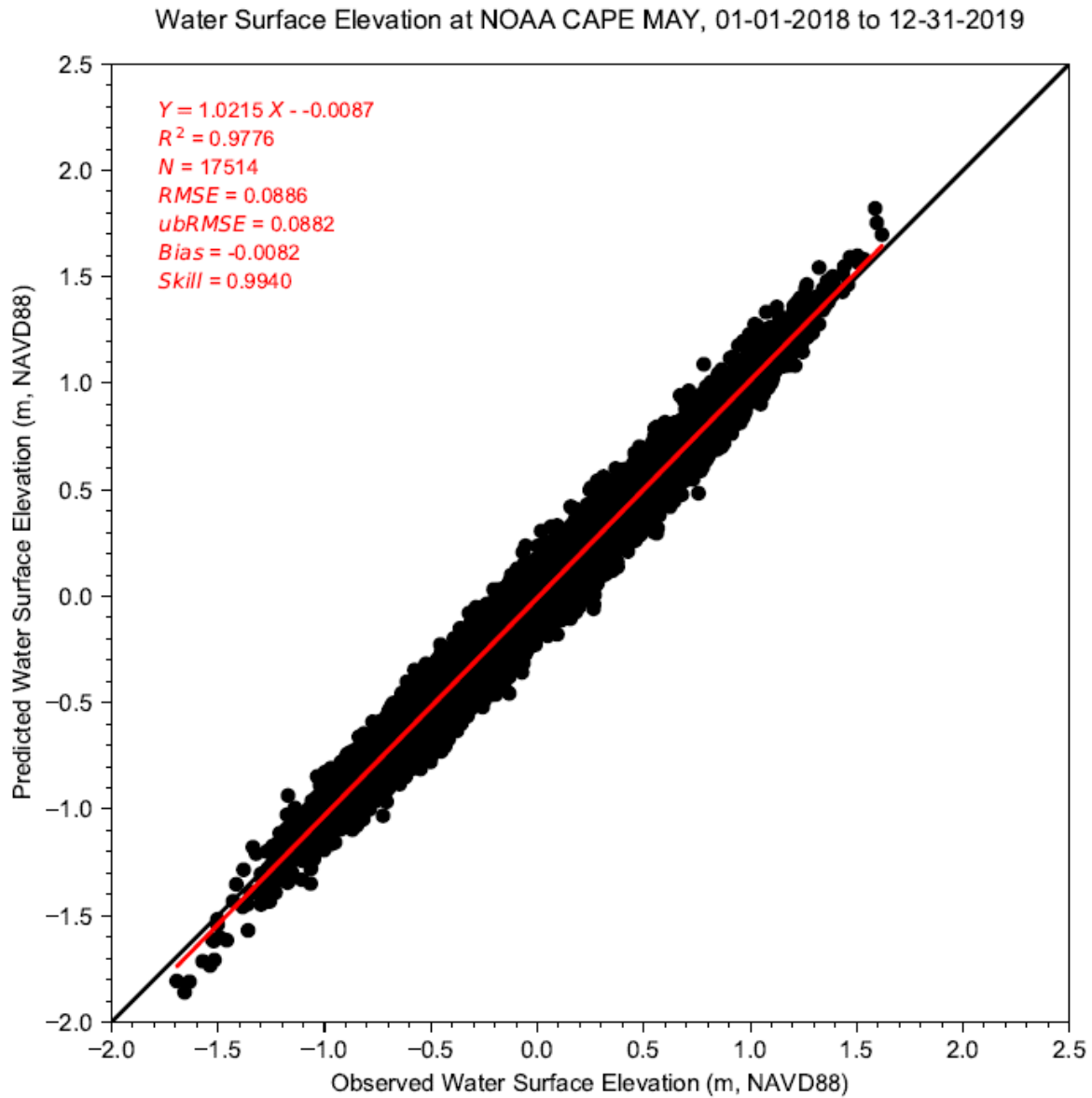
Figure H-9: Observed and Predicted Water Surface Elevation at NOAA NEWBOLD

Appendix I: Comparison of observed and predicted water surface elevation



Note: NOAA hourly verified data were used. Station ID: 8557380
Run ID: EFDC_HYDRO_G72_2023-01-06

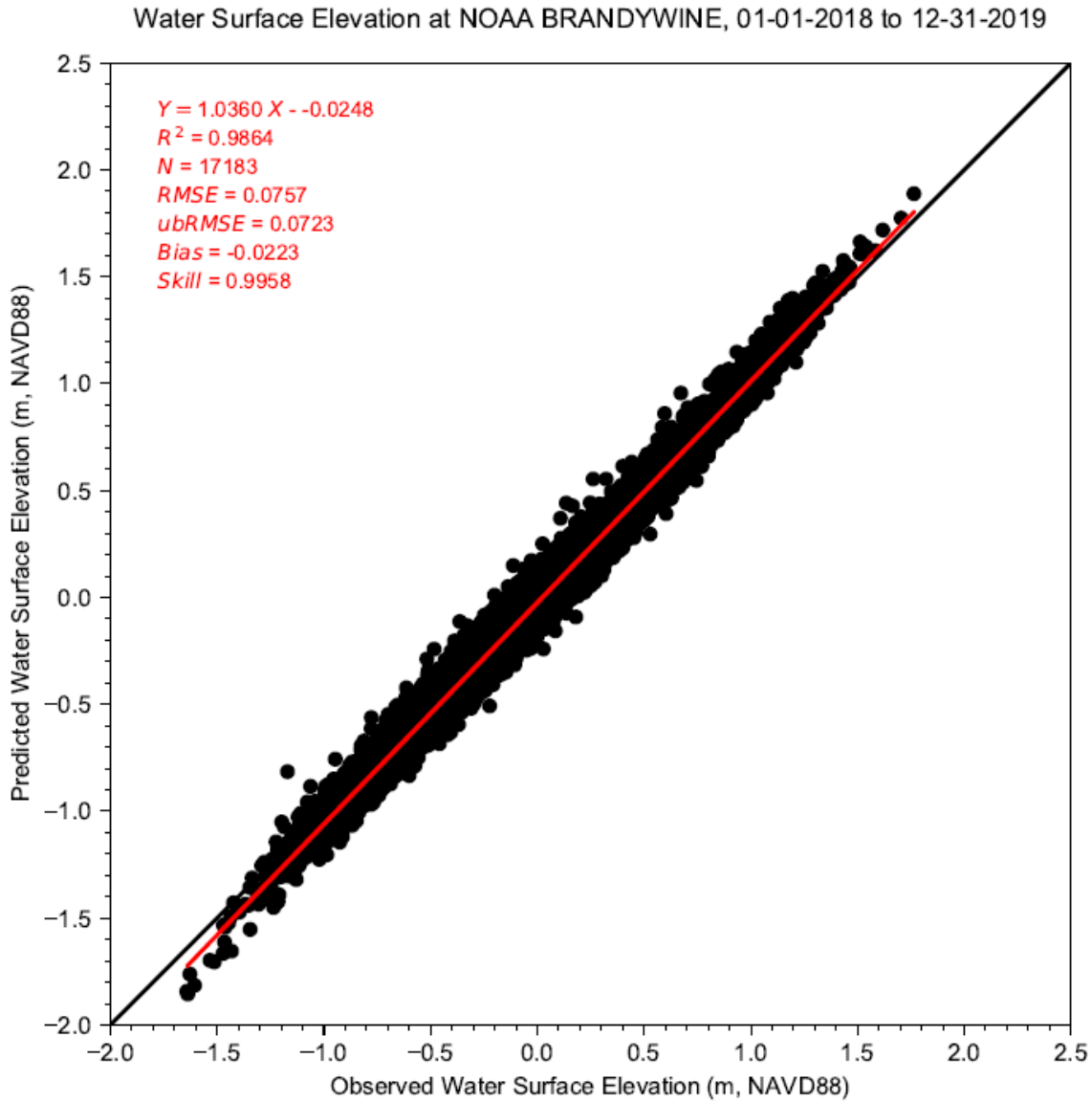
Figure I-1: Comparison of Observed and Predicted Water Surface Elevation at NOAA LEWES



Note: NOAA hourly verified data were used. Station ID: 8536110

Run ID: EFDC_HYDRO_G72_2023-01-06

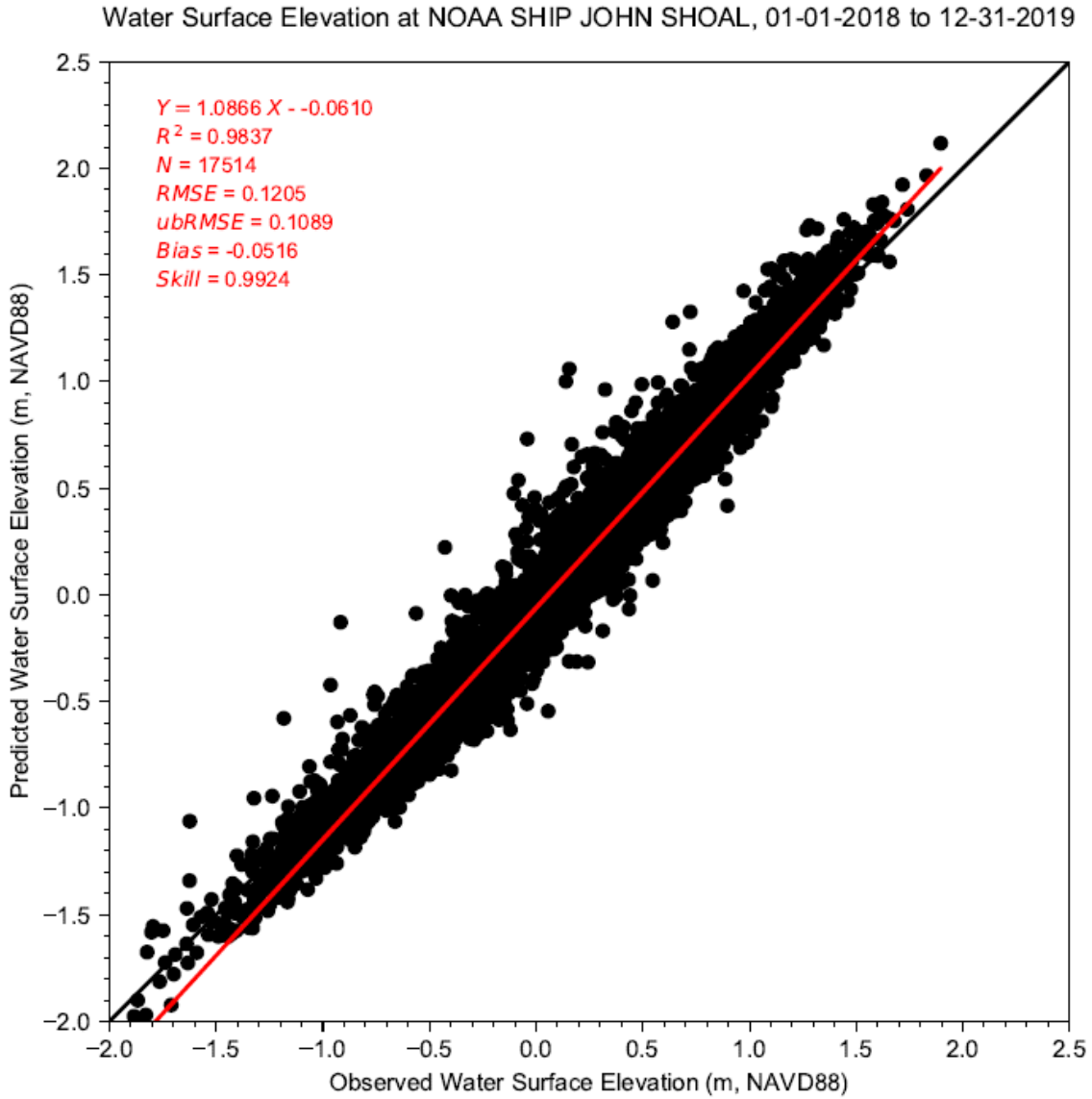
Figure I-2: Comparison of Observed and Predicted Water Surface Elevation at NOAA CAPE MAY



Note: NOAA hourly verified data were used. Station ID: 8555889

Run ID: EFDC_HYDRO_G72_2023-01-06

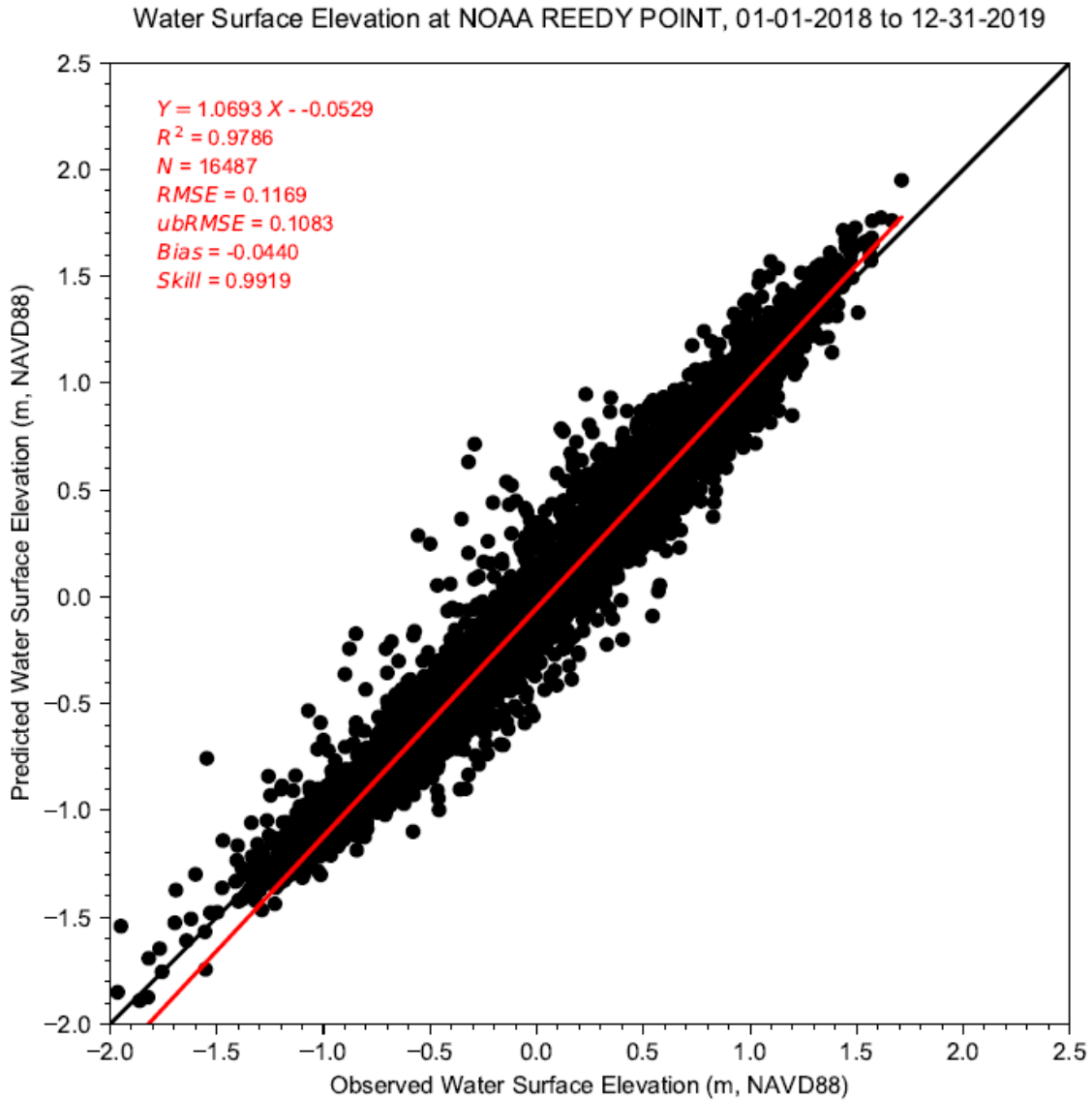
Figure I-3: Comparison of Observed and Predicted Water Surface Elevation at NOAA BRANDYWINE



Note: NOAA hourly verified data were used. Station ID: 8537121

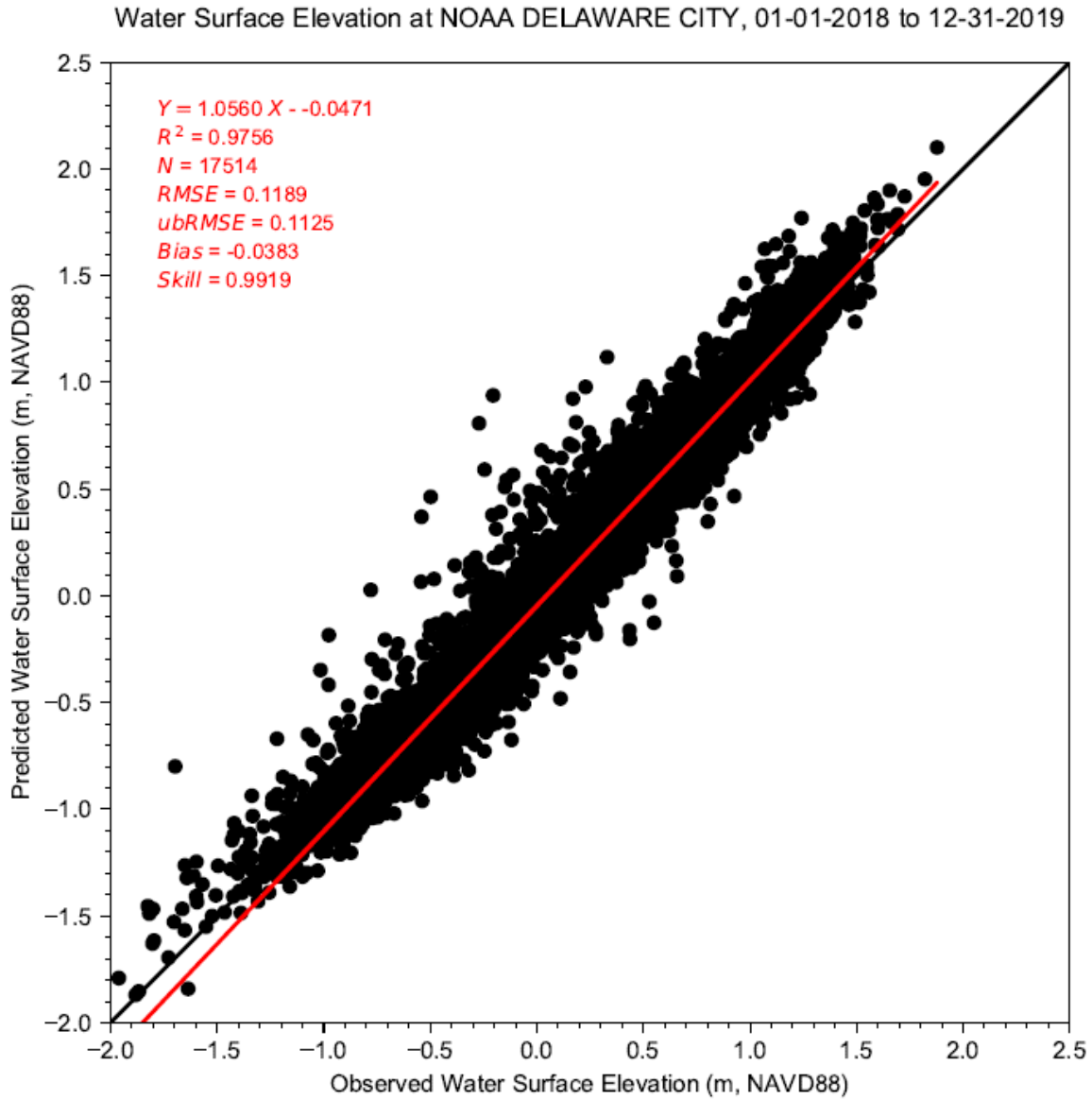
Run ID: EFDC_HYDRO_G72_2023-01-06

Figure I-4: Comparison of Observed and Predicted Water Surface Elevation at NOAA SHIP JOHN SHOAL



Note: NOAA hourly verified data were used. Station ID: 8551910
Run ID: EFDC_HYDRO_G72_2023-01-06

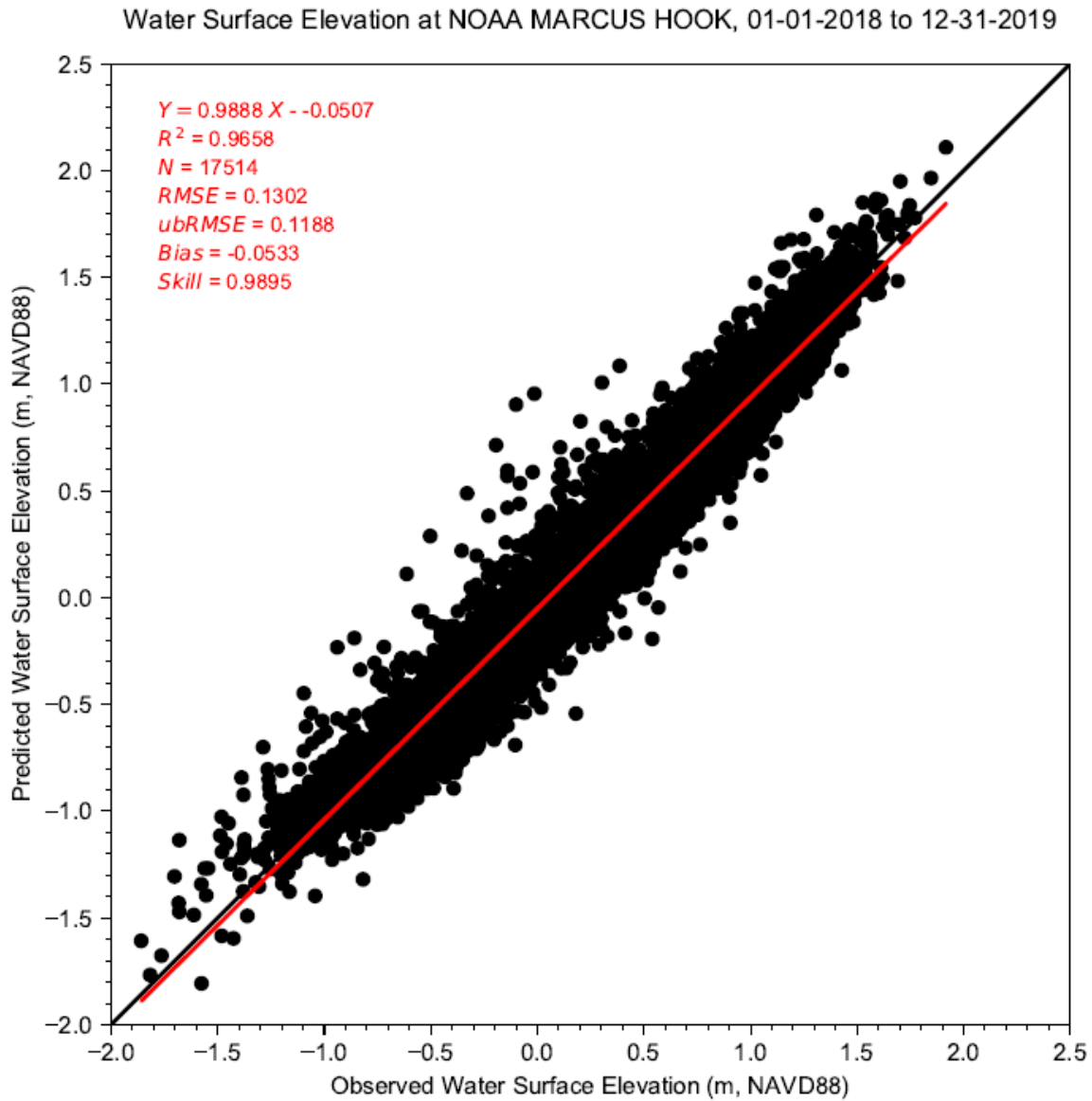
Figure I-5: Comparison of Observed and Predicted Water Surface Elevation at NOAA REEDY POINT



Note: NOAA hourly verified data were used. Station ID: 8551762

Run ID: EFDC_HYDRO_G72_2023-01-06

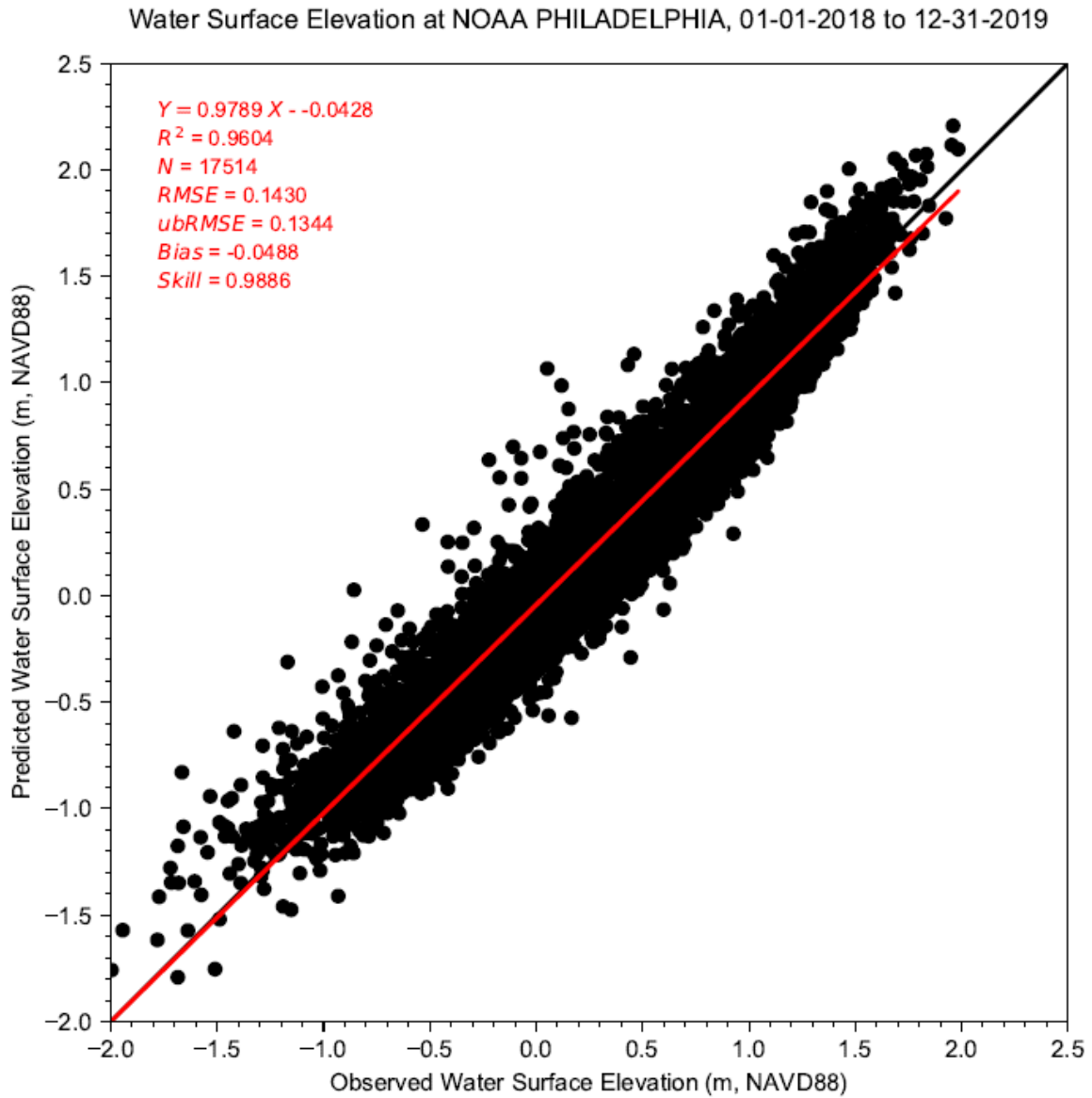
Figure I-6: Comparison of Observed and Predicted Water Surface Elevation at NOAA DELAWARE CITY



Note: NOAA hourly verified data were used. Station ID: 8540433

Run ID: EFDC_HYDRO_G72_2023-01-06

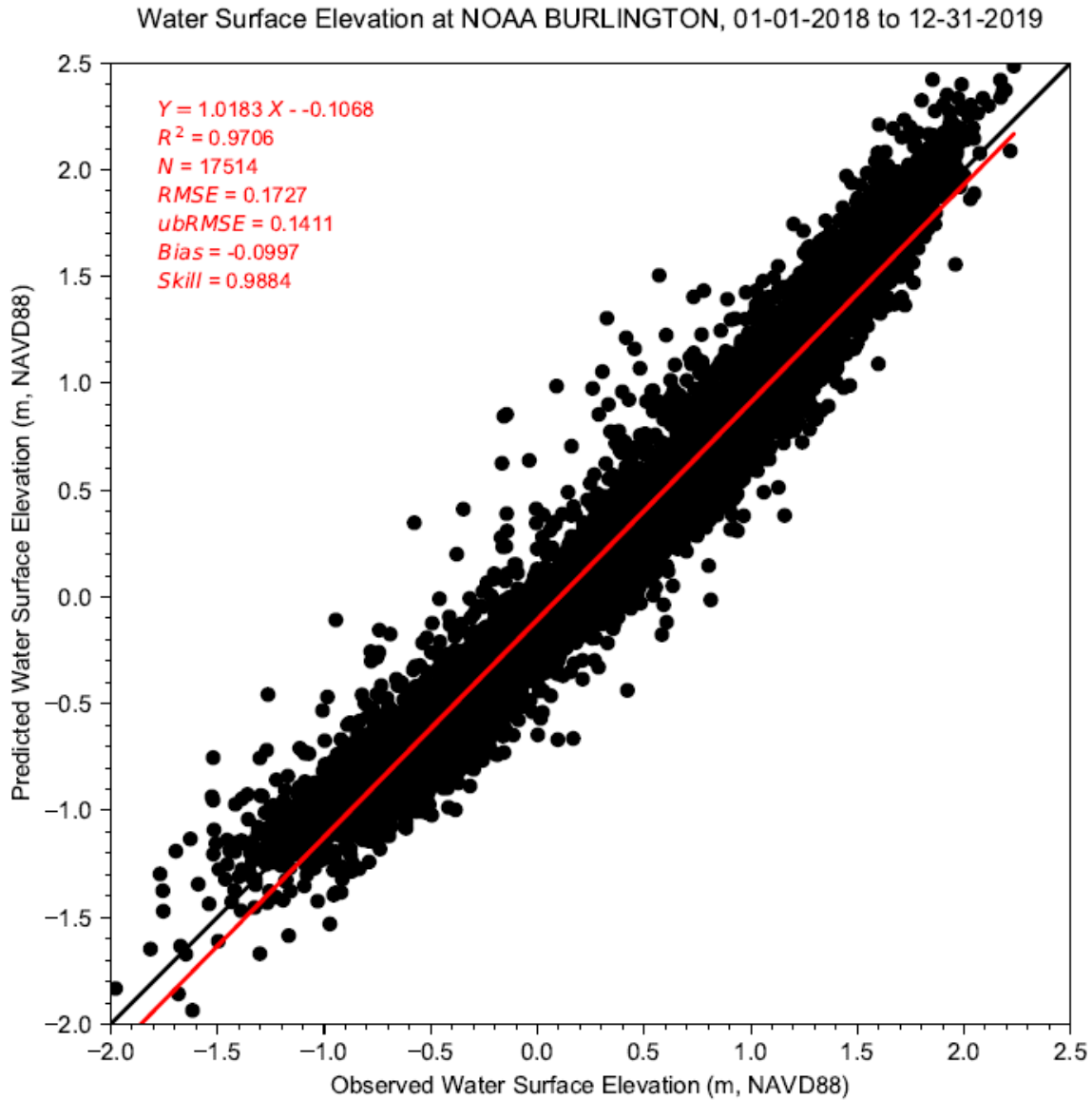
Figure I-7: Comparison of Observed and Predicted Water Surface Elevation at NOAA MARCUS HOOK



Note: NOAA hourly verified data were used. Station ID: 8545240

Run ID: EFDC_HYDRO_G72_2023-01-06

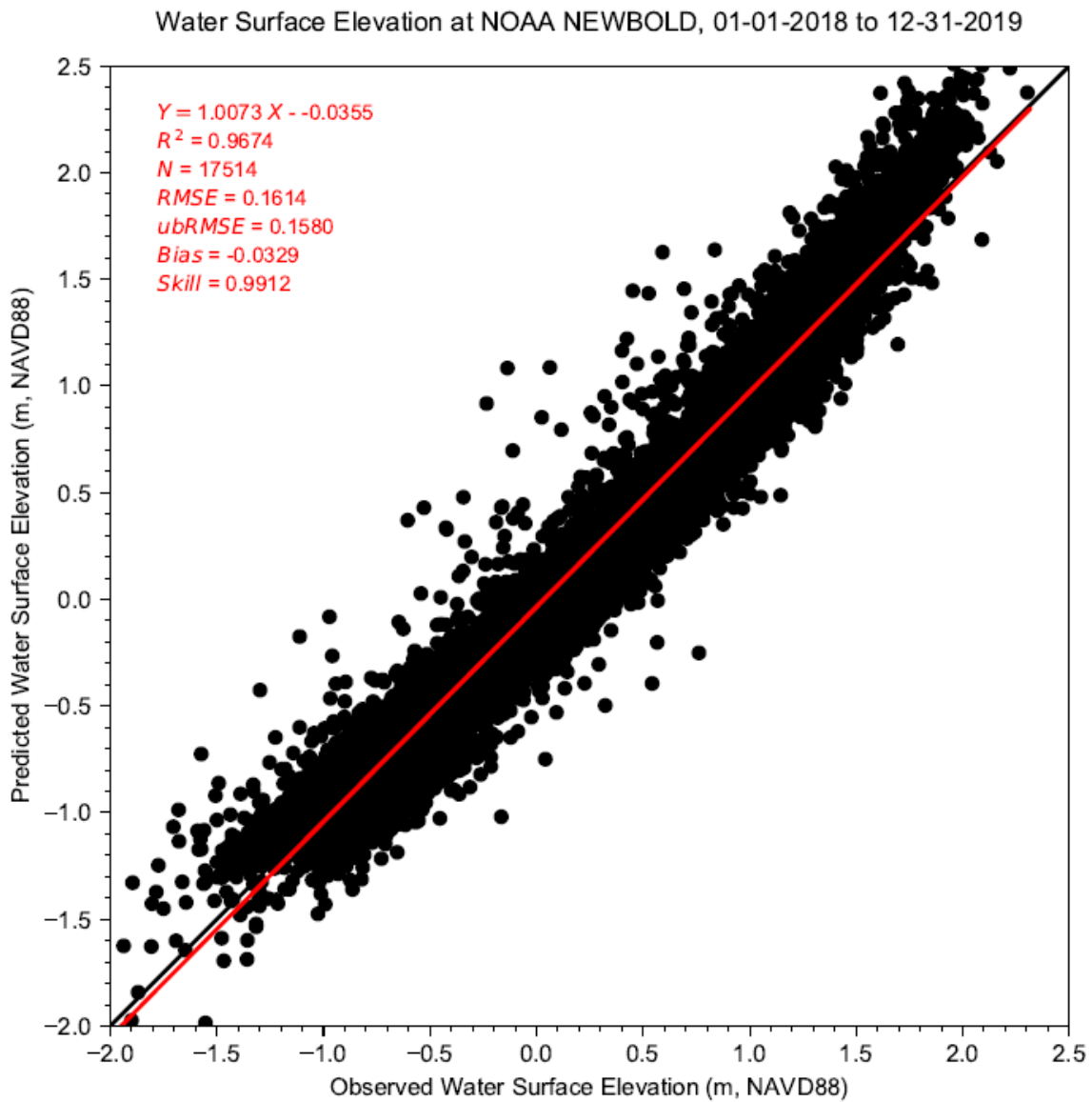
Figure I-8: Comparison of Observed and Predicted Water Surface Elevation at NOAA PHILADELPHIA



Note: NOAA hourly verified data were used. Station ID: 8539094

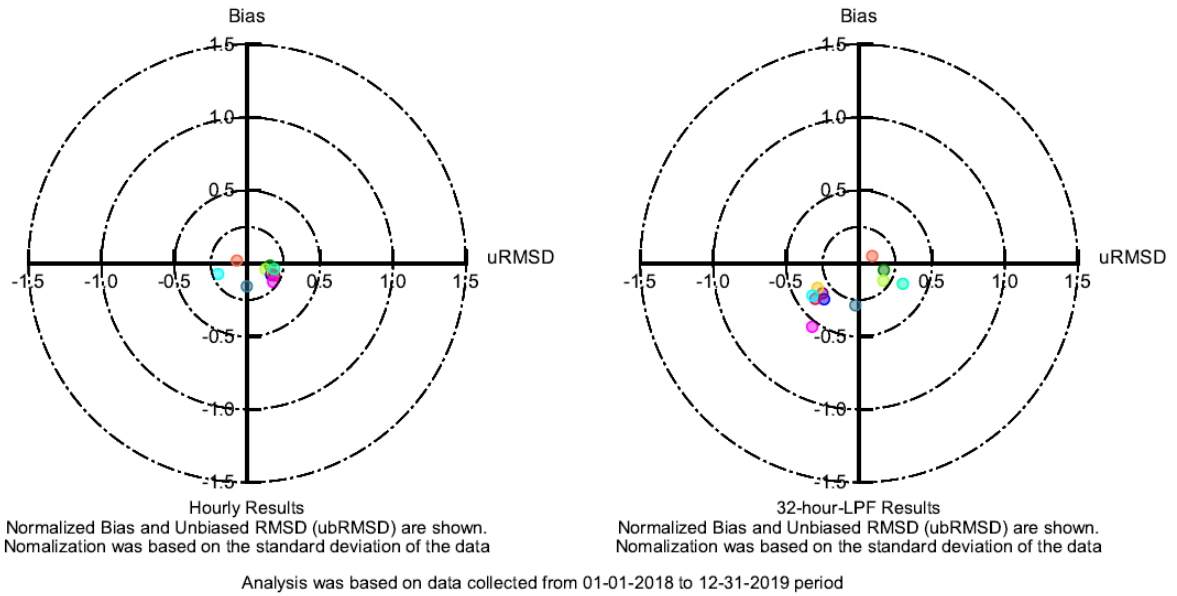
Run ID: EFDC_HYDRO_G72_2023-01-06

Figure I-9: Comparison of Observed and Predicted Water Surface Elevation at NOAA BURLINGTON



Note: NOAA hourly verified data were used. Station ID: 8548989
Run ID: EFDC_HYDRO_G72_2023-01-06

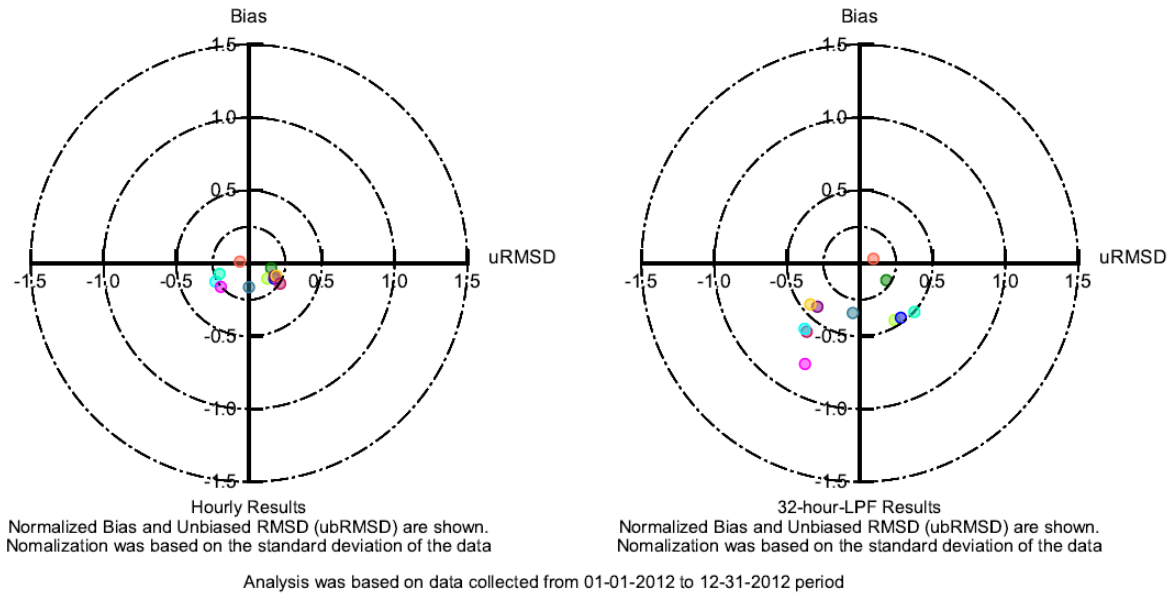
Figure I-10: Comparison of Observed and Predicted Water Surface Elevation at NOAA NEWBOLD



- NOAA LEWES
- NOAA SHIP JOHN SHOAL
- NOAA DELAWARE CITY
- NOAA MARCUS HOOK
- NOAA BURLINGTON
- NOAA CAPE MAY
- NOAA REEDY POINT
- NOAA CHESAPEAKE CITY
- NOAA PHILADELPHIA
- NOAA NEWBOLD
- NOAA BRANDYWINE

Note: NOAA hourly verified data were used.
Run ID: EFDC_HYDRO_G72_2023-01-06

Figure I-11: Target Diagram for Predicted Hourly and 32-hour-LPF Water Surface Elevations for 2018-2019 Period.

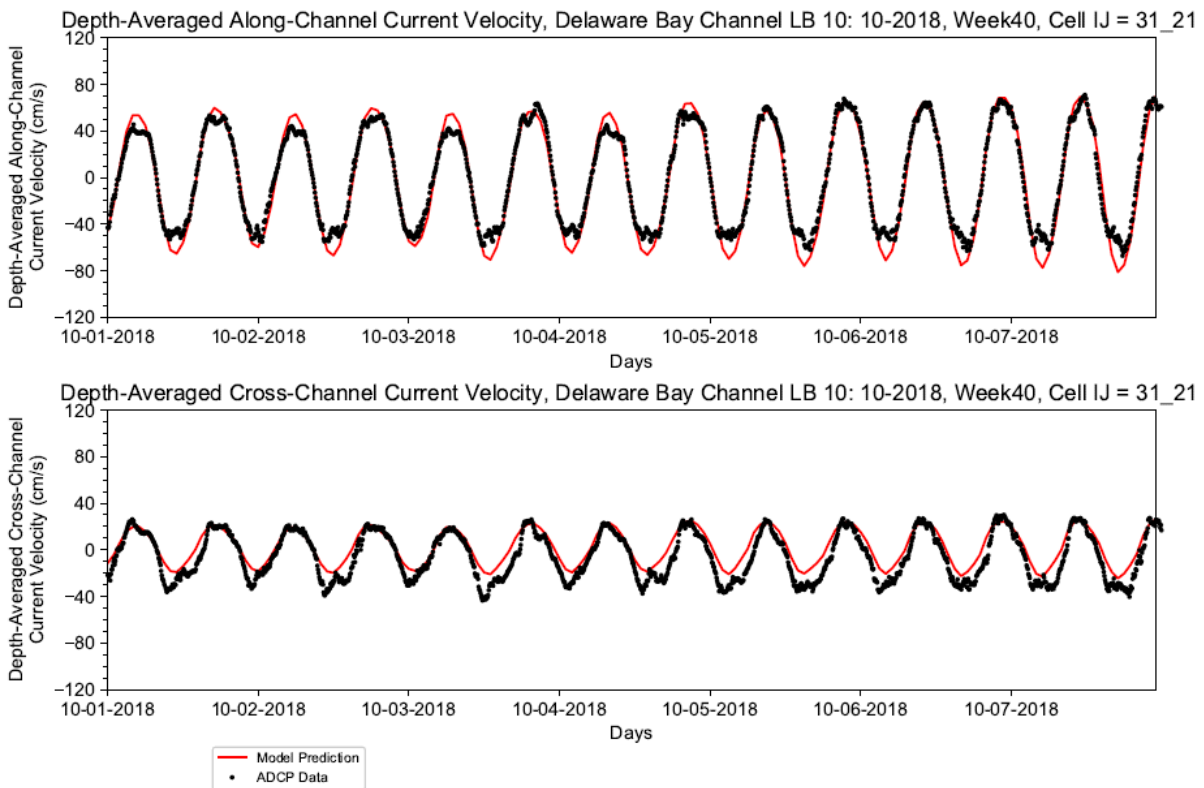


- NOAA LEWES
- NOAA SHIP JOHN SHOAL
- NOAA DELAWARE CITY
- NOAA MARCUS HOOK
- NOAA BURLINGTON
- NOAA CAPE MAY
- NOAA REEDY POINT
- NOAA CHESAPEAKE CITY
- NOAA PHILADELPHIA
- NOAA NEWBOLD
- NOAA BRANDYWINE

Note: NOAA hourly verified data were used.
 Run ID: EFDC_HYDRO_G72_2023-01-06

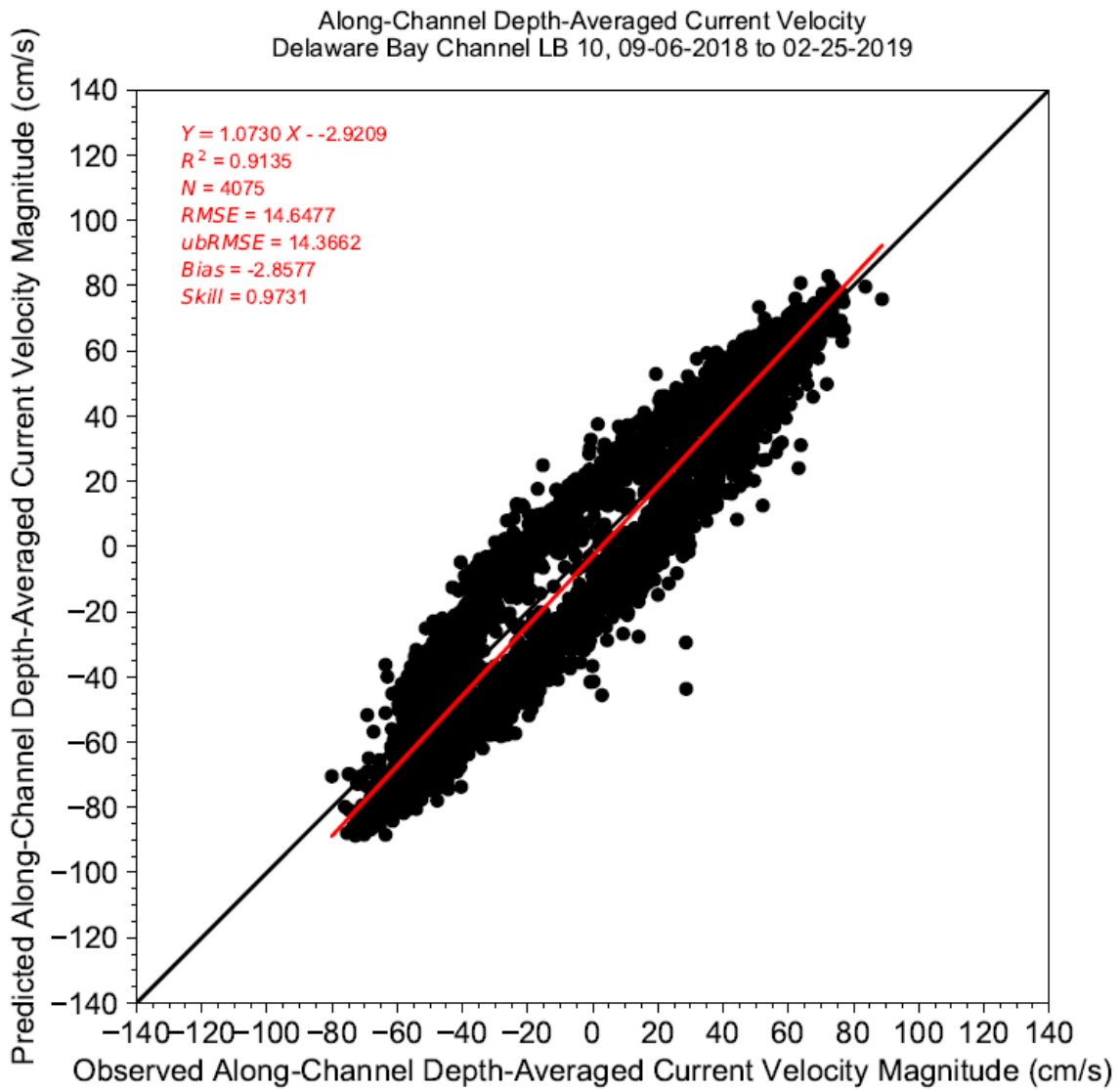
Figure I-12: Target Diagram for Predicted Hourly and 32-hour-LPF Water Surface Elevations for 2012 Period

Appendix J: Observed and predicted depth-averaged current velocity magnitude at NOAA current velocity stations



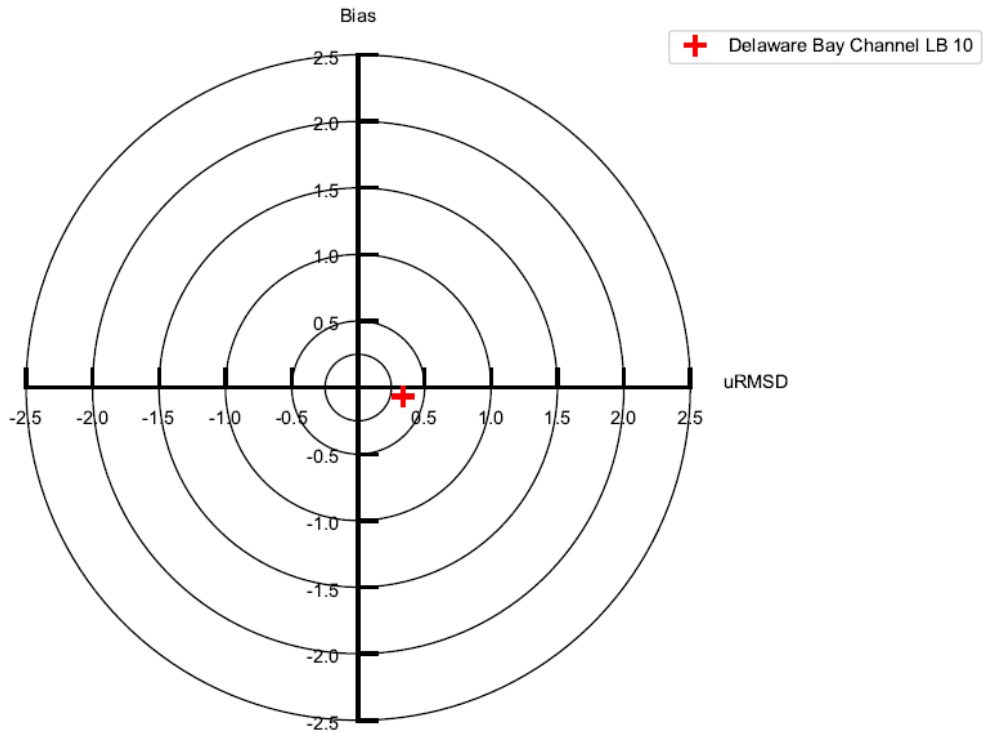
Note: Station ID: DB0502, Delaware Bay Channel LB 10
Run ID: EFDC_HYDRO_G72_2023-01-06

Figure J-1: Observed and Predicted Depth-Averaged Along-Channel and Cross-Channel Current Velocities at Delaware Bay Channel LB 10



Note: Station ID: DB0502, Delaware Bay Channel LB 10
Run ID: EFDC_HYDRO_G72_2023-01-06

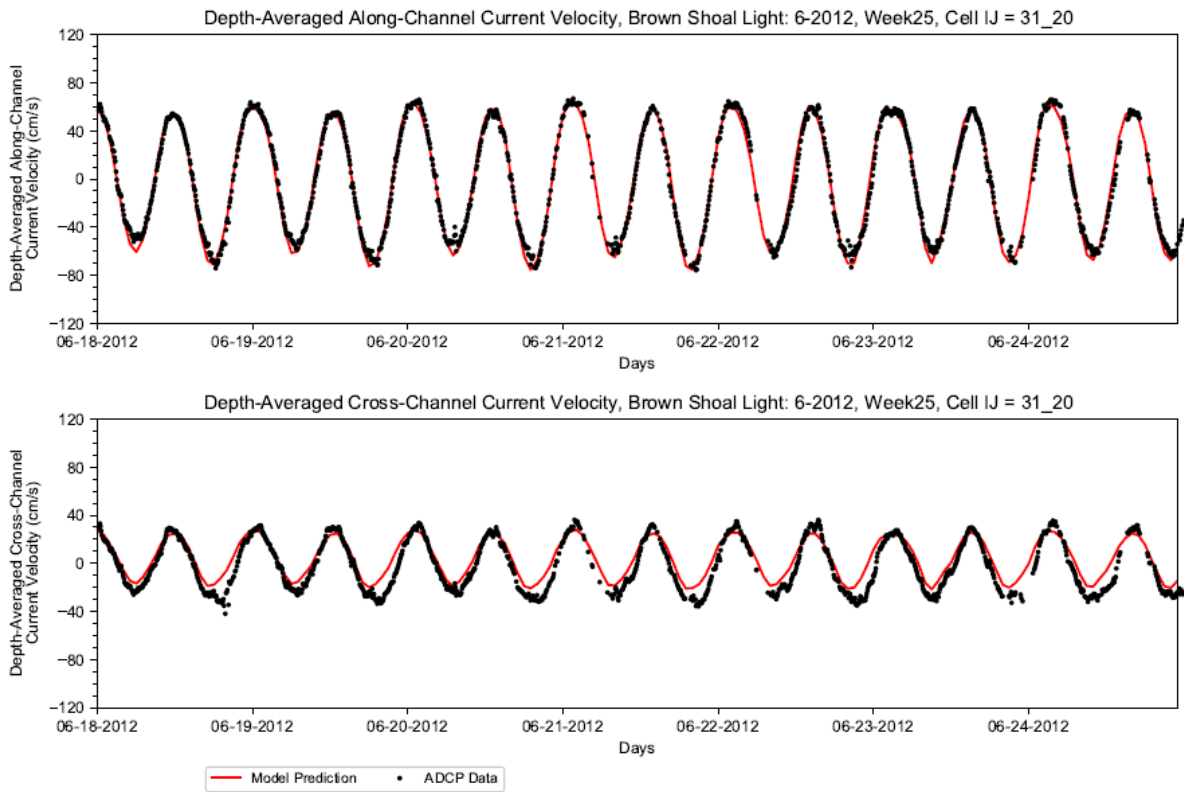
Figure J-2: Comparison of Observed and Predicted Along-Channel Depth-Averaged Current Velocity Magnitude at Delaware Bay Channel LB 10 during 09-06-2018 to 02-25-2019 period



Normalized Bias and Unbiased RMSD (ubRMSD) are shown.
Normalization was based on the standard deviation of the data
N = 4075, Normalized Bias = -0.0672, Normalized Unbiased RMSD = 0.338, Reference STDV (data) = 42.5042

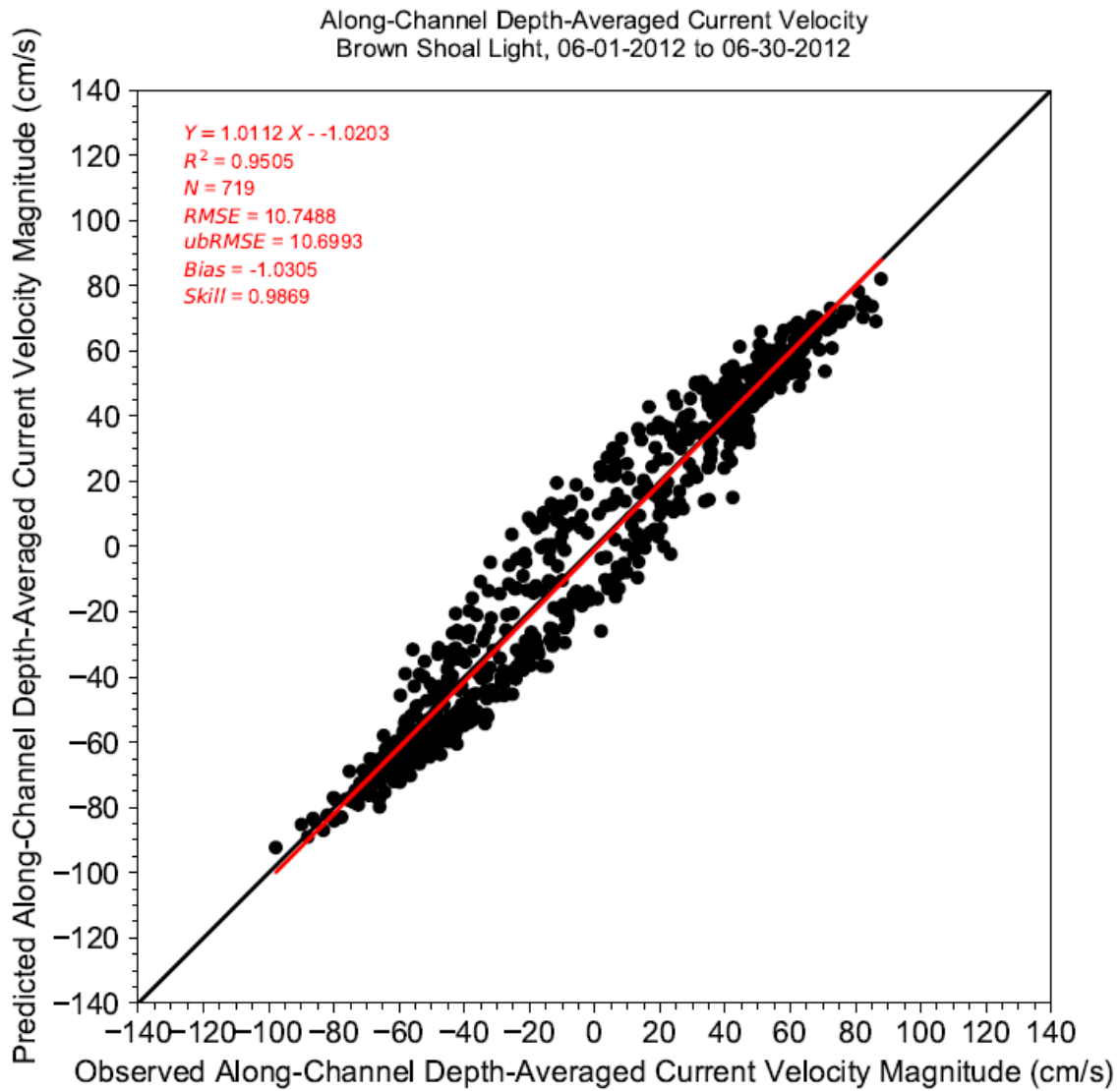
Note: Station ID: DB0502, Delaware Bay Channel LB 10
Run ID: EFDC_HYDRO_G72_2023-01-06
Period: 09-06-2018 to 02-25-2019

Figure J-3: Target Diagram for Predicted Along-Channel Depth-Averaged Current Velocity at Delaware Bay Channel LB 10



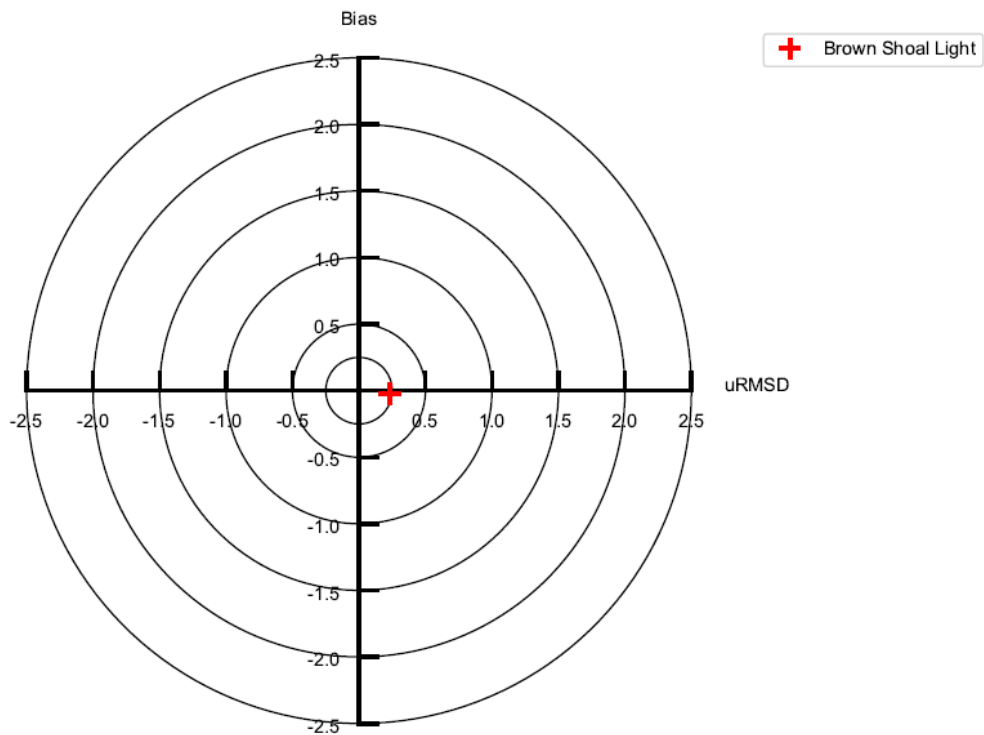
Note: Station ID: DB0501, Brown Shoal Light
Run ID: EFDC_HYDRO_G72_2023-01-06

Figure J-4: Observed and Predicted Depth-Averaged Along-Channel and Cross-Channel Current Velocities at Brown Shoal Light



Note: Station ID: DB0501. Brown Shoal Light
Run ID: EFDC_HYDRO_G72_2023-01-06
Period: 06-01-2012 to 06-30-2012

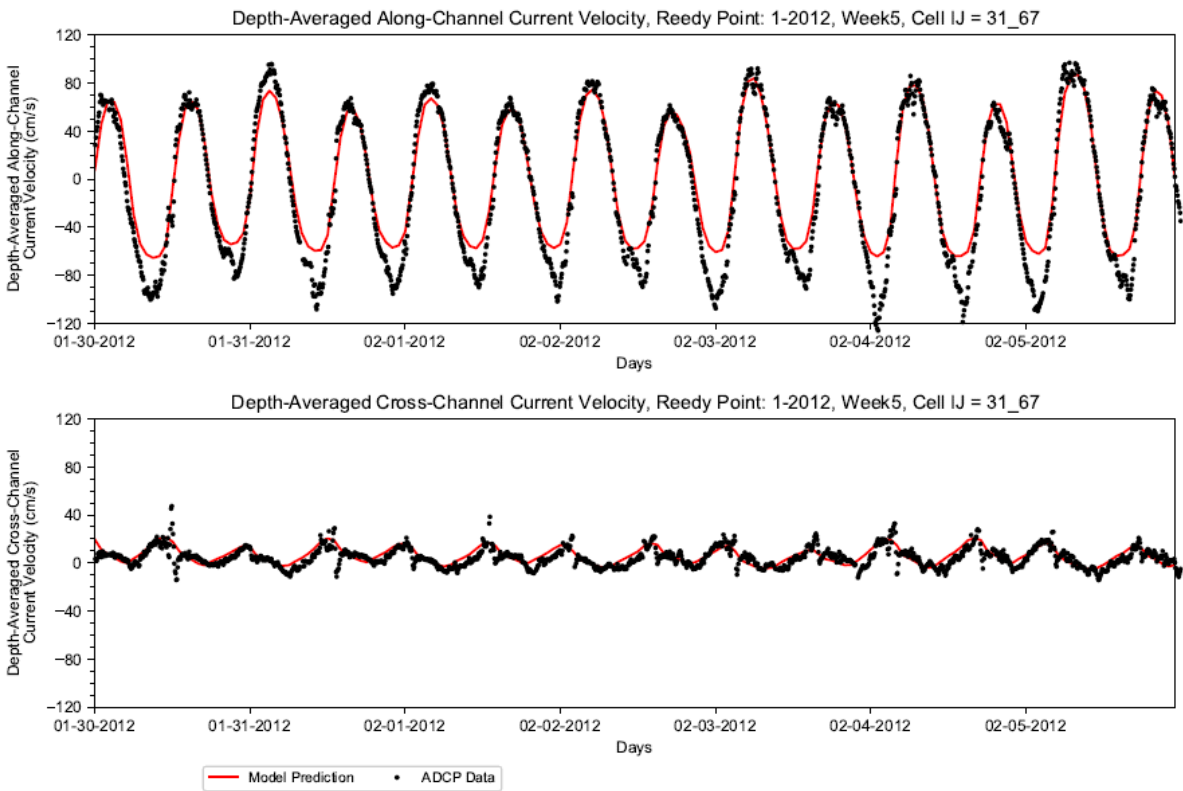
Figure J-5: Comparison of Observed and Predicted Along-Channel Depth-Averaged Current Velocity Magnitude at Brown Shoal Light during 06-01-2012 to 06-30-2012 period



Normalized Bias and Unbiased RMSD (uBRMSD) are shown.
Normalization was based on the standard deviation of the data
N = 719, Normalized Bias = -0.0222, Normalized Unbiased RMSD = 0.231, Reference STDV (data) = 46.3235

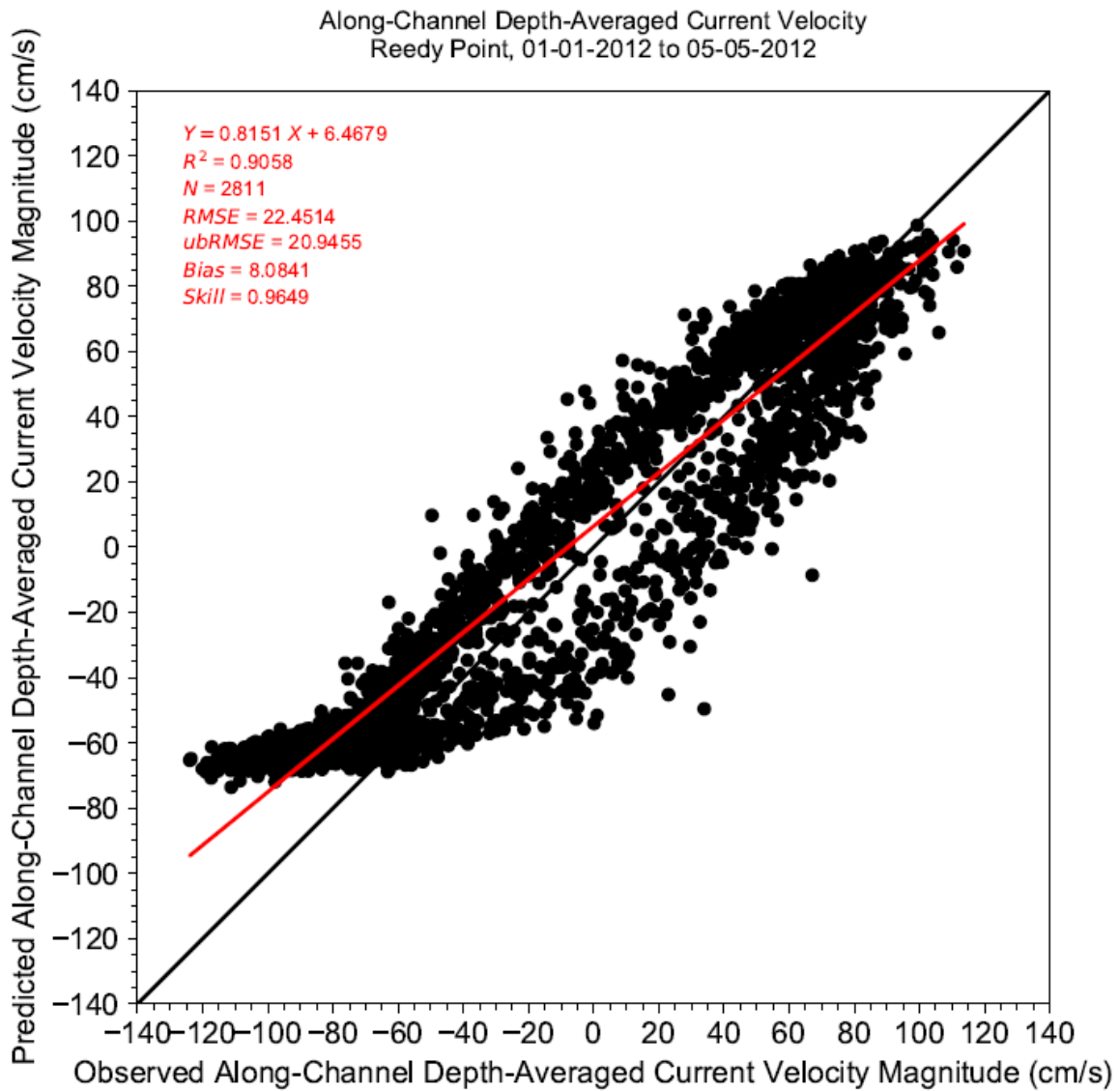
Note: Station ID: DB0501, Brown Shoal Light
Run ID: EFDC_HYDRO_G72_2023-01-06
Period: 06-01-2012 to 06-30-2012

Figure J-6: Target Diagram for Predicted Depth-Averaged Current Velocity at Brown Shoal Light



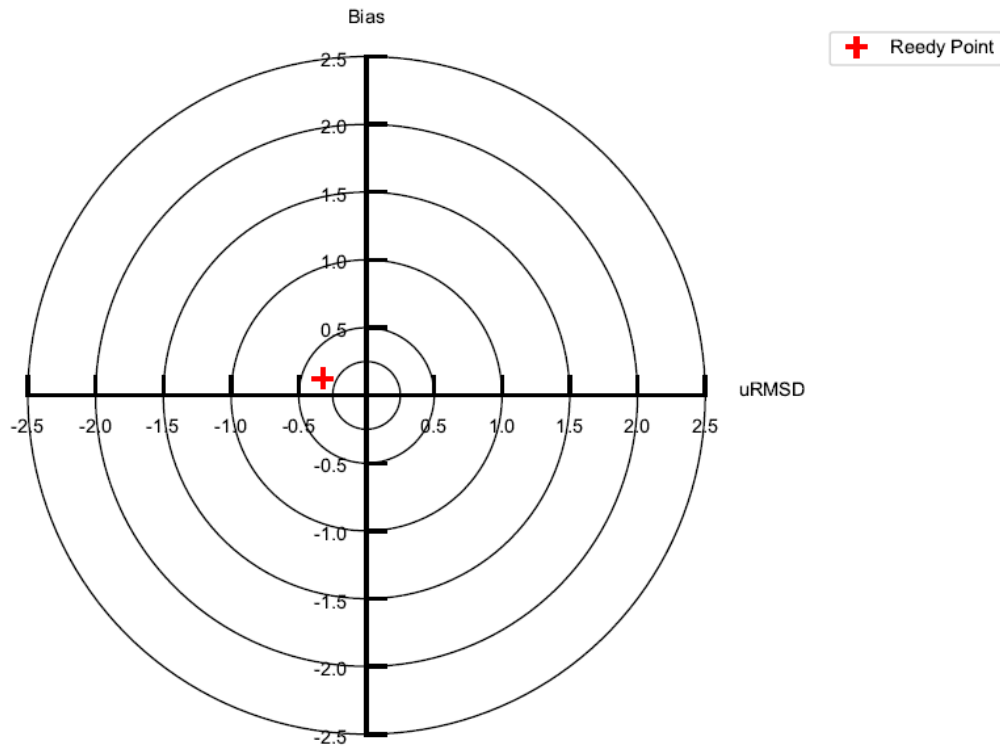
Note: Station ID: DB0201, Reedy Point
Run ID: EFDC_HYDRO_G72_2023-01-06

Figure J-7: Observed and Predicted Depth-Averaged Along-Channel and Cross-Channel Current Velocities at Reedy Point



Note: Station ID: DB0201, Reedy Point
Run ID: EFDC_HYDRO_G72_2023-01-06
Period: 01-01-2012 to 05-05-2012

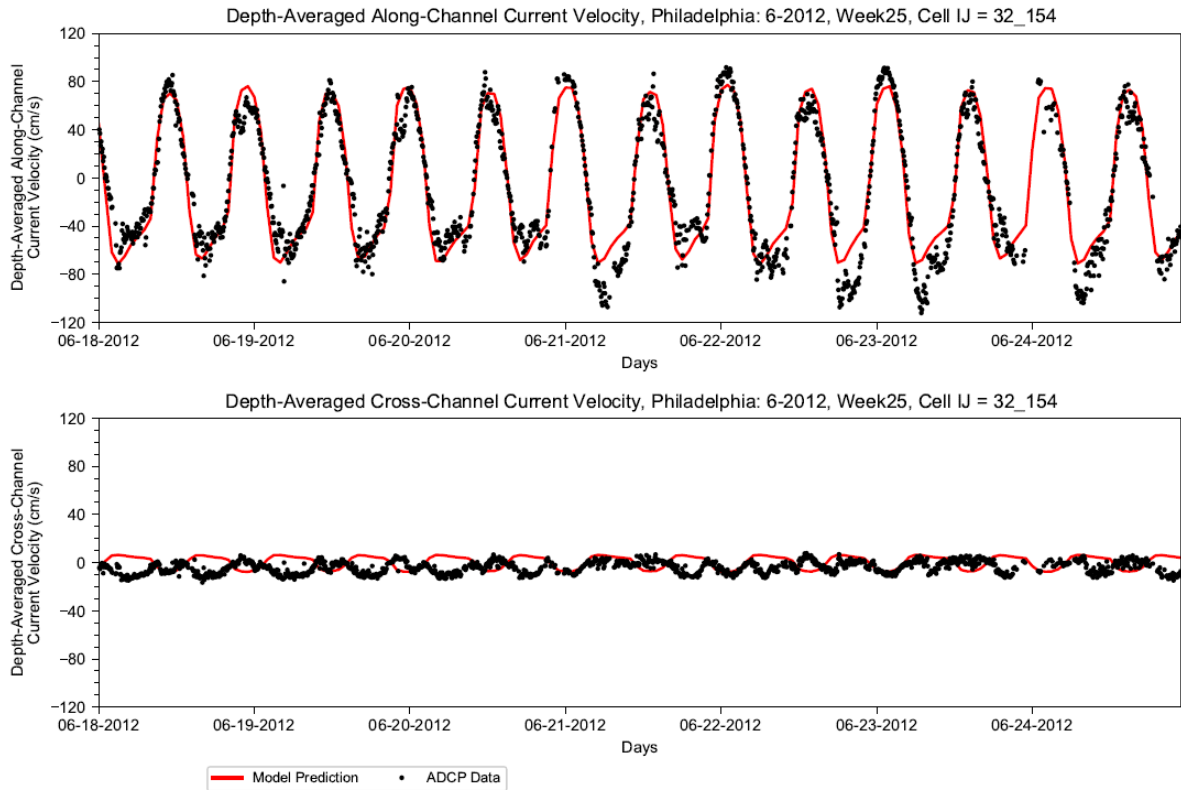
Figure J-8: Comparison of Observed and Predicted Along-Channel Depth-Averaged Current Velocity Magnitude at Reedy Point during 01-01-2012 to 05-05-2012 period



Normalized Bias and Unbiased RMSD (ubRMSD) are shown.
Normalization was based on the standard deviation of the data
N = 2811, Normalized Bias = 0.124, Normalized Unbiased RMSD = -0.3213, Reference STDV (data) = 65.1842

Note: Station ID: DB0201, Reedy Point
Run ID: EFDC_HYDRO_G72_2023-01-06
Period: 01-01-2012 to 05-05-2012

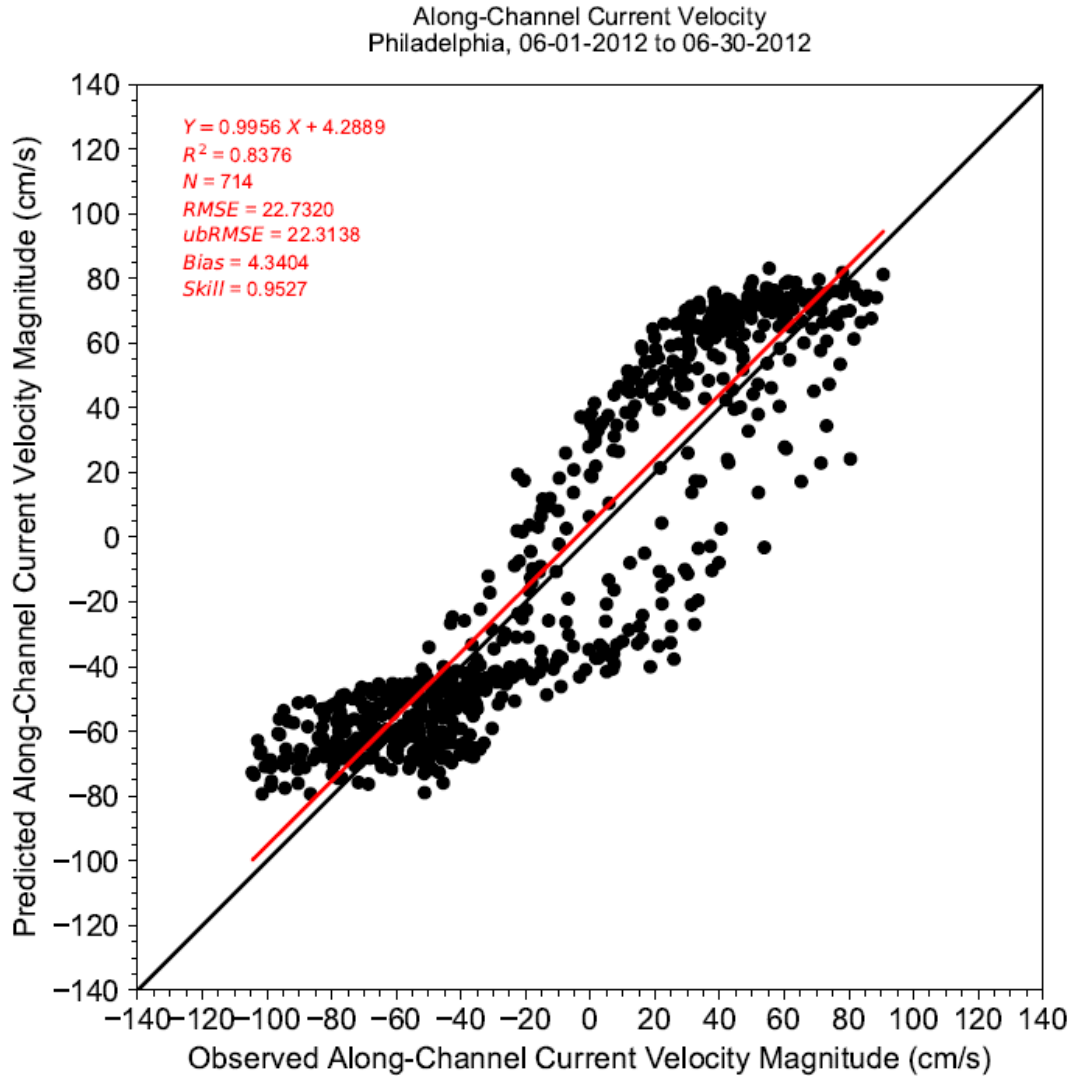
Figure J-9: Target Diagram for Predicted Depth-Averaged Current Velocity at Reedy Point



Note: Station ID: DB0301, Philadelphia
 Run ID: EFDC_HYDRO_G72_2023-01-06

Use caution for model-to-data comparisons of depth-averaged current velocity collected at NOAA Philadelphia (db0301). Current velocity data were collected at a fixed depth, and the sensor is shooting sideways across the river. Sensor depth is 4.5 m, and it is located at the west bank (PA side). Signals from bin# 34, which is approximately 138 m from the sensor, were used for the comparison with model results for predicted depth-averaged velocity at cell (32, 154) inside the ship channel. It was assumed that the ADCP depth of 4.5 m is representative of the depth-averaged value at that location. The depth of the ship channel is approximately 45 ft (13.7 m) below MLLW.

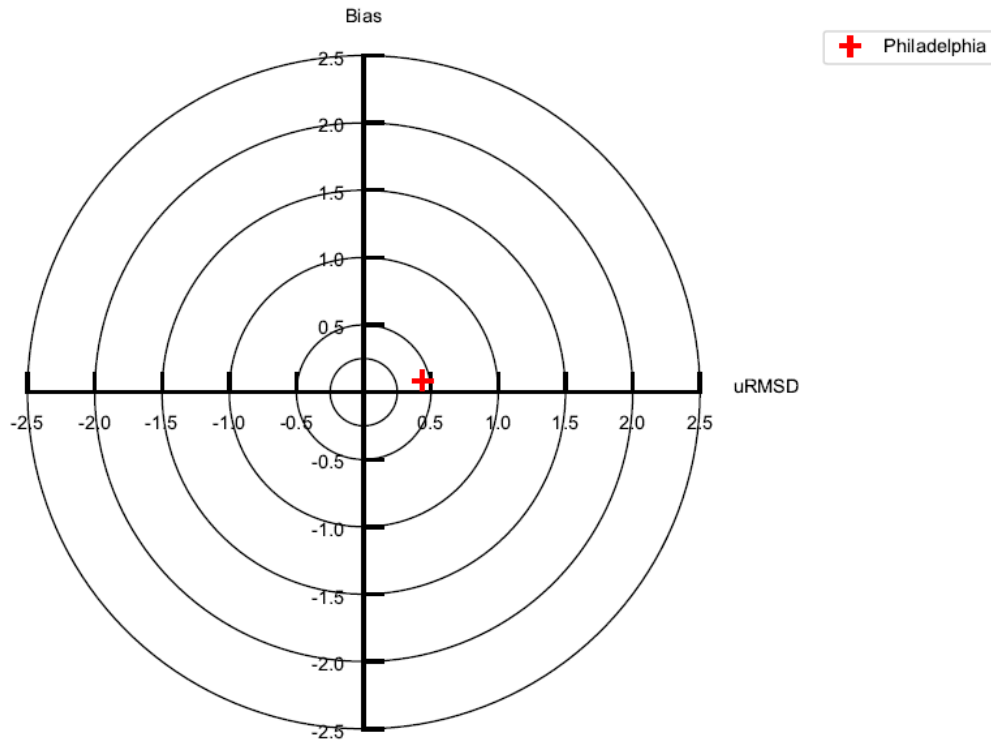
Figure J-10: Observed and Predicted Depth-Averaged Along-Channel and Cross-Channel Current Velocities at Philadelphia



Note: Station ID: DB0301, Philadelphia
 Run ID: EFDC_HYDRO_G72_2023-01-06

Use caution for model-to-data comparisons of depth-averaged current velocity collected at NOAA Philadelphia (db0301). Current velocity data were collected at a fixed depth, and the sensor is shooting sideways across the river. Sensor depth is 4.5 m, and it is located at the west bank (PA side). Signals from bin# 34, which is approximately 138 m from the sensor, were used for the comparison with model results for predicted depth-averaged velocity at cell (32, 154) inside the ship channel. It was assumed that the ADCP depth of 4.5 m is representative of the depth-averaged value at that location. The depth of the ship channel is approximately 45 ft (13.7 m) below MLLW.

Figure J-11: Comparison of Observed and Predicted Along-Channel Current Velocity Magnitude at Philadelphia during 06-01-2012 to 06-30-2012 period



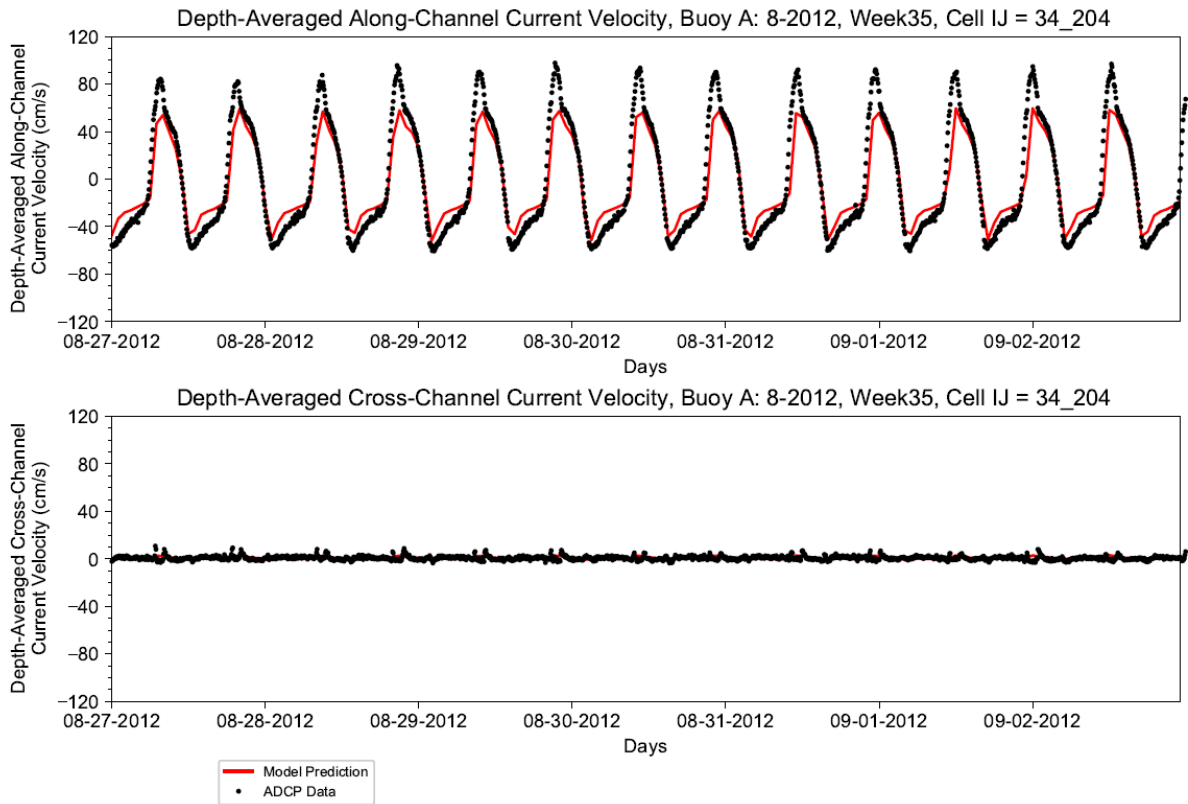
Normalized Bias and Unbiased RMSD (ubRMSD) are shown.
 Normalization was based on the standard deviation of the data
 N = 714, Normalized Bias = 0.0852, Normalized Unbiased RMSD = 0.4381, Reference STDV (data) = 50.9345

Note: Station ID: DB0301, Philadelphia
 Run ID: EFDC_HYDRO_G72_2023-01-06

Use caution for model-to-data comparisons of depth-averaged current velocity collected at NOAA Philadelphia (db0301). Current velocity data were collected at a fixed depth, and the sensor is shooting sideways across the river. Sensor depth is 4.5 m, and it is located at the west bank (PA side). Signals from bin# 34, which is approximately 138 m from the sensor, were used for the comparison with model results for predicted depth-averaged velocity at cell (32, 154) inside the ship channel. It was assumed that the ADCP depth of 4.5 m is representative of the depth-averaged value at that location. The depth of the ship channel is approximately 45 ft (13.7 m) below MLLW.

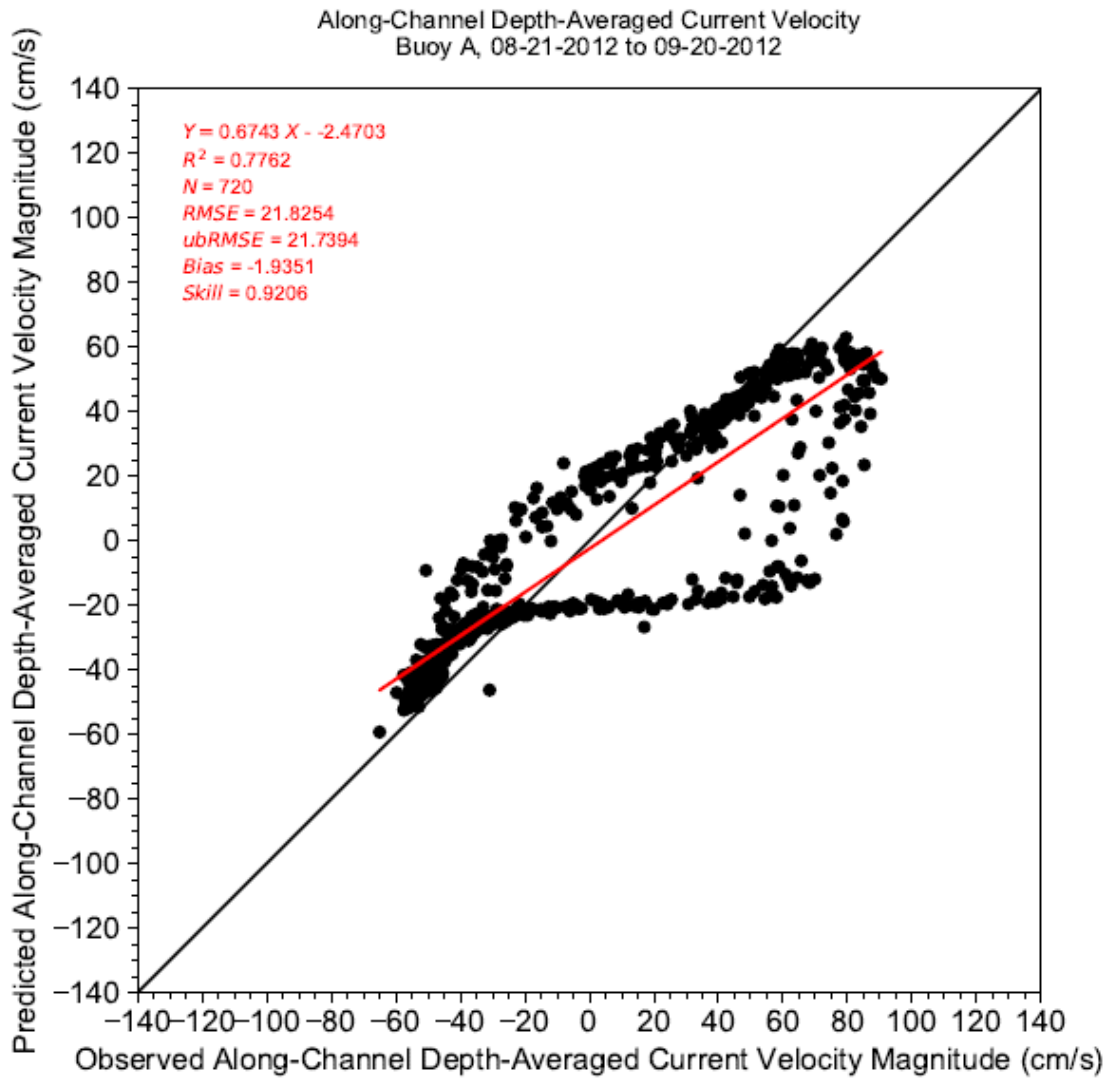
Figure J-12: Target Diagram for Predicted Depth-Averaged Current Velocity at Philadelphia

Appendix K: Observed and predicted depth-averaged current velocity magnitude at PWD buoy locations



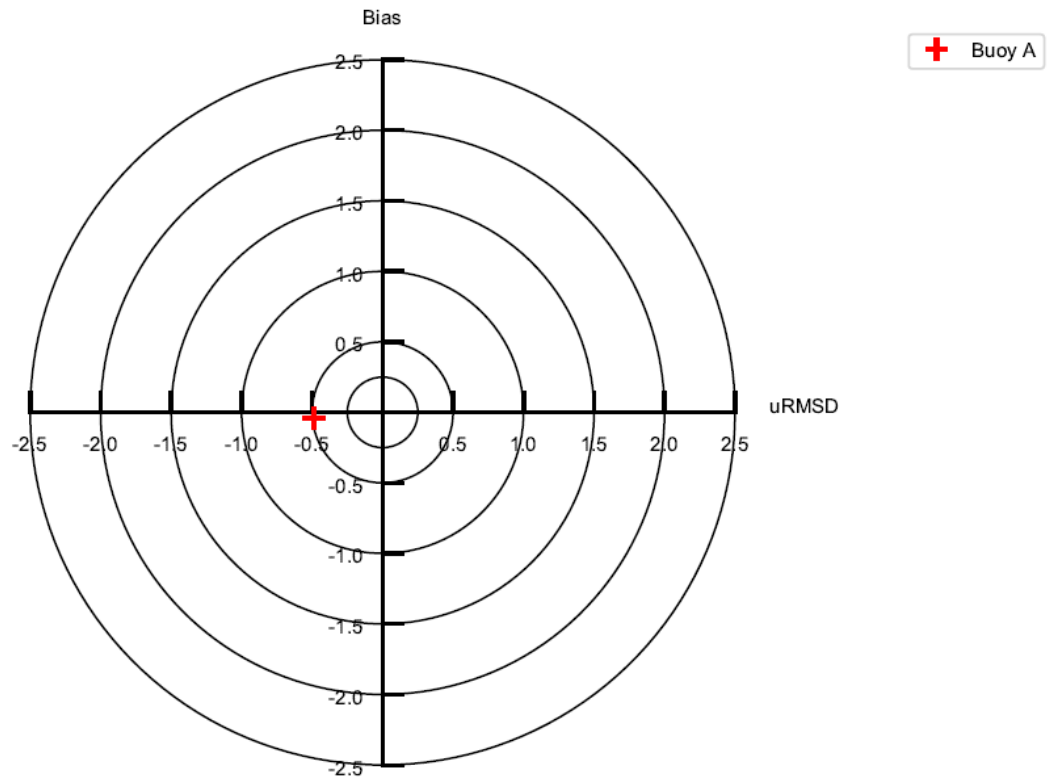
Note: ADCP current velocity data collected during August 21 through September 20, 2012, from Deployment #3, were used in this analysis. Data were provided by PWD to DRBC on December 14, 2022. This is an example figure showing results for the one-week period from September 3 to September 9, 2012.

Figure K-1: Observed and Predicted Depth-Averaged Along and Cross-Channel Current Velocity at Buoy A



Note: ADCP current velocity data collected during August 21 through September 20, 2012, from Deployment #3, were used in this analysis. Data were provided by PWD to DRBC on December 14, 2022.

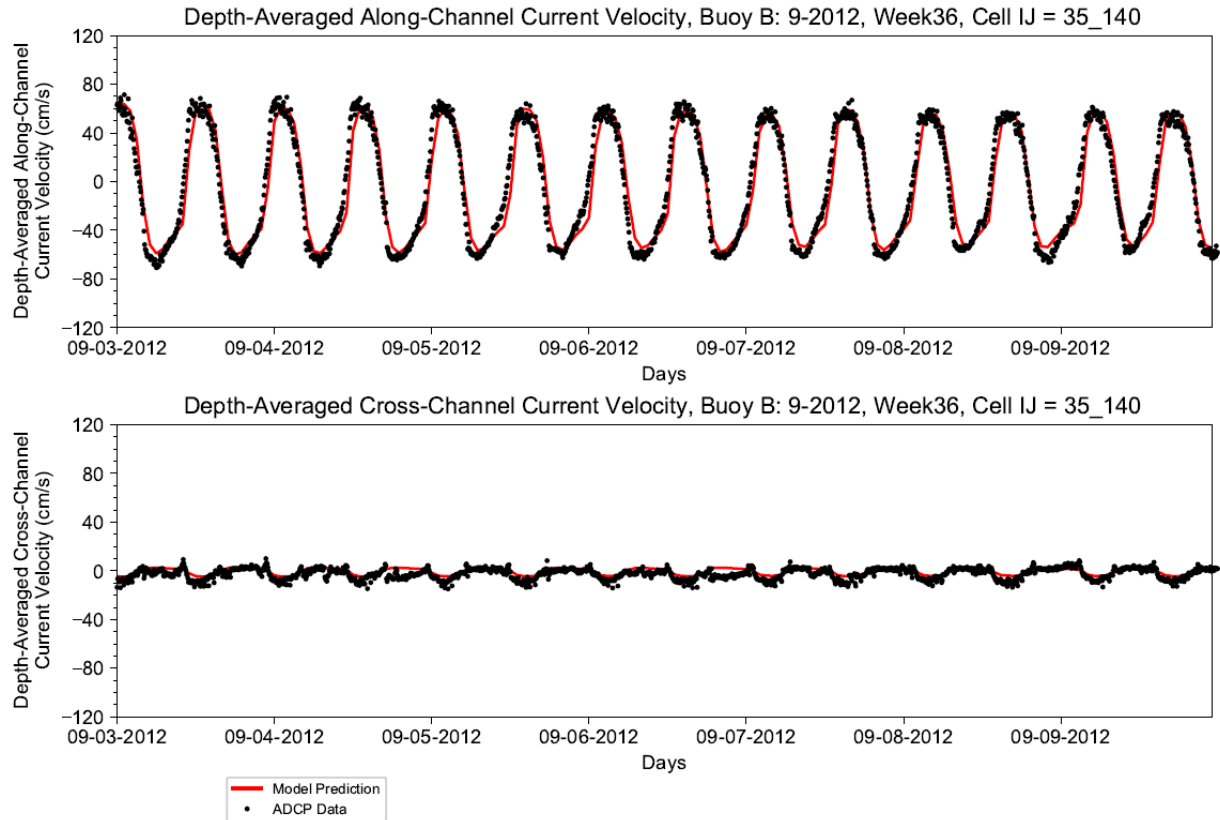
Figure K-2: Comparison of Observed and Predicted Along-Channel Depth-Averaged Current Velocity Magnitude at Buoy A during 08-21-2012 to 09-20-2012 period



Normalized Bias and Unbiased RMSD (ubRMSD) are shown.
Normalization was based on the standard deviation of the data
N = 720, Normalized Bias = -0.0423, Normalized Unbiased RMSD = -0.4874, Reference STDV (data) = 44.6714

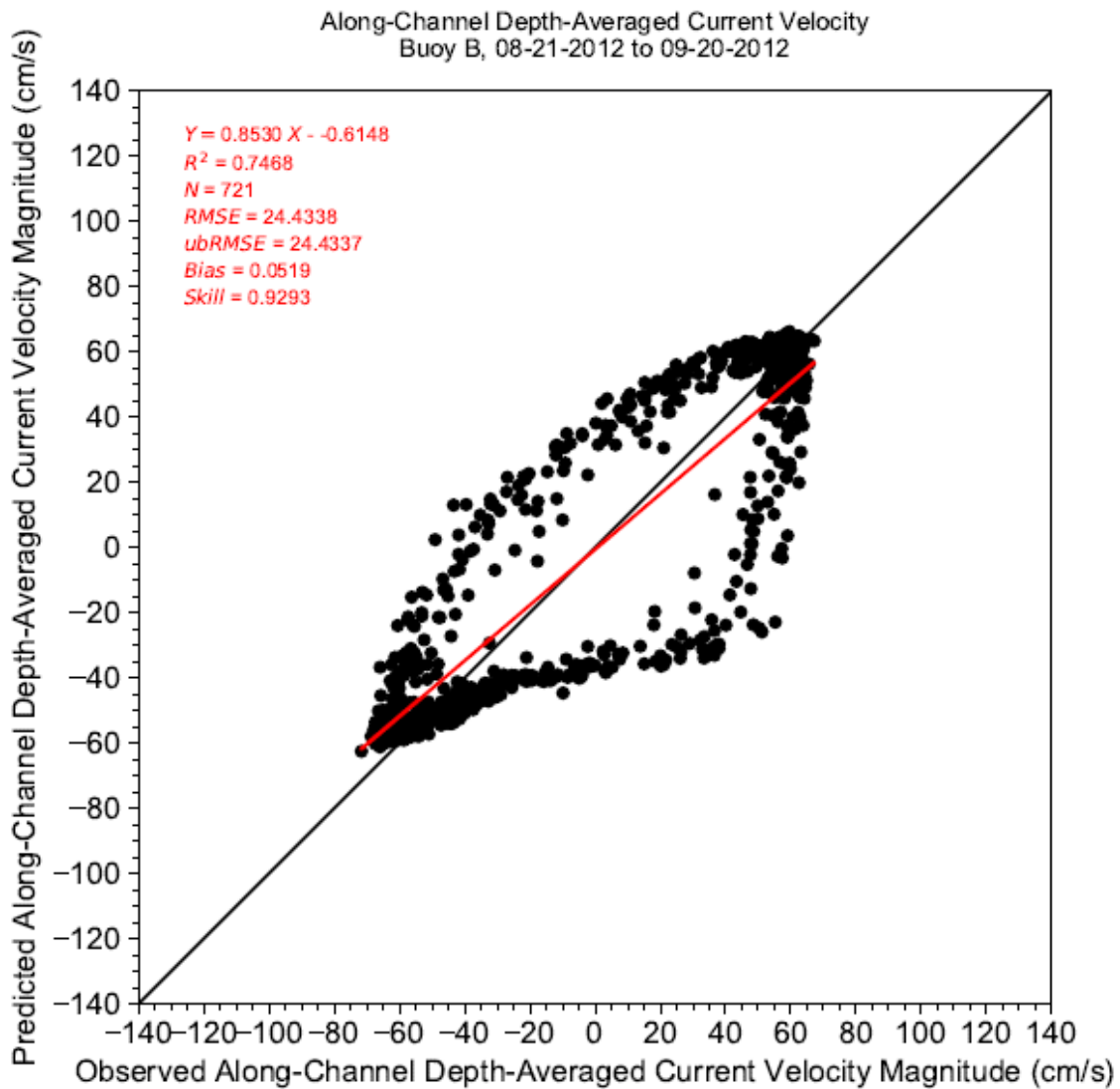
Note: ADCP current velocity data collected during August 21 through September 20, 2012, from Deployment #3, were used in this analysis. Data were provided by PWD to DRBC on December 14, 2022.

Figure K-3: Target Diagram for Predicted Along-Channel Depth-Averaged Current Velocity at Buoy A



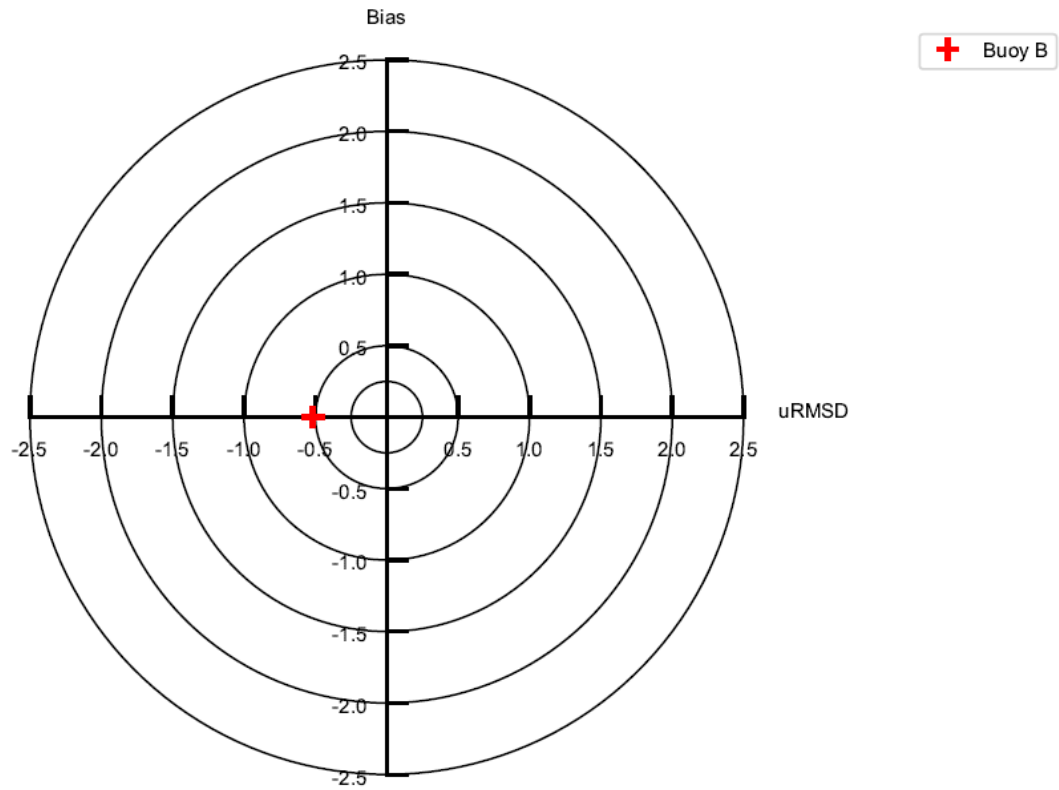
Note: ADCP current velocity data collected during August 21 through September 20, 2012, from Deployment #3, were used in this analysis. Data were provided by PWD to DRBC on December 14, 2022. This is an example figure showing results for the one-week period from September 3 to September 9, 2012.

Figure K-4: Observed and Predicted Depth-Averaged Along and Cross-Channel Current Velocity at Buoy B



Note: ADCP current velocity data collected during August 21 through September 20, 2012, from Deployment #3, were used in this analysis. Data were provided by PWD to DRBC on December 14, 2022.

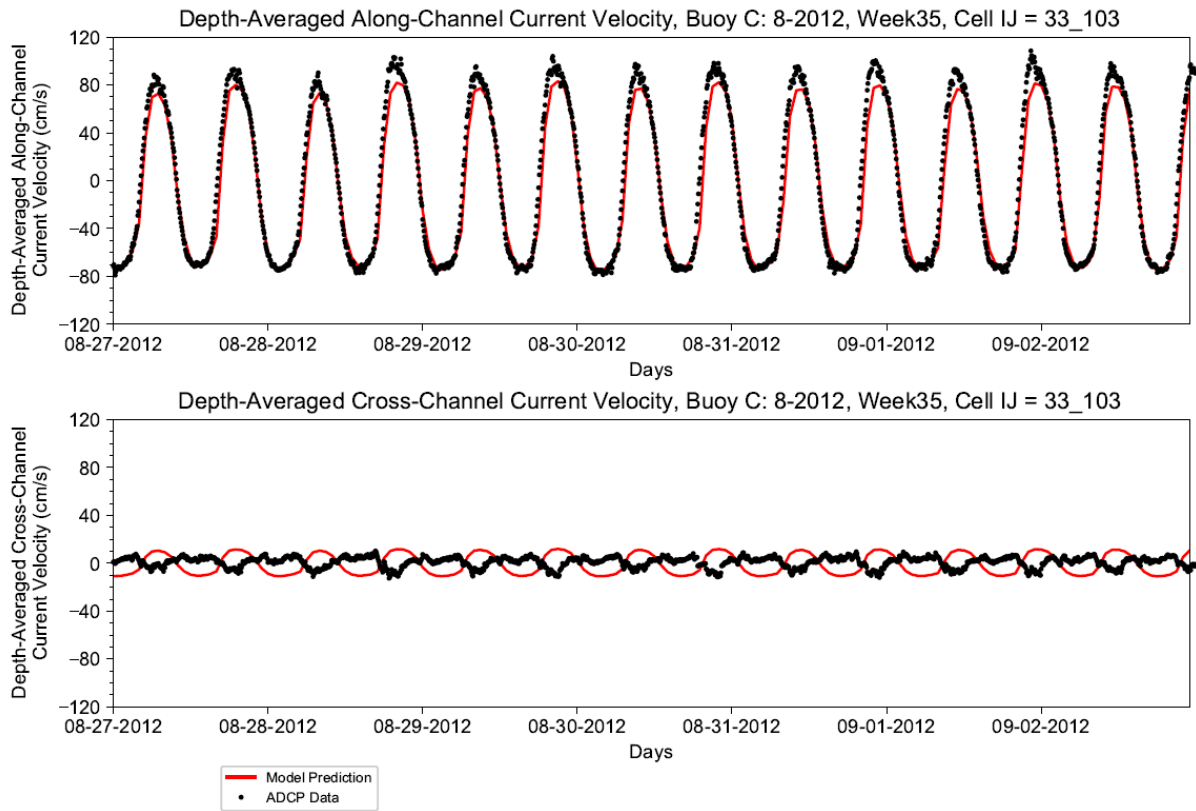
Figure K-5: Comparison of Observed and Predicted Along-Channel Depth-Averaged Current Velocity Magnitude at Buoy B during 08-21-2012 to 09-20-2012 period



Normalized Bias and Unbiased RMSD (ubRMSD) are shown.
Normalization was based on the standard deviation of the data
N = 721, Normalized Bias = 0.0015, Normalized Unbiased RMSD = -0.5183, Reference STDV (data) = 47.1999

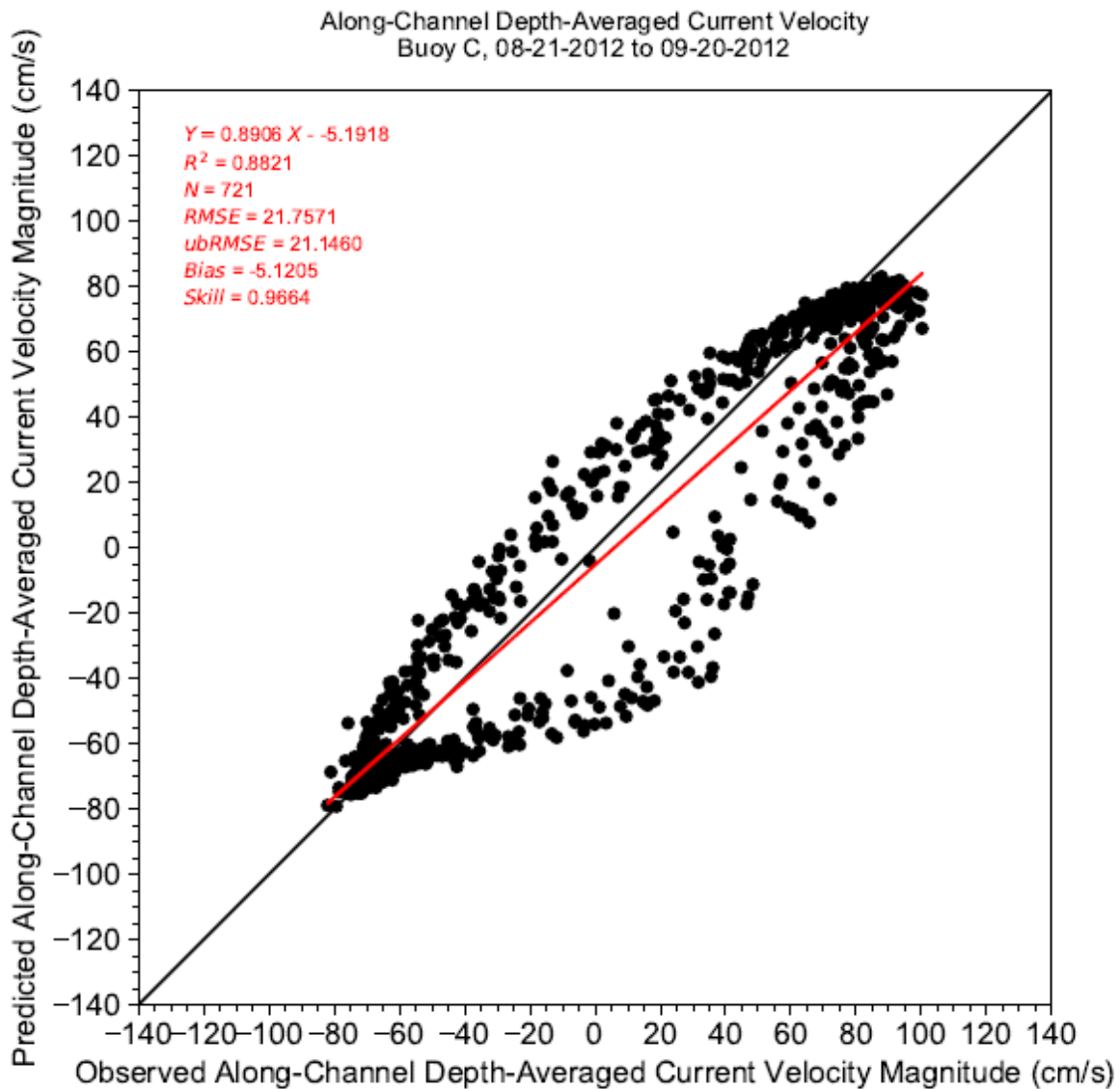
Note: ADCP current velocity data collected during August 21 through September 20, 2012, from Deployment #3, were used in this analysis. Data were provided by PWD to DRBC on December 14, 2022.

Figure K-6: Target Diagram for Predicted Along-Channel Depth-Averaged Current Velocity at Buoy B



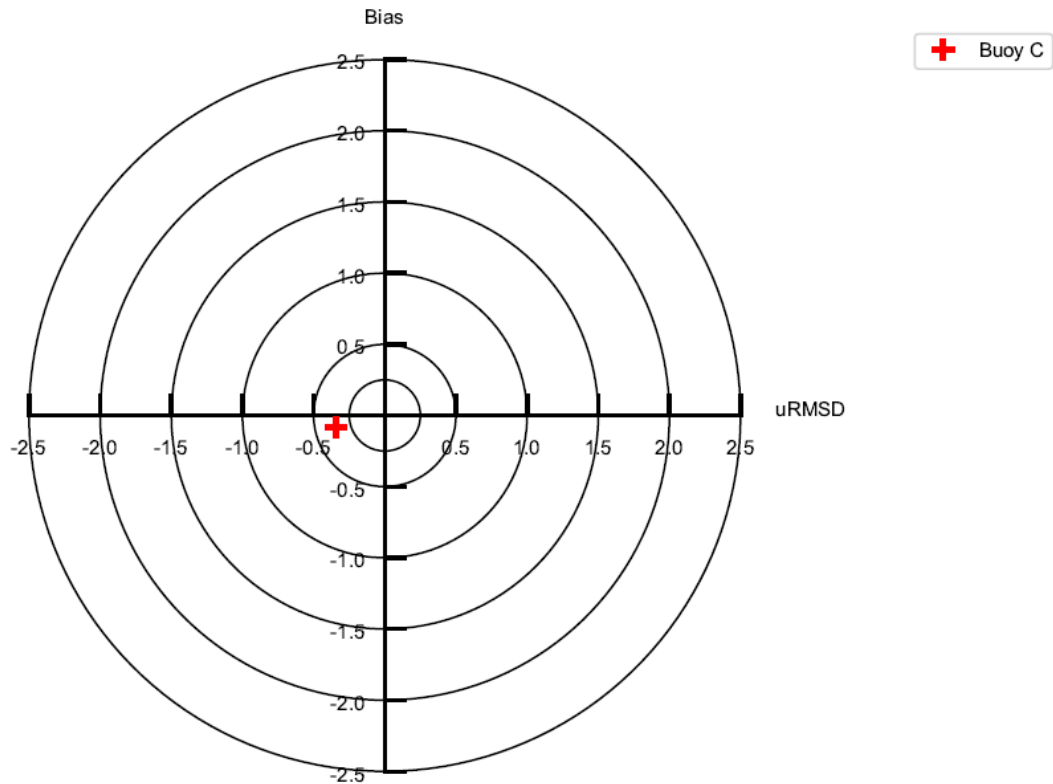
Note: ADCP current velocity data collected during August 21 through September 20, 2012, from Deployment #3, were used in this analysis. Data were provided by PWD to DRBC on December 14, 2022. This is an example figure showing results for the one-week period from September 3 to September 9, 2012.

Figure K-7: Observed and Predicted Depth-Averaged Along and Cross-Channel Current Velocity at Buoy C



Note: ADCP current velocity data collected during August 21 through September 20, 2012, from Deployment #3, were used in this analysis. Data were provided by PWD to DRBC on December 14, 2022.

Figure K-8: Comparison of Observed and Predicted Along-Channel Depth-Averaged Current Velocity Magnitude at Bouy C during 08-21-2012 to 09-20-2012 period



Normalized Bias and Unbiased RMSD (ubRMSD) are shown.
Normalization was based on the standard deviation of the data
N = 721, Normalized Bias = -0.0826, Normalized Unbiased RMSD = -0.3437, Reference STDV (data) = 61.6167

Note: ADCP current velocity data collected during August 21 through September 20, 2012, from Deployment #3, were used in this analysis. Data were provided by PWD to DRBC on December 14, 2022.

Figure K-9: Target Diagram for Predicted Along-Channel Depth-Averaged Current Velocity at Buoy C

Appendix L: Summary of harmonic analysis for current velocity at NOAA stations

Table L-1: Summary of Harmonic Analysis for Along-Channel Depth-Averaged Current Velocity

Station	Station ID	Symbol	RM	Amplitude (m/s)			Phase (degree)			Phase (hours)		
				EFDC Predicted	Data	Difference (cm/s)	EFDC Predicted	Data	Difference (deg.)	EFDC Predicted	Data	Difference (hr.)
Brown Shoal Light	db0501	M2	5.8	0.637	0.567	7.07	154.98	136.93	18.05	5.347	4.724	0.623
	db0501	S2	5.8	0.067	0.116	-4.90	191.55	182.55	9.00	6.385	6.085	0.300
	db0501	N2	5.8	0.123	0.196	-7.30	126.87	101.09	25.78	4.461	3.555	0.906
	db0501	K1	5.8	0.059	0.078	-1.92	302.55	292.67	9.88	20.115	19.458	0.657
	db0501	M4	5.8	0.017	0.002	1.52	487.70	309.18	178.52	8.413	5.334	3.080
	db0501	O1	5.8	0.031	0.026	0.42	294.57	290.64	3.93	21.127	20.845	0.282
	db0501	M6	5.8	0.018	0.007	1.03	321.86	238.53	83.33	3.702	2.743	0.958
Delaware Bay Channel LB 10	db0502	M2	6.9	0.627	0.503	12.38	153.47	132.21	21.26	5.295	4.561	0.734
	db0502	S2	6.9	0.117	0.125	-0.72	214.82	159.83	54.99	7.161	5.328	1.833
	db0502	N2	6.9	0.000	0.000	0.00	0.00	0.00	0.00	0.000	0.000	0.000
	db0502	K1	6.9	0.038	0.027	1.06	330.67	319.74	10.93	21.984	21.258	0.727
	db0502	M4	6.9	0.020	0.005	1.51	476.54	319.90	156.64	8.221	5.519	2.702
	db0502	O1	6.9	0.037	0.040	-0.33	295.07	292.91	2.16	21.163	21.008	0.155
	db0502	M6	6.9	0.014	0.023	-0.96	315.12	211.95	103.17	3.624	2.438	1.187
Reedy Point	db0201	M2	58.3	0.748	0.871	-12.34	68.70	56.21	12.49	2.370	1.939	0.431
	db0201	S2	58.3	0.066	0.086	-2.01	111.87	101.86	10.01	3.729	3.395	0.334
	db0201	N2	58.3	0.000	0.000	0.00	0.00	0.00	0.00	0.000	0.000	0.000
	db0201	K1	58.3	0.054	0.101	-4.71	162.05	164.62	-2.57	10.774	10.945	-0.171
	db0201	M4	58.3	0.083	0.102	-1.87	124.79	29.50	95.29	2.153	0.509	1.644
	db0201	O1	58.3	0.038	0.039	-0.10	168.82	171.54	-2.72	12.108	12.303	-0.195
	db0201	M6	58.3	0.053	0.056	-0.25	400.51	319.57	80.94	4.606	3.675	0.931
Philadelphia	db0301	M2	79.3	0.715	0.605	10.99	123.27	107.27	16.00	4.253	3.701	0.552
	db0301	S2	79.3	0.049	0.118	-6.87	173.14	173.43	-0.29	5.771	5.781	-0.010
	db0301	N2	79.3	0.094	0.173	-7.89	94.67	71.81	22.86	3.329	2.525	0.804
	db0301	K1	79.3	0.051	0.085	-3.34	195.61	188.26	7.35	13.005	12.516	0.489
	db0301	M4	79.3	0.170	0.068	10.13	270.21	203.85	66.36	4.661	3.517	1.145
	db0301	O1	79.3	0.027	0.073	-4.58	181.09	168.51	12.58	12.988	12.086	0.902
	db0301	M6	79.3	0.069	0.041	2.82	228.06	173.97	54.09	2.623	2.001	0.622

Notes: Use caution for model-to-data comparisons of depth-averaged current velocity collected at NOAA Philadelphia (db0301). Current velocity data were collected at a fixed depth, and the sensor is shooting sideways across the river. Sensor depth is 4.5 m, and it is located at the west bank (PA side). Signals from bin# 34, which is approximately 138 m from the sensor, were used for comparison with model results for predicted depth-averaged velocity at cell (32, 154) inside the ship channel. It was assumed that the ADCP depth of 4.5 m is representative of the depth-averaged value at that location. The depth of the ship channel is approximately 45 ft (13.7m) below MLLW. Although model skill score is acceptable, large uncertainty exists at this location because of this assumption and the grid resolution.

Appendix M: Harmonics analysis for current velocity at NOAA stations

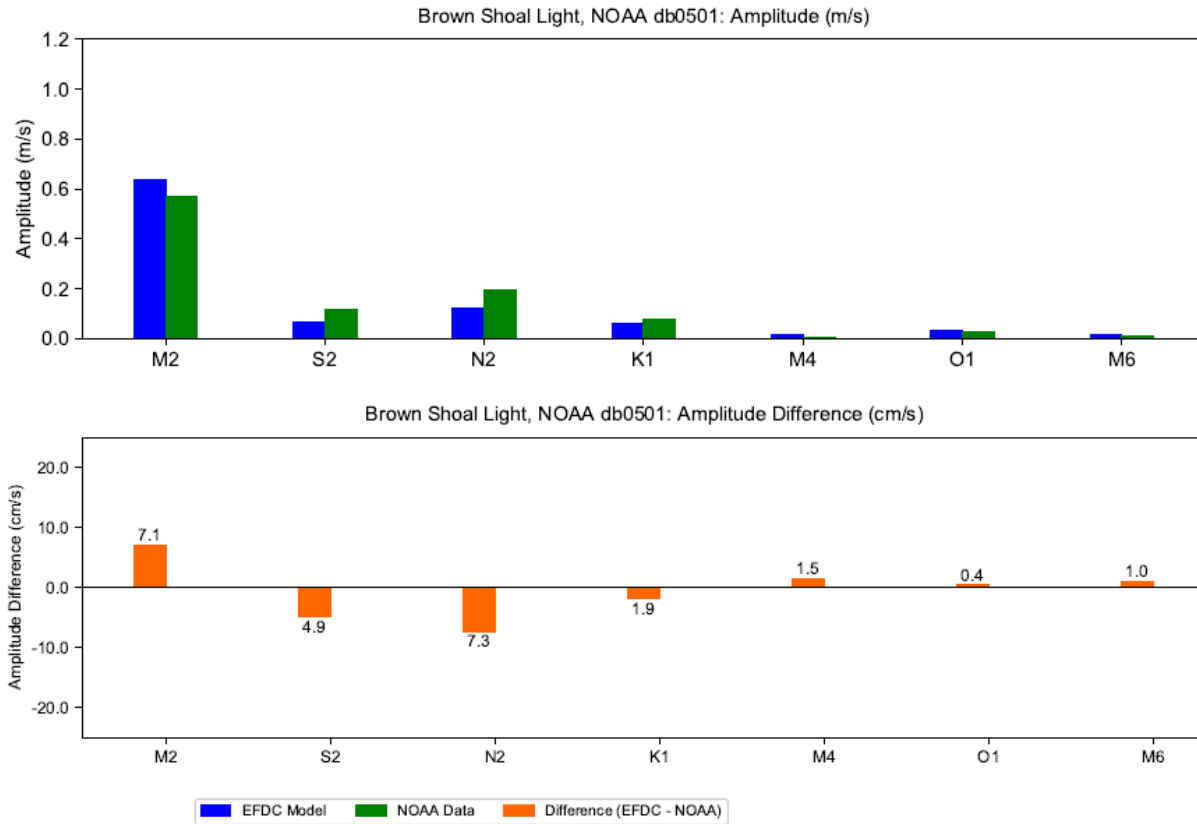


Figure M-1: Harmonics Analysis for Predicted Along-Channel Depth-Averaged Current Velocity Amplitude at Brown Shoal Light, NOAA Station db0501 based on Data Collected from to 06-01-2012_to_06-30-2012 Period

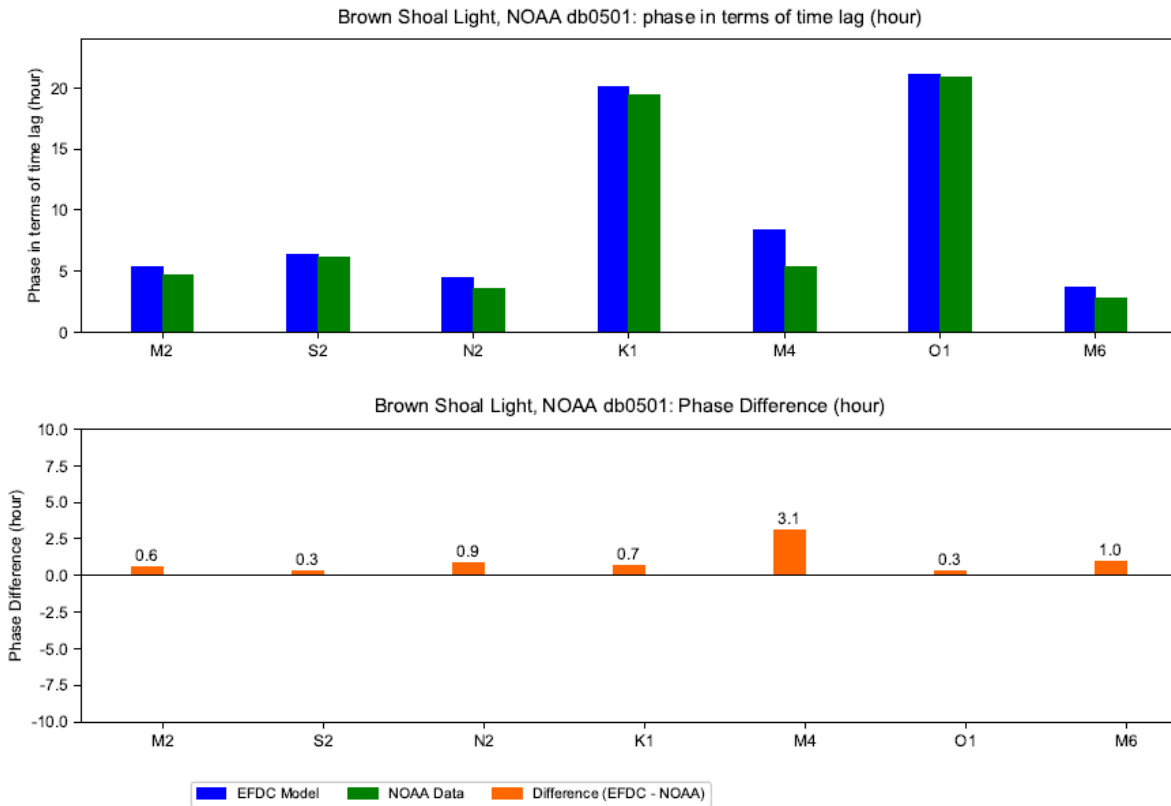


Figure M-2: Harmonics Analysis for Predicted Along-Channel Depth-Averaged Current Velocity Phase at Brown Shoal Light, NOAA Station db0501 based on Data Collected from to 06-01-2012_to_06-30-2012 Period

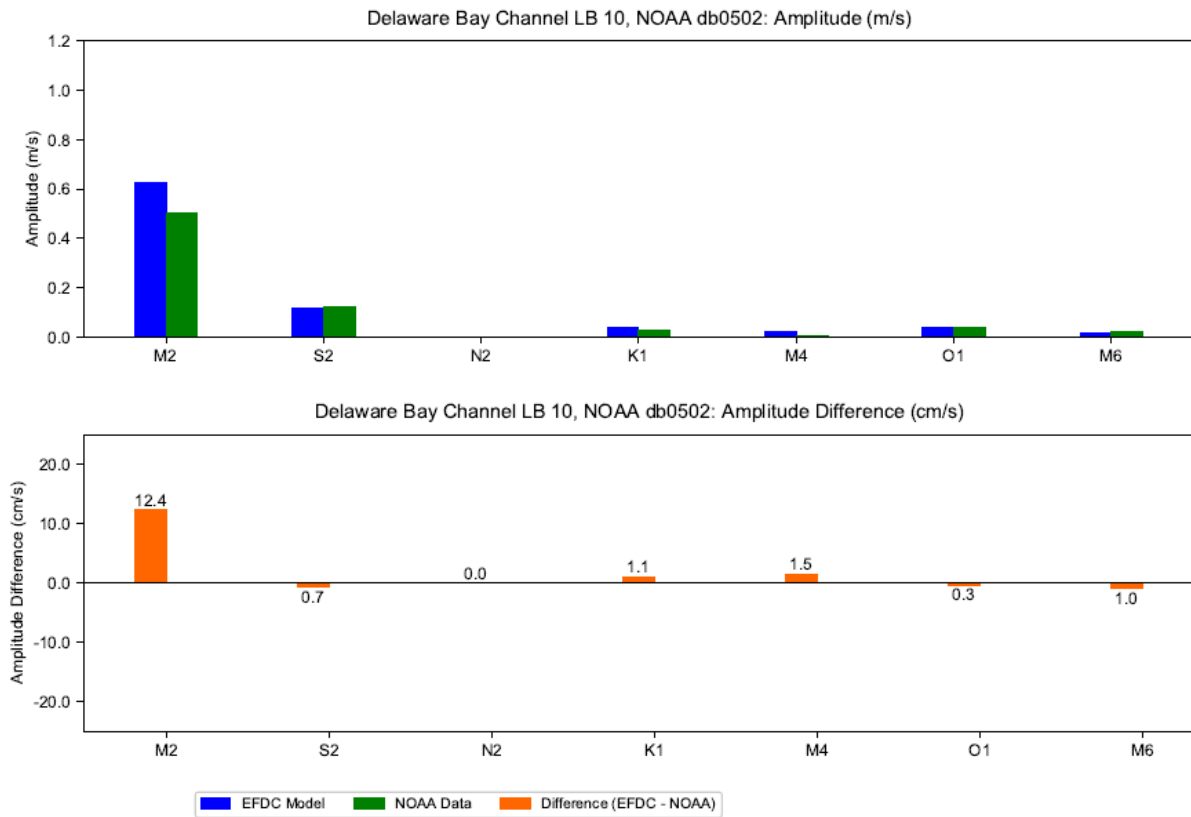


Figure M-3: Harmonics Analysis for Predicted Along-Channel Depth-Averaged Current Velocity Amplitude at Delaware Bay Channel LB 10, NOAA Station db0502 based on Data Collected from 02-01-2019 to 02-25-2019 Period

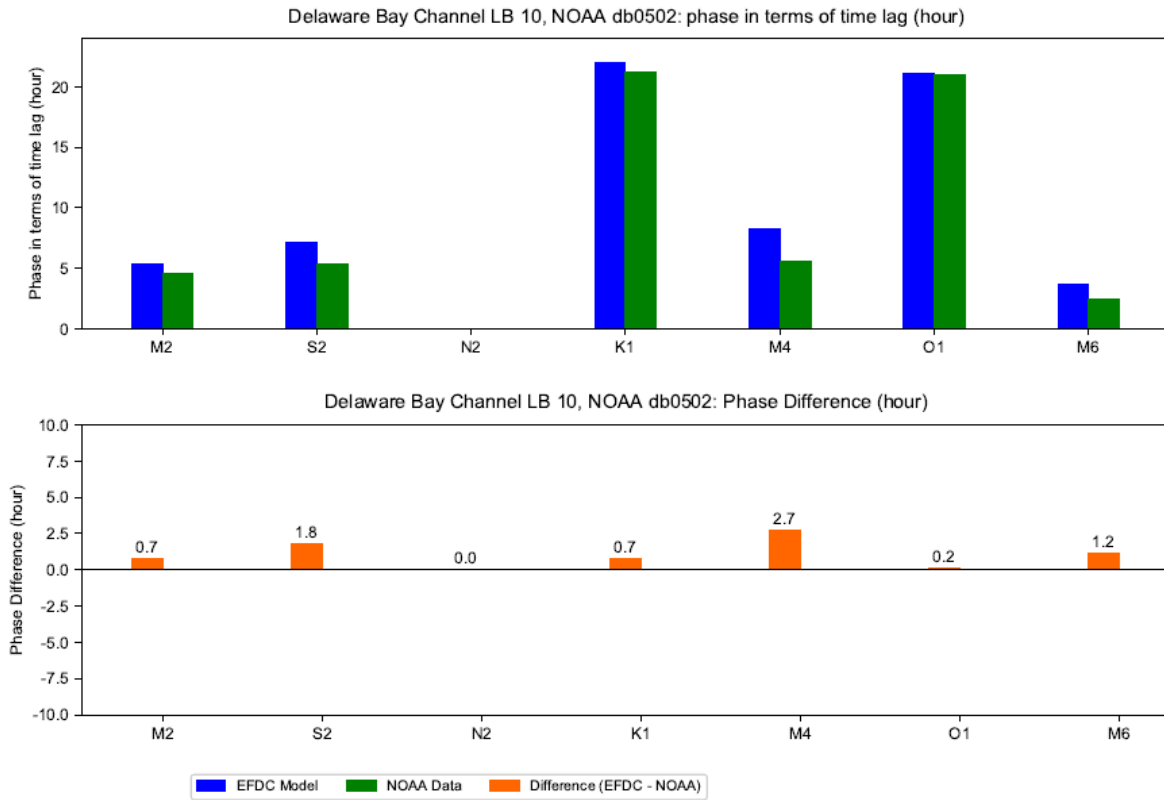


Figure M-4: Harmonics Analysis for Predicted Along-Channel Depth-Averaged Current Velocity Phase at Delaware Bay Channel LB 10, NOAA Station db0502 based on Data Collected from 02-01-2019 to 02-25-2019 Period

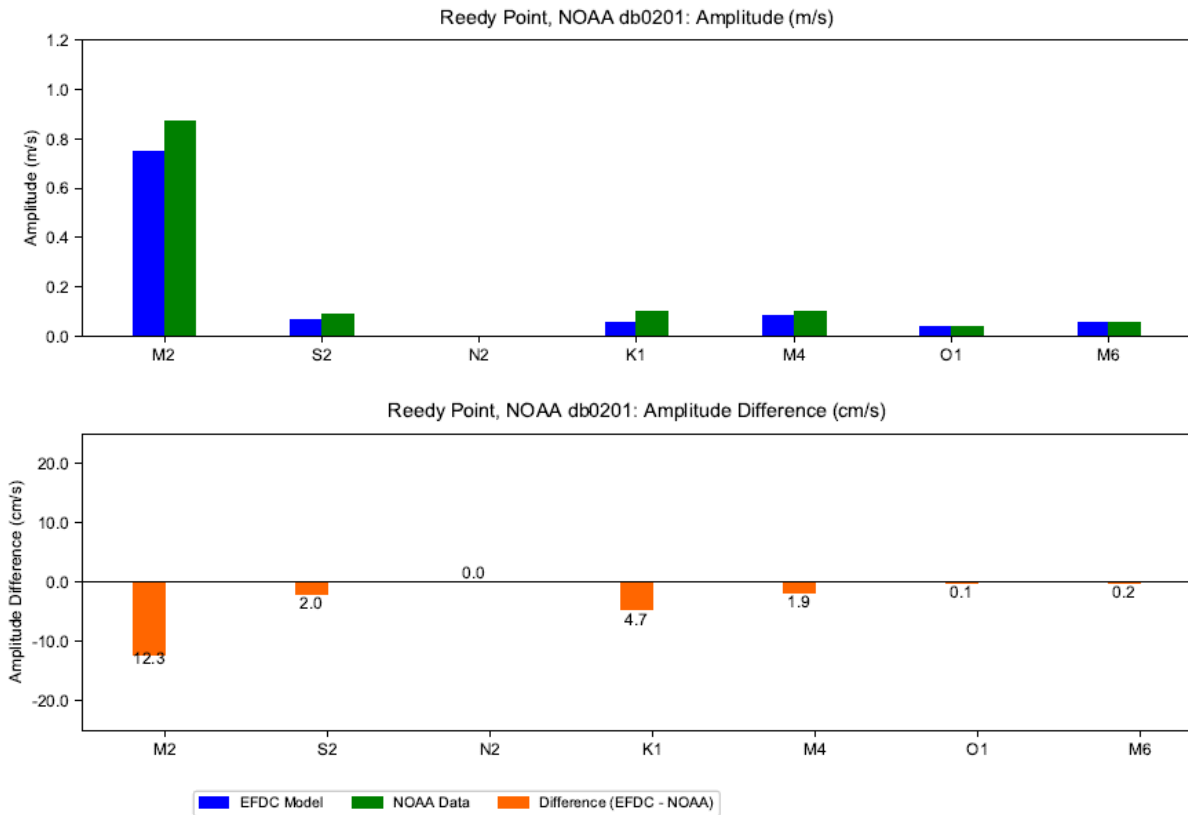


Figure M-5: Harmonics Analysis for Predicted Along-Channel Depth-Averaged Current Velocity Amplitude at Reedy Point, NOAA Station db0201 based on Data Collected from 03-28-2012 to 04-16-2012 Period

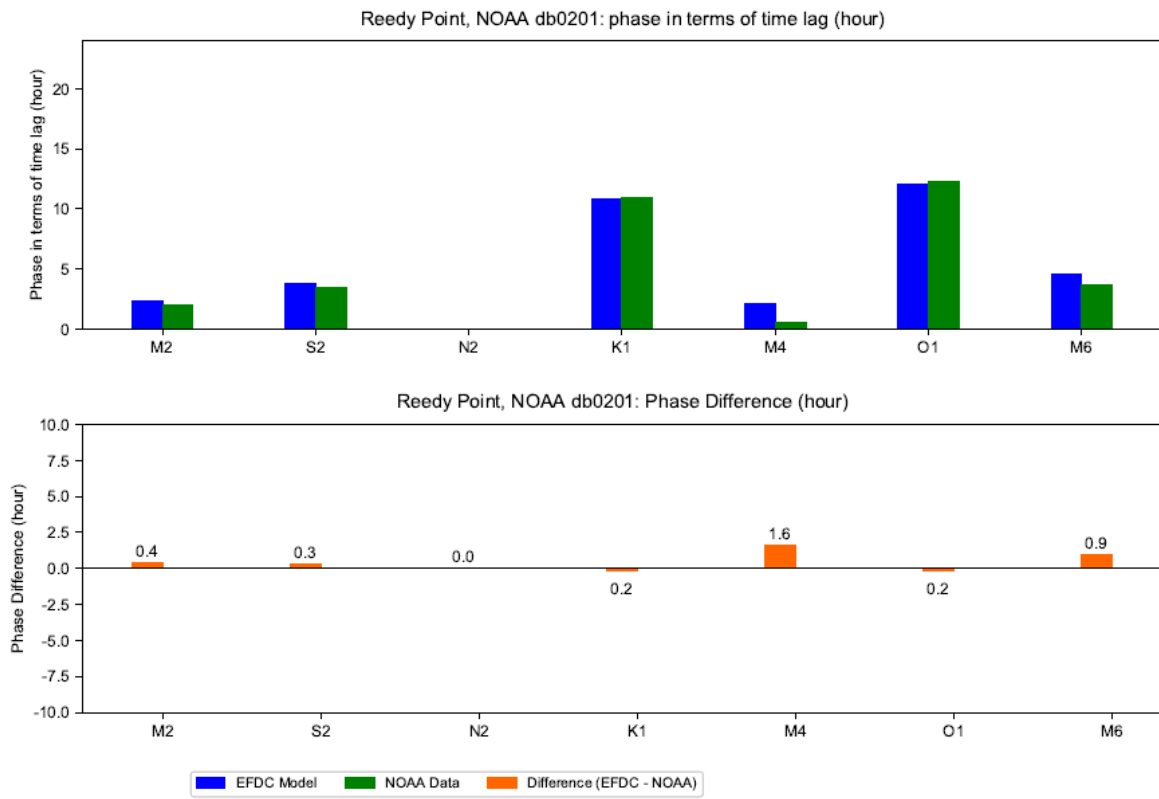


Figure M-6: Harmonics Analysis for Predicted Along-Channel Depth-Averaged Current Velocity Phase at Reedy Point, NOAA Station db0201 based on Data Collected from 03-28-2012 to 04-16-2012 Period

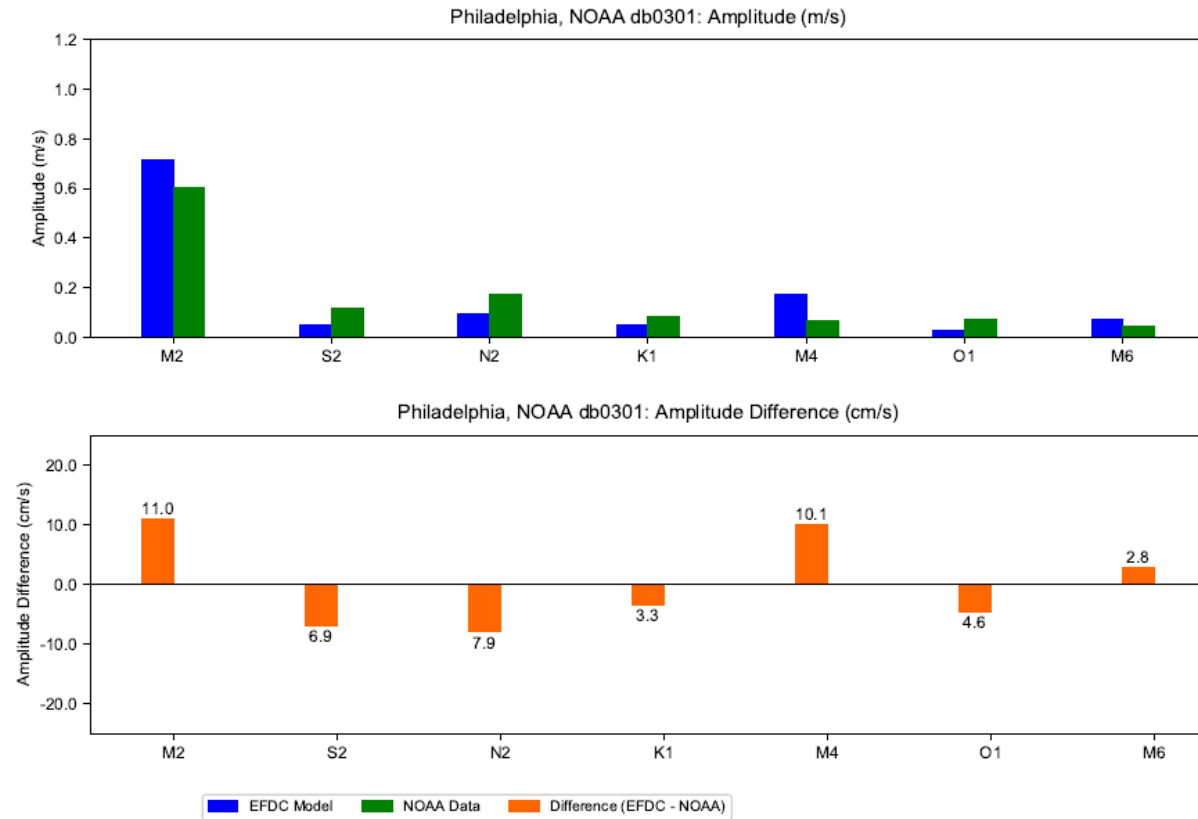


Figure M-7: Harmonics Analysis for Predicted Along-Channel Depth-Averaged Current Velocity Amplitude at Philadelphia, NOAA Station db0301 based on Data Collected from 06-01-2012 to 06-30-2012 Period

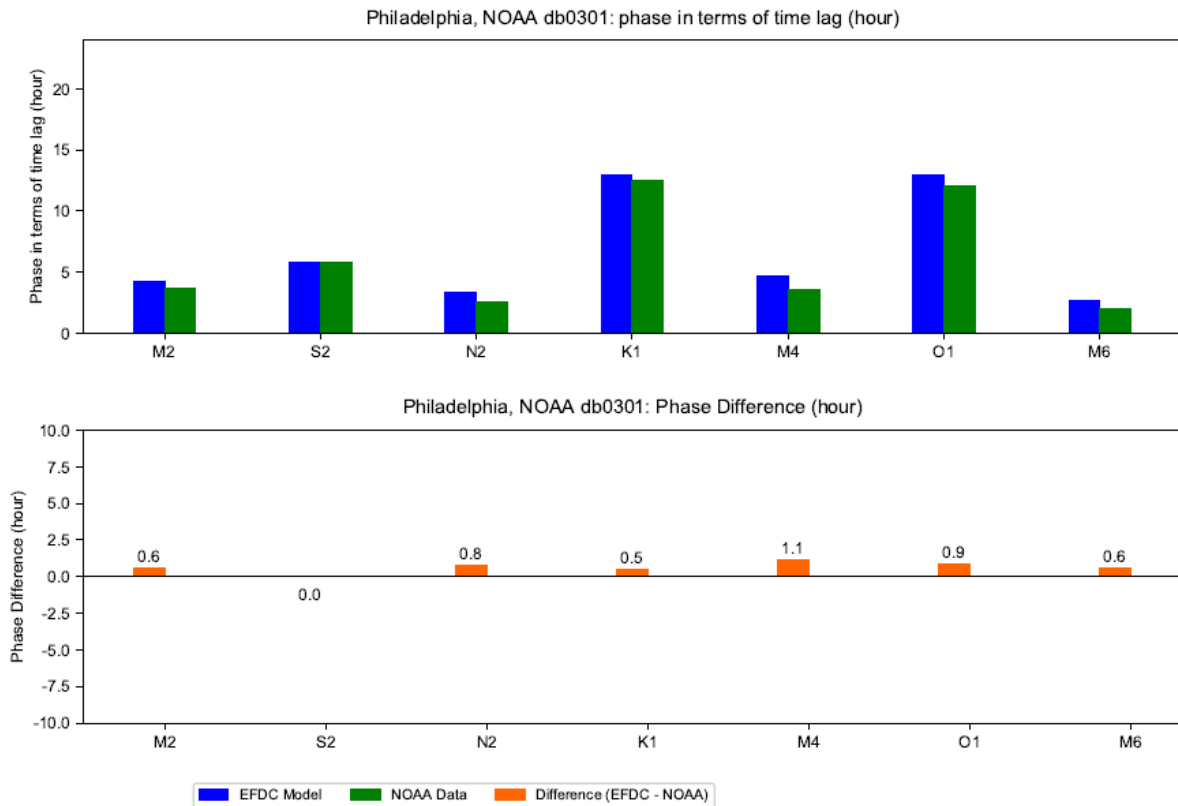


Figure M-8: Harmonics Analysis for Predicted Along-Channel Depth-Averaged Current Velocity Phase at Philadelphia, NOAA Station db0301 based on Data Collected from 06-01-2012 to 06-30-2012 Period

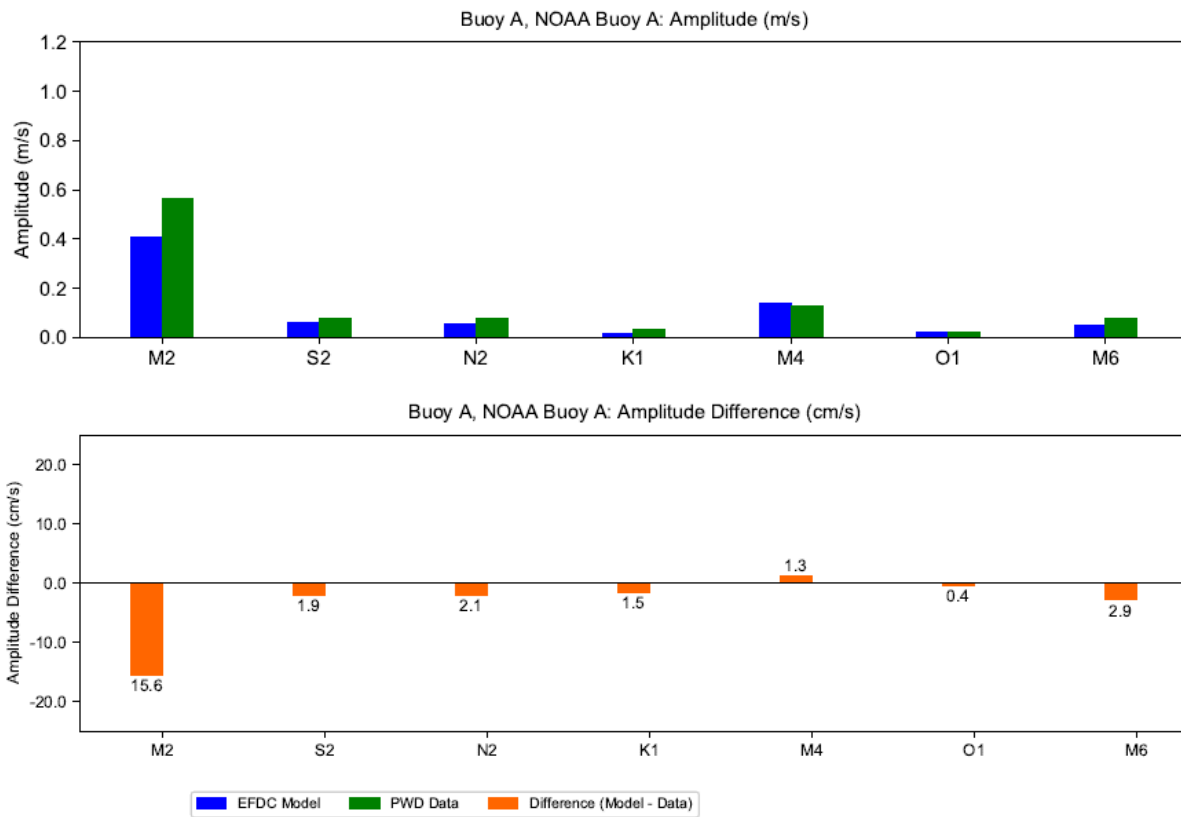
Appendix N: Summary of harmonic analysis for current velocity at PWD stations

Table N-1: Summary of Harmonic Analysis for Along-Channel Depth-Averaged Current Velocity at PWD Stations

Station	Symbol	RM	Amplitude (m/s)			Phase (degree)			Phase (hours)		
			EFDC Predicted	Data	Difference (cm/s)	EFDC Predicted	Data	Difference (deg.)	EFDC Predicted	Data	Difference (hr.)
Buoy A	M2	117.4	0.407	0.562	-15.57	134.27	116.70	17.57	4.633	4.026	0.606
	S2	117.4	0.059	0.078	-1.95	194.83	172.40	22.43	6.494	5.747	0.748
	N2	117.4	0.057	0.078	-2.11	143.07	119.13	23.94	5.031	4.189	0.842
	K1	117.4	0.016	0.031	-1.52	210.18	210.00	0.18	13.974	13.962	0.012
	M4	117.4	0.140	0.127	1.29	293.56	242.29	51.27	5.064	4.180	0.884
	O1	117.4	0.020	0.024	-0.40	172.04	178.71	-6.67	12.339	12.817	-0.478
	M6	117.4	0.051	0.079	-2.85	288.32	249.47	38.85	3.316	2.869	0.447
Buoy B	M2	93.7	0.599	0.621	-2.21	120.40	93.48	26.92	4.154	3.225	0.929
	S2	93.7	0.087	0.083	0.44	180.58	149.25	31.33	6.019	4.975	1.044
	N2	93.7	0.079	0.075	0.43	129.73	98.77	30.96	4.562	3.473	1.089
	K1	93.7	0.028	0.046	-1.85	199.74	208.39	-8.65	13.280	13.855	-0.575
	M4	93.7	0.106	0.061	4.47	257.71	217.72	39.99	4.446	3.756	0.690
	O1	93.7	0.031	0.041	-1.06	165.83	142.32	23.51	11.893	10.207	1.686
	M6	93.7	0.054	0.055	-0.10	212.61	139.39	73.22	2.445	1.603	0.842
Buoy C	M2	77	0.764	0.811	-4.76	103.20	85.37	17.83	3.561	2.945	0.615
	S2	77	0.107	0.104	0.35	160.29	133.82	26.47	5.343	4.461	0.882
	N2	77	0.101	0.105	-0.46	111.06	87.23	23.83	3.905	3.067	0.838
	K1	77	0.040	0.055	-1.52	193.34	197.72	-4.38	12.854	13.145	-0.291
	M4	77	0.093	0.084	0.87	184.66	143.10	41.56	3.186	2.469	0.717
	O1	77	0.044	0.055	-1.13	158.85	165.55	-6.70	11.393	11.873	-0.481
	M6	77	0.059	0.066	-0.70	150.13	101.42	48.71	1.727	1.166	0.560

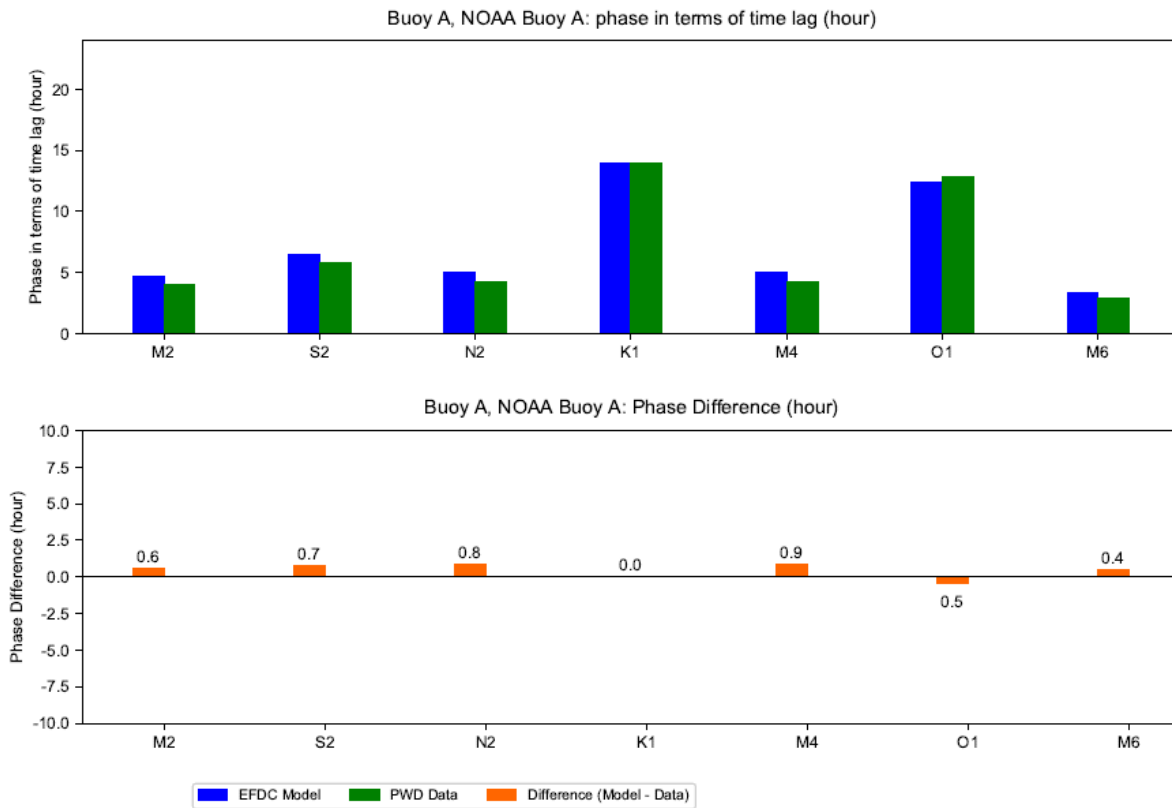
Note: ADCP current velocity data collected during August 21 through September 20, 2012, from Deployment #3, were used in this analysis. Data were provided by PWD to DRBC on December 14, 2022.

Appendix O: Harmonics analysis for current velocity at PWD stations



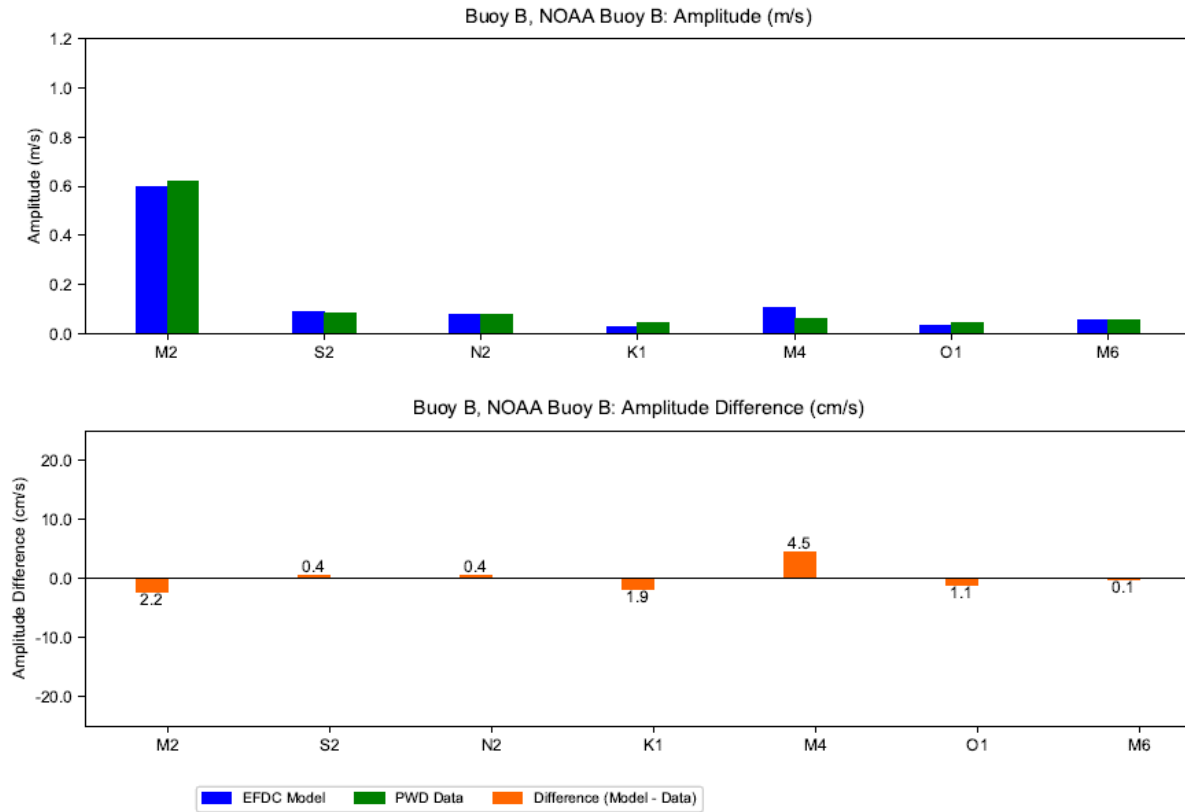
Note: ADCP current velocity data collected during August 21 through September 20, 2012, from Deployment #3, were used in this analysis. Data were provided by PWD to DRBC on December 14, 2022.

Figure O-1: Harmonics Analysis for Predicted Along-Channel Depth-Averaged Current Velocity Amplitude at Buoy A Location



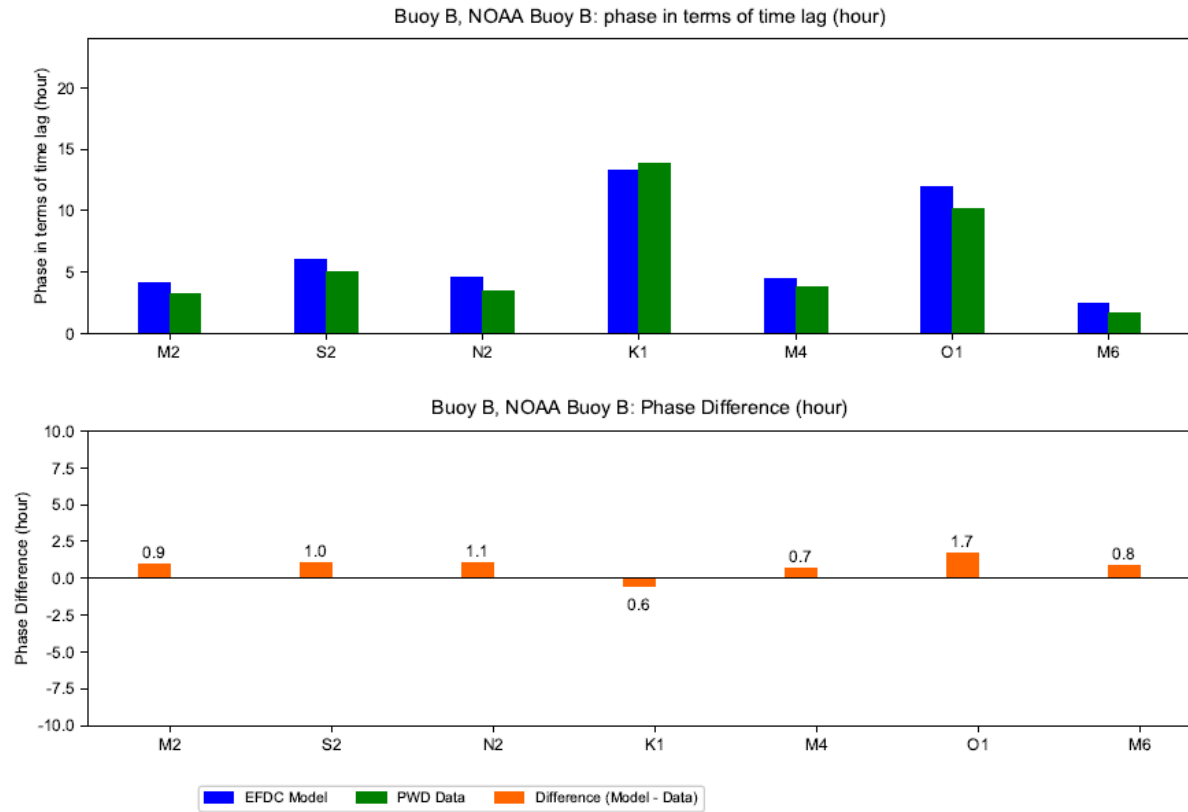
Note: ADCP current velocity data collected during August 21 through September 20, 2012, from Deployment #3, were used in this analysis. Data were provided by PWD to DRBC on December 14, 2022.

Figure O-2: Harmonics Analysis for Predicted Along-Channel Depth-Averaged Current Velocity Phase at Buoy A Location



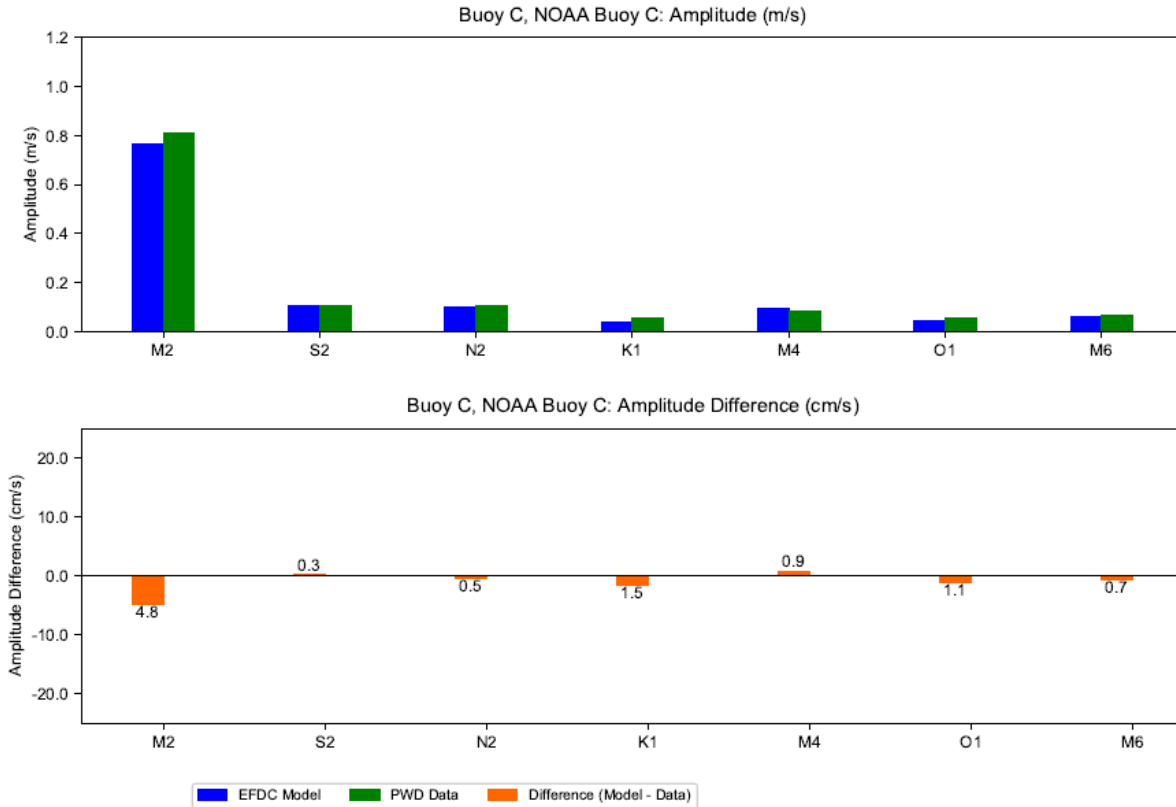
Note: ADCP current velocity data collected during August 21 through September 20, 2012, from Deployment #3, were used in this analysis. Data were provided by PWD to DRBC on December 14, 2022.

Figure O-3: Harmonics Analysis for Predicted Along-Channel Depth-Averaged Current Velocity Amplitude at Buoy B Location



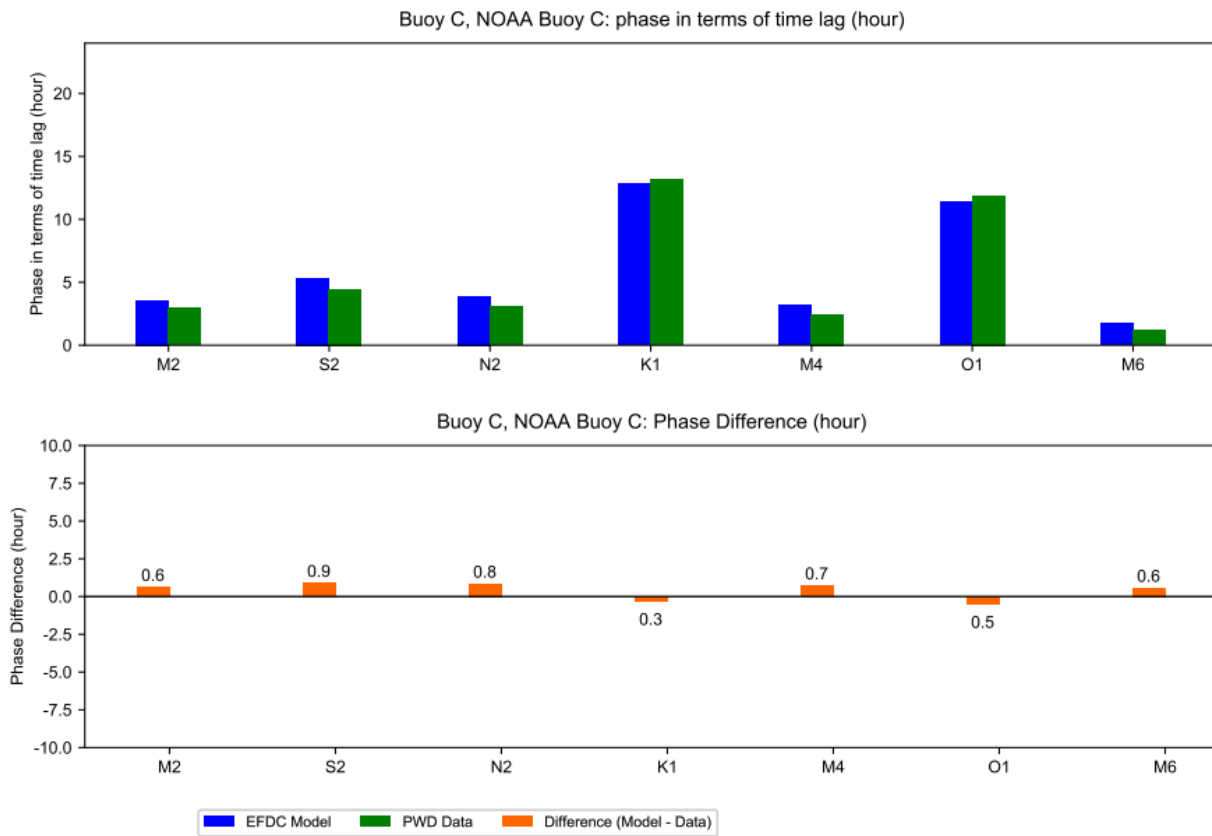
Note: ADCP current velocity data collected during August 21 through September 20, 2012, from Deployment #3, were used in this analysis. Data were provided by PWD to DRBC on December 14, 2022.

Figure O-4: Harmonics Analysis for Predicted Along-Channel Depth-Averaged Current Velocity Phase at Buoy B Location



Note: ADCP current velocity data collected during August 21 through September 20, 2012, from Deployment #3, were used in this analysis. Data were provided by PWD to DRBC on December 14, 2022.

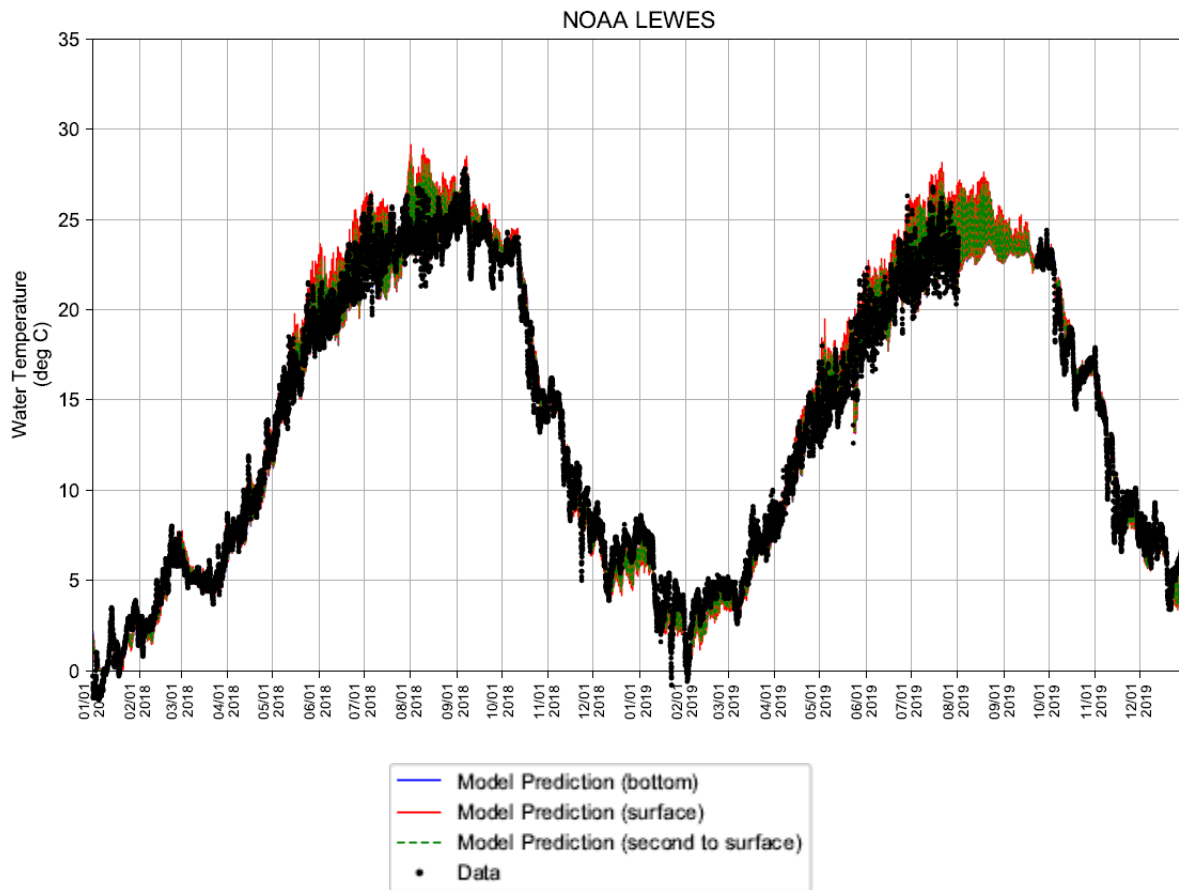
Figure O-5: Harmonics Analysis for Predicted Along-Channel Depth-Averaged Current Velocity Amplitude at Buoy C Location



Note: ADCP current velocity data collected during August 21 through September 20, 2012, from Deployment #3, were used in this analysis. Data were provided by PWD to DRBC on December 14, 2022.

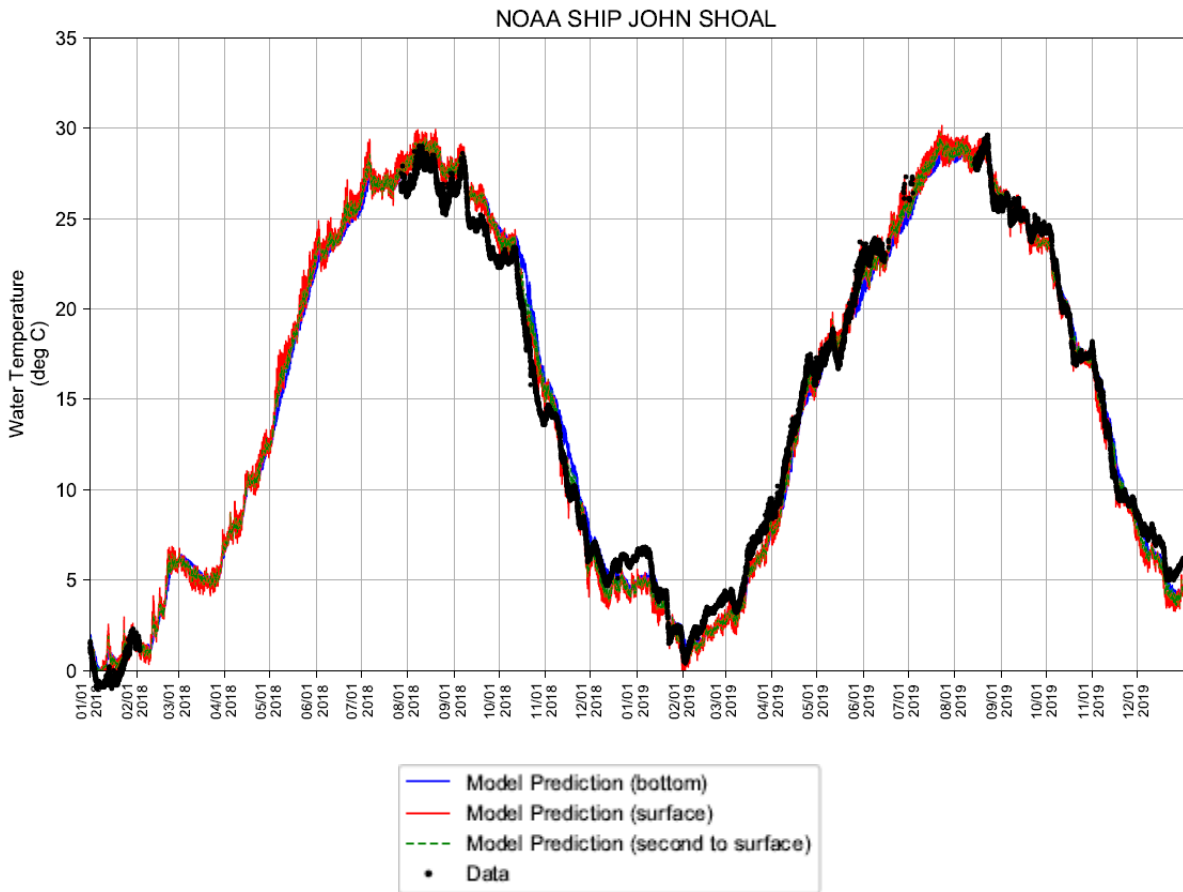
Figure O-6: Harmonics Analysis for Predicted Along-Channel Depth-Averaged Current Velocity Phase at Buoy C Location

Appendix P: Observed and predicted water temperature



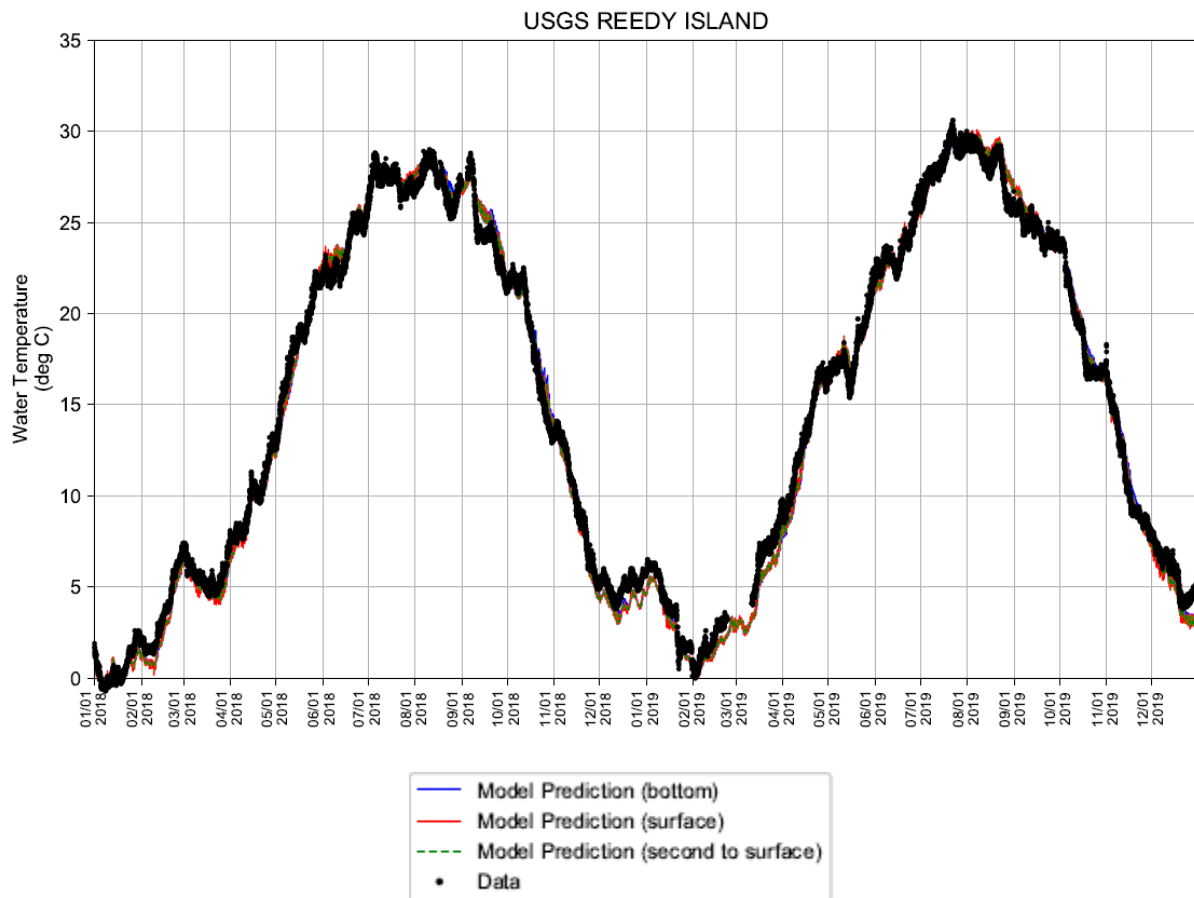
Station ID: 8557380, NOAA LEWES
Run ID: EFDC_HYDRO_G72_2023-01-06

Figure P-1: Observed and Predicted Water Temperature at NOAA LEWES



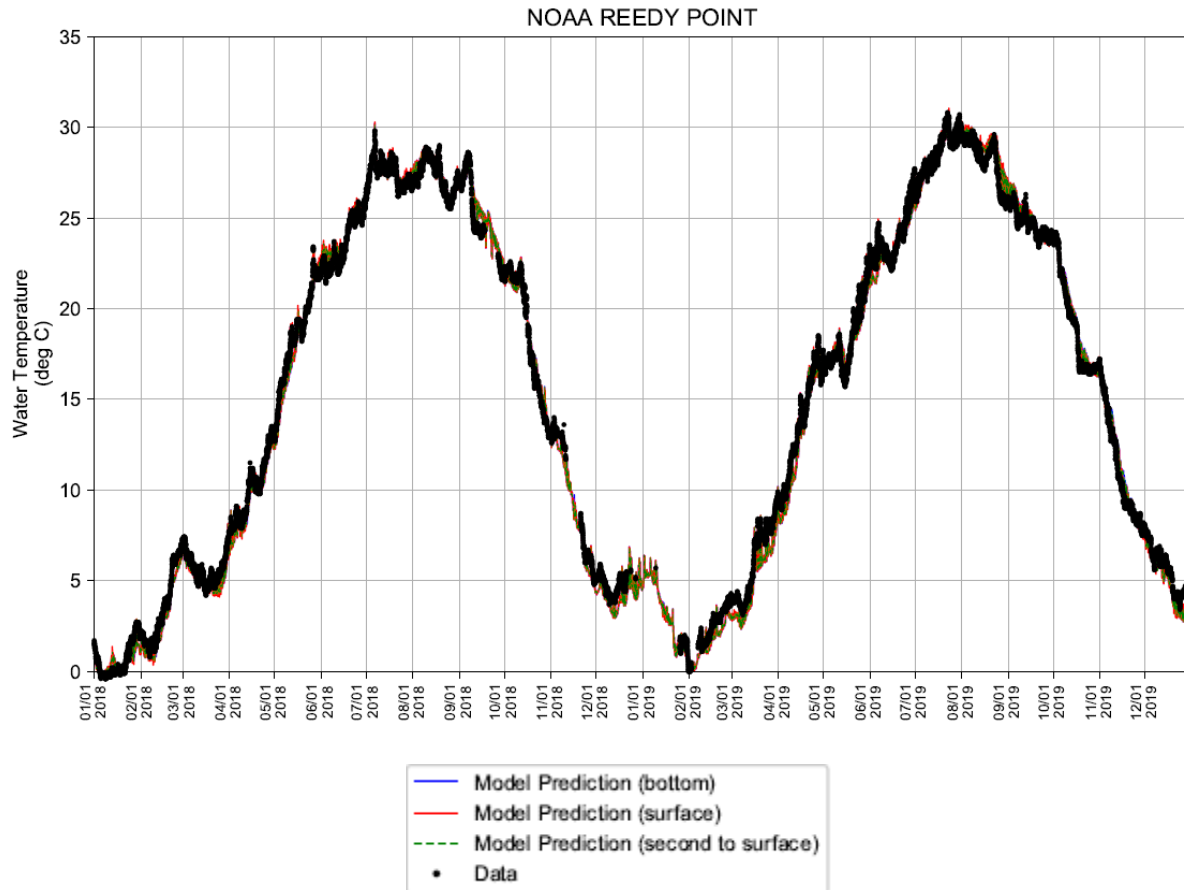
Station ID: 8537121, NOAA SHIP JOHN SHOAL
Run ID: EFDC_HYDRO_G72_2023-01-06

Figure P-2: Observed and Predicted Water Temperature at NOAA SHIP JOHN SHOAL



Station ID: 01482800, USGS REEDY ISLAND
Run ID: EFDC_HYDRO_G72_2023-01-06

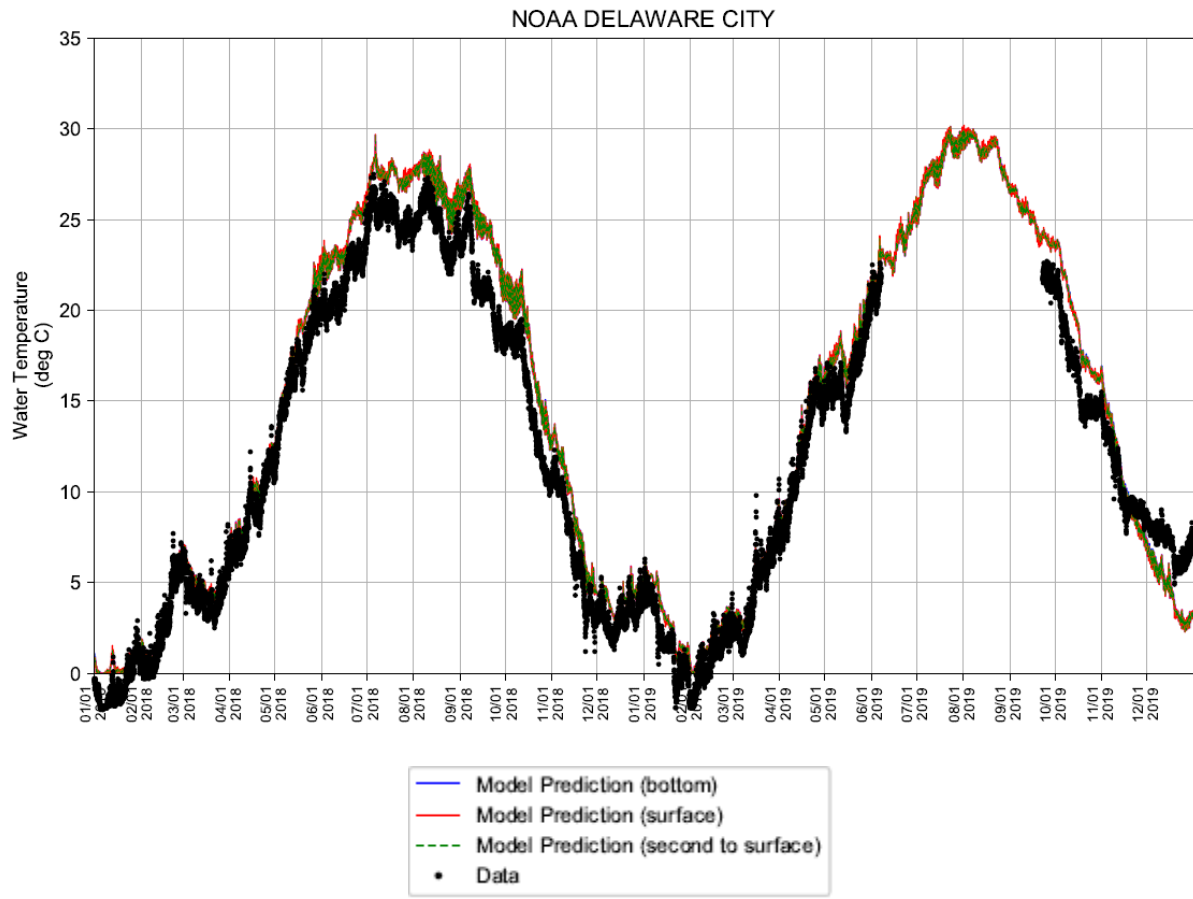
Figure P-3: Observed and Predicted Water Temperature at USGS REEDY ISLAND



Station ID: 8551910, NOAA REEDY POINT

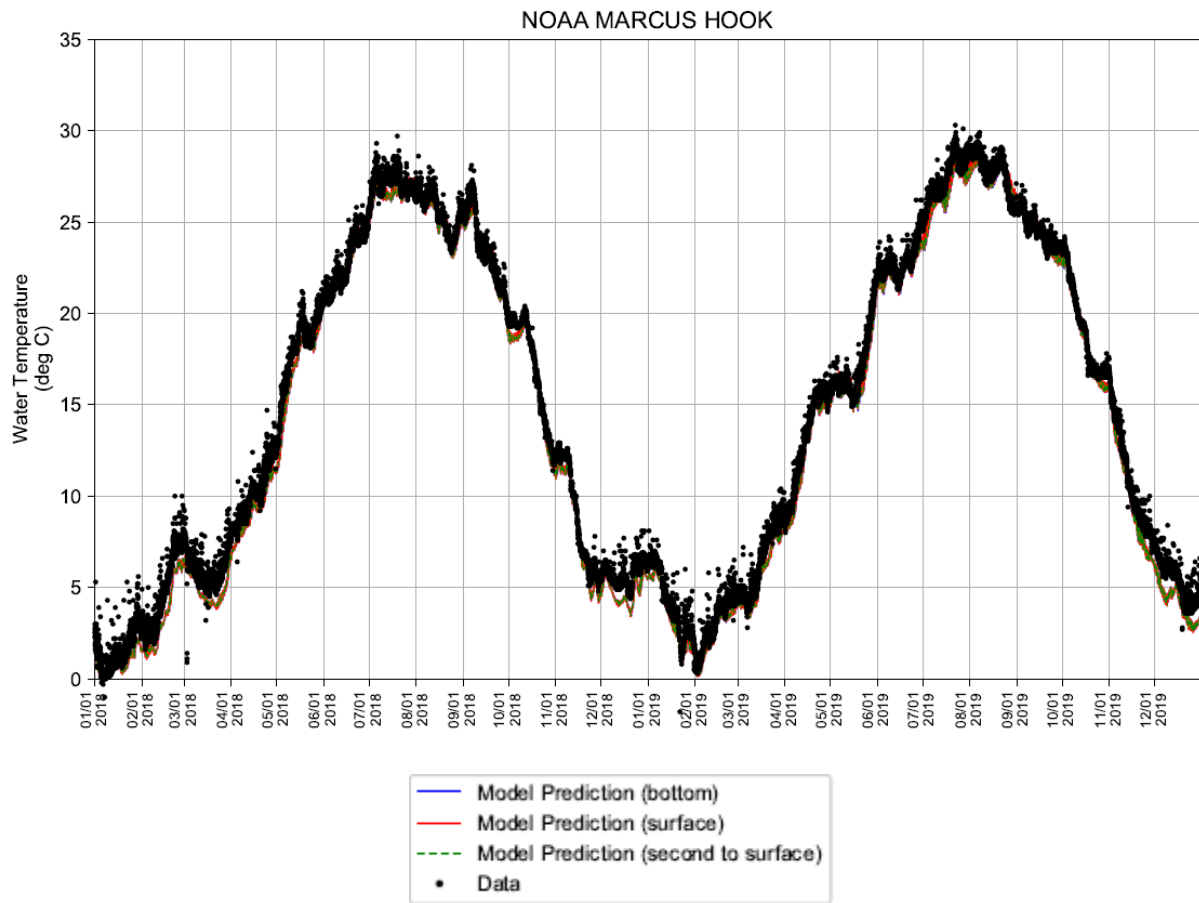
Run ID: EFDC_HYDRO_G72_2023-01-06

Figure P-4: Observed and Predicted Water Temperature at NOAA REEDY POINT



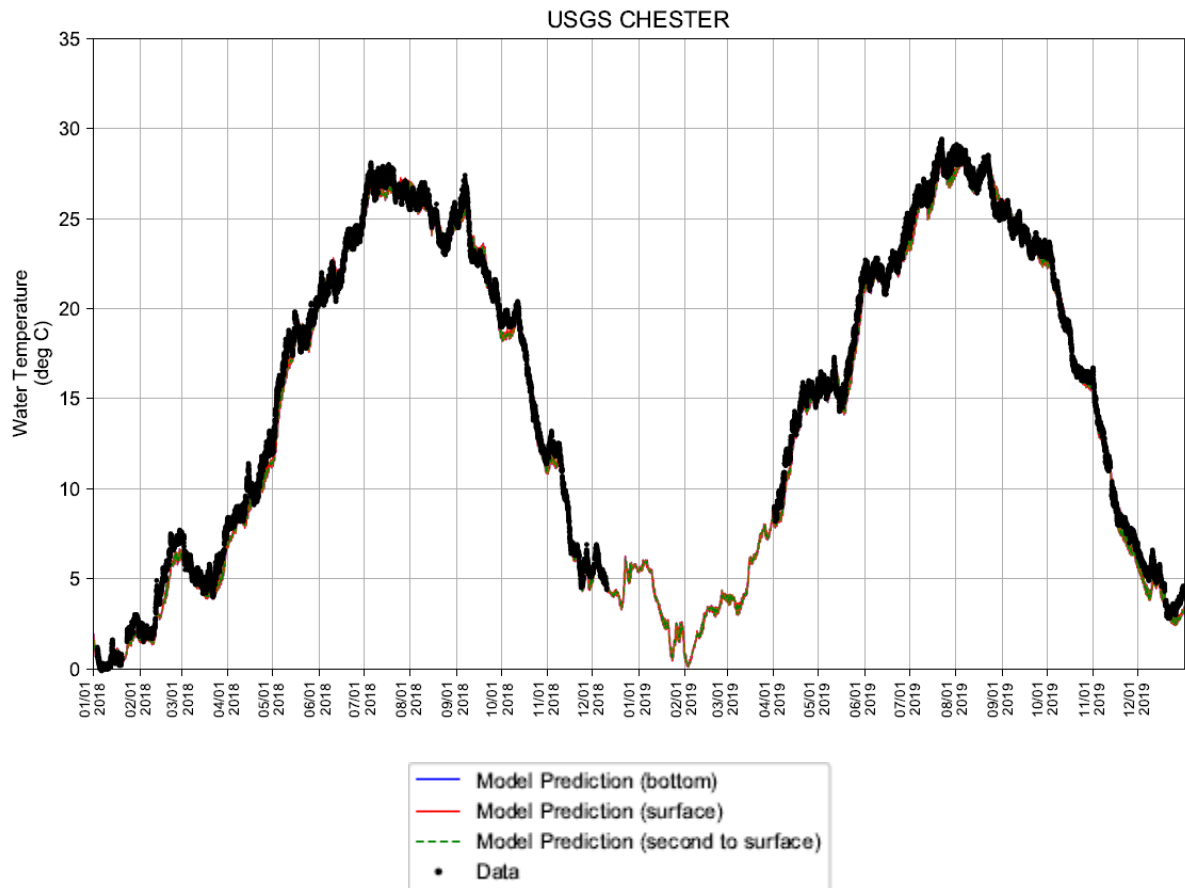
Station ID: 8551762, NOAA DELAWARE CITY
Run ID: EFDC_HYDRO_G72_2023-01-06

Figure P-5: Observed and Predicted Water Temperature at NOAA DELAWARE CITY



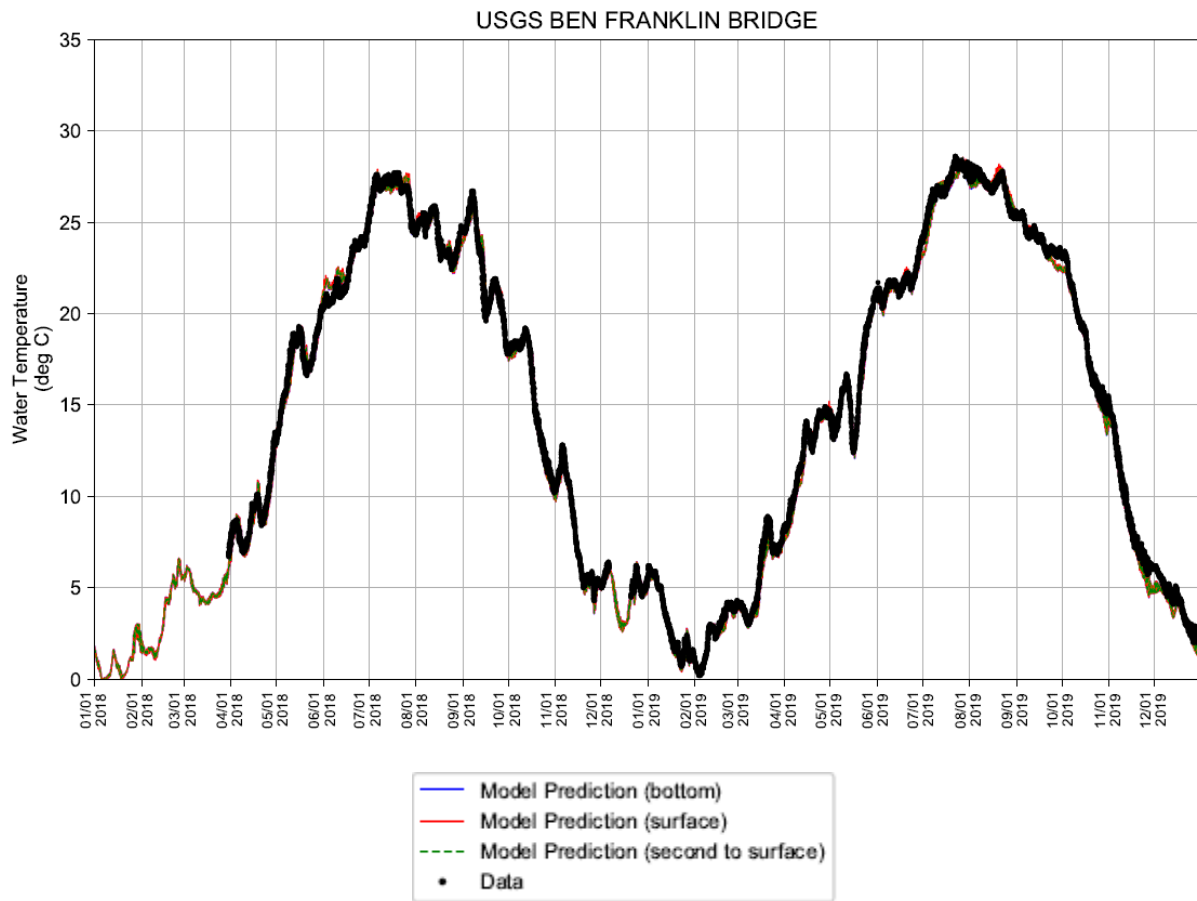
Station ID: 8540433, NOAA MARCUS HOOK
Run ID: EFDC_HYDRO_G72_2023-01-06

Figure P-6: Observed and Predicted Water Temperature at NOAA MARCUS HOOK



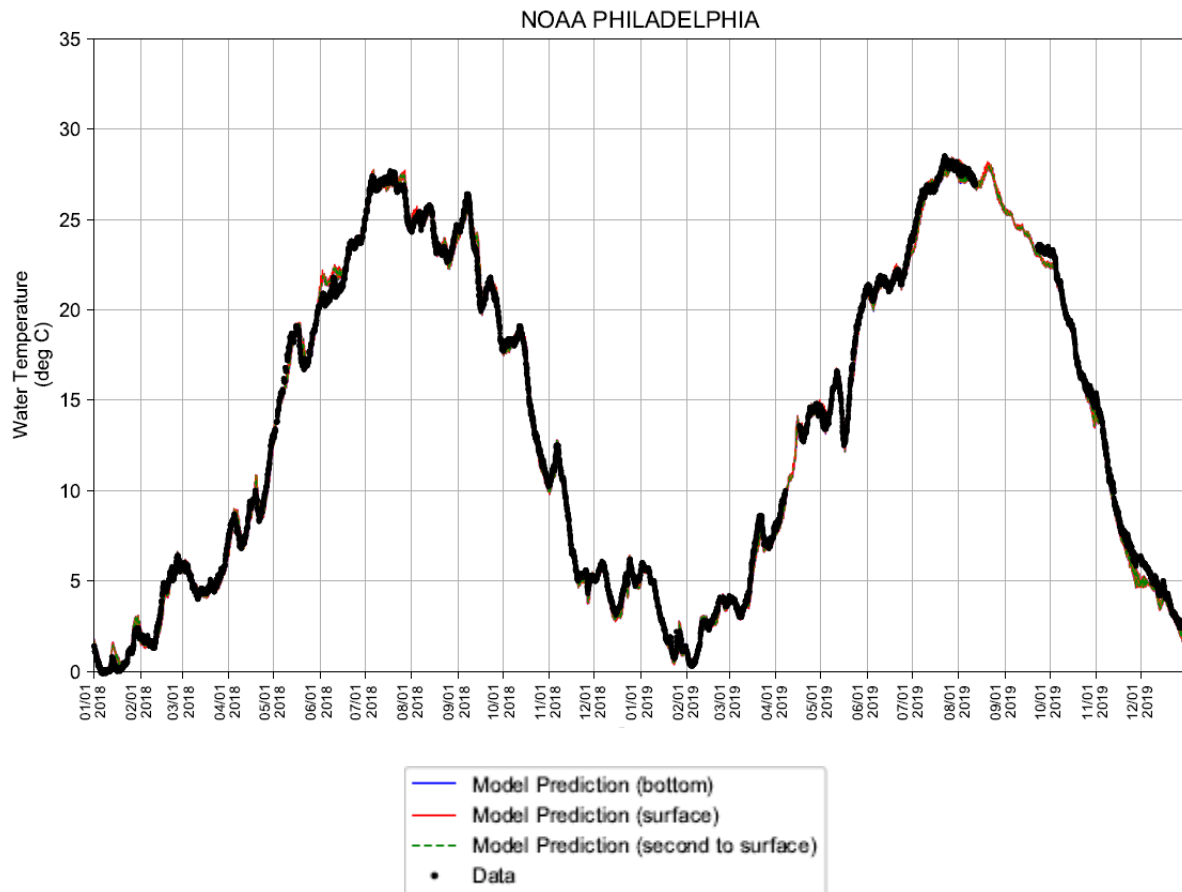
Station ID: 01477050, USGS CHESTER
Run ID: EFDC_HYDRO_G72_2023-01-06

Figure P-7: Observed and Predicted Water Temperature at USGS CHESTER



Station ID: 01467200, USGS BEN FRANKLIN BRIDGE
Run ID: EFDC_HYDRO_G72_2023-01-06

Figure P-8: Observed and Predicted Water Temperature at USGS BEN FRANKLIN BRIDGE



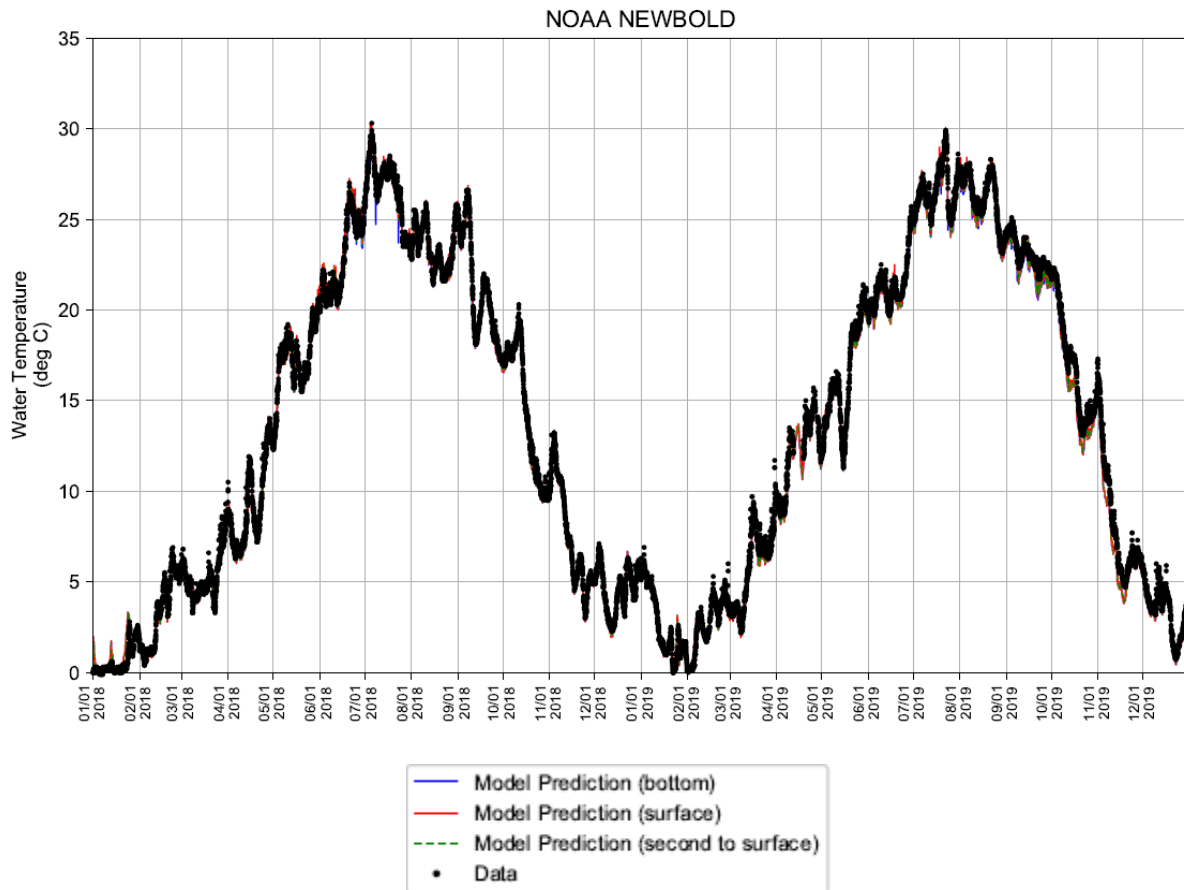
Station ID: 8545240, NOAA PHILADELPHIA
Run ID: EFDC_HYDRO_G72_2023-01-06

Figure P-9: Observed and Predicted Water Temperature at NOAA PHILADELPHIA



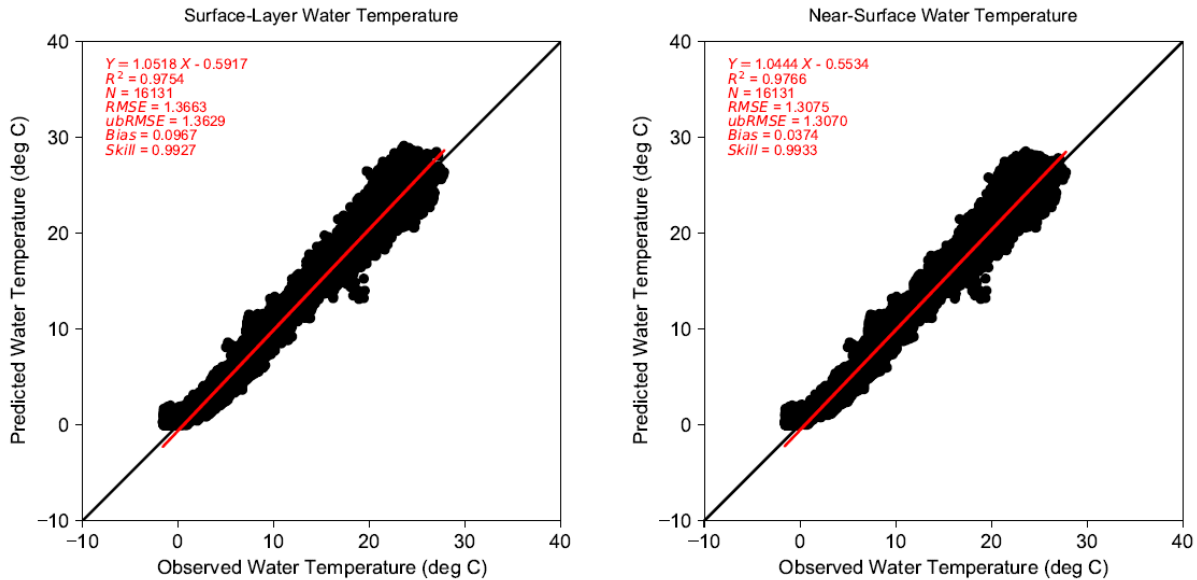
Station ID: 8539094, NOAA BURLINGTON
Run ID: EFDC_HYDRO_G72_2023-01-06

Figure P-10: Observed and Predicted Water Temperature at NOAA BURLINGTON



Station ID: 8548989, NOAA NEWBOLD
Run ID: EFDC_HYDRO_G72_2023-01-06

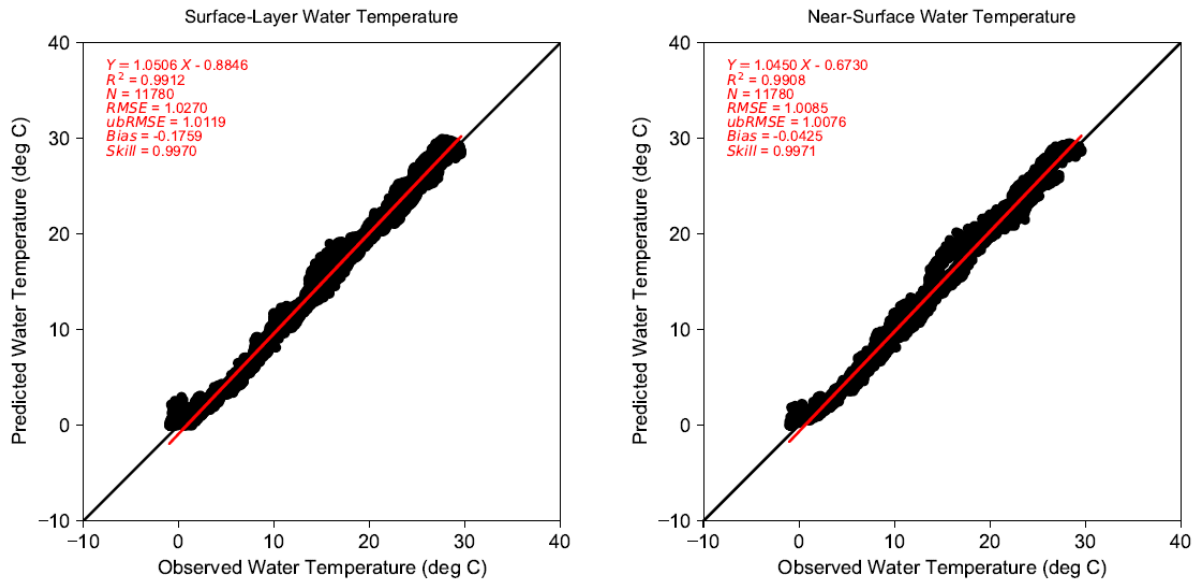
Figure P-11: Observed and Predicted Water Temperature at NOAA NEWBOLD



Notes: Water Temperature data were based on NOAA and USGS continuous data. Model results were paired to data at hourly time intervals for this analysis. Data were collected at a depth that could correspond to either the surface layer of the model or the layer immediately below (i.e., near-surface), so model results from both vertical layers were compared.

Period: 01-01-2018 to 12-31-2019

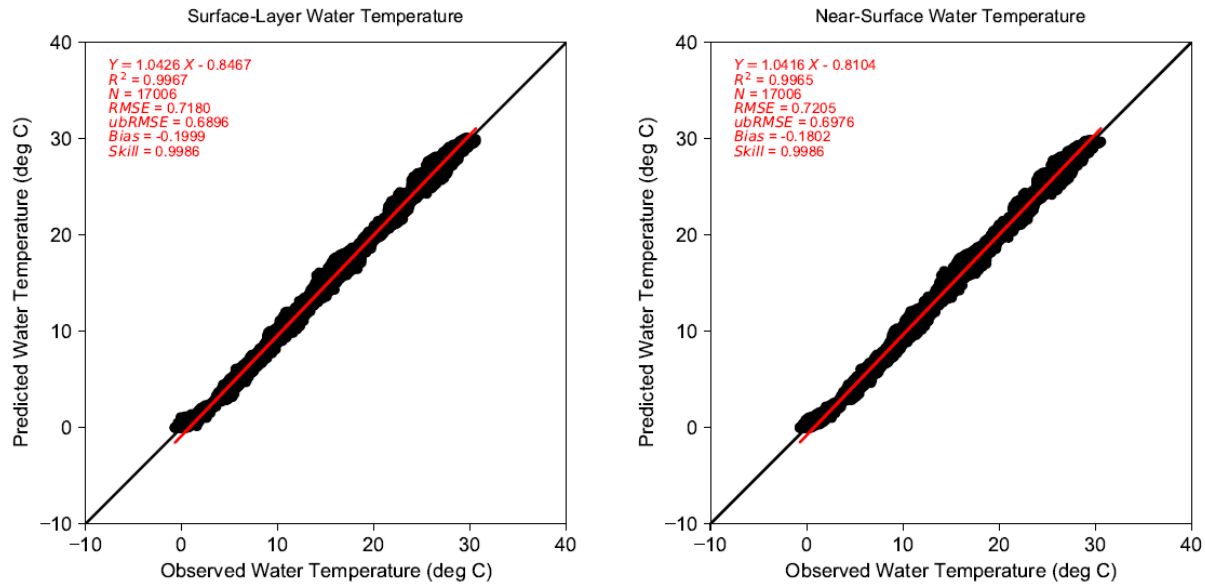
Figure P-12: Comparison of Observed and Predicted Water Temperature at NOAA LEWES during 01-01-2018 to 12-31-2019 period



Notes: Water Temperature data were based on NOAA and USGS continuous data. Model results were paired to data at hourly time intervals for this analysis. Data were collected at a depth that could correspond to either the surface layer of the model or the layer immediately below (i.e., near-surface), so model results from both vertical layers were compared.

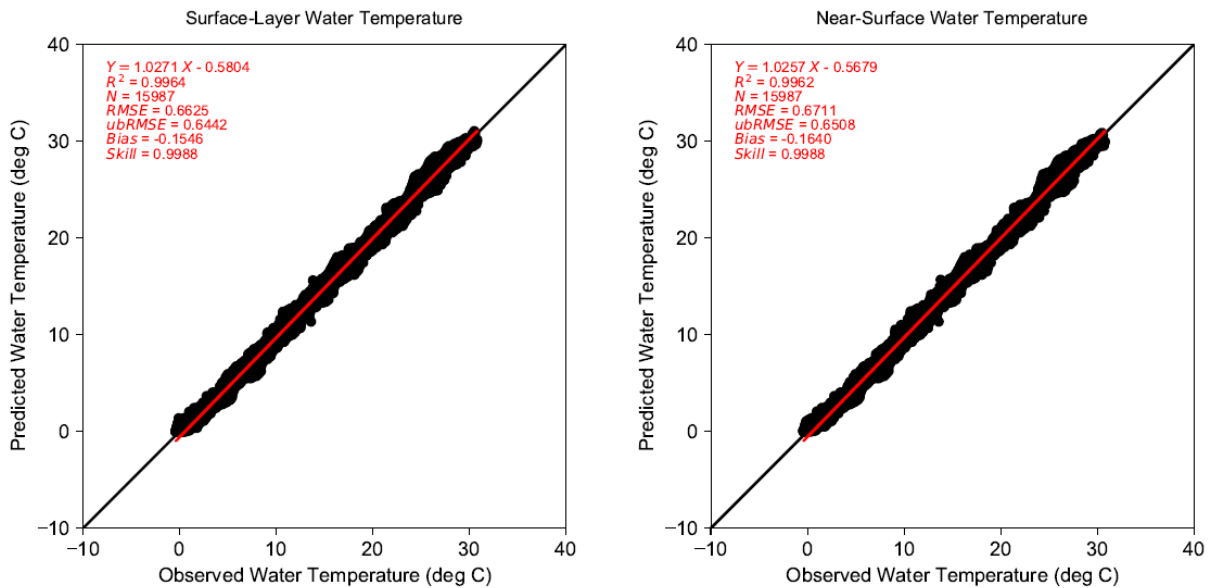
Period: 01-01-2018 to 12-31-2019

Figure P-13: Comparison of Observed and Predicted Water Temperature at NOAA SHIP JOHN SHOAL during 01-01-2018 to 12-31-2019 period



Notes: Water Temperature data were based on NOAA and USGS continuous data. Model results were paired to data at hourly time intervals for this analysis. Data were collected at a depth that could correspond to either the surface layer of the model or the layer immediately below (i.e., near-surface), so model results from both vertical layers were compared. Here model results from both vertical layers were compared. Period: 01-01-2018 to 12-31-2019

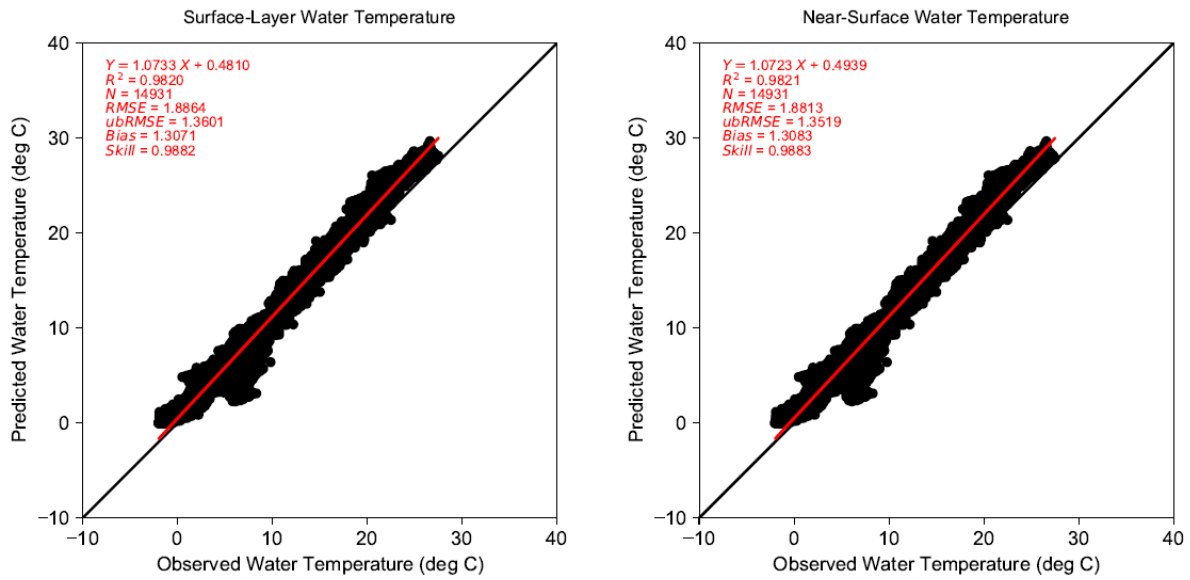
Figure P-14: Comparison of Observed and Predicted Water Temperature at USGS REEDY ISLAND during 01-01-2018 to 12-31-2019 period



Notes: Water Temperature data were based on NOAA and USGS continuous data. Model results were paired to data at hourly time intervals for this analysis. Data were collected at a depth that correspond to either the surface layer of the model or the layer immediately below (i.e., near-surface), so model results from both vertical layers were compared.

Period: 01-01-2018 to 12-31-2019

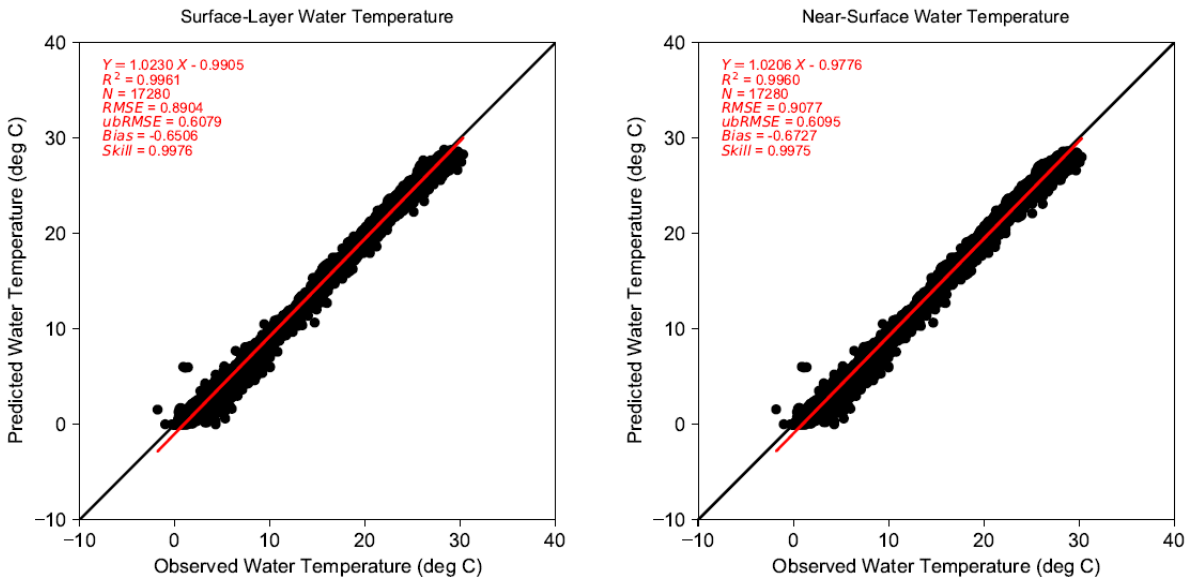
Figure P-15: Comparison of Observed and Predicted Water Temperature at NOAA REEDY POINT during 01-01-2018 to 12-31-2019 period



Notes: Water Temperature data were based on NOAA and USGS continuous data. Model results were paired to data at hourly time intervals for this analysis. Data were collected at a depth that could correspond to either the surface layer of the model or the layer immediately below (i.e., near-surface), so model results from both vertical layers were compared.

Period: 01-01-2018 to 12-31-2019

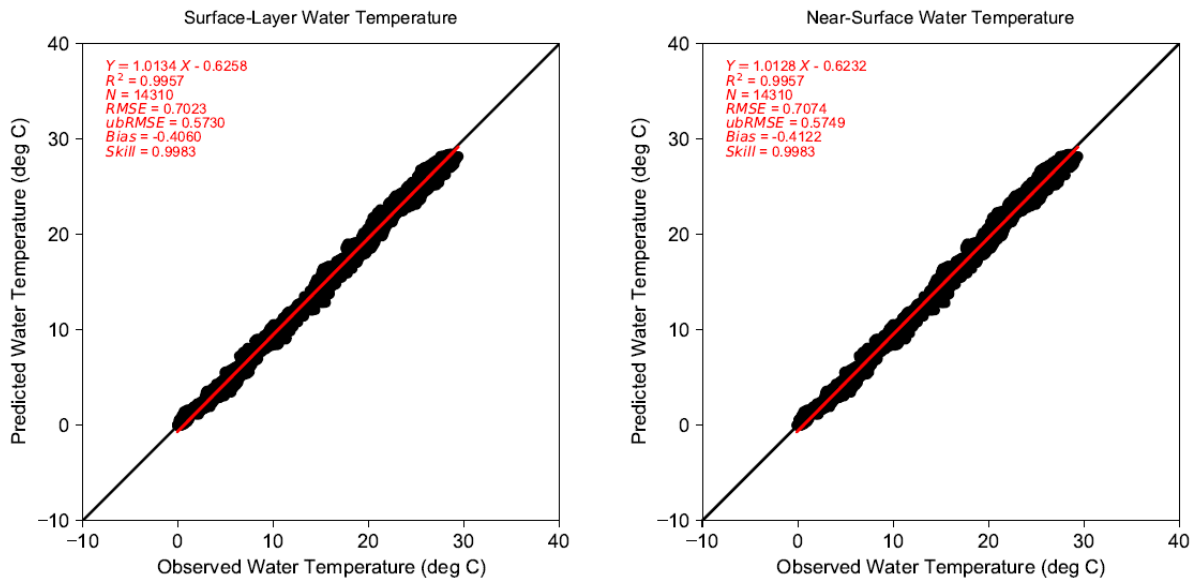
Figure P-16: Comparison of Observed and Predicted Water Temperature at NOAA DELAWARE CITY during 01-01-2018 to 12-31-2019 period



Notes: Water Temperature data were based on NOAA and USGS continuous data. Model results were paired to data at hourly time intervals for this analysis. Data were collected at a depth that could correspond to either the surface layer of the model or the layer immediately below (i.e., near-surface), so model results from both vertical layers were compared.

Period: 01-01-2018 to 12-31-2019

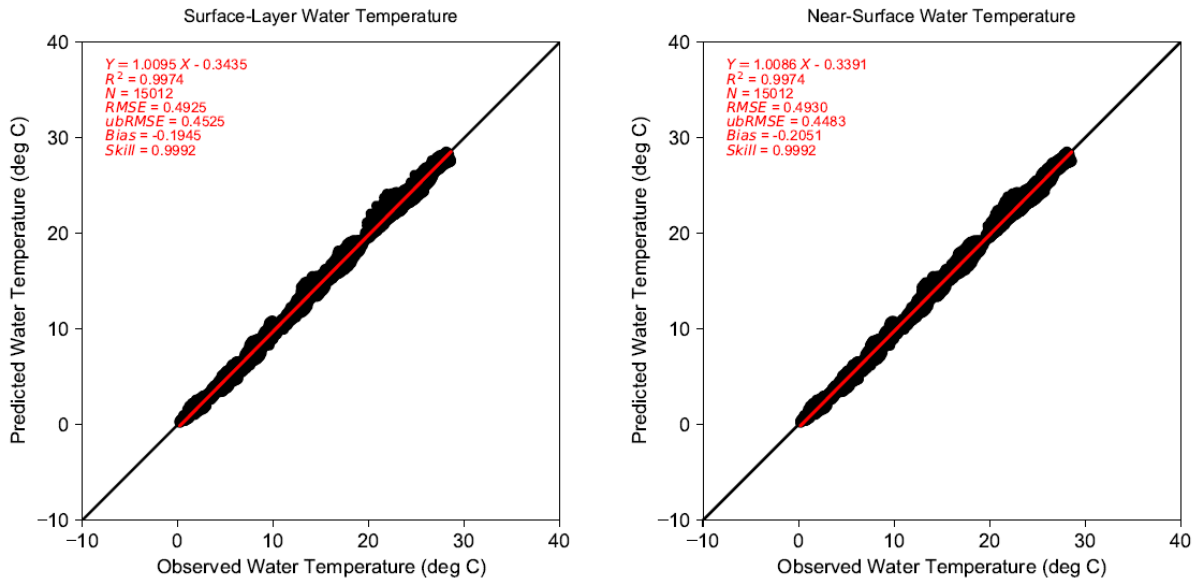
Figure P-17: Comparison of Observed and Predicted Water Temperature at NOAA MARCUS HOOK during 01-01-2018 to 12-31-2019 period



Notes: Water Temperature data were based on NOAA and USGS continuous data. Model results were paired to data at hourly time intervals for this analysis. Data were collected at a depth that could correspond to either the surface layer of the model or the layer immediately below (i.e., near-surface). Here model results from both vertical layers were compared.

Period: 01-01-2018 to 12-31-2019

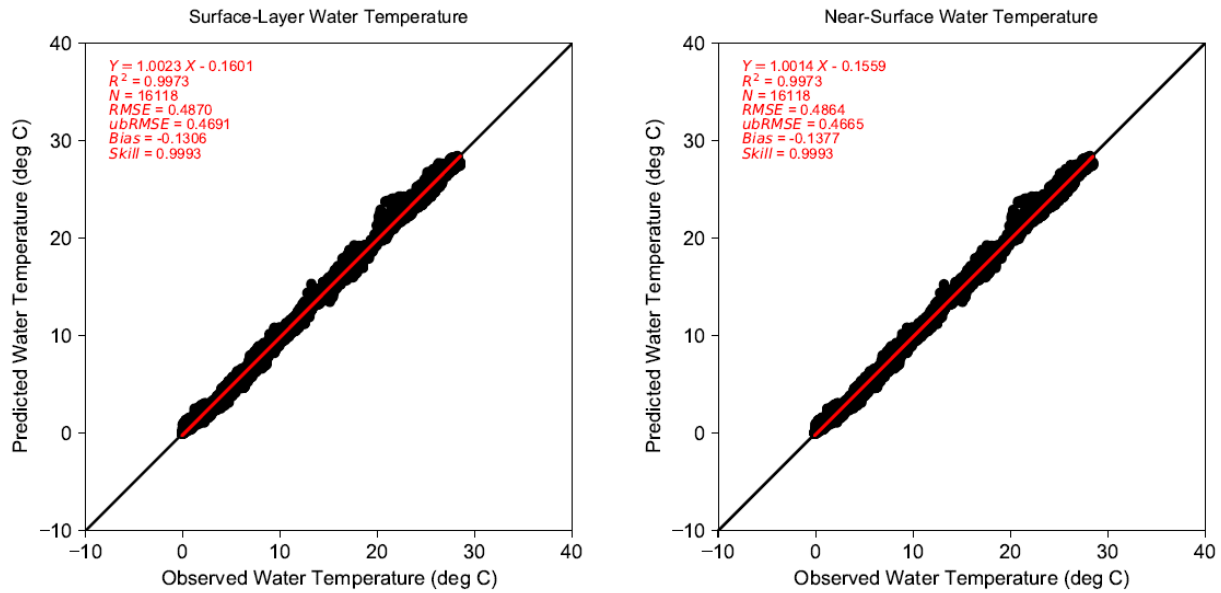
Figure P-18: Comparison of Observed and Predicted Water Temperature at USGS CHESTER during 01-01-2018 to 12-31-2019 period



Notes: Water Temperature data were based on NOAA and USGS continuous data. Model results were paired to data at hourly time intervals for this analysis. Data were collected at a depth that could correspond to either the surface layer of the model or the layer immediately below (i.e., near-surface). Here model results from both vertical layers were compared.

Period: 01-01-2018 to 12-31-2019

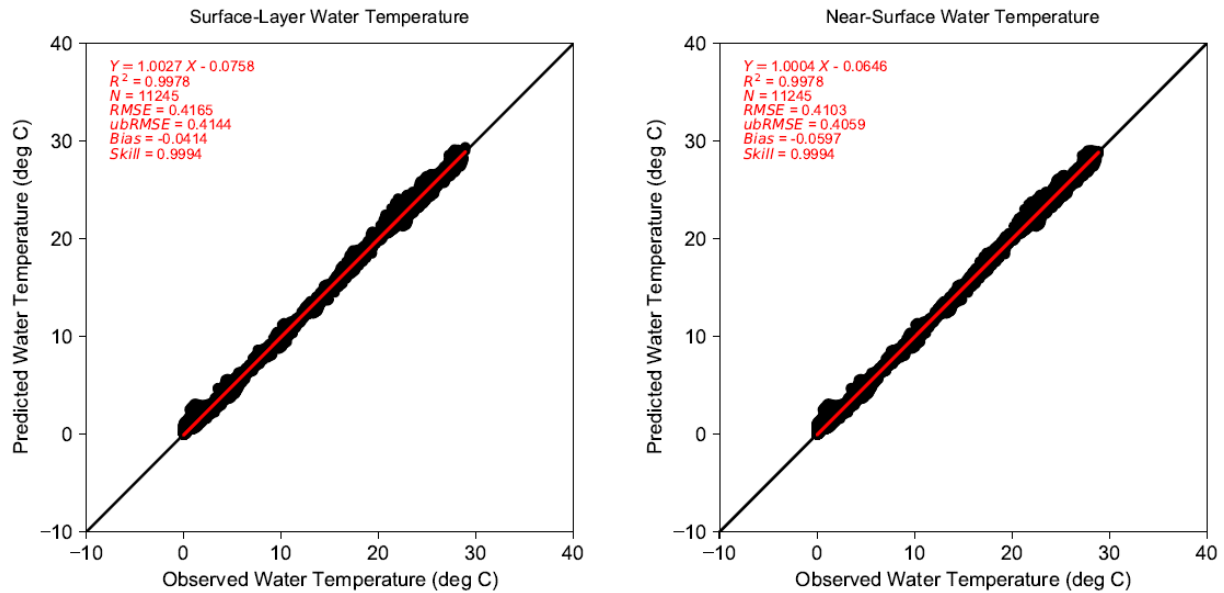
Figure P-19: Comparison of Observed and Predicted Water Temperature at USGS BEN FRANKLIN BRIDGE during 01-01-2018 to 12-31-2019 period



Notes: Water Temperature data were based on NOAA and USGS continuous data. Model results were paired to data at hourly time intervals for this analysis. Data were collected at a depth that could correspond to either the surface layer of the model or the layer immediately below (i.e., near-surface), so model results from both vertical layers were compared.

Period: 01-01-2018 to 12-31-2019

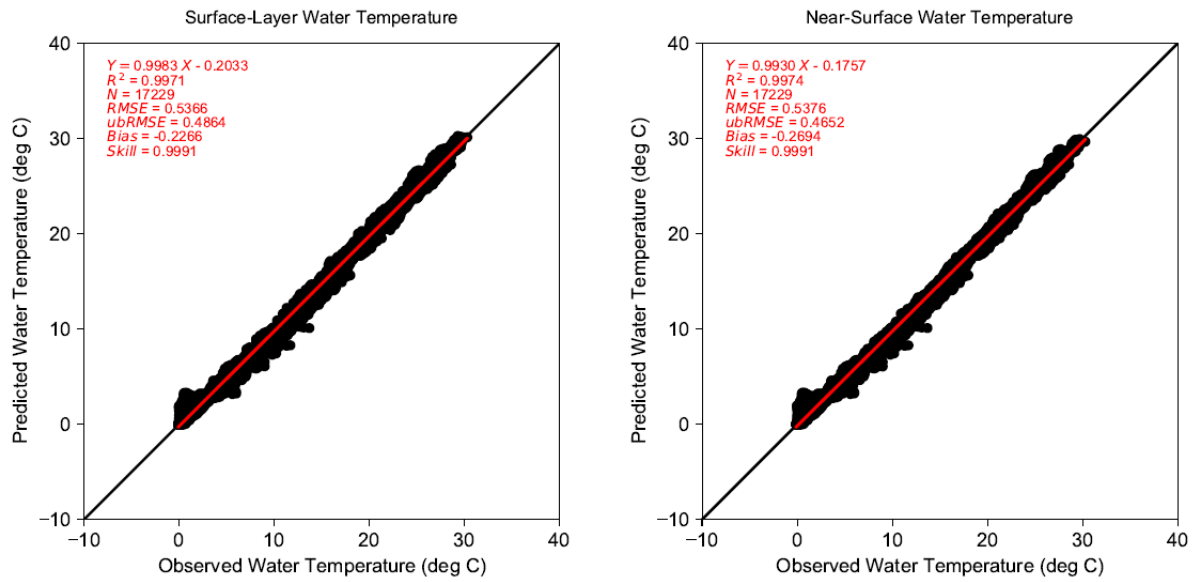
Figure P-20: Comparison of Observed and Predicted Water Temperature at NOAA PHILADELPHIA during 01-01-2018 to 12-31-2019 period



Notes: Water Temperature data were based on NOAA and USGS continuous data. Model results were paired to data at hourly time intervals for this analysis. Data were collected at a depth that could correspond to either the surface layer of the model or the layer immediately below (i.e., near-surface), so model results from both vertical layers were compared.

Period: 01-01-2018 to 12-31-2019

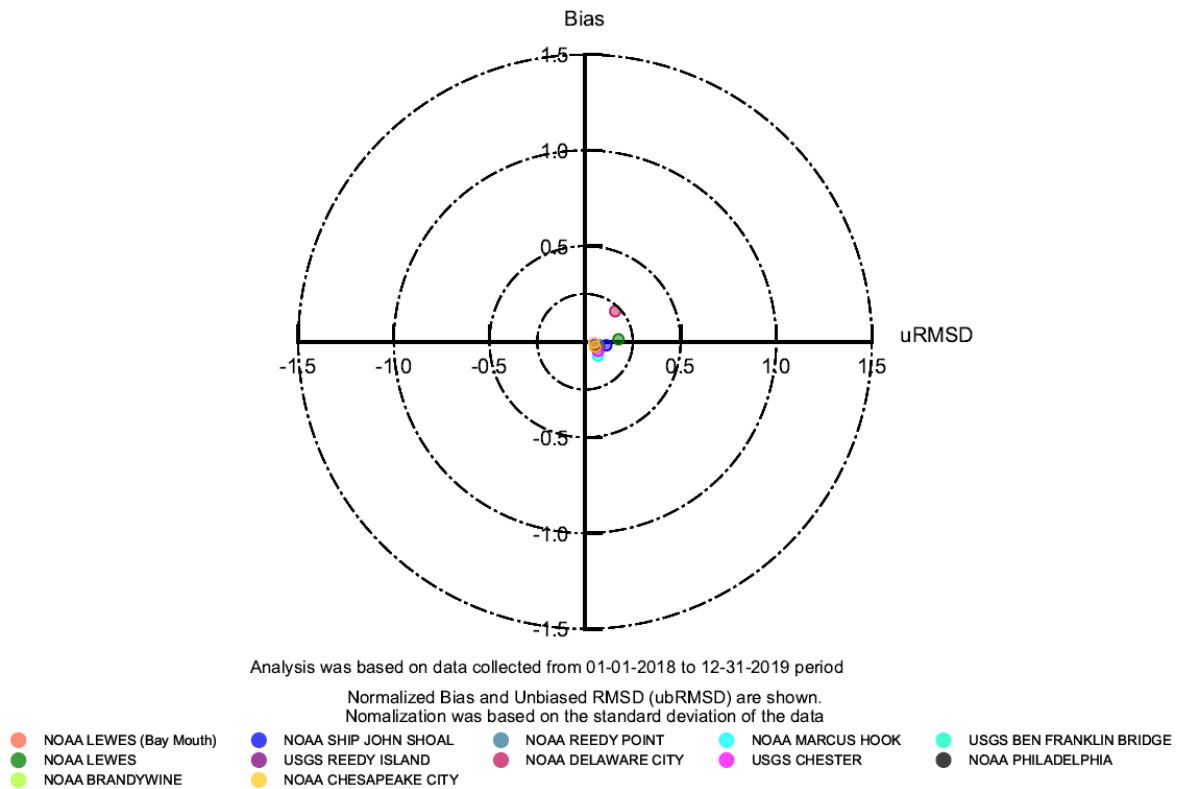
Figure P-21: Comparison of Observed and Predicted Water Temperature at NOAA BURLINGTON during 01-01-2018 to 12-31-2019 period



Notes: Water Temperature data were based on NOAA and USGS continuous data. Model results were paired to data at hourly time intervals for this analysis. Data were collected at a depth that could correspond to either the surface layer of the model or the layer immediately below (i.e., near-surface), so model results from both vertical layers were compared.

Period: 01-01-2018 to 12-31-2019

Figure P-22: Comparison of Observed and Predicted Water Temperature at NOAA NEWBOLD during 01-01-2018 to 12-31-2019 period



Notes: Water Temperature data were based on NOAA and USGS continuous data. Model results were paired to data at hourly time intervals for this analysis

Period: 01-01-2018 to 12-31-2019

Run ID: EFDC_HYDRO_G72_2023-01-06

Figure P-23: Target Diagram for Hourly Near Surface Predicted Water Temperature for 2018-2019 Period

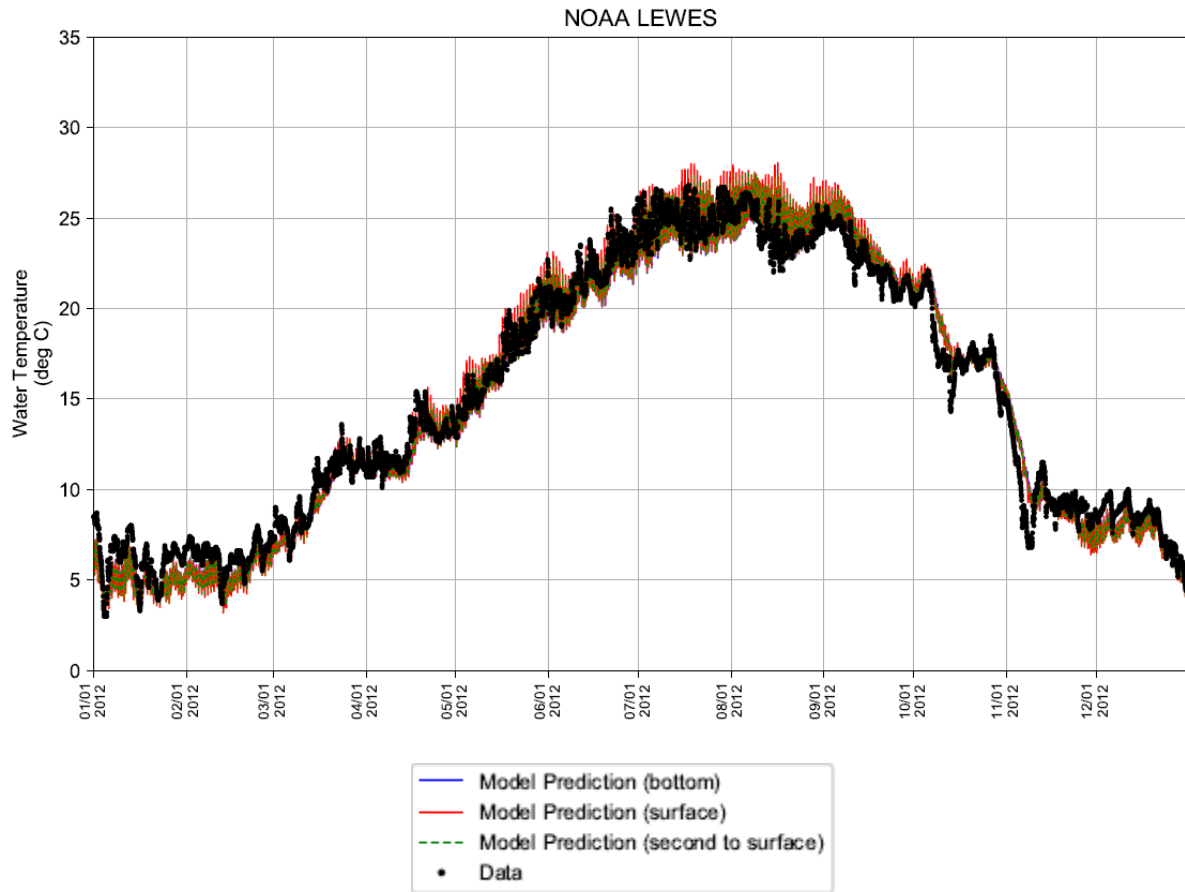


Figure P-24: Observed and Predicted Water Temperature at NOAA LEWES during 2012 Period

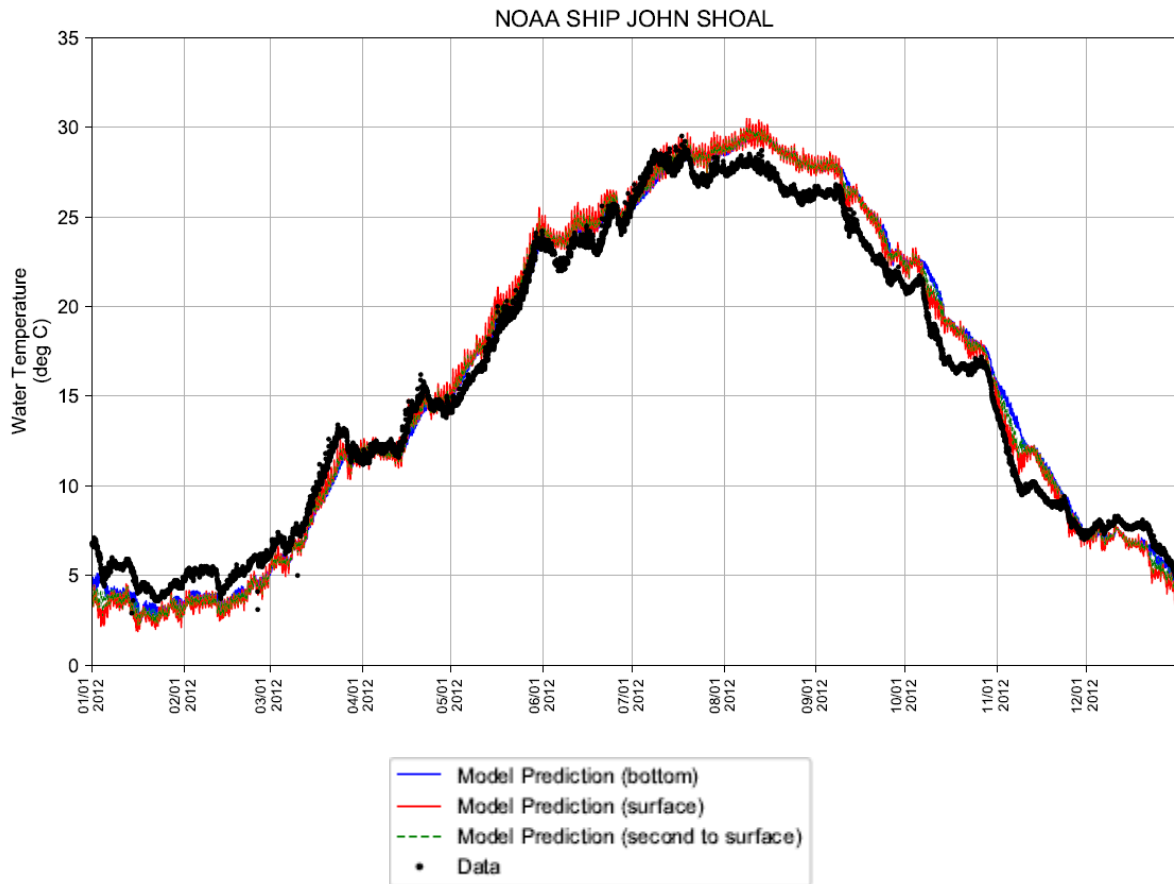


Figure P-25: Observed and Predicted Water Temperature at NOAA Station 8537121 SHIP JOHN SHOAL during 2012 Period

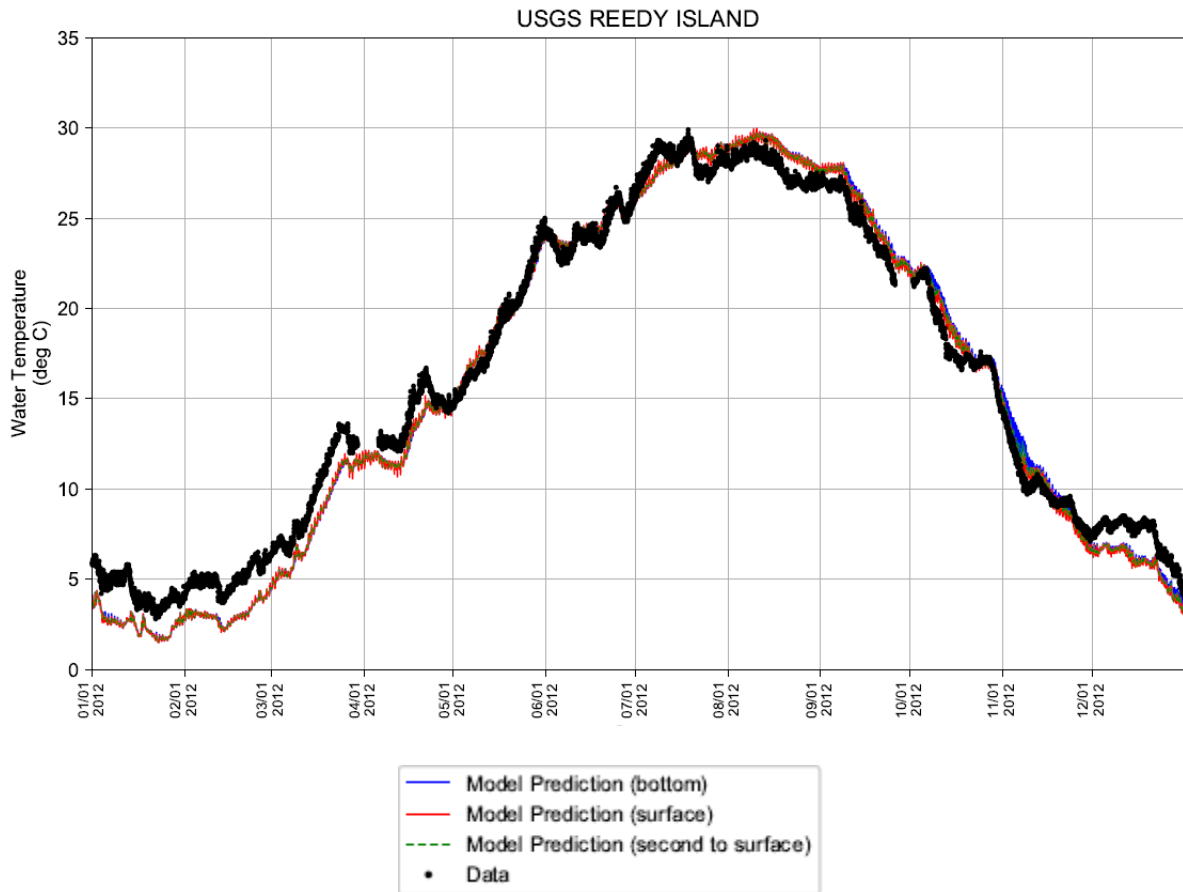


Figure P-26: Observed and Predicted Water Temperature at USGS REEDY ISLAND during 2012 Period

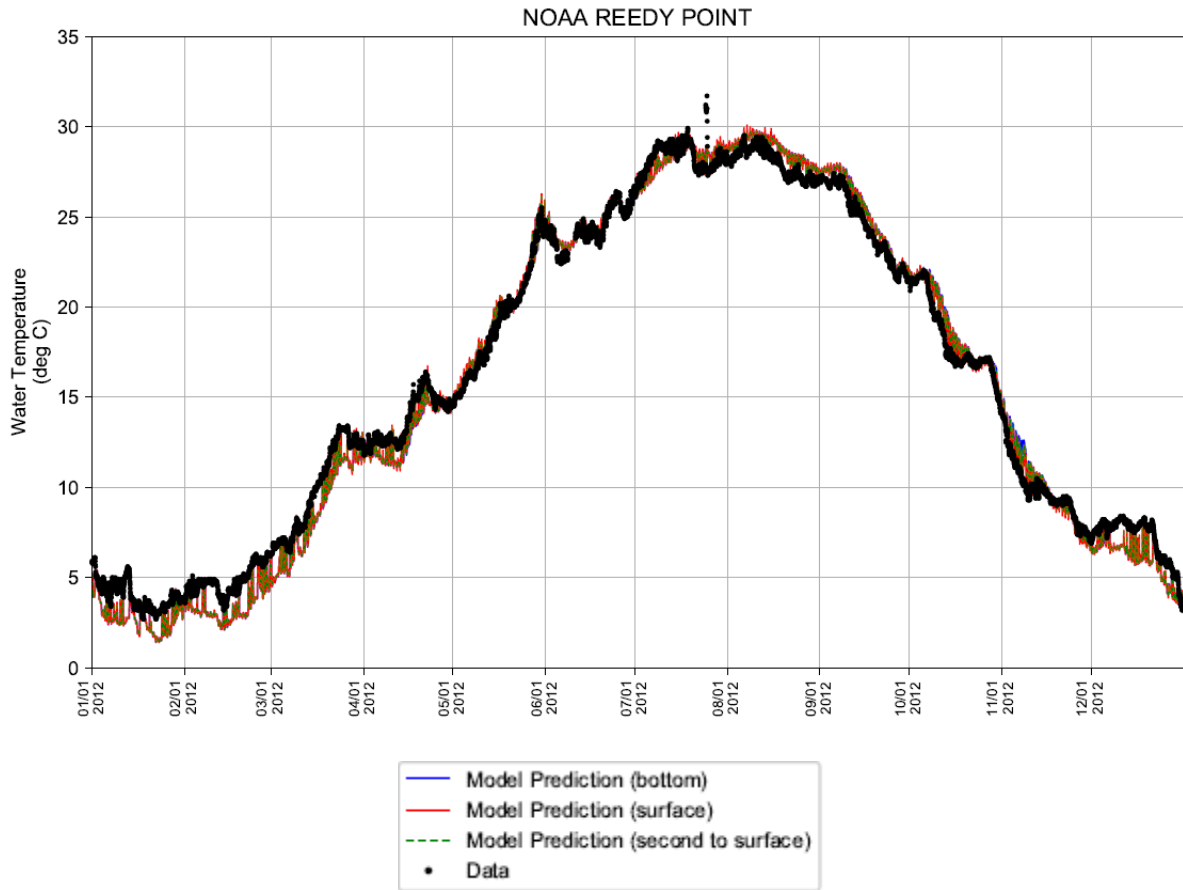


Figure P-27: Observed and Predicted Water Temperature at NOAA REEDY POINT during 2012 Period

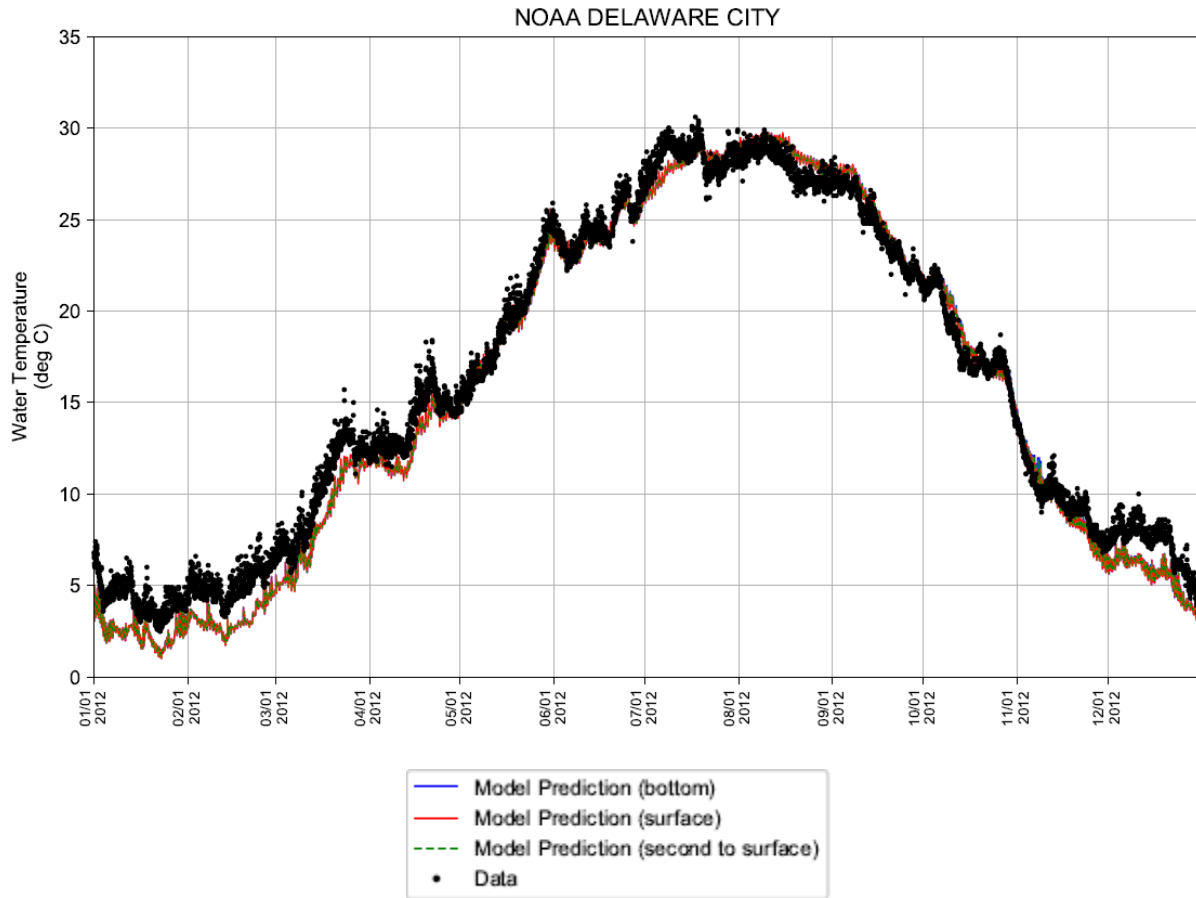


Figure P-28: Observed and Predicted Water Temperature at NOAA DELAWARE CITY during 2012 Period

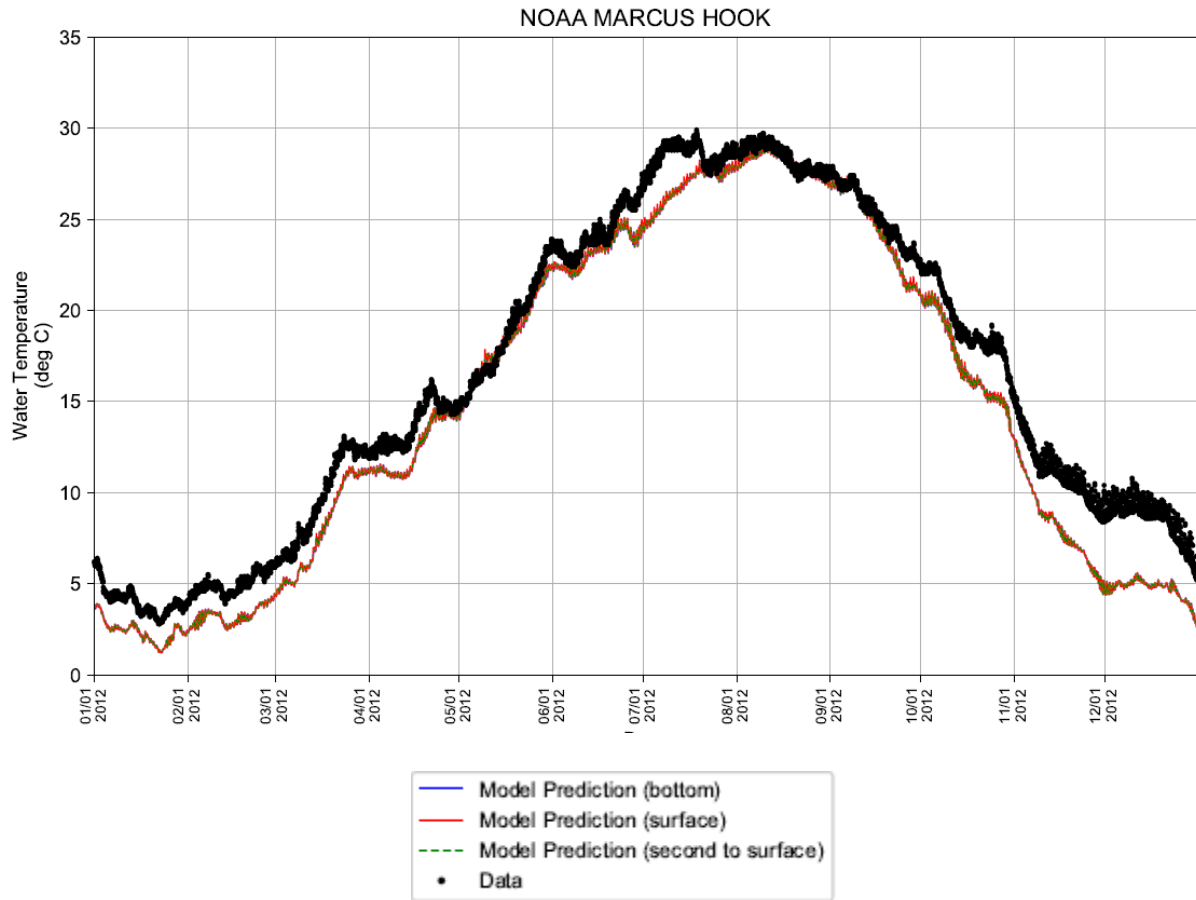


Figure P-29: Observed and Predicted Water Temperature at NOAA MARCUS HOOK during 2012 Period

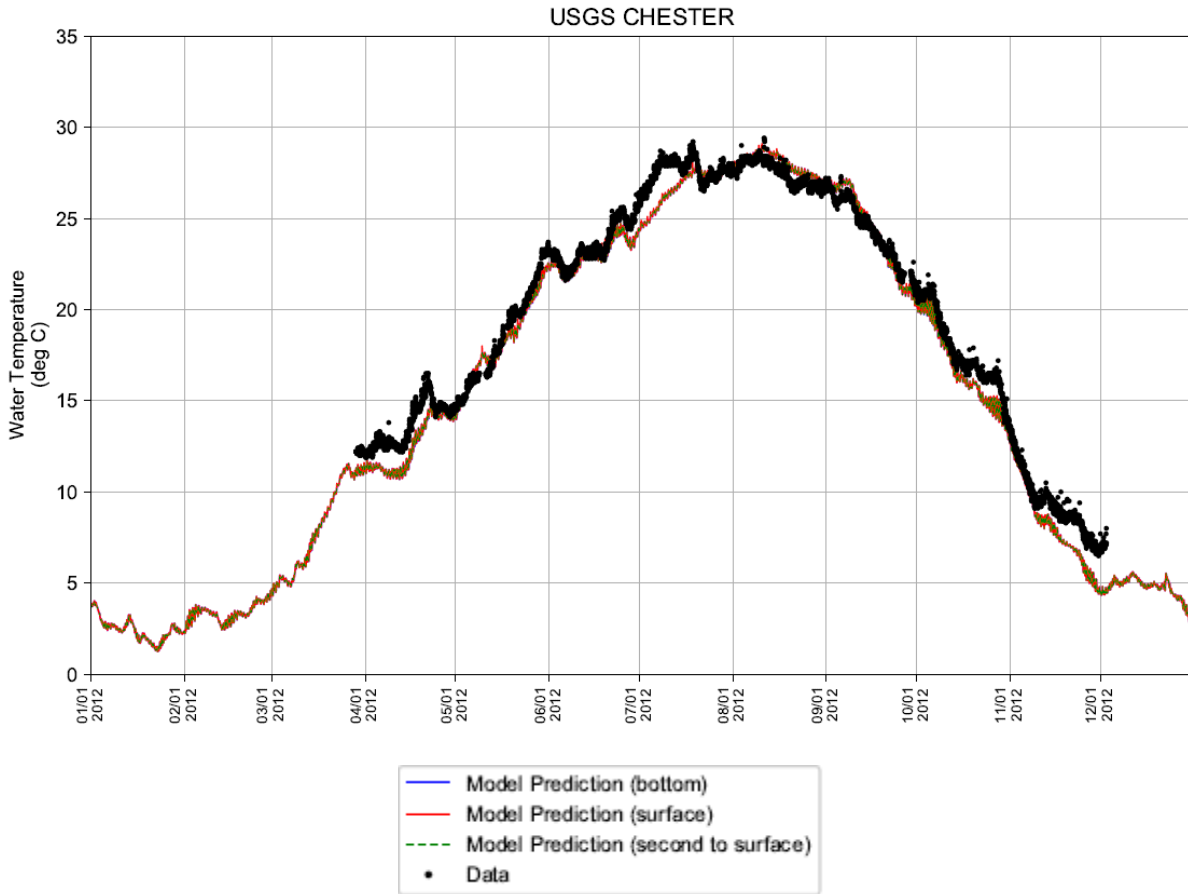


Figure P-30: Observed and Predicted Water Temperature at USGS CHESTER during 2012 Period

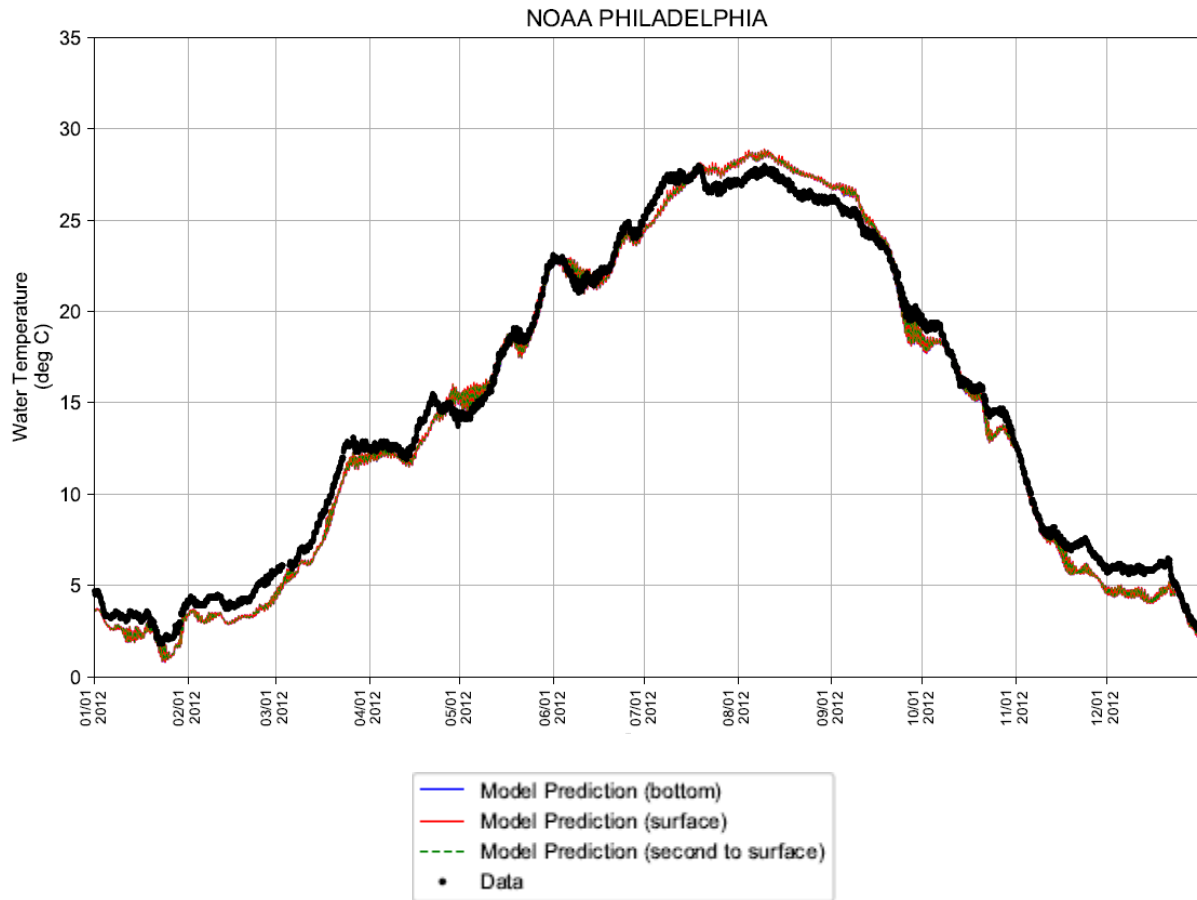


Figure P-31: Observed and Predicted Water Temperature at NOAA Station 8545240 PHILADELPHIA during 2012 Period

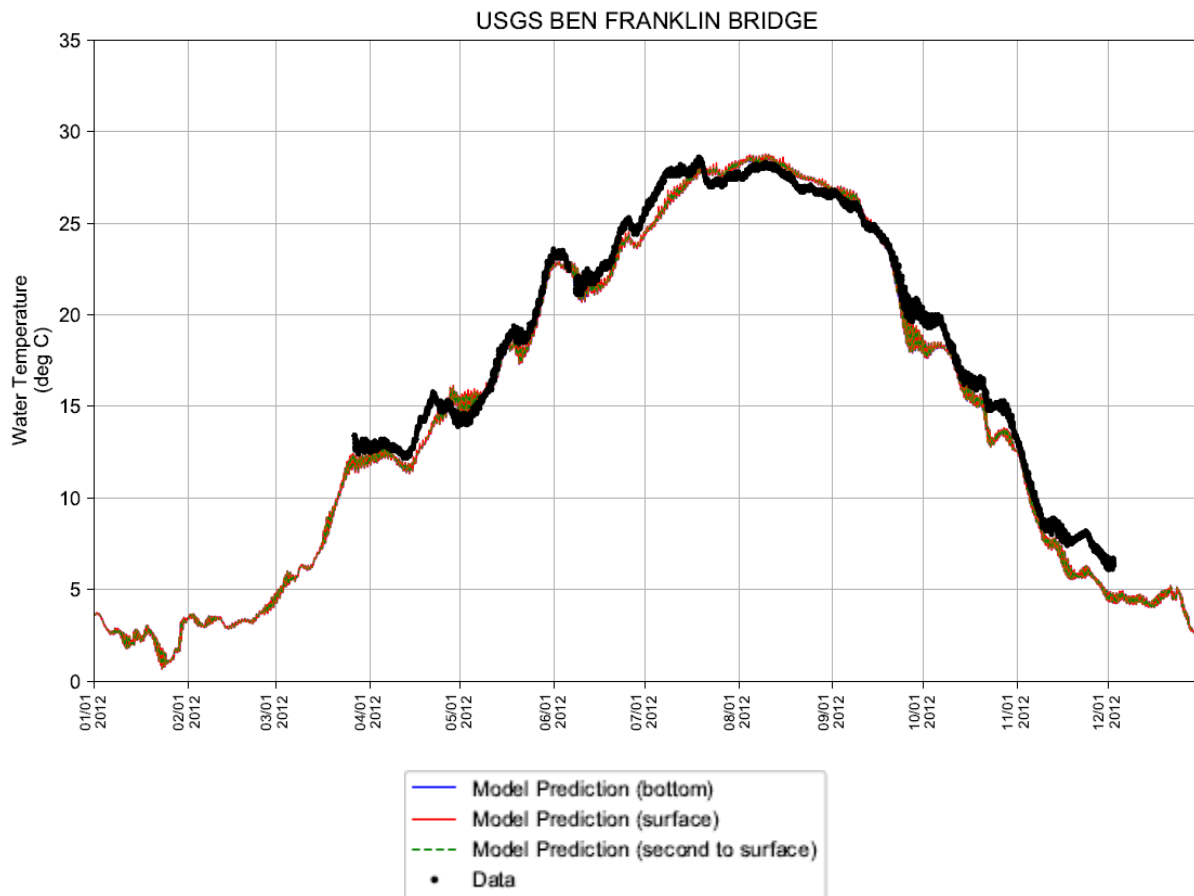


Figure P-32: Observed and Predicted Water Temperature at USGS 01467200 BEN FRANKLIN BRIDGE during 2012 Period

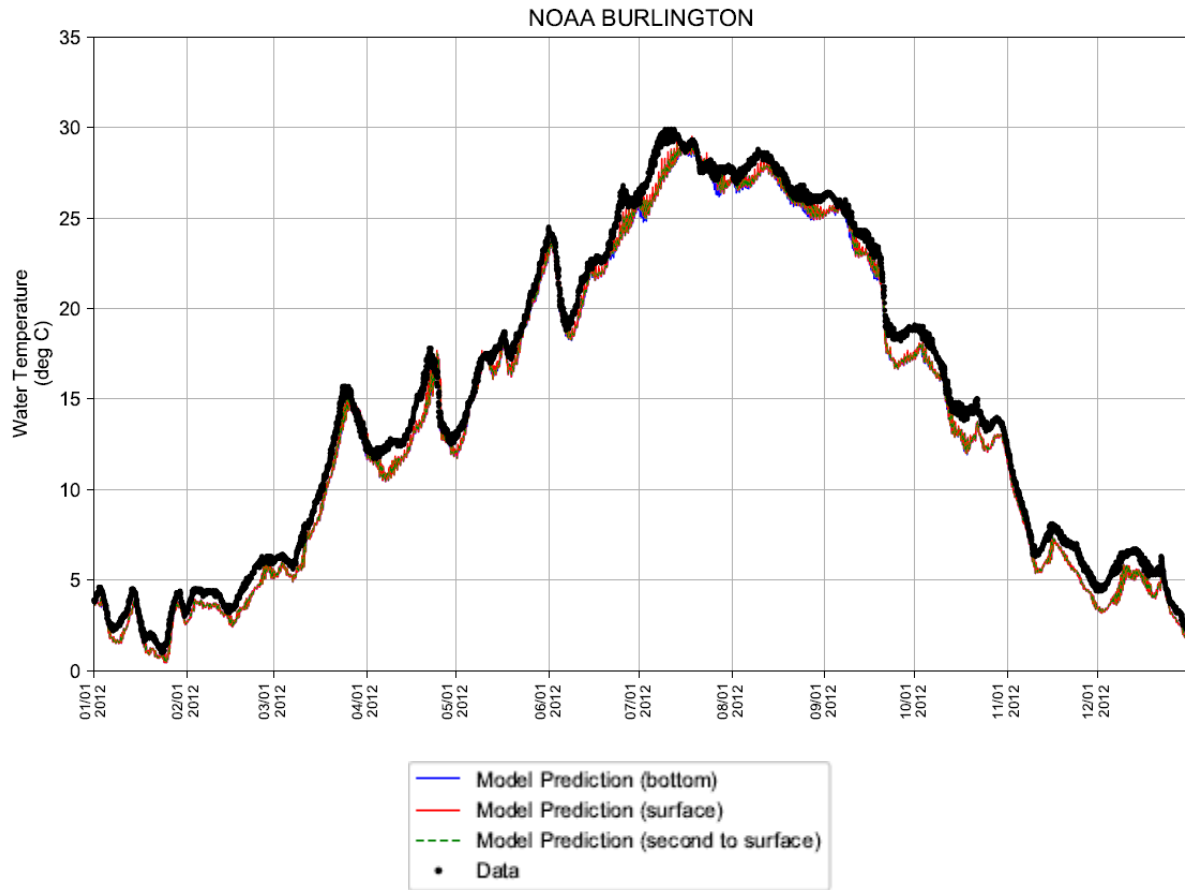


Figure P-33: Observed and Predicted Water Temperature at NOAA BURLINGTON during 2012 Period

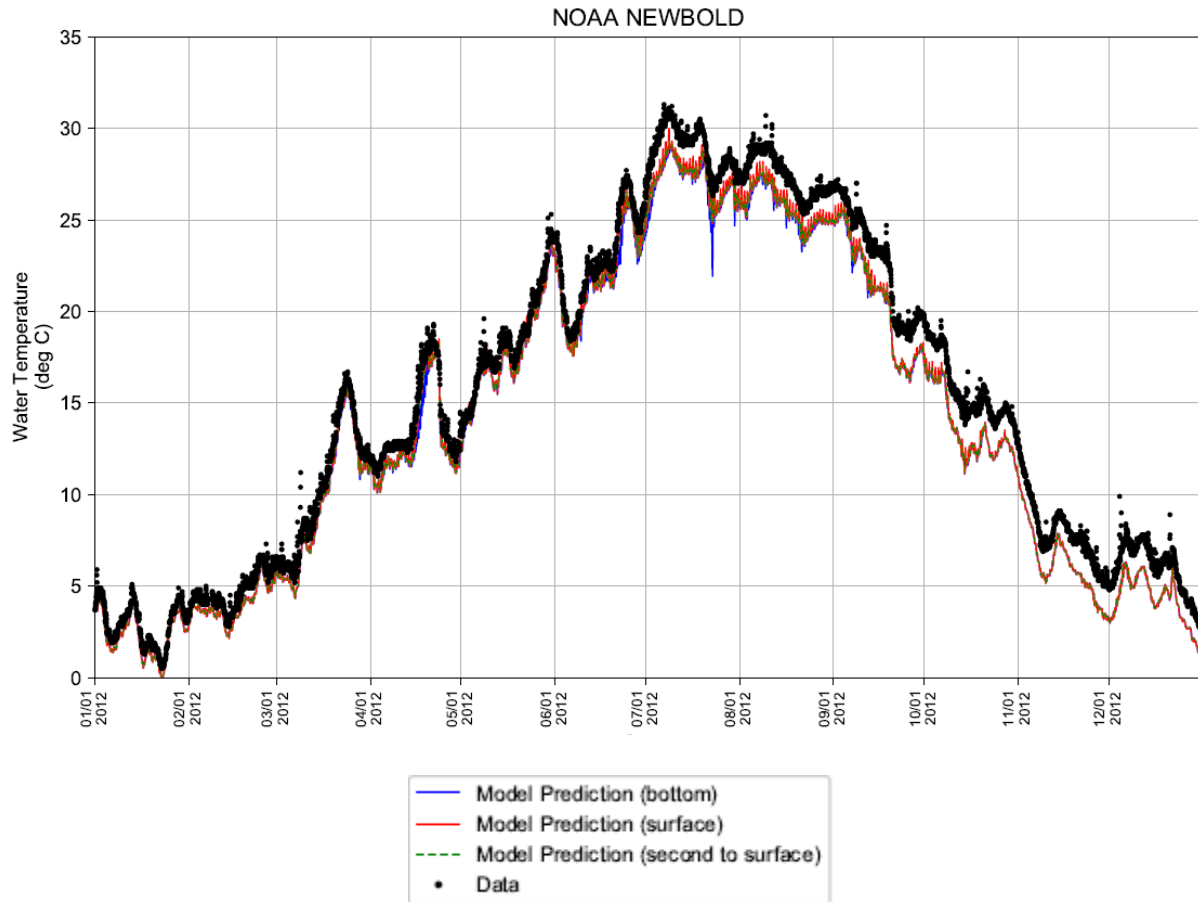


Figure P-34: Observed and Predicted Water Temperature at NOAA NEWBOLD during 2012 Period

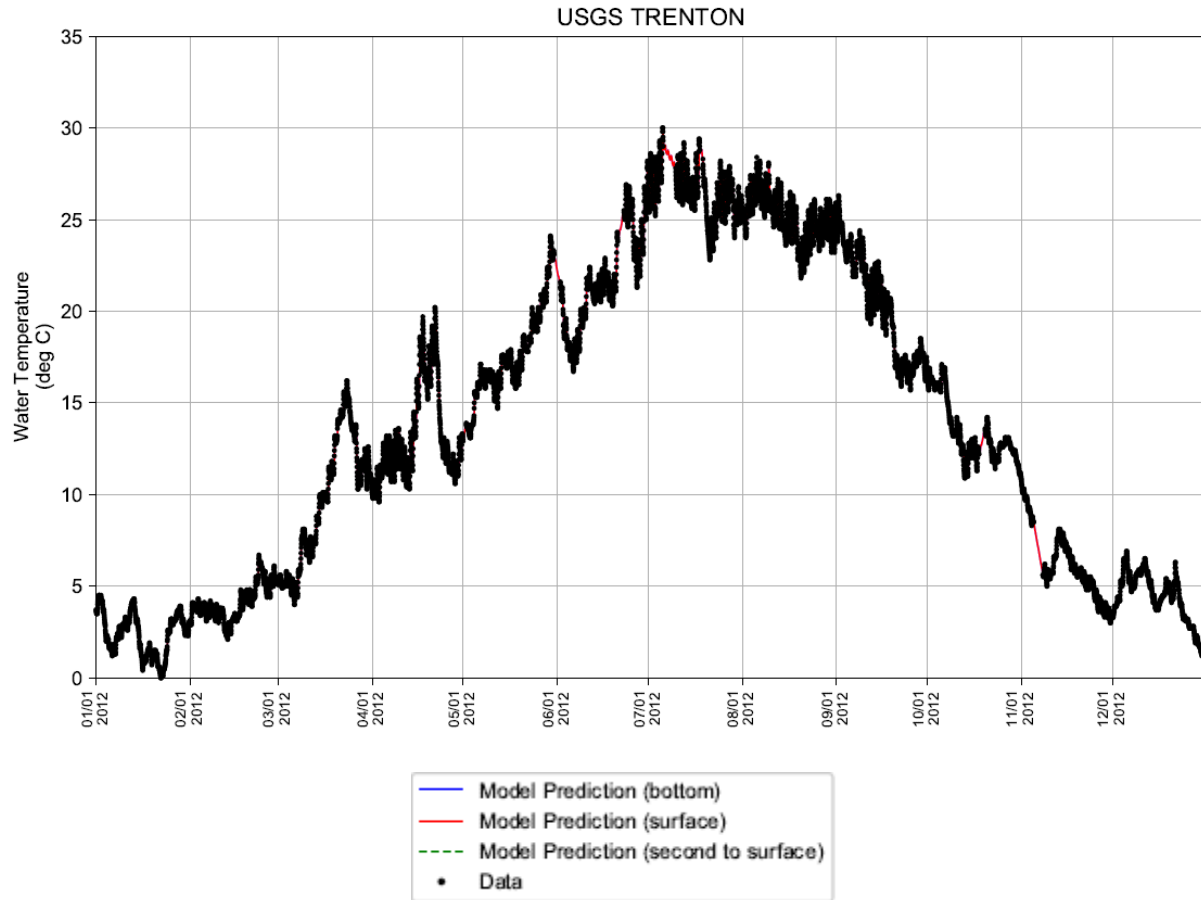
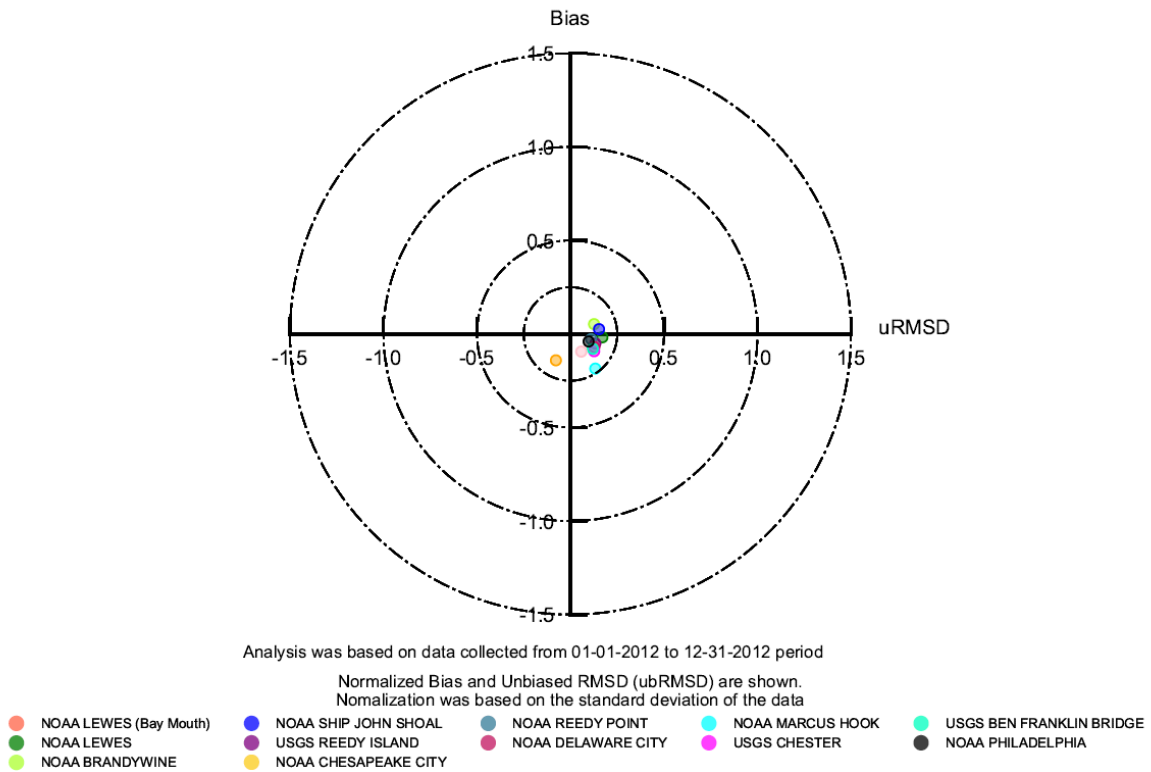


Figure P-35: Observed and Model Boundary Condition for Water Temperature at USGS TRENTON during 2012 Period



Notes: Water Temperature data were based on NOAA and USGS continuous data. Model results were paired to data at hourly time intervals for this analysis
 Period: 01-01-2012 to 12-31-2012
 Run ID: EFDC_HYDRO_G72_2023-01-06

Figure P-36: Target Diagram for Hourly Near-Surface Predicted Water Temperature for 2012 Period

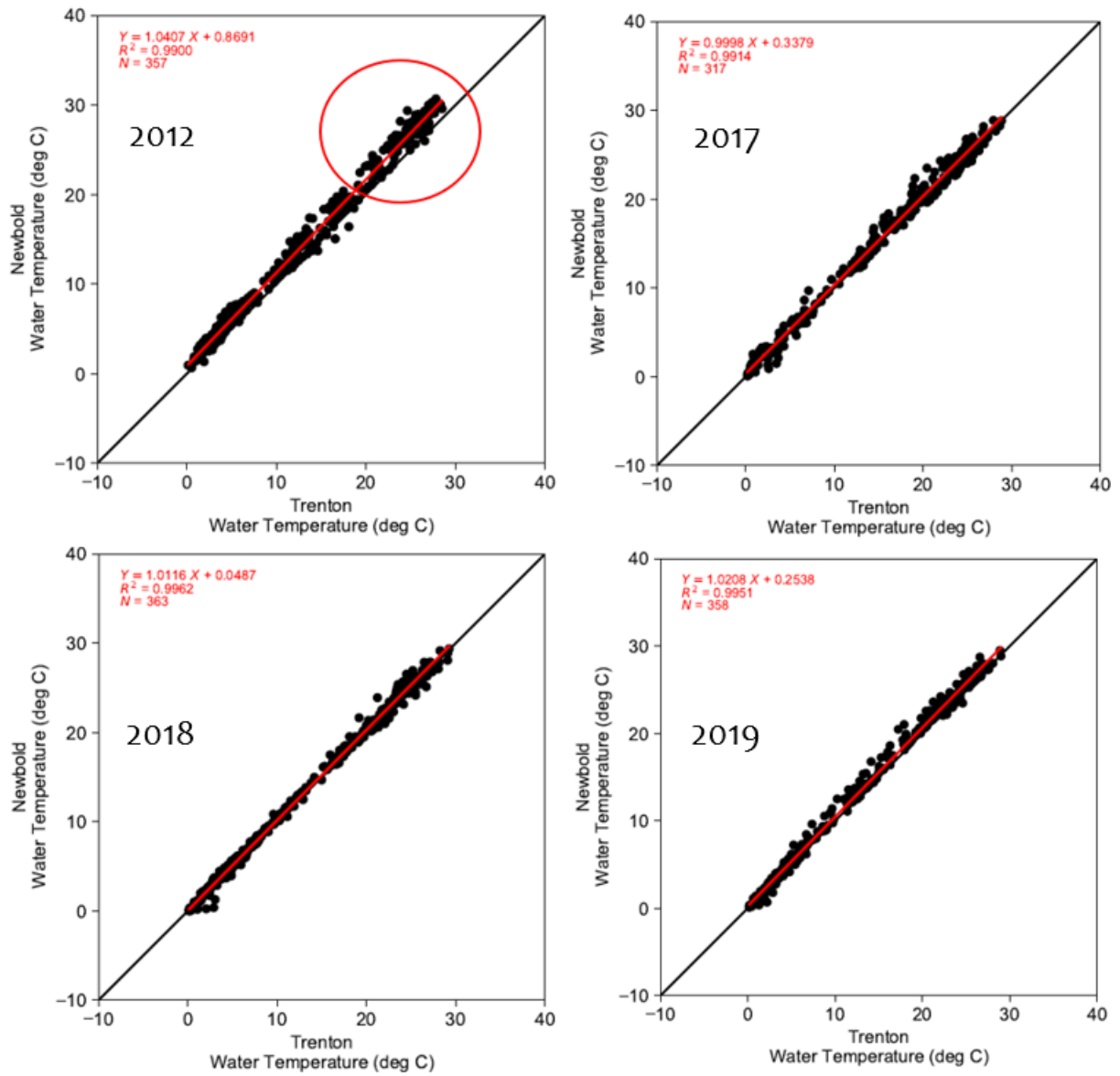
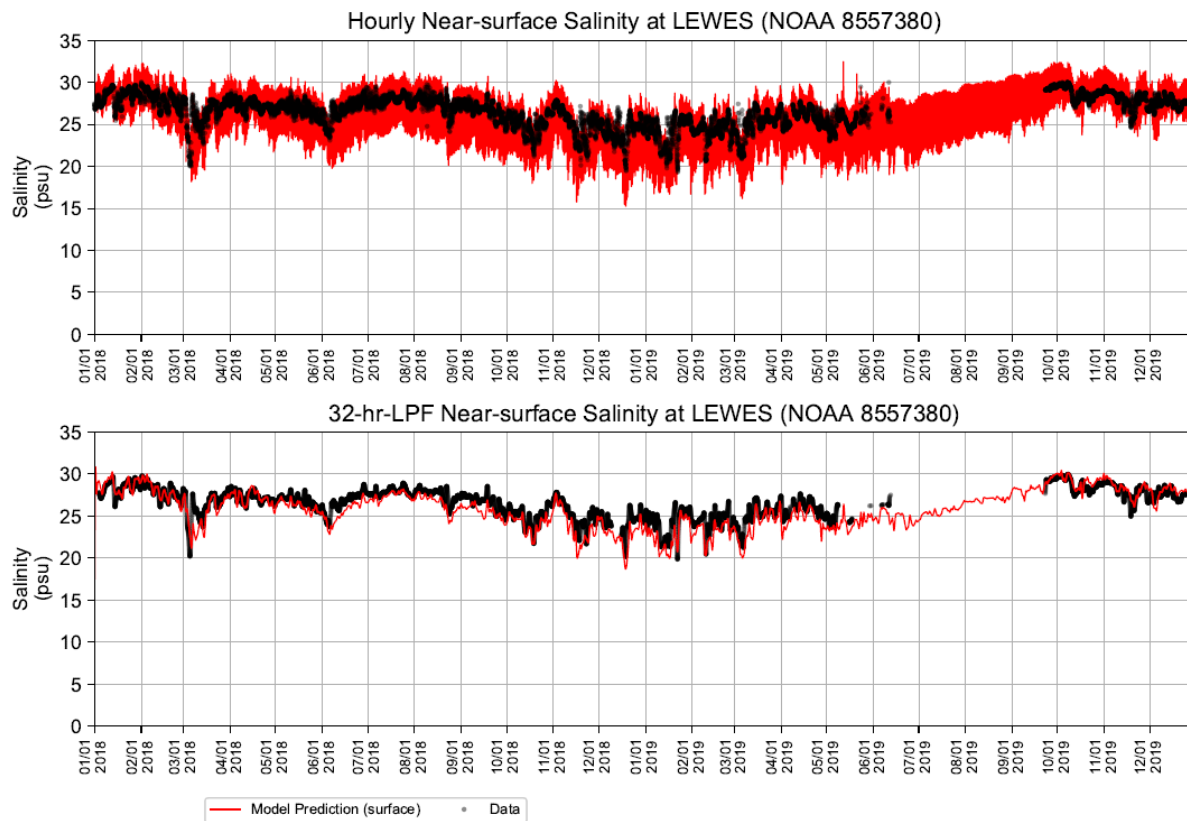


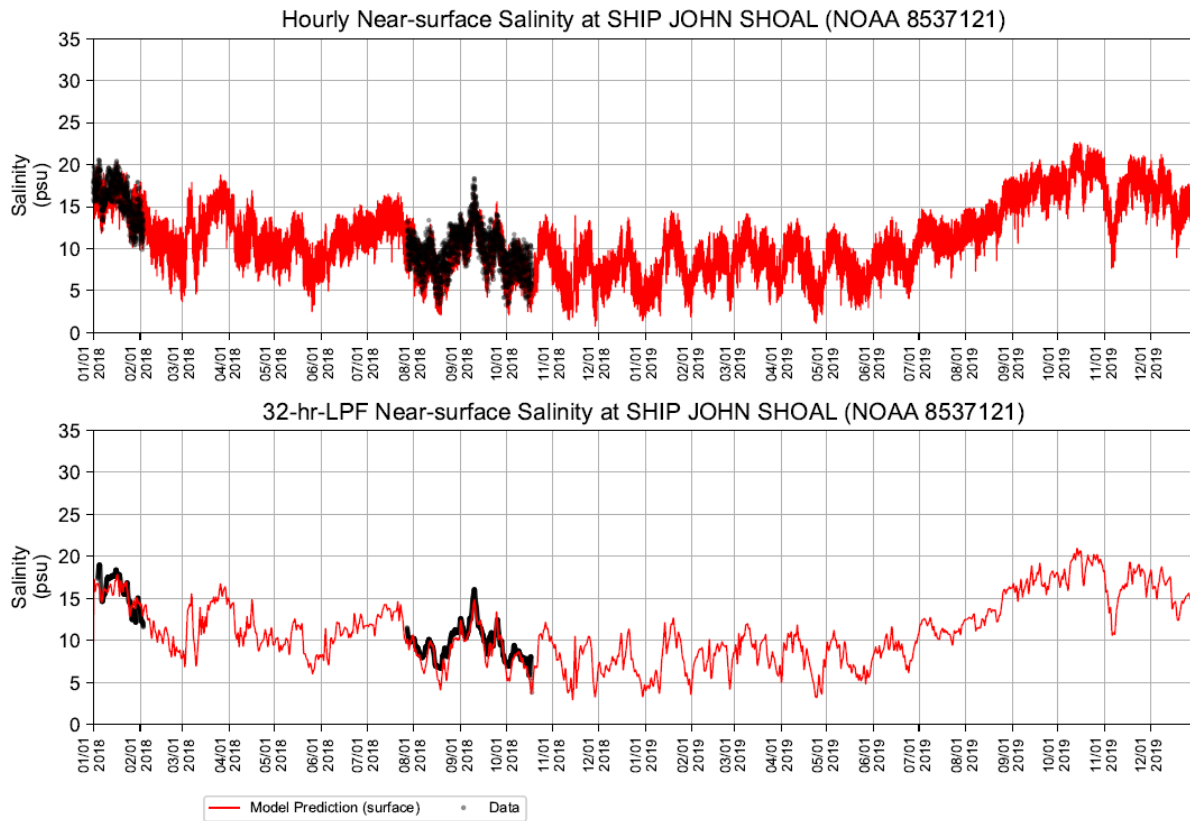
Figure P-37: Daily Water Temperature at Newbold and Trenton

Appendix Q: Observed and predicted hourly and 32-hour-low-pass-filtered salinity for 2018, 2019, and 2012 periods



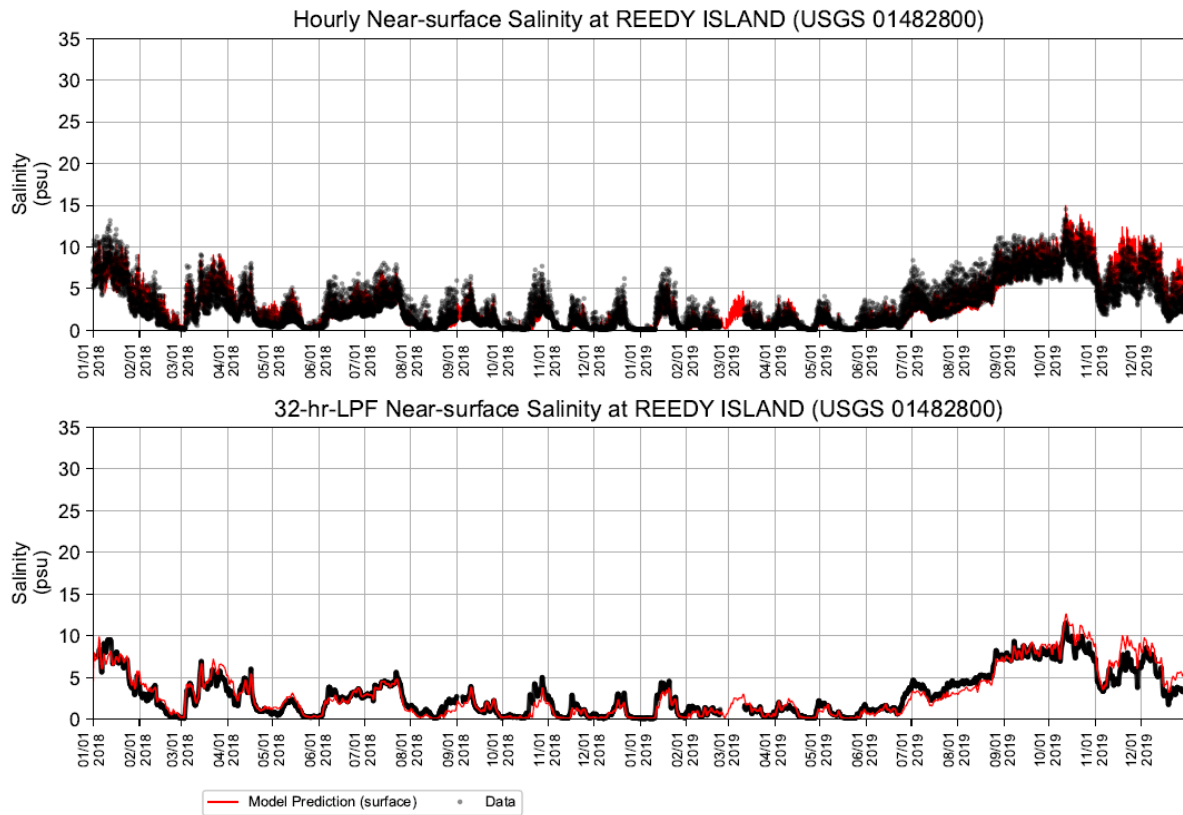
Notes: Salinity data were derived from conductivity or specific conductance and water temperature based on Method 2520B described in Standard Methods for the Examination of Water and Wastewater, 19th Ed. 1995.
Run ID: EFDC_HYDRO_G72_2023-01-06

Figure Q-1: Observed and Predicted Near-surface Salinity at LEWES for 2018 to 2019 Period



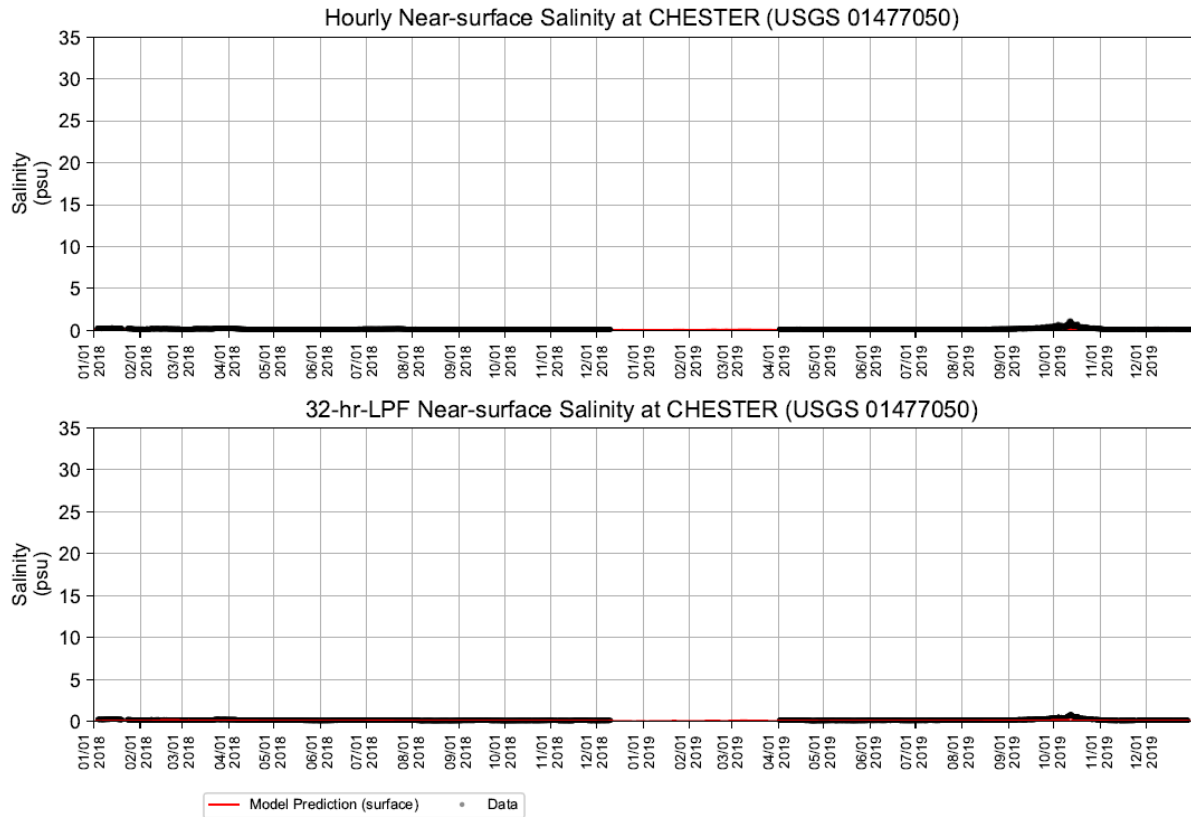
Notes: Salinity data were derived from conductivity or specific conductance and water temperature based on Method 2520B described in *Standard Methods for the Examination of Water and Wastewater, 19th Ed. 1995*.
Run ID: EFDC_HYDRO_G72_2023-01-06

Figure Q-2: Observed and Predicted Near-surface Salinity at SHIP JOHN SHOAL for 2018 to 2019 Period



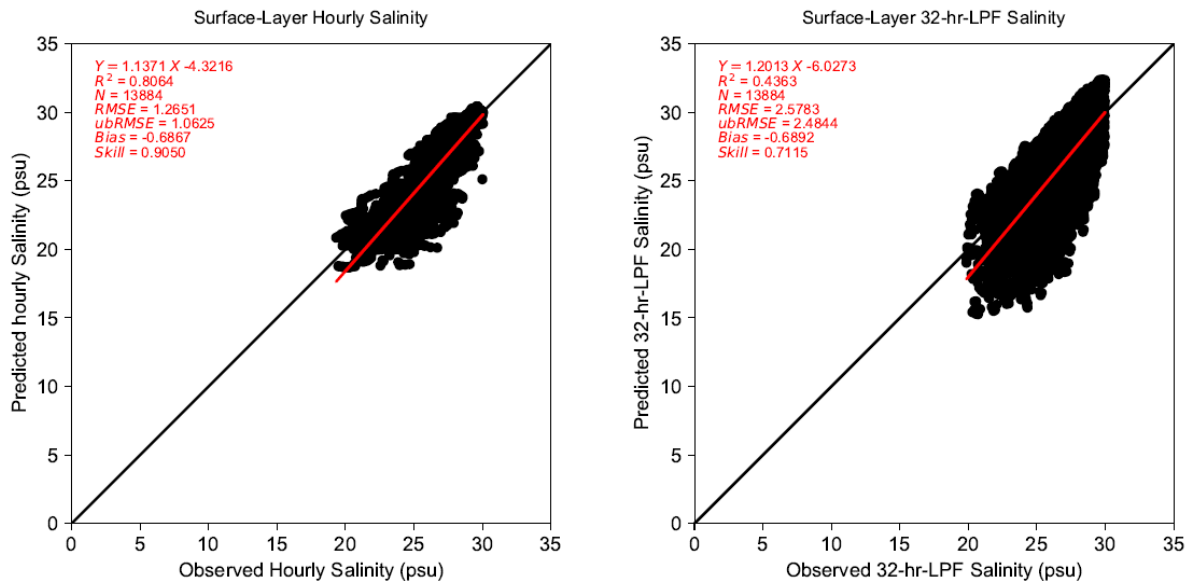
Notes: Salinity data were derived from conductivity or specific conductance and water temperature based on Method 2520B described in *Standard Methods for the Examination of Water and Wastewater, 19th Ed. 1995*.
Run ID: EFDC_HYDRO_G72_2023-01-06

Figure Q-3: Observed and Predicted Near-surface Salinity at REEDY ISLAND for 2018 to 2019 Period



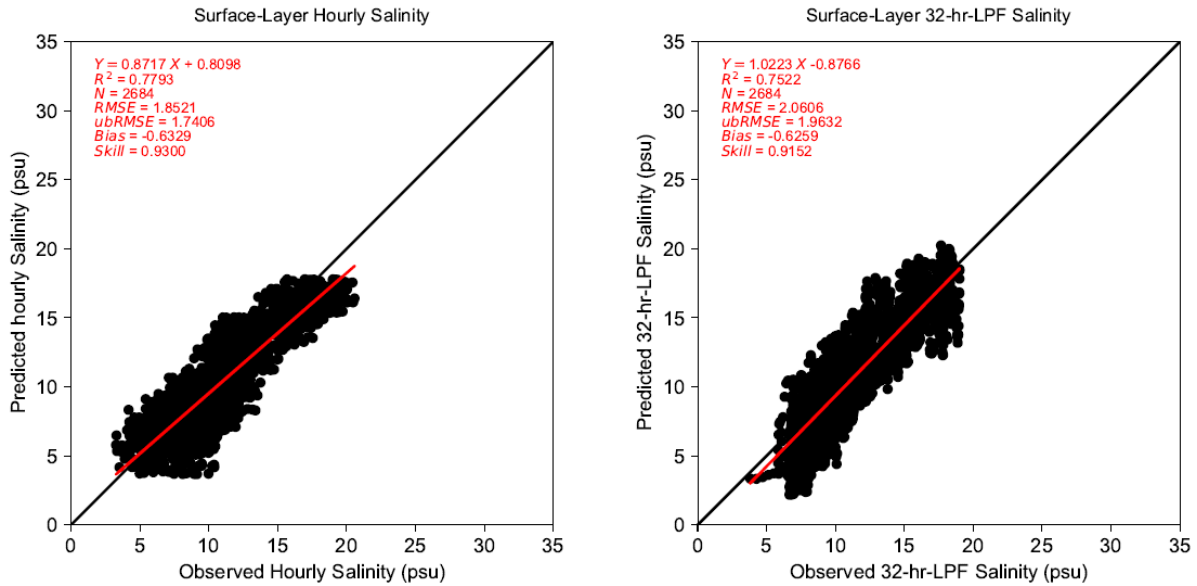
Notes: Salinity data were derived from conductivity or specific conductance and water temperature based on Method 2520B described in Standard Methods for the Examination of Water and Wastewater, 19th Ed. 1995.
Run ID: EFDC_HYDRO_G72_2023-01-06

Figure Q-4: Observed and Predicted Near-surface Salinity at CHESTER for 2018 to 2019 Period



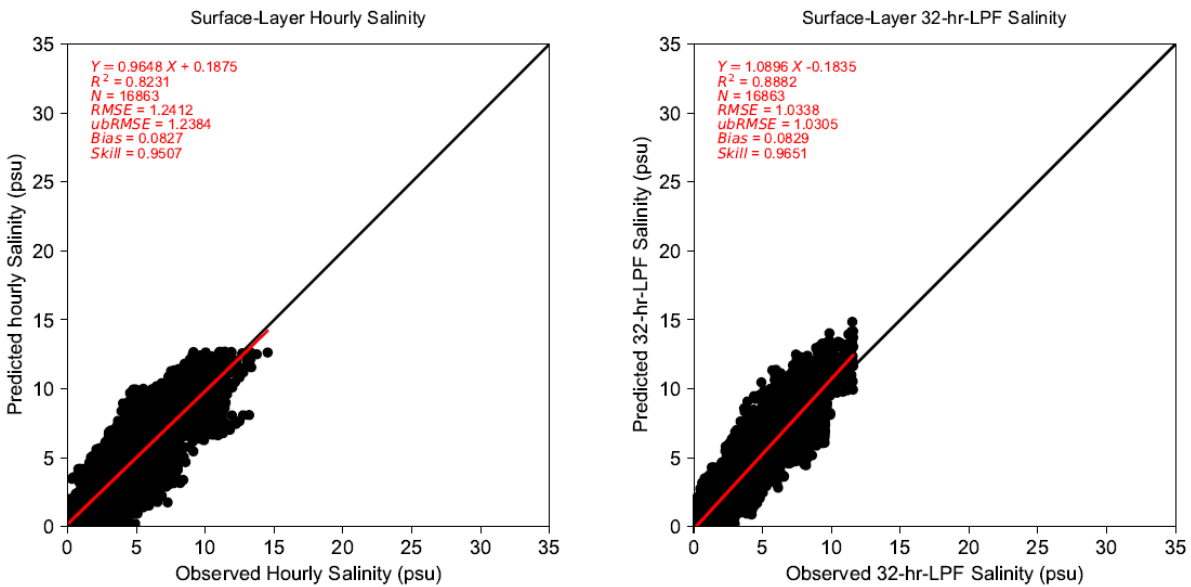
Notes: Salinity data were derived from conductivity or specific conductance and water temperature based on Method 2520B described in Standard Methods for the Examination of Water and Wastewater, 19th Ed. 1995.
 Run ID: EFDC_HYDRO_G72_2023-01-06

Figure Q-5: Comparison of Observed and Predicted Hourly and 32-hour-Low-pass-filtered Salinity at LEWES (NOAA 8557380) during 01-01-2018 to 12-31-2019 period



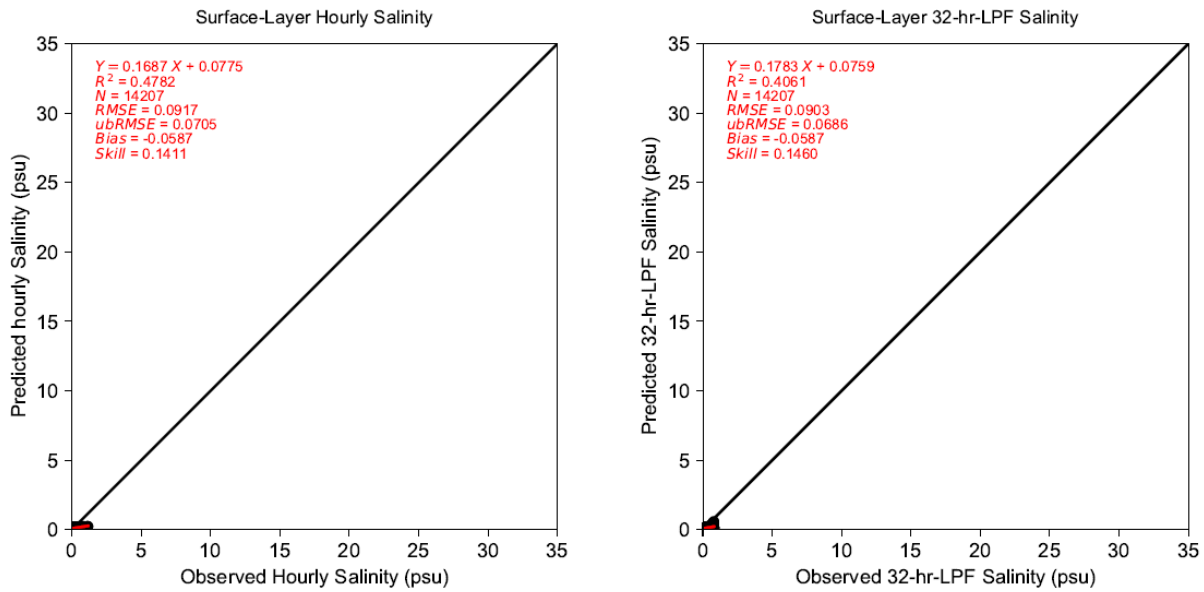
Notes: Salinity data were derived from conductivity or specific conductance and water temperature based on Method 2520B described in Standard Methods for the Examination of Water and Wastewater, 19th Ed. 1995.
 Run ID: EFDC_HYDRO_G72_2023-01-06

Figure Q-6: Comparison of Observed and Predicted Hourly and 32-hour-Low-pass-filtered Salinity at SHIP JOHN SHOAL (NOAA 8537121) during 01-01-2018 to 12-31-2019 period



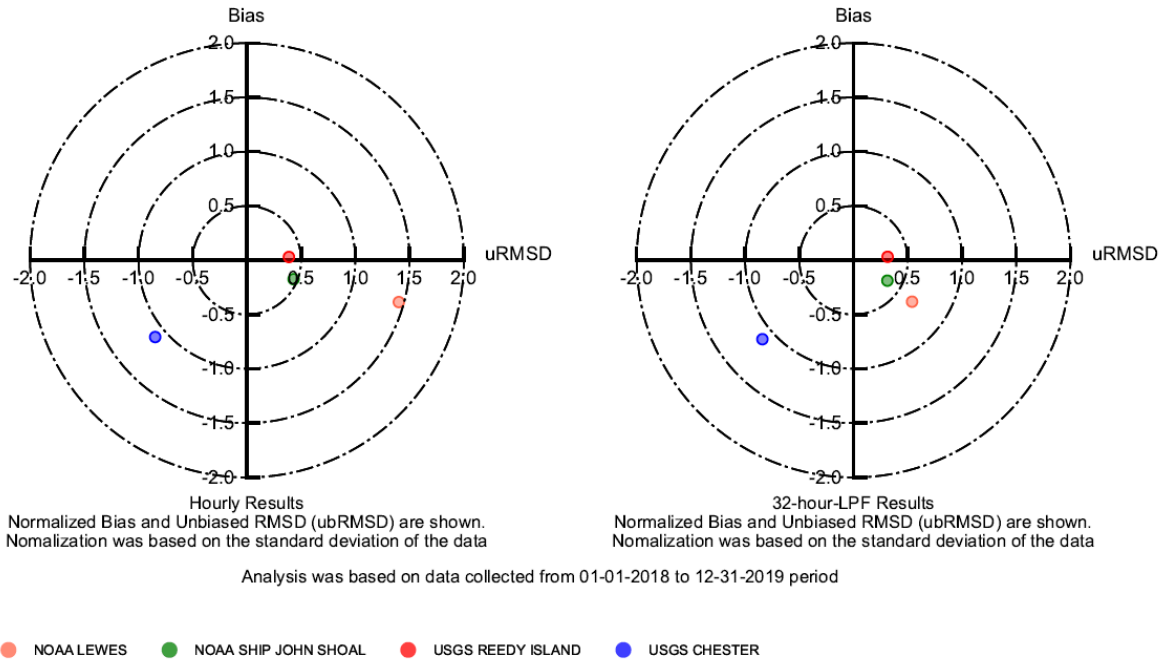
Notes: Salinity data were derived from conductivity or specific conductance and water temperature based on Method 2520B described in *Standard Methods for the Examination of Water and Wastewater, 19th Ed. 1995*.
 Run ID: EFDC_HYDRO_G72_2023-01-06

Figure Q-7: Comparison of Observed and Predicted Hourly and 32-hour-Low-pass-filtered Salinity at REEDY ISLAND (USGS 01482800) during 01-01-2018 to 12-31-2019 period



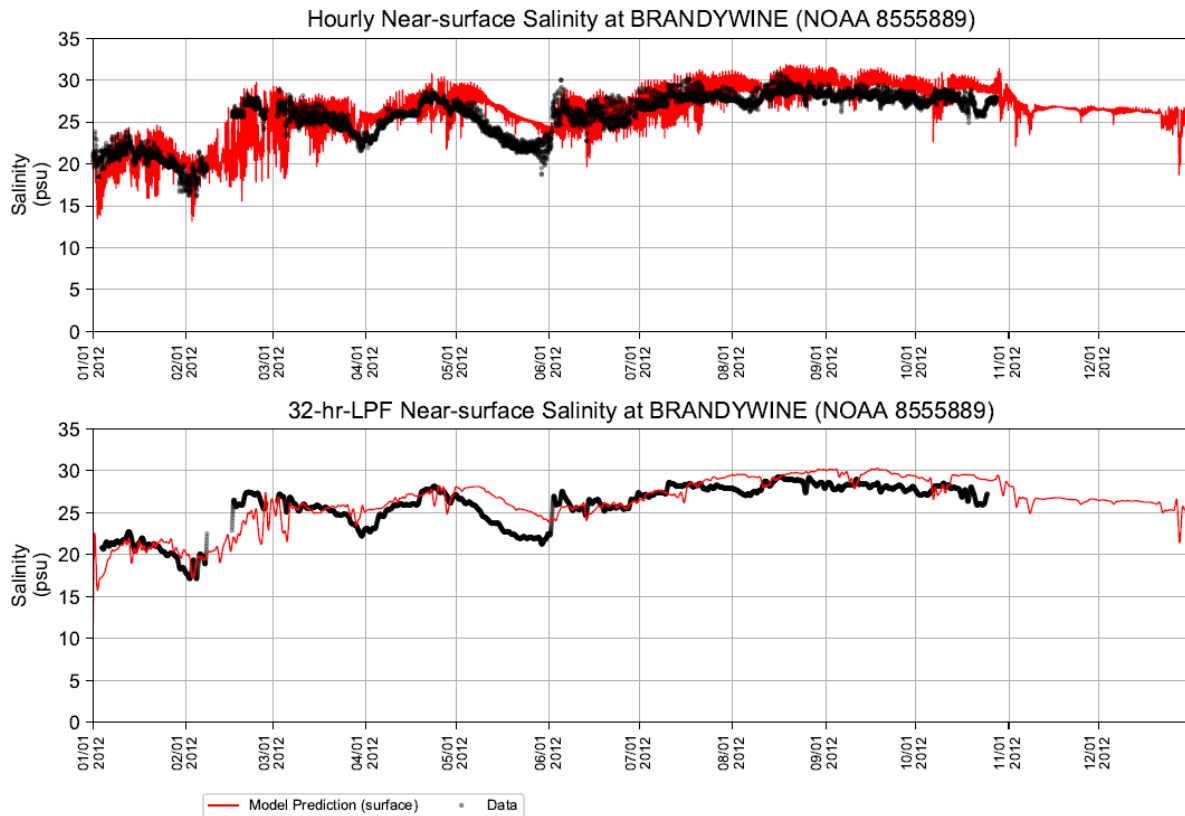
Notes: Salinity data were derived from conductivity or specific conductance and water temperature based on Method 2520B described in Standard Methods for the Examination of Water and Wastewater, 19th Ed. 1995.
 Run ID: EFDC_HYDRO_G72_2023-01-06

Figure Q-8: Comparison of Observed and Predicted Hourly and 32-hour-Low-pass-filtered Salinity at CHESTER (USGS 01477050) during 01-01-2018 to 12-31-2019 period



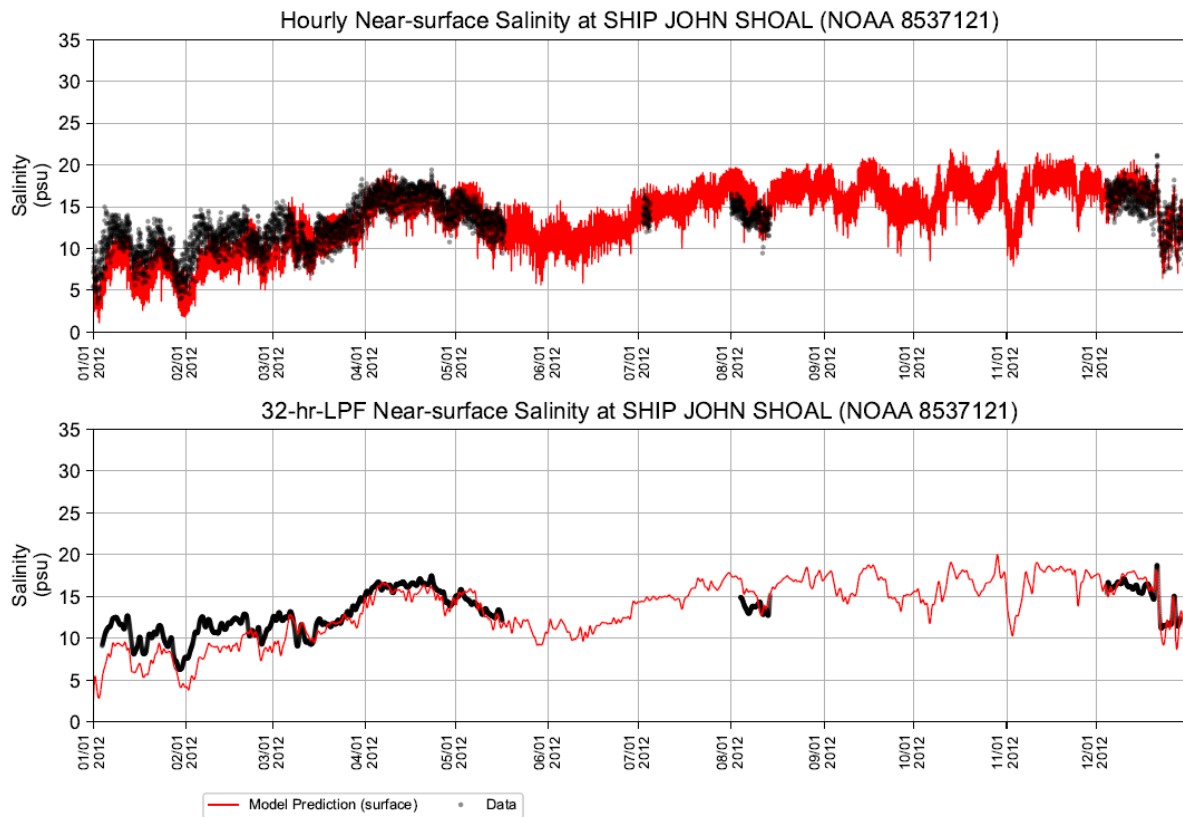
Notes: Salinity data were derived from conductivity or specific conductance and water temperature based on Method 2520B described in Standard Methods for the Examination of Water and Wastewater, 19th Ed. 1995.
Run ID: EFDC_HYDRO_G72_2023-01-06

Figure Q-9: Target Diagram for Predicted Hourly and 32-hour-LPF Near-Surface Salinity for 2018 to 2019 Period



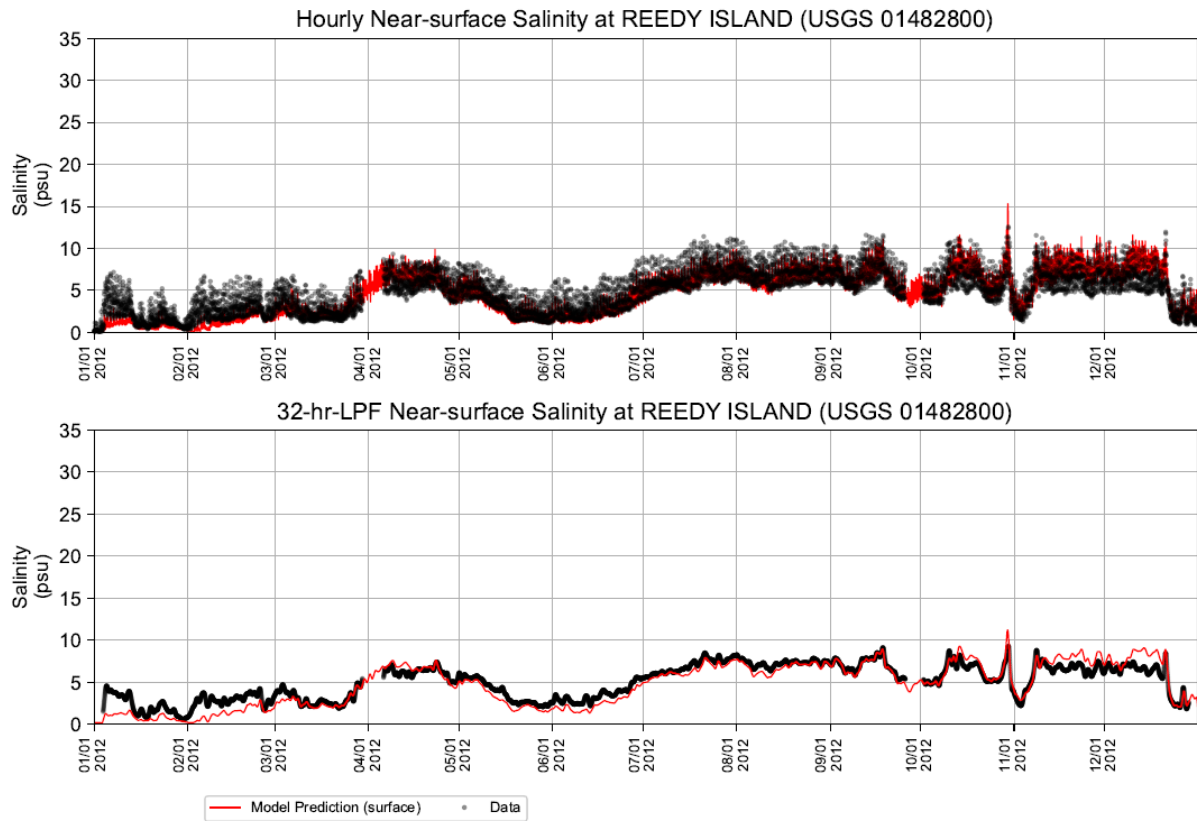
Notes: Salinity data were derived from conductivity or specific conductance and water temperature based on Method 2520B described in *Standard Methods for the Examination of Water and Wastewater, 19th Ed. 1995*.
Run ID: EFDC_HYDRO_G72_2023-01-06

Figure Q-10: Observed and Predicted Near-surface Salinity at BRANDYWINE for 2012 Period



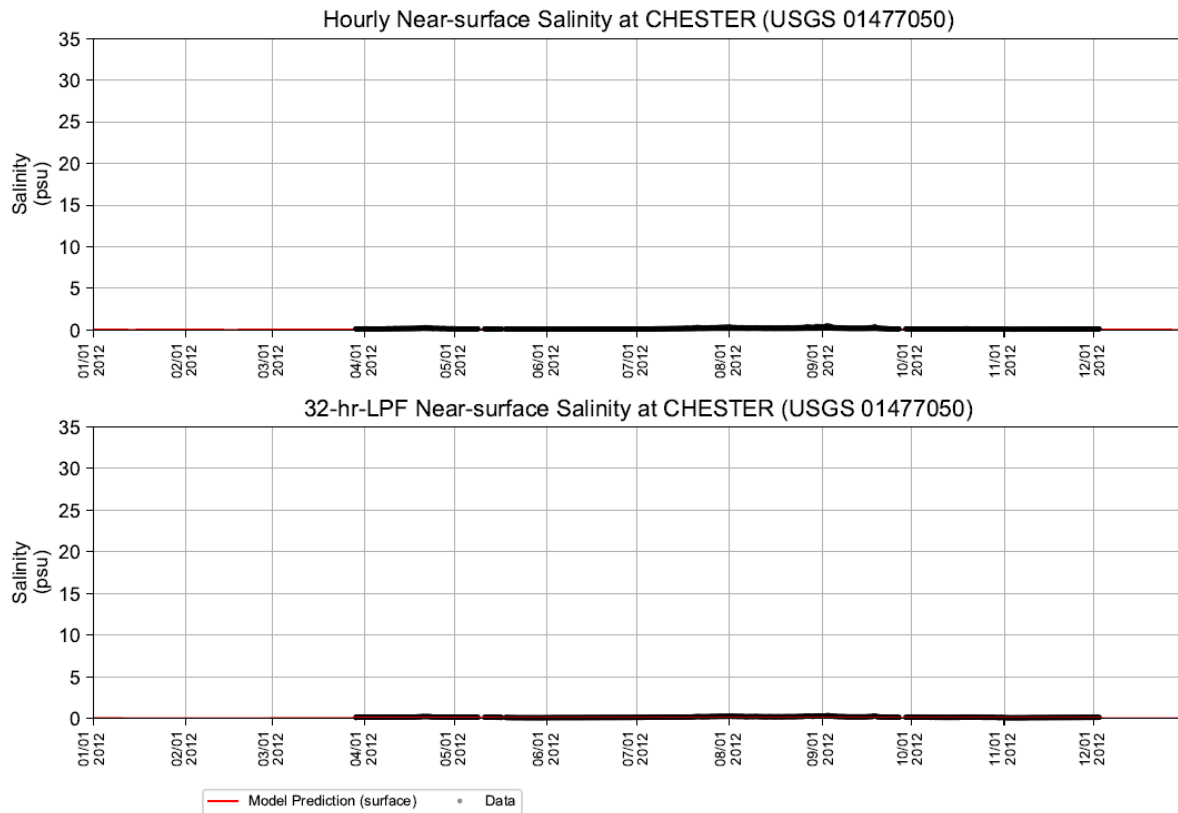
Notes: Salinity data were derived from conductivity or specific conductance and water temperature based on Method 2520B described in Standard Methods for the Examination of Water and Wastewater, 19th Ed. 1995.
Run ID: EFDC_HYDRO_G72_2023-01-06

Figure Q-11: Observed and Predicted Near-surface Salinity at SHIP JOHN SHOAL for 2012 Period



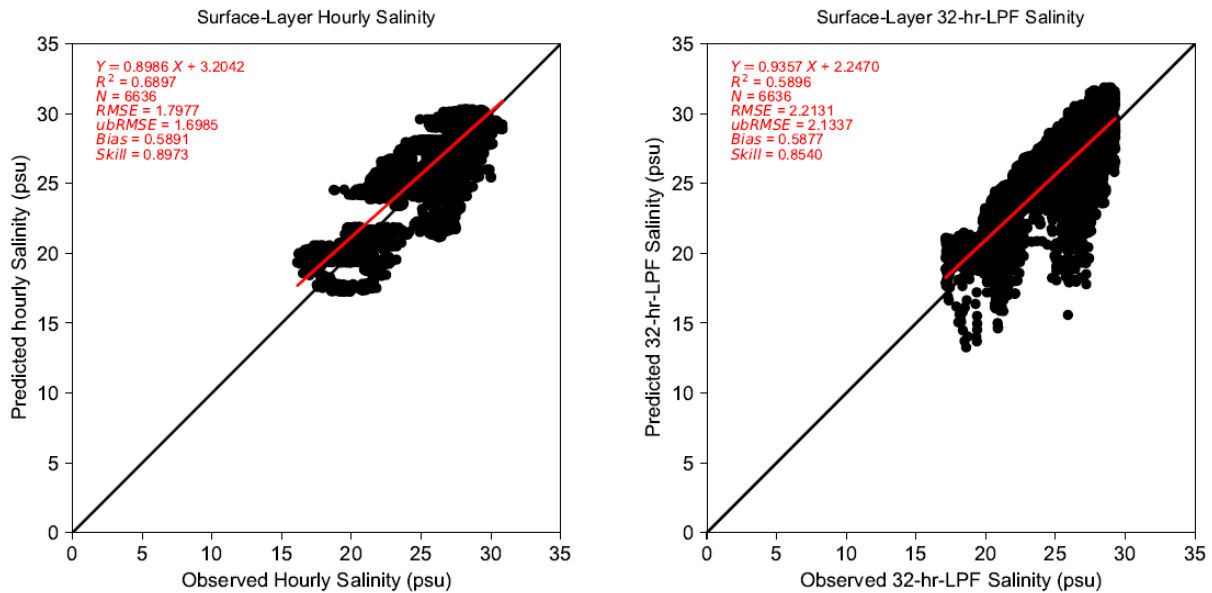
Notes: Salinity data were derived from conductivity or specific conductance and water temperature based on Method 2520B described in *Standard Methods for the Examination of Water and Wastewater, 19th Ed. 1995*.
Run ID: EFDC_HYDRO_G72_2023-01-06

Figure Q-12: Observed and Predicted Near-surface Salinity at REEDY ISLAND for 2012 Period



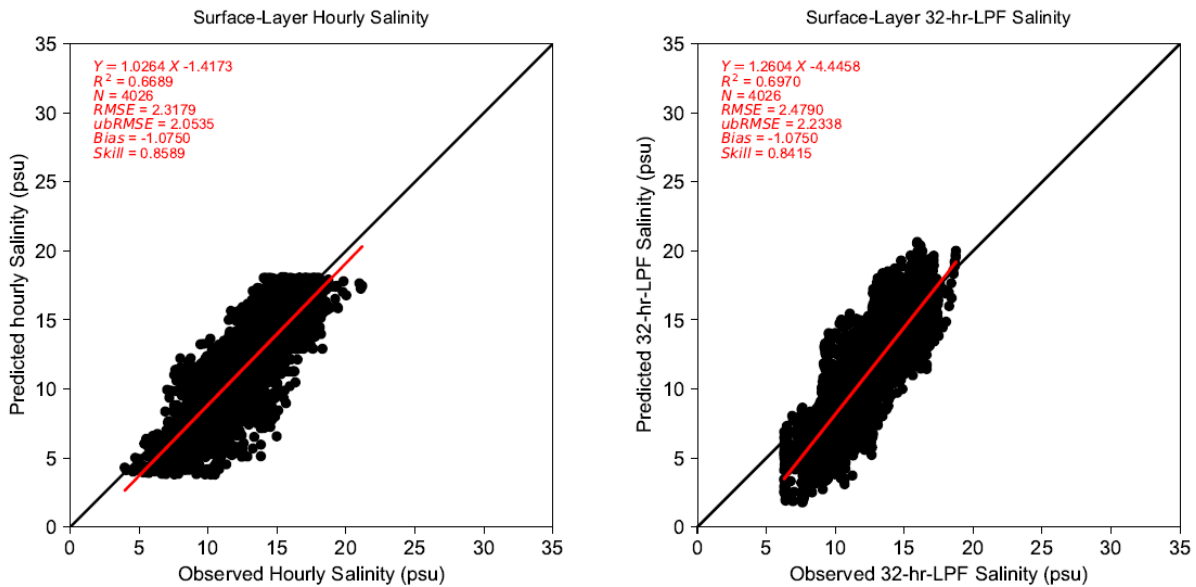
Notes: Salinity data were derived from conductivity or specific conductance and water temperature based on Method 2520B described in *Standard Methods for the Examination of Water and Wastewater, 19th Ed. 1995*.
 Run ID: EFDC_HYDRO_G72_2023-01-06

Figure Q-13: Observed and Predicted Near-surface Salinity at CHESTER for 2012 Period



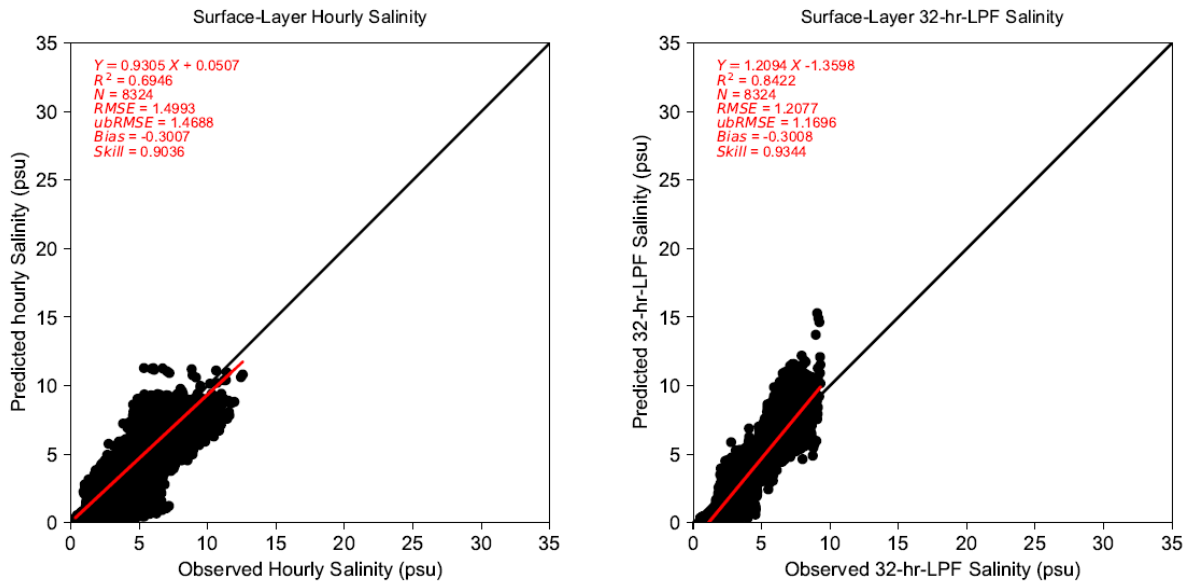
Notes: Salinity data were derived from conductivity or specific conductance and water temperature based on Method 2520B described in Standard Methods for the Examination of Water and Wastewater, 19th Ed. 1995.
 Run ID: EFDC_HYDRO_G72_2023-01-06

Figure Q-14: Comparison of Observed and Predicted Hourly and 32-hour-Low-pass-filtered Salinity at BRANDYWINE (NOAA 8555889) during 01-01-2012 to 12-31-2012 period



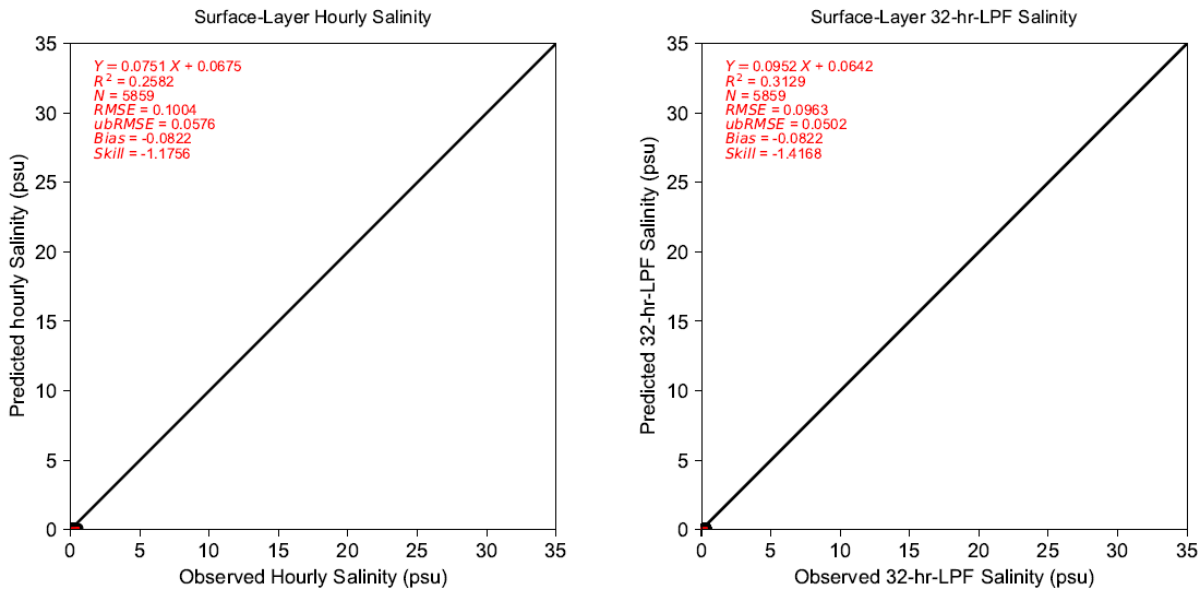
Notes: Salinity data were derived from conductivity or specific conductance and water temperature based on Method 2520B described in Standard Methods for the Examination of Water and Wastewater, 19th Ed. 1995.
 Run ID: EFDC_HYDRO_G72_2023-01-06

Figure Q-15: Comparison of Observed and Predicted Hourly and 32-hour-Low-pass-filtered Salinity at SHIP JOHN SHOAL (NOAA 8537121) during 01-01-2012 to 12-31-2012 period



Notes: Salinity data were derived from conductivity or specific conductance and water temperature based on Method 2520B described in *Standard Methods for the Examination of Water and Wastewater, 19th Ed. 1995*.
 Run ID: EFDC_HYDRO_G72_2023-01-06

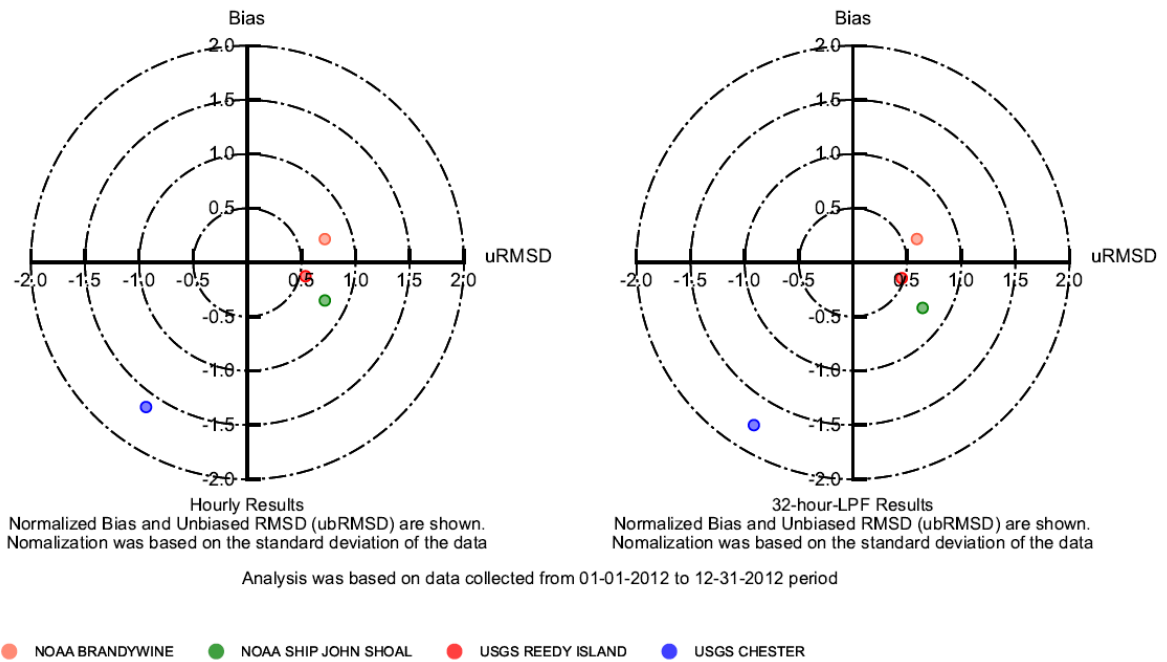
Figure Q-16. Comparison of Observed and Predicted Hourly and 32-hour-Low-pass-filtered Salinity at REEDY ISLAND (USGS 01482800) during 01-01-2012 to 12-31-2012 period



Notes: Salinity data were derived from conductivity or specific conductance and water temperature based on Method 2520B described in Standard Methods for the Examination of Water and Wastewater, 19th Ed. 1995. Salinity intrusion during this period was farther downstream, so the observed salinity reflects the background level from upland sources.

Run ID: EFDC_HYDRO_G72_2023-01-06

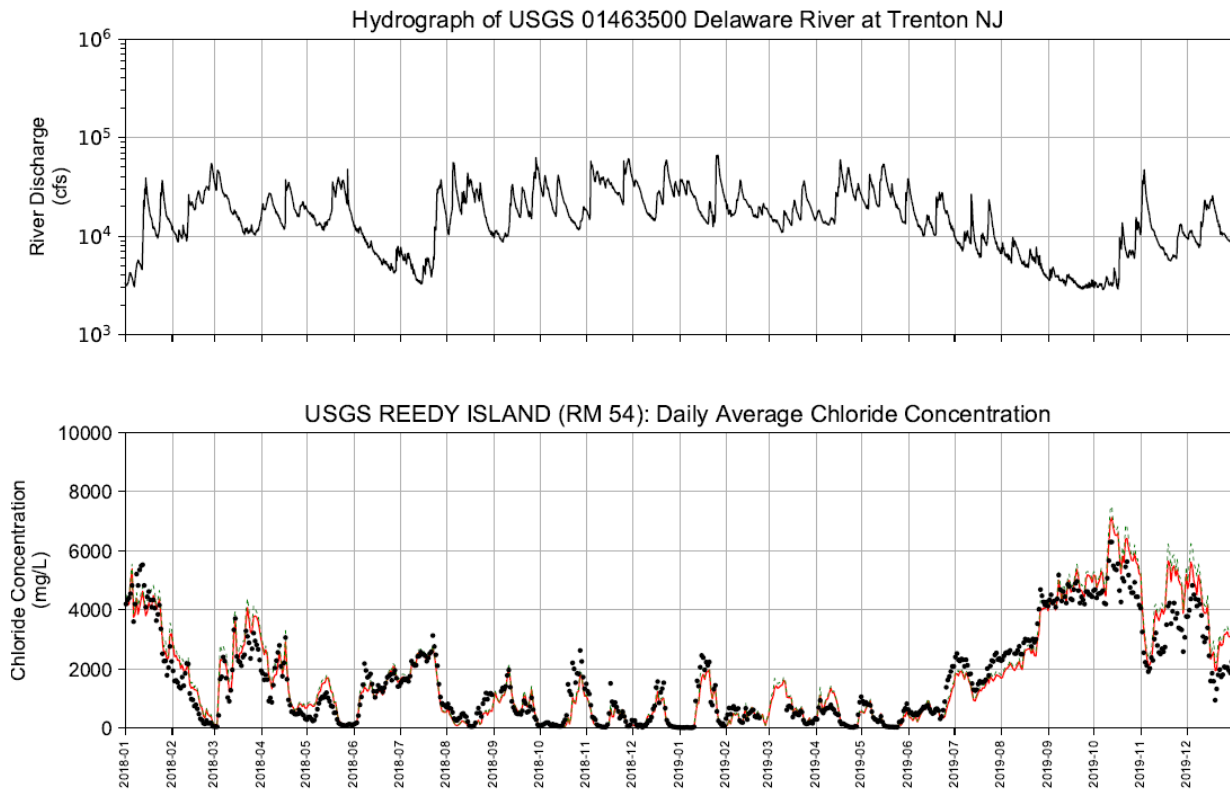
Figure Q-17. Comparison of Observed and Predicted Hourly and 32-hour-Low-pass-filtered Salinity at CHESTER (USGS 01477050) during 01-01-2012 to 12-31-2012 period



Notes: Salinity data were derived from conductivity or specific conductance and water temperature based on Method 2520B described in Standard Methods for the Examination of Water and Wastewater, 19th Ed. 1995.
Run ID: EFDC_HYDRO_G72_2023-01-06

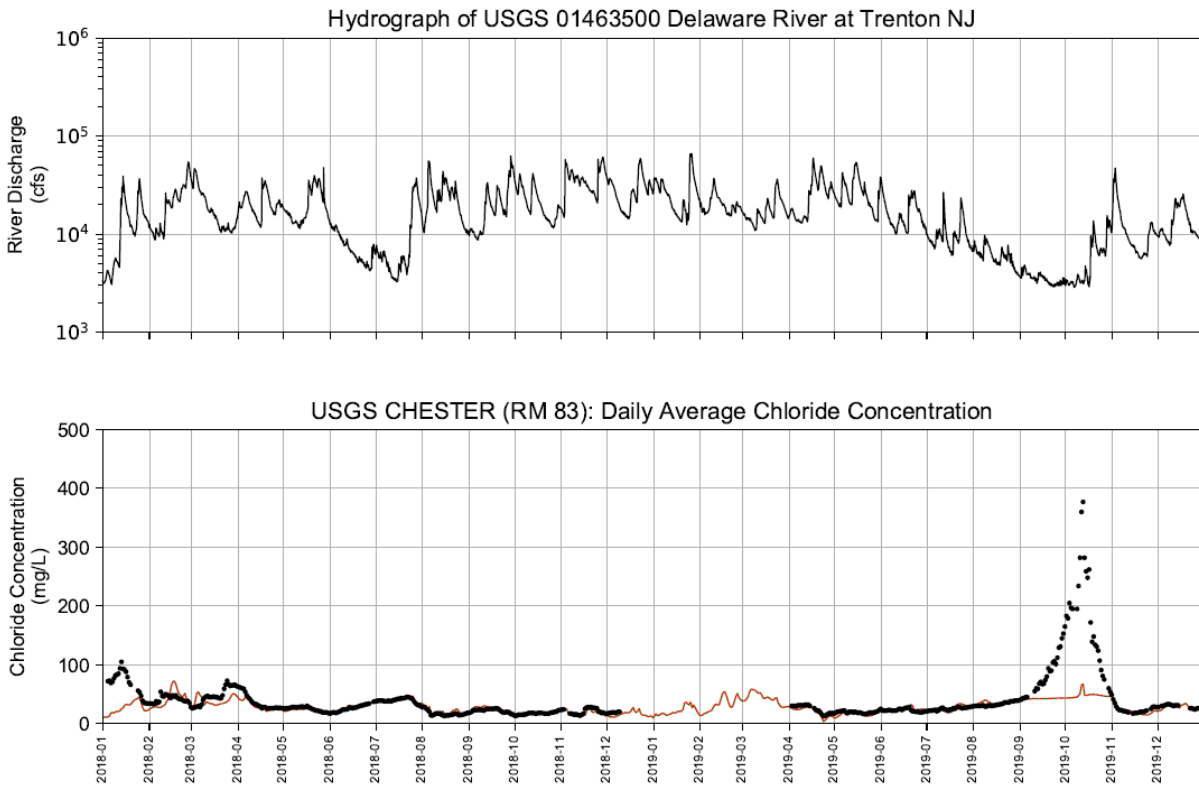
Figure Q-18: Target Diagram for Predicted Hourly and 32-hour-LPF Near-Surface Salinity for 2012 Period

Appendix R: Observed and predicted daily average chloride for 2018, 2019, and 2012



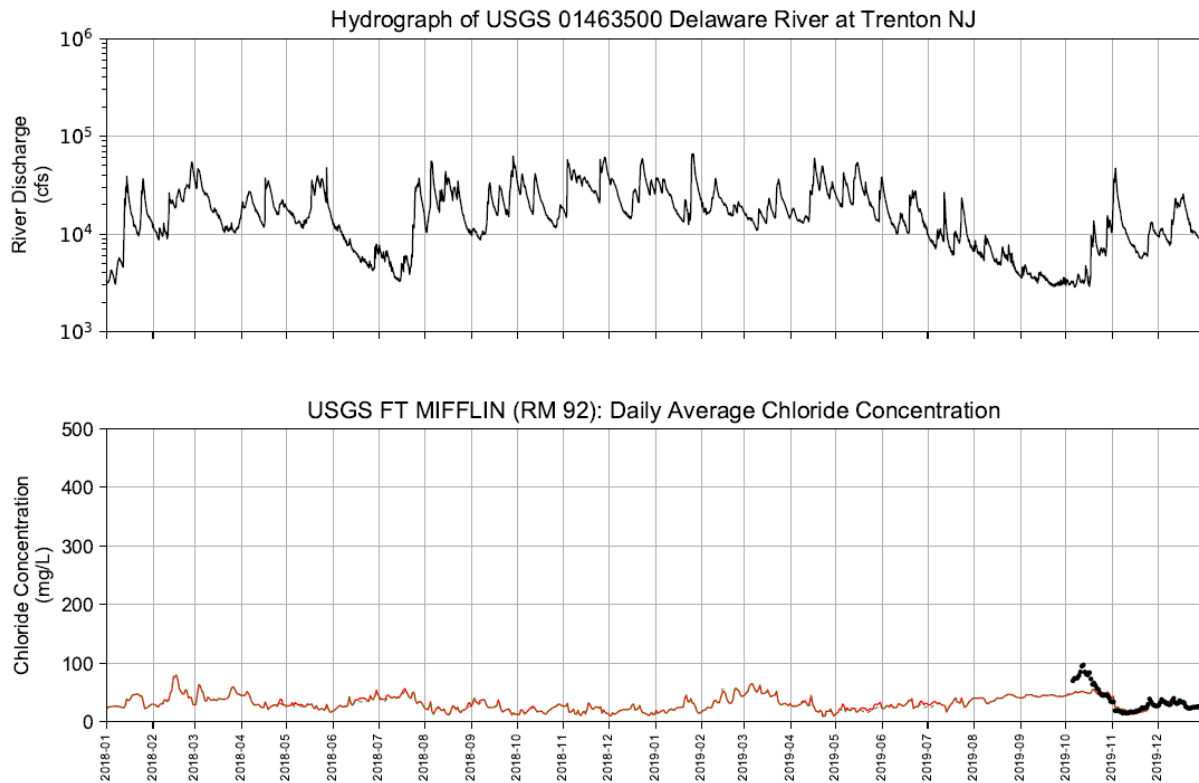
Notes: Chloride concentration data were derived from specific conductance based on USGS (Paulson, 1970).
Station ID: USGS01482800, USGS REEDY ISLAND (RM 54.1)
Run ID: EFDC_HYDRO_G72_2023-01-06

Figure R-1: Observed and Predicted Daily Average Chloride Concentration at USGS Station USGS REEDY ISLAND (RM 54.1) for 2018 to 2019 Period



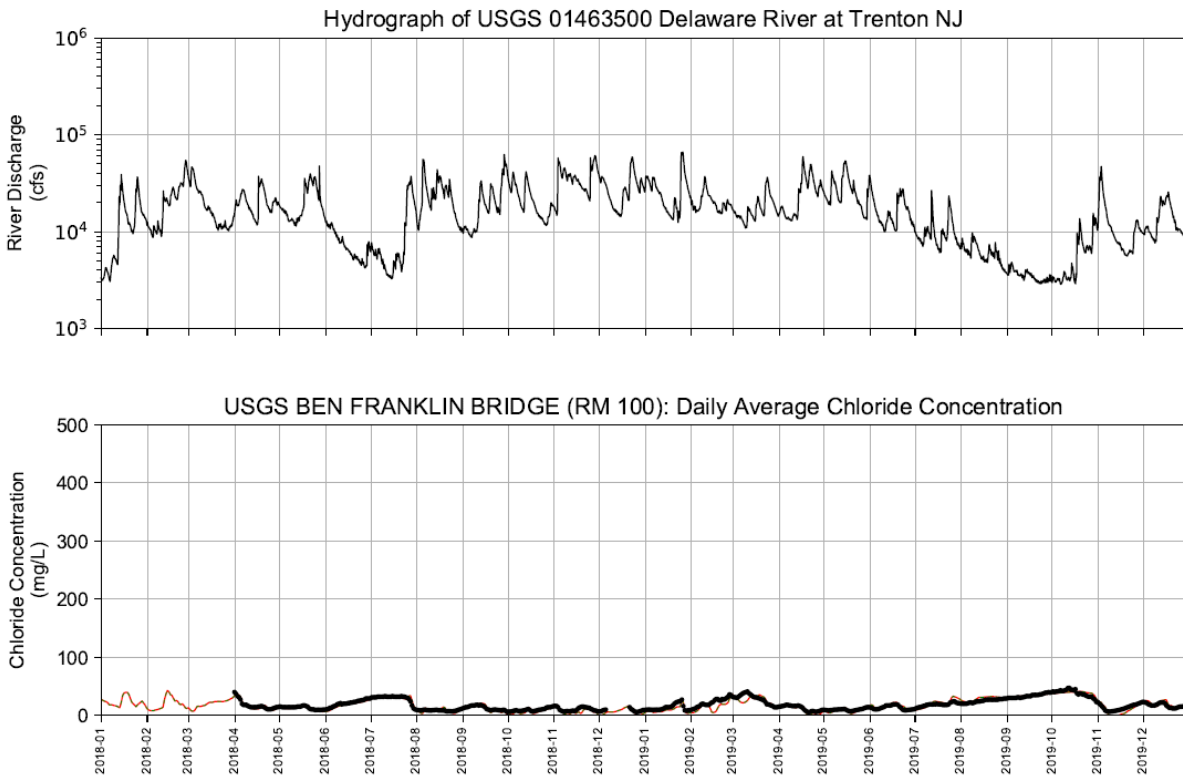
Notes: Chloride concentration data were derived from specific conductance based on USGS (1970s).
Station ID: USGS01477050, USGS CHESTER (RM 83.6)
Run ID: EFDC_HYDRO_G72_2023-01-06

Figure R-2: Observed and Predicted Daily Average Chloride Concentration at USGS Station USGS CHESTER (RM 83.6) for 2018 to 2019 Period



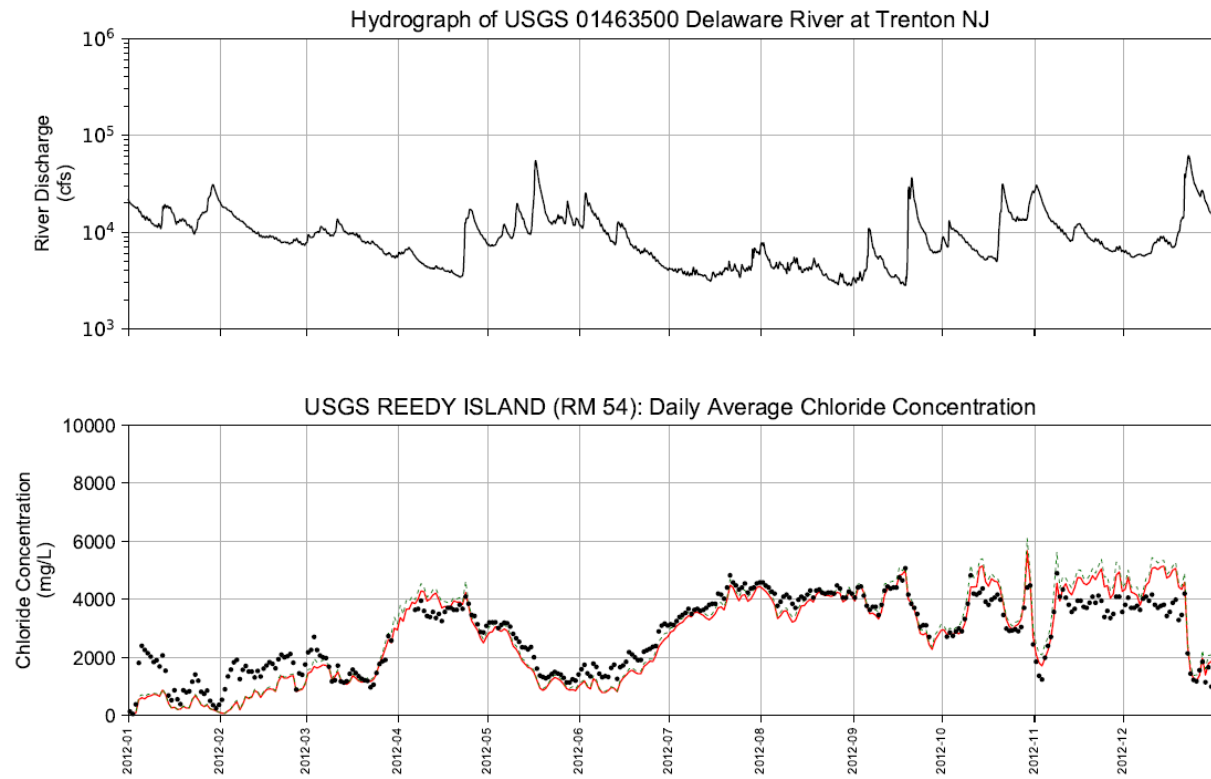
Notes: Chloride concentration data were derived from specific conductance based on USGS (1970s).
Station ID: USGS01474703, USGS FT MIFFLIN (RM 91.9)
Run ID: EFDC_HYDRO_G72_2023-01-06

Figure R-3: Observed and Predicted Daily Average Chloride Concentration at USGS Station USGS FT MIFFLIN (RM 91.9) for 2018 to 2019 Period



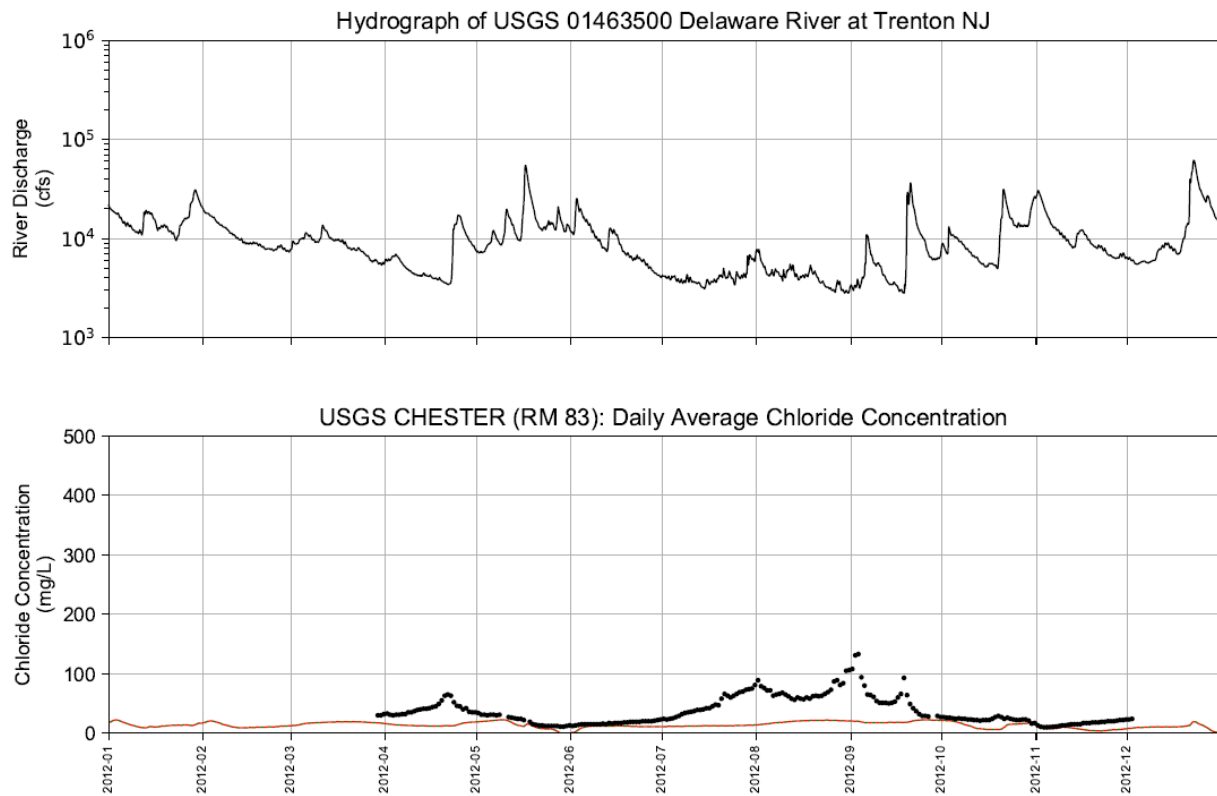
Notes: Chloride concentration data were derived from specific conductance based on USGS (1970s).
Station ID: USGS01467200, USGS BEN FRANKLIN BRIDGE (RM 100)
Run ID: EFDC_HYDRO_G72_2023-01-06

Figure R-4: Observed and Predicted Daily Average Chloride Concentration at USGS Station USGS BEN FRANKLIN BRIDGE (RM 100) for 2018 to 2019 Period



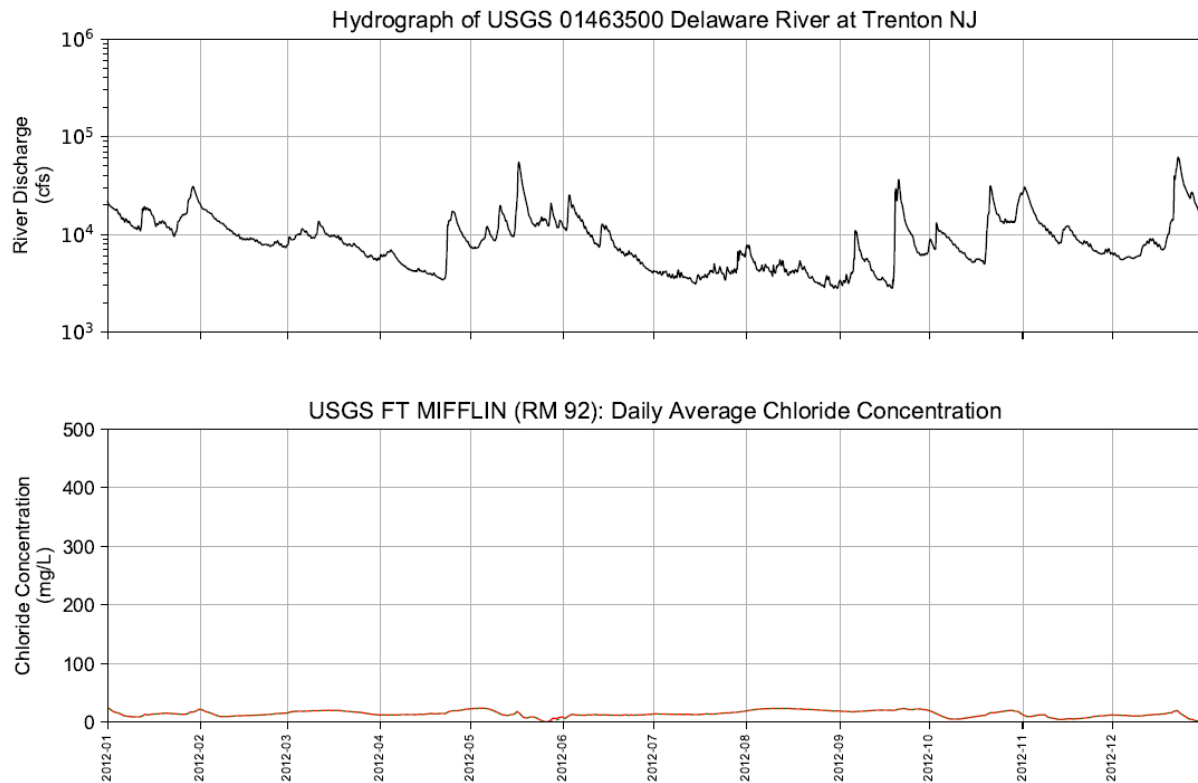
Notes: Chloride concentration data were derived from specific conductance based on USGS (1970s).
Station ID: USGS01482800, USGS REEDY ISLAND (RM 54.1)
Run ID: EFDC_HYDRO_G72_2023-01-06

Figure R-5: Observed and Predicted Daily Average Chloride Concentration at USGS Station USGS REEDY ISLAND (RM 54.1) for 2012 Period



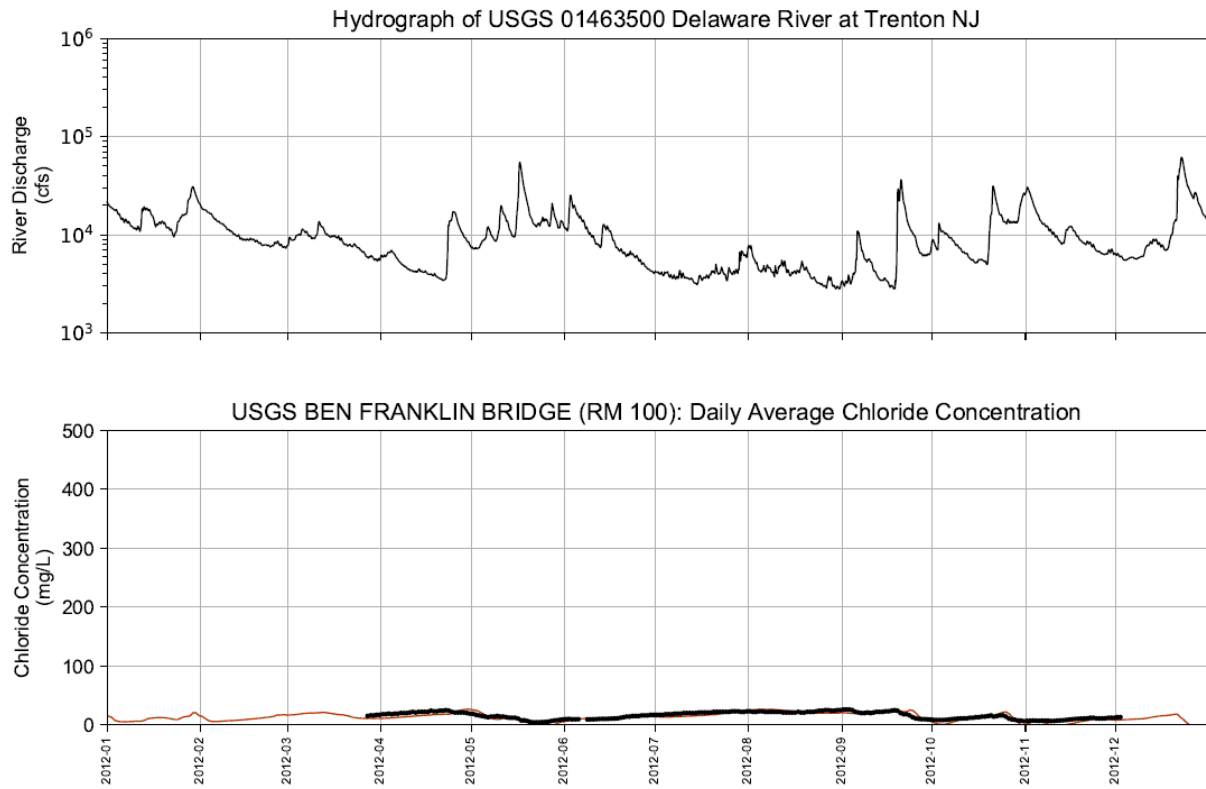
Notes: Chloride concentration data were derived from specific conductance based on USGS (1970s).
Station ID: USGS01477050, USGS CHESTER (RM 83.6)
Run ID: EFDC_HYDRO_G72_2023-01-06

Figure R-6: Observed and Predicted Daily Average Chloride Concentration at USGS Station USGS CHESTER (RM 83.6) for 2012 Period



Notes: Chloride concentration data were derived from specific conductance based on USGS (1970s).
Station ID: USGS01474703, USGS FT MIFFLIN (RM 91.9). No data for 2012 period.
Run ID: EFDC_HYDRO_G72_2023-01-06

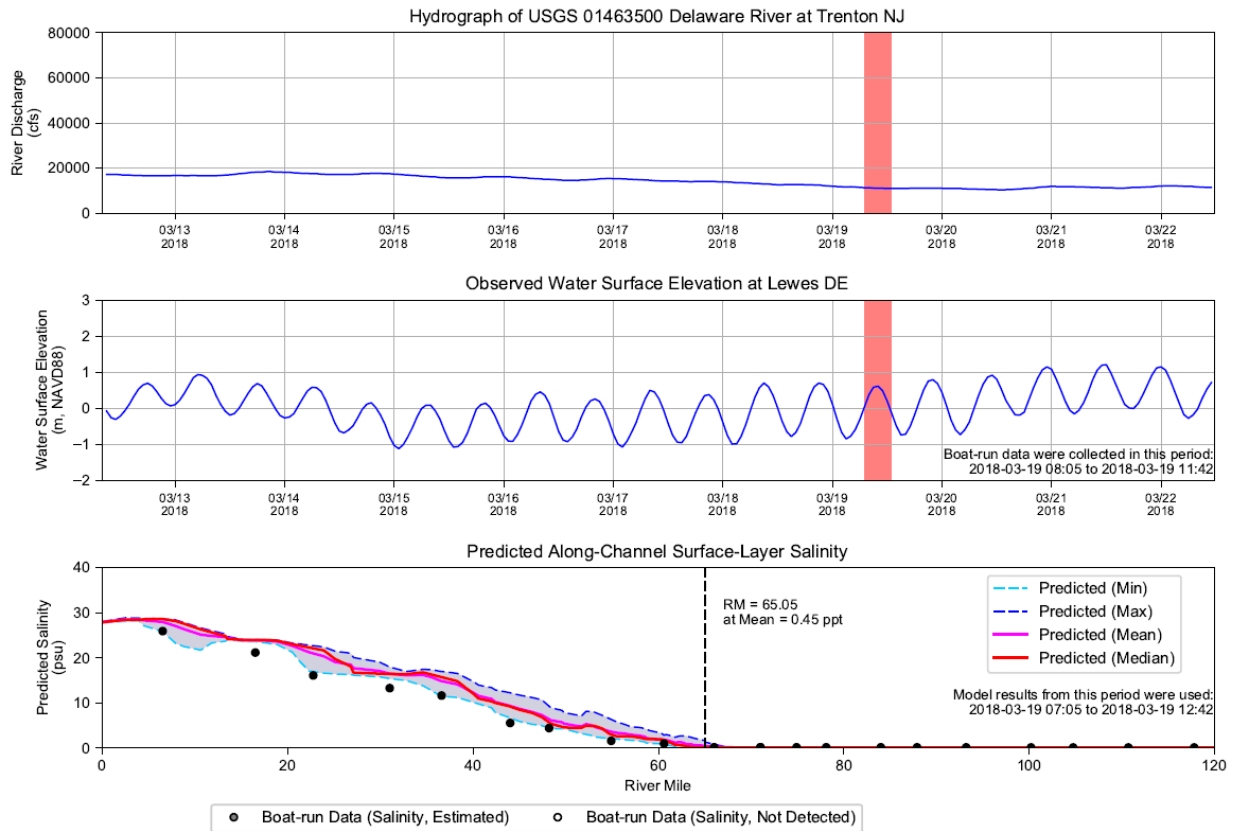
Figure R-7: Observed and Predicted Daily Average Chloride Concentration at USGS Station USGS FT MIFFLIN (RM 91.9)



Notes: Chloride concentration data were derived from specific conductance based on USGS (1970s).
Station ID: USGS01467200, USGS BEN FRANKLIN BRIDGE (RM 100)
Run ID: EFDC_HYDRO_G72_2023-01-06

Figure R-8: Observed and Predicted Daily Average Chloride Concentration at USGS Station USGS BEN FRANKLIN BRIDGE (RM 100) for 2012 Period

Appendix S: Longitudinal profile of salinity in Delaware River and Bay for 2018, 2019, and 2012

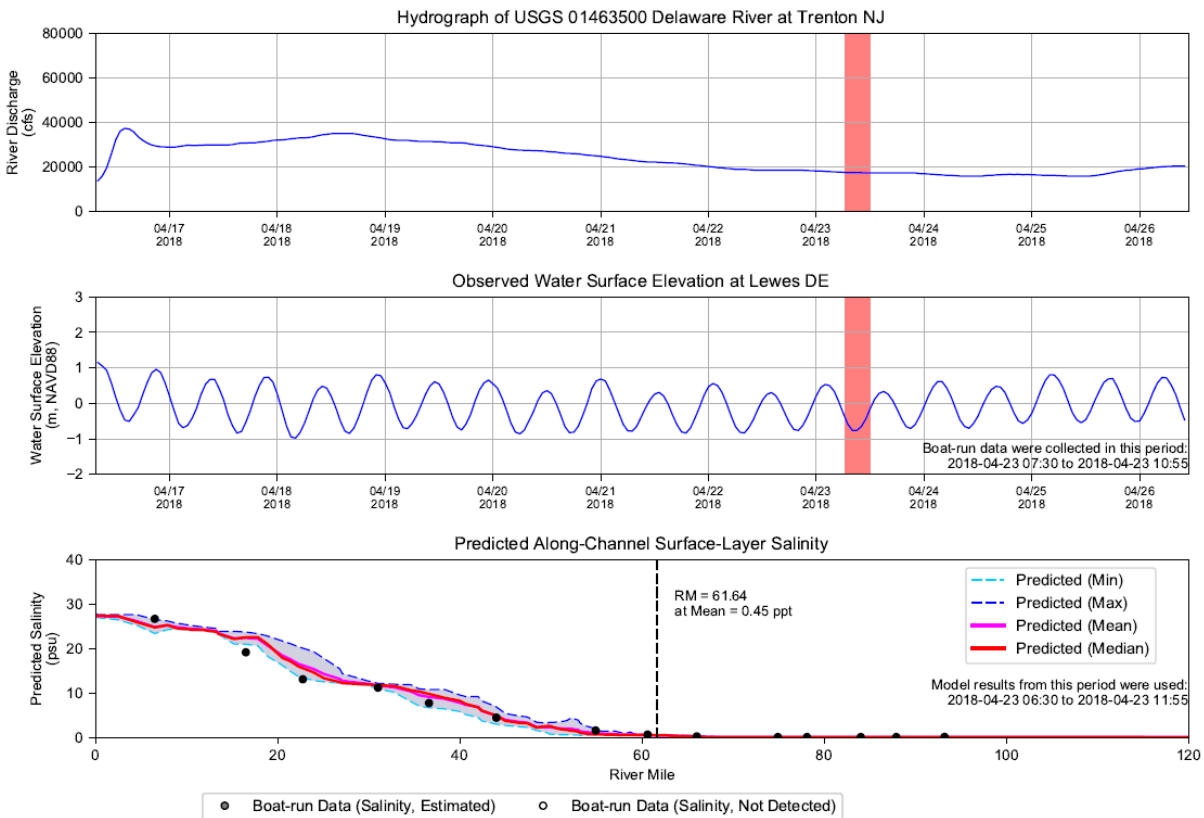


Notes:

Salinity and Chloride data collected by boat-run survey were used. Data that were measured to be under the detention limit were set to half of the detection limit. Red shaded areas indicate the boat-run survey period: 2018-03-19 08:05 to 2018-03-19 11:42. Model results along the navigation channel during the period of 2018-03-19 07:05 to 2018-03-19 12:42 were used in this analysis.

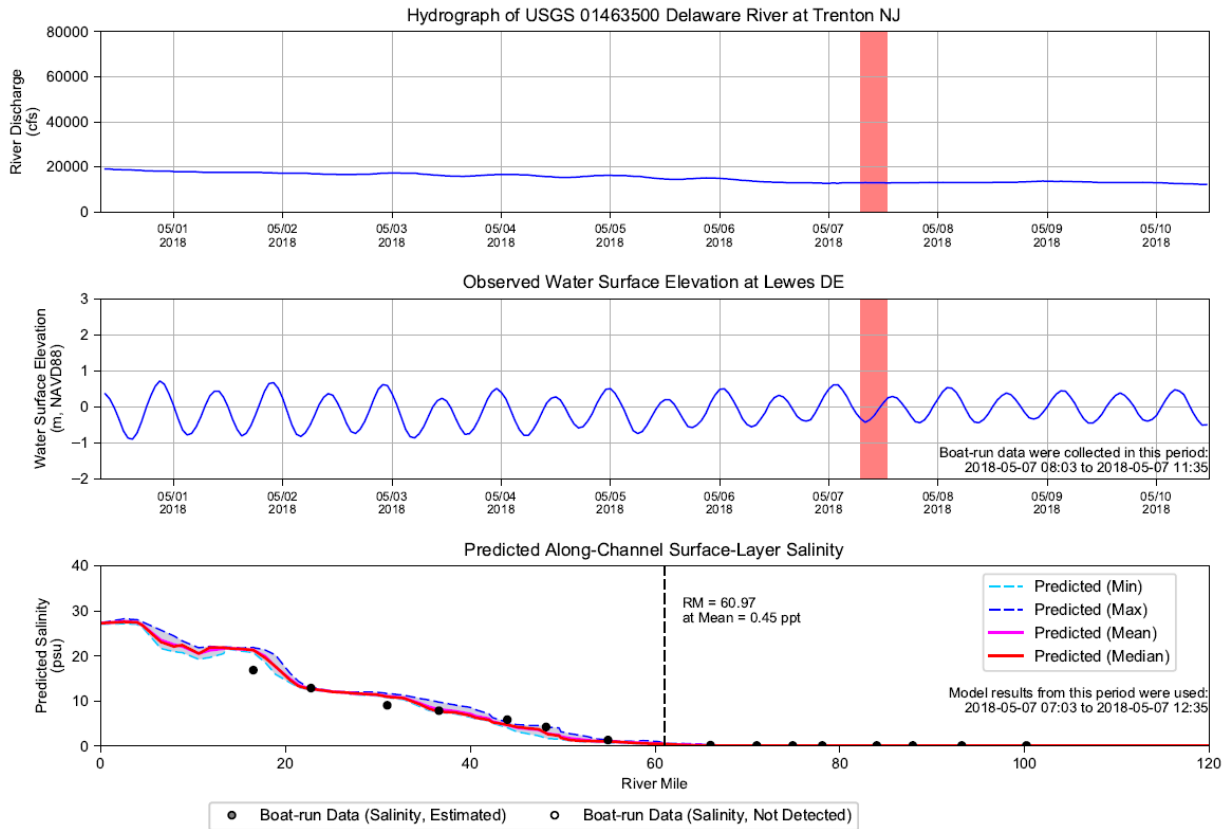
Run ID: EFDC_HYDRO_G72_2023-01-06

Figure S-1: Longitudinal Profile of Salinity in Delaware River and Bay. Survey period: 2018-03-19 08:05 to 2018-03-19 11:42.



Notes: Salinity and Chloride data collected by boat-run survey were used. Data that were measured to be under the detention limit were set to half of the detection limit. Red shaded areas indicate the boat-run survey period: 2018-04-23 07:30 to 2018-04-23 10:55. Model results along the navigation channel during the period of 2018-04-23 06:30 to 2018-04-23 11:55 were used in this analysis.
Run ID: EFDC_HYDRO_G72_2023-01-06

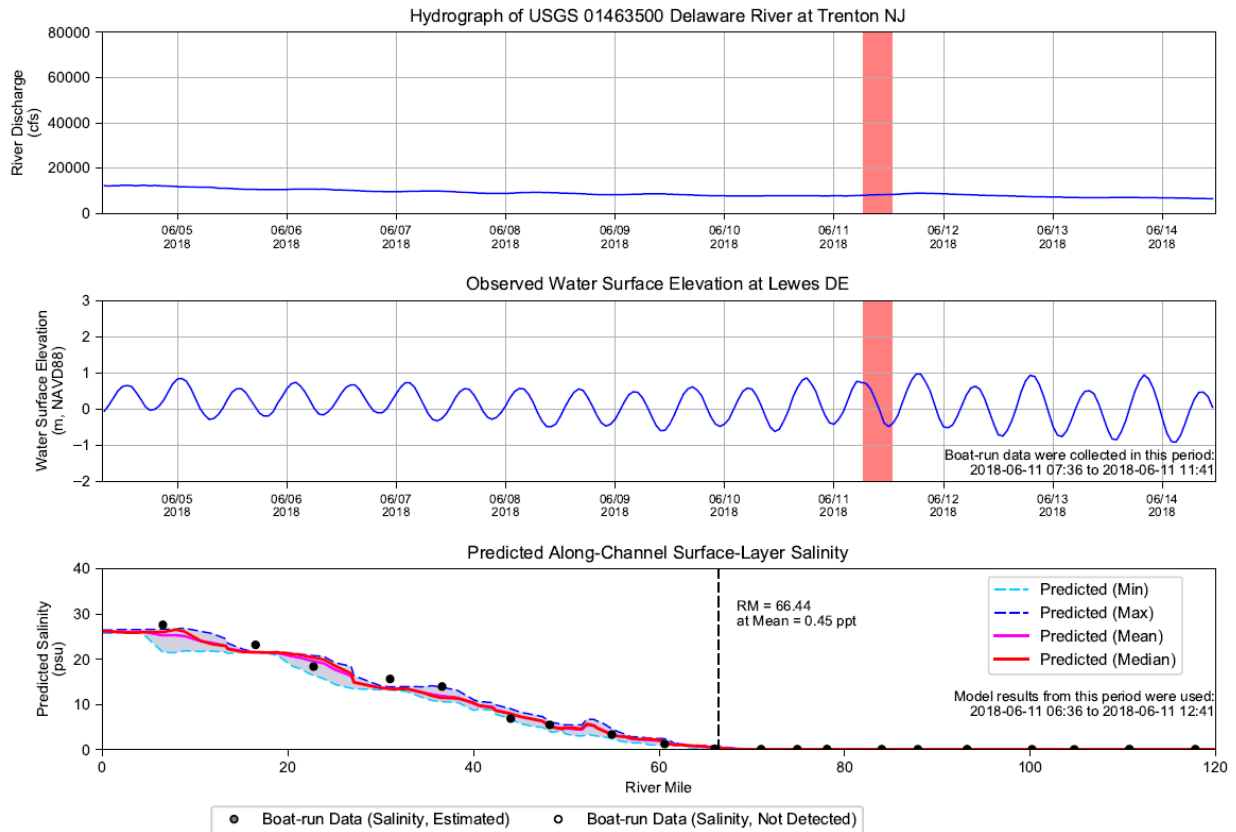
Figure S-2: Longitudinal Profile of Salinity in Delaware River and Bay. Survey period: 2018-04-23 07:30 to 2018-04-23 10:55.



Notes: Salinity and Chloride data collected by boat-run survey were used. Data that were measured to be under the detention limit were set to half of the detection limit. Red shaded areas indicate the boat-run survey period: 2018-05-07 08:03 to 2018-05-07 11:35. Model results along the navigation channel during the period of 2018-05-07 07:03 to 2018-05-07 12:35 were used in this analysis.

Run ID: EFDC_HYDRO_G72_2023-01-06

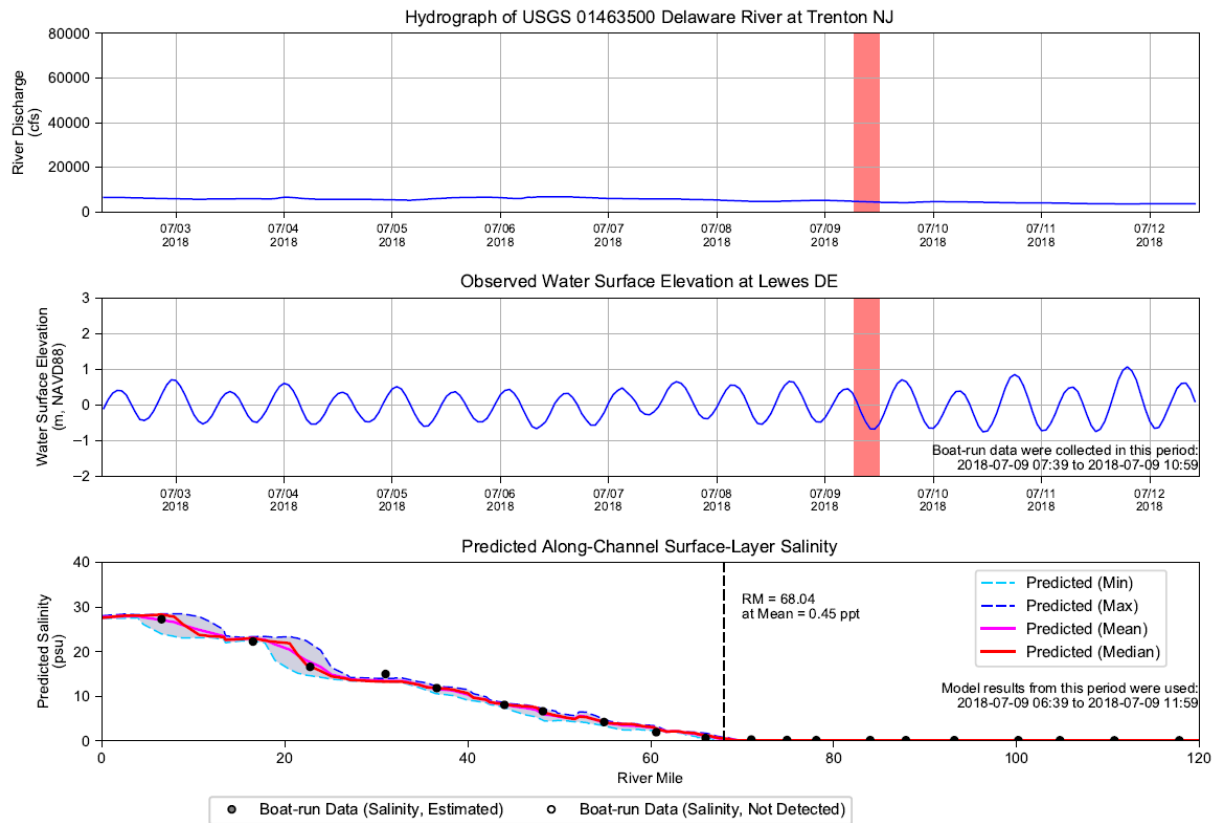
Figure S-3: Longitudinal Profile of Salinity in Delaware River and Bay. Survey period: 2018-05-07 08:03 to 2018-05-07 11:35.



Notes: Salinity and Chloride data collected by boat-run survey were used. Data that were measured to be under the detention limit were set to half of the detection limit. Red shaded areas indicate the boat-run survey period: 2018-06-11 07:36 to 2018-06-11 11:41. Model results along the navigation channel during period of 2018-06-11 06:36 to 2018-06-11 12:41 were used in this analysis.

Run ID: EFDC_HYDRO_G72_2023-01-06

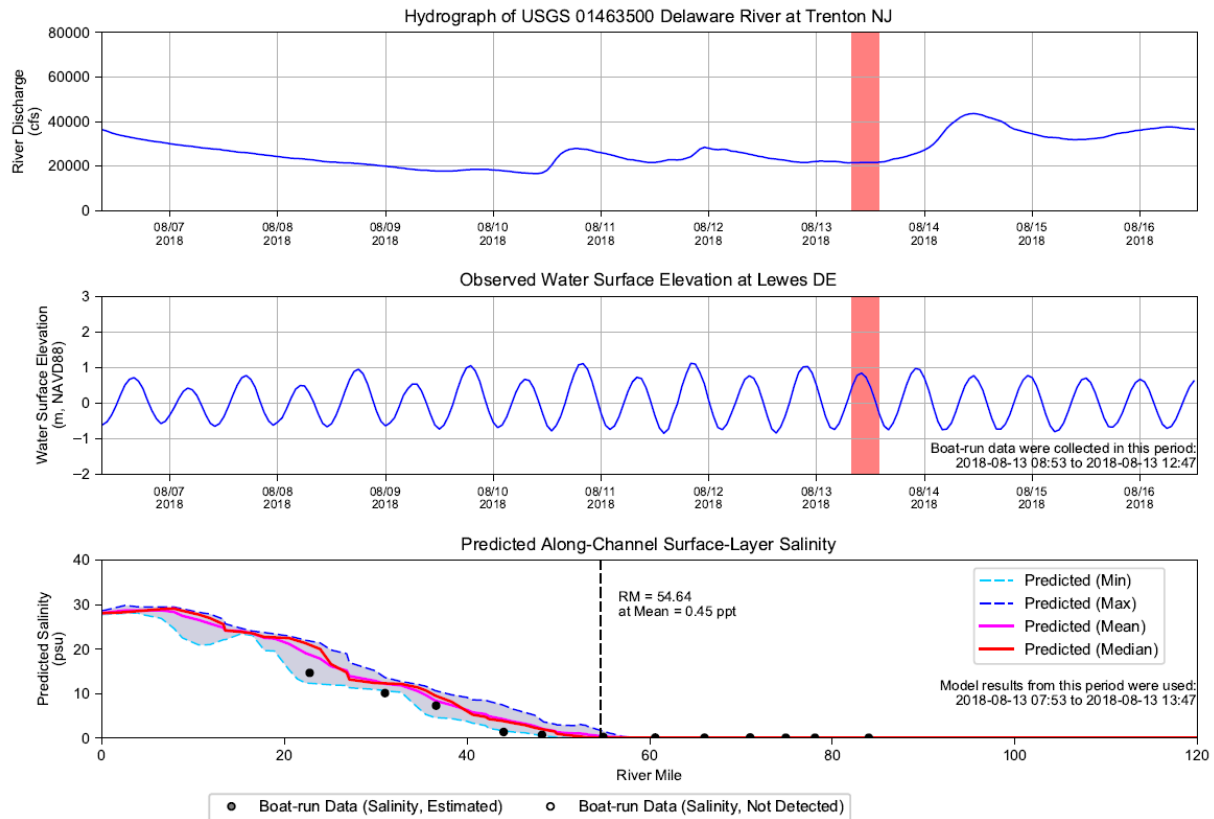
Figure S-4: Longitudinal Profile of Salinity in Delaware River and Bay. Survey period: 2018-06-11 07:36 to 2018-06-11 11:41.



Notes: Salinity and Chloride data collected by boat-run survey were used. Data that were measured to be under the detention limit were set to half of the detection limit. Red shaded areas indicate the boat-run survey period: 2018-07-09 07:39 to 2018-07-09 10:59. Model results along the navigation channel during period of 2018-07-09 06:39 to 2018-07-09 11:59 were used in this analysis.

Run ID: EFDC_HYDRO_G72_2023-01-06

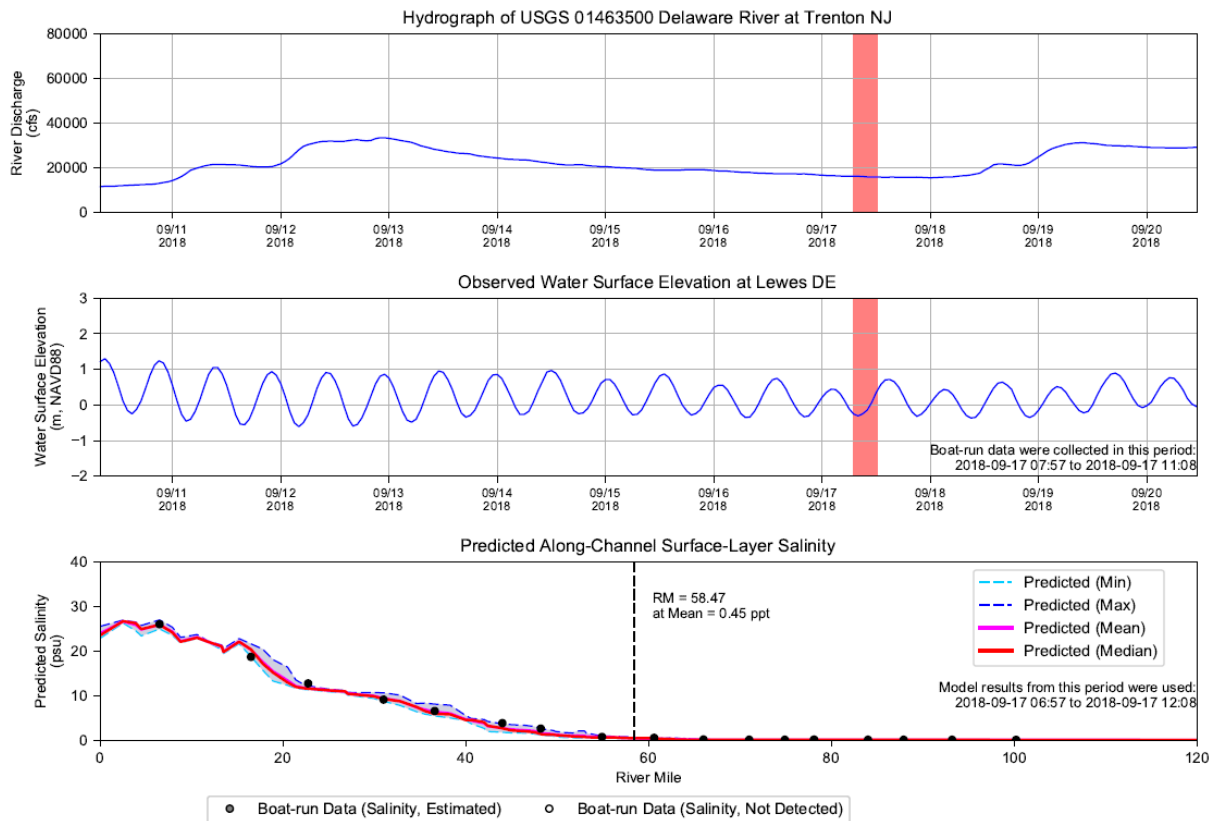
Figure S-5: Longitudinal Profile of Salinity in Delaware River and Bay. Survey period: 2018-07-09 07:39 to 2018-07-09 10:59.



Notes: Salinity and Chloride data collected by boat-run survey were used. Data that were measured to be under the detention limit were set to half of the detection limit. Red shaded areas indicate the boat-run survey period: 2018-08-13 08:53 to 2018-08-13 12:47. Model results along the navigation channel during period of 2018-08-13 07:53 to 2018-08-13 13:47 were used in this analysis.

Run ID: EFDC_HYDRO_G72_2023-01-06

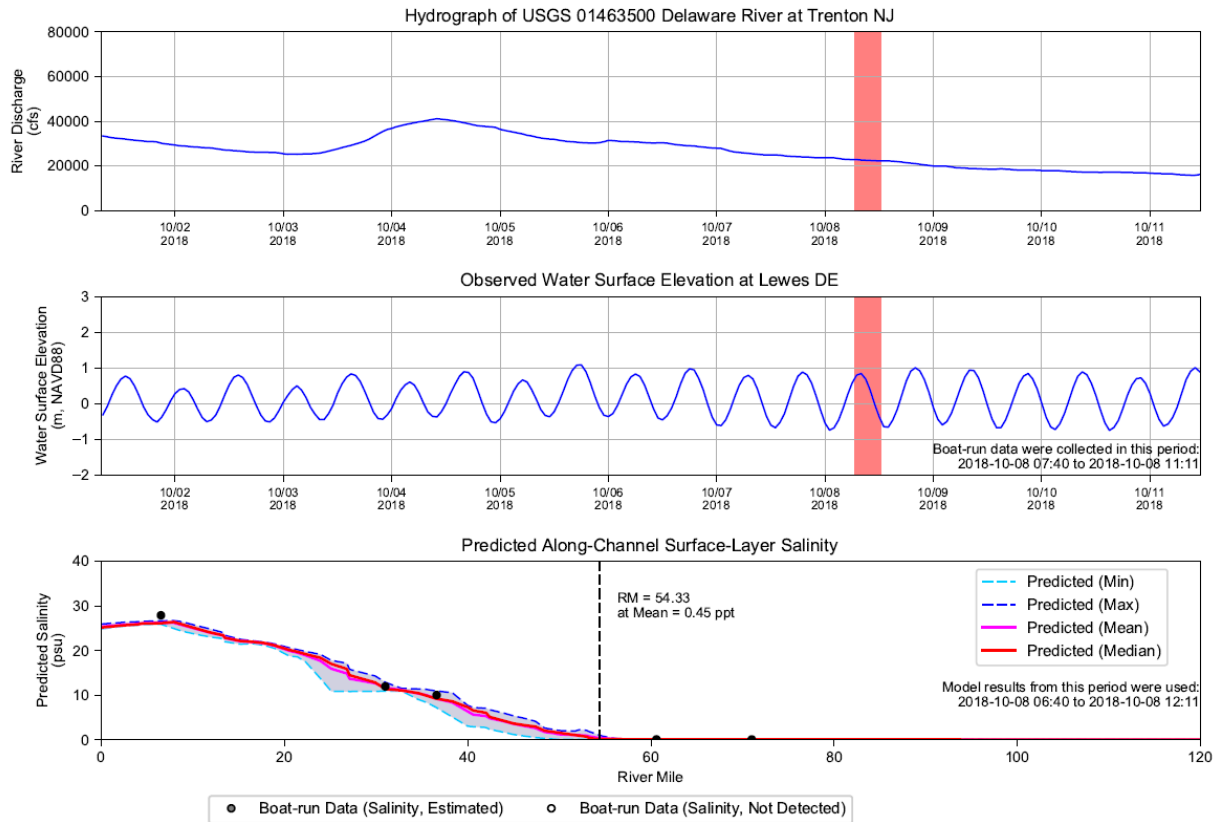
Figure S-6: Longitudinal Profile of Salinity in Delaware River and Bay. Survey period: 2018-08-13 08:53 to 2018-08-13 12:47.



Notes: Salinity and Chloride data collected by boat-run survey were used. Data that measured to be under the detention limit were set to half of the detection limit. Red shaded areas indicate the boat-run survey period: 2018-09-17 07:57 to 2018-09-17 11:08. Model results along the navigation channel during period of 2018-09-17 06:57 to 2018-09-17 12:08 were used in this analysis.

Run ID: EFDC_HYDRO_G72_2023-01-06

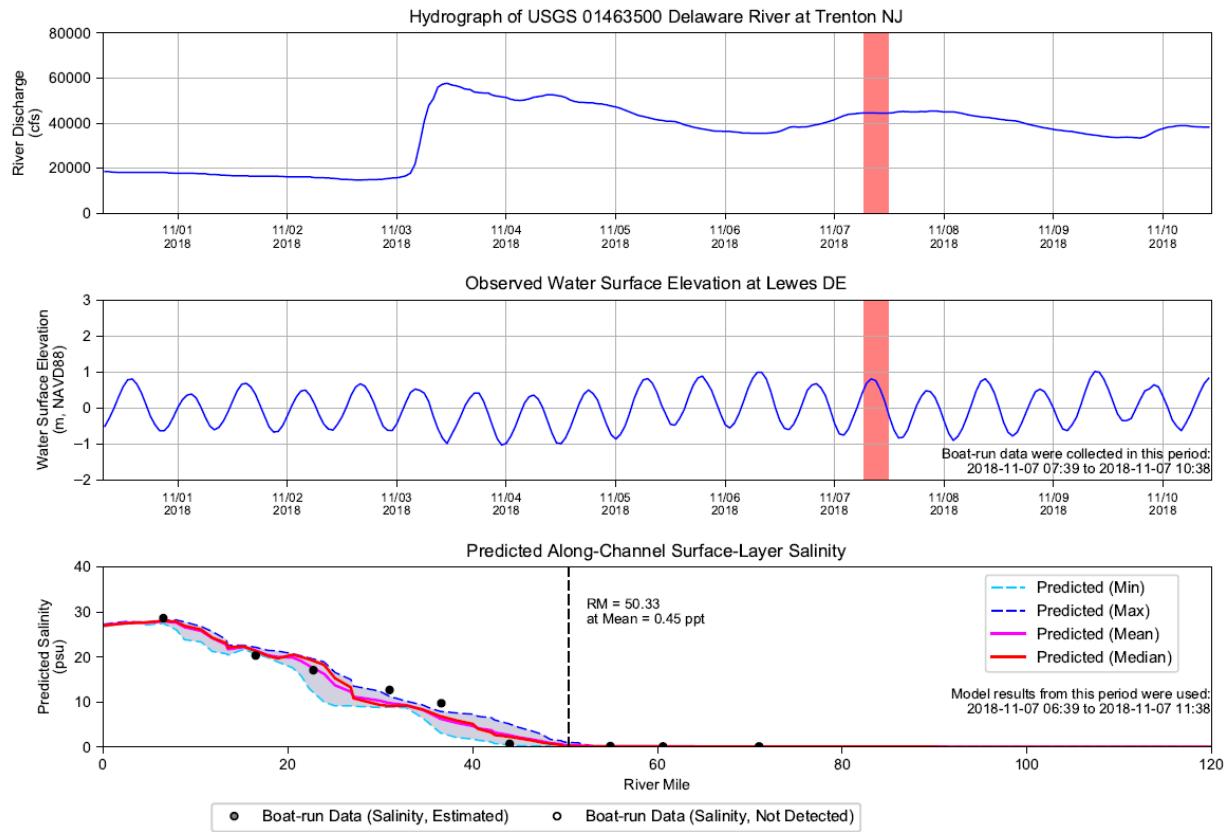
Figure S-7: Longitudinal Profile of Salinity in Delaware River and Bay. Survey period: 2018-09-17 07:57 to 2018-09-17 11:08.



Notes: Salinity and Chloride data collected by boat-run survey were used. Data that were measured to be under the detection limit were set to half of the detection limit. Red shaded area indicates the boat run survey period: 2018-10-08 07:40 to 2018-10-08 11:11. Model results along the navigation channel during period of 2018-10-08 06:40 to 2018-10-08 12:11 were used in this analysis.

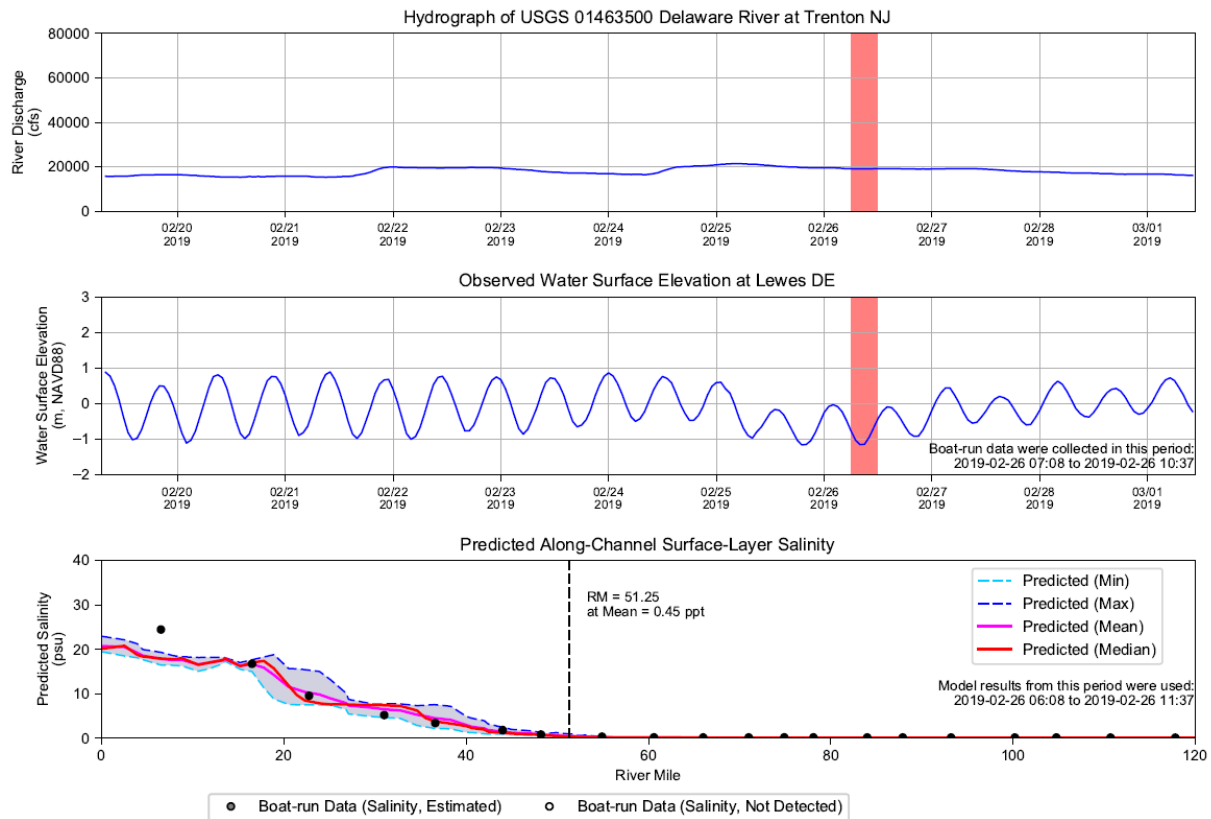
Run ID: EFDC_HYDRO_G72_2023-01-06

Figure S-8: Longitudinal Profile of Salinity in Delaware River and Bay. Survey period: 2018-10-08 07:40 to 2018-10-08 11:11.



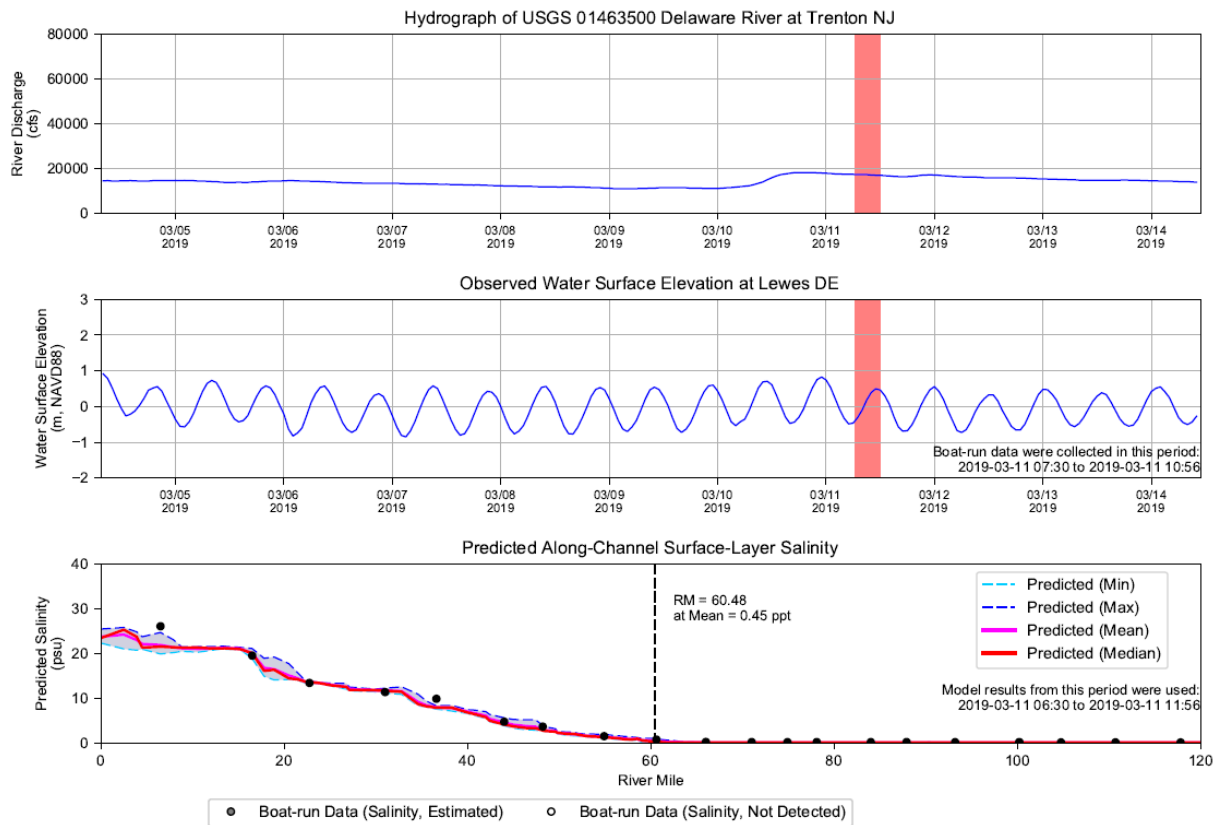
Notes: Salinity and Chloride data collected by boat-run survey were used. Data that were measured to be under the detention limit were set to half of the detection limit. Red shaded areas indicate the boat-run survey period: 2018-11-07 07:39 to 2018-11-07 10:38. Model results along the navigation channel during period of 2018-11-07 06:39 to 2018-11-07 11:38 were used in this analysis
Run ID: EFDC_HYDRO_G72_2023-01-06

Figure S-9: Longitudinal Profile of Salinity in Delaware River and Bay. Survey period: 2018-11-07 07:39 to 2018-11-07 10:38.



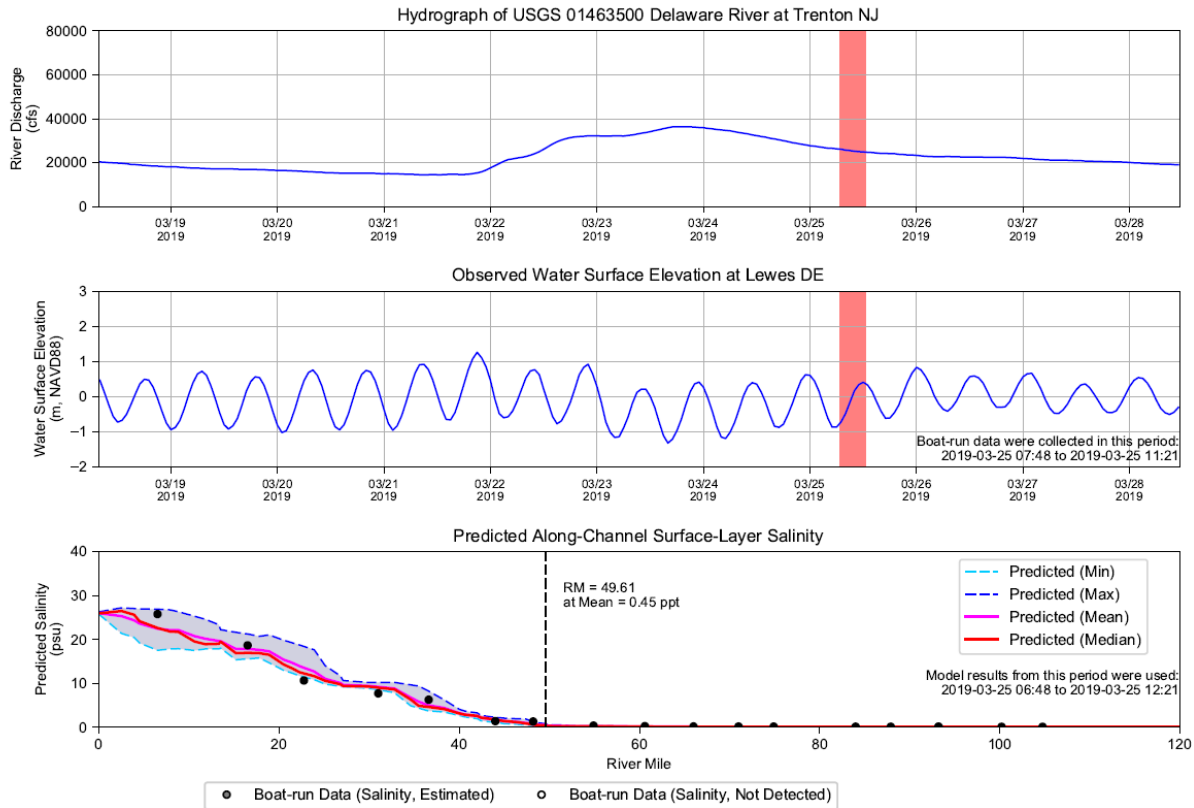
Notes: Salinity and Chloride data collected by boat-run survey were used. Data that were measured to be under the detention limit were set to half of the detection limit. Red shaded areas indicate the boat run survey period: 2019-02-26 07:08 to 2019-02-26 10:37. Model results along the navigation channel during period of 2019-02-26 06:08 to 2019-02-26 11:37 were used in this analysis
Run ID: EFDC_HYDRO_G72_2023-01-06

Figure S-10: Longitudinal Profile of Salinity in Delaware River and Bay. Survey period: 2019-02-26 07:08 to 2019-02-26 10:37.



Notes: Salinity and Chloride data collected by boat-run survey were used. Data that were measured to be under the detention limit were set to half of the detection limit. Red shaded areas indicate the boat-run survey period: 2019-03-11 07:30 to 2019-03-11 10:56. Model results along the navigation channel during period of 2019-03-11 06:30 to 2019-03-11 11:56 were used in this analysis.
Run ID: EFDC_HYDRO_G72_2023-01-06

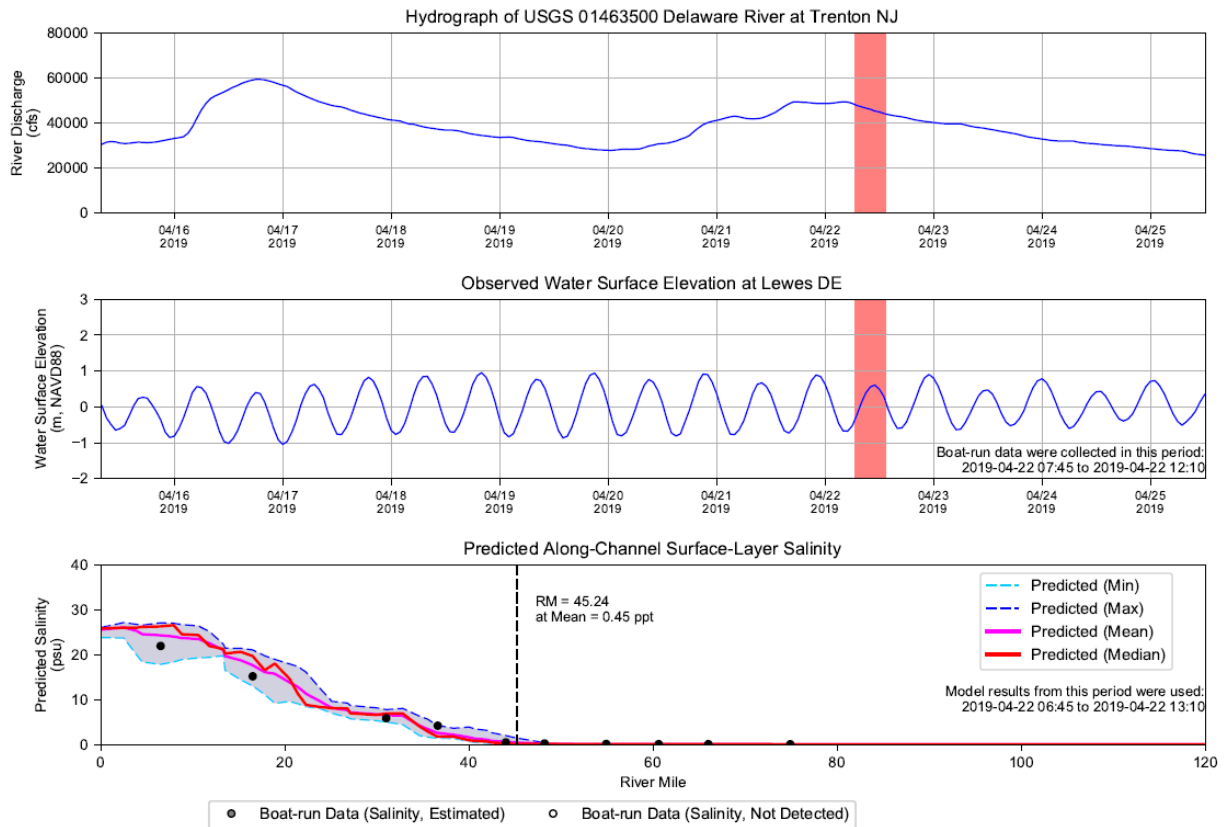
Figure S-11: Longitudinal Profile of Salinity in Delaware River and Bay. Survey period: 2019-03-11 07:30 to 2019-03-11 10:56.



Notes: Salinity and Chloride data collected by boat-run survey were used. Data that were measured to be under the detention limit were set to half of the detection limit. Red shaded areas indicate the boat-run survey period: 2019-03-25 07:48 to 2019-03-25 11:21. Model results along the navigation channel during period of 2019-03-25 06:48 to 2019-03-25 12:21 were used in this analysis

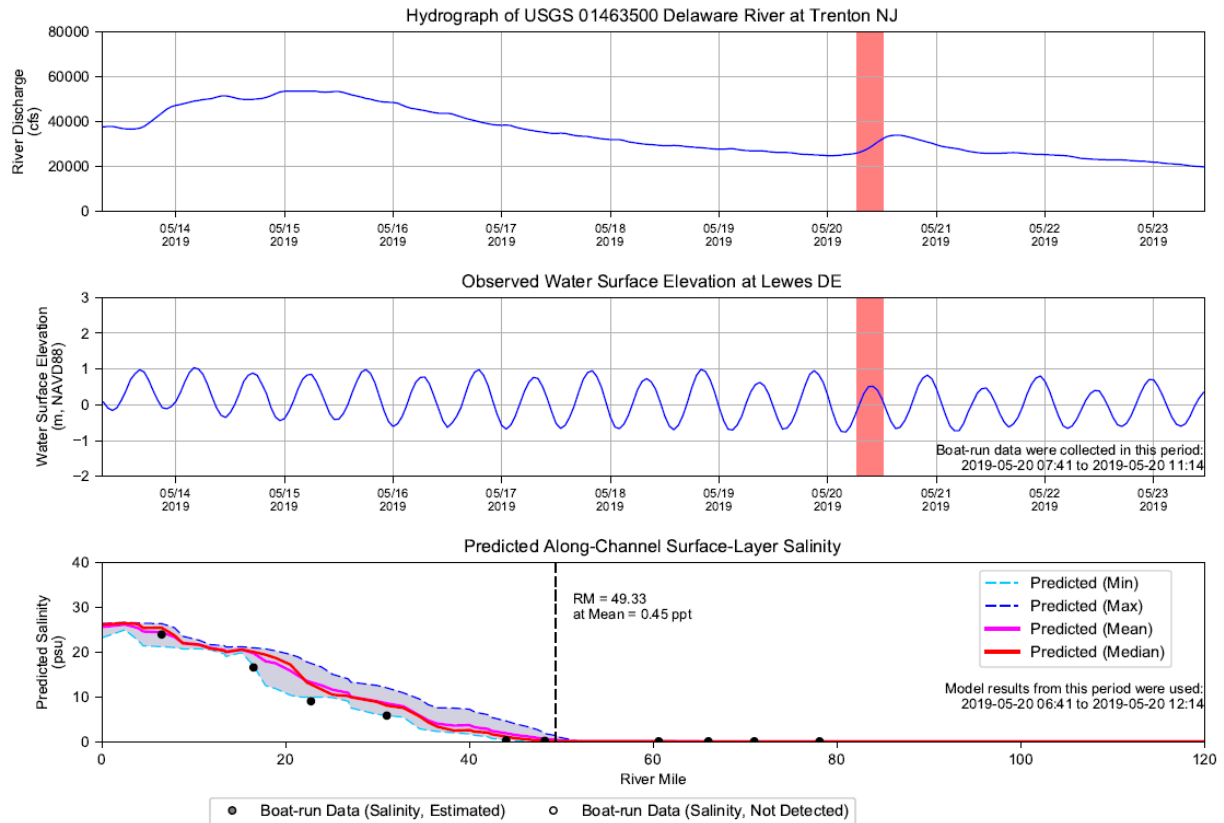
Run ID: EFDC_HYDRO_G72_2023-01-06

Figure S-12: Longitudinal Profile of Salinity in Delaware River and Bay. Survey period: 2019-03-25 07:48 to 2019-03-25 11:21.



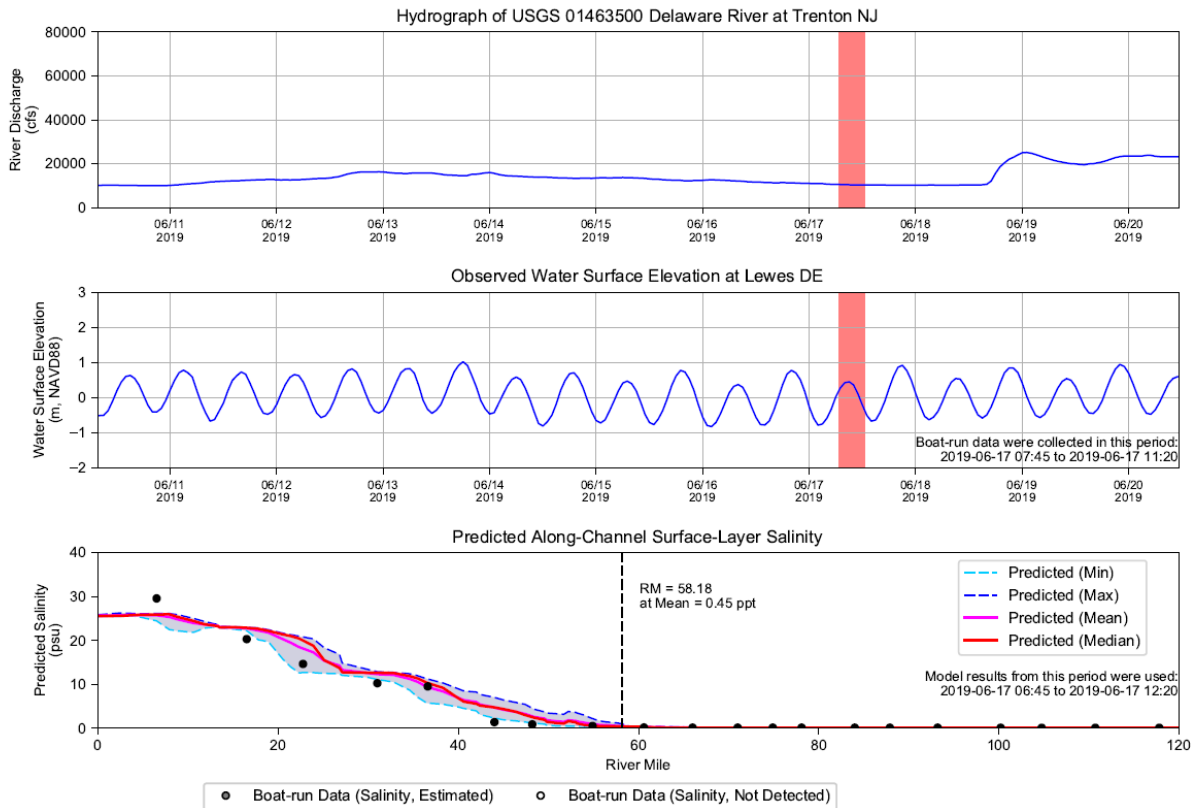
Notes: Salinity and Chloride data collected by boat-run survey were used. Data that were measured to be under the detention limit were set to half of the detection limit. Red shaded areas indicate the boat-run survey period: 2019-04-22 07:45 to 2019-04-22 12:10. Model results along the navigation channel during period of 2019-04-22 06:45 to 2019-04-22 13:10 were used in this analysis
Run ID: EFDC_HYDRO_G72_2023-01-06

Figure S-13: Longitudinal Profile of Salinity in Delaware River and Bay. Survey period: 2019-04-22 07:45 to 2019-04-22 12:10.



Notes: Salinity and Chloride data collected by boat-run survey were used. Data that were measured to be under the detention limit were set to half of the detection limit. Red shaded areas indicate the boat-run survey period: 2019-05-20 07:41 to 2019-05-20 11:14. Model results along the navigation channel during period of 2019-05-20 06:41 to 2019-05-20 12:14 were used in this analysis
Run ID: EFDC_HYDRO_G72_2023-01-06

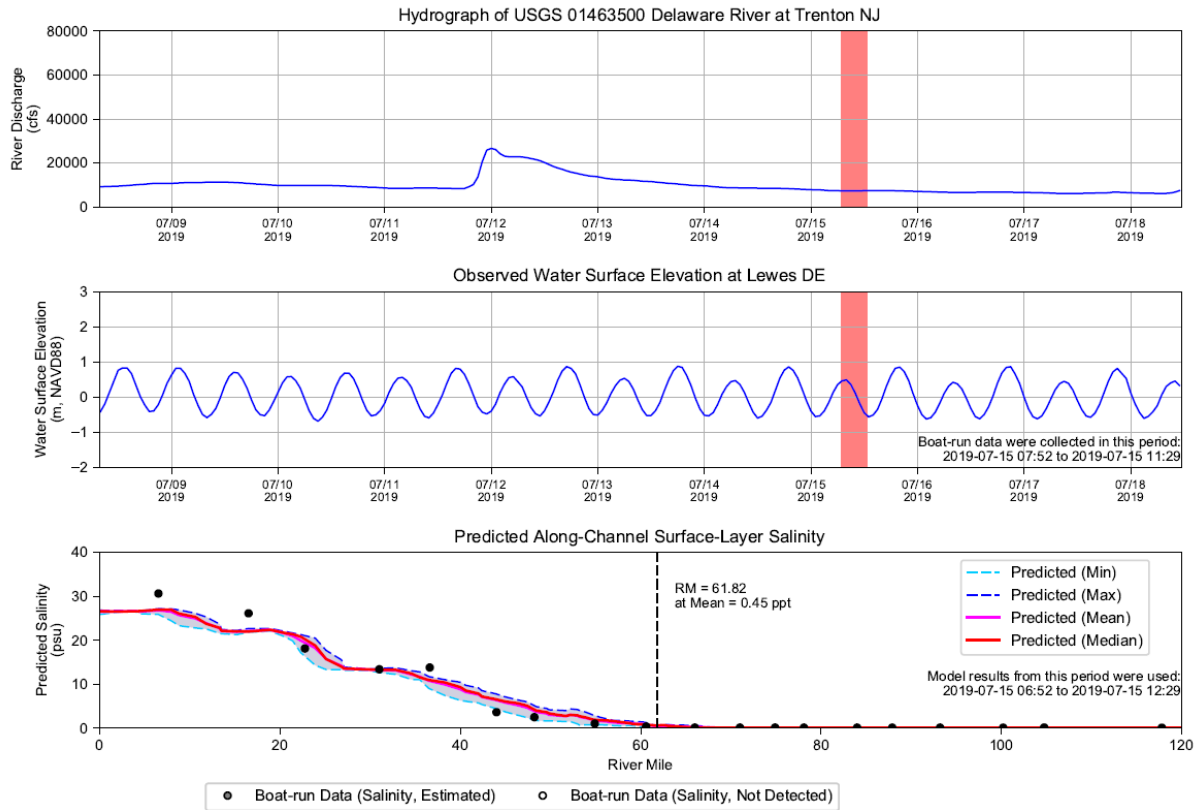
Figure S-14: Longitudinal Profile of Salinity in Delaware River and Bay. Survey period: 2019-05-20 07:41 to 2019-05-20 11:14.



Notes: Salinity and Chloride data collected by boat-run survey were used. Data that were measured to be under the detention limit were set to half of the detection limit. Red shaded areas indicate the boat-run survey period: 2019-06-17 07:45 to 2019-06-17 11:20. Model results along the navigation channel during period of 2019-06-17 06:45 to 2019-06-17 12:20 were used in this analysis

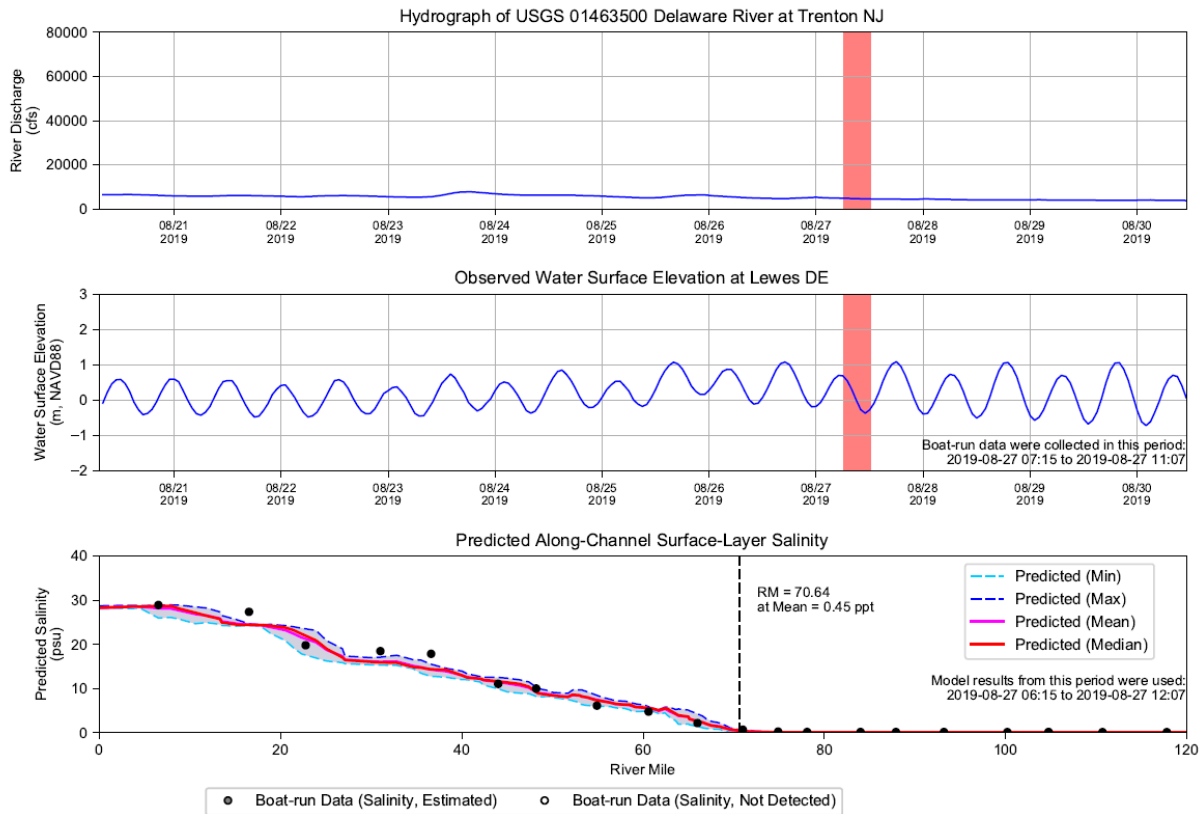
Run ID: EFDC_HYDRO_G72_2023-01-06

Figure S-15: Longitudinal Profile of Salinity in Delaware River and Bay. Survey period: 2019-06-17 07:45 to 2019-06-17 11:20.



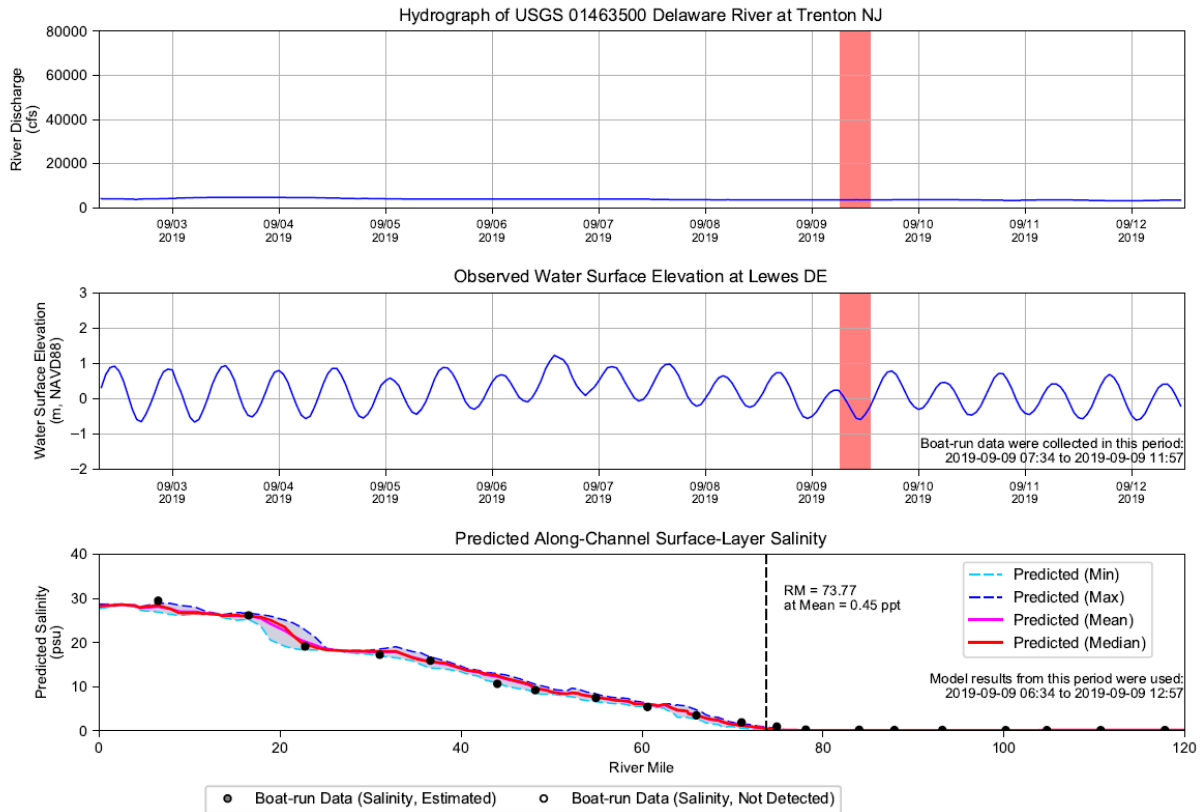
Notes: Salinity and Chloride data collected by boat-run survey were used. Data that were measured to be under the detention limit were set to half of the detection limit. Red shaded areas indicate the boat run survey period: 2019-07-15 07:52 to 2019-07-15 11:29. Model results along the navigation channel during period of 2019-07-15 06:52 to 2019-07-15 12:29 were used in this analysis
Run ID: EFDC_HYDRO_G72_2023-01-06

Figure S-16: Longitudinal Profile of Salinity in Delaware River and Bay. Survey period: 2019-07-15 07:52 to 2019-07-15 11:29.



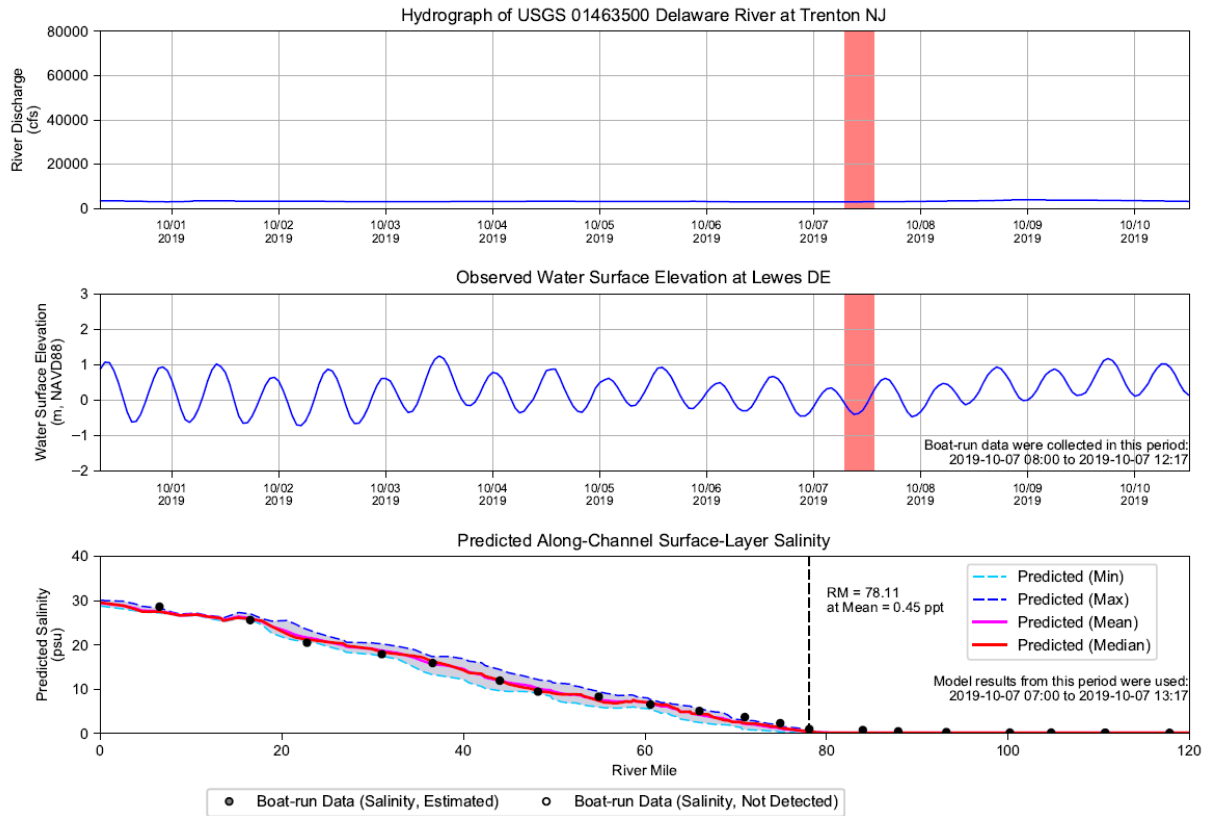
Notes: Salinity and Chloride data collected by boat-run survey were used. Data that were measured to be under the detention limit were set to half of the detection limit. Red shaded areas indicate the boat-run survey period: 2019-08-27 07:15 to 2019-08-27 11:07. Model results along the navigation channel during period of 2019-08-27 06:15 to 2019-08-27 12:07 were used in this analysis
 Run ID: EFDC_HYDRO_G72_2023-01-06

Figure S-17: Longitudinal Profile of Salinity in Delaware River and Bay. Survey period: 2019-08-27 07:15 to 2019-08-27 11:07.



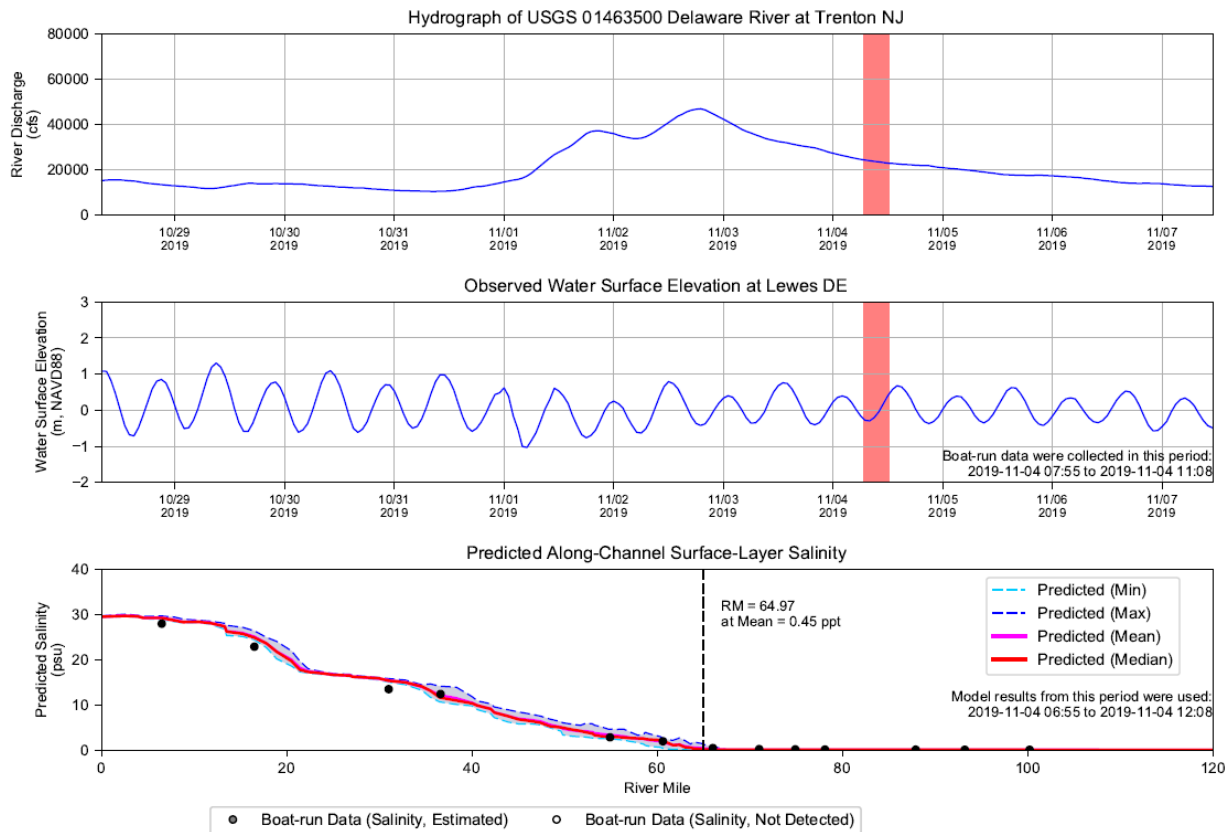
Notes: Salinity and Chloride data collected by boat-run survey were used. Data that were measured to be under the detention limit were set to half of the detection limit. Red shaded areas indicate the boat-run survey period: 2019-09-09 07:34 to 2019-09-09 11:57. Model results along the navigation channel during period of 2019-09-09 06:34 to 2019-09-09 12:57 were used in this analysis
Run ID: EFDC_HYDRO_G72_2023-01-06

Figure S-18: Longitudinal Profile of Salinity in Delaware River and Bay. Survey period: 2019-09-09 07:34 to 2019-09-09 11:57.



Notes: Salinity and Chloride data collected by boat-run survey were used. Data that were measured to be under the detention limit were set to half of the detection limit. Red shaded areas indicate the boat-run survey period: 2019-10-07 08:00 to 2019-10-07 12:17. Model results along the navigation channel during period of 2019-10-07 07:00 to 2019-10-07 13:17 were used in this analysis
Run ID: EFDC_HYDRO_G72_2023-01-06

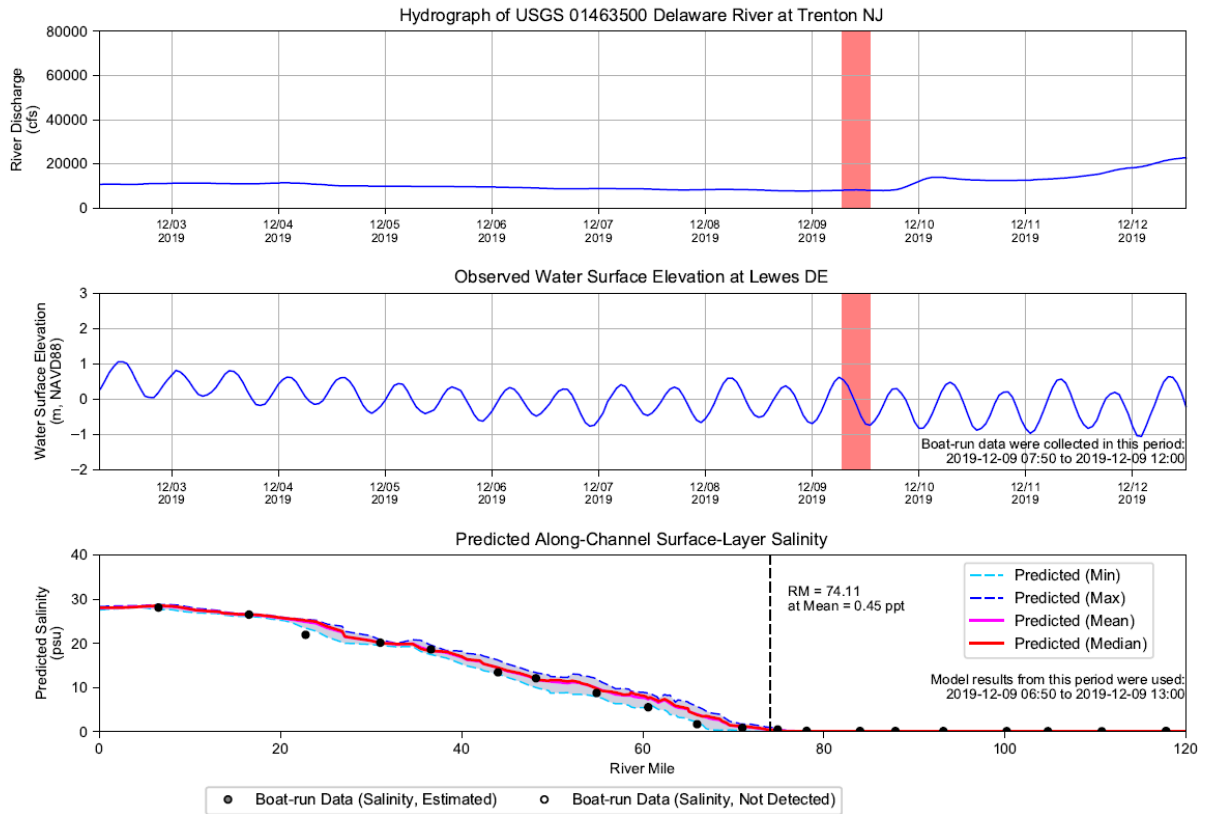
Figure S-19: Longitudinal Profile of Salinity in Delaware River and Bay. Survey period: 2019-10-07 08:00 to 2019-10-07 12:17.



Notes: Salinity and Chloride data collected by boat-run survey were used. Data that were measured to be under the detention limit were set to half of the detection limit. Red shaded areas indicate the boat-run survey period: 2019-11-04 07:55 to 2019-11-04 11:08. Model results along the navigation channel during period of 2019-11-04 06:55 to 2019-11-04 12:08 were used in this analysis

Run ID: EFDC_HYDRO_G72_2023-01-06

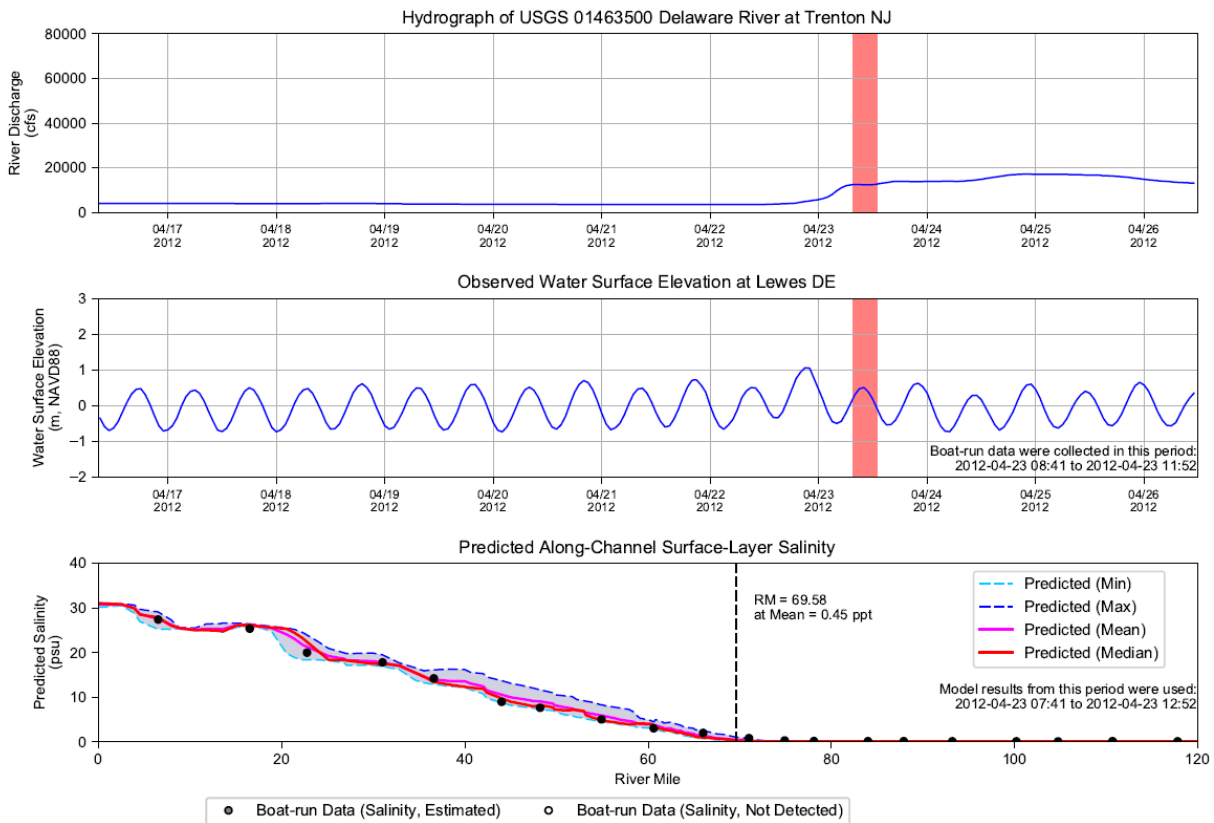
Figure S-20: Longitudinal Profile of Salinity in Delaware River and Bay. Survey period: 2019-11-04 07:55 to 2019-11-04 11:08.



Notes: Salinity and Chloride data collected by boat-run survey were used. Data that were measured to be under the detention limit were set to half of the detection limit. Red shaded areas indicate the boat-run survey period: 2019-12-09 07:50 to 2019-12-09 12:00. Model results along the navigation channel during period of 2019-12-09 06:50 to 2019-12-09 13:00 were used in this analysis.

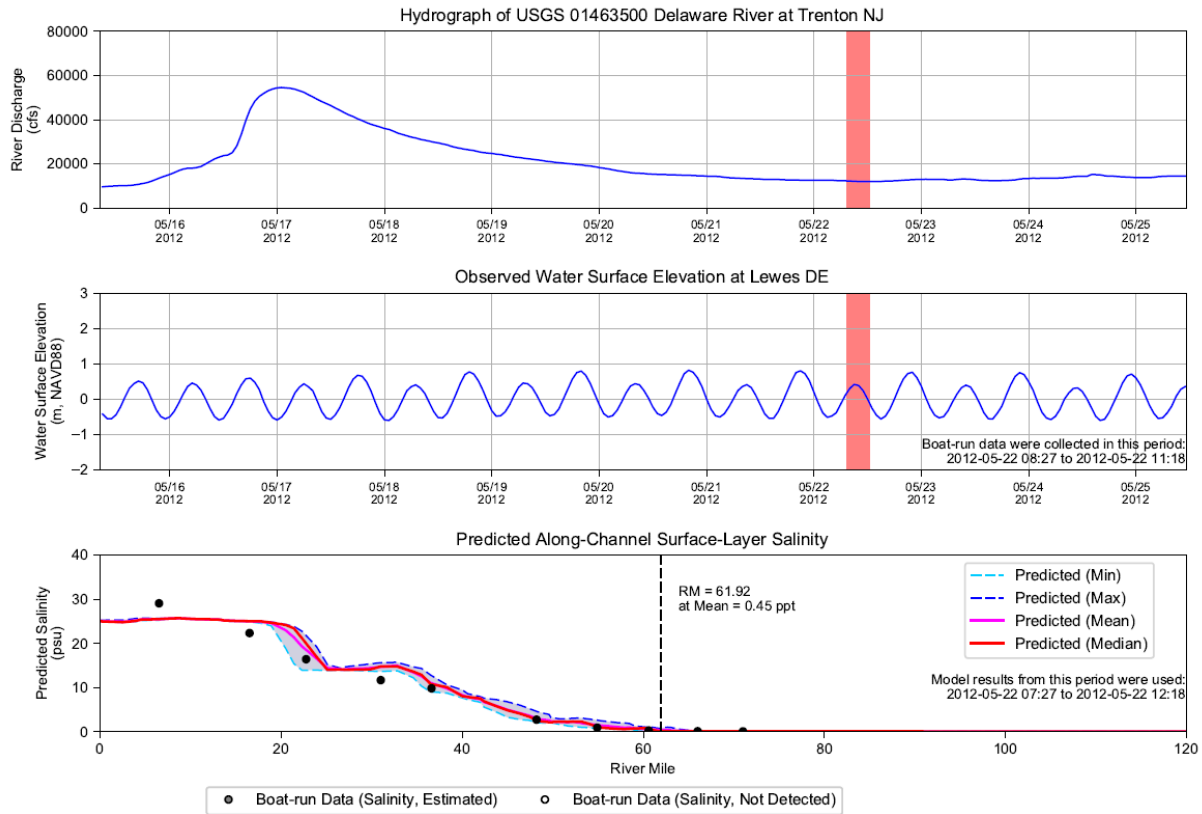
Run ID: EFDC_HYDRO_G72_2023-01-06

Figure S-21: Longitudinal Profile of Salinity in Delaware River and Bay. Survey period: 2019-12-09 07:50 to 2019-12-09 12:00.



Notes: Salinity and Chloride data collected by boat-run survey were used. Data that were measured to be under the detention limit were set to half of the detection limit. Red shaded areas indicate the boat-run survey period: 2012-04-23 08:41 to 2012-04-23 11:52. Model results along the navigation channel during period of 2012-04-23 07:41 to 2012-04-23 12:52 were used in this analysis
Run ID: EFDC_HYDRO_G72_2023-01-06

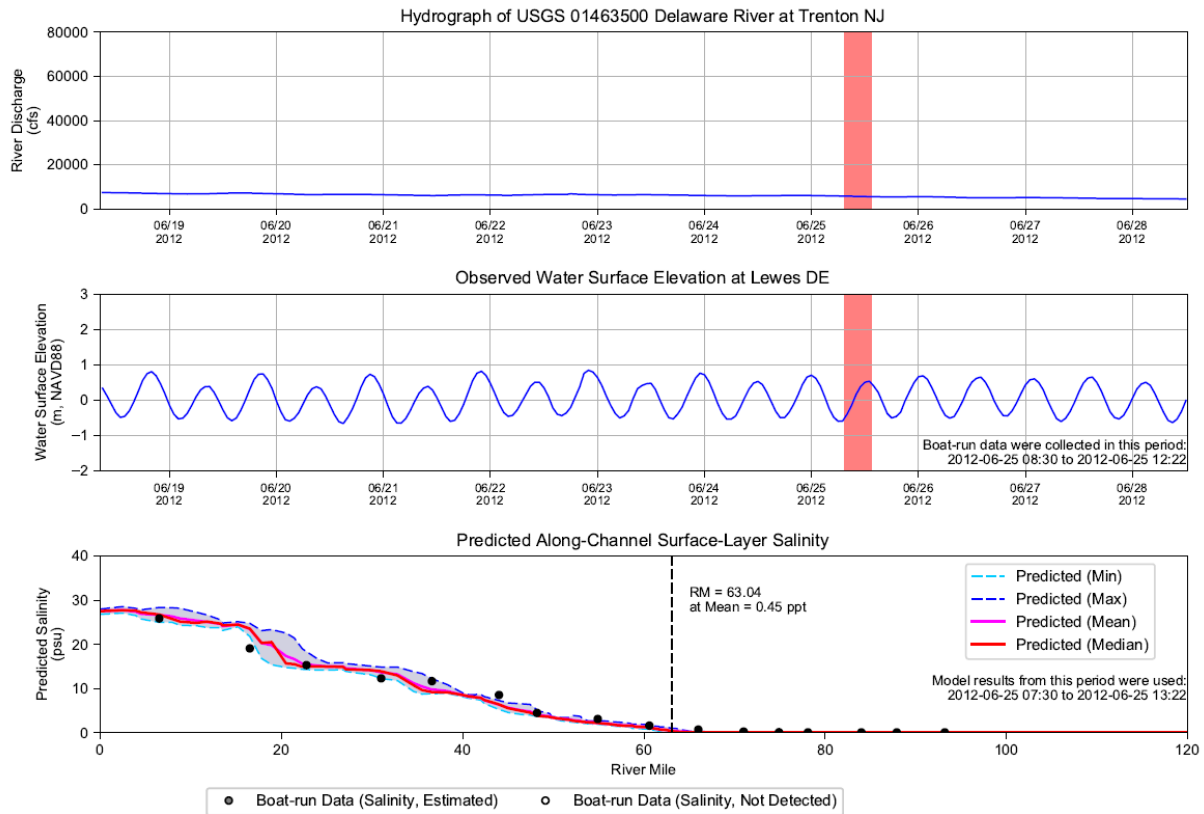
Figure S-22: Longitudinal Profile of Salinity in Delaware River and Bay. Survey period: 2012-04-23 08:41 to 2012-04-23 11:52.



Notes: Salinity and Chloride data collected by boat-run survey were used. Data that were measured to be under the detention limit were set to half of the detection limit. Red shaded areas indicate the boat-run survey period: 2012-05-22 08:27 to 2012-05-22 11:18. Model results along the navigation channel during period of 2012-05-22 07:27 to 2012-05-22 12:18 were used in this analysis.

Run ID: EFDC_HYDRO_G72_2023-01-06

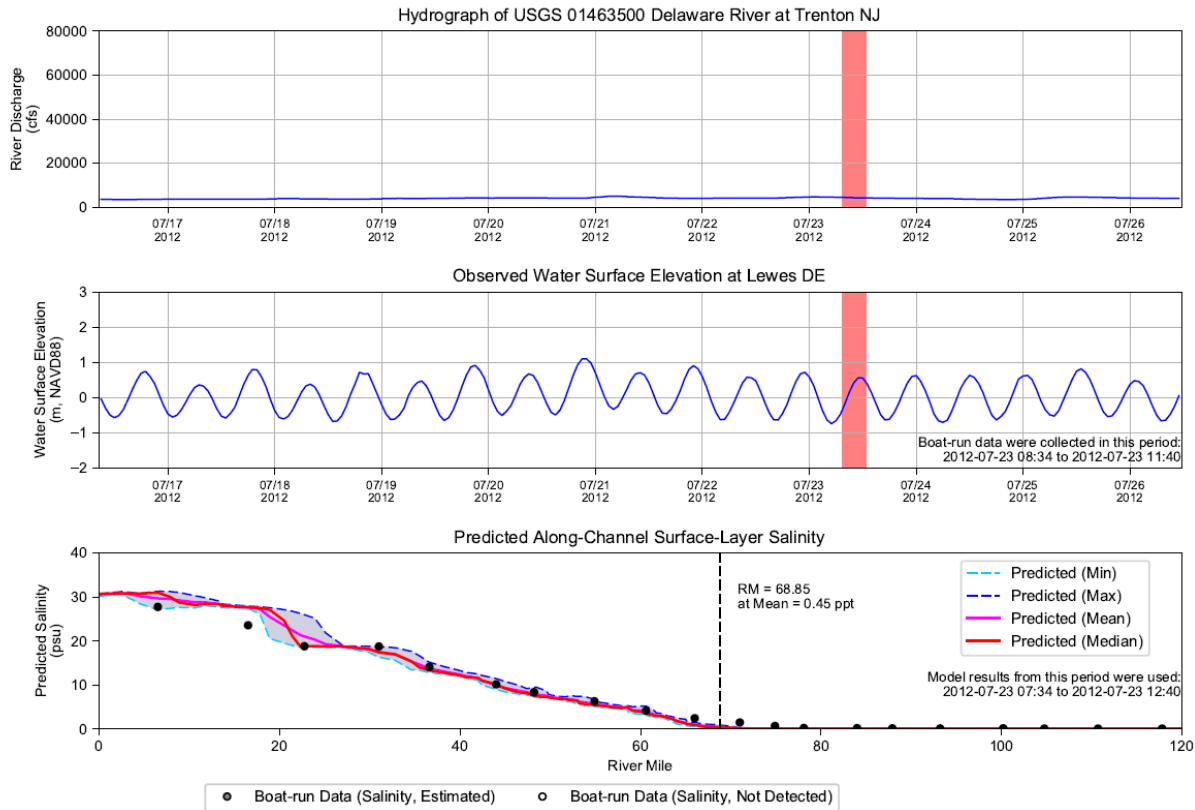
Figure S-23: Longitudinal Profile of Salinity in Delaware River and Bay. Survey period: 2012-05-22 08:27 to 2012-05-22 11:18.



Notes: Salinity and Chloride data collected by boat-run survey were used. Data that were measured to be under the detention limit were set to half of the detection limit. Red shaded areas indicate the boat-run survey period: 2012-06-25 08:30 to 2012-06-25 12:22. Model results along the navigation channel during period of 2012-06-25 07:30 to 2012-06-25 13:22 were used in this analysis.

Run ID: EFDC_HYDRO_G72_2023-01-06

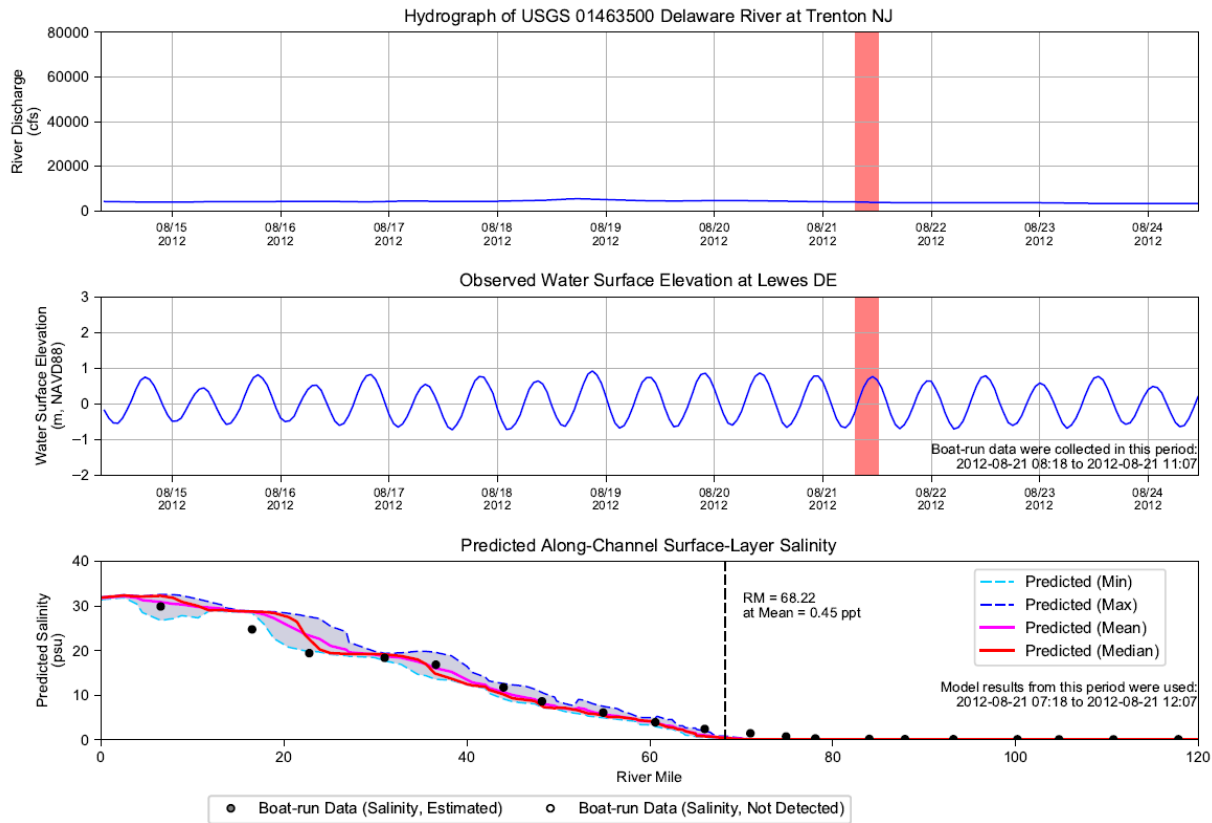
Figure S-24: Longitudinal Profile of Salinity in Delaware River and Bay. Survey period: 2012-06-25 08:30 to 2012-06-25 12:22.



Notes: Salinity and Chloride data collected by boat-run survey were used. Data that were measured to be under the detention limit were set to half of the detection limit. Red shaded areas indicate the boat-run survey period: 2012-07-23 08:34 to 2012-07-23 11:40. Model results along the navigation channel during period of 2012-07-23 07:34 to 2012-07-23 12:40 were used in this analysis.

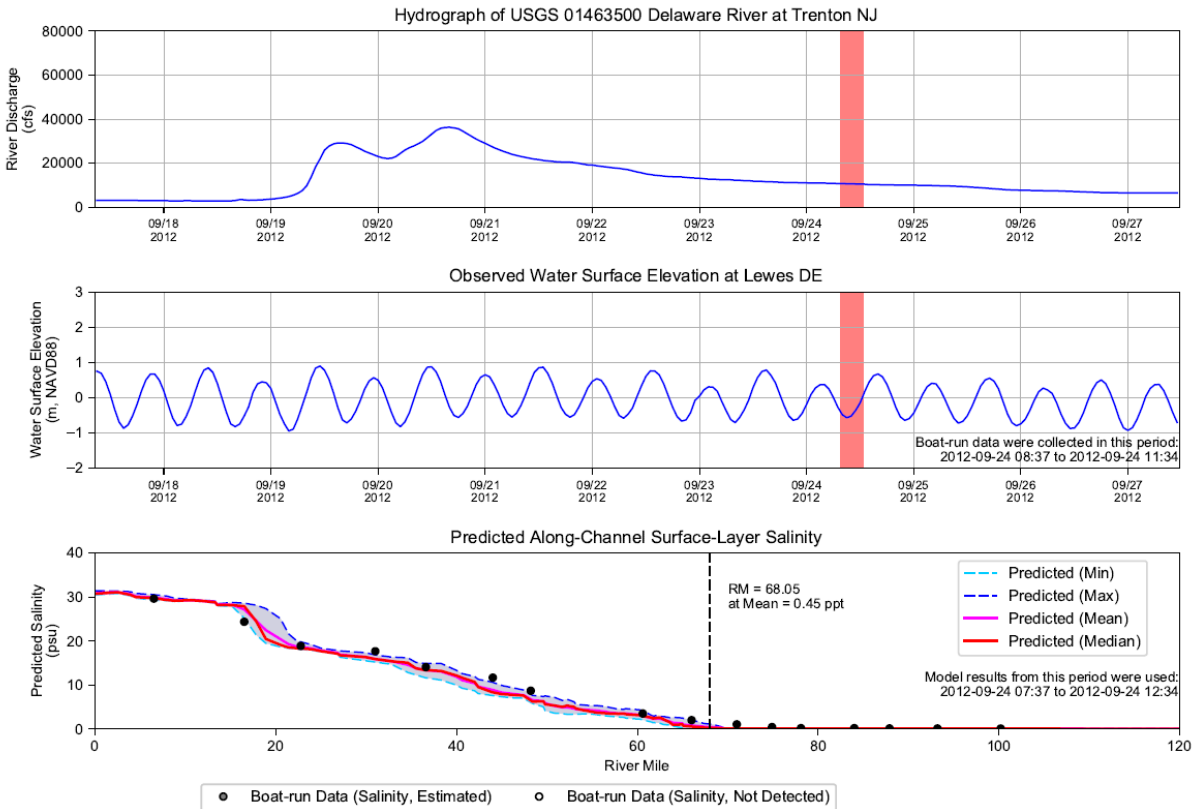
Run ID: EFDC_HYDRO_G72_2023-01-06

Figure S-25: Longitudinal Profile of Salinity in Delaware River and Bay. Survey period: 2012-07-23 08:34 to 2012-07-23 11:40.



Notes: Salinity and Chloride data collected by boat-run survey were used. Data that were measured to be under the detention limit were set to half of the detection limit. Red shaded areas indicate the boat-run survey period: 2012-08-21 08:18 to 2012-08-21 11:07. Model results along the navigation channel during period of 2012-08-21 07:18 to 2012-08-21 12:07 were used in this analysis
Run ID: EFDC_HYDRO_G72_2023-01-06

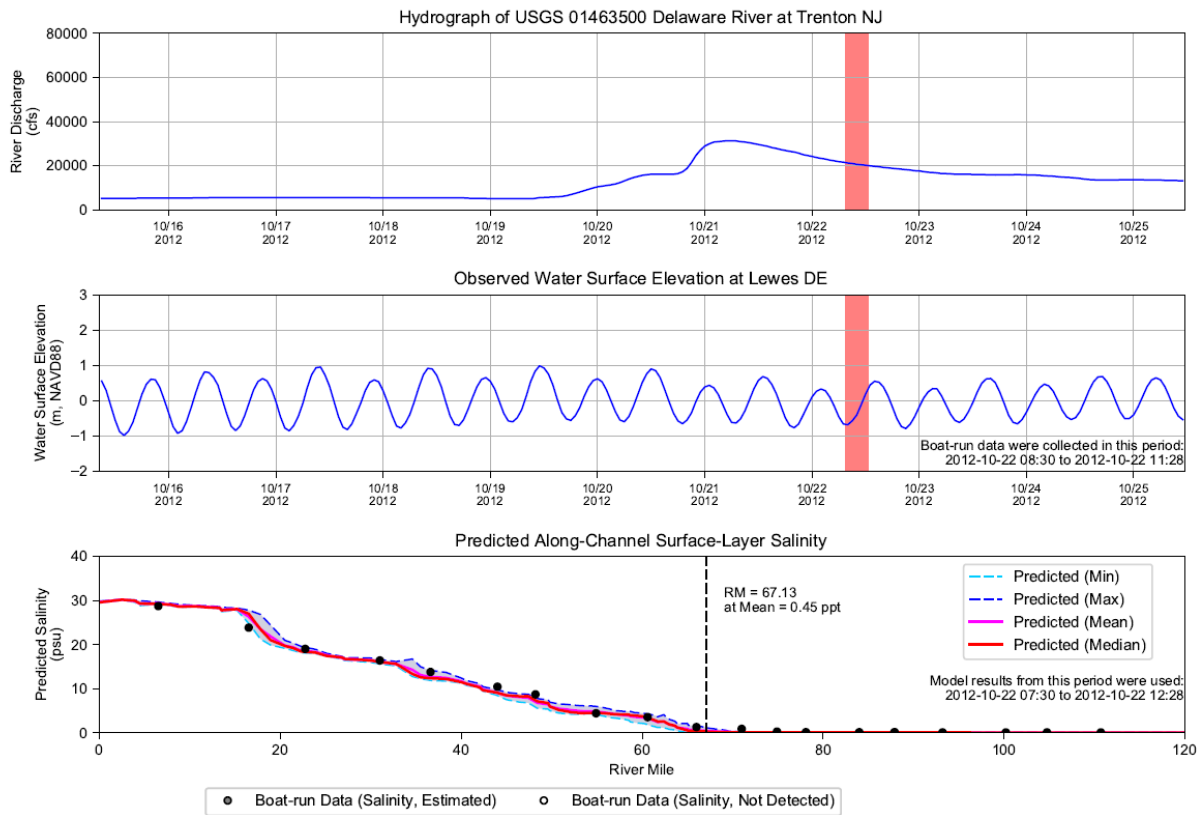
Figure S-26: Longitudinal Profile of Salinity in Delaware River and Bay. Survey period: 2012-08-21 08:18 to 2012-08-21 11:07.



Notes: Salinity and Chloride data collected by boat-run survey were used. Data that were measured to be under the detention limit were set to half of the detection limit. Red shaded areas indicate the boat-run survey period: 2012-09-24 08:37 to 2012-09-24 11:34. Model results along the navigation channel during period of 2012-09-24 07:37 to 2012-09-24 12:34 were used in this analysis.

Run ID: EFDC_HYDRO_G72_2023-01-06

Figure S-27: Longitudinal Profile of Salinity in Delaware River and Bay. Survey period: 2012-09-24 08:37 to 2012-09-24 11:34.

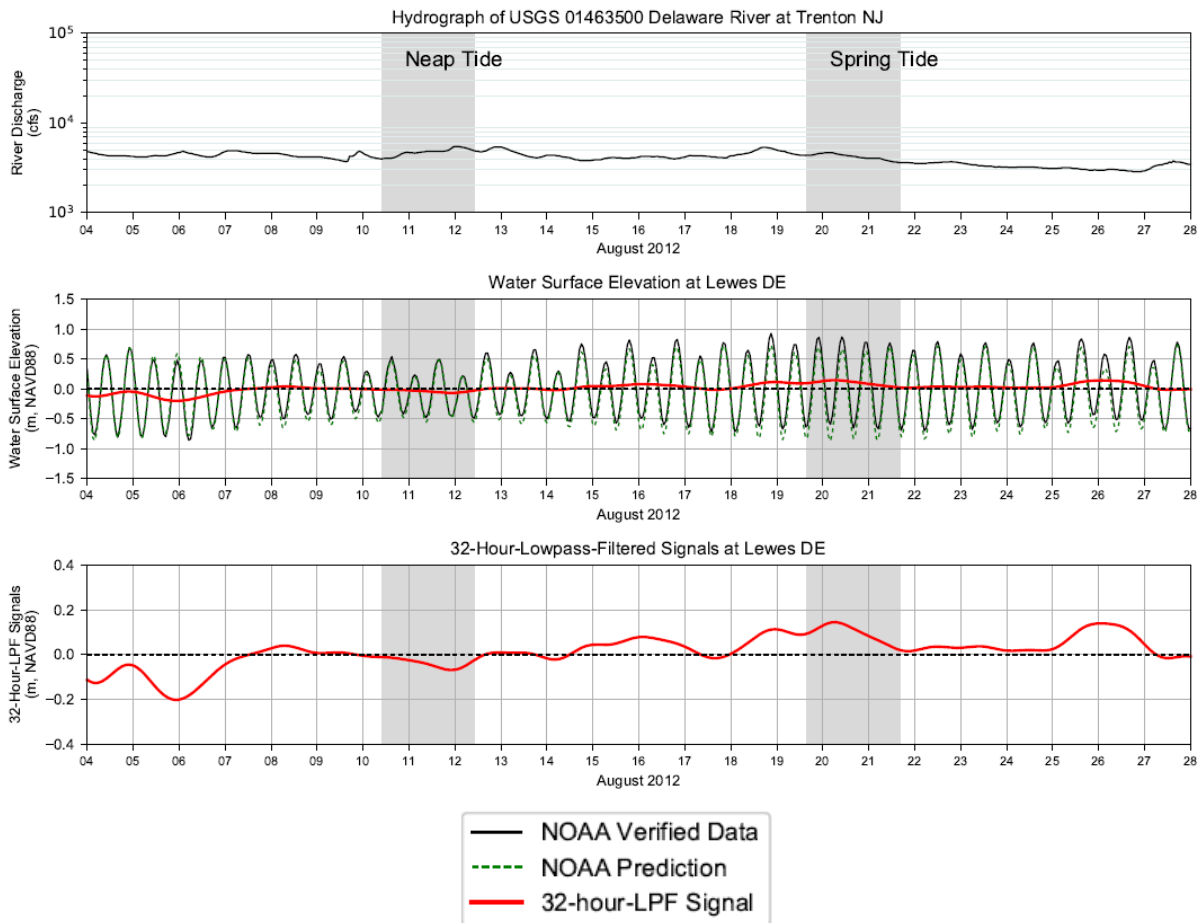


Notes: Salinity and Chloride data collected by boat-run survey were used. Data that were measured to be under the detection limit were set to half of the detection limit. Red shaded areas indicate the boat-run survey period: 2012-10-22 08:30 to 2012-10-22 11:28. Model results along the navigation channel during period of 2012-10-22 07:30 to 2012-10-22 12:28 were used in this analysis

Run ID: EFDC_HYDRO_G72_2023-01-06

Figure S-28: Longitudinal Profile of Salinity in Delaware River and Bay. Survey period: 2012-10-22 08:30 to 2012-10-22 11:28.

Appendix T: Evaluation of vertical resolution



Selected time window for neap tide: 08-10-2012 10:00 to 08-12-2012 10:00

Selected time window for spring tide: 08-19-2012 16:00 to 08-21-2012 16:00

Figure T-1: River Flow at Trenton and Observed Tide at Lewes during August 2012 Period

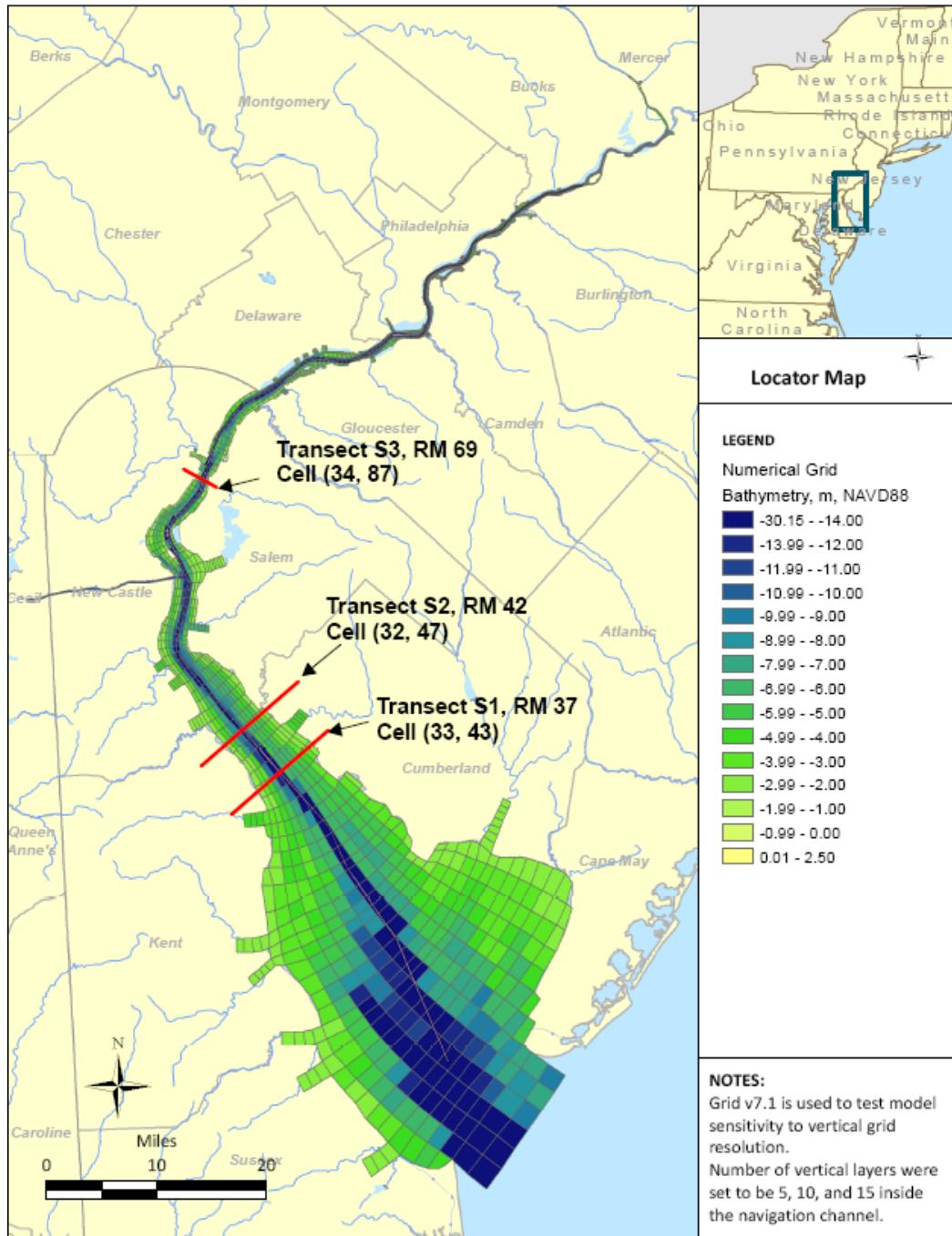


Figure T-2: Numerical Grid with Selected Cells and Transect Locations Used for Vertical Grid Resolution Sensitivity Analysis

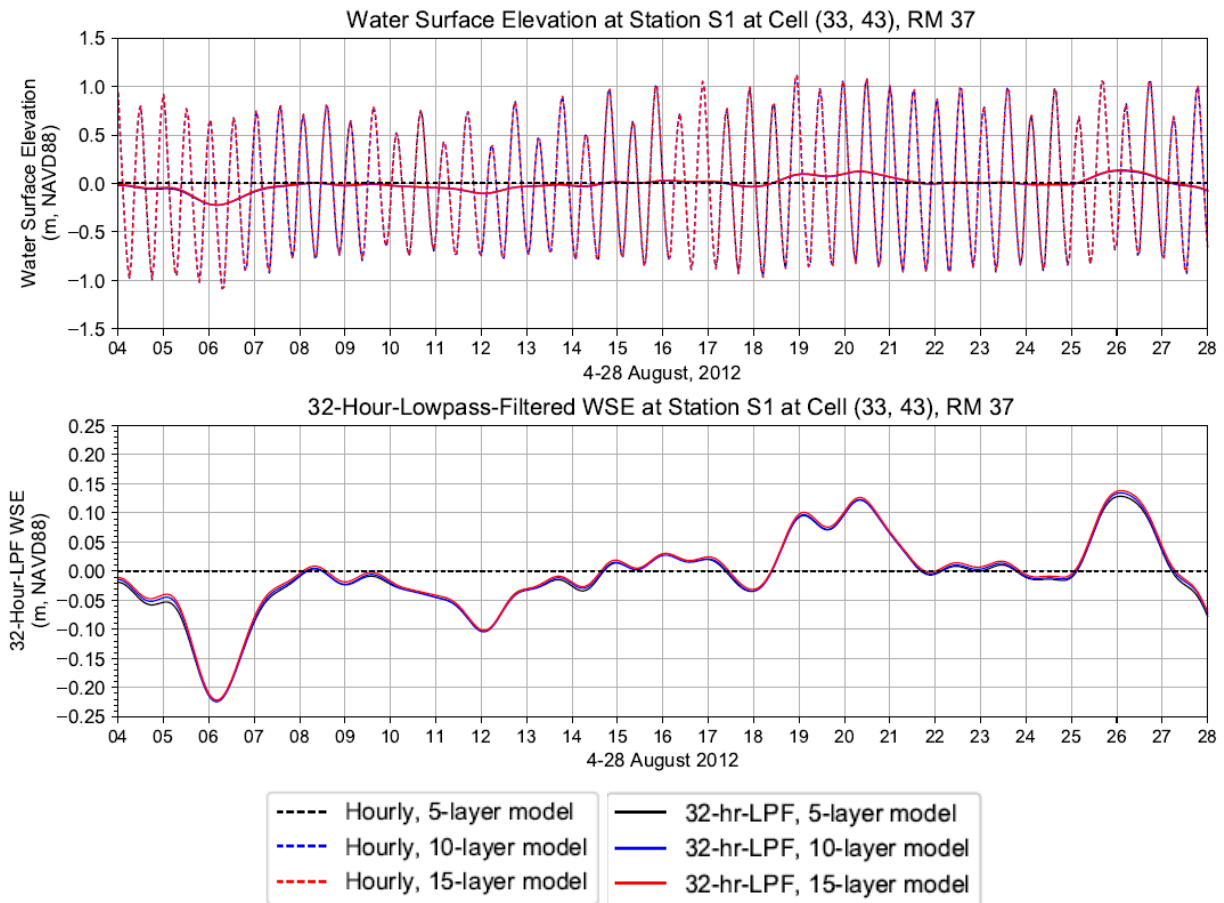


Figure T-3: Simulated Hourly and 32-hour-Lowpass-Filtered Water Surface Elevation during 08-04-2012 to 08-28-2012 at Station S1 at Cell (33, 43), RM 37

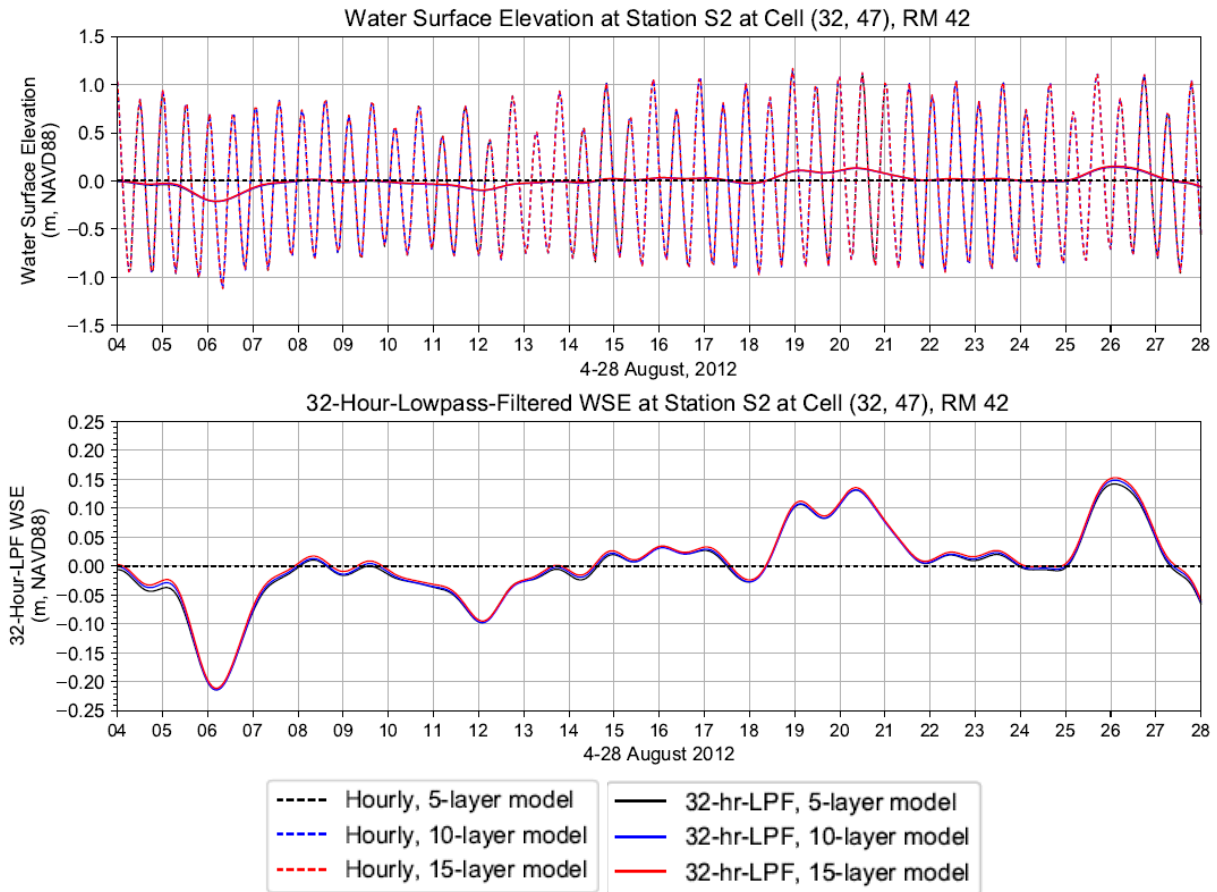


Figure T-4: Simulated Hourly and 32-hour-Lowpass-Filtered Water Surface Elevation during 08-04-2012 to 08-28-2012 at Station S2 at Cell (32, 47), RM 42

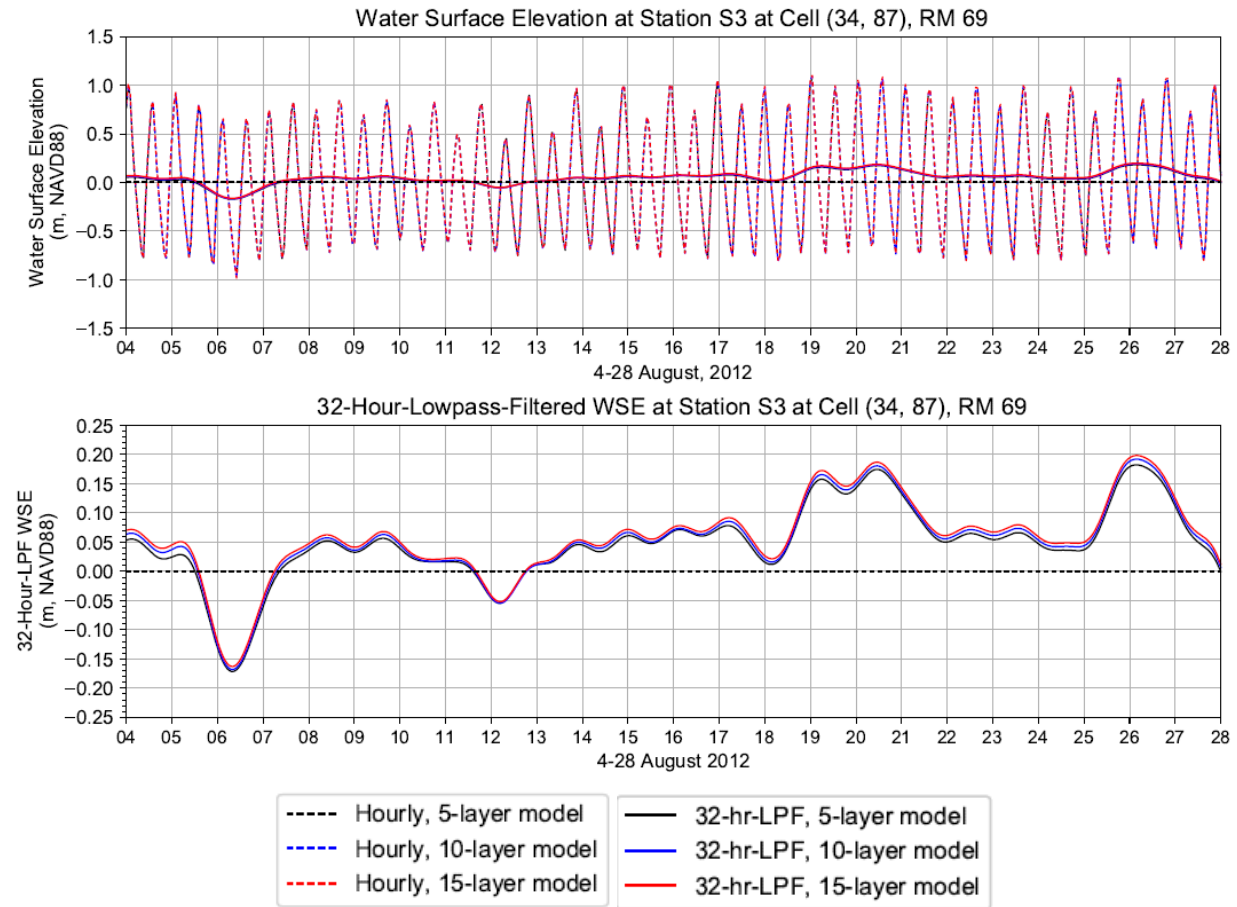


Figure T-5: Simulated Hourly and 32-hour-Lowpass-Filtered Water Surface Elevation during 08-04-2012 to 08-28-2012 at Station S3 at Cell (34, 87), RM 69

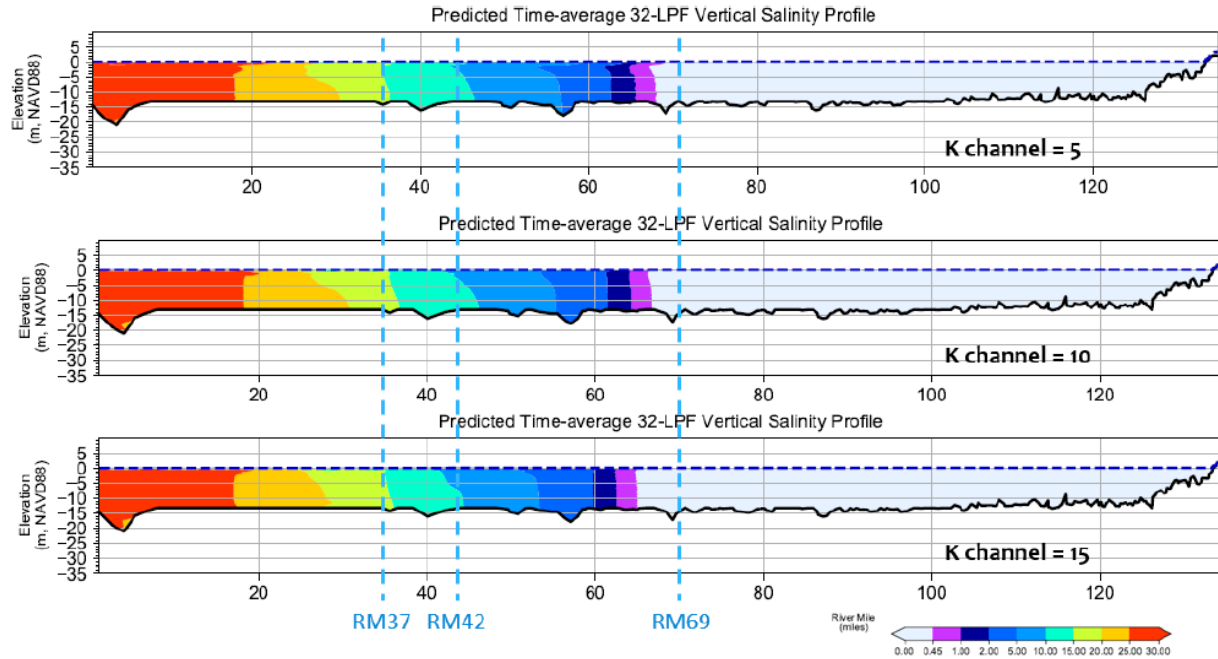


Figure O-6: Longitudinal and Vertical Distribution of Tidally Averaged Salinity (32-Lowpass-Filtered Results) - Spring Tide Time period: 08-19-2012 16:00 to 08-21-2012 16:00

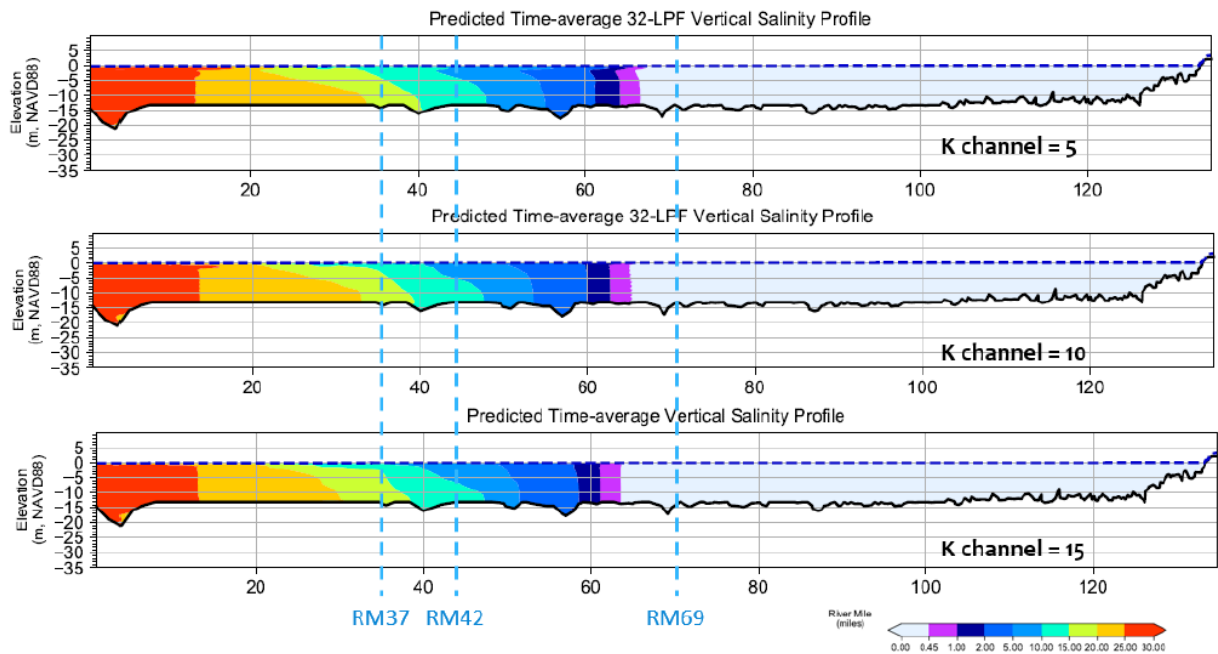


Figure T-7: Longitudinal and Vertical Distribution of Tidally Averaged Salinity (32-Lowpass-Filtered Results) - Neap Tide Time period: 08-10-2012 10:00 to 08-12-2012 10:00

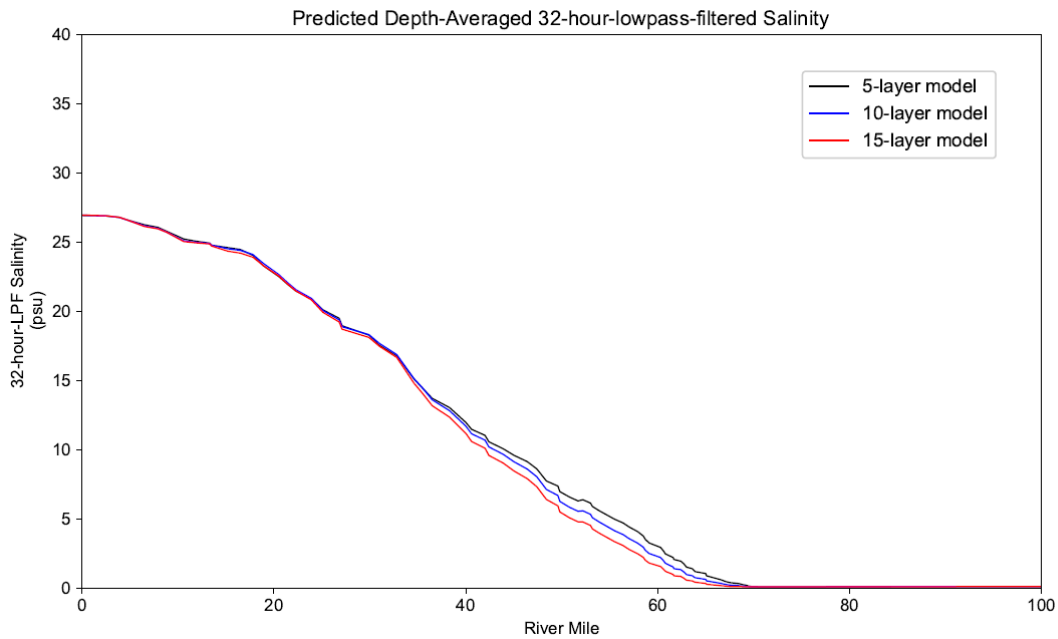


Figure T-8: Comparison of Predicted Depth-Averaged 32-hour-lowpass-filtered Salinity Time-Averaged Values during Period of 08-19-2012 to 08-21-2012 are Shown, Spring Tide

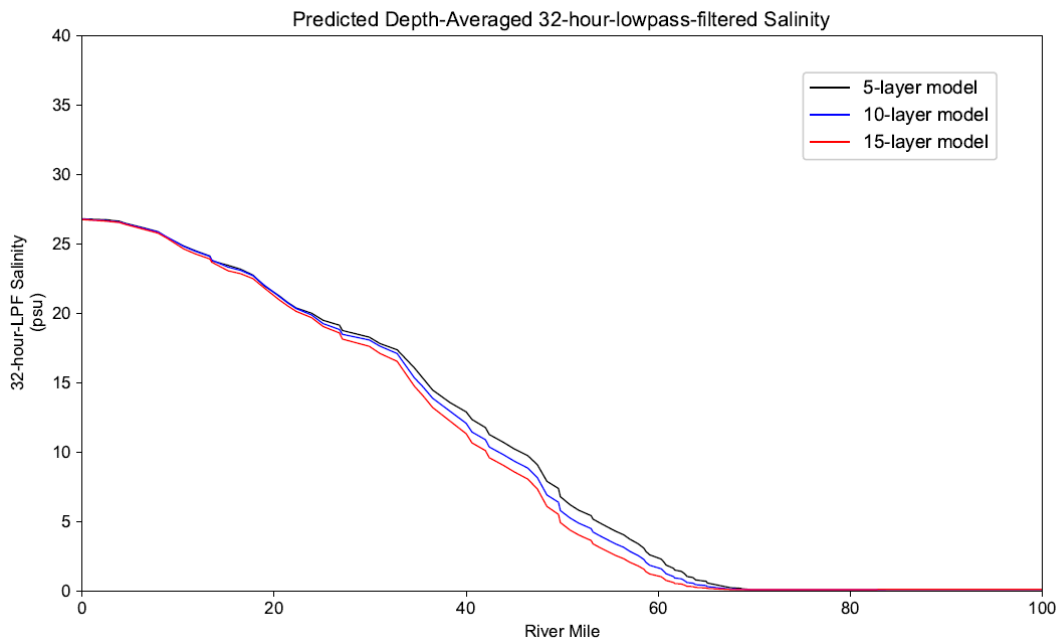


Figure T-9: Comparison of Predicted Depth-Averaged 32-hour-lowpass-filtered Salinity Time-Averaged Values during Period of 08-10-2012 to 08-12-2012 are Shown, Neap Tide

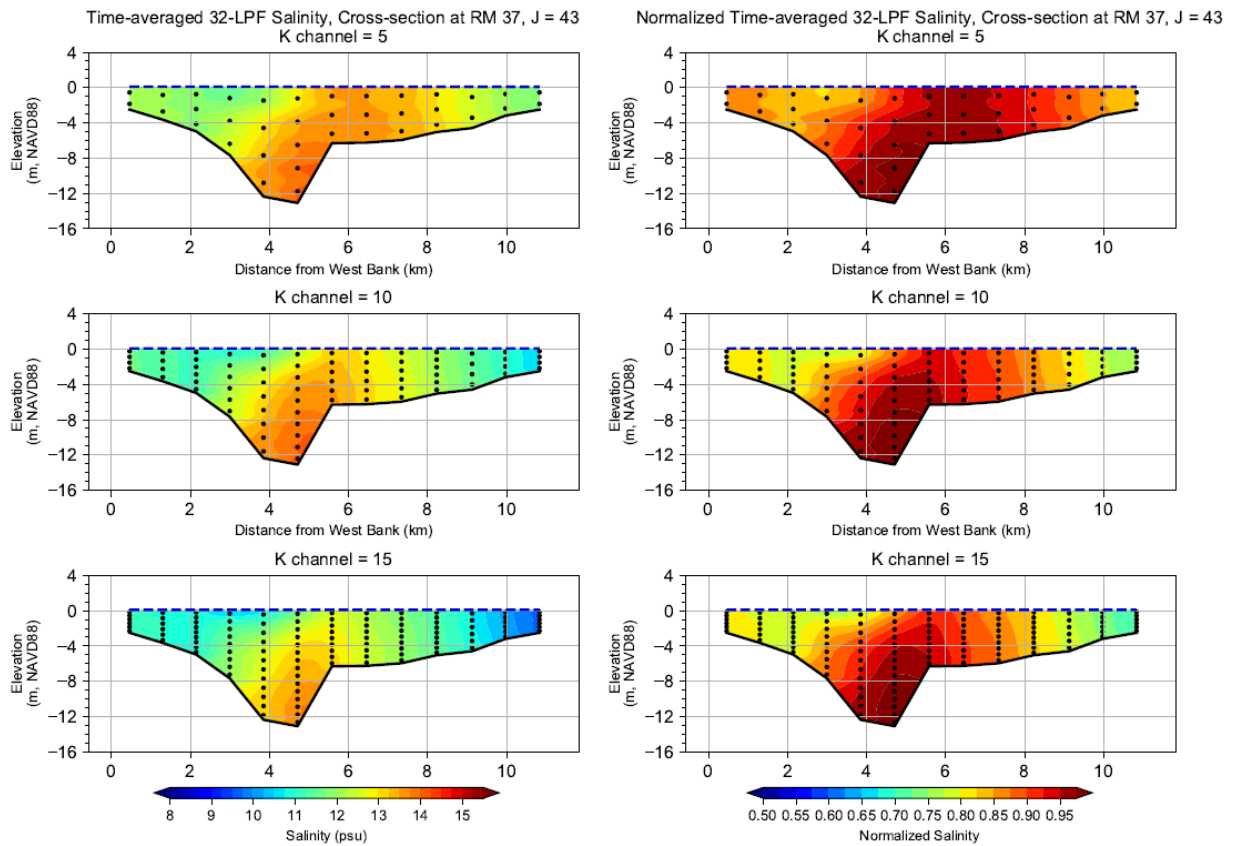


Figure T-10: Vertical Slide of Normalized Time-averaged 32-LPF Salinity at Cross-section at RM 37, J = 43 during 08-19-2012 to 08-21-2012 Period, Spring Tide. Salinity was normalized against the maximum salinity of the cross-section.

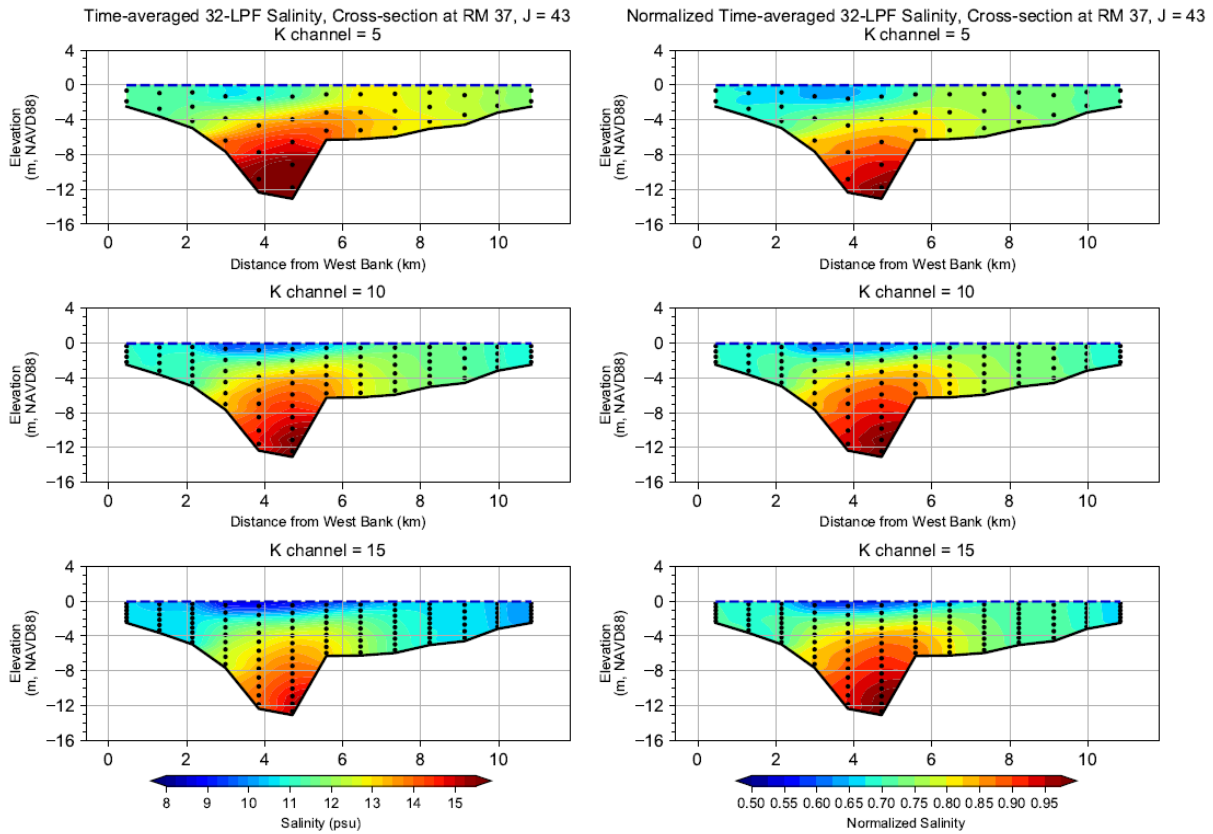


Figure T-11: Vertical Slide of Normalized Time-averaged 32-LPF Salinity at Cross-section at RM 37, J = 43 during 08-10-2012 to 08-12-2012 Period, Neap Tide. Salinity was normalized against the maximum salinity of the cross-section.

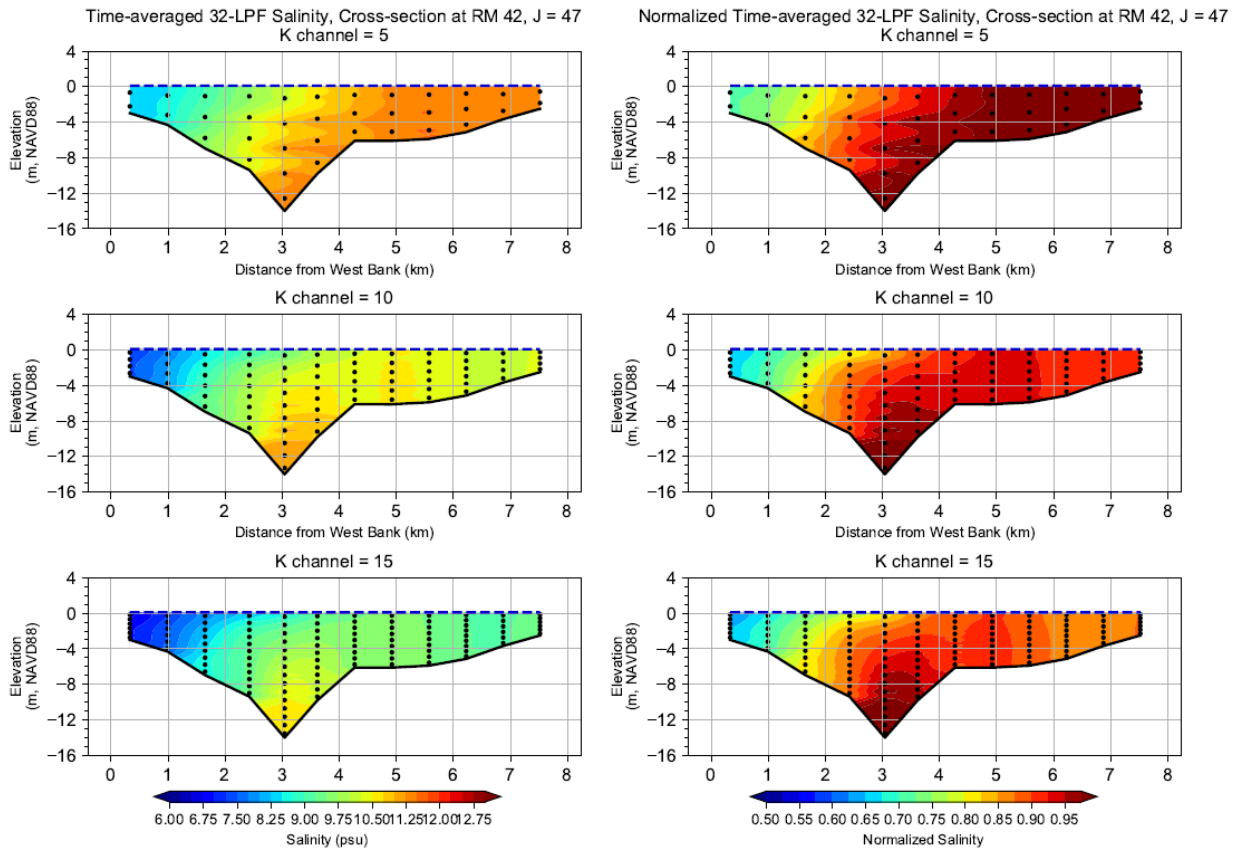


Figure T-12: Vertical Slide of Normalized Time-averaged 32-LPF Salinity at Cross-section at RM 42, J = 47 during 08-19-2012 to 08-21-2012 Period, Spring Tide. Salinity was normalized against the maximum salinity of the cross-section.

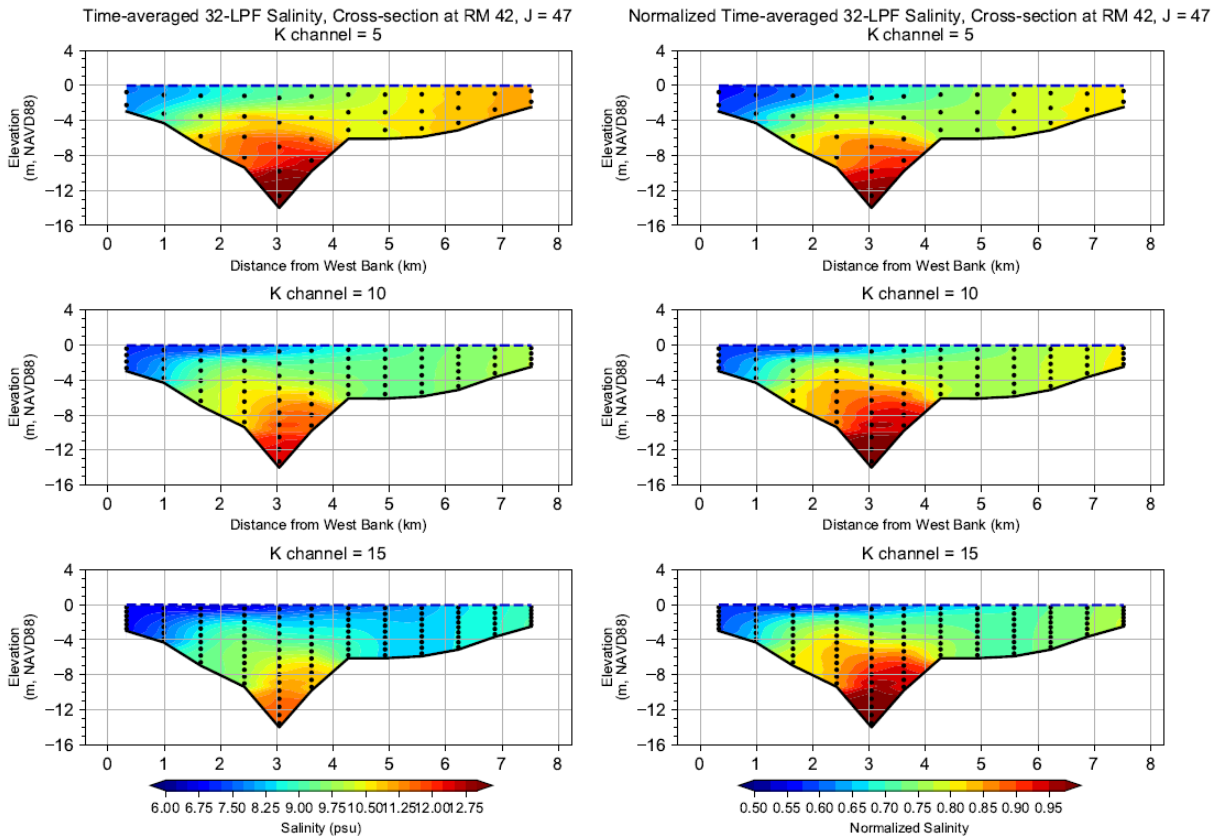


Figure T-13: Vertical Slide of Normalized Time-averaged 32-LPF Salinity at Cross-section at RM 42, J = 47 during 08-10-2012 to 08-12-2012 Period, Neap Tide. Salinity was normalized against the maximum salinity of the cross-section.

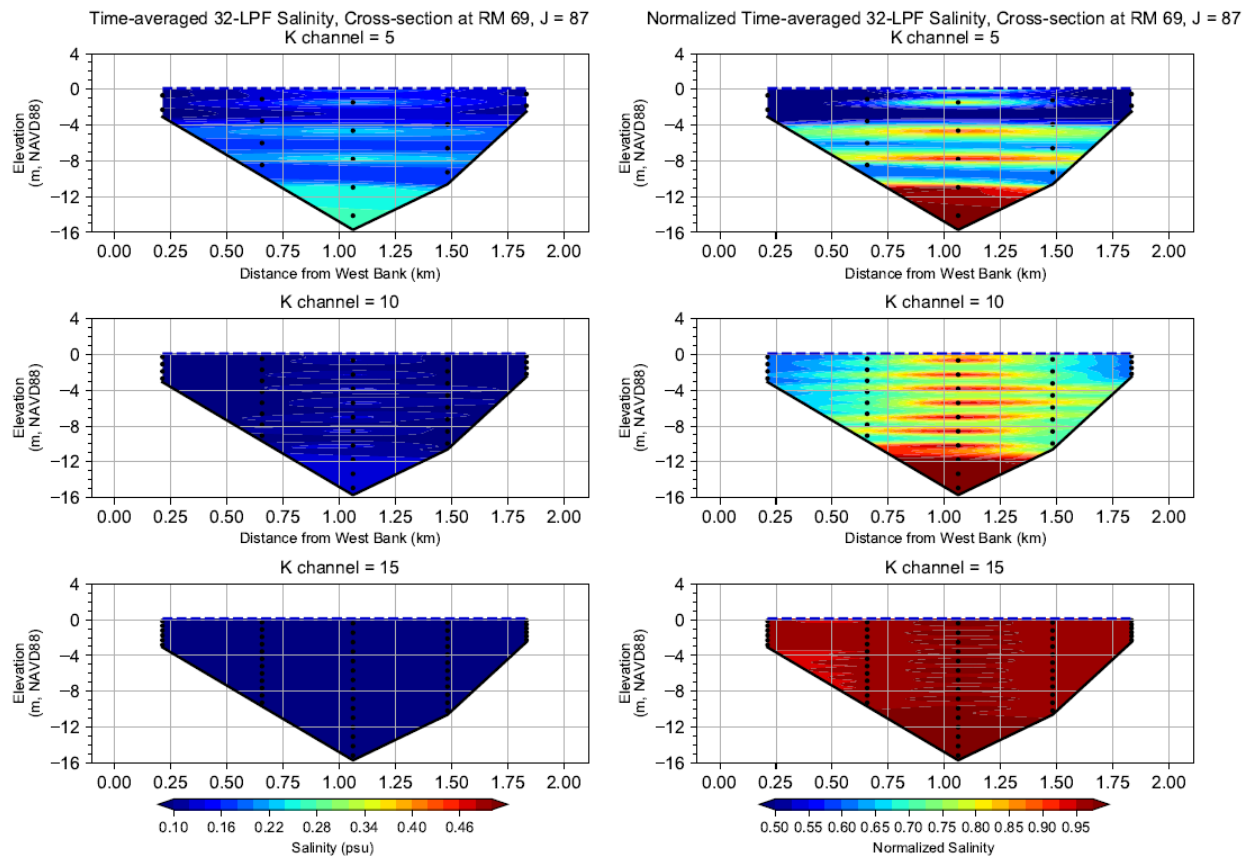


Figure T-14: Vertical Slide of Normalized Time-averaged 32-LPF Salinity at Cross-section at RM 69, J = 87 during 08-19-2012 to 08-21-2012 Period, Spring Tide. Salinity was normalized against the maximum salinity of the cross-section.

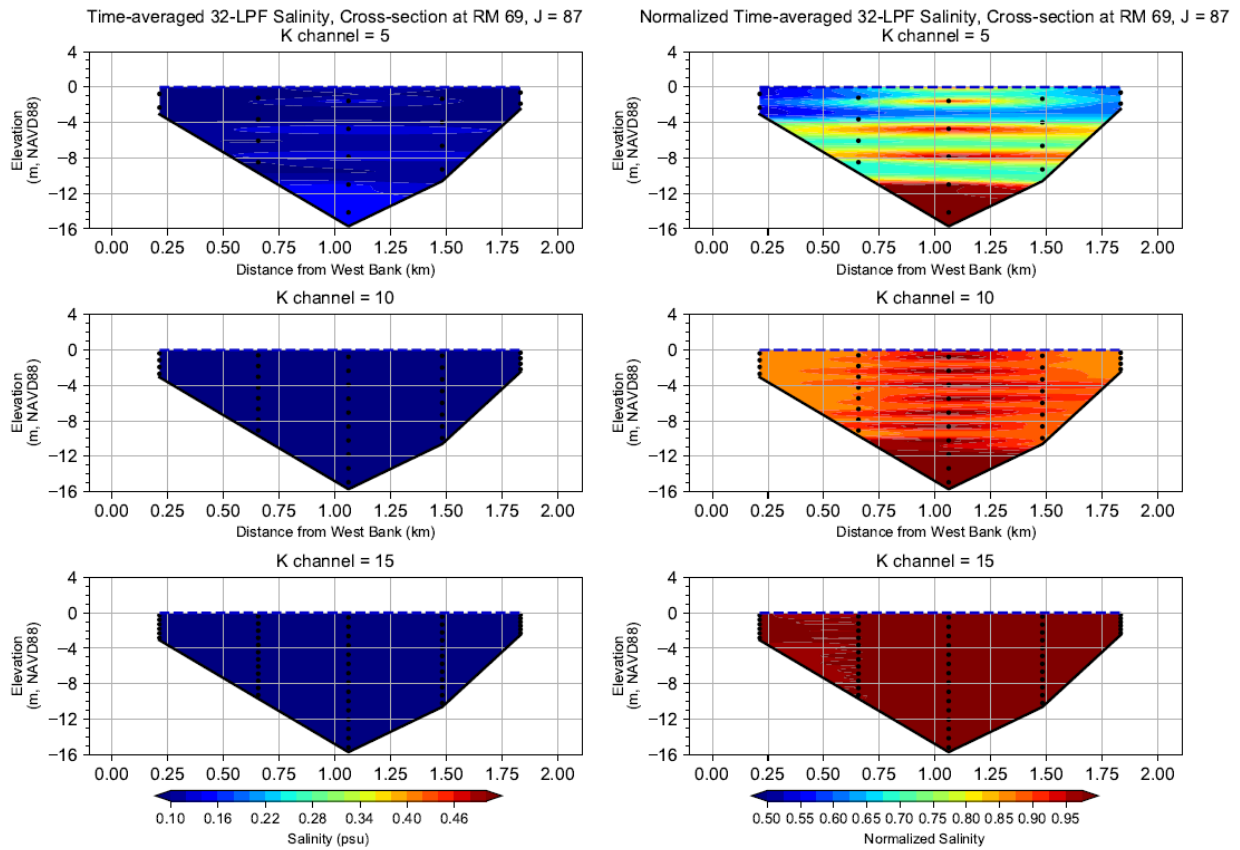


Figure T-15: Vertical Slide of Normalized Time-averaged 32-LPF Salinity at Cross-section at RM 69, J = 87 during 08-10-2012 to 08-12-2012 Period, Neap Tide. Salinity was normalized against the maximum salinity of the cross-section.

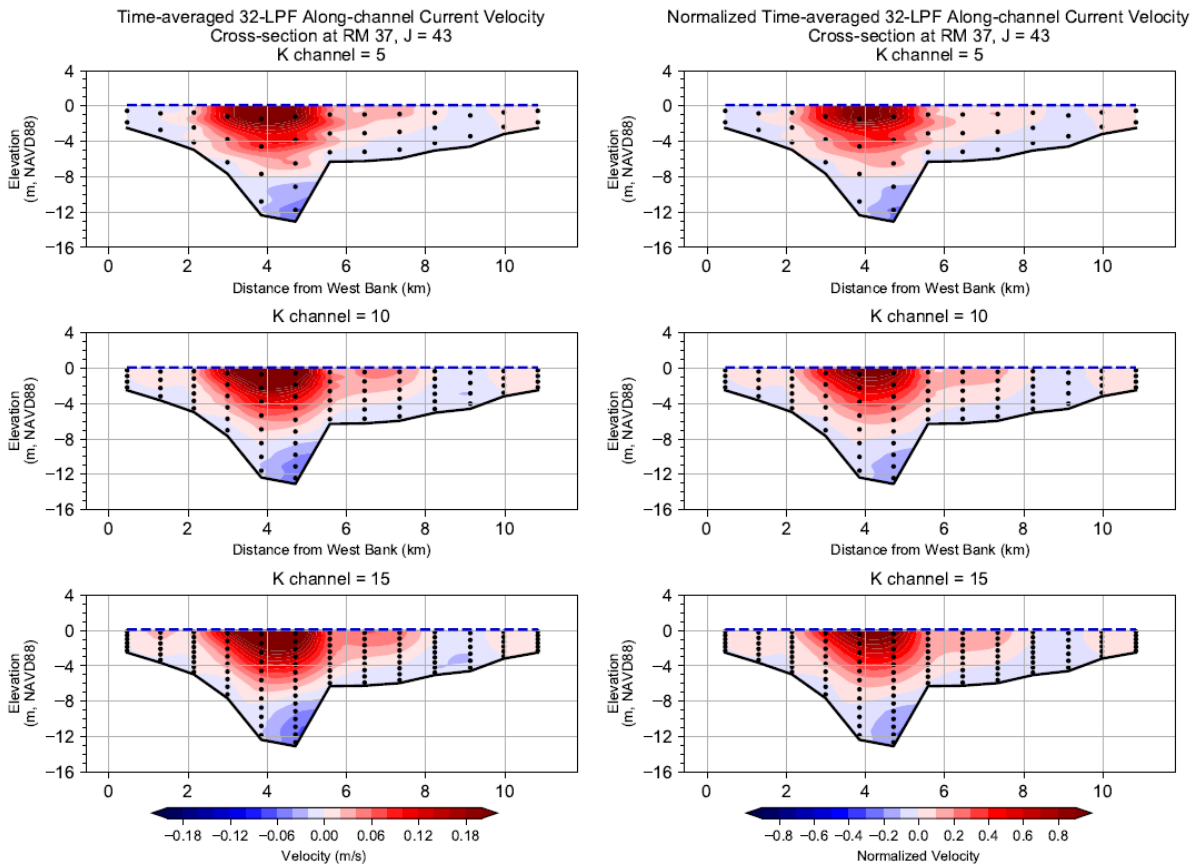


Figure T-16: Vertical Slide of Normalized Time-averaged 32-LPF Along-channel Current Velocity at Cross-section at RM 37, J = 43 during 08-19-2012 to 08-21-2012 Period, Spring Tide. Positive is moving seaward. Velocity was normalized against the maximum velocity of the cross-section.

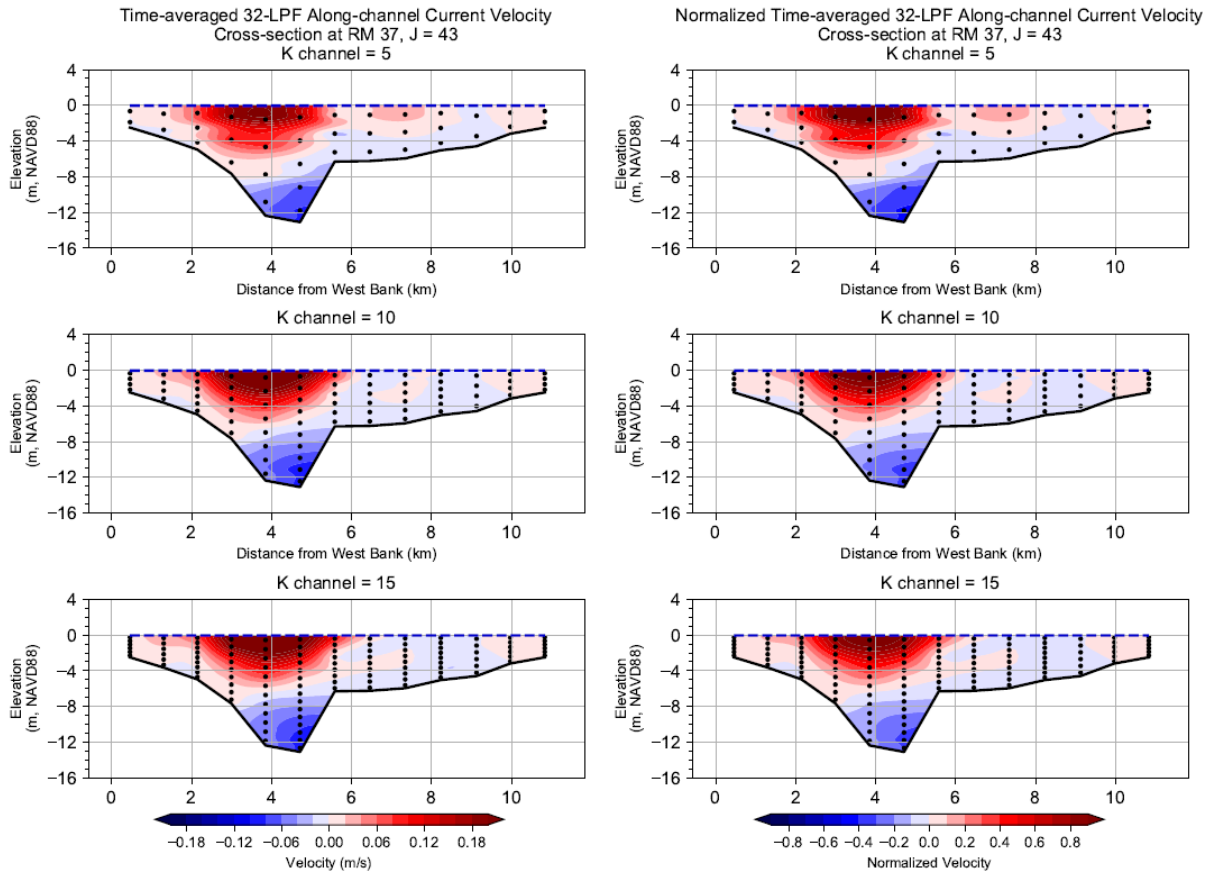


Figure T-17: Vertical Slide of Normalized Time-averaged 32-LPF Along-channel Current Velocity at Cross-section at RM 37, J = 43 during 08-10-2012 to 08-12-2012 Period, Neap Tide. Positive is moving seaward. Velocity was normalized against the maximum velocity of the cross-section.

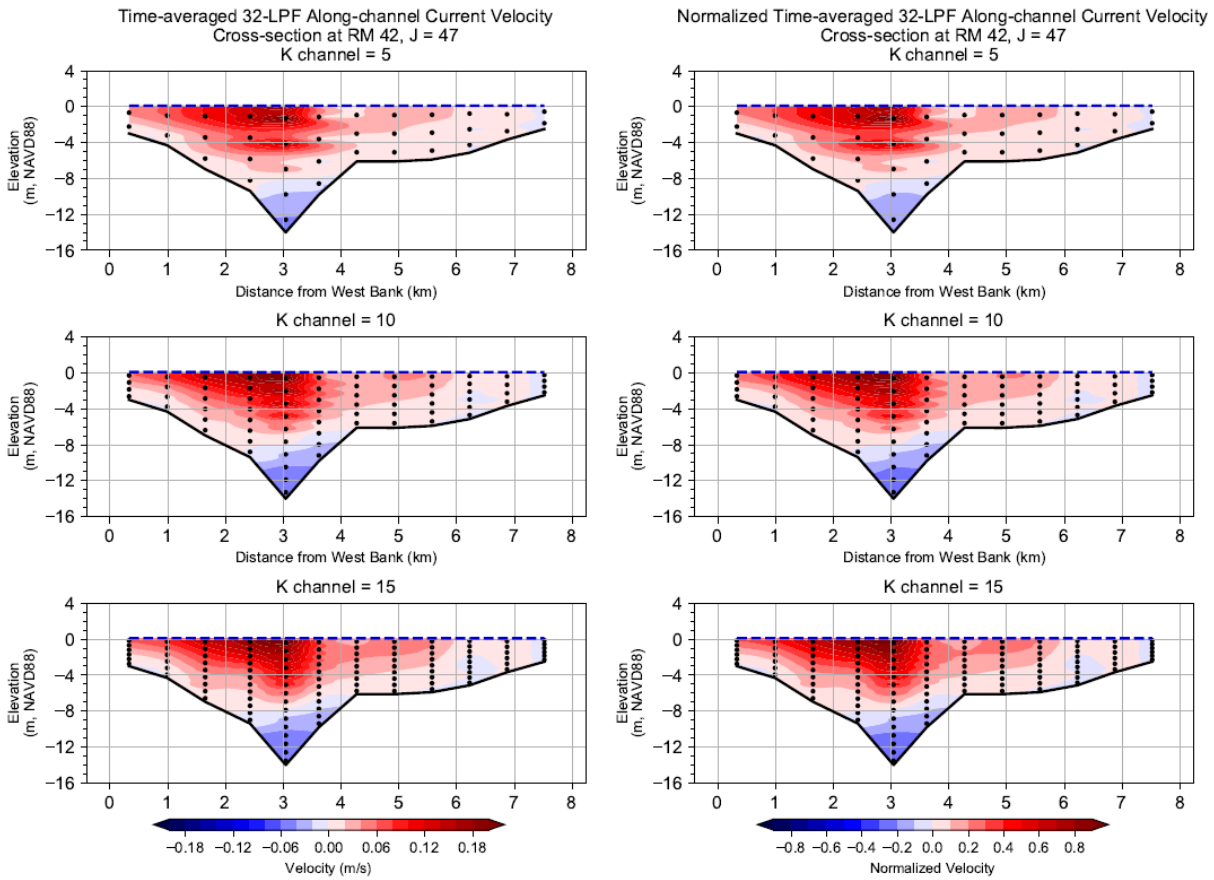


Figure T-18: Vertical Slide of Normalized Time-averaged 32-LPF Along-channel Current Velocity at Cross-section at RM 42, J = 47 during 08-19-2012 to 08-21-2012 Period, Spring Tide. Positive is moving seaward. Velocity was normalized against the maximum velocity of the cross-section.

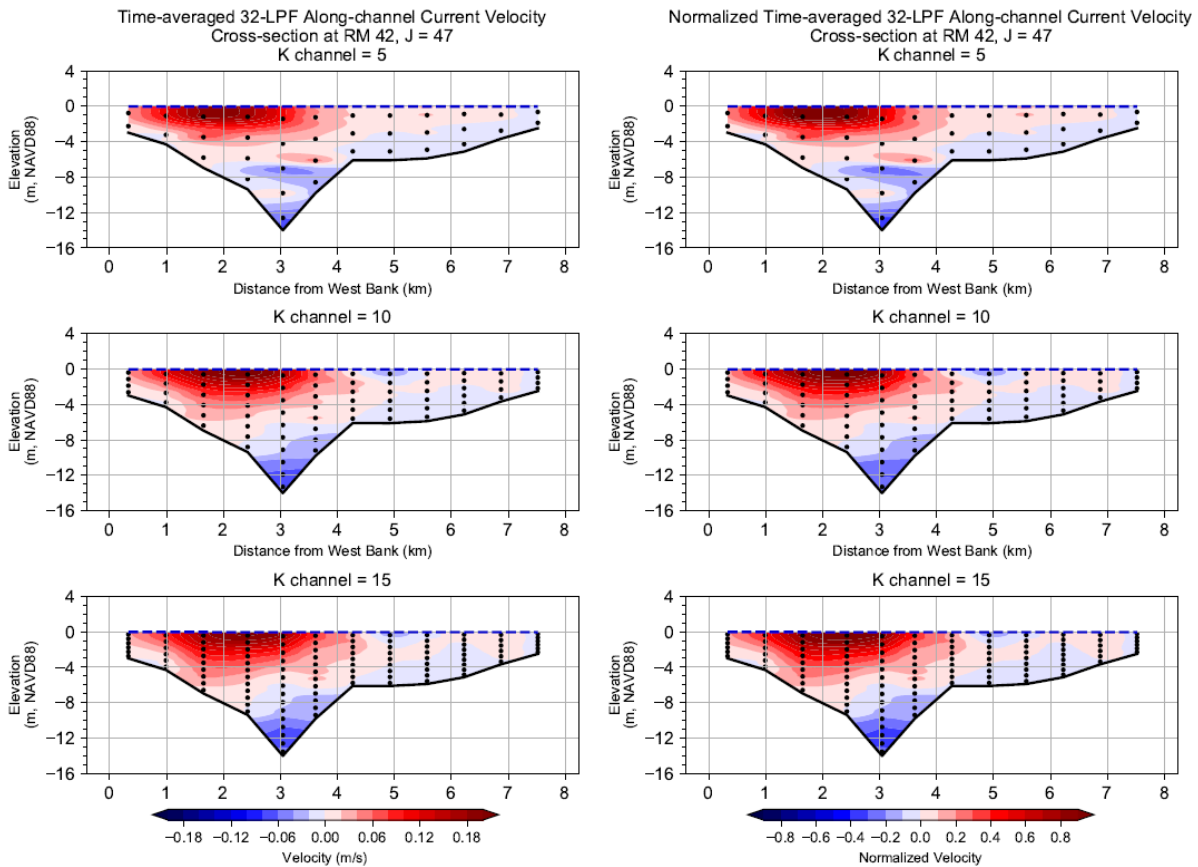


Figure T-19: Vertical Slide of Normalized Time-averaged 32-LPF Along-channel Current Velocity at Cross-section at RM 42, J = 47 during 08-10-2012 to 08-12-2012 Period, Neap Tide. Positive is moving seaward. Velocity was normalized against the maximum velocity of the cross-section.

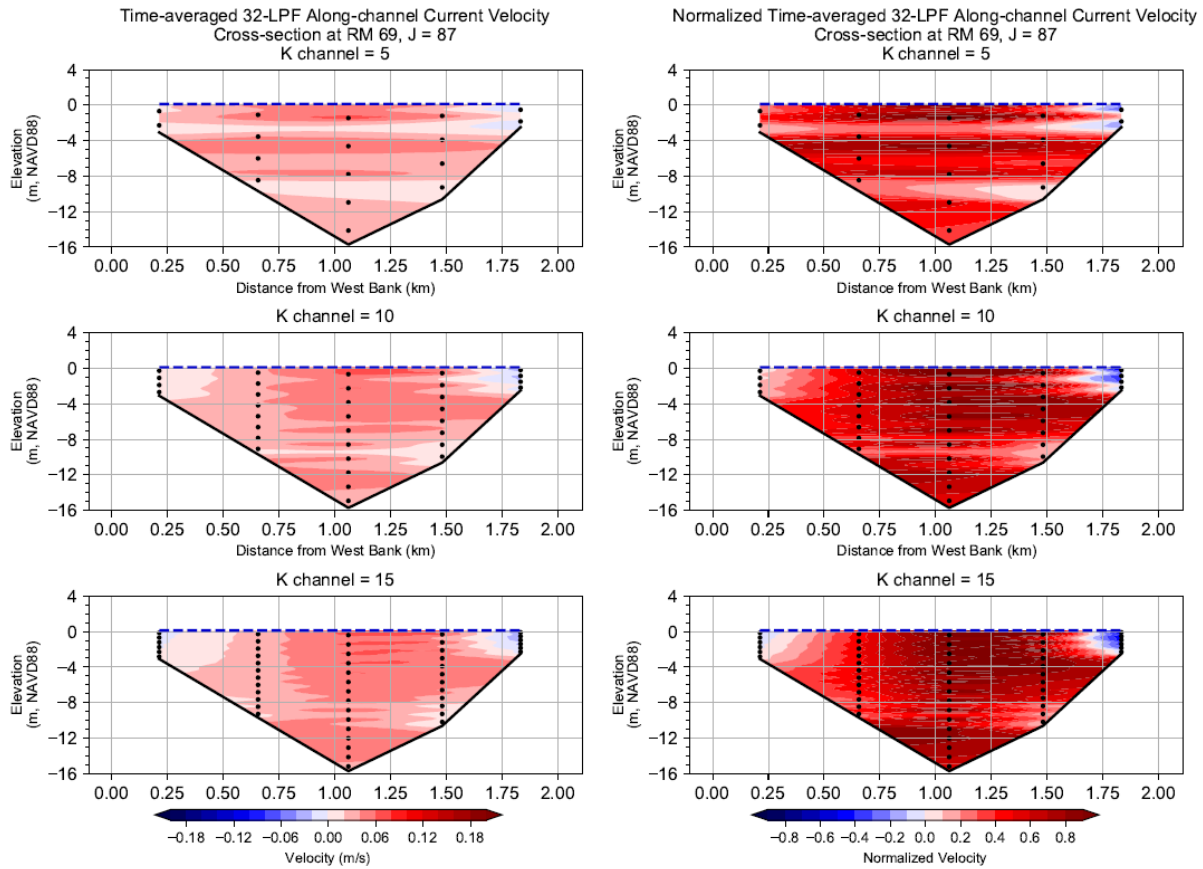


Figure T-20: Vertical Slide of Normalized Time-averaged 32-LPF Along-channel Current Velocity at Cross-section at RM 69, J = 87 during 08-19-2012 to 08-21-2012 Period, Spring Tide. Positive is moving seaward. Velocity was normalized against the maximum velocity of the cross-section.

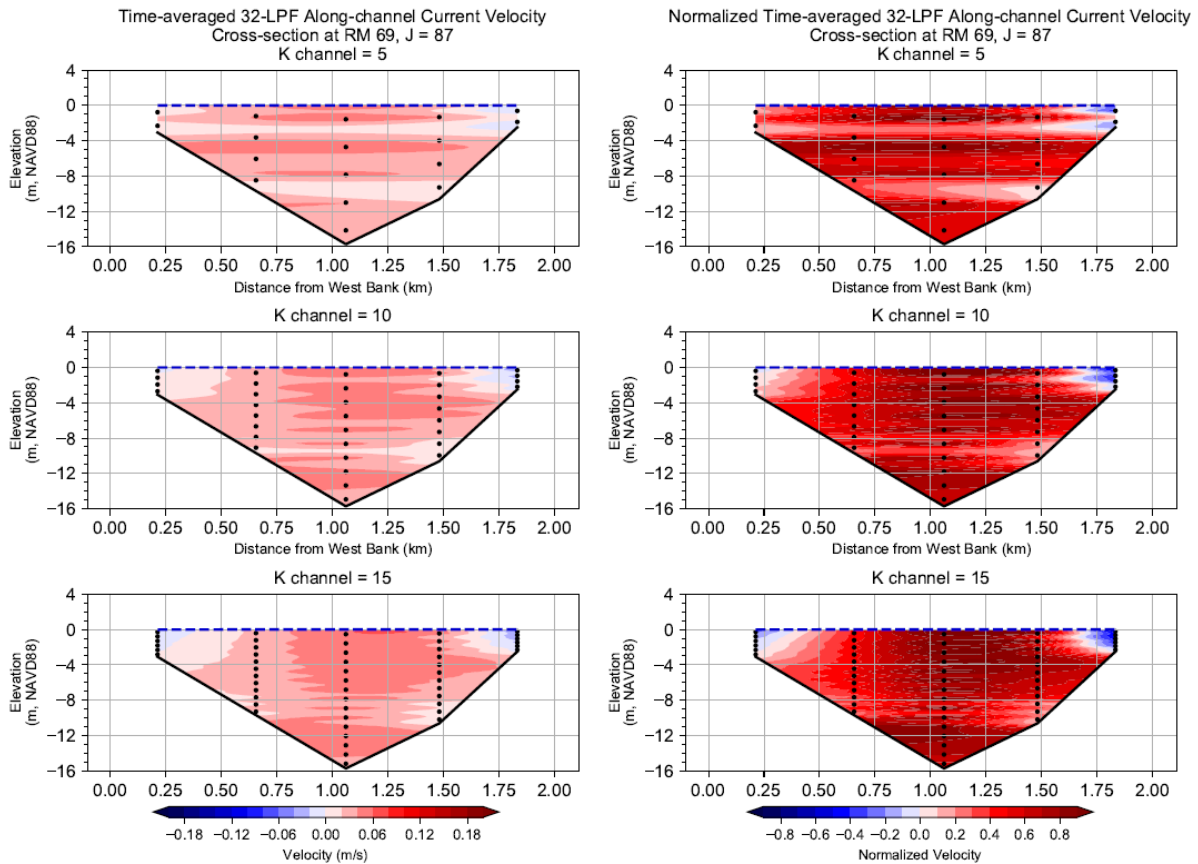
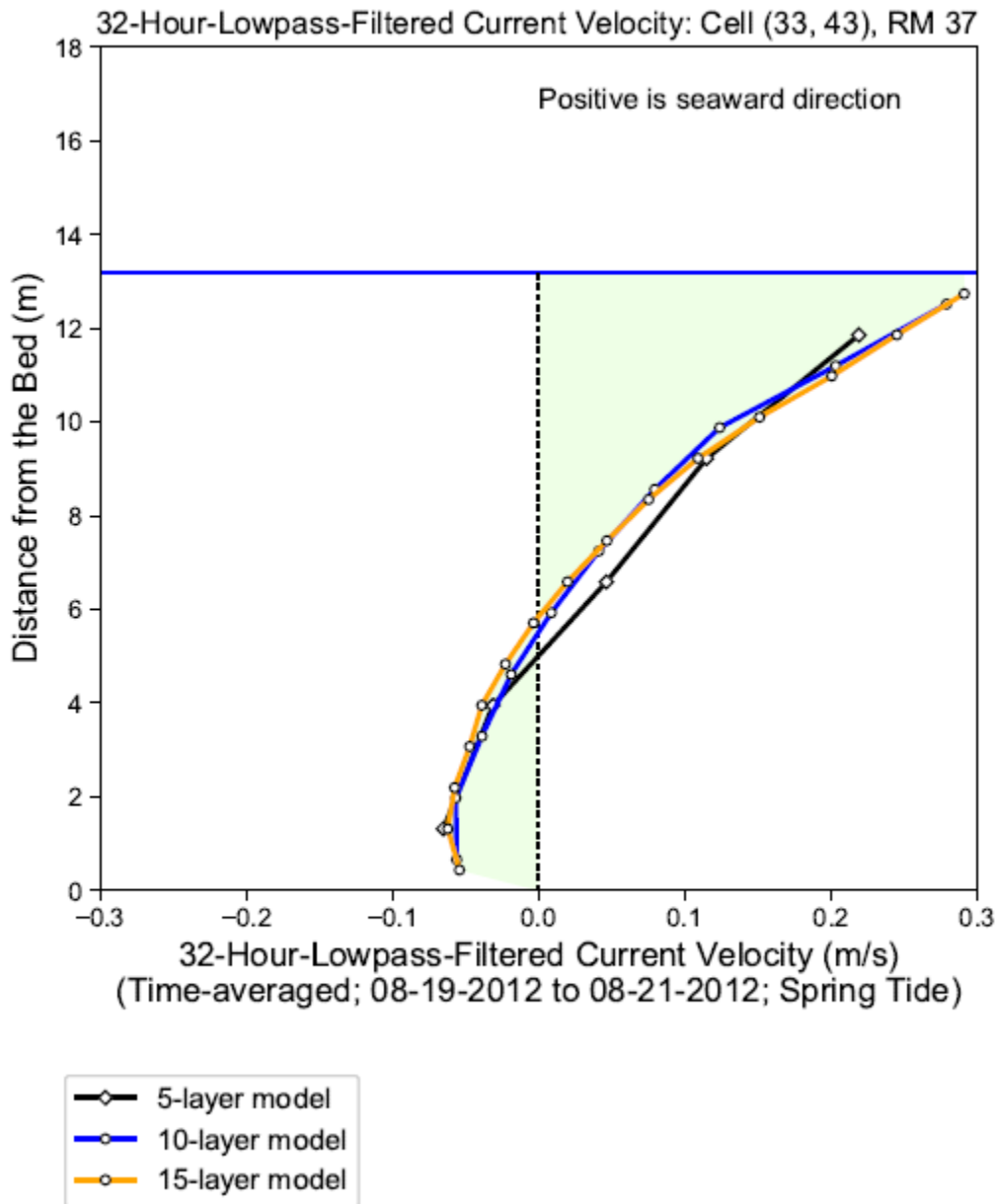
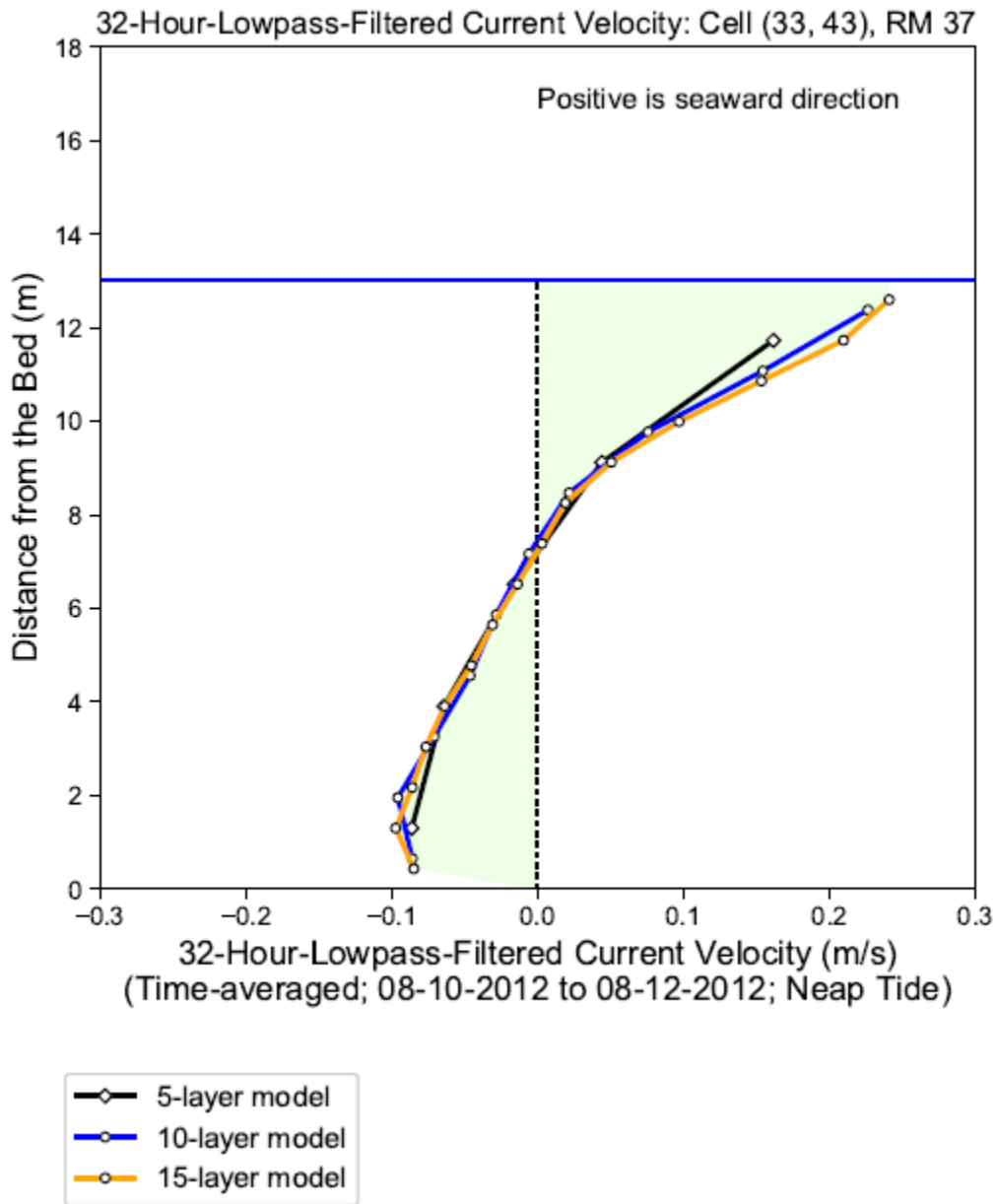


Figure T-21: Vertical Slide of Normalized Time-averaged 32-LPF Along-channel Current Velocity at Cross-section at RM 69, J = 87 during 08-10-2012 to 08-12-2012 Period, Neap Tide. Positive is moving seaward. Velocity was normalized against the maximum velocity of the cross-section.



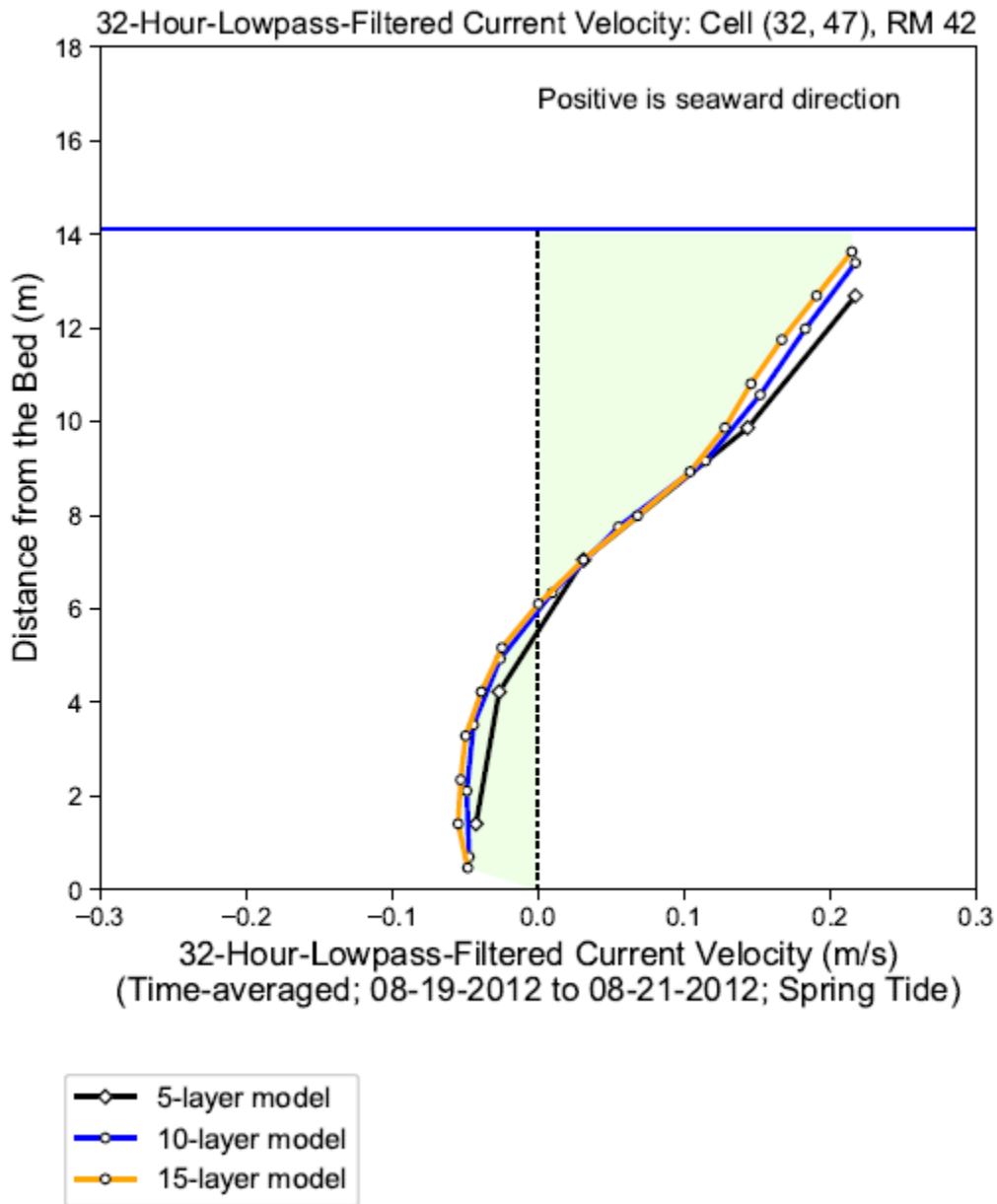
Notes: 32-hour-Low-pass-filtered results were calculated first and then averaged over the time period to represent the mean vertical structure. Shaded area represents the profile of the 15-layer model.

Figure T-22: Simulated 32-Hour-Lowpass-Filtered Along-channel Current Velocity during 08-19-2012 to 08-21-2012; Spring Tide at Station S1 at Cell (33, 43), RM 37.



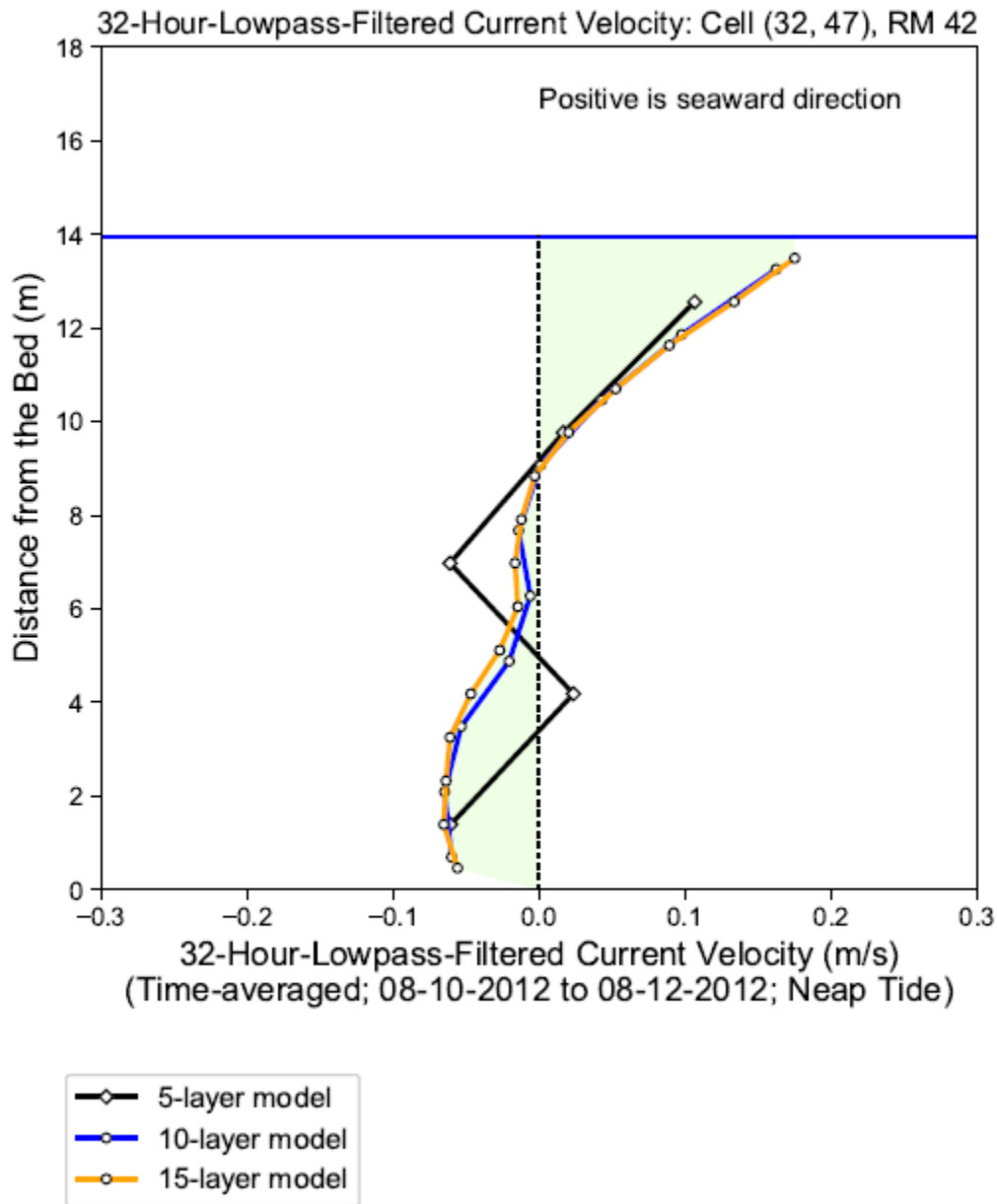
Notes: 32-hour-Low-pass-filtered results were calculated first and then averaged over the time period to represent the mean vertical structure. Shaded area represents the profile of the 15-layer model.

Figure T-23: Simulated 32-Hour-Lowpass-Filtered Along-channel Current Velocity during 08-10-2012 to 08-12-2012; Neap Tide at Station S1 at Cell (33, 43), RM 37.



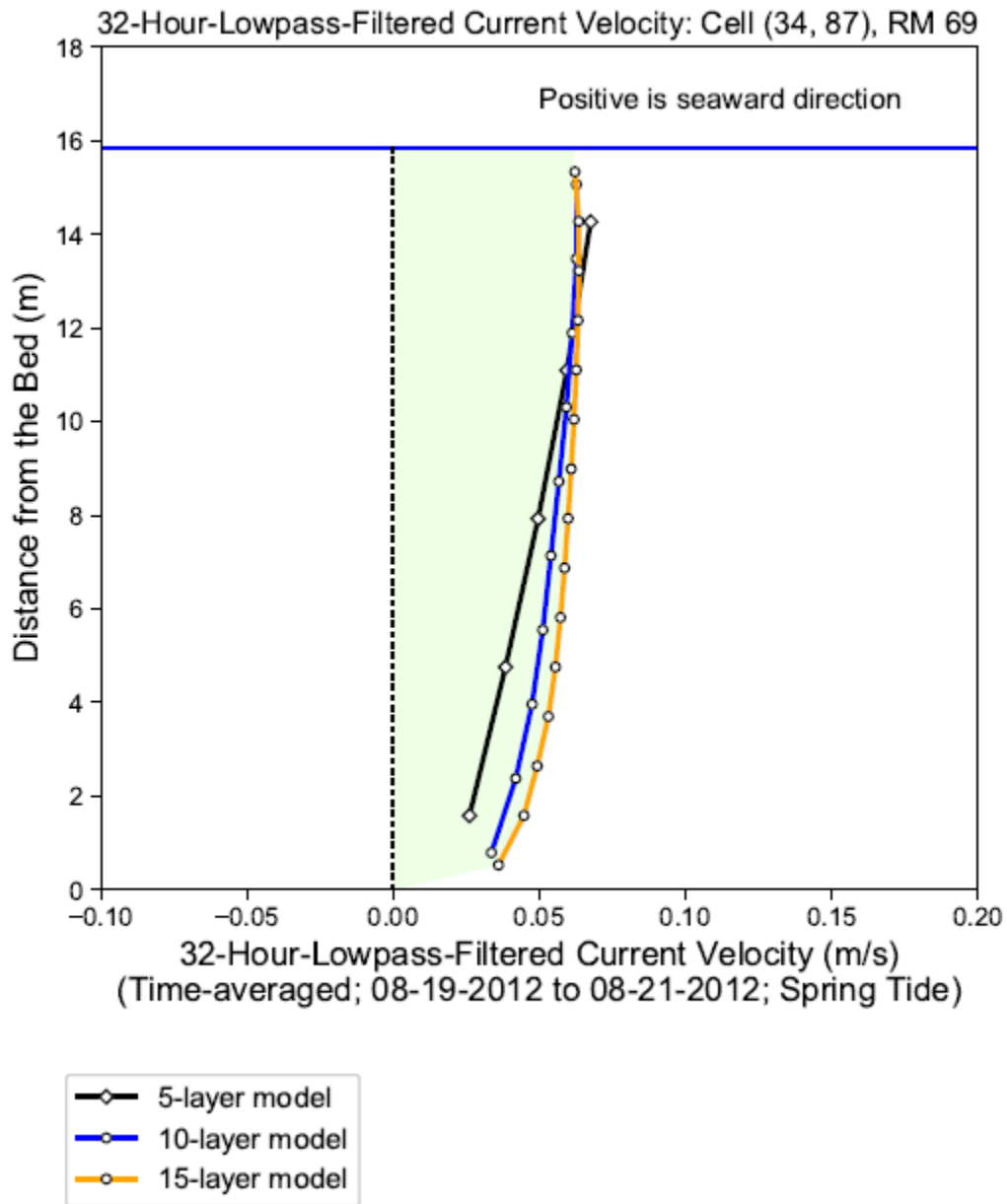
Notes: 32-hour-Low-pass-filtered results were calculated first and then averaged over the time period to represent the mean vertical structure. Shaded area represents the profile of the 15-layer model.

Figure T-24: Simulated 32-Hour-Lowpass-Filtered Along-channel Current Velocity during 08-19-2012 to 08-21-2012; Spring Tide at Station S2 at Cell (32, 47), RM 42.



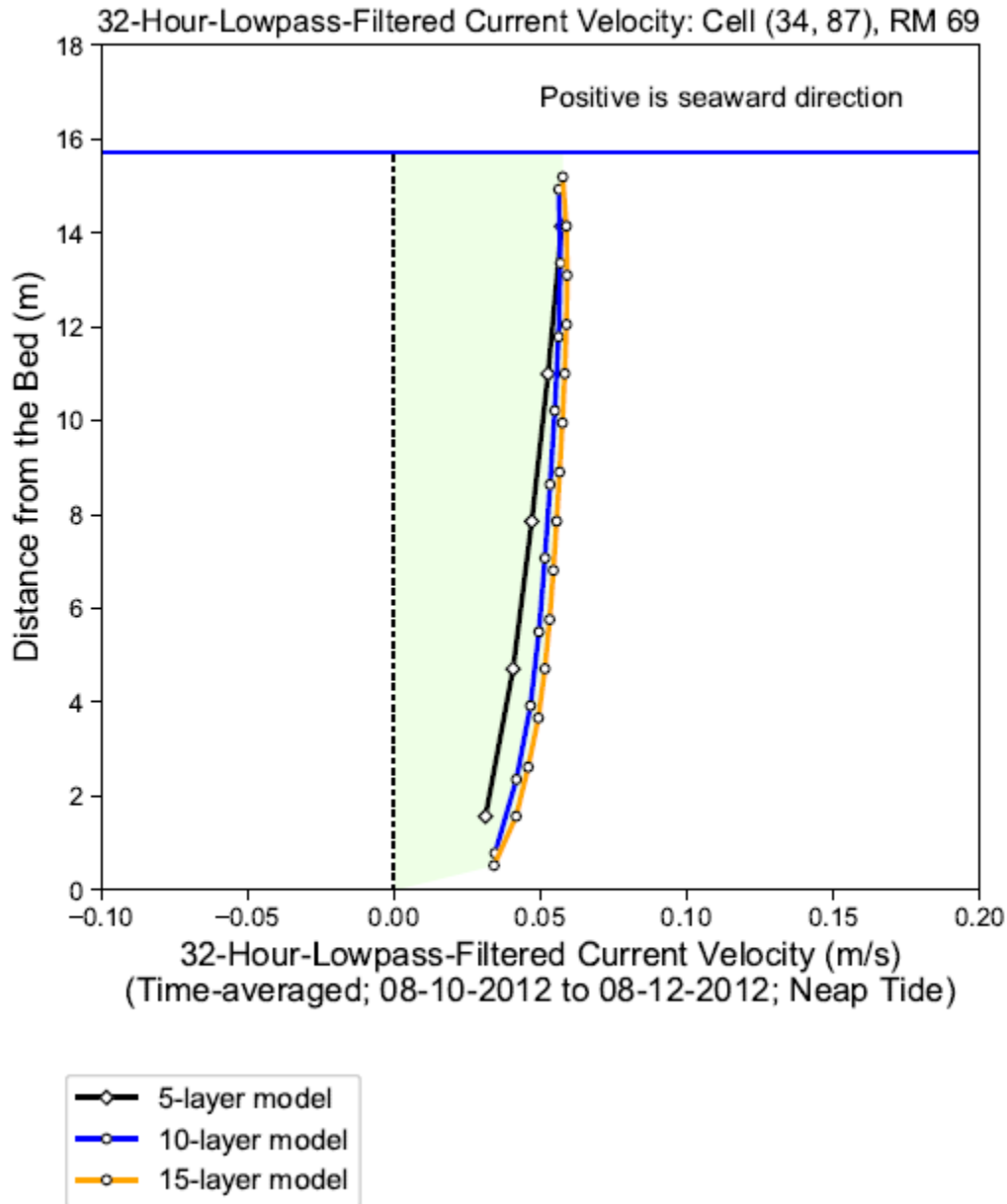
Notes: 32-hour-Low-pass-filtered results were calculated first and then averaged over the time period to represent the mean vertical structure. Shaded area represents the profile of the 15-layer model.

Figure T-25: Simulated 32-Hour-Lowpass-Filtered Along-channel Current Velocity during 08-10-2012 to 08-12-2012; Neap Tide at Station S2 at Cell (32, 47), RM 42.



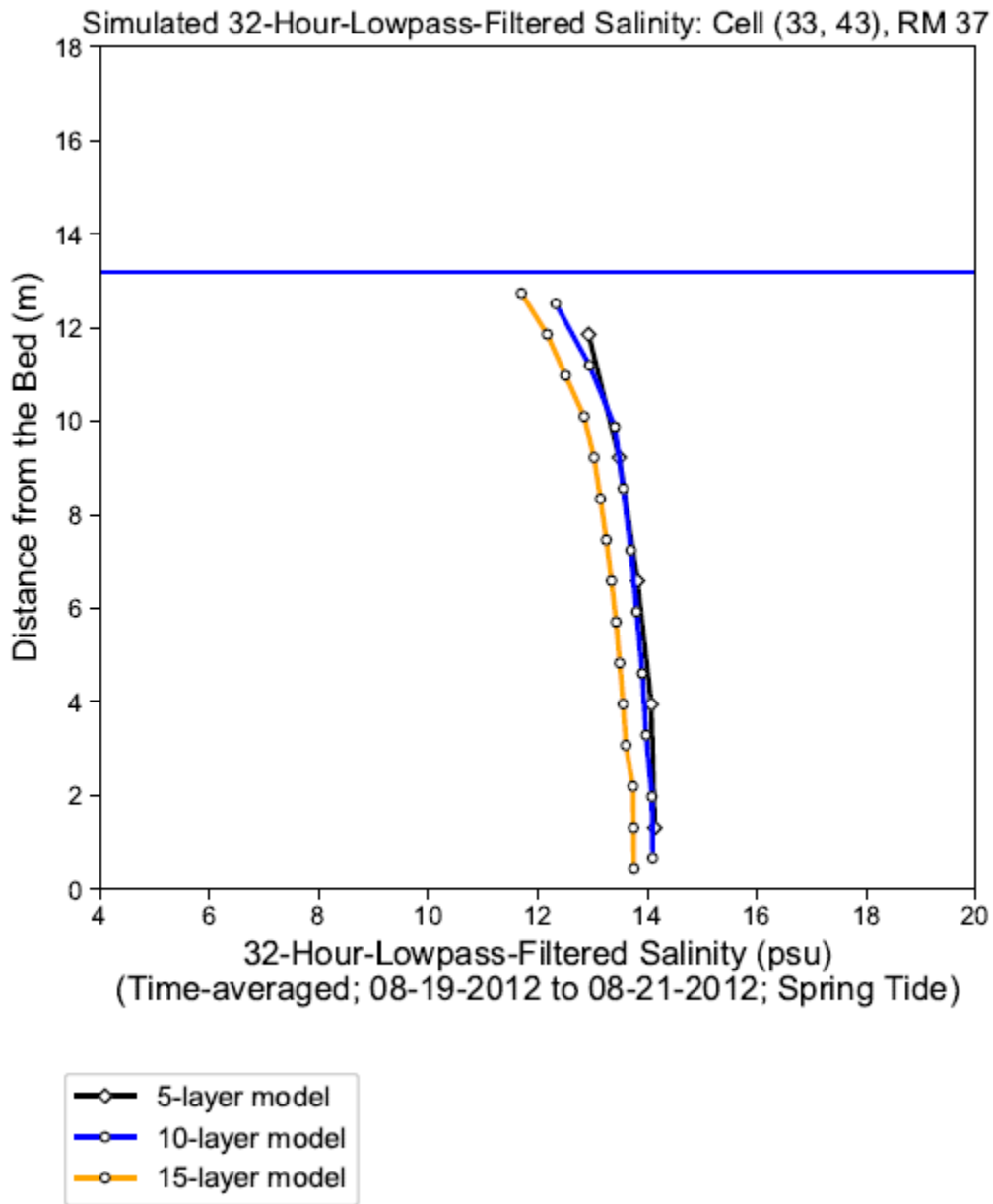
Notes: 32-hour-Low-pass-filtered results were calculated first and then averaged over the time period to represent the mean vertical structure. Shaded area represents the profile of the 15-layer model.

Figure T-26: Simulated 32-Hour-Lowpass-Filtered Along-channel Current Velocity during 08-19-2012 to 08-21-2012; Spring Tide at Station S3 at Cell (34, 87), RM 69.



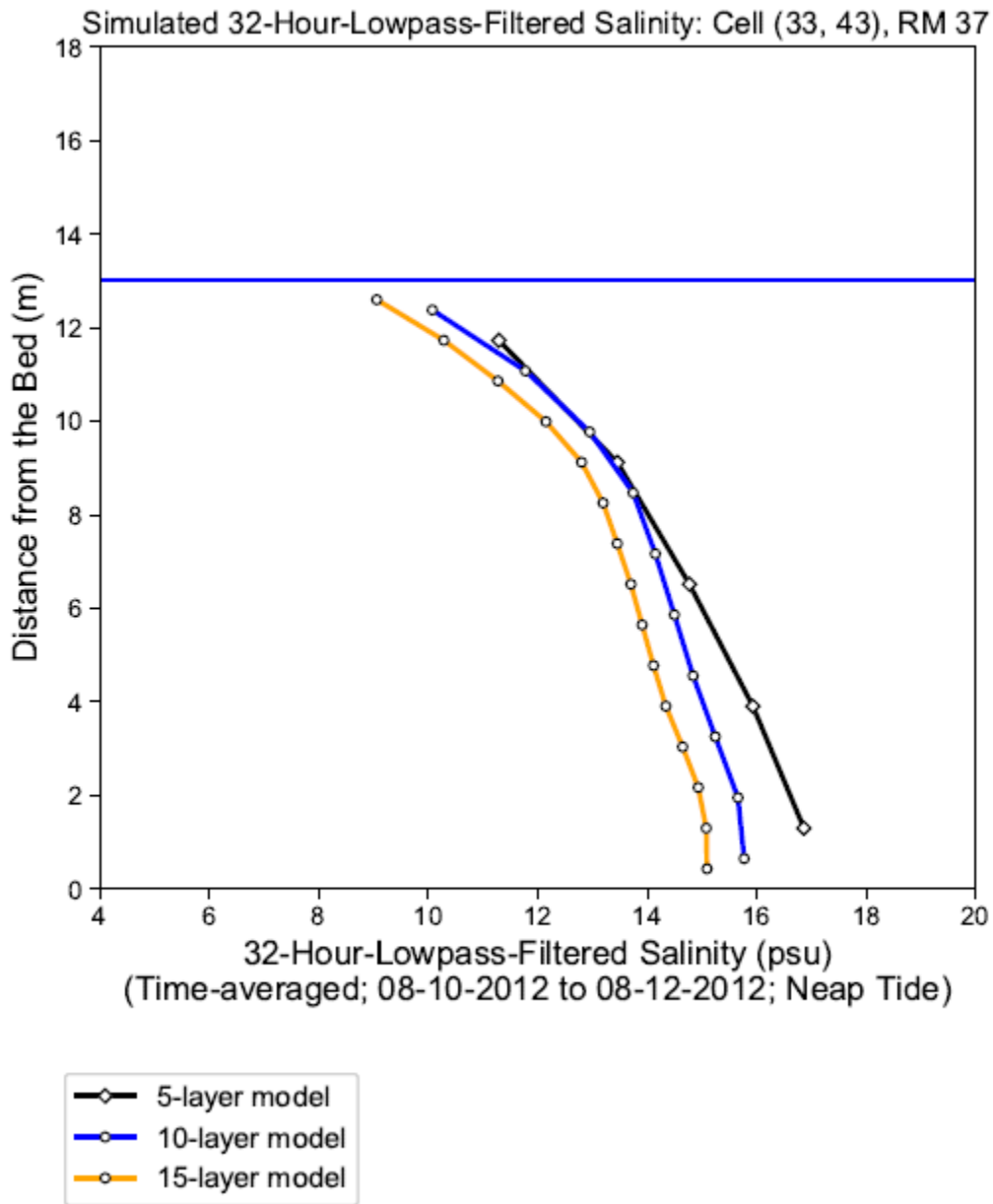
Notes: 32-hour-Low-pass-filtered results were calculated first and then averaged over the time period to represent the mean vertical structure. Shaded area represents the profile of the 15-layer model.

Figure T-27: Simulated 32-Hour-Lowpass-Filtered Along-channel Current Velocity during 08-10-2012 to 08-12-2012; Neap Tide at Station S3 at Cell (34, 87), RM 69.



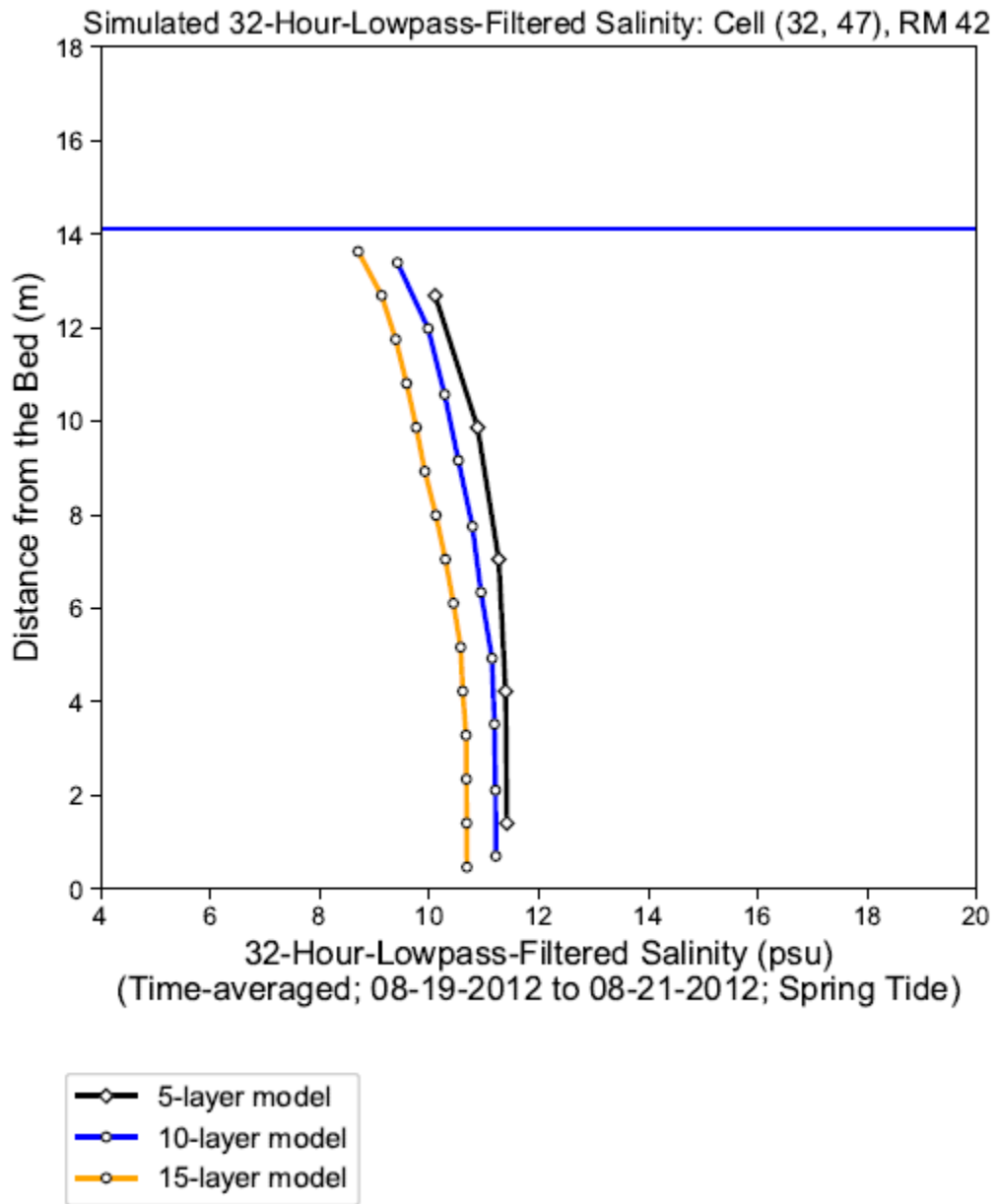
Notes: 32-hour-Low-pass-filtered results were calculated first and then averaged over the time period to represent the mean vertical structure.

Figure T-28: Simulated 32-Hour-Lowpass-Filtered Salinity during 08-19-2012 to 08-21-2012; Spring Tide at Station S1 at Cell (33, 43), RM 37.



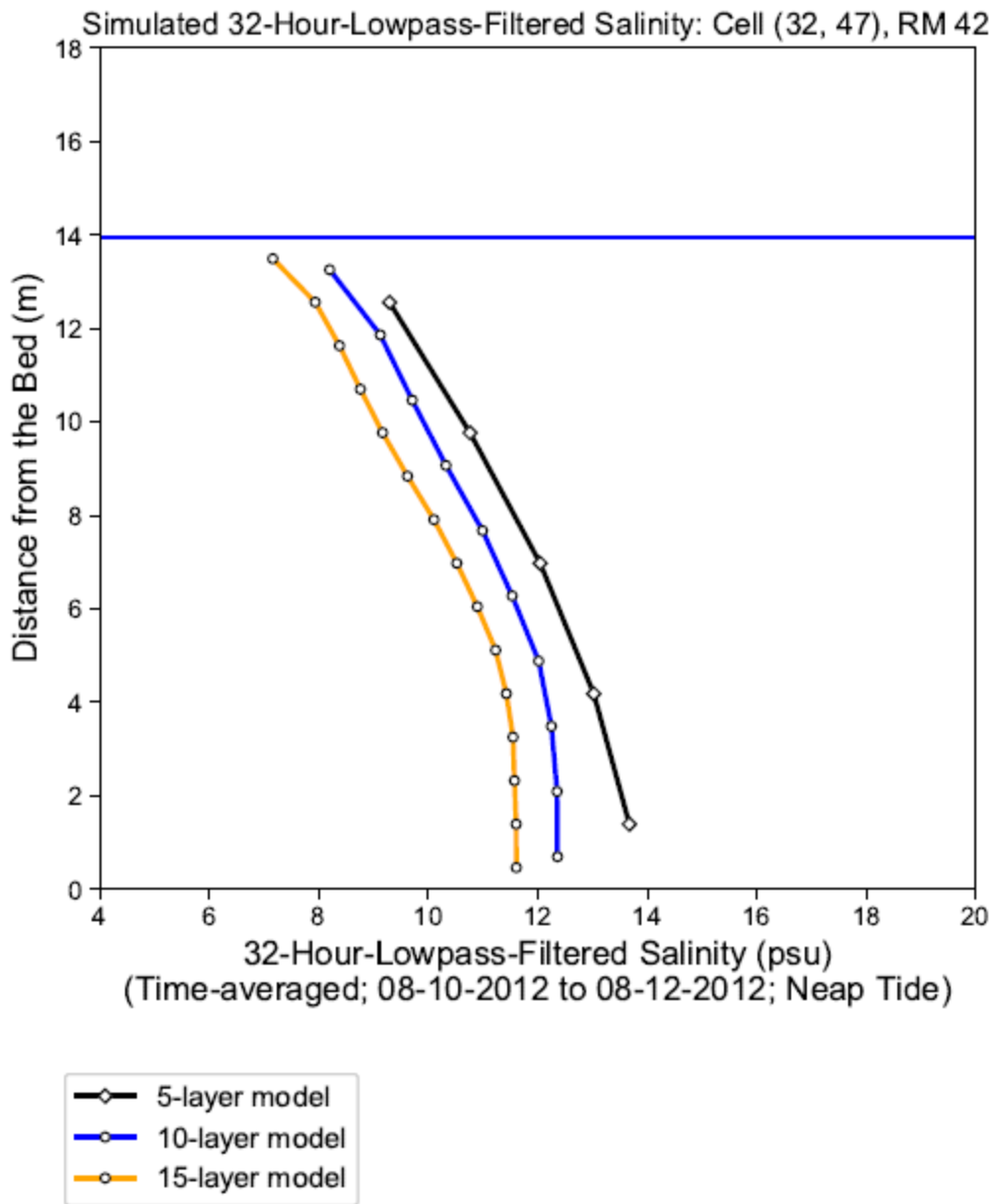
Notes: 32-hour-Low-pass-filtered results were calculated first and then averaged over the time period to represent the mean vertical structure.

Figure T-29: Simulated 32-Hour-Lowpass-Filtered Salinity during 08-10-2012 to 08-12-2012; Neap Tide at Station S1 at Cell (33, 43), RM 37.



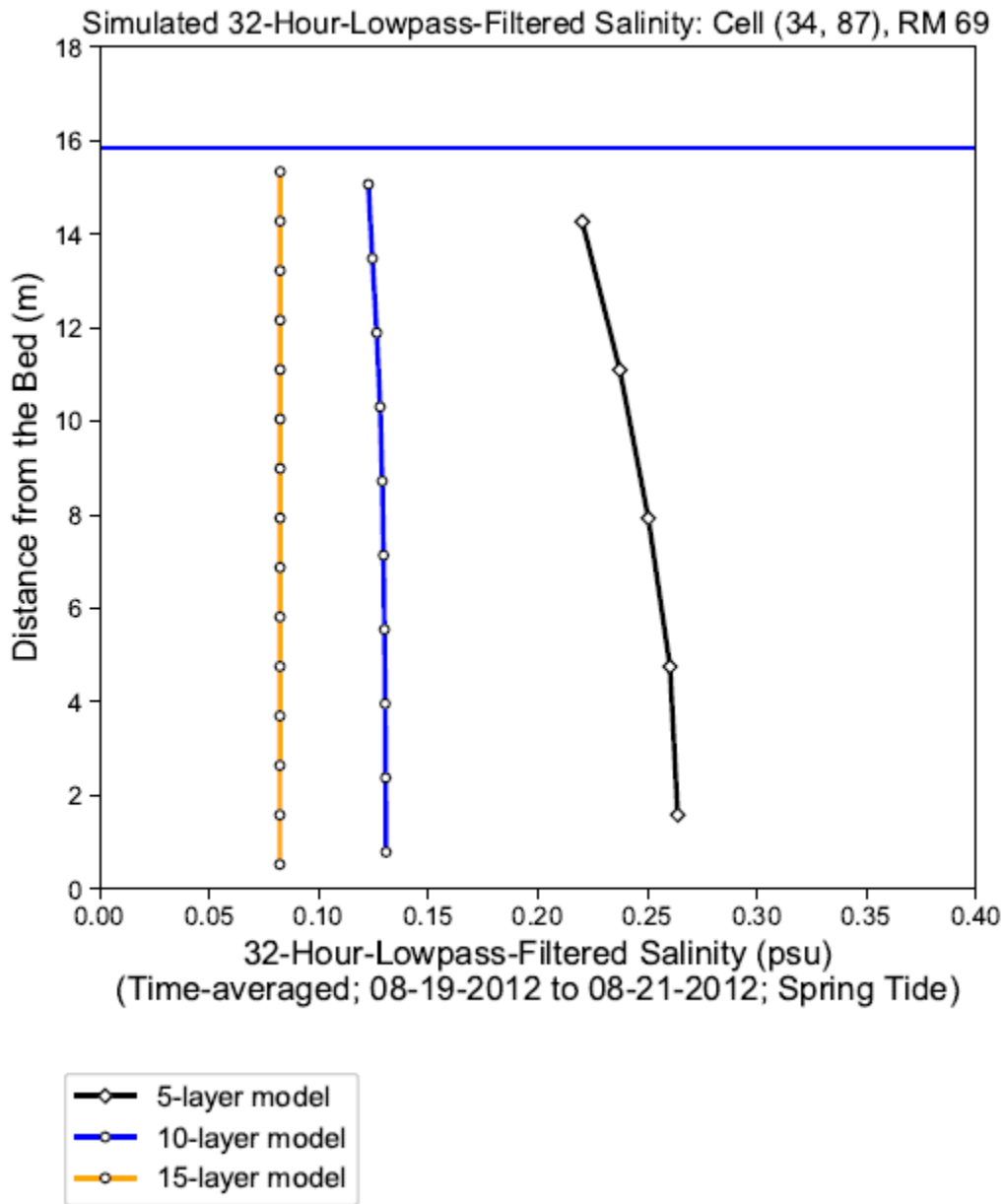
Notes: 32-hour-Low-pass-filtered results were calculated first and then averaged over the time period to represent the mean vertical structure.

Figure T-30: Simulated 32-Hour-Lowpass-Filtered Salinity during 08-19-2012 to 08-21-2012; Spring Tide at Station S2 at Cell (32, 47), RM 42.



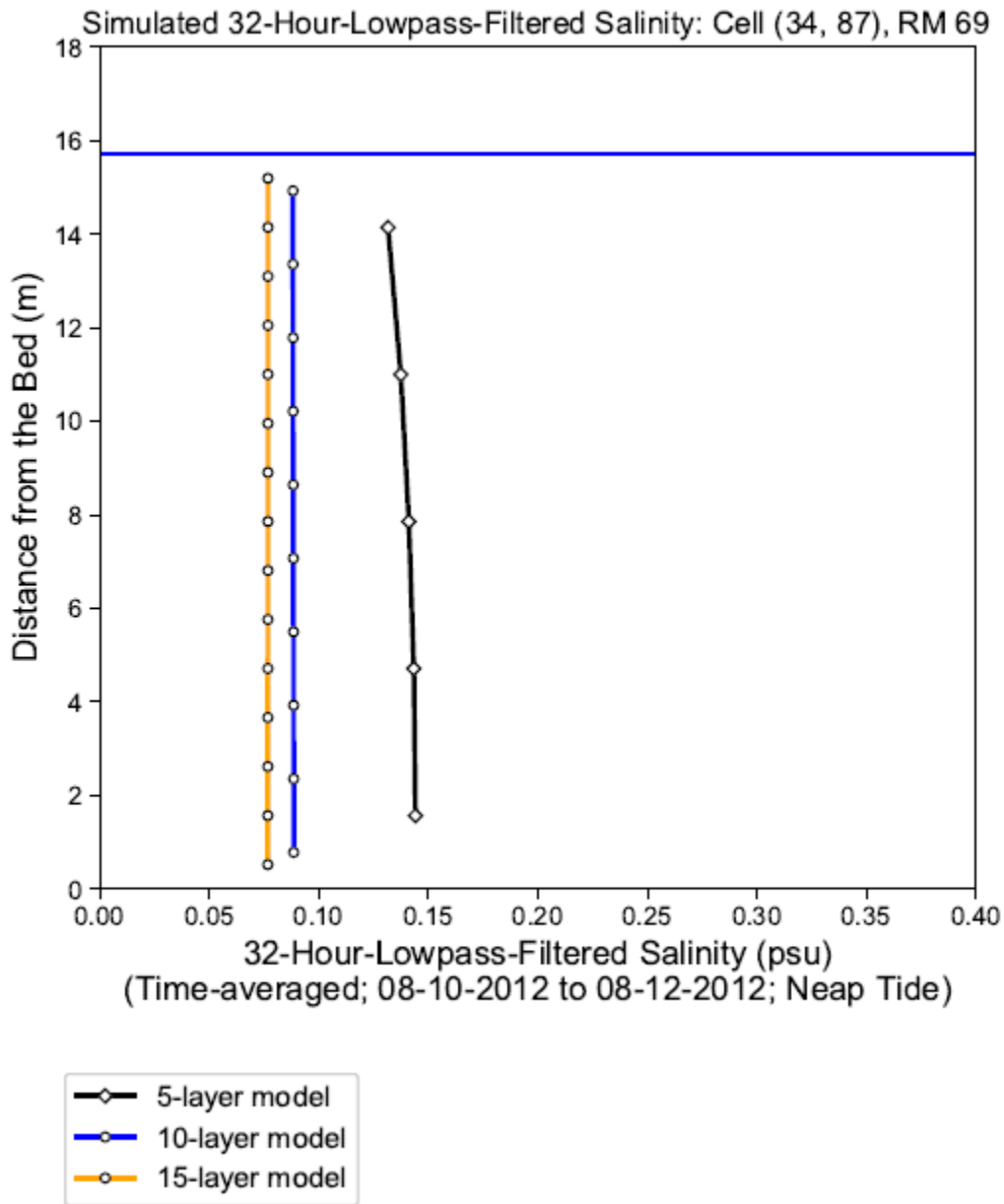
Notes: 32-hour-Low-pass-filtered results were calculated first and then averaged over the time period to represent the mean vertical structure.

Figure T-31: Simulated 32-Hour-Lowpass-Filtered Salinity during 08-10-2012 to 08-12-2012; Neap Tide at Station S2 at Cell (32, 47), RM 42.



Notes: 32-hour-Low-pass-filtered results were calculated first and then averaged over the time period to represent the mean vertical structure.

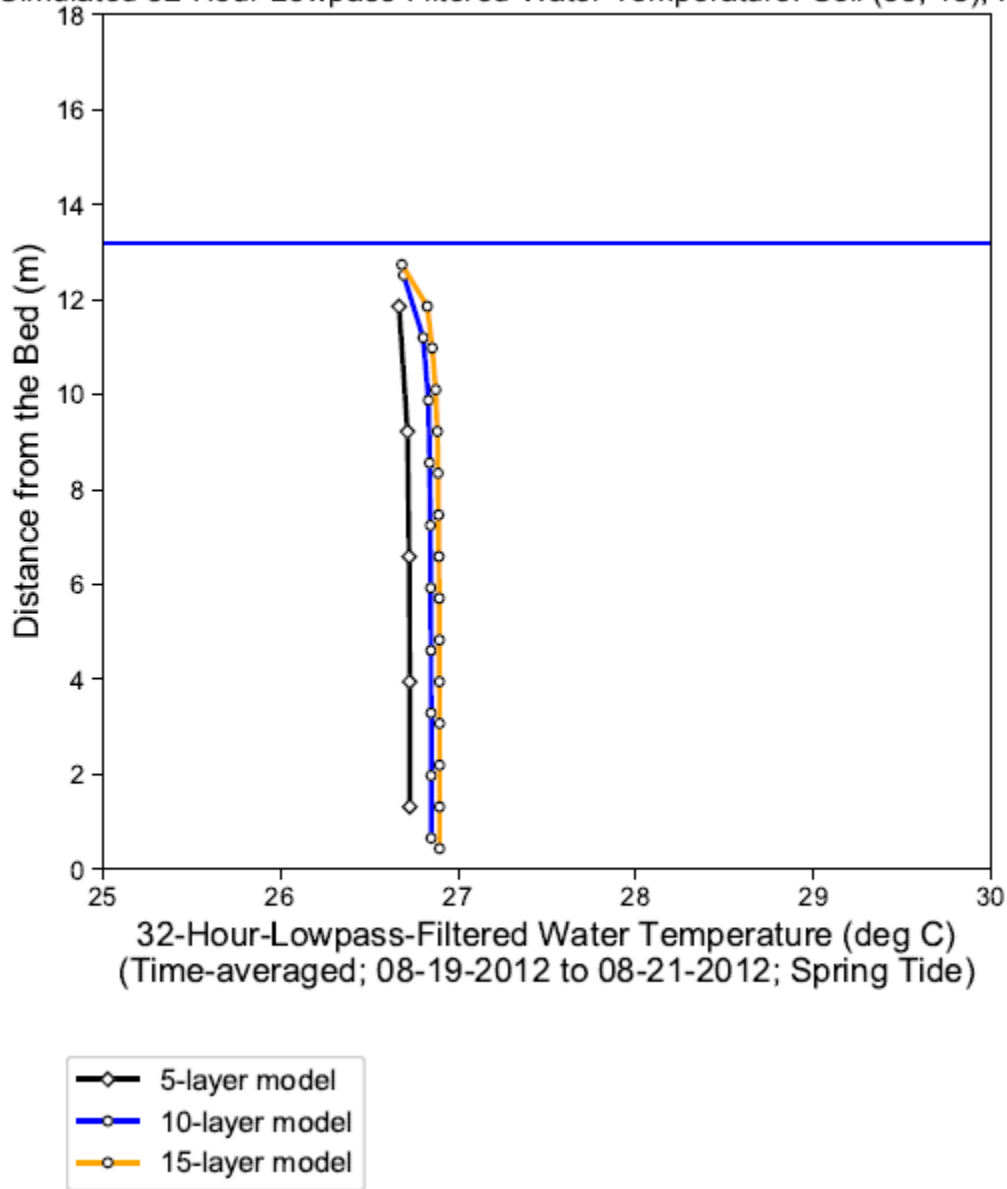
Figure T-32: Simulated 32-Hour-Lowpass-Filtered Salinity during 08-19-2012 to 08-21-2012; Spring Tide at Station S3 at Cell (34, 87), RM 69.



Notes: 32-hour-Low-pass-filtered results were calculated first and then averaged over the time period to represent the mean vertical structure.

Figure T-33: Simulated 32-Hour-Lowpass-Filtered Salinity during 08-10-2012 to 08-12-2012; Neap Tide at Station S3 at Cell (34, 87), RM 69.

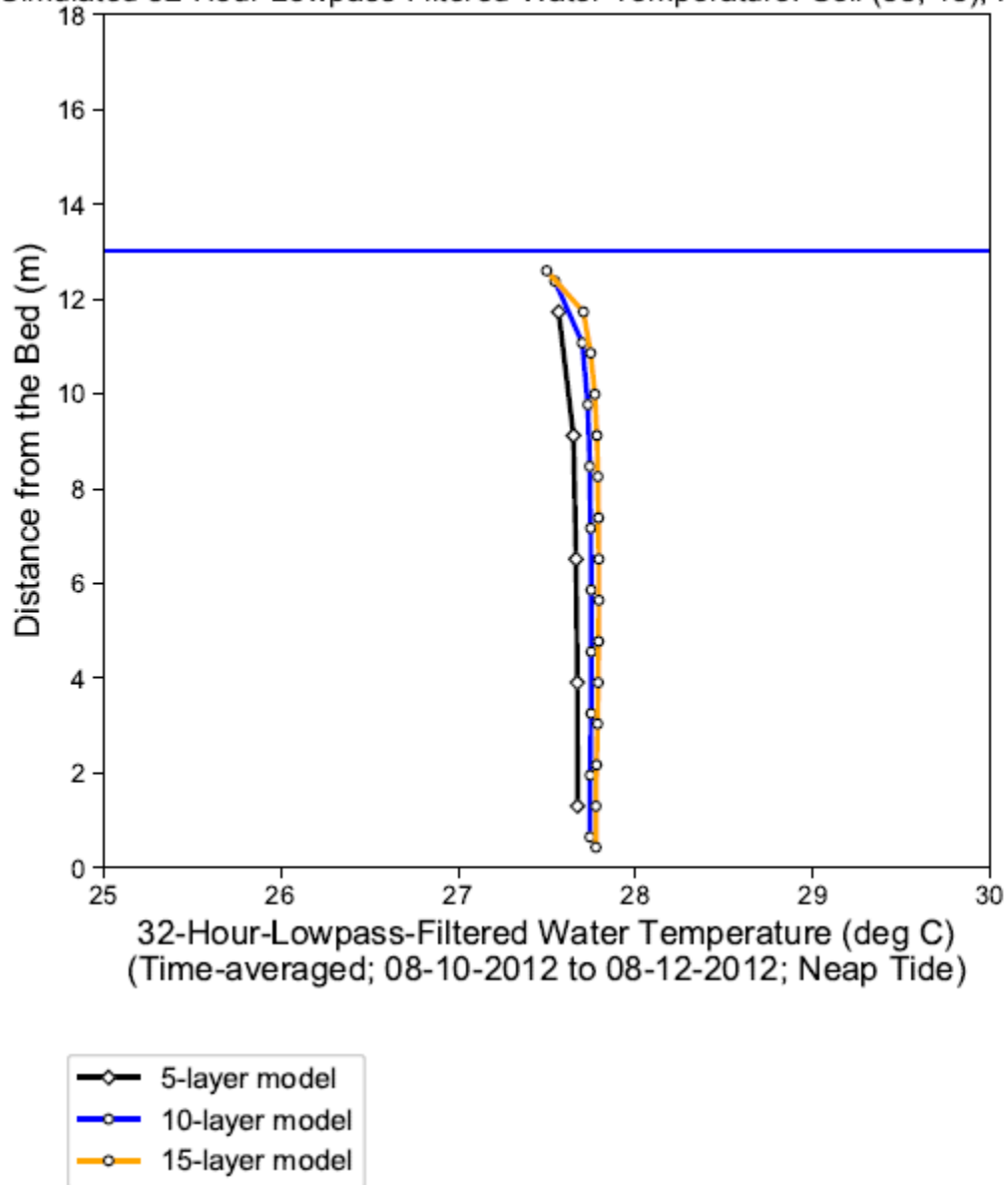
Simulated 32-Hour-Lowpass-Filtered Water Temperature: Cell (33, 43), RM 37



Notes: 32-hour-Low-pass-filtered results were calculated first and then averaged over the time period to represent the mean vertical structure.

Figure T-34: Simulated 32-Hour-Lowpass-Filtered Water Temperature during 08-19-2012 to 08-21-2012; Spring Tide at Station S1 at Cell (33, 43), RM 37.

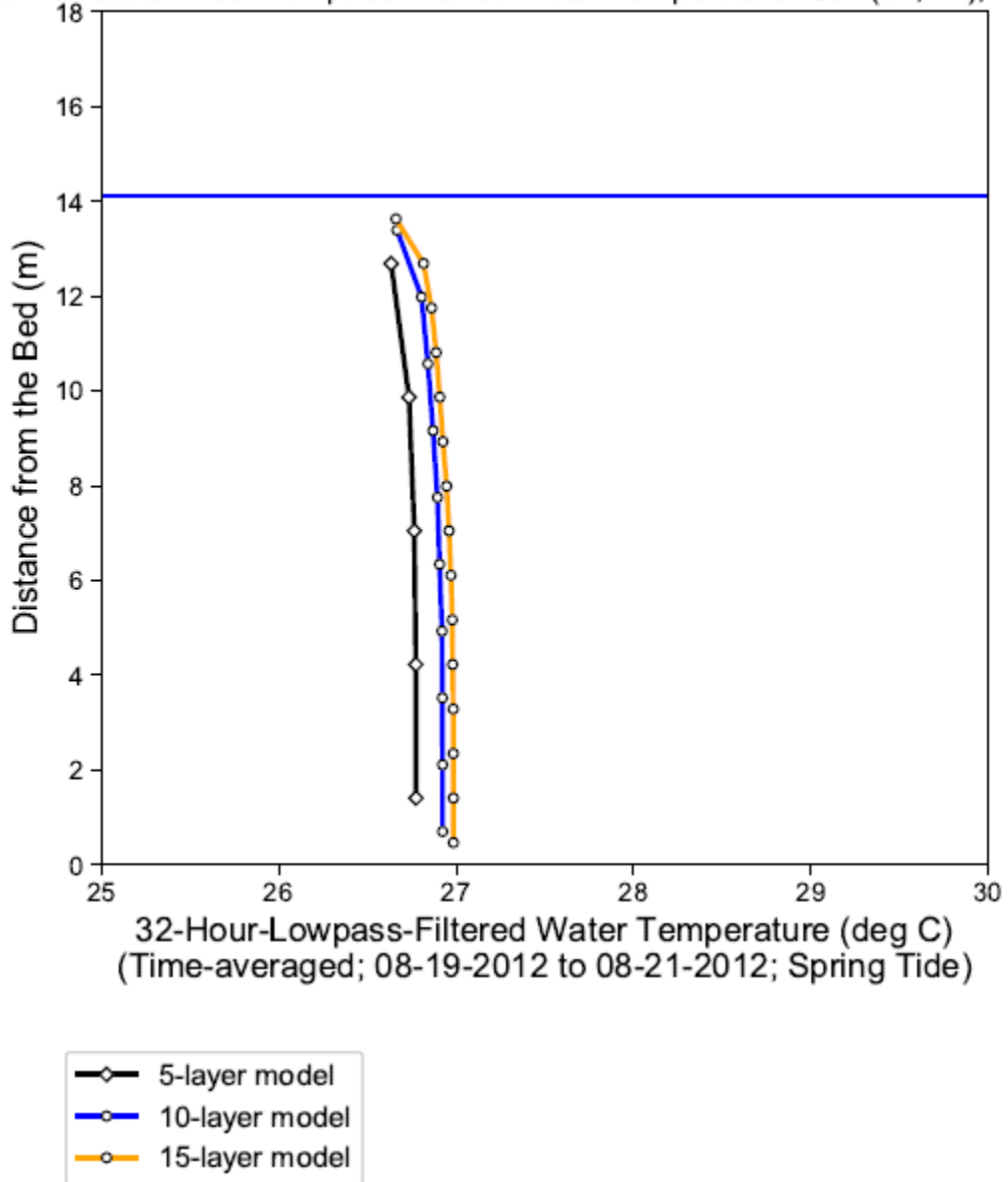
Simulated 32-Hour-Lowpass-Filtered Water Temperature: Cell (33, 43), RM 37



Notes: 32-hour-Low-pass-filtered results were calculated first and then averaged over the time period to represent the mean vertical structure.

Figure T-35: Simulated 32-Hour-Lowpass-Filtered Water Temperature during 08-10-2012 to 08-12-2012; Neap Tide at Station S1 at Cell (33, 43), RM 37.

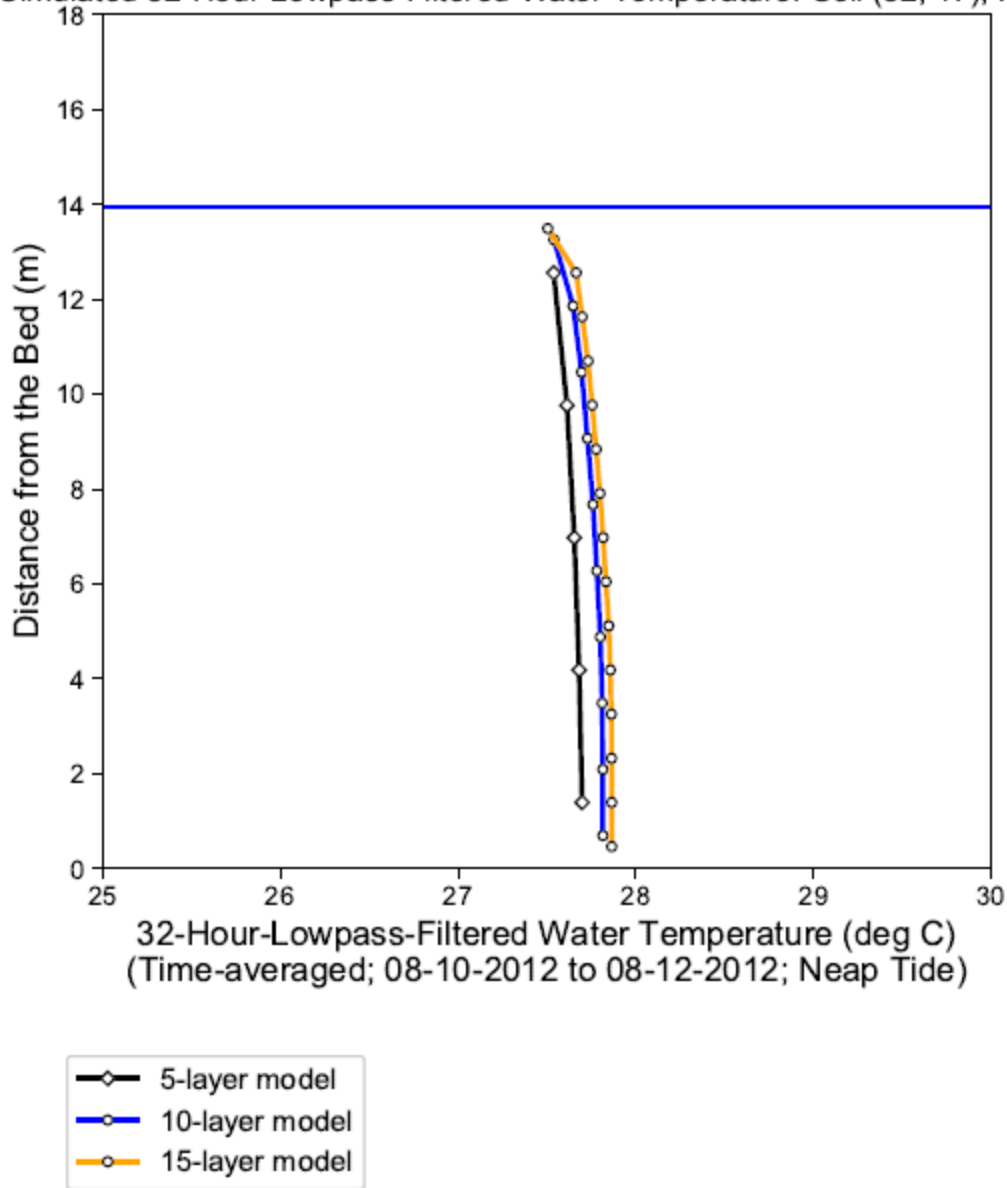
Simulated 32-Hour-Lowpass-Filtered Water Temperature: Cell (32, 47), RM 42



Notes: 32-hour-Low-pass-filtered results were calculated first and then averaged over the time period to represent the mean vertical structure.

Figure T-36: Simulated 32-Hour-Lowpass-Filtered Water Temperature during 08-19-2012 to 08-21-2012; Spring Tide at Station S2 at Cell (32, 47), RM 42.

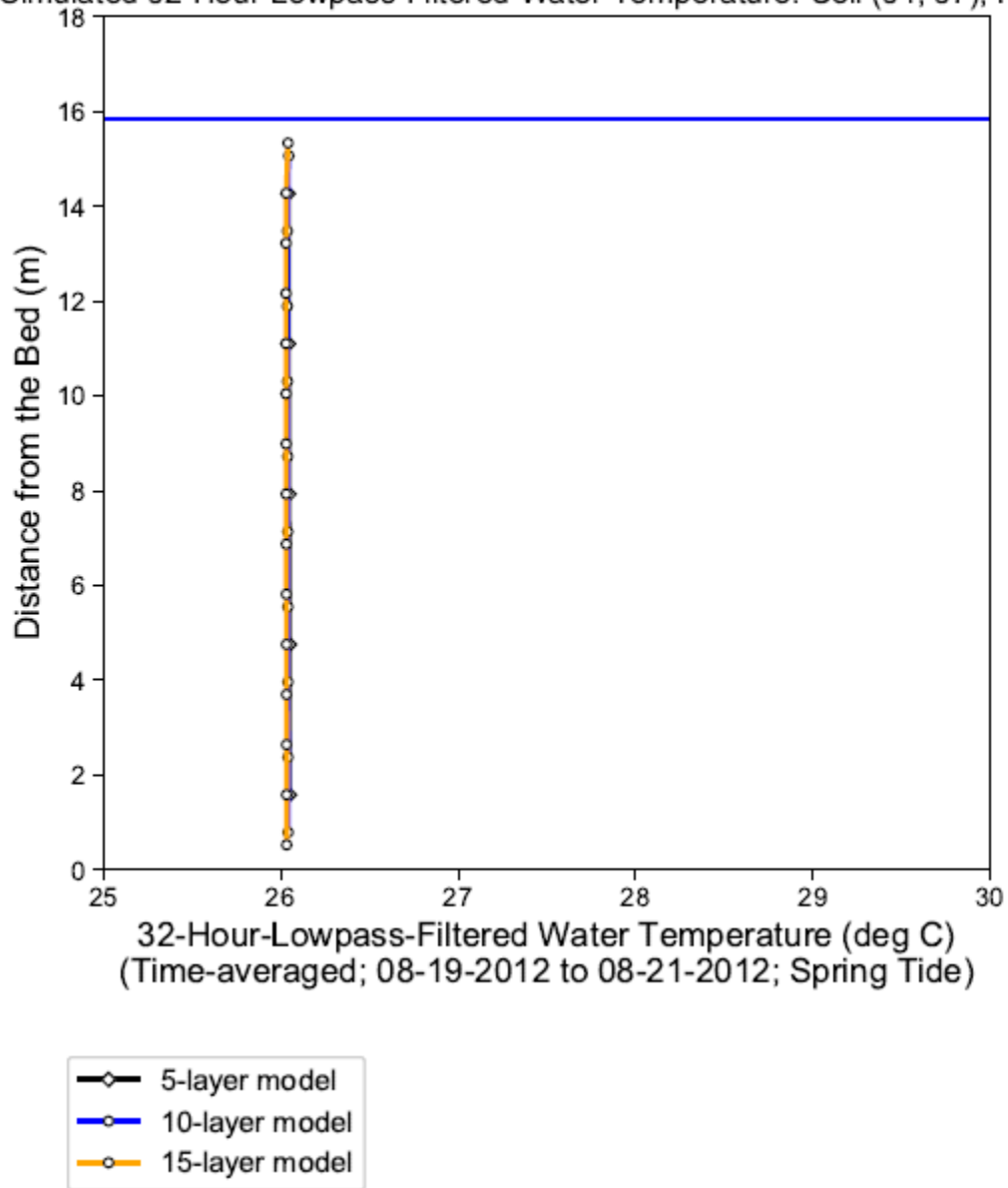
Simulated 32-Hour-Lowpass-Filtered Water Temperature: Cell (32, 47), RM 42



Notes: 32-hour-Low-pass-filtered results were calculated first and then averaged over the time period to represent the mean vertical structure.

Figure T-37: Simulated 32-Hour-Lowpass-Filtered Water Temperature during 08-10-2012 to 08-12-2012; Neap Tide at Station S2 at Cell (32, 47), RM 42.

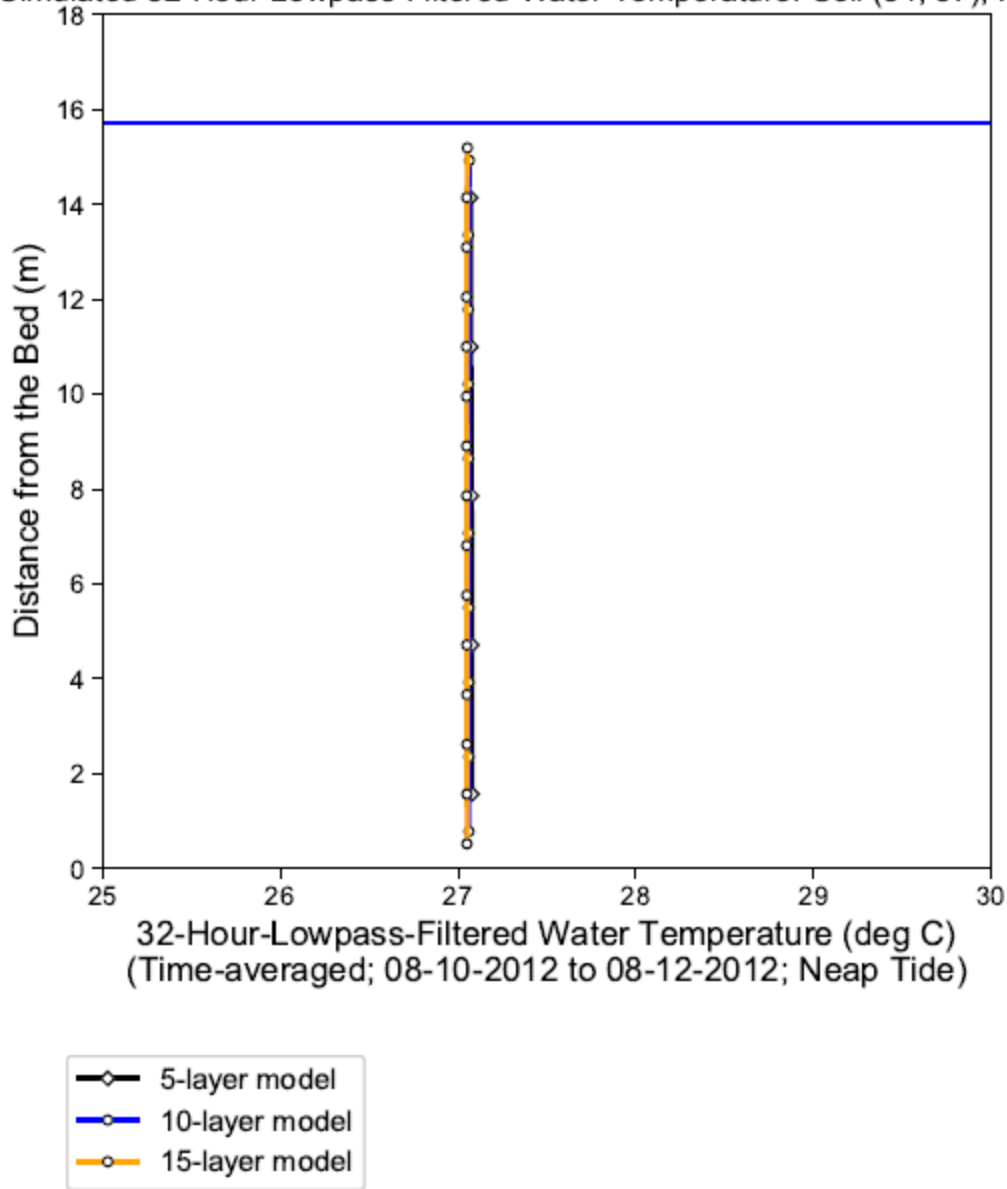
Simulated 32-Hour-Lowpass-Filtered Water Temperature: Cell (34, 87), RM 69



Notes: 32-hour-Low-pass-filtered results were calculated first and then averaged over the time period to represent the mean vertical structure.

Figure T-38: Simulated 32-Hour-Lowpass-Filtered Water Temperature during 08-19-2012 to 08-21-2012; Spring Tide at Station S3 at Cell (34, 87), RM 69.

Simulated 32-Hour-Lowpass-Filtered Water Temperature: Cell (34, 87), RM 69



Notes: 32-hour-Low-pass-filtered results were calculated first and then averaged over the time period to represent the mean vertical structure.

Figure T-39: Simulated 32-Hour-Lowpass-Filtered Water Temperature during 08-10-2012 to 08-12-2012; Neap Tide at Station S3 at Cell (34, 87), RM 69.

End of Document